UNIVERSITAT DE
BARCELONA

Simulación molecular aplicada a inhibidores de 11β hidroxiesteroide deshidrogenasa tipo 1 y efecto de temperatura en Citoglobina

Constantí Seira Castán

ADVERTIMENT. La consulta d'aquesta tesi queda condicionada a l'acceptació de les següents condicions d'ús: La difusió d'aquesta tesi per mitjà del servei TDX (**www.tdx.cat**) i a través del Dipòsit Digital de la UB (**diposit.ub.edu**) ha estat autoritzada pels titulars dels drets de propietat intel·lectual únicament per a usos privats emmarcats en activitats d'investigació i docència. No s'autoritza la seva reproducció amb finalitats de lucre ni la seva difusió i posada a disposició des d'un lloc aliè al servei TDX ni al Dipòsit Digital de la UB. No s'autoritza la presentació del seu contingut en una finestra o marc aliè a TDX o al Dipòsit Digital de la UB (framing). Aquesta reserva de drets afecta tant al resum de presentació de la tesi com als seus continguts. En la utilització o cita de parts de la tesi és obligat indicar el nom de la persona autora.

ADVERTENCIA. La consulta de esta tesis queda condicionada a la aceptación de las siguientes condiciones de uso: La difusión de esta tesis por medio del servicio TDR (**www.tdx.cat**) y a través del Repositorio Digital de la UB (**diposit.ub.edu**) ha sido autorizada por los titulares de los derechos de propiedad intelectual únicamente para usos privados enmarcados en actividades de investigación y docencia. No se autoriza su reproducción con finalidades de lucro ni su difusión y puesta a disposición desde un sitio ajeno al servicio TDR o al Repositorio Digital de la UB. No se autoriza la presentación de su contenido en una ventana o marco ajeno a TDR o al Repositorio Digital de la UB (framing). Esta reserva de derechos afecta tanto al resumen de presentación de la tesis como a sus contenidos. En la utilización o cita de partes de la tesis es obligado indicar el nombre de la persona autora.

WARNING. On having consulted this thesis you're accepting the following use conditions: Spreading this thesis by the TDX (**www.tdx.cat**) service and by the UB Digital Repository (**diposit.ub.edu**) has been authorized by the titular of the intellectual property rights only for private uses placed in investigation and teaching activities. Reproduction with lucrative aims is not authorized nor its spreading and availability from a site foreign to the TDX service or to the UB Digital Repository. Introducing its content in a window or frame foreign to the TDX service or to the UB Digital Repository is not authorized (framing). Those rights affect to the presentation summary of the thesis as well as to its contents. In the using or citation of parts of the thesis it's obliged to indicate the name of the author.

UNIVERSITAT DE BARCELONA

Simulación molecular aplicada a inhibidores de 11β hidroxiesteroide deshidrogenasa tipo 1 y efecto de temperatura en Citoglobina

Constantí Seira Castán

UNIVERSITAT DE BARCELONA
FACULTAT DE FARMACIA I CIENCIES DE L'ALIMENTACIÓ
DEPARTAMENT DE NUTRICIÓ, CIÈNCIES DE L'ALIMENTACIÓ I GASTRONOMIA

Simulación molecular aplicada a inhibidores de 11β hidroxiesteroide deshidrogenasa tipo 1 y efecto de temperatura en Citoglobina

CONSTANTÍ SEIRA CASTAN

BARCELONA, 2018

UNIVERSITAT DE BARCELONA
FACULTAT DE FARMACIA I CIÈNCIES DE L'ALIMENTACIÓ
DEPARTAMENT DE NUTRICIÓ, CIENCIES DE L'ALIMENTACIÓ I GASTRONOMIA
PROGRAMA DE DOCTORAT EN RECERCA, DESENVOLUPAMENT I CONTROL DE MEDICAMENTS

Simulación molecular aplicada a inhibidores de 11β hidroxiesteroide deshidrogenasa tipo 1 y efecto de temperatura en Citoglobina

Memoria presentada por Constantí Seira Castan
para optar al título de Doctor por la Universidad de Barcelona
dirigida por:

Dr. Axel Bidon-Chanal Badia
Director

Dr. Francisco Javier Luque Garriga
Director

Constantí Seira Castan
Doctorando

Dr. Axel Bidon-Chanal Badia
Tutor

CONSTANTÍ SEIRA CASTAN
BARCELONA, 2018

Als meus pares

“Somos pocos pero aún quedamos,

aún quedamos unos pocos,

que no somos como ellos”

Def Con Dos, 6 dementes contra el mundo

Agradecimientos

Primer de tot, moltes gràcies al meu Director i Tutor de la Tesi, el Dr. Axel Bidon-Chanal, per introduir-me en el món desconegut de la química teòrica, per ajudar-me en aquest repte, que no em pensava pas que pogués assolir, corregir-me els “errors totals” i pels viatges amb cotxe. És un orgull (o una maledicció depenent a qui li preguntis) ser el teu últim doctorand i espero que el meu vídeo post-tesi s’iguali amb el teu.

També agrair al Professor Francisco Javier Luque, la seva disponibilitat i col·laboració com a co-director d’aquesta tesi doctoral, concedint-me part del seu temps i per deixar-me formar part d’aquesta gran família que és el grup d’investigació Computational Biology & Drug Design.

Moltes gràcies al Dr. Ramón Pouplana, per acceptar-me al màster, pels consells, i per les calçotades a Sant Climent.

Per altra banda, agrair als Dr. Barril, Campanera i Curutchet per oferir-me ajuda a l’hora de resoldre problemes quan ho he necessitat; especialment a aquest últim per haver-nos fet partíceps d’un document imperdible que segueixo custodiant com si fos un templari.

Muchas gracias también al Dr. Santiago Vázquez, Profesor agregado del Departamento de Farmacología i Química Terapéutica por su colaboración en las publicaciones de la primera parte de esta tesis doctoral.

Por último (pero no por eso menos importante) agradecer a la Dra. Mª Luisa Garcia por su ayuda en temas burocráticos, siempre engorrosos.

Un cop agraïts els “jefes” .... més de 4 anys donen per molt, i segurament em deixi algú a l’hora de donar-li les gràcies, com que no tinc la memòria del Toni pels noms aliens posaré els que recordo (i els que em recordarà ell).

Gràcies a la Salo AKA “Khaleesi de Sants” per la paciència i els bons consells.

Gràcies al Jordi per l'ajuda quan no entenia res (encara menys que ara), pels penals no xiulats i per les converses de primats involucionats.

Gràcies a la Marina AKA "mamita loca/a mãe de Roque" pels cafès "en chel", els aniversaris accidentats i els carnavals absurds.

Grazie Ornella porque aunque me odiesss y te caiga mal ... no puedessss vivir sin mí ... y lo sabesssss.

Gràcies a la Rosana, per l'empenta a l'hora d'avançar en les publicacions, i la col·laboració inestimable (això dit de l'Arda Turan de la Química Computacional a la Messi de la Química Farmacèutica).

Gracias a Sonia faaaan por ser tan faaaaaan ... bueno de todo en general y de cualquier cosa en particular, y porque ya lleva acertadas 2 "teorías de Romero" (2 de 15588536959).

Obrigado Dr Syl Pinke AKA "a mãe da pequena Iara" para ser a bonequinha mentirosa mais bonita que meus olhos jamais verão.

Merci à Théo Sánchez pour rafraîchir mon français rouillé.

Gracias a Javi Vázquez, por sus intentos de ligar con francesas ("ye mapol") y por las conversaciones simiescas.

Gràcies als "Barrilers": Serena, Sergi, Guillermo, Galdeano, Miriam, Moira, Macej, Daniel, Kevin, Yvonne, Melpomeni, Montse, Aida, Salvatore i qui m'hagi deixat per els seminaris compartits.

Obrigado Gleice (e seu marido Dannyson) por tentar apresentar Deus na minha vida sem sucesso.

Grazie Tiziana per insegnarmi a dire correttamente Tom Hanks e per le conversazioni in metropolitana.

Grazie Carmine AKA “Carmain” per lo zaino, per farci conoscere il “Miseria e nobilta” e per rispettare la mia coinquilina.

Obrigado Railda e Louri, para a cachaça de Jambú, as cervejas e por não me deixar envenenar seu casamento.

Gràcies a la Laia (uhuuuummm) per els riures al despatx, per ser la “lover advisor” del F.O. i perquè quan deu assentir segur que li fa perdre el senderi al Fede (Pedron).

Gracias a Mauro por llevar el “uhummmmm” al otro lado del charco.

Gracias a Fede (Isoglio) por que nunca pensaba que iba a abrazarme a un argentino hasta que Sergi Roberto marcó el sexto y por los “encuentros inesperados”.

Grazie Alessandro per insegnarmi tutte le parolacce dell’italiano.

Gracias a Camila por los debates inacabables y por presentarnos a Róber.

Grazie Stella, per aver testato la pazienza di tutti senza finire all’obitorio.

Grazie Emanuele per essere il mio amuleto di buona fortuna e sfortuna ma non per strofinare le mie palle senza permesso.

Gracias a David Vílchez, AKA Broncano/Marron por experimentar “la sensación” y no hacer (excesivo) usufructo de ella.

Thank you Elnaz for the patience and for letting Sheitan be part of your life.

Gracias Natalia por ser tan amable y paciente llevando a Bruno en tu interior.

Gràcies Irene per ser més simpática que "podemita" animant els dinars.

Grazie Salvatore poiché dopo predecessori indegni hai ripristinato il prestigio dell'Università di Bari.

Grazie Roberta, Valeria e Nora per avermi fatto capire che il caffè di qua non è buono per il palato italiano.

Gracias al "TITÁN" Will ZAMora, el Hércules caribeño, el Conan de Costa Rica, el Capitán América Latina, el hombre que no va al Gym, si no que el Gym viene a él, papito de Iara y miembro fundador del F.O., por las cenas (¡me encanta el vino!) , por enseñarme a hablar un poco de Patois y por dejarnos a los simples mortales alguna muchacha libre a la que conquistarrrr.

Gràcies a Toni AKA Toñinder#Guay/Tonino Ciccione, també co-fundador del F.O., per ser tan bon company i millor persona i per contagiar, ni que sigui una mica, a capsigranys com jo d'aquesta bondat, per tenir paciència (infinita) amb alguns habitants de Naboo y per el viatges a Ikea fent un "Tetris".

Moltes gracis a na Carol AKA Dr. Estarellas (la más bonita de todas las estrellas para los amigos, la maldad hecha belleza para los enemigos) per ésser sa meva segona mamà, per s'ajuda en es pósters i perquè ara ja només li caldrà cuidar de l'Elsa.

A Giulia, perchè lei "Sends me into hyperspace when I see her pretty face".

I finalment als meus pares, per tot.

Resumen

Esta tesis doctoral contempla dos objetivos. El primero consiste en el estudio de relaciones estructura-actividad en diseño de fármacos, que en su mayoría incluyen el grupo adamantano debido a sus propiedades estructurales y fisicoquímicas, sobre la enzima 11β-hidroxiesteroide deshidrogenasa tipo 1. El interés en dicho enzima obedece al papel que desempeña en el contexto de enfermedades metabólicas como la diabetes y el síndrome metabólico, además de proporcionar un nuevo enfoque en el tratamiento de las disfunciones cognitivas relacionadas con la edad, incluyendo la enfermedad de Alzheimer. Así, en la tesis se describen las aproximaciones realizadas para el diseño de compuestos implicados en la inhibición de dicho enzima desde la perspectiva del trabajo realizado en modelización molecular y estudio del modo de unión de los inhibidores propuestos. Dicha investigación ha sido realizada en colaboración con diversos Departamentos, entre ellos el de Farmacología, Toxicología y Química Terapèutica de la Facultad de Farmacia y Ciencias de la Alimentación de la Universidad de Barcelona, donde se llevó a cabo la síntesis de los compuestos, obteniéndose resultados prometedores para diferentes conjuntos de compuestos.

El segundo objetivo se centra en el estudio del proceso de migración de ligandos en globinas concretamente en el caso particular de citoglobina, cuarto miembro de la familia de la globinas. El interés principal ha radicado en el estudio mediante trabajos de modelización molecular del efecto que provoca la temperatura en el transporte de ligandos sobre citoglobina. En particular, se ha examinado la relación entre estructura, dinámica y función comparando la citoglobina humana con la del pez *Chaenocephalus aceratus* y *Dissostichus mawsoni* haciendo énfasis en la influencia de la temperatura sobre la topología de sus cavidades internas. Asimismo, también se realizó un análisis cualitativo sobre la migración de O_2 a través de los diferentes sistemas estudiados. Dicho estudio ha puesto en evidencia la vital importancia del enlace (o la ausencia del mismo) de hidrógeno entre la serina 30 y el triptófano 151 como factor clave en la estabilidad de la proteína y la formación, tamaño y continuidad de sus canales.

Summary

This doctoral thesis has two objectives. The first is the study of structure-activity relationships in drug design, which mostly include the adamantane group due to its structural and physicochemical properties, on the enzyme 11β-hydroxysteroid dehydrogenase type 1. The interest in this enzyme is due to the role that it plays in the context of metabolic diseases such as diabetes and metabolic syndrome, and provides a new approach in the treatment of age-related cognitive dysfunctions, including Alzheimer's disease. Accordingly, the thesis describes the approximations made for the design of compounds involved in the inhibition of this enzyme from the perspective of the work done in molecular modeling and of the predicted binding mode of the proposed inhibitors. This research has been carried out in collaboration with several Departments, among them Pharmacology, Toxicology and Therapeutical Chemistry of the Faculty of Pharmacy and Food Sciences of the University of Barcelona, where the synthesis of the compounds was carried out, obtaining promising results for different sets of compounds.

The second aim involves the study of the migration process of ligands in globins focusing on the particular case of cytoglobin, fourth member of the globin family. The main interest has been focused in the study, by means of molecular modelling, of the effect of temperature on the transport of ligands in cyoglobin. The relationship between structure, dynamics and function has been examined by comparing human cytoglobin with the *Chaenocephalus aceratus and Dissostichus mawsoni*, with emphasis on the influence of temperature on the topology of its internal cavities. A qualitative study on the migration of O_2 through the different systems was also carried out, disclosing the vital importance of hydrogen bonding (or lack thereof) between serine 30 and tryptophan 151 as a key factor in the stability of the protein and the conformation, size and continuity of its internal tunnel cavities.

Abreviaturas

AMBER	*Assited Model Building with Energy Refinement*
ADME	*Absorption, Distribution, Metabolism and Excretion process*
B3LYP	*Becke three-parmeter Lee-Yang-Parr Exchange-correlation functional*
caCygb	*Chanenocephalus aceratus Cytoglobin*
cAMP	*Cyclic adenosine monophosphate*
CHARMM	*Chemistry at HARvard Macromolecular Mechanics*
CYP450	*Cytochrome P-450*
DFT	*Density Functional Theory*
ER	*Endoplasmic Reticulum*
EMA	*European Medicines Agency*
ER	*Endoplasmic Reticulum*
FDA	*Food & Drugs Administration*
GAFF	*General AMBER Force Field*
GBSA	*Generalized Born model augment with the hydrophobic solvent accesible Surface Area term*
GC	*GlucoCorticoid*
GPCR	*G Protein-Coupled Receptor*
GR	*Glucoorticoid Receptor*
HPC	*hipotalámic-pituitaric-suprarrenal axis*
hCygb_c1	*human Cytoglobin tryptophan conformation 1*
hCygb_c2	*human Cytoglobin tryptophan conformation 2*
hCygb_S30M	*human Cytoglobin mutation Metionine-Serine*
HF	*Hartree-Fock method*
11β-HSD1	*11β-hydroxysteroid dehydrogenase type 1*
11β-HSD2	*11β-hydroxysteroid dehydrogenase type 2*
IC_{50}	*half-maximal Inhibitory Concentration*
Lba	*leghemoglobin*
LKT	*Leukotriene*
MD	*Molecular Dynamics*
MM	*Molecular Mechanics*

MetS	*Metabolic Syndrome*
Mb	*Mioglobin*
MR	*Mineralocorticoid Receptor*
MST	*Miertus -Scrocco Tomasi solvation model*
NADPH	*Nicotinamide Adenine Dinucleotide Phosphate*
ND	*Not Determined*
Ngb	*Neuroglobin*
NSAID	*Nonsteroidal anti-inflammatory drug*
PD	*Pharmacodynamics*
PDB	*Protein Data Bank*
PG	*Prostaglandin*
PK	*PharmacoKinetic*
QM	*Quantum Mechanics*
QM/MM	*Quantum Mechanics Molecular Mechanics*
RMDS	*Root-Mean Square Deviation*
ROS	*Reactive Oxygen Species*
TIP3P	*Transferrable Intermolecular Potential with 3 points*

Índice

ÍNDICE

1- INTRODUCCIÓN **1**

1.1 Inhibición de la enzima 11β-hydroxisteroide deshidrogenasa **3**

1.1.1 Glucocorticoides y su actividad fisiológica **3**
1.1.2 Estructura y función de la enzima 11β-hydroxisteroide deshidrogenasa **5**
1.1.3 11β-HSD1 como diana terapéutica pleotrópica **8**
1.1.4 Diabetes mielitus tipo 2, obesidad y síndrome metabólico **9**
1.1.5 El papel de 11β-HSD1 en inflamación **11**
1.1.6 11β-HSD1 en la disfunción cognitiva producida por el envejecimiento **12**
1.1.7 Estrategias terapéuticas de inhibición de 11β-HSD1 **12**
1.1.8 Inhibidores de 11β-HSD1 basados en la estructura del adamantano **17**

1.2 Análisis de los canales internos de citoglobina **21**

1.2.1 Globinas y difusión de ligandos **21**
1.2.2 Citoglobinas **25**
1.2.3 Efecto de la temperatura en globinas **29**
1.2.4 Aproximaciones computacionales a enzimas psicrofílicas **31**

2- OBJETIVOS **35**

2.1 Estudio de relaciones estructura-actividad en diseño de fármacos, aplicado a 11β-hidroxiesteroide deshidrogenasa tipo 1 **37**

2.2 Influencia de la temperatura en la topología de las cavidades internas y la migración de ligandos en citoglobinas **38**

3- RESULTADOS **39**

3.1.1 Artículo 1: *"Searching for novel applications of the benzohomoadamantane scaffold in medicinal chemistry: Synthesis of novel 11b-HSD1 inhibitors"* **43**

3.1.2 Artículo 2: "*Novel 11b-HSD1 inhibitors: C-1 versus C-2 substitution and effect of the introduction of an oxygen atom in the adamantane scaffold*" **59**

3.1.3 Artículo 3: *"Design, synthesis and in vivo proof-of-concept of novel pyrrolidine-based 11β-HSD1 inhibitors for age-related cognitive dysfunction"* **91**

3.1.4 Artículo 4: "*Rational design in the discovery of novel N-acylpyrrolidine-based 11β-HSD1 inhibitors.*" **(Sent publication)** **141**

3.2.1 Artículo 5(capítulo): *"Understanding the kinetics of ligand binding to globins with molecular dynamics simulations: The necessity of multiple state models"* **169**

3.2.2 Artículo 6: "*Influence of Temperature on the Topological Features of Inner Cavities, ligand migration and model comparison in Cytoglobin"* **(Sent publication)** **177**

4- DISCUSIÓN **193**

4.1 Análisis de los inhibidores propuestos en la publicaciones de 11β-hidroxiesteroide deshidrogenasa tipo1 **195**

- 4.1.1 **Substitución en C1/C2** **198**
- 4.1.2 **Inversión de N-pirrolidinas modificadas** **199**

4.2 Estudio del proceso de migración de ligandos en globinas **204**

- 4.2.1 **Análisis de métodos para el estudio de la unión de ligandos con globinas en modelos de estado múltiple** **204**
- 4.2.2 **Influencia de la temperatura sobre las características topológicas del las cavidades internas en citoglobinas y estudio de la migración de ligandos diatómicos** **206**
- 4.2.3 **Estudio comparativo de los modelos de C. Aceratus y D. Mawsoni** **210**

5- CONCLUSIONES 213
5.1 Estudio computacional de la inhibición de 11β-HSD1 215
5.2.1 Análisis de métodos para el estudio de la unión de ligandos con globinas en modelos de estado múltiple 216
5.2.2 Influencia de la temperatura sobre las características topológicas del las cavidades internas en citoglobinas y estudio de la migración de ligandos diatómicos 216
5.2.3 Estudio comparativo de los modelos de C. Aceratus y D. Mawsoni 216

BIBLIOGRAFÍA 217

Capítulo 1. Introducción

Este capítulo se desarrolla en dos partes, que definen el ámbito de los estudios realizados en esta tesis doctoral. La primera parte presenta la enzima 11β-hidroxiesteroide deshidrogenasa 1 (11b-HSD1) en el contexto de las enfermedades metabólicas como diabetes y síndrome metabólico, así como la descripción de las aproximaciones realizadas para el diseño de compuestos inhibidores de dicha enzima. La segunda parte se centra en el estudio de citoglobina, destacando en particular el efecto de la temperatura sobre las propiedades topológicas de cavidades internas y la dinámica de la proteína con objeto de comprender su adaptación funcional a distintos entornos.

1.1 Inhibición de la enzima 11β-hydroxiesteroide deshidrogenasa

En esta sección se presentarán los efectos de los glucocorticoides en el organismo y su regulación por la enzima 11β-HSD1, así como su relevancia en el desarrollo de múltiples enfermedades, tales como síndrome metabólico, inflamación, disfunción cognitiva, y diabetes tipo 2. Asimismo, se describirá la estructura y función de dicha enzima. Finalmente, se presentarán las estrategias empleadas en el diseño de inhibidores de 11β-HSD1.

1.1.1 Glucocorticoides y su actividad fisiológica

Los glucocorticoides son hormonas con un rol clave en la modulación de la respuesta inmune e inflamatoria, regulando el metabolismo energético y la homeostasis cardiovascular, así como también las respuestas del organismo al estrés. Contrarrestando la acción de la insulina, los glucocorticoides C estimulan la gluconeogénesis, inhiben la secreción de insulina de las células β y la captación periférica de glucosa. Además, contribuyen a la lipólisis, con la posterior movilización de ácidos grasos y proteólisis. En consecuencia, se puede afirmar que generalmente los glucocorticoides inducen estados catabólicos.[1,2]

Dentro de los glucocorticoides, cabe destacar el cortisol o hidrocortisona (**Esquema 1**). El cortisol humano activo es sintetizado por la corteza suprarrenal con un ritmo circadiano fuerte. Su secreción es controlada por el eje hipotalámico-pituitario-suprarrenal (HPS) e inducida en condiciones de estrés. El cortisol sérico pasa a las membranas celulares y ejerce sus funciones intracelulares uniéndose a receptores de glucorticoides (GRs), que son receptores nucleares activados por ligandos. Los GRs regulan, directa o indirectamente, la expresión de una gran cantidad de genes implicados en diversos procesos fisiológicos, incluyendo el receptor activador-proliferador de peroxisoma γ (PPAR-γ), la proteína de unión al potenciador de CCAAT (factores de transcripción que promueven la expresión de ciertos genes a través de la interacción con sus promotores) y el factor nuclear κB (NF-κB), entre otros.[3,4] Por otra parte, los glucocorticoides se unen a los receptores de mineralocorticoides (MR), que regulan la presión sanguínea y el equilibrio de sodio en el riñón.[5]

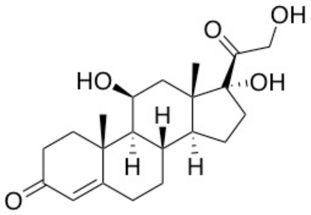

***Esquema 1**. Estructura química del cortisol.*

El conjunto de actividades mediadas por cortisol depende de la concentración local de cortisol activo en tejidos específicos, la cual se ajusta mediante el metabolismo previo a la unión con GRs, que a su vez está controlado por las enzimas 11β-HSD. La cortisona plasmática proporciona una reserva inactiva, que puede convertirse en glucocorticoides activos en sitios donde la actividad de la 11β-HSD1 reductasa es predominante. Ello confiere un mecanismo de regulación, que permite un control más efectivo de la activación de determinados procesos celulares.

1.1.2 Estructura y función de la enzima 11β-hydroxiesteroide deshidrogenasa

Los enzimas microsomales 11β-HSD pertenecen a la familia deshidrogenasa/reductasa de cadena corta, que controlan la homeostasis de glucocorticoide, juntamente con el HPS. En humanos y roedores, se han identificado dos isoenzimas, 11β-HSD1 y 11β-HSD2, que catalizan la interconversión de 11β-hidroxiglucocorticoides activos y sus equivalentes 11-ceto inactivos (**Figura 1**).

Figura 1. *Esquema de la interconversión entre 11β-hidroxiglucocorticoides activos y sus equivalentes 11-ceto inactivos*

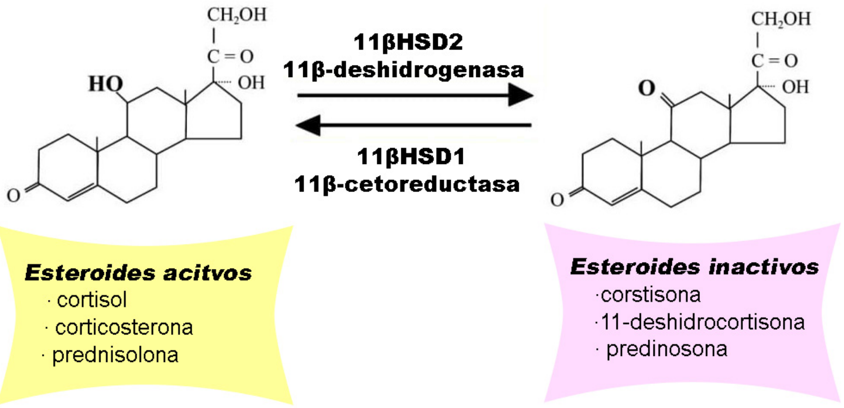
CH₂OH
C=O
OH
HO
O
11βHSD2
11β-deshidrogenasa
11βHSD1
11β-cetoreductasa
CH₂OH
C=O
OH
O
O
Esteroides acitvos
· cortisol
· corticosterona
· prednisolona
Esteroides inactivos
·corstisona
·11-deshidrocortisona
· predinosona

El enzima 11β-HSD1 cataliza la reducción (activación) dependiente de NADPH de la cortisona (humana) 11-cetosteroide y la 11-dehidrocorticosterona (roedor) a cortisol y corticosterona, respectivamente. Está altamente expresado en muchos tejidos diana, como hígado, tejido adiposo, músculo esquelético, macrófagos, y cerebro. La hexosa-6-fosfato deshidrogenasa, también localizada en el retículo endoplasmático, proporciona concentraciones adecuadas de NADPH, que favorecen el comportamiento de la 11β-HSD1 como reductasa in vivo.[6,7] Además, la mayor afinidad de la 11β-HSD1 hacia la cortisona hace que el cortisol aumente esta actividad oxoreductiva. En condiciones in vitro, sin embargo, el 11β-HSD1 es bidireccional y también puede actuar como una deshidrogenasa. A su vez, el enzima 11β-HSD2 es una deshidrogenasa dependiente de NAD^+ y cataliza la oxidación (inactivación) de los 11β-hidroxiglucocorticoides en riñón, colon, placenta, páncreas, glándulas salivales y tejido inflamado.[8] En los tejidos con mineralocorticoides, los receptores de mineralocorticoiedes (RM) tienen la misma afinidad de unión por el cortisol que la aldosterona; esto implica que la enzima 11β-HSD2 impide su activación por cortisol y permite que la aldosterona actúe como ligando, al inactivar el cortisol a cortisona.

La enzima 11β-HSD1 es una proteína de 34 kD compuesta por 292 aminoácidos y que forma homodímeros y tetrámeros en solución, que, actúan como forma activa.[9,10] La enzima está compuesta por 4 regiones principales: un dominio transmembrana en la región N-terminal unido al retículo endoplasmático, un dominio de unión a un cofactor, caracterizado por un plegamiento Rossman, un conjunto de residuos clave que componen el sitio catalítico, y una región esencial para la dimerización enzimática en el extremo C-terminal (**Figura 2**).

Figura 2*. Estructura de rayos X de 11β-HSD1 (código 4BB6) unido al cofactor NADPH y uno de los inhibidores.*

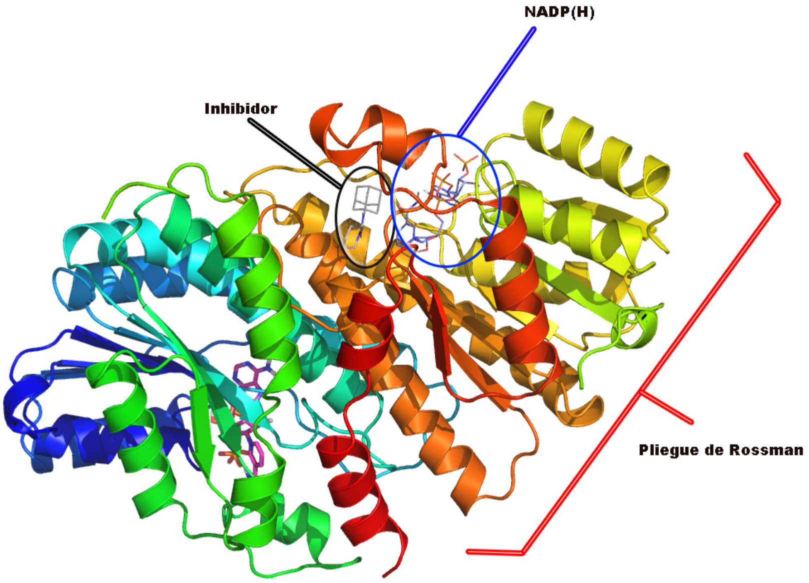

El plegamiento Rossman está altamente conservado en la familia de enzimas deshidrogenasa/reductasa de cadena corta, a la que pertenece la 11β-HSD1. Esta estructura tridimensional consiste en hojas β paralelas de siete cadenas flanqueadas por tres hélices α en los lados izquierdo y derecho de cada una de ellas.[11] En 11β-HSD1, el sitio de unión del cofactor se encuentra en el pliegue de Rossman, y se cierra en la ubicación del sitio catalítico del sustrato (**Figura 3**).

Figura 3. *Centro activo de 11β-HSD1 (código 4BB6)*

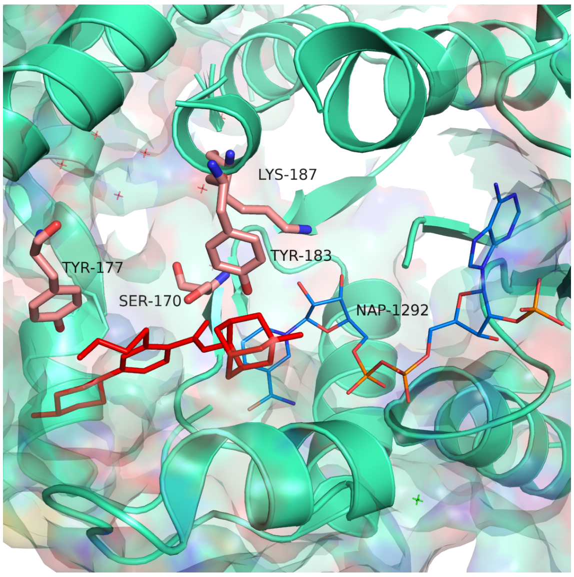

El sitio catalítico del sustrato muestra la secuencia de aminoácidos Tyr-X-X-X-Lys (específicamente Tyr183 y Lys187, donde X-X-X es una determinada combinación de aminoácidos: ver **Figura 3**). El motivo XXX a menudo incluye un residuo de serina conservado (Ser170), que participa activamente en la unión del ligando, estabilizando la orientación del sustrato dentro del sitio catalítico y asistiendo la transferencia de protones hacia y desde los intermediarios reducidos y oxidados. Por otra parte, Lys187 forma puentes de hidrógeno con la nicotinamida ribosa de NADP (H) y disminuye el pKa del grupo hidroxilo del residuo vecino Tyr183, que se une también al sustrato y al cofactor. La también conocida como tríada catalítica Tyr183 - Ser170 - Lys187 interacciona así con el sustrato y promueve la transferencia de protones al oxígeno cetónico reactivo de la cortisona para generar el cortisol glucorticoide activo. Cabe remarcar que la cortisona no es el único sustrato de la 11β-HSD1, ya que se han identificado varios sustratos adicionales tales como esteroides 7-oxigenados, 7-ceto colesterol y compuestos carbonílicos inespecíficos no esteroideos, acentuado el papel que ejerce en la desintoxicación de sustancias exógenas.[12,13,14]

1.1.3 11β-HSD1 como diana terapéutica pleotrópica

La producción endógena de glucocorticoides y su metabolismo desempeña un papel fundamental en la etiología de varios trastornos. Si bien ello ha servido como base para estudiar la inhibición farmacológica de 11β-HSD1 como modulador de la acción local de glucocorticoides, ello requiere inhibir selectivamente esta isoforma específica para evitar efectos nocivos asociados con la unión a 11β-HSD2 u otras enzimas hidroxiesteroide deshidrogenasas. Así, por ejemplo, una actividad deficiente de 11β-HSD2 (como resultado de mutación génica, o por inhibición de esta isoforma) resulta en una inactivación deteriorada del cortisol y un exceso de mineralocorticoides, conduciendo a hipocalemia e hipernatremia, que pueden inducir hipertensión.[15,16]

Aunque se ha demostrado que la actividad de 11β-HSD1 en el cerebro no contribuye al recambio sistémico de cortisol/cortisona, la inhibición de 11β-HSD1 obedece a su expresión en áreas del cerebro relevantes para el control metabólico.[17,18] Por ello, debe considerarse con precaución ya que existe el riesgo de una producción compensatoria de cortisol a través de la regulación positiva del eje HPS[19](**Figura 4**).

Figura 4. *Biosíntesis de cortisol por glándula suprarrenal bajo control de eje HPS, y metabolismo específico de tejido de GC por enzimas 11β-HSD. CRH: hormona liberadora de corticotropina; ACTH: hormona adrenocorticotrófica.*

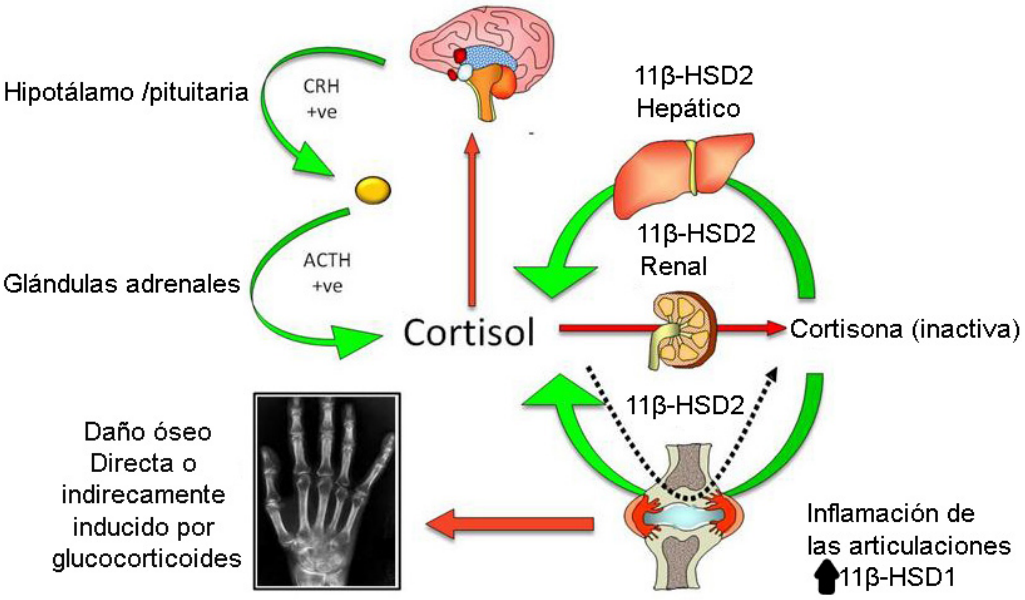
Hipotálamo /pituitaria
CRH
+ve
11β-HSD2
Hepático
Glándulas adrenales
ACTH
+ve
11β-HSD2
Renal
Cortisol
Cortisona (inactiva)
11β-HSD2
Daño óseo
Directa o
indirecamente
inducido por
glucocorticoides
Inflamación de
las articulaciones
↑11β-HSD1

1.1.4 Diabetes mielitus tipo 2, obesidad y síndrome metabólico

La diabetes mielitus tipo 2 (DM2) es un trastorno metabólico a largo plazo que se caracteriza por niveles elevados de azúcar en la sangre, resistencia a insulina y falta relativa de insulina. Los síntomas comunes incluyen aumento de la sed, micción frecuente y pérdida de peso inexplicable, pudiendo también incluir aumento del hambre, sensación de cansancio y llagas que no cicatrizan. Las complicaciones a largo plazo incluyen enfermedades del corazón, derrames cerebrales, retinopatía diabética que puede resultar en ceguera, insuficiencia renal y flujo sanguíneo pobre en las extremidades, que puede conducir a amputaciones (**Figura 5**).

Figura 5*. Representación esquemática del mecanismo de la diabetes*

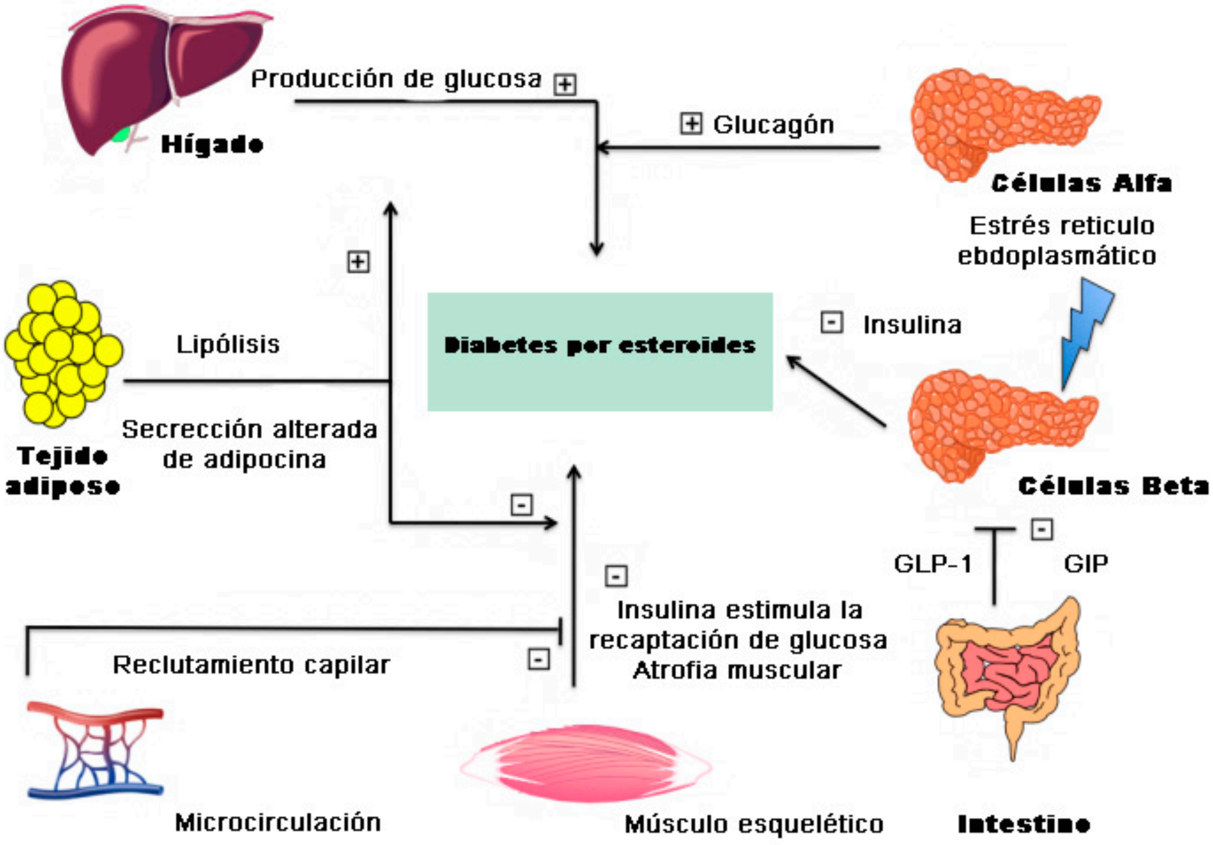
Producción de glucosa ⊞
Hígado
⊞ Glucagón
Células Alfa
Estrés reticulo ebdoplasmático
⊞
Lipólisis
Diabetes por esteroides
⊟ Insulina
Tejido adiposo
Secrección alterada de adipocina
Células Beta
⊟
⊟
GLP-1
GIP
⊟
Insulina estimula la recaptación de glucosa
Atrofia muscular
Reclutamiento capilar
⊟
Microcirculación
Músculo esquelético
Intestino

Se produce principalmente como resultado de la obesidad y falta de suficiente ejercicio. Algunas personas son genéticamente más propensas a padecerla que otras, representando alrededor del 90% de los casos de diabetes, mientras que el otro 10% se debe principalmente a diabetes mellitus tipo 1 y diabetes gestacional. En la diabetes mellitus tipo 1 hay una falta absoluta de insulina debido a la descomposición de las células pancreáticas de los islotes de Langerhans. La tasa de incidencia ha aumentado notablemente desde 1960 en paralelo con la obesidad. A partir de 2013 hubo aproximadamente 368 millones de personas diagnosticadas con la enfermedad en comparación con alrededor de 30 millones en 1985. Típicamente comienza a mediana edad aunque las tasas están aumentando entre la población joven. Se asocia a una esperanza de vida diez años menor y fue una de las primeras enfermedades descritas, siendo determinada la importancia de la insulina en la enfermedad en la década de 1920.

El síndrome metabólico (SM) es un compendio de al menos tres de los siguientes factores:

· Obesidad abdominal (central)
· Presión arterial elevada
· Glucosa plasmática en ayunas elevada
· Altos niveles séricos de triglicéridos
· Niveles bajos de lipoproteínas de alta densidad (HDL)

Principalmente se asocia con el riesgo de desarrollar enfermedad cardiovascular y diabetes tipo 2. La prevalencia en los Estados Unidos es aproximadamente del 34% de la población adulta, aumentando con la edad. Se cree que el síndrome es causado por un trastorno subyacente de la utilización y almacenamiento de la energía. Actualmente la estrategia terapéutica predominante para la prevención o la gestión de DM2 y SM es el tratamiento individual de los factores de riesgo en lugar de hacerlo con el trastorno en su conjunto.

Al contrario de lo que sucede en el síndrome de Cushing, donde los niveles elevados de cortisol circulante causan los cambios fenotípicos, en el SM los niveles circulantes de GC no suelen ser elevados, a pesar de que hasta hace poco la creencia extendida era que el principal contribuyente a la sintomatología era el nivel de cortisol libre en el plasma y las densidades locales intercelulares e intracelulares de GC regulados por las enzimas 11β-HSD son responsables de anormalidades metabólicas.

Diversos estudios han demostrado la relevancia de la enzima 11β-HSD1 en SM. Los experimentos en ratones con sobreexpresión 11β-HSD1 dirigida al tejido adiposo desarrollaron un fenotipo similar al del síndrome de Cushing, incluyendo resistencia a la insulina, obesidad visceral, dislipidemia e hipertensión, sin un aumento en los niveles plasmáticos de glucorticoides.[20,21]

Por otro lado, la sobreexpresión de 11β-HSD1 en tejido hepático condujo a la aparición de SM, pero sin alteración de la tolerancia a la glucosa y la obesidad. En contraste, en el modelo *knock-out* [11β-HSD1 (- / -)] los ratones habían reducido sus niveles de triglicéridos y ácidos grasos no esterificados, mejorando su tolerancia a la glucosa y unos valores de HDLs más altos en una dieta con alto contenido de grasa. [22,23,24] Paralelamente, la sobreexpresión de 11β-HSD2 en tejido adiposo reduce la masa corporal y aumenta la tolerancia a la glucosa y la sensibilidad a insulina.[25]

Finalmente, se ha observado una asociación de la activación glucocorticoide dependiente de 11β-HSD1 (en hígado y tejido adiposo) con resistencia a insulina y leptina, obesidad visceral, dislipidemia, diabetes tipo 2 y complicaciones cardiovasculares, características del SM.[26] La actividad anormal de la 11β-HSD1 reductasa hepática parece desempeñar un papel importante en los síndromes de resistencia a la insulina. La sobreexpresión de 11β-HSD1 dentro del tejido adiposo en ratones transgénicos da como resultado la resistencia a la insulina, hiperlipidemia y obesidad visceral, mientras que los ratones *knock-out* 11β-HSD1 muestran niveles disminuidos de triglicéridos y colesterol, así como resistencia a la hiperglucemia inducida por el estrés. Por tanto, la inhibición de la 11β-HSD1 hepática puede ser un objetivo prometedor para el tratamiento de la resistencia a la insulina en enfermedades metabólicas.[27,28,29]

1.1.5 El rol de 11β-HSD1 en la inhibición de la inflamación

La modulación de las enzimas 11β-HSD, y en particular la inhibición de 11β-HSD1 en tejido adiposo e hígado, son de especial interés como estrategias terapéuticas en el tratamiento de la SM y sus trastornos asociados.

Los efectos antiinflamatorios de los glucocorticoides han sido estudiados previamente.[30] La terapia a corto plazo con glucocorticoides, principalmente cortisona, ha sido descrita ampliamente para tratar la inflamación aguda. Sin embargo, los glucocorticoides endógenos son inmunomoduladores en lugar de simplemente agentes antiinflamatorios.[2,31] Los glucocorticoides aumentan o inhiben las respuesta inmune en función de la concentración y la etapa del proceso inflamtorio, al afectar la migración de las células inmunitarias, sus estados diferenciados y la producción de una serie de citoquinas inflamatorias.[32] En última instancia, forman una respuesta inflamatoria que avanza dependiendo del entorno local.

Con respecto a 11β-HSD1, se expresa en ciertas células inmunitarias, como los monocitos diferenciados y en la mayoría de las poblaciones de linfocitos, contribuyendo a mejorar las respuestas inmunes celulares.[33] En los procesos inflamatorios crónicos, tales como artritis reumatoide, aterosclerosis y rinitis, existe un desequilibrio en la expresión/actividad de las dos isoformas de 11β-HSD.[8,34,35] Se ha sugerido que la desregulación del control recíproco normal de 11β-HSD1 y 11β-HSD2 pueden contribuir al fracaso de la resolución durante estados inflamatorios crónicos. Por tanto, el control de la biodisponibilidad de glucocorticoides dentro de las células inmunes por 11β-HSD1 proporciona un punto de control para la atenuación de respuestas inmunes no deseadas.[36,37]

También se debe tener en cuenta que los trastornos metabólicos como la obesidad y la DM2 se asocian con una respuesta inmune desregulada, reforzando así el potencial de la inhibición de 11β-HSD1 como nueva estrategia terapéutica en estas condiciones.[38]

1.1.6 11β-HSD1 en la disfunción cognitiva producida por el envejecimiento

La región del hipocampo es un área cerebral que tiene un rol importante en la formación de recuerdos de larga duración y ejerce un de control sobre el eje HPS.[39] En esta región en particular se expresa únicamente 11β-HSD1, junto con GRs y MRs. Teniendo en cuenta el fenotipo del síndrome de Cushing, la regulación deficiente del eje HPS con los niveles fenotipo del síndrome de Cushing, la regulación deficiente del eje HPS con los niveles crónicamente elevados de GCs resultantes produce efectos perjudiciales en áreas específicas del cerebro, resultando en algunos casos en disfunción cognitiva. Concretamente, las concentraciones excesivas de glucocorticoides en el cerebro incrementan la muerte neuronal debido a factores como el aumento de los niveles de proteína precursora amiloide, la hipoxia y las concentraciones excitotóxicas de glutamato [40]

El deterioro cognitivo relacionado con glucocorticoides es evidente en el envejecimiento. [41,42,43] De hecho, los glucocorticoides están implicados en la patogénesis del deterioro cognitivo relacionado con la edad y el Alzheimer.[44,45,46] Se cree que la baja concentración intracelular de glucocorticoides en el hipocampo activa los MR, cuya estimulación conduce a un aumento de la memoria, mientras que la alta concentración de glucocorticoides lo satura. [47] Por otra parte, la inhibición de 11β-HSD1 reduce la carga de la placa β-amiloide y sus niveles en plasma de los modelos animales de Alzheimer.[48,49]

1.1.7 Estrategias terapéuticas de inhibición de 11β-HSD1

En los últimos años, se ha producido un rápido crecimiento de las publicaciones relacionadas con 11β-HSD1 por su potencial valor terapéutico. Así, muchos grupos de investigación en el mundo académico y en la industria farmacéutica han realizado diversos estudios para determinar el papel de 11β-HSD1 en el desarrollo de múltiples enfermedades y, por tanto, descubrir inhibidores adecuados para tratar estos trastornos.[50]

La gran mayoría de los inhibidores desarrollados presentan una funcionalidad como aceptor de puente de hidrógeno, incluyendo grupos amida, lactama, urea, carbamato, sulfona, sulfonamida o heterociclos, que a su vez están flanqueados por radicales lipófilos voluminosos tales como ciclohexano, adamantano o anillos de benceno. Una gran parte de los candidatos se pueden clasificar en base a la presencia de grupos específicos: arilsulfonamidas, triazoles, piperazinas, sulfonamidas, piperidinas, carboxamidas, tiazolonas, amidas heterocíclicas, ureas.[51.52]

El análisis de las estructuras cristalográficas disponibles para complejos de 11β-HSD1 en la base de datos de proteínas (PDB), que asciende a 40 estructuras, permite identificar diversos puntos claves para descubrir nuevos ligandos potenciales, tal como se ilustra en la **Figura 6** para el complejo con el inhibidor RL104.

* La zona aceptora de enlaces de hidrógeno reproduce la función ceto del substrato endógeno, interactuando con los residuos del centro activo.
* Los grupos lipofílicos voluminosos se sitúan en las cavidades hidrofóbicas situadas en el sitio catalítico, generalmente cerca del área de unión de la unidad de nicotinamida de NADPH.
* El sitio catalítico está abierto a la región del disolvente, lo que permite que la zona de unión se adapte para los ligandos de mayor tamaño. En dicha región, la tirosina 177 juega un papel esencial en la interacción con las regiones hidrófobas de las moléculas adyacentes.

***Figura 6**. Modo de unión del ligando RL104 (marrón) próximo al cofactor NAPDH (en amarillo), los residuos claves en la unión (azul) la tirosina 177 (rosa) y algunos de los pertenecientes a las cavidades hidrofóbicas (verde).*

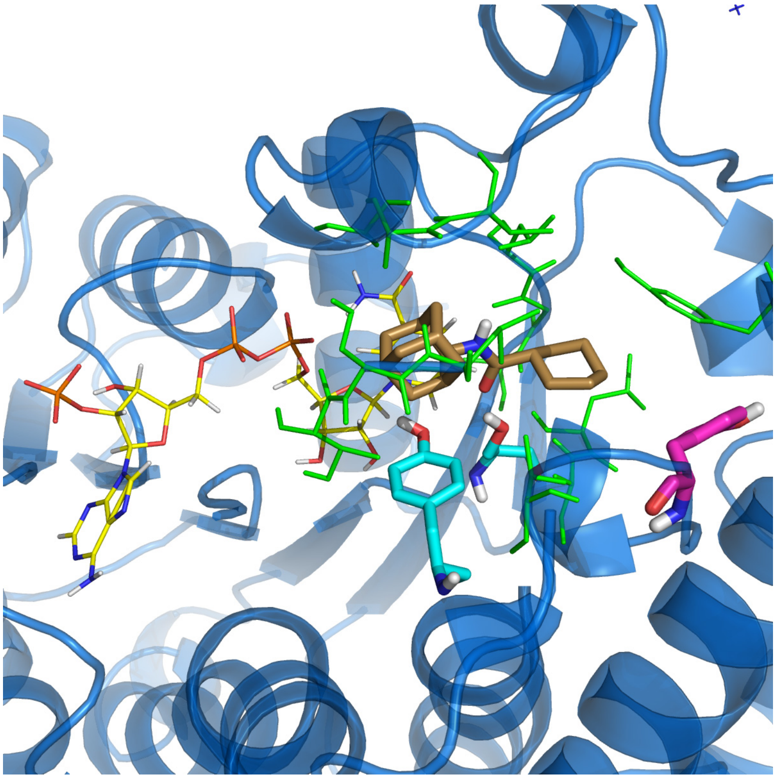

La literatura de patentes que rodea el desarrollo de nuevos inhibidores de 11β-HSD1 ha sido extremadamente prolífica en la última década. Existen más de 250 solicitudes de patentes publicadas, así como varias publicaciones del mundo académico y de la industria que incluyen inhibidores biológicamente activos.[53,54,55,56] Ello se muestra en la **Tabla 1**, que incluye la lista de inhibidores que han superado los estudios clínicos de 11β-HSD1.[57,58,59,60,61]

Tabla 1. *Conjunto de fármacos que han sido o se están ensayando en análisis clínicos como inhibidores de 11β-HSD1.*

Compuesto	**Compañía**	**Estado**
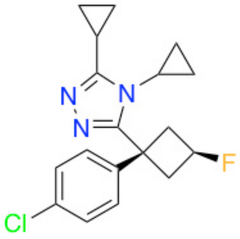 **MK-0916**	**Merck**	**Fase II**
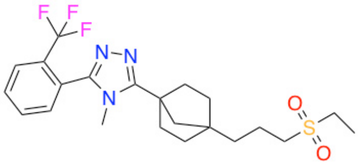 **MK-0736**	**Merck**	**Fase II**
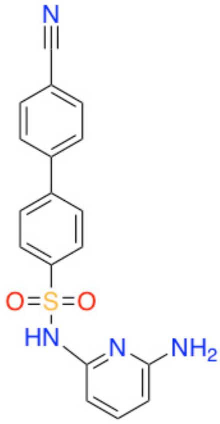 N O=S=O HN N NH2 **PF-915275**	**Pfizer**	**Fase II**
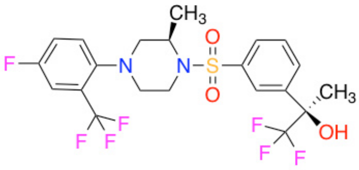 CH3 F N N O S O CH3 OH F F F F F F **HSD-016**	**Wyeth**	**Fase I**

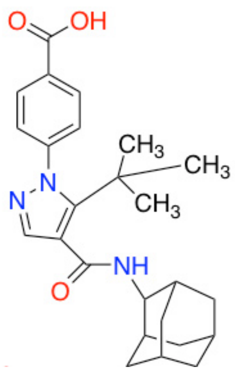 **AZD-8329**	**AstraZeneca**	**Fase I**
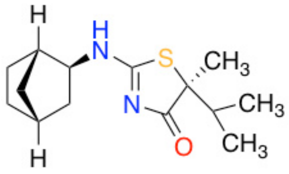 **AMG-221/BVT-83370**	**Amgen/Biovitrum**	
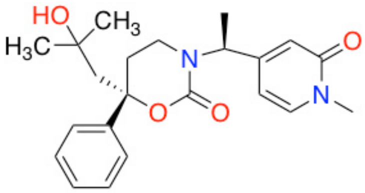 **BI 13558**	**Boehringer Ingelheim**	**Fase I**
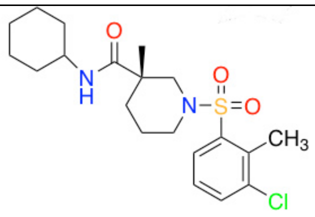 **INCB13739**	**Incyte**	**Fase II**
RO5093151	**Hoffman-La Roche**	**Fase II**
P2202	**Eli Lilly & Piramal**	**Fase II**

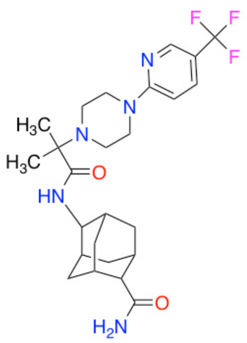 **ABT-384**	**Abbott**	**Fase II**
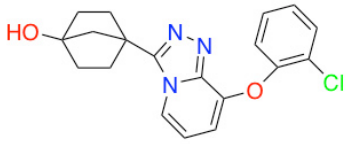 **BMS-770767**	**Bristol-Meyers Squibb**	**Fase II**
UE2343	**University of Edinburgh** **Actinogen**	**Fase II** **(reclutamiento)**
ASP36629	**Astellas Pharma**	**Fase II**
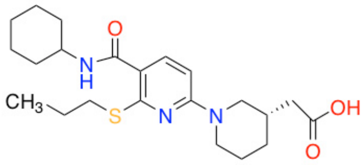 **AZD-4017**	**Astra Zeneca**	**Fase II**

1.1.8 Inhibidores de 11β-HSD1 basados en la estructura del adamantano

El grupo adamantano está presente en muchos inhibidores de 11β-HSD1 descritos en la literatura científica y de patentes, y algunos han sido ensayados en análisis clínicos (véase **Tabla 1**). En los ejemplos mostrados anteriormente, los inhibidores que contienen un grupo adamantano presentan una funcionalidad como aceptores de enlaces de hidrógeno unida a un extremo del grupo adamantano, que se adapta a una de las cavidades hidrófobas del sitio catalítico. A pesar de estas características de unión generales, se han sintetizado y analizado diferentes tipos de compuestos basados en adamantano, desde amidas y ureas hasta triazoles y tiazolonas (ver **Tabla 2**).

La aparición del anillo de adamantano en muchos inhibidores de 11β-HSD1 sugiere que éstos forman interacciones con los residuos de las cavidades hidrofóbicas. Dejando a un lado la mayor o menor afinidad que pueda tener el ligando en cuestión hacia el sitio de unión de la enzima, el hecho de que el adamantano posea una alta lipofilia puede provocar problemas de solubilidad y estabilidad metabólica. Los resultados farmacológicos preliminares muestran que el aumento de la hidrofobicidad de los inhibidores generalmente implica una mejora del potencial inhibidor de 11β-HSD1, aunque ello puede limitar el comportamiento en los ensayos de farmacodinámica (PD).

Tabla 2. *Selección de inhibidores de 11β-HSD1 en proceso de desarrollo*

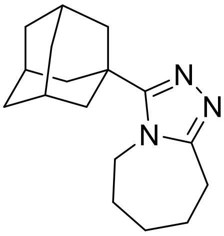	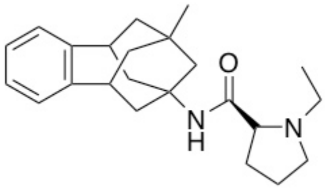	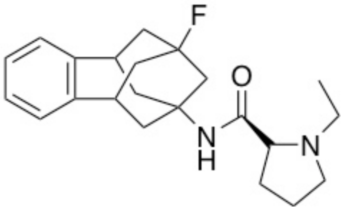
MK544	**EV15**	**EV22**
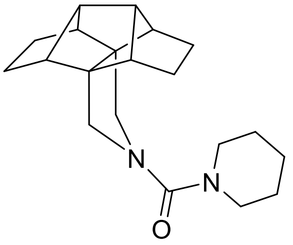	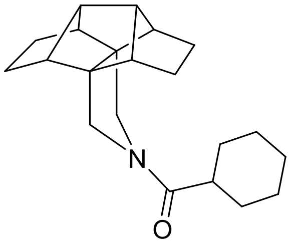	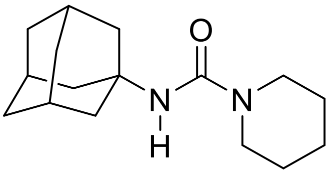
EV26	**EV28**	**RL103**
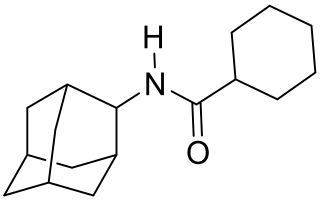	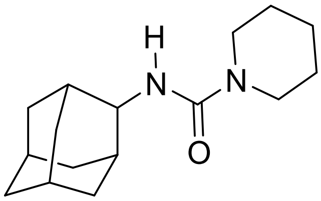	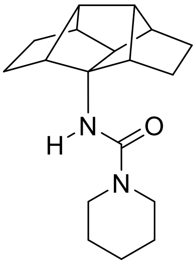
RL104	**RL106**	**RL115**

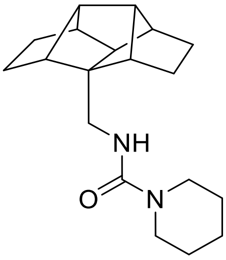	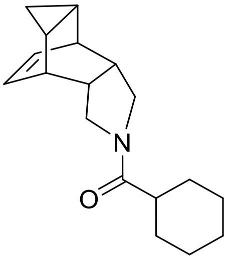	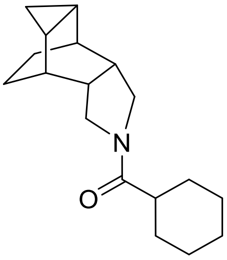
RL116	**RL117**	**RL118**
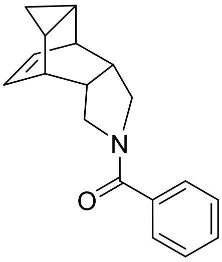	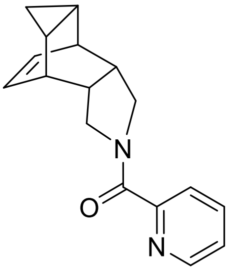	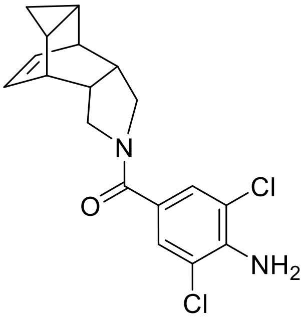
RL130	**RL131**	**RL134**
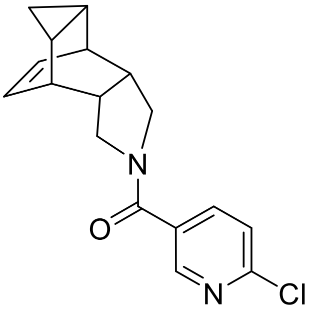	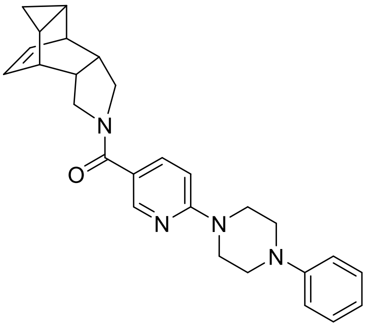	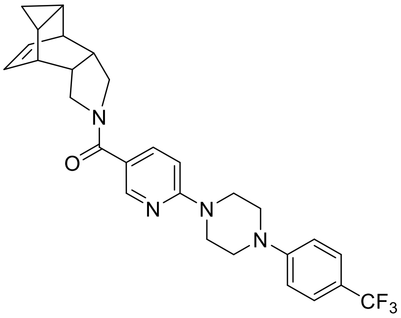
RL136	**RL138**	**RL139**
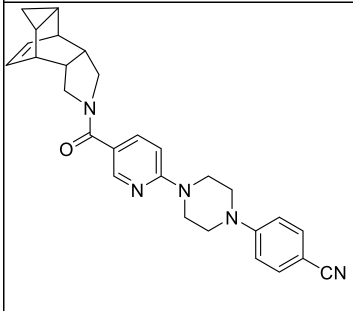	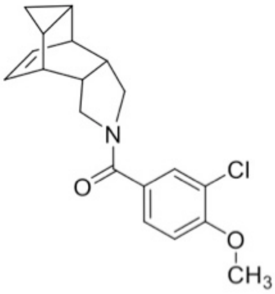	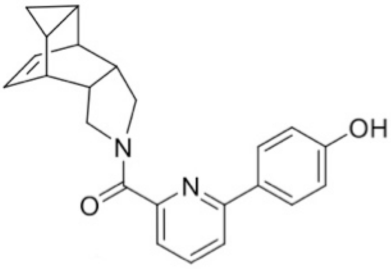
RL140	**RL144**	**RL147**

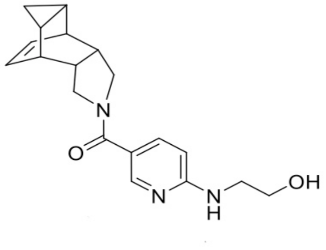	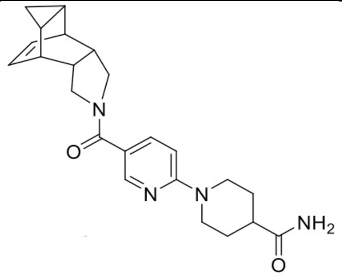	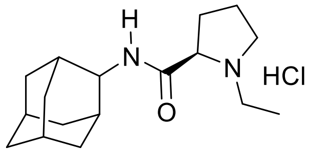
RL148	**RL150**	**PF- 877423**

Con el fin de mejorar los perfiles de farmacocinética (PK) y PD, diversos grupos de investigación académicos e industriales han intentado desenvolupar diferentes enfoques. [62,63,64] Por una parte, se ha explorado la introducción de grupos polares en posiciones clave, tales como amidas, sulfonamidas y grupos hidroxilo, con el objetivo de aumentar la solubilidad en agua. Por otro lado, la sustitución del grupo adamantano por otras estructuras, como el biciclo [2.2.2] de octano, mejora los perfiles de PK y PD en los tejidos diana. Merck siguió esta estrategia en un programa de desarrollo con éxito, lo que les llevó a la síntesis de MK-0736. Estos descubrimientos sugieren que es posible optimizar el resto de adamantano lipófilo de manera eficaz para la administración clínica dirigida al desarrollo de inhibidores de11β-HSD1 con mejor perfil terapéutico

1.2 Unión de ligandos en globinas y estudio de la influencia de la temperatura sobre las características topológicas de las cavidades internas en citoglobinas

La siguiente sección se centra en la descripción de las propiedades estructurales y funcionales de globinas, particularmente de la citoglobina, haciendo especial énfasis en el efecto de la temperatura sobre las variaciones topológicas de sus cavidades, además de su impacto en la difusión de ligandos gaseosos.

1.2.1 Globinas y difusión de ligandos

Las globinas son proteínas que poseen una estructura formada por un grupo prostético hemo (**Figura 7**), que les capacita para mostrar afinidad y sensibilidad elevadas a pequeñas moléculas, como, O_2, CO y NO. Forman parte de la superfamilia de las globinas, entre las que existen diferencias remarcables que afectan al plegamiento trdimensional, el entorno químico del sitio de unión y el modo de unión al grupo hemo, así como la naturaleza de las interacciones entre éste y la proteína.

***Figura** 7. Representación del grupo hemo*

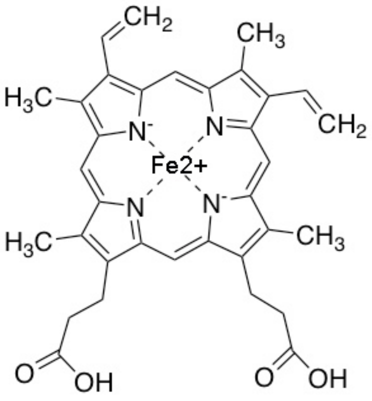

Las globinas tienen una estructura terciaria común, formada por tres hélices alfa que se disponen sobre otras tres hélices alfa. Este motivo se conoce como apilamiento helicoidal 3-sobre-3 (**Figura 8**), pese a que en determinadas globinas se ha descubierto un apilamiento tipo 2-sobre-2, propio del grupo de hemoglobinas truncadas 2/2Hbs, con una secuencia de unos 20 o 30 aminoácidos más corta respecto a mioglobina (Mb).

Figura 8 *A) Apilamiento helicoidal 3-sobre-3 de mioglobina (código 1VXA), B) Apilamiento tipo 2-sobre-2 hemoglobina (código 1IDR).*

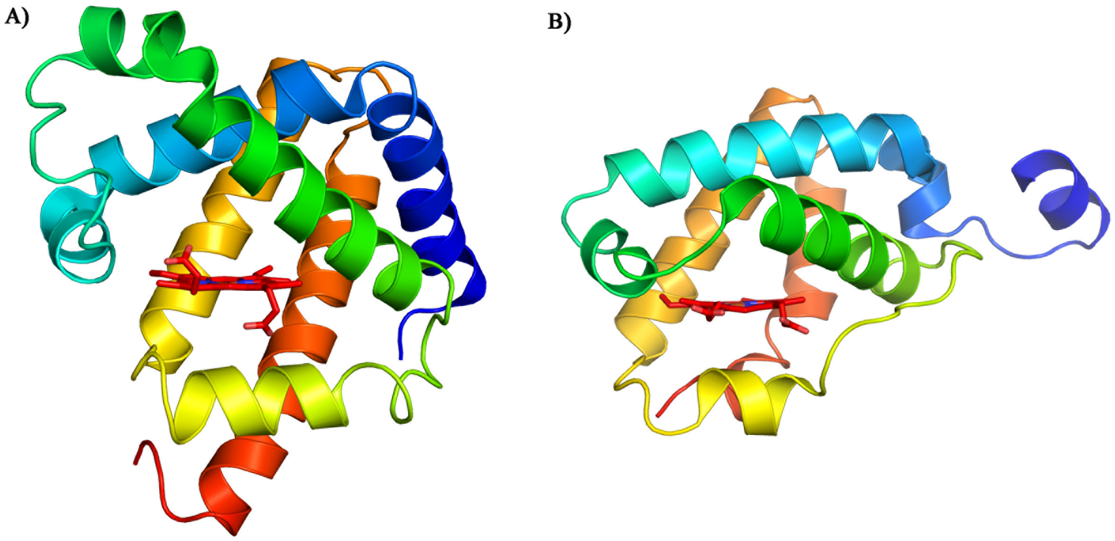

Entre ellas presentan una elevada variabilidad a nivel de secuencia, aunque algunos residuos se conservan en zonas concretas, destacando especialmente el residuo de His proximal (HisF8), que está presente en todas las globinas conocidas. Sin embargo, la evolución ha propiciado que determinados aminoácidos se sitúen en zonas sensibles de la estructura tridimensional de cada globina, regulando en gran parte la difusión y la afinidad de ligandos, así como la función biológica de dichas hemoglobinas.

Un ejemplo de ello es la mioglobina (Mb), que además de ser de las primeras globinas descubiertas también se encuentra en el grupo de las más estudiadas hasta el punto de ser conocida como "*el átomo de hidrógeno de la Biología*". A mediados del siglo XX Kendrew resolvió su estructura 3D, lo que le valió la consecución del Premio Nobel de Química en

1962. Aunque existen múltiples estudios previos, todavía hoy es motivo de debate y análisis por su complejidad, relevancia y función biológica.

El plegamiento de las globinas implica una naturaleza y distribución espacial de los residuos determinada, dando lugar a la existencia de una red de canales y cavidades en la matriz proteica que modulan el acceso selectivo de ligandos. La accesibilidad de los ligandos puede verse modificada por la existencia de barreras asociadas a la transición entre diversas cavidades o por la presencia de aminoácidos que pueden actuar como puerta de acceso entre túneles. Por otra parte, la existencia de aminoácidos dadores de puente de hidrógeno en el sitio de unión, que normalmente se sitúan en la cavidad distal, modulan la energía de enlace entre el ligando y el grupo hemo. Cuanto mayor es el número de puentes de hidrógeno entre la proteína y el ligando unido al hemo, mayor es la energía asociada a la unión ligando-receptor lo cual se conoce como efecto distal.

Por otra parte, la reactividad del grupo hemo se ve influenciada por la histidina proximal, que acaba resultando en una modulación de la actividad por ligando, conocida como efecto proximal. Existen casos en que el plano de anillo imidazólico de la histidina proximal se encuentra orientado con una conformación alternada respecto a los nitrógenos pirrólicos del hemo (como sucede en la Leghemoglobin A, abreviada como Lba), mientras que en otros está eclipsado (como en la Mb). En el primer caso se facilita la donación de carga por parte de la histidina al átomo de hierro del hemo, hecho que conlleva una retrodonación pi de éste al ligando que incrementa la fuerza del enlace Fe-ligando. En consecuencia, aunque los entornos distales son parecidos, la constante de velocidad asociada a la rotura del enlace Fe-ligando de Lba es inferior a la de Mb.

Este conjunto de diferencias en la estructura de la cavidad del gupo hemo da lugar a propiedades diferenciadas entre las globinas. Por este motivo, desenvolupan funciones diversas como el tranporte y almacenamiento de gases, el papel de sensores en la modulación de determinados procesos, la oxidación de compuestos orgánicos, el tranporte de electrones y la catálisis de reacciones entre especies reactivas de oxígeno y nitrógeno.[65] Estos procesos vienen determinados por la afinidad selectiva de las diversas globinas por los diferentes ligandos moleculares.

Al mismo tiempo, la afinidad depende de la relación entre las constante cinéticas k_{on} y k_{off} para distintos ligandos di y triatómicos (**Figura 9**). Estas constantes tienen unidades de M^{-1} s^{-1} y s^{-1} respectivamente; en equilibrio la fórmula que relaciona el proceso de asociación (R + L → RL, siendo R el Receptor y L el el ligando) y disociación (RL → R + L) es la siguiente:

$$k_{on}[R][L] = k_{off}[RL]$$

Figura 9. *Proceso de asociación (k_{on}) y disociación (k_{off}) en globinas*

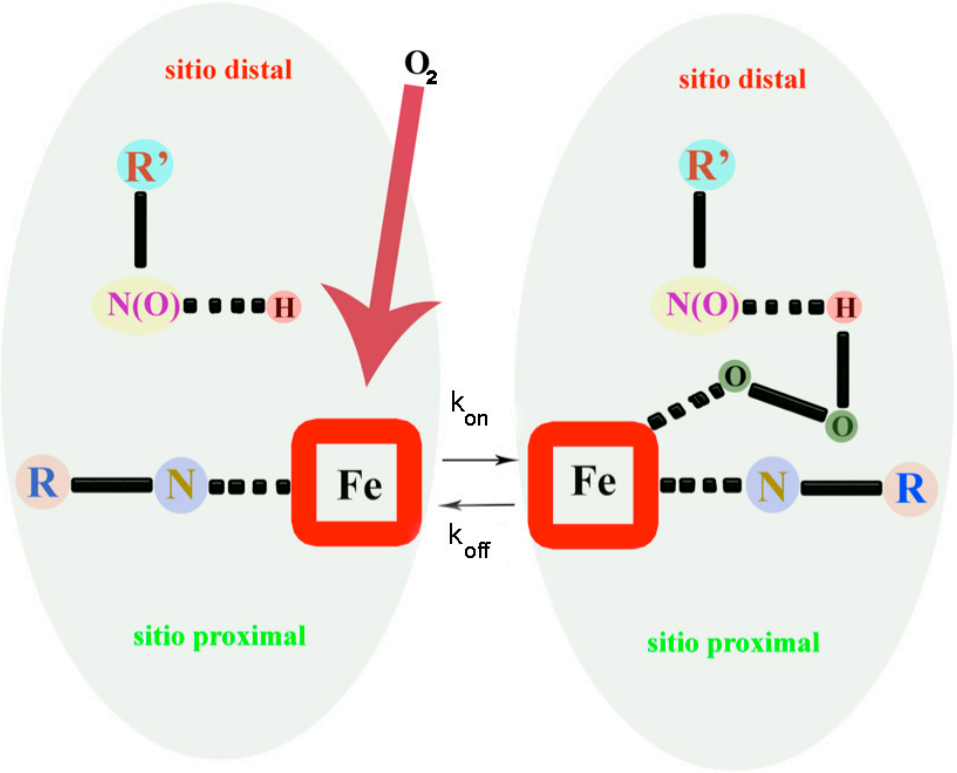
sitio distal
O_2
R'
N(O)
H
R
N
Fe
sitio proximal
k_{on}
k_{off}
sitio distal
R'
N(O)
H
O
O
Fe
N
R
sitio proximal

El proceso de asociación, que viene modulado por $\mathrm{k_{on}}$, depende principalmente de la accesibilidad del ligando a la cavidad distal, donde se produce la coordinación con la posición axial disponible del grupo prostético hemo. Puesto que la formación del enlace con el Fe se produce generalmente de forma rápida, la asociación viene determinada principalmente por la migración del ligando a través de la proteína. El proceso de migración se produce a través de cavidades contiguas por las que el ligando deberá difundir, superando barreras energéticas asociadas a las fluctuaciones térmicas de los residuos que forman dichas cavidades.[66] En ocasiones dichas cavidades forman un sistema de túneles que pueden estar modulados por distintos mecanismos, como la existencia de residuos que limitan o facilitan el acceso de ligandos.

A su vez, el proceso de disociación, modulado por $\mathrm{k_{off}}$, está determinado por diversos factores ligados a la estabilidad del enlace ligando-Fe, como por ejemplo la interacción del ligando con residuos dadores de puente de hidrógeno en la cavidad distal u otras interacciones no covalentes con residuos distales. Al mismo tiempo, cuando se completa la ruptura del enlace ligando-Fe, la probabilidad de que el ligando salga de la cavidad distal y su difusión a través de la matriz proteica, es posible que afecte al proceso de disociación.[67]

La función biológica de las hemoglobinas puede verse influenciada por otros procesos, como por ejemplo la formación de una estructura cuaternaria en condiciones fisiológicas. Si bien algunas de ellas se encuentran en forma de monómero (como la Mb), en otras la estructura fisiológica implica diversas subunidades, formando agregados poliméricos (como la Hb de mamíferos), cuya estructura tetramérica va ligada al efecto alostérico presente a la unión de $\mathrm{O_2}$.

1.2.2 Citoglobina

En los últimos años se han descubierto la neuroglobina y la citoglobina como nuevos miembros de la familia de las proteínas respiratorias con el grupo hemo en el ser humano y otros vertebrados. Poco después del descubrimiento de la neuroglobina (Ngb)[68], expresada principalmente en tejidos nerviosos vertebrados y la retina, se aisló una cuarta globina vertebrada en células estrelladas de rata usando un enfoque proteómico que se denominó STAP[69] (activación de células estrelladas asociadas a una proteína). Esta nueva proteína mostró una actividad peroxidasa respecto al peróxido de hidrógeno y al hidroperóxido de ácido linoleico. Paralelamente, la secuencia de esta globina se identificó en ratón, ser humano y pez cebra y, dado que se expresa en todos los tipos de tejidos humanos, se denominó citoglobina (Cygb; **Figura 10**).

Ngb y Cygb son estructuralmente similares a Mb,[70] aunque contienen cavidades distintas que pueden influir en la unión del ligando.[71] Los estudios cinéticos y estructurales muestran que Ngb y Cygb pertenecen a la clase de las globinas hexacoordinadas con una cinética de unión al ligando bifásico.[72] Aunque Ngb está relacionada evolutivamente con las globinas nerviosas de los invertebrados[73], Cygb comparte una ascendencia común más reciente con la Mb. Ngb se expresa principalmente en el cerebro y en otros tejidos, como por ejemplo la retina. La evidencia actual apunta a un papel importante de Ngb en la homeostasis del oxígeno neuronal y la protección de la hipoxia, aunque puede participar en otras funciones. Por otra parte, Cygb se expresa predominantemente en fibroblastos y de células similares, pero también en distintas clases de células nerviosas. Se sabe mucho menos sobre su función, aunque en fibroblastos podría estar implicada en la síntesis de colágeno.

***Figura 10**. Comparación de citoglobina con otras globinas conocidas.*

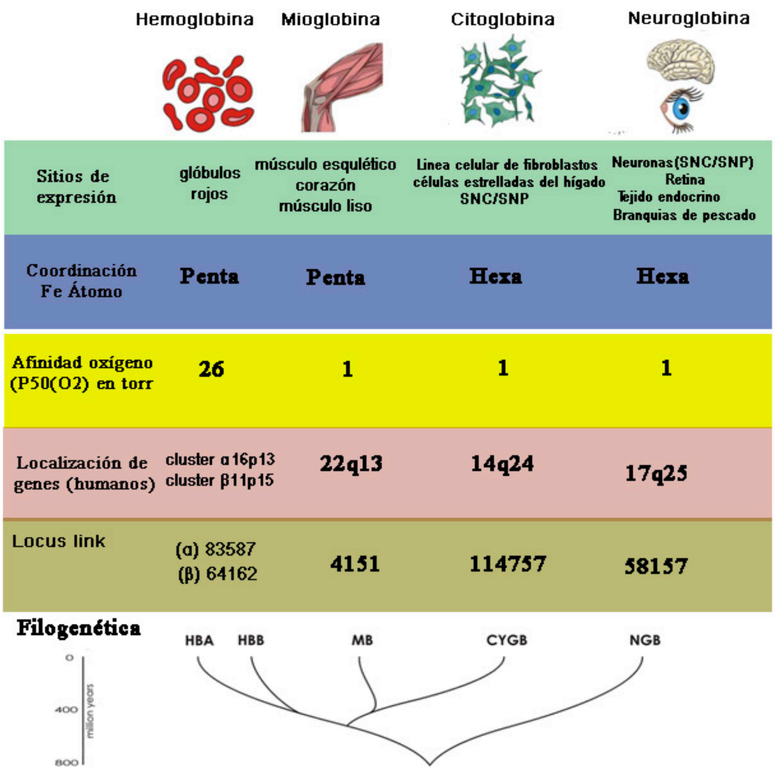

	Hemoglobina	Mioglobina	Citoglobina	Neuroglobina
Sitios de expresión	glóbulos rojos	músculo esquelético corazón músculo liso	Linea celular de fibroblastos células estrelladas del hígado SNC/SNP	Neuronas(SNC/SNP) Retina Tejido endocrino Branquias de pescado
Coordinación Fe Átomo	Penta	Penta	Hexa	Hexa
Afinidad oxígeno (P50(O2) en torr	26	1	1	1
Localización de genes (humanos)	cluster α 16p13 cluster β 11p15	22q13	14q24	17q25
Locus link	(α) 83587 (β) 64162	4151	114757	58157

La Cygb humana consta de 190 aminoácidos, mostrando extensiones de aproximadamente 20 aminoácidos tanto en los extremos carbonilo como en los terminales amino con respecto a las globinas estándar **(Figura 11)**. A nivel de secuencia de aminoácidos Cygb comparte el 30% de similitud con la mioglobina (Mb), lo que sugiere que Cygb y Mb provienen de un antepasado común.

***Figura 11**. Representación de la estructura de rayos X de la citoglobina. Código PDB 3AG0*

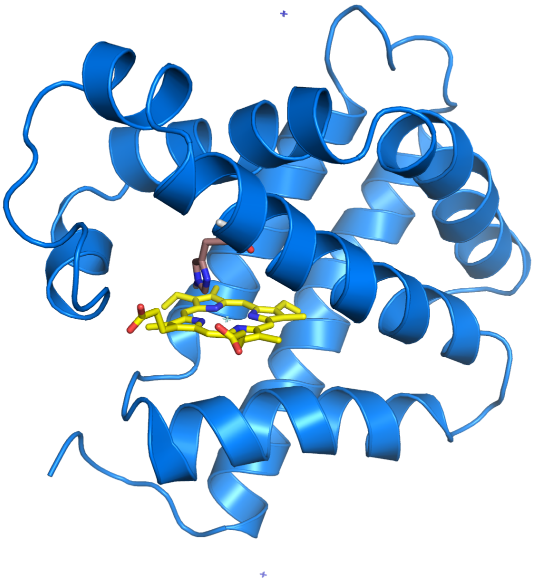

La secuencia de aminoácidos se estructura principalmente siguiendo el patrón de "loops" de la globina desde la hélice de A a la H, incluyendo residuos clave como la histidina proximal (F8) y distal (E7) histidinas, y la fenilalanina CD1, entre las hélices C y D.

Junto con Ngb, Cygb es el primer ejemplo de globina hexacoordinada[74,75,76], con histidina en humanos y otros vertebrados (**Figura 12**). En ausencia de ligandos exógenos el hierro del grupo hemo se coordina con la histidina distal (HisE7). Se han encontrado hemoglobinas bis-histidyl hexacoordinadas (Hbs) en animales, cianobacterias y plantas, y en su estado ferroso se unen reversiblemente a ligandos diatómicos exógenos con altas afinidades.[77] La unión de ligandos exógenos es posible sólo con el desplazamiento concomitante de la HisE7 distal, un mecanismo regulador que se ha sugerido que requiere un cambio conformacional sustancial.[78,79] A pesar de la presencia generalizada de Hbs bis-histidil hexacoordinadas, su función fisiológica es aún en gran medida desconocida, aunque estudios recientes han sugerido su participación en la detoxificación de NO, desempeñando un papel protector durante la hipoxia.[80,81]

Figura 12. *Hexacoordinación del* O_2 *con la HisE7*

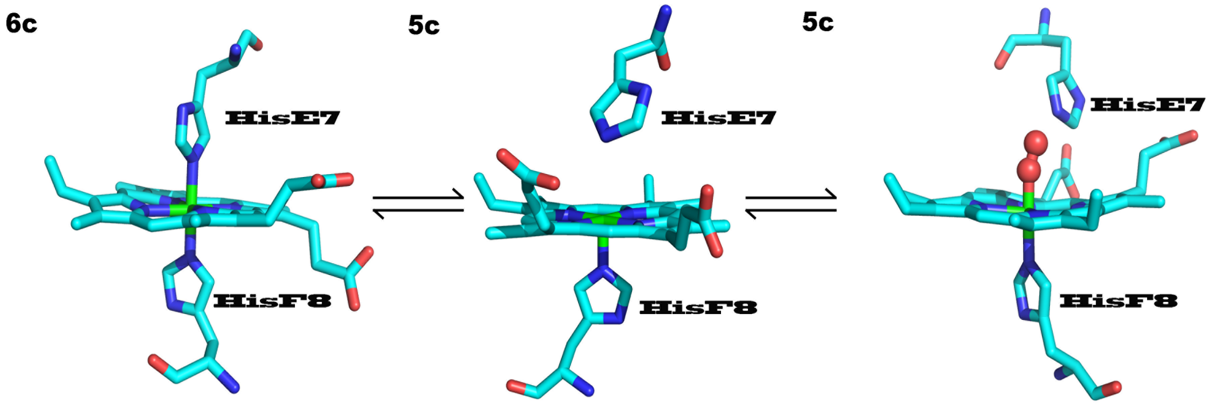

La Cygb muestra algunas características estructurales peculiares, como el extremo N-terminal y el C-terminal, que pueden mediar interacciones proteína-proteína específicas. Además, la estructura cristalina de Cygb bis-histidil hexacoordinada muestra una cavidad con matriz de proteína apolar extendida, conectada al exterior a través de un estrecho túnel anidado entre las hélices G y H.

Figura 13 *Cavidad presente en Cygb de C. aceratus a 283.15 K con perspectiva lateral y rotación de 90º*

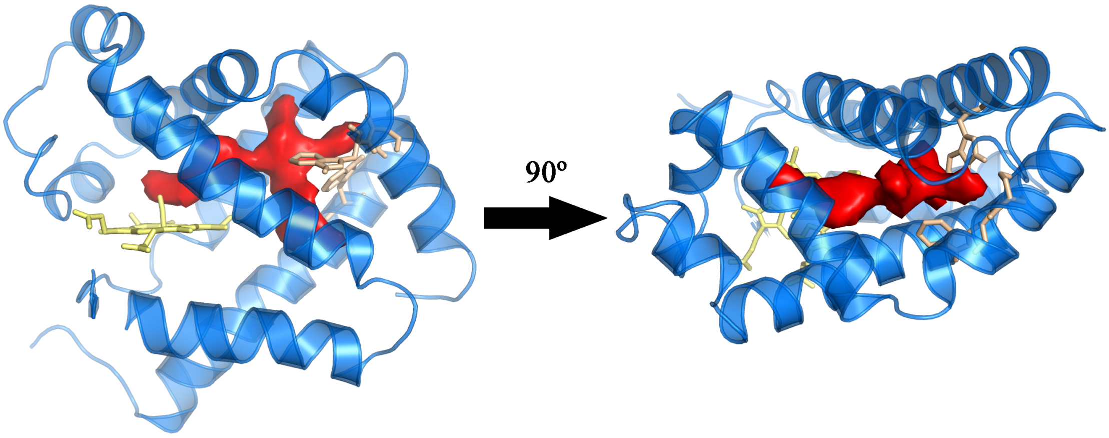

Por otro lado, la cavidad interna difiere de las reconocidas al tener un rol en Mb, Ngb, Hb truncada y mini-Hb *C. Lacteus*, y puede implicar que el ligando diatómico se desplace por su interior después del proceso de fotolización del mismo, lo cual plantea una discusión sobre el papel funcional de la Cygb.[82]

Entender la implicación de las cavidades y los cambios conformacionales que modulan la difusión y la unión del ligando es crucial para la comprensión de los mecanismos que son relevantes para la función o funciones de la Hbs. Aunque se han propuesto varias hipótesis para la Cygb, hasta el momento no se han obtenido pruebas claras en favor de ninguna de ellas. Además de un papel en la regulación del nivel de NO y en las especies reactivas de oxígeno, se ha propuesto la intervención de Cygb en el almacenamiento de oxígeno o sensor de proteínas, o como una enzima implicada en la síntesis de colágeno.[83,84] También se ha discutido su rol en cáncer[85] como gen supresor de tumores, tras el hallazgo de que la región promotora del gen que codifica la Cygb está hipermetilada, y como tal está subexpresada en tumores.

Además, se descubrió una estructura dimérica para Cygb, con enlaces disulfuro intermoleculares[86] entre los residuos Cys38 y Cys83. Estudios previos también han sugerido que la Cygb podría formar un enlace disulfuro intramolecular que permitiría adaptar varias configuraciones diferentes. Se sugirió que los cambios conformacionales inducidos por enlaces disulfuro podría ser crítico para las funciones fisiológicas de Cygb.[87]

1.2.3 Efecto de la temperatura en globinas

La inmensa mayoría de los organismos vivos sobreviven en condiciones estándar de temperatura y presión, pero existen organismos extremófilos diseñados para sobrevivir bajo condiciones ambientales extremas.[88,89,90,91] Se dividen en hipertermófilos, que pueden sobrevivir a temperturas próximas a los 120 ºC, y los organismos adaptados al frío, llamados psicrófilos, que lo hacen a temperaturas inferiores a 15 ºC.

Los hipertermófilos son en su mayoría bacterias o arqueas encontradas en erupciones volcánicas o en respiraderos geotérmicos. Son considerados los organismos más antiguos originados en la tierra, cuando las condiciones ambientales no eran adecuadas para la vida normal. No obstante, existe un contínuo debate su posible evolución para adaptarse a ambientes extremófilos.[92] Los psicrófilos, por otro lado, sobreviven bajo condiciones de temperatura extremadamente bajas, debido a que poseen una peculiar característica que les permite interaccionar y conservar la estabilidad en algunos casos por debajo del punto de congelación del agua.

Cabe pensar que las proteínas presentes en estos microorganismos presentan características específicas que posibilitan la adaptación a condiciones de temperatura extremas. Estas proteínas son especialmente atractivas, ya que pueden ser una alternativa adecuada a los catalizadores en condiciones difíciles y tienen aplicaciones biotecnológicas.

Hoy en día, hay gran interés en conocer las bases físicas de la termoestabilidad en las proteínas hipertérmicas y psicófilas en comparación con sus contrapartes mesófilas. Las simulaciones de dinámica molecular (MD) son una herramienta valiosa para descubrir la complejidad extrema menos obvia en el orden de las matrices proteicas a escala atomística que contribuye a su termoestabilidad. Hasta la fecha no se ha identificado ningún mecanismo que pueda ser considerado responsable de esta característica, aunque se han reconocido muchos factores que alteran la estabilidad de las proteínas en diversos aspectos.[93]

Desde el punto de vista de la cinética química, un problema clave con la reducción de la temperatura es que la entalpía de activación da lugar a una disminución exponencial en las tasas de reacción enzimática, según la teoría del estado de transición:

$$\kappa_{rxn} = \kappa\left(\frac{\kappa T}{h}\right) e^{\frac{-\Delta G}{\kappa T}} = \kappa\left(\frac{\kappa T}{h}\right) e^{\frac{\Delta S}{\kappa T}\cdot} e^{\frac{-\Delta H}{\kappa T}}$$

donde κ_{rxn} es la velocidad de reacción y T la temperatura, κ es un coeficiente de transmisión, k y h son las constantes de Boltzmann y Planck, respectivamente, y ΔG es la energía libre de activación, que se puede descomponer en contribuciones entrópicas y entálpicas.

Una disminución de la temperatura de 37º C a 0º C supone una reducción de entre 20 y 250 veces la actividad de una enzima mesófila. La supervivencia a bajas temperaturas requiere, por lo tanto, que la cinética enzimática se "adapte" a estas condiciones como estrategia para mantener la estabilidad en un ambiente frío.

Los organismos psicrófilos sintetizan enzimas lábiles al calor que poseen una alta actividad específica y eficiencia catalítica a bajas temperaturas. Las enzimas adaptadas al frío tienen generalmente una estabilidad térmica reducida en comparación con los ortólogos mesófilos, presumiblemente para contrarrestar el aumento de la rigidez estructural a temperaturas más bajas. Sin embargo, el cambio en la estabilidad estructural no parece seguir ninguna regla general, sino que es más bien una combinación de varios factores. Sin embargo, una característica común en enzimas adaptadas al frío es que poseen una entalpía menor y una entropía de activación más negativa que sus homólogos mesófilos y termófilos.[94] Por otra parte, las energías libre de activación suelen ser similares a las que presentan enzimas de organismos mesófilos. La entalpía de activación más baja hace que la tasa sea menos dependiente de la temperatura y se cree que es la adaptación primaria de las enzimas psicrófilas.

Diversos estudios también sugieren que la flexibilidad molecular es una característica esencial para el buen funcionamiento de la proteína. En particular, la flexibilidad proteica rige la unión de ligandos y la liberación subsiguiente de productos, lo cual es esencial para su función biológica. Por lo tanto, un conocimiento adecuado de la estructura y flexibilidad de las proteínas juega un papel vital en la comprensión de las complejidades y funciones moleculares. Así, se ha propuesto que la adaptación al frío está asociada a un incremento de la flexibilidad del sitio activo, que podría conducir a entalpías de activación inferiores a expensas de requerir más ordenación de los sustratos y el sitio activo, es decir, un cambio entrópico más negativo. Sin embargo, no hay resultados experimentales concluyentes para esta hipótesis.

1.2.4 Aproximaciones computacionales a enzimas psicrofílicas

El origen de la optimización de la velocidad catalítica en las enzimas adaptadas al frío, en términos de relaciones estructura-función, sigue siendo incierto. La comprensión de tales relaciones no sólo proporcionaría información sobre los procesos evolutivos de adaptación, sino que también permitiría el diseño racional de enzimas adaptadas a bajas temperaturas.

Las simulaciones por ordenador podrían proporcionar una forma única de analizar la reacción energética de enzimas ortólogos con diferentes tipos de adaptación a bajas temperaturas. Sin embargo, para que esta estrategia sea viable deben cumplirse varios criterios. En primer lugar, el análisis de factores indirectos o circunstanciales (flexibilidad, electrostática, hidrofobicidad, etc.) por sí solo no es suficiente para obtener pruebas concluyentes. En su lugar, los perfiles de energía libre a lo largo del camino de reacción deben obtenerse con alta precisión. Por otra parte, el equilibrio entalpía-entropía de activación (crucial para diferentes enzimas) debe ser reproducido por las simulaciones para ello es necesario conocerla dependencia de la energía libre de activación con la temperatura. Esto implica calcular un gran número de perfiles de energía libre a diferentes temperaturas para que las entalpías y entropías de activación se puedan extraer con alta precisión. Claramente, este amplio muestreo por simulaciones de dinámica molecular (MD) impide el uso del método QM/MM, aunque el método empírico de enlace de valencia (EVB) proporciona una alternativa eficiente.[95] Finalmente, siempre que los equilibrios entalpía-entropía de activación observados experimentalmente sean representados por las simulaciones, debe ser posible descomponerlos en sus componentes energéticos subyacentes, y finalmente traducirlos en diferencias entre las estructuras 3D de la enzima y sus fluctuaciones.

Objetivos

2.1 Estudio de relaciones estructura-actividad en diseño de fármacos sobre 11β-hidroxiesteroide deshidrogenasa tipo 1

Aprovechando la amplia experiencia del grupo de investigación del Dr. S. Vázquez en la síntesis de esqueletos carbonados policíclicos, se inició un proyecto de colaboración relacionado con el descubrimiento de nuevos inhibidores de 11β-HSD1 portadores de motivos tipo adamantano como homólogos hidrófobos. En particular, se planteó la hipótesis de que la sustitución del grupo adamantano por otras estructuras de grupos policíclicos hidrofóbicos, que se adapten mejor al tamaño y forma de la cavidad, puede ofrecer compuestos con perfiles de PK y PD mejorados.

Bajo estas premisas, el objetivo general ha sido examinar el efecto de diversos cambios estructurales sobre el modo de unión de los compuestos al enzima 11β-HSD1. Concretamente, se han considerado los siguientes puntos:

1.- Evaluación de una familia de compuestos de estructura general benzo-homoadamantano.

2.- Análisis de familias de compuestos con un esqueleto lipofílico de mayor tamaño que el grupo adamantano.

3.- Estudio del efecto de la sustitución del adamantano en C-2.

4.- Análisis comparativo en función de los diferentes grupos funcionales de los ligandos diseñados.

2.2 Influencia de la temperatura en la topología de las cavidades internas y la migración de ligandos en citoglobinas

En este capítulo se pretende examinar el efecto de la topología de cavidades internas sobre la migración de ligandos, y en particular profundizar en la sensibilidad estructural de diversas citoglobinas a cambios en la temperatura. En concreto, los objetivos han sido:

1.- Determinar el impacto de la temperatura en la dinámica de las proteínas y el número y la naturaleza de las cavidades internas.
2.- Estudiar y evaluar las propiedades estructurales, dinámicas y topológicas de Cygb humana y del pez antártico C. aceratus.

Resultados

La investigación llevada a cabo en esta tesis doctoral se ha plasmado en 6 publicaciones científicas que se indican a continuación separadas por cada uno de los dos objetivos principales, y se reproducen en las páginas siguientes.

3.1 Diseño de inhibidores de 11β-HSD1.

En relación a este objetivo, mi contribución se ha centrado en el desarrollo de los estudios de modelización y simulación reportados en cada una de las publicaciones, que tenían por objeto guiar y/o interpretar los trabajos de síntesis química y evaluación farmacológica llevados a cabo con el Prof. S. Vázquez, profesor de la Facultad de Farmacia.

Valverde, E., Seira, C., McBride, A., Binnie, M., Luque, F. J., Webster, S. P., … Vázquez, S. (2015). Searching for novel applications of the benzohomoadamantane scaffold in medicinal chemistry: Synthesis of novel 11β-HSD1 inhibitors. *Bioorganic and Medicinal Chemistry*, *23*(24), 7607–7617. http://doi.org/10.1016/j.bmc.2015.11.004

Leiva, R., Seira, C., McBride, A., Binnie, M., Luque, F. J., Bidon-Chanal, A., … Vázquez, S. (2015). Novel 11 β -HSD1 inhibitors: C-1 versus C-2 substitution and effect of the introduction of an oxygen atom in the adamantane scaffold. *Bioorganic and Medicinal Chemistry Letters*, *25*(19), 4250–4253. http://doi.org/10.1016/j.bmcl.2015.07.097

Leiva, R., Griñan-Ferré, C., Seira, C., Valverde, E., McBride, A., Binnie, M., … Vázquez, S. (2017). Design, synthesis and in vivo study of novel pyrrolidine-based 11β-HSD1 inhibitors for age-related cognitive dysfunction. *European Journal of Medicinal Chemistry*, *139*, 412-428. http://doi.org/10.1016/j.ejmech.2017.08.003

Seira, C., Leiva, R., McBride, A., Luque, F. J., Webster, S. P., Vázquez, S, Bidon-Chanal, A., *Rational design in the discovery of novel N-acylpyrrolidine-based 11β-HSD1 inhibitors.* **(**en preparación**)**

3.2 Efecto de la temperatura en migración de ligando en citoglobina

En relación a estos estudios, mi contribución se ha centrado en el desarrollo y análisis de diversos tipos de simulación por dinámica molecular destinados a identificar las características estructurales y dinámicas de citoglobina a diversas temperaturas, así como de su impacto en la topología de cavidades internas y su implicación en migración de ligandos.

Estarellas, C., Seira, C., Luque, F. J., Bidon-Chanal Badia, A. (2015). Understanding the kinetics of ligand binding to globins with molecular dynamics simulations: The necessity of multiple state models. *Drug Discovery Today: Technologies*, *17*, 22–27. http://doi.org/10.1016/j.ddtec.2015.09.002

Seira, C., Bolognesi, M., Luque, F. J., Viappiani, C., Bidon-Chanal, A *Influence of temperature on the topological features of inner cavities, ligand migration and model comparison in Cytoglobin*. **(**en preparación**)**

3.1.1 Artículo 1: *Searching for novel applications of the benzohomoadamantane scaffold in medicinal chemistry: Synthesis of novel 11β-HSD1 inhibitors.*

Resumen

Las propiedades estructurales y fisicoquímicas del núcleo de adamantano explican su uso como *scaffold* químico en múltiples fármacos. En los últimos años, hemos desarrollado nuevos *scaffolds* policíclicos como sustitutos del grupo adamantano con resultados esperanzadores en varios objetivos. El adamantano es una característica estructural común en varios inhibidores de 11β-hidroxiesteroide deshidrogenasa tipo 1 (11β-HSD1), se ha explorado la capacidad del 6,7,8,9,10,11-hexahidro-5H-5,9: 7 , 11-dimetanobenzo [9] annulen-7-yl scaf-fold para actuar como un sustituto del núcleo adamantano en una nueva serie de inhibidores de 11β-HSD1. Es de destacar que, dentro de esta familia de compuestos, un derivado está dotado de actividad inhibidora submicromolar de 11β-HSD1. Los estudios de modelado molecular apoyan la unión de los compuestos al centro activo de la enzima. Sin embargo, un ligero ajuste de la hidrofobicidad del núcleo de tamaño expandido puede ser beneficioso para aumentar la potencia inhibidora.

Bioorganic & Medicinal Chemistry 23 (2015) 7607–7617

Contents lists available at ScienceDirect

Bioorganic & Medicinal Chemistry

journal homepage: www.elsevier.com/locate/bmc

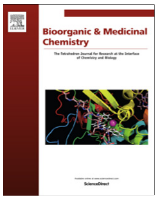

Searching for novel applications of the benzohomoadamantane scaffold in medicinal chemistry: Synthesis of novel 11β-HSD1 inhibitors

Elena Valverde[a,†], Constantí Seira[b,†], Andrew McBride[c], Margaret Binnie[c], F. Javier Luque[b], Scott P. Webster[c], Axel Bidon-Chanal[b], Santiago Vázquez[a,*]

[a] *Laboratori de Química Farmacèutica (Unitat Associada al CSIC), Facultat de Farmàcia, and Institute of Biomedicine (IBUB), Universitat de Barcelona, Av. Joan XXIII, s/n, Barcelona E-08028, Spain*

[b] *Departament de Fisicoquímica, Facultat de Farmàcia and Institute of Biomedicine (IBUB), Universitat de Barcelona, Av. Prat de la Riba, 171, 08921 Santa Coloma de Gramenet, Spain*

[c] *Endocrinology Unit, Centre for Cardiovascular Science, University of Edinburgh, Queen's Medical Research Institute, EH16 4TJ, United Kingdom*

ARTICLE INFO

Article history:
Received 2 September 2015
Revised 30 October 2015
Accepted 5 November 2015
Available online 5 November 2015

Keywords:
Adamantane
Cage compounds
11β-HSD1 inhibitors
Drug discovery
Molecular dynamics

ABSTRACT

The structural and physicochemical properties of the adamantane nucleus account for its use as a chemical scaffold in multiple drugs. In the last years, we have developed new polycyclic scaffolds as surrogates of the adamantane group with encouraging results in multiple targets. As adamantane is a common structural feature in several 11β-hydroxysteroid dehydrogenase type 1 (11β-HSD1) inhibitors, we have explored the ability of the 6,7,8,9,10,11-hexahydro-5*H*-5,9:7,11-dimethanobenzo[9]annulen-7-yl scaffold to act as a surrogate of the adamantane nucleus in a novel series of 11β-HSD1 inhibitors. Of note, within this family of compounds one derivative is endowed with submicromolar 11β-HSD1 inhibitory activity. Molecular modeling studies support the binding of the compounds to the active site of the enzyme. However, a fine tuning of the hydrophobicity of the size-expanded nucleus may be beneficial for the inhibitory potency.

© 2015 Elsevier Ltd. All rights reserved.

1. Introduction

Over the last eight decades, adamantane-like compounds have attracted organic and medicinal chemists.[1] The structural and physicochemical properties of the adamantane nucleus account for its use as a chemical scaffold in multiple drugs.[2] Seven drugs featuring the adamantane motif have reached the market, including amantadine and rimantadine, two antivirals that constituted the birth of the medicinal chemistry of adamantane derivatives.[3] Later, memantine was launched and became a blockbuster drug, and is the only NMDA receptor antagonist approved for the treatment of Alzheimer's disease.[4] The role of adamantane-based scaffolds in enzyme inhibition is reflected in vildagliptin and saxagliptin, which are dipeptidyl peptidase IV (DPP-IV) inhibitors clinically approved for diabetes treatment.[5] Soluble epoxide hydrolase (sEH) and 11β-hydroxysteroid dehydrogenase (11β-HSD) are other enzyme targets for adamantane-based compounds,[6] with important roles in the metabolic syndrome though without any inhibitor on the market yet (Fig. 1).

Glucocorticoids are hormones that intervene in the body's response to stress, regulate carbohydrate, protein and lipid metabolism and modulate inflammatory and immune responses.[7] It has been hypothesized that elevated intracellular concentrations of cortisol in adipose tissue and liver can lead to glucose intolerance and insulin resistance and contribute to the development of the metabolic syndrome, which is a major risk factor for cardiovascular disease and type II diabetes.[8] The link between glucocorticoid excess and metabolic syndrome is manifested in Cushing's syndrome patients, who have elevated glucocorticoid levels with a phenotype similar to the metabolic syndrome.[9] In humans, glucocorticoid homeostasis is primarily controlled by the hypothalamic-pituitary-adrenal (HPA) axis and biosynthesis is mediated by the 11β-HSD enzymes. The two isoforms of this enzyme (11β-HSD1 and 11β-HSD2) catalyze the interconversion between active cortisol and inactive cortisone (Fig. 2). 11β-HSD1 is mainly expressed in liver, adipose tissue and brain and in vivo acts mainly as a reductase, whilst 11β-HSD2 is found chiefly in mineralocorticoid target tissues such as kidney and colon.

---

[*] Corresponding author. Tel.: +34 934 024 533.
E-mail address: svazquez@ub.edu (S. Vázquez).

[†] They have contributed equally to this work.

http://dx.doi.org/10.1016/j.bmc.2015.11.004
0968-0896/© 2015 Elsevier Ltd. All rights reserved.

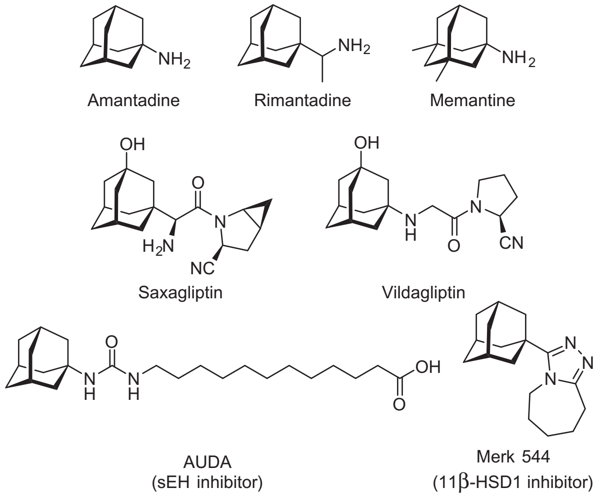

Figure 1. Representative structures of adamantane-based drugs.

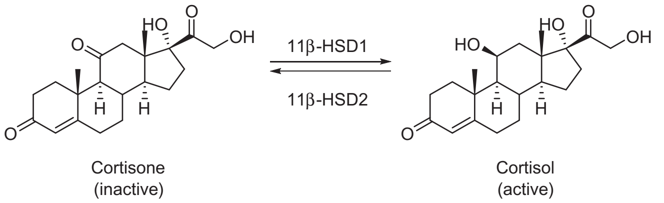

Figure 2. Interconversion of cortisone to cortisol in humans by 11β-HSD enzymes.

Although circulating cortisol levels are not increased in metabolic syndrome patients, it has been proposed that its production is altered through an increase in 11β-HSD1 expression and activity, notably in metabolic tissues.[10] Therefore, inhibition of 11β-HSD1 may represent a valuable therapeutic strategy in patients with metabolic syndrome. Indeed, from its discovery as a therapeutic target, many companies and academic groups have put forth great efforts into pursuing new and improved inhibitors.[6a,b,11–13]

The active site of 11β-HSD1 is flexible and largely hydrophobic with key residues (Ser170, Tyr183) mediating important hydrogen bonding interactions.[12] As a result, many known inhibitors contain bulky lipophilic groups, such as adamantane ring systems, adjacent usually to an amide group.[6b,11,13] Nevertheless, the widespread use of lipophilic moieties in most inhibitors presents potential problems of poor solubility and also metabolic instability, which can occur via hydroxylation at the 5-position of the adamantyl group.[14] Consequently, many research teams have pursued alternative strategies to avert this issue, by attaching polar groups at key positions and often using other adamantane-like polycyclic scaffolds.[15]

In the last few years, our research group has synthesized new polycyclic scaffolds as surrogates of the adamantane group with encouraging results on multiple targets. These include ring-contracted, ring-expanded, ring-rearranged and oxa-ring analogs of amantadine, rimantadine and memantine with anti-influenza, NMDA receptor antagonist and trypanocidal activities (Fig. 3), proving the capacity of these polycycles to substitute the adamantane ring.[16] Recently, we described a new series of benzopolycyclic amines, such as **3**, which are active as NMDA receptor antagonists.[17]

Here we investigate the substitution of the adamantane moiety of a series of known 11β-HSD1 inhibitors by using a carbocyclic system with the general structure **I**, which involves the size expansion via insertion of a benzene ring, in conjunction with a diversity of carbocyclic or heterocyclic subunits (**A**–**D**) reported in previous studies on the right-hand side (RHS) of the molecule (Fig. 4).[15c,18,19]

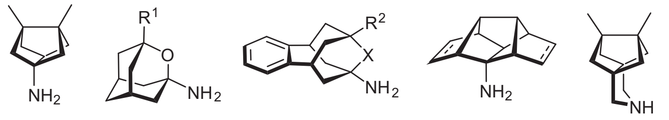

Figure 3. Structures of ring-contracted, ring-expanded and oxa analogs of adamantane (X = O, CH_2).

2. Results and discussion

2.1. Design of new derivatives

A hybrid strategy was used to design new compounds whereby the inhibitor was partitioned into the hydrophobic adamantane-like unit and a ring, linked via an amido or urea-like unit. The adamantane-like moiety was replaced by the 6,7,8,9,10,11-hexahydro-5*H*-5,9:7,11-dimethanobenzo[9]annulen-7-yl polycycle, which introduced a phenyl ring in the hydrophobic cage. This strategy had a dual purpose. First, a phenyl ring together with polar groups attached to the polycycle (OH, OMe, F) were introduced in an effort to modify the pharmacokinetic properties of the compounds, and particularly to affect the metabolism at specific ring positions. Second, since 2-substituted adamantanes are more potent 11β-HSD1 inhibitors than their synthetically more accessible 1-substituted counterparts,[19] the insertion of the phenyl ring was expected to lead to new binding interactions with the enzyme. It is worth noting that inspection of the available X-ray structures and preliminary docking studies (see below) indicate that the active site of the enzyme is large enough to accommodate the enlarged polycycle. A series of functional chemical groups previously tested in 11β-HSD1 inhibitors were integrated into the RHS moiety, while the amido linker was retained to enable the formation of key hydrogen bonds in the binding site.

2.2. Chemistry

The novel compounds were synthesized according to Schemes 1–3 starting from amines **6**–**9** (Fig. 5), easily available following the procedures previously described by our group.[17]

From amines **6**, **7** and **8**, the synthetic pathways for the amide end products **10**, **11** and **15**–**20** are outlined in Scheme 1. Benzamides **10** and **11** were obtained from **6** and **7**, respectively, by coupling with the commercially available 4-amino-3,5-dichlorobenzoic acid. For the synthesis of the PF-877423 analogs, **6**, **7** and **8** were coupled with *N*-Boc-protected D-proline to furnish amides **12**, **13** and **14**, respectively. Cleavage of the protecting group under acidic conditions furnished the pyrrolidines **15**–**17** in very high yields. Finally, *N*-alkylation with ethyl bromide and triethylamine gave the three PF-877423 analogs **18**–**20**.

In a similar manner, amide **21** was prepared through an amide coupling reaction with cyclohexanecarboxylic acid in 96% yield (Scheme 2). Of note, we have recently disclosed that the introduction of such a substituent within a series of substituted adamantane derivatives was beneficial for inhibitory activity.[19] The key step in the synthesis of the thiazolone ring system in compound **23** was accomplished by a substitution/cyclization reaction between the thiourea **22** and ethyl 2-bromoisobutyrate, although with very low overall yield (Scheme 2).

Lastly, a series of four ureas were synthesized in medium to low yields from amines **6**–**9** by reaction with piperidine-1-carbonyl chloride, as is shown in Scheme 3.

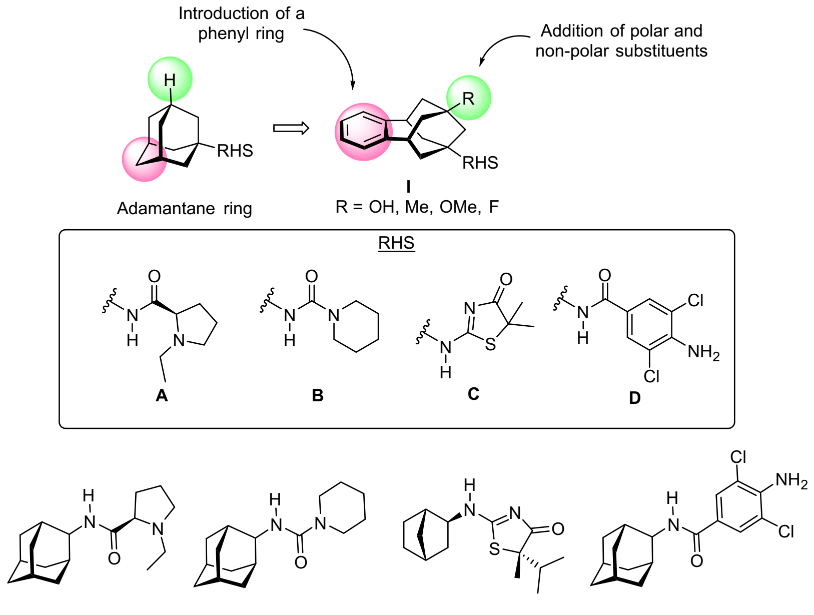
Introduction of a phenyl ring
Addition of polar and non-polar substituents
H
RHS
Adamantane ring
R
RHS
I
R = OH, Me, OMe, F
RHS
A
B
C
D

A, Pfizer's PF-877423 **B**, Vitae's inhibitor **C**, Amgen's AMG-221 **D**, Our previous work

Figure 4. New 11β-HSD1 inhibitors with general structure **I** and selected known nanomolar inhibitors taken as model compounds.

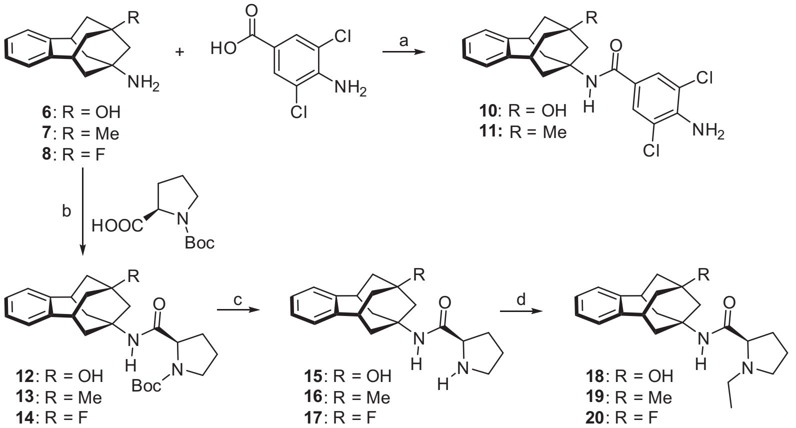
6: R = OH
7: R = Me
8: R = F
a
10: R = OH
11: R = Me
b
12: R = OH
13: R = Me
14: R = F
c
15: R = OH
16: R = Me
17: R = F
d
18: R = OH
19: R = Me
20: R = F

Scheme 1. Reagents and conditions: (a) HOBt, EDC, Et_3N, EtOAc, rt, 21 h, 95% for **10**, 53% for **11**; (b) HATU, Et_3N, DMF, rt, 18 h or HOBt, EDC, Et_3N, EtOAc, rt, 18 h, 50% for **12**, 84% for **13**, 92% for **14**; (c) 85 wt % *o*-phosphoric acid, CH_2Cl_2, 3-18 h, 87% for **15**, quantitative for **16** and **17**; (d) ethyl bromide, KI, Et_3N, DMF, rt, 18 h, 72% for **18**, 44% for **19**, 35% for **20**.

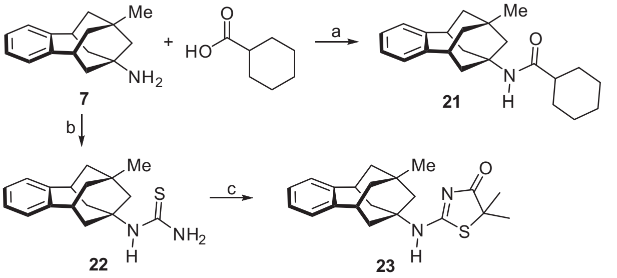
7
a
21
b
22
c
23

Scheme 2. Reagents and conditions: (a) HOBt, EDC, Et_3N, EtOAc, rt, 18 h, 96%; (b) (i) benzoyl isothiocyanate, $CHCl_3$, rt, 18 h, (ii) MeOH, THF, K_2CO_3, H_2O, rt, 18 h; (c) ethyl 2-bromoisobutyrate, DIPEA, EtOH, microwave heating (130 °C), 3 h, 7% overall.

The structure of all new compounds was confirmed by elemental analysis and/or accurate mass measurement, IR, ^1H NMR, ^{13}C NMR and mass spectral analysis.

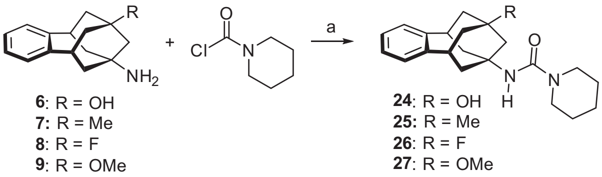
6: R = OH
7: R = Me
8: R = F
9: R = OMe
a
24: R = OH
25: R = Me
26: R = F
27: R = OMe

Scheme 3. Reagents and conditions: (a) Et_3N, CH_2Cl_2, rt, 18 h, 64% for **24**, 59% for **25**, 26% for **26**, 38% for **27**.

2.3. In vitro cellular inhibition of 11β-HSD1

A preliminary in vitro compound screen was performed to evaluate if the synthesized compounds were able to inhibit human 11β-HSD1 using a microsomal assay (see Section 4). Five compounds (**16**, **19**, **20**, **21** and **26**) were found to have an inhibitory effect larger than 50% at a single dose of 10 μM (Table 1). This highlights the relevant role played by the polar moiety at the RHS.

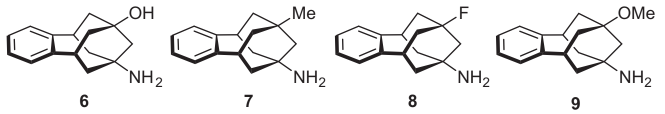

Figure 5. Amines **6–9** used as left-hand side of the putative new 11β-HSD1 inhibitors synthesized in this work.

Table 1
Enzyme inhibition data[a]

Compound	R	RHS	% of inhibition	IC_{50} (μM)
10	OH	D	31	ND
11	CH_3	D	36	ND
15	OH	**A** (N = H)	15	ND
16	CH_3	**A** (N = H)	57	ND
18	OH	A (N-Et)	24	ND
19	CH_3	A (N-Et)	77 ± 6	1.0 ± 0.3
20	F	A (N-Et)	76	0.35 ± 0.2
21	CH_3	Cyclohexyl	52	ND
23	CH_3	C	35	ND
24	OH	B	30	ND
25	CH_3	B	36	ND
26	F	B	62	ND
27	OCH_3	B	41	ND
PF-877423	—	A (N-Et)	93	0.004

[a] 11β-HSD1 inhibition was determined in mixed sex, Human Liver Microsomes (Celsis In-vitro Technologies) by measuring the conversion of ^{3}H-cortisone to ^{3}H-cortisol in a cortisol-Scintillation Proximity Assay. Percentage inhibition was determined relative to a no inhibitor control (see Section 4 for further details).

Within this series of benzopolycyclic derivatives, the combination of a fluorine atom at C-9 with the *N*-ethyl-D-proline subunit in compound **20** gave the highest inhibitory activity. Also, the introduction of polar (OH or OCH_3) groups in the C-9 position of the polycycle scaffold is deleterious to the inhibitory activity.

2.4. Molecular modeling studies

Preliminary docking calculations performed with Glide,[20] supported the ability of the size-expanded polycycles to fill the binding cavity of human 11β-HSD1 (for details about molecular simulations, see Section 4). Thus, the best scored poses of the most potent inhibitors, **19** and **20**, mimicked the binding mode of PF-877423, retaining the hydrogen bond formed between the amide carbonyl oxygen with the hydroxyl group of Ser170, whereas the hydrophobic cage filled the site occupied by the adamantane unit of PF-877423. Furthermore, the docking scores of **19** (8.1 kcal/mol) and **20** (8.2 kcal/mol) compared well with PF-877423 (7.8 kcal/mol). However, compounds **19** and **20** are around 100/200-fold less potent than PF-877423 (Table 1). Therefore, the substitution of the adamantane moiety by the size-expanded polycycle is detrimental for the binding to the enzyme.

To check this hypothesis, the structural integrity of the best poses of compounds **19** and **20** was explored by means of molecular dynamics (MD) simulations. Three independent 50 ns MD simulations were run for each ligand-receptor complex. All the simulations were stable, as noted in root-mean square deviation (RMSD) profiles ranging from 1.5 to 2.4 Å for the protein backbone, and from 2.5 to 3.5 Å for the residues in the binding site, thus reflecting enhanced flexibility of the loops that enclose the binding pocket. The ligand pose was preserved throughout the simulations (Fig. 6), and the hydrogen bond formed between the inhibitor and Ser170 was maintained in all cases (average distance of 2.8 ± 0.2 Å). Finally, the relative binding affinities were estimated from SIE calculations, which revealed that compounds **19** and **20** should be stronger binders (by 0.5 and 1.1 kcal/mol, respectively) compared to PF-877423.

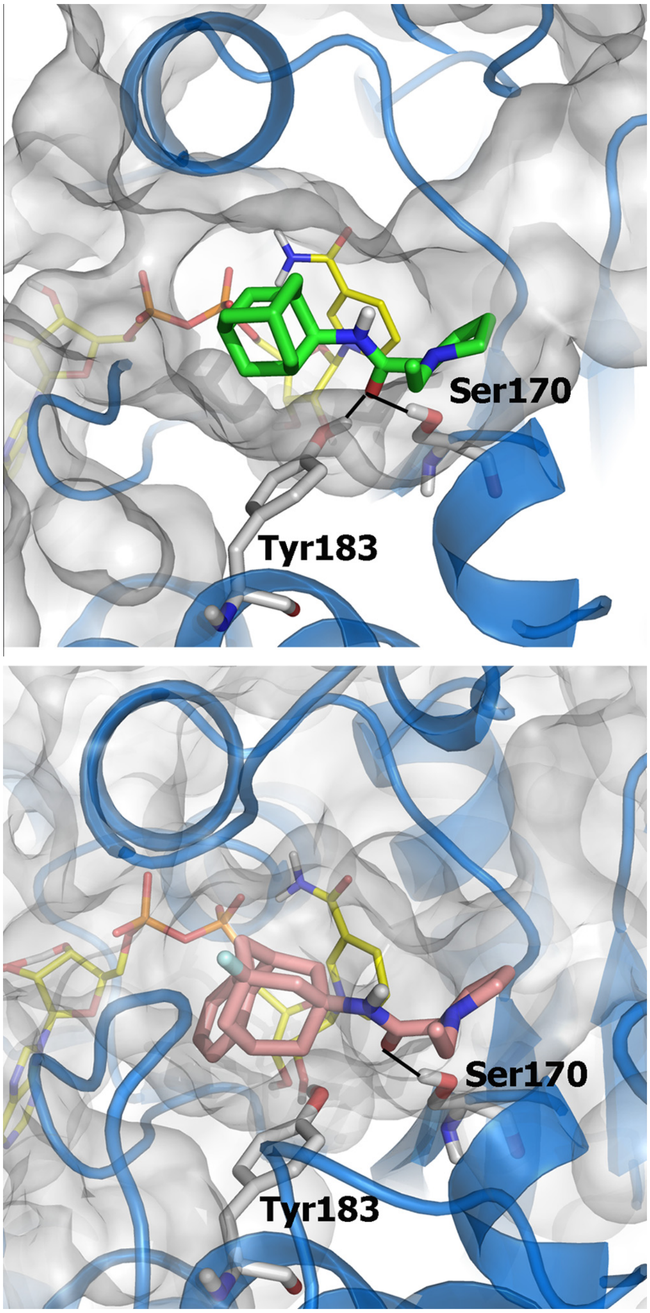

Figure 6. Representative snapshots taken from the MD simulations of the complexes between human 11β-HSD1 and compounds PF-877423 (top; green sticks) and **20** (bottom; pink sticks). Residues Tyr183 and Ser170 are shown as gray sticks, the NADP cofactor as yellow-based sticks and the protein backbone as blue cartoon. The hydrogen bond between the inhibitor and Ser170 is shown as a black line. For the sake of clarity only polar hydrogens are shown. The shape of the binding cavity is shown as a white contour.

The analysis of the trajectories allowed us to gain insight into the structure-activity relationships of these compounds. In particular, the beneficial effect of the methyl/fluorine substituents (R in **I**; see Fig. 4 and Table 1) can be ascribed to the fact that they fill a small hydrophobic pocket shaped by the side chains of Leu126, Ala226, Val227 and the Cα atom of Ser125 (see Fig. 7A). The closest distances from the fluorine atom to these residues typically range from 3.6 to 4.8 Å. This explains the lower inhibitory potency found for compounds bearing the more polar hydroxyl group or the bulkier methoxy substituent (Table 1). On the other hand, the C-1 substitution pattern used for the linkage between

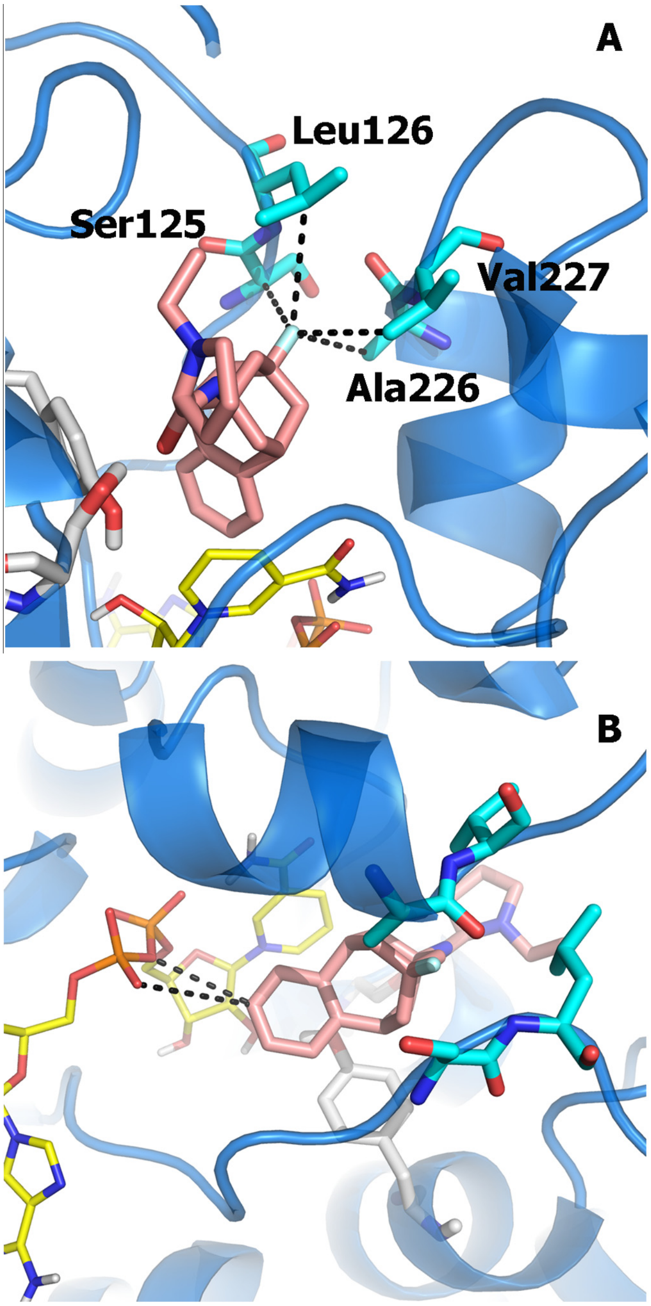

Figure 7. (A) Representation of the contacts between the fluorine atom in the hydrophobic pocket formed by Ser125, Leu126, Ala226 and Val227 (shown as blue-colored sticks). (B) Spatial arrangement of the benzene ring of compound **19** and the phosphate group of the cofactor (shown as yellow sticks). The van der Waals contacts are highlighted by dashed lines.

the size-expanded polycycle and the RHS moiety seems to be detrimental for the activity. This is reflected in the conformational change of Tyr183 found for simulations with compounds **19** and **20**, in contrast with the arrangement observed in the simulations run for PF-877423 (see Fig. 6A and B). While Tyr183 forms transient hydrogen-bond interactions with the amide carbonyl group of PF-877423 (Fig. 6A), the conformational change triggered by the C-1 fused compound prevents the formation of similar interactions (Fig. 6B), which should weaken the binding affinity. Finally, the lower inhibitory activity can also stem from an exceedingly large expansion of the polycycle ring, since the benzene moiety is too close to the phosphate group of the cofactor, as noted in distances ranging from 4.2 to 5.0 Å (see Fig. 7B). Accordingly, one can assume that water molecules hydrating the phosphate oxygens are expelled from the binding pocket, with a concomitant loss of stabilizing interactions with the cofactor, which are not counterbalanced by interactions with the benzene ring.

While the preceding results support the assumption that insertion of the benzene ring is not beneficial for the binding, the reduction in inhibitory potency may also arise from a decrease in water solubility due to the increased hydrophobicity of the polycycle,[21] which should lower the effective concentration of the compound in the human liver microsome assay. To this end, the octanol/water partition coefficient ($\log P_{o/w}$) was determined using quantum mechanical IEF/MST calculations,[22] for the most favorable conformations of compounds **19**, **20** and PF-877423. As expected, the results point out that the expansion of the polycycle increases the $\log P_{o/w}$ by 1.5 (**19**) and 0.9 (**20**) units relative to PF-877423.

Taken together, the results suggest that the size-expansion strategy outlined here may lead to effective inhibitors of human 11β-HSD1. Nevertheless, a proper balance of the hydrophobicity afforded by the size-expanded polycycle is necessary to optimize the pharmacological profile. Hence, the incorporation of nucleus with enhanced polarity appears to be a suitable strategy for developing novel inhibitors.

3. Conclusions

Thirteen new polycyclic compounds have been synthesized from easily available amines **6**–**9** as 11β-HSD1 inhibitors. Five of the novel compounds displayed reasonable enzyme inhibition and the most potent of them (**20**) possessed submicromolar inhibitory potency. Contrary to our previous results where adamantane may be replaced by the polycycle 6,7,8,9,10,11-hexahydro-5,7:9,11-dimethano-5*H*-benzocyclononen-7-yl scaffold,[17] the adoption of this strategy was found to be less successful in the case of human 11β-HSD1 inhibitors. Further work fine tuning the size expansion and the polarity of the nucleus may lead to novel series of 11β-HSD1 inhibitors. Also, taking into account that very recently it has been shown that C-2 substituted adamantyl inhibitors are more potent than their C-1 analogs,[19] work is in progress to synthesize and evaluate novel amides derived from 6,7,8,9,10,11-hexahydro-5,7:9,11-dimethano-5*H*-benzocyclononen-8-amine.

4. Experimental

4.1. Chemistry

4.1.1. General

Melting points were determined in closed-end capillary tubes. NMR spectra were recorded in the following spectrometers: ^{1}H NMR (400 or 500 MHz), ^{13}C NMR (100.6 or 125.7 MHz). Chemical shifts (δ) are reported in ppm related to internal tetramethylsilane (TMS) and coupling constants are reported in Hertz (Hz). Assignments given for the NMR spectra are based on DEPT, COSY ^{1}H/^{1}H, HETCOR ^{1}H/^{13}C (HSQC and HMBC sequences for one bond and long range ^{1}H/^{13}C heterocorrelations, respectively) and NOESY experiments for selected compounds. For the MS and GC/MS analyses the samples were introduced directly or through a gas chromatograph. For GC/MS analyses a 30-meter column [5% diphenyl-95% dimethylpolysiloxane, conditions: 10 psi, initial temperature: 35 °C (2 min), then heating at a range of 8 °C/min till 300 °C, then isothermic at 300 °C] was used. The electron impact (70 eV) or chemical ionization (CH_4) techniques were used. Only significant ions are given: those with higher relative ratio, except for the ions with higher m/z values. Accurate mass measurements were obtained using ESI technique. Absorption values in the IR spectra (KBr or ATR) are given as wave-numbers (cm^{-1}). Only the more intense bands are given. Column chromatography was performed on aluminum oxide, neutral, Brockmann I (60 Å, 50–200 μm). For the thin layer chromatography (TLC) aluminum-backed sheets with aluminum oxide 60 Å were used and spots were visualized with UV light and/or 1% aqueous solution of $KMnO_4$.

4.1.2. 4-Amino-3,5-dichloro-*N*-(9-hydroxy-6,7,8,9,10,11-hexahydro-5*H*-5,9:7,11-dimethanobenzo[9]annulen-7-yl)benzamide, 10

To a solution of amine **6** (270.0 mg, 1.18 mmol) in EtOAc (15 mL) and DMF (1 mL) were added 4-amino-3,5-dichlorobenzoic acid (220.9 mg, 1.07 mmol), 1-hydroxybenzotriazole (HOBt) (216.7 mg, 1.6 mmol), 1-ethyl-3-(3-dimethylaminopropyl)carbodiimide (EDC) (248.0 mg, 1.6 mmol) and triethylamine (0.327 mL, 2.2 mmol) and the reaction mixture was stirred at room temperature for 21 h. To the resulting suspension was then added water (20 mL) and the phases were separated. The organic phase was washed with 5% aqueous $NaHCO_3$ solution (15 mL) and brine (15 mL), dried over anhyd Na_2SO_4 and filtered. Evaporation in vacuo of the combined organic phases gave **10** (422.0 mg, 95% yield) as a white solid. The analytical sample was obtained by crystallization from DCM, mp 236–237 °C. IR (ATR) ν: 3362, 2923, 2853, 2160, 1976, 1643, 1606, 1547, 1519, 1492, 1452, 1321, 1299, 1269, 1230, 1201, 1101, 1020, 864, 748, 570 cm^{-1}. ^1H NMR (500 MHz, $CDCl_3$) δ: 1.58 (broad s, 1H, OH), 1.81 [d, J = 12.5 Hz, 2H, 10(13)-H_b], 2.00 [m, 2H, 10(13)-H_a], 2.12 [d, J = 13 Hz, 2H, 6(12)-H_b], 2.19 (s, 2H, 8-H_2), 2.27 [ddd, J = 13.0 Hz, J' = 6.5 Hz, J'' = 1.0 Hz, 2H, 6(12)-H_a], 3.23 [tt, J = 6.5 Hz, J' = 1.5 Hz, 2H, 5(11)-H], 4.73 (broad s, 2H, Ar-NH_2), 5.72 (broad s, 1H, CONH), 7.09 [m, 2H, 1(4)-H], 7.13 [m, 2H, 3(2)-H], 7.54 [s, 2H, 16(20)]. ^{13}C NMR (125.7 MHz, $CDCl_3$) δ: 38.6 [CH_2, C6(12)], 40.0 [CH, C5(11)], 42.5 [CH_2, C10(13)], 48.4 (CH_2, C8), 57.4 (C, C7), 70.9 (C, C9), 118.9 [C, C17(19)], 125.4 (C, C15), 126.7 [C, C16(20)], 126.8 [CH, C2(3)], 128.1 [CH, C1(4)], 142.6 (C, C18), 145.1 [d, C, C4a(C11a)], 164.2 (C, CO). GC-MS (EI), rt = 47.7 min, m/z (%); significant ions: 418 (21), 416 ($M^{\cdot+}$, 32), 212 (43), 207 (36), 205 (46), 194 (16), 190 (63), 188 (100), 179 (15), 160 (15), 155 (33), 154 (29), 142 (16), 141 (17), 129 (19), 128 (20), 124 (16), 115 (16). Anal. Calcd for $C_{22}H_{22}Cl_2N_2O_2$: C, 63.32; H, 5.31; N, 6.71. Found: C, 63.32; H, 5.35; N, 6.52.

4.1.3. 4-Amino-3,5-dichloro-*N*-(9-methyl-6,7,8,9,10,11-hexahydro-5*H*-5,9:7,11-dimethanobenzo[9]annulen-7-yl)benzamide, 11

To a solution of amine **7** (200.0 mg, 0.88 mmol) in ethylacetate (10 mL) and DMF (1 mL) were added 4-amino-3,5-dichlorobenzoic acid (165.0 mg, 0.80 mmol), 1-hydroxybenzotriazole (HOBt) (162 mg, 1.2 mmol), 1-ethyl-3-(3-dimethylaminopropyl)carbodiimide (EDC) (186.0 mg, 1.2 mmol) and triethylamine (0.25 mL, 1.76 mmol) and the reaction mixture was stirred at room temperature for 22 h. To the resulting suspension was then added water (20 mL) and the phases were separated. The organic phase was washed with 5% aqueous $NaHCO_3$ solution (15 mL) and brine (15 mL), dried over anhyd Na_2SO_4 and filtered. Evaporation in vacuo of the combined organic phases gave an orange solid (320.0 mg). Column chromatography (Al_2O_3, 100% DCM) gave **11** (176.7 mg, 53% yield) as a white solid. The analytical sample was obtained washing the solid with *n*-pentane, mp 173–175 °C. IR (ATR) ν: 3460, 3352, 2920, 2852, 1627, 1610, 1532, 1484, 1452, 1322, 1306, 1270, 1232, 1126, 1091, 1049, 1006, 947, 908, 880, 837, 789, 757, 720, 695, 663, 581 cm^{-1}. ^1H NMR (500 MHz, $CDCl_3$) δ: 0.95 (s, 3H, C9-CH_3), 1.58 [dt, J = 13.5 Hz, J' = 1.5 Hz, 2H, 10(13)-H_b], 1.69 [ddm, J = 13.5 Hz, J' = 6.5 Hz, 2H, 10(13)-H_a], 1.93 (s, 2H, 8-H_2), 2.15 [dt, J = 13.0 Hz, J' = 1.5 Hz, 2H, 6(12)-H_b], 2.25 [ddm, J = 13.0 Hz, J' = 6.5 Hz, 2H, 6(12)-H_a], 3.11 [tt, J = 6.5 Hz, J' = 1.5 Hz, 2H, 5(11)-H], 4.71 (broad s, 2H, NH_2), 5.68 (broad s, 1H, NH), 7.04–7.11 [complex signal, 4H, 1(4)-H, 2(3)-H], 7.54 [s, 2H, 16(20)]. ^{13}C NMR (125.7 MHz, $CDCl_3$) δ: 32.2 (CH_3, C9-CH_3), 33.7 (C, C9), 39.1 [CH_2, C6(12)], 41.0 [CH, C5(11)], 41.1 [CH_2, C10(13)], 47.3 (CH_2, C8), 55.0 (C, C7), 118.8 [C, C17(19)], 125.7 (C, C15), 126.3 [CH, C2(3)], 126.6 [CH, C16(20)], 128.0 [CH, C1(4)], 142.4 (C, C18), 146.1 [d, C, C4a(C11a)], 164.1 (C, CO). GC-MS (EI), rt = 40.6 min, m/z (%); significant ions: 416 (25), 415 (11), 414 ($M^{\cdot+}$, 38), 211 (20), 210 (100), 195 (26), 190 (48), 188 (74), 182 (19), 181 (19), 160 (12), 156 (14), 155 (78), 154 (30), 143 (13), 142 (14), 141 (18), 129 (18), 128 (19), 124 (15), 115 (14). Anal. Calcd for $C_{23}H_{24}Cl_2N_2O_2$: C, 66.51; H, 5.82; N, 6.74. Calcd for $C_{23}H_{24}Cl_2N_2O_2 \cdot 0.1C_5H_{12}$: C, 66.79; H, 6.01; N, 6.63. Found: C, 66.82; H, 6.04; N, 6.54%.

4.1.4. (2*R*)-*tert*-Butyl 2-[(9-hydroxy-6,7,8,9,10,11-hexahydro-5*H*-5,9:7,11-dimethanobenzo[9]annulen-7-yl)carbamoyl]pyrrolidine-1-carboxylate, 12

To a solution of amine **6** (500.0 mg, 2.18 mmol) in DMF (10 mL) were added Boc-D-proline (445.8 mg, 2.07 mmol), HATU (328.4 mg, 2.18 mmol) and triethylamine (0.6 mL, 4.36 mmol) and the resulting solution was stirred at room temperature overnight. The reaction mixture was then diluted with EtOAc: benzene 2 : 1 (25 mL) and washed with 0.5 N HCl aqueous solution (2 × 25 mL), brine (25 mL), saturated $NaHCO_3$ aqueous solution (2 × 25 mL) and brine (25 mL). The organic phase was separated, dried over anhyd Na_2SO_4, filtered and concentrated in vacuo to give an orange oil (765.0 mg). Column chromatography (Al_2O_3, hexane/EtOAc mixture) gave **12** (438.0 mg, 50% yield) as a white solid. The analytical sample was obtained by crystallization from EtOAc/pentane, mp 98–103 °C. IR (ATR) ν: 3408, 3327, 2975, 2927, 1677, 1538, 1451, 1400, 1366, 1300, 1247, 1163, 1119, 1088, 1045, 978, 922, 862, 758 cm^{-1}. ^1H NMR (500 MHz, $CDCl_3$) δ: 1.45 [s, 9 H, OC(CH_3)$_3$], 1.73 (m, 2H, 17-H_2), 1.76 [d, J = 13.0 Hz, 2H, 10(13)-H_b], 1.83 (broad signal, 1H, 16-H_a), 1.93–2.31 [complex signal, 9 H, 10(13)-H_a, 6(12)-H_2, 8-H_2, 16-H_b], 3.17 [t, J = 6.5 Hz, 2H, 5(11)-H], 3.37 (m, 2H, 18-H_2), 4.21 (m, 1H, 15-H), 5.81 (broad s, 1H, OH), 6.94 (broad s, 1H, NH), 7.06 [m, 4H, 1(4)-H], 7.10 [m, 2H, 2(3)-H]. ^{13}C NMR (125.7 MHz, $CDCl_3$) δ (mixture of two rotamers): 23.7 (CH_2) and 24.1 (CH_2) (two rotamers, C17), 28.4 [CH_3, OC(CH_3)$_3$], 31.1 (broad CH_2, C16), 38.4 [CH_2, C6(12)], 40.0 [CH, C5(11)], 42.4 [CH_2, C10(13)], 47.1 (CH_2, C18), 48.2 (CH_2, C8), 56.6 (C, C7), 61.2 (CH) and 61.9 (CH) (C15, two rotamers), 70.8 (C, C9), 80.4 (C, C20), 126.6 [CH, C2(3)], 128.1 [CH, C1(4)], 145.2 [d, C, C4a(C11a)], 154.7 (C) and 156.1 (C) (NCO, two rotamers), 170.9 (C) and 171.6 (C) (CO, two rotamers). HRMS-ESI + m/z $[M+H]^+$ calcd for $[C_{25}H_{34}N_2O_4+H]^+$: 427.2591, found: 427.2593.

4.1.5. (2*R*)-*N*-(9-Hydroxy-6,7,8,9,10,11-hexahydro-5*H*-5,9:7,11-dimethanobenzo[9]annulen-7-yl)pyrrolidine-2-carboxamide, 15

A solution of Boc-protected pyrrolidine **12** (438.5 mg, 1.03 mmol) in DCM (5 mL) and 85% *o*-phosphoric acid (1.05 mL, 15.4 mmol) was stirred at room temperature for 3 h. To the reaction mixture was then added water (8 mL) and the pH was adjusted to ~12 with 5 N NaOH solution. The phases were separated, the aqueous phase was extracted with further DCM (2 × 8 mL) and the combined organic phases were dried over anhyd Na_2SO_4 and filtered. Evaporation in vacuo of the combined organic layers gave **15** (290.8 mg, 87% yield) as a white solid, mp 175–180 °C. IR (ATR) ν: 3441, 3368, 3262, 2945, 2863, 1639, 1521, 1507, 1475, 1434, 1401, 1378, 1361, 1336, 1300, 1230, 1194, 1115, 1050, 887, 846, 799, 767, 731, 698, 552 cm^{-1}. ^1H NMR (500 MHz, $CDCl_3$) δ: 1.66 (complex signal, 2H, 17-H_2), 1.78 [d, J = 13 Hz, 2H, 10(13)-H_b], 1.85 (m, 1H, 16-H_a), 1.90–1.99 [complex signal, 4H, 6(12)-H_b, 10(13)-H_a], 2.04–2.11 (complex signal, 4H, 8-H, 16-H_b), 2.15–2.25 [complex signal, 2H, 6(12)-H_a], 2.83

(dt, *J* = 10.5 Hz, *J*′ = 6.5 Hz, 1H, 18-H_a), 2.97 (dt, *J* = 10.5 Hz, *J*′ = 6.5 Hz, 1H, 18-H_b), 3.17 [broad t, *J* = 6.5 Hz, 2H, 5(11)-H], 3.59 (dd, *J* = 9 Hz, *J*′ = 5.5 Hz, 1H, 15-H), 7.06 [m, 2H, 1(4)-H], 7.08 [m, 2H, 2(3)-H], 7.60 (broad s, 1H, NH). ^{13}C NMR (125.7 MHz, $CDCl_3$) δ: 26.1 (CH_2, C17), 30.8 (CH_2, C16), 38.5 (CH_2) and 38.6 (CH_2) (C6 and C12), 40.1 [CH, C5(11)], 42.4 [CH_2, C10(13)], 47.2 (CH_2, C18), 48.1 (CH_2, C8), 55.9 (C, C7), 61.0 (CH, C15), 70.7 (C, C9), 126.6 [CH, C2(3)], 128.1 [CH, C1(4)], 145.3 [C, C4a(C11a)], 174.1 (C, CO). Anal. Calcd for $C_{20}H_{26}N_2O_2$: C, 73.59; H, 8.03; N, 8.58. Calcd for $C_{20}H_{26}N_2O_2 \cdot 0.15DCM$: C, 71.36; H, 7.82; N, 8.26. Found: C, 71.48; H, 7.78; N, 8.07.

4.1.6. (2*R*)-1-Ethyl-*N*-(9-hydroxy-6,7,8,9,10,11-hexahydro-5*H*-5,9:7,11-dimethanobenzo[9]annulen-7-yl)pyrrolidine-2-carboxamide, 18

A solution of pyrrolidine **15** (170.0 mg, 0.52 mmol) in DMF (3 mL) was cooled to 5 °C with an ice bath. Then KI (8.6 mg, 0.052 mmol) and triethylamine (0.278 mL, 2.08 mmol) were added, followed by the dropwise addition of ethyl bromide (0.04 mL, 0.55 mmol). The reaction mixture was stirred at room temperature in an ice-water bath overnight. The resulting suspension was then filtered and the solids were washed with EtOAc (10 mL). The combined filtrates were washed with saturated aqueous $NaHCO_3$ solution (10 mL) and brine (10 mL). The organic phase was separated, dried over anhyd Na_2SO_4, filtered and concentrated in vacuo to give **18** (133.0 mg, 72% yield) as a white solid. The analytical sample was obtained by crystallization from EtOAc/pentane, mp 150–152 °C. IR (ATR) *v*: 3388, 2931, 2871, 1647, 1511, 1440, 1384, 1358, 1335, 1304, 1234, 1194, 1117, 1088, 1060, 761, 647 cm^{-1}. ^1H NMR (500 MHz, $CDCl_3$) δ: 1.04 (t, *J* = 7.5 Hz, 3H, NCH_2CH_3), 1.59–1.82 [complex signal, 3H, 16-H_a, 17-H_2], 1.77 [d, *J* = 12.5 Hz, 2H, 10(13)-H_b], 1.92 [d, *J* = 13 Hz, 2H, 6(12)-H_b], 1.97 [dd, *J* = 12.5 Hz, *J*′ = 6.5 Hz, 2H, 10(13)-H_a], 2.02 (broad s, 1H, OH), 2.11 (m, 1H, 16-H_b), 2.14 (s, 2H, 8-H_2), 2.17–2.30 [complex signal, 3H, 6(12)-H_a, 19-H_a], 2.45 (m, 1H, 18-H_a), 2.58 (m, 1H, 18-H_b), 3.85 (dd, *J* = 10.0 Hz, *J*′ = 4.5 Hz, 1H, 15-H), 3.12 (m, 1H, 19-H_b), 3.18 [dt, *J* = 6.5 Hz, *J*′ = 1.5 Hz, 2H, 5(11)-H], 7.07 [m, 2H, 1(4)-H], 7.11 [m, 2H, 2(3)-H], 7.45 (broad s, 1H, NH). ^{13}C NMR (125.7 MHz, $CDCl_3$) δ: 14.8 (CH_3, NCH_2CH_3), 24.1 (CH_2, C17), 30.7 (CH_2, C16), 38.6 (CH_2) and 38.7 (CH_2) (C6 and C12), 40.1 [CH, C5(11)], 42.4 [CH_2, C10(13)], 48.1 (CH_2, C8), 49.7 (CH_2, C18), 53.8 (CH_2, NCH_2CH_3), 55.8 (C, C7), 67.8 (CH, C15), 70.7 (C, C9), 126.6 [CH, C2(3)], 128.1 [CH, C1(4)], 145.3 [d, C, C4a(C11a)], 174.3 (C, CO). Anal. Calcd for $C_{22}H_{30}N_2O_2$: C, 74.54; H, 8.53; N, 7.90. Calcd for $C_{22}H_{30}N_2O_2 \cdot 0.1EtOAc$: C, 74.06; H, 8.55; N, 7.71. Found: C, 73.93; H, 8.64; N, 7.71.

4.1.7. (2*R*)-*tert*-Butyl-2-[(9-methyl-6,7,8,9,10,11-hexahydro-5*H*-5,9:7,11-dimethanobenzo[9]annulen-7-yl)carbamoyl]pyrrolidine-1-carboxylate, 13

To a solution of amine **7** (388.0 mg, 1.71 mmol) in EtOAc (20 mL) were added Boc-D-proline (336.0 mg, 1.56 mmol), HOBt (316.0 mg, 2.34 mmol), EDC (363.0 mg, 2.34 mmol) and triethylamine (0.48 mL, 3.43 mmol) and the mixture was stirred at room temperature overnight. To the resulting suspension was then added water (15 mL) and the phases were separated. The organic phase was washed with saturated aqueous $NaHCO_3$ solution (15 mL) and brine (15 mL), dried over anhyd Na_2SO_4 and filtered. Evaporation in vacuo of the combined organic layers gave **13** (556.0 mg, 84% yield) as a white solid, that was washed with pentane for obtaining an analytical sample, mp 168–169 °C. IR (ATR) *v*: 3296, 2917, 1706, 1684, 1657, 1560, 1450, 1385, 1363, 1287, 1238, 1179, 1161, 1123, 1089, 1048, 1009, 982, 920, 756, 673, 574 cm^{-1}. ^1H NMR (400 MHz, $CDCl_3$) δ (two rotamers): 0.91 (s, 3H, C9-CH_3), 1.46 [s, 9 H, $OC(CH_3)_3$], 1.53 [broad d, *J* = 13.5 Hz, 2H, 10(13)-H_b], 1.65 [broad dd, *J* = 13.5 Hz, *J*′ = 6.5 Hz, 2H, 10(13)-H_a], 1.75–1.88 (complex signal, 4H, 8-H_2, 17-H_2), 2.01 [broad d, *J* = 13 Hz, 2H, 6(12)-H_b], 2.13 [m, 2H, 6(12)-H_a], 2.3 (very broad signal, 1H, 16-H_b), 3.06 [t, *J* = 6 Hz, 2H, 5(11)-H], 3.39 (broad m, 2H, 18-H_2), 4.11 (very broad signal, 1H, 15-H), 6.77 (broad s, 1H, NH), 7.05 [m, 4H, Ar-H]. ^{13}C NMR (100.6 MHz, $CDCl_3$) δ (two rotamers): 24.2 (broad CH_2, C17), 28.4 [CH_3, $C(CH_3)_3$], 31.1 (broad CH_2, C16), 32.2 (CH_3, C9-CH_3), 33.6 (C, C9), 38.9 and 39.0 [CH_2, C6(12)], 41.0 and 41.1 [CH, C5(11)], 41.11 and 41.15 [CH_2, C10(13)], 47.0 (CH_2, C8), 47.2 (broad signal, CH_2, C18), 54.1 (C, C7), 60.6 and 61.9 (CH, C15), 126.2 [CH, C2(3)], 127.9 [CH, C1(4)], 146.2 [broad C, C4a (C11a)], 170.8 (very broad C, CO). MS-DIP (EI), *m*/*z* (%); significant ions: 424 ($M^{\cdot+}$, <1), 211 ($C_{16}H_{19}^{+}$, 14), 171 (22), 170 (14), 155 (19), 140 (8), 115 (22), 114 (100), 70 (60), 57 (22). HRMS-ESI + *m*/*z* [*M* +H]$^+$ calcd for [$C_{26}H_{36}N_2O_3$+H^+]: 425.2799, found: 425.2803.

4.1.8. (2*R*)-*N*-(9-Methyl-6,7,8,9,10,11-hexahydro-5*H*-5,9:7,11-dimethanobenzo[9]annulen-7-yl)pyrrolidine-2-carboxamide, 16

A solution of Boc-protected pyrrolidine **13** (556.1 mg, 1.31 mmol) in DCM (6 mL) and 85% *o*-phosphoric acid (1.33 mL, 19.6 mmol) was stirred at room temperature for 18 h. To the reaction mixture was then added water (15 mL) and the aqueous phase was basified until pH ∼ 12 with 5 N NaOH solution. The phases were separated and the aqueous phase was extracted with further DCM (2 × 10 mL). The combined organic layers were dried over anhyd Na_2SO_4, filtered and evaporated in vacuo to give **16** (419.5 mg, quantitative yield) as a white solid. The analytical sample was obtained by crystallization from EtOAc/pentane, mp 116–119 °C. IR (ATR) *v*: 3289, 3257, 3017, 2920, 2897, 2864, 2839, 1646, 1515, 1492, 1467, 1450, 1359, 1345, 1307, 1245, 1208, 1153, 1135, 1110, 1090, 1046, 1006, 948, 914, 877, 856, 800, 754, 700, 613, 644, 558, 488 cm^{-1}. ^1H NMR (500 MHz, $CDCl_3$) δ: 0.91 (s, 3H, C9-CH_3), 1.53 [d, *J* = 13.0 Hz, 2H, 10(13)-H_b], 1.66 [complex signal, 4H, 17-H_2, 10(13)-H_a], 1.86 (complex signal, 3H, 8-H_2, 16-H_a), 1.99 [dq, *J* = 13.0 Hz, *J*′ = 1.5 Hz, 2H, 6(12)-H_b], 2.07 (m, 1H, 16-H_b), 2.17 [m, 2H, 6(12)-H_a], 2.84 (dt, *J* = 10.5 Hz, *J*′ = 6.5 Hz, 1H, 18-H_a), 2.97 (dt, *J* = 10.5 Hz, *J*′ = 6.5 Hz, 1H, 18-H_b), 3.06 [tq, *J* = 6.5 Hz, *J*′ = 1.5 Hz, 2H, 5(11)-H], 3.60 (dd, *J* = 9.0 Hz, *J*′ = 5.5 Hz, 1H, 15-H), 7.02–7.08 [complex signal, 4H, Ar-H], 7.50 (broad s, 1H, NH). ^{13}C NMR (125.7 MHz, $CDCl_3$) δ: 26.1 (CH_2, C17), 30.8 (CH_2, C16), 32.2 (CH_3, C9-CH_3), 33.5 (C, C9), 38.9 (CH_2) and 39.0 (CH_2) (C6 and C12), 41.0 [CH, C5(11)], 41.1 (CH_2) and 41.2 (CH_2) (C10 and C13), 47.0 (CH_2, C8), 47.2 (CH_2, C18), 53.3 (C, C7), 61.1 (CH, C15), 126.2 [CH, C2(3)], 127.9 [CH, C1(4)], 146.3 [d, C, C4a(C11a)], 173.9 (C, CO). GC-MS (CI), rt = 27.0 min, *m*/*z* (%); significant ions: 324 ($M^{\cdot+}$, <1), 211 ($C_{16}H_{19}^{+}$, 1), 155 (4), 70 (100). Anal. Calcd for $C_{21}H_{28}N_2O$: C, 77.74; H, 8.70; N, 8.63. Calcd for $C_{21}H_{28}N_2O \cdot 0.2EtOAc \cdot 0.15Pentane$: C, 76.75; H, 8.97; N, 7.94. Found: C, 76.78; H, 8.95; N, 7.89.

4.1.9. (2*R*)-1-Ethyl-*N*-(9-methyl-6,7,8,9,10,11-hexahydro-5*H*-5,9:7,11-dimethanobenzo[9]annulen-7-yl)pyrrolidine-2-carboxamide, 19·tartrate

A solution of pyrrolidine **16** (504.0 mg, 1.55 mmol) in DMF (10 mL) was cooled to 5 °C with an ice bath. Then KI (26.0 mg, 0.16 mmol) and triethylamine (0.87 mL, 6.2 mmol) were added, followed by the dropwise addition of ethyl bromide (0.12 mL, 1.63 mmol). The reaction mixture was stirred at room temperature in an ice-water bath overnight. To the resulting solution were added EtOAc (5 mL) and water (20 mL). The phases were separated and the aqueous layer was extracted with further EtOAc (2 × 15 mL). The combined organic phases were washed with saturated aqueous $NaHCO_3$ solution (15 mL) and brine (15 mL), dried over anhyd Na_2SO_4, filtered and concentrated in vacuo to give a clear oil (446.0 mg). Column chromatography (Al_2O_3, hexane/EtOAc mixtures) gave **19** (255.0 mg, 44% yield) as a white solid. A solution of L-(+)-tartaric acid (108.8 mg, 0.72 mmol) in methanol

(2 mL) was added to **19** directly. The solvent was removed under vacuo to give **19** as its tartrate salt. The analytical sample was obtained by crystallization from methanol/diethyl ether, mp 177–179 °C. IR (ATR) ν: 3426, 3250, 3023, 2915, 1694, 1667, 1573, 1453, 1361, 1306, 1243, 1217, 1116, 1080, 948, 893, 800, 761, 666 cm^{-1}. ^{1}H NMR (500 MHz, CD_3OD) δ: 0.94 (s, 3H, C9-CH_3), 1.27 (t, J = 7.5 Hz, 3H, $\mathrm{NCH_2C}H_3$), 1.50 [d, J = 13.5 Hz, 2H, 10(13)-H$_b$], 1.69 [dd, J = 13.0 Hz, J' = 6.0 Hz, 2H, 10(13)-H$_a$], 1.80 (s, 2H, 8-H$_2$), 1.93–1.99 [complex signal, 3H, 16-H$_a$, 17-H$_2$], 2.11 [m, 2H, 6(12)-H$_a$], 2.17 [d, J = 13 Hz, 2H, 6(12)-H$_b$], 2.46 (m, 1H, 16-H$_b$), 3.08 [tt, J = 6.5 Hz, J' = 2 Hz, 2H, 5(11)-H], 3.13 (m, 1H, 18-H$_a$), 3.19 (q, J = 7.5 Hz, 2H, $\mathrm{NC}H_2\mathrm{CH_3}$), 3.66 (m, 1H, 18-H$_b$), 3.96 (dd, J = 9 Hz, J' = 6.5 Hz, 1H, 15-H), 4.41 (s, 2H, tartrate-C*H*), 7.02–7.065 [complex signal, 4H, Ar-H]. ^{13}C NMR (125.7 MHz, CD_3OD) δ: 11.5 (CH_3, $\mathrm{NCH_2}C\mathrm{H_3}$), 24.0 ($CH_2$, C17), 31.2 ($CH_2$, C16), 32.8 ($CH_3$, C9-*C*$H_3$), 34.5 (C, C9), 39.5 ($CH_2$) and 39.6 ($CH_2$) (C6 and C12), 42.4 [CH and CH_2, C5(11), C10(13)], 48.0 (CH_2, C8), 51.3 (CH_2, $\mathrm{N}C\mathrm{H_2CH_3}$), 55.6 ($CH_2$, C18), 56.1 (C, C7), 68.6 (CH, C15), 74.1 (CH, tartrate-*C*H), 127.5 [CH, C2(3)], 129.0 [CH, C1(4)], 147.4 [C, C4a(C11a)], 168.6 (C, CO), 176.6 (C, tartrate-CO). GC–MS (CI), rt = 18.5 min, *m*/*z* (%); significant ions: 393 (M+41, 7), 381 (M+29, 18), 354 (27), 353 (M+1, 100), 211 (12), 98 (26). Anal. Calcd for $C_{27}H_{38}N_2O_7$: C, 64.52; H, 7.62; N, 5.57. Calcd for $C_{27}H_{38}N_2O_7\cdot 1H_2O$: C, 62.29; H, 7.74; N, 5.38. Found: C, 62.50; H, 7.50; N, 5.13.

4.1.10. (2*R*)-1-Ethyl-*N*-(9-fluoro-6,7,8,9,10,11-hexahydro-5*H*-5,9:7,11-dimethanobenzo[9]annulen-7-yl)pyrrolidine-2-carboxamide, 20·tartrate

Boc-D-proline (55.0 mg, 0.26 mmol), HOBt (52.0 mg, 0.38 mmol), EDC (59.0 mg, 0.38 mmol) and triethylamine (0.14 mL, 1.02 mmol) were added to a solution of amine **8·HCl** (75.0 mg, 0.28 mmol) in EtOAc (4 mL) and the mixture was stirred at room temperature overnight. To the resulting suspension was then added water (5 mL) and the phases were separated. The organic phase was washed with saturated aqueous $NaHCO_3$ solution (5 mL) and brine (5 mL), dried over anhyd Na_2SO_4 and filtered. Evaporation in vacuo of the combined organic layers gave **17** (110.0 mg, 92% yield) as a beige solid. The product was used in next step without further purification or characterization.

A solution of Boc-protected pyrrolidine **14** (110.0 mg, 1.26 mmol) in DCM (2 mL) and 85% o-phosphoric acid (0.26 mL, 3.90 mmol) was stirred at room temperature for 4 h. To the reaction mixture was then added water (5 mL) and the aqueous phase was basified until pH ∼ 12 with 5 N NaOH solution. The phases were separated and the aqueous phase was extracted with further DCM (2 × 5 mL). The combined organic layers were dried over anhyd Na_2SO_4, filtered and evaporated in vacuo to give **17** (82.0 mg, quantitative yield) as a maroon gum. The product was used in next step without further characterization or purification.

A solution of pyrrolidine **17** (82.0 mg, 0.25 mmol) in DMF (1.5 mL) was cooled to 5 °C with an ice bath. Then KI (4.0 mg, 0.03 mmol) and triethylamine (0.14 mL, 1.00 mmol) were added, followed by the dropwise addition of a solution of ethyl bromide (29.0 mg, 0.26 mmol) in DMF (0.5 mL). The reaction mixture was stirred at room temperature in an ice-water bath overnight. To the resulting solution was added EtOAc (5 mL) and water (5 mL). The phases were separated and the aqueous layer was extracted with further EtOAc (2 × 5 mL). The combined organic phases were washed with saturated aqueous $NaHCO_3$ solution (5 mL) and brine (5 mL), dried over anhyd Na_2SO_4, filtered and concentrated in vacuo to give an orange oil (74.0 mg). Column chromatography (SiO_2, DCM/methanol mixtures) gave **20** (33.0 mg, 35% yield) as a white solid. A solution of L-(+)-tartaric acid (11.0 mg, 0.07 mmol) in methanol (1 mL) was added to **20** directly. The solvents were removed under vacuo to give **20** as its tartrate salt, mp 94–96 °C. IR (ATR) ν: 3500–2800 (3432, 3381, 3285, 3063, 2923, 2856), 2553, 2363, 2182, 1962, 1721, 1667, 1563, 1441, 1395, 1358, 1341, 1301, 1235, 1118, 1074, 997, 863, 757, 663 cm^{-1}. ^{1}H NMR (500 MHz, CD_3OD) δ: 1.28 (t, J = 7.5 Hz, 3H, $\mathrm{NCH_2C}H_3$), 1.84 [d, J = 11.5 Hz, 2H, 10(13)-H$_b$], 1.99 (complex signal, 2H, 16-H$_a$, 17-H$_a$), 2.08 [d, J = 13 Hz, 2H, 6(12)-H$_b$], 2.16 [complex signal, 6 H, 6(12)-H$_a$, 10(13)-H$_a$, 17-H$_a$], 2.24 (d, J = 6.5 Hz, 2H, 8-H), 2.50 (m, 1H, 16-H$_b$], 3.17 (complex signal, 3H, $\mathrm{NC}H_2\mathrm{CH_3}$, 18-H$_a$), 3.27 [m, 2H, 5(11)-H], 3.68 (m, 1H, 18-H$_b$), 3.95 (dd, J = 8.5 Hz, J' = 7 Hz, 1H, 15-H), 4.45 (s, 2H, tartrate-C*H*), 7.11 [complex signal, 4H, Ar-H]. ^{13}C NMR (125.7 MHz, CD_3OD) δ: 11.4 (CH_3, $\mathrm{NCH_2}C\mathrm{H_3}$), 24.0 ($CH_2$, C17), 31.1 ($CH_2$, C16), 39.1 [$CH_2$, d, $^4J_{C-F}$ = 7.4 Hz, C6(12)], 40.9 [CH, d, $^3J_{C-F}$ = 12.9 Hz, C5(11)], 41.2 [CH_2, d, $^2J_{C-F}$ = 20.1 Hz, C10(13)], 46.6 (CH_2, d, $^2J_{C-F}$ = 18.9 Hz, C8), 51.4 (CH_2, $\mathrm{N}C\mathrm{H_2CH_3}$), 55.6 ($CH_2$, C18), 59.3 (C, d, $^3J_{C-F}$ = 11.2 Hz, C7), 68.6 (CH, C15), 73.8 (CH, tartrate-*C*H), 94.6 (C, d, $^1\mathrm{J}_{C-F}$ = 177.6 Hz, C9), 128.1 [CH, C2(3)], 129.2[CH, C1(4)], 146.1 [C, C4a(C11a)], 168.4 (C, CO), 176.9 (C, tartrate-CO). MS (DEPEI), rt = 18.5 min, *m*/*z* (%); significant ions: 99 (27), 98 (100), 97 (26), 96 (11), 76 (13), 71 (10), 70 (34), 69 (14), 68 (11). HRMS-ESI + *m*/*z* $[M+H]^+$ calcd for $[C_{22}H_{29}FN_2O+H^+]$: 357.2337, found: 357.2338.

4.1.11. *N*-(9-Methyl-5,6,8,9,10,11-hexahydro-7H-5,9:7,11-dimethanobenzo[9]annulen-7-yl)cyclohexanecarboxamide, 21

To a solution of amine **7** (204.8 mg, 0.90 mmol) in EtOAc (15 mL) were added cyclohexanecarboxylic acid (104.9 mg, 0.82 mmol), HOBt (166.1 mg, 1.23 mmol), EDC (190.5 mg, 1.23 mmol) and triethylamine (0.251 mL, 1.80 mmol) and the reaction mixture was stirred at room temperature overnight. To the resulting suspension was then added water (15 mL) and the phases were separated. The organic phase was washed with saturated aqueous $NaHCO_3$ solution (15 mL) and brine (15 mL), dried over anhyd Na_2SO_4 and filtered. Evaporation in vacuo of the combined organic layers gave **21** (265.0 mg, 96% yield) as a white solid. The analytical sample was obtained by crystallization with EtOAc/pentane, mp 197–198 °C. IR (ATR) ν: 3299, 3060, 2917, 2850, 1645, 1545, 1490, 1447, 1381, 1361, 1335, 1316, 1261, 1214, 1091, 1047, 1005, 960, 942, 894, 753, 675, 665 cm^{-1}. ^{1}H NMR (500 MHz, $CDCl_3$) δ: 0.91 (s, 3H, 14-H), 1.15–1.27 [complex signal, 4H, 18-H$_2$, 17(19)-H$_a$], 1.37 [m, 2H, 16(20)-H$_a$], 1.53 [broad d, J = 13.5 Hz, 2H, 10(13)-H$_b$], 1.65 [m, 2H, 10(13)-H$_a$], 1.72–1.83 [m, complex signal, 4H, 16(20)-H$_b$, 17(19)-H$_b$], 1.85 (s, 2H, 8-H$_2$), 1.93 (tt, J = 11.5 Hz, J' = 3.5 Hz, 1H, 15-H]), 1.97 [dt, J = 13 Hz, J' = 1.5 Hz, 2H, 6(12)-H$_b$], 2.16 [ddm, J = 13.0 Hz, J' = 6.5 Hz, 2H, 6(12)-H$_a$], 3.06 [tt, J = 6.5 Hz, J' = 1.5 Hz, 2H, 5(11)-H], 5.14 (broad s, 1H, NH), 7.02–7.08 [complex signal, 4H, Ar-H]. ^{13}C NMR (125.7 MHz, $CDCl_3$) δ: 25.7 [CH_2, C17(19)], 25.8 (CH_2, C18), 29.8 [CH_2, C16(20)], 32.2 (CH_3, C14), 33.6 (C, C9), 39.1 [CH_2, C6(12)], 41.0 [CH, C5(11)], 41.1 [CH_2, C10(13)], 46.4 (CH, C16), 47.2 (CH_2, C8), 54.0 (C, C7), 126.2 [CH, C2(3)], 127.9 [CH, C1(4)], 146.2 [d, C, C4a(C11a)], 175.3 (C, CO). GC–MS (EI), rt = 27.7 min, *m*/*z* (%); significant ions: 338 (18), 337 ($M^{\cdot+}$, 68), 282 (49), 212 (22), 211 (92), 210 (61), 169 (18), 156 (19), 155 (100), 154 (20), 143 (34), 141 (30), 129 (27), 128 (23), 83 (17), 55 (22). Anal. Calcd for $C_{23}H_{31}NO$: C, 81.85; H, 9.26; N, 4.15. Found: C, 81.82; H, 9.34; N, 4.14.

4.1.12. *N*-(9-Methyl-5,6,8,9,10,11-hexahydro-7H-5,9:7,11-dimethanobenzo[9]annulen-7-yl)thiourea, 22

To a solution of amine **7** (500.0 mg, 2.21 mmol) in $CHCl_3$ (20 mL) was added benzoyl isothiocyanate (0.327 mL, 2.43 mmol) and the reaction mixture was stirred at room temperature overnight. The resulting solution was concentrated in vacuo to give a brown gum (1.11 g). To a solution of this gum (1.11 g, aprox. 2.85 mmol) in methanol (22 mL) and THF (10 mL) were added K_2CO_3 (1.97 g, 14.26 mmol) and water (10 mL) and the mixture was stirred at room temperature overnight. The resulting suspension was filtered and the solids were washed with methanol

(15 mL) to give **22** (330.3 mg, 52% overall yield) as a white solid, mp 197–199 °C. IR (ATR) *ν*: 3481, 3209, 3135, 3097, 3012, 2916, 2840, 1618, 1529, 1491, 1450, 1359, 1302, 1238, 1209, 1134, 1090, 1048, 1022, 941, 815, 799, 758, 719, 708, 643, 611 cm^{-1}. ^{1}H NMR (400 MHz, DMSO-d$_6$) *δ*: 0.88 (s, 3H, 14-H), 1.36 [broad d, *J* = 13.0 Hz, 2H, 10(13)-H$_b$], 1.61 [ddd, *J* = 13.0 Hz, *J*′ = 6.0 Hz, *J*″ = 1.2 Hz, 2H, 10(13)-H$_a$], 1.77 (s, 2H, 8-H$_2$), 2.06 [ddd, *J* = 12.0 Hz, *J*′ = 5.6 Hz, *J*″ = 2.0 Hz, 2H, 6(12)-H$_a$], 3.04 [m, 2H, 5(11)-H], 6.76 (bs, 2H, NH$_2$), 7.02–7.09 (complex signal, 4H, Ar-H), 7.31 (bs, 1H, NH). ^{13}C NMR (100.6 MHz, DMSO-d$_6$) *δ*: 32.1 (CH$_3$, C14), 33.2 [CH$_2$, C10(13)], 38.2 [CH, C5(11)], 41.0 [CH$_2$, C6(12)], 47.5 (CH$_2$, C8), 50.1 (C, C7), 55.0 (C, C9), 126.1 [CH, C2(3)], 127.7 [CH, C1(4)], 146.2 [d, C, C4a(C11a)], 181.2 (C, CS). MS-DIP (EI), *m*/*z* (%); significant ions: 287 (15), 286 (M$^{\cdot+}$, 66), 285 (66), 212 (10), 211 [(C$_{16}$H$_{19}$)$^+$, 50], 210 (14), 169 (15), 156 (17), 155 (100), 154 (12), 153 (12), 143 (37), 141 (33), 129 (29), 128 (24), 117 (11), 115 (24). HRMS-ESI + *m*/*z* [*M*+H]$^+$ calcd for [C$_{17}$H$_{22}$N$_2$S+H$^+$]: 287.1576, found: 287.1578.

4.1.13. 5,5-Dimethyl-2-[(9-methyl-5,6,8,9,10,11-hexahydro-7H-5,9:7,11-dimethanobenzo[9]annulen-7-yl)amino]thiazol-4(5H)-one, 23

Thiourea **22** (300.0 mg, 1.05 mmol), ethyl 2-bromoisobutyrate (0.29 mL, 1.95 mmol), DIPEA (0.36 mL) and abs. ethanol (3.5 mL) were placed into a microwave vial. The white suspension was heated to 130 °C, 250 psi and 250 W for 3 h. The solvents were then removed under vacuo and the resulting solid was partitioned between DCM (10 mL) and 0.5 N HCl solution (10 mL) and the phases were separated. The aqueous phase was extracted with further DCM (3 × 10 mL), and the combined organic phases were dried over anhyd Na$_2$SO$_4$ and filtered. Evaporation in vacuo of the combined organic layers gave a white solid (315.0 mg). Column chromatography (Al$_2$O$_3$, DCM/methanol mixtures) gave **23** (47.0 mg, 13% yield) as a white solid. The analytical sample was obtained washing the solid with pentane, mp 294–299 °C. IR (ATR) *ν*: 3223, 2906, 1673, 1586, 1540, 1505, 1458, 1376, 1361, 1293, 1281, 1255, 1235, 1182, 1128, 1091, 1033, 1005, 951, 756, 651, 633, 602, 534 cm^{-1}. ^{1}H NMR (500 MHz, CDCl$_3$) *δ*: 0.93 (s, 3H, C-C*H*$_3$), 1.53 [d, *J* = 13.5 Hz, 2H, 10(13)-H$_b$], 1.62 [s, 6 H, C (C*H*$_3$)$_2$], 1.67 [ddm, *J* = 12.5 Hz, *J*′ = 6.5 Hz, 2H, 10(13)-H$_a$], 1.95 (s, 2H, 8-H$_2$), 2.17 [d, *J* = 12.5 Hz, 2H, 6(12)-H$_b$], 2.29 [dd, *J* = 12.5 Hz, *J*′ = 6.5 Hz, 2H, 6(12)-H$_a$], 3.09 [t, *J* = 6.5 Hz, 2H, 5(11)-H], 5.75 (broad s, 1H, NH), 7.04 [m, H, 1(4)-H], 7.08 [m, H, 2(3)-H]. ^{13}C NMR (125.7 MHz, CDCl$_3$) *δ*: 27.9 [CH$_3$, C(*C*H$_3$)$_2$], 32.0 (CH$_3$, C-*C*H$_3$), 33.9 (C, C9), 38.9 [CH$_2$, C6(12)], 40.8 [CH$_2$, C10(13)], 40.9 [CH, C5(11)], 47.1 (CH$_2$, C8), 59.4 (C, C7), 61.0 [C, *C*(CH$_3$)$_2$], 126.5 [CH, C2(3)], 128.0 [CH, C1(4)], 145.7 [d, C, C4a(C11a)], 176.2 (C, CN), 193.8 (C, CO). GC-MS (EI), rt = 28.7 min, *m*/*z* (%); significant ions: 355 (24), 354 (M$^{\cdot+}$, 100), 285 (34), 211 [(C$_{16}$H$_{19}$)$^+$, 35], 210 (11), 169 (14), 156 (15), 155 (100), 154 (10), 143 (35), 141 (29), 129 (27), 128 (21), 117 (11), 115 (18). Anal Calcd for C$_{21}$H$_{26}$N$_2$OS: C, 71.15; H, 7.39; N, 7.90, S 9.04. Calcd for C$_{21}$H$_{26}$N$_2$OS·0.75CH$_3$OH·0.1DCM: C, 67.81; H, 7.60; N, 7.24, S 8.28. Found: C, 67.98; H, 7.22; N, 7.29, S 7.88.

4.1.14. *N*-(9-Hydroxy-6,7,8,9,10,11-hexahydro-5*H*-5,9:7,11-dimethanobenzo[9]annulen-7-yl)piperidine-1-carboxamide, 24

To a solution of aminoalcohol **6** (270.0 mg, 1.18 mmol) in DCM (10 mL) were added 1-piperidinecarbonyl chloride (0.162 mL, 1.30 mmol) and triethylamine (0.328 mL, 2.36 mmol) and the reaction mixture was stirred at room temperature overnight. Saturated aqueous NaHCO$_3$ solution (15 mL) was added and the phases were separated. The aqueous phase was extracted with further DCM (2 × 15 mL), and the combined organic phases were dried over anhyd Na$_2$SO$_4$, filtered and concentrated in vacuo to give a yellow solid (472.0 mg). Column chromatography (Al$_2$O$_3$, DCM/methanol mixtures) gave **24** (288.0 mg, 64% overall yield) as a white solid, that was washed with pentane for obtaining an analytical sample, mp 188–190 °C. IR (ATR) *ν*: 3419, 2934, 2899, 2852, 1635, 1502, 1444, 1414, 1375, 1356, 1334, 1291, 1249, 1201, 1161, 1148, 1111, 1067, 1028, 992, 969, 907, 848, 762, 728, 625, 570, 544 cm^{-1}. ^{1}H NMR (500 MHz, CDCl$_3$) *δ*: 1.48–1.59 [complex signal, 6 H, 16(18)-H$_2$, 17-H$_2$], 1.76 [d, *J* = 13.0 Hz, 2H, 10(13)-H$_b$], 1.90–2.02 [complex signal, 4H, 6(12)-H$_b$, 10(13)-H$_a$], 2.09 (s, 2H, 8-H$_2$), 2.17 [ddd, *J* = 13.0 Hz, *J*′ = 6.5 Hz, *J*″ = 1.5 Hz, 2H, 6(12)-H$_a$], 3.16 [tt, *J* = 6.5 Hz, *J*′ = 1.5 Hz, 2H, 5(11)-H], 3.23 [m, 4H, 15(19)-H$_2$], 7.05 [m, 2H, 1(4)-H], 7.09 [m, 2H, 3(2)-H]. ^{13}C NMR (125.7 MHz, CDCl$_3$) *δ*: 24.3 (CH$_2$, C17), 25.5 [CH$_2$, C16(18)], 39.4 [CH$_2$, C6(12)], 40.1 [CH, C5(11)], 42.4 [CH$_2$, C10(13)], 44.9 [CH$_2$, C15(19)], 49.1 (CH$_2$, C8), 56.3 (C, C7), 71.0 (C, C9), 126.5 [CH, C2(3)], 128.0 [CH, C1(4)], 145.4 [d, C, C4a(C11a)], 156.4 (C, CO). MS-DIP (EI), *m*/*z* (%); significant ions: 341 (11), 340 (M$^{\cdot+}$, 48), 255 (41), 212 (9), 157 (13), 155 (22), 144 (13), 141 (13), 129 (35), 128 (33), 127 (43), 115 (21), 112 (20), 86 (19), 85 (70), 84 (100), 69 (20), 57 (10), 56 (14). Anal. Calcd for C$_{21}$H$_{28}$N$_2$O$_2$: C, 74.08; H, 8.29; N, 8.23. Calcd for C$_{21}$H$_{28}$N$_2$O$_2$·0.45CH$_3$OH·0.2C$_5$H$_{12}$: C, 73.01; H, 8.79; N, 7.59. Found: C, 73.17; H, 8.43; N, 7.23.

4.1.15. *N*-(9-Methyl-6,7,8,9,10,11-hexahydro-5*H*-5,9:7,11-dimethanobenzo[9]annulen-7-yl)piperidine-1-carboxamide,25

To a solution of amine **7** (300.0 mg, 1.32 mmol) in DCM (15 mL) were added 1-piperidinecarbonyl chloride (0.247 mL, 1.98 mmol) and triethylamine (0.367 mL, 2.64 mmol) and the reaction mixture was stirred at room temperature overnight. Saturated aqueous NaHCO$_3$ solution (15 mL) was added and the phases were separated. The aqueous phase was extracted with further DCM (2 × 15 mL), and the combined organic phases were dried over anhyd Na$_2$SO$_4$, filtered and concentrated in vacuo to give a yellow solid (419.0 mg). Column chromatography (Al$_2$O$_3$, DCM/methanol mixtures) gave **25** (265.0 mg, 59% yield) as a white solid. The analytical sample was obtained washing with pentane, mp 170–171 °C. IR (ATR) *ν*: 3361, 2914, 2850, 1617, 1525, 1479, 1439, 1404, 1360, 1343, 1275, 1261, 1228, 1211, 1168, 1022, 978, 949, 852, 758, 576 cm^{-1}. ^{1}H NMR (500 MHz, CDCl$_3$) *δ*: 0.91 (s, 3H, C9-C*H*$_3$), 1.49–1.59 [complex signal, 8 H, 10(13)-H$_b$, 16(18)-H$_2$, 17-H$_2$], 1.65 [ddm, *J* = 13.5 Hz, *J*′ = 6.5 Hz, 2H, 10(13)-H$_a$], 1.84 (s, 2H, 8-H), 2.00 [d, *J* = 13.0 Hz, 2H, 6(12)-H$_b$], 2.16 [ddm, *J* = 13.0 Hz, *J*′ = 6.5 Hz, 2H, 6(12)-H$_a$], 3.06 [tt, *J* = 6.5 Hz, *J*′ = 1.5 Hz, 2H, 5(11)-H], 3.22–3.25 [complex signal, 4H, 15(19)-H], 4.25 (s, 1H, NH), 7.03 [m, 2H, 1(4)-H], 7.06 [m, 2H, 3(2)-H]. ^{13}C NMR (125.7 MHz, CDCl$_3$) *δ*: 24.4 (CH$_2$, C17), 25.6 [CH$_2$, C16(18)], 32.3 (CH$_3$, C9-*C*H$_3$), 33.7 (C, C9), 39.8 [CH$_2$, C6(12)], 41.2 [CH, C5(11)], 41.3 [CH$_2$, C10(13)], 44.9 [CH$_2$, C15(19)], 48.0 (CH$_2$, C8), 53.6 (C, C7), 126.1 [CH, C2(3)], 127.9 [CH, C1(4)], 146.4 [d, C, C4a(C11a)], 156.6 (C, CO). MS-DIP (EI), *m*/*z* (%); significant ions: 254 (18), 253 [(M-C$_5$H$_{11}$N)$^{\cdot+}$, 100], 238 (25), 195 (10), 182 (14), 155 (32), 143 (13), 141 (15), 129 (17), 128 (15), 115 (15). Anal. Calcd for C$_{22}$H$_{30}$N$_2$O: C, 78.06; H, 8.93; N, 8.28. Found: C, 78.05; H, 9.11; N, 8.06.

4.1.16. *N*-(9-Fluoro-5,6,8,9,10,11-hexahydro-7H-5,9:7,11-dimethanobenzo[9]annulen-7-yl)piperidine-1-carboxamide, 26

To a solution of amine **8** (177.5 mg, 0.79 mmol) in DCM (9 mL), were added 1-piperidinecarbonyl chloride (0.1 mL, 0.80 mmol) and triethylamine (0.213 mL, 1.54 mmol) and the reaction mixture was stirred at room temperature overnight. Saturated aqueous NaHCO$_3$ solution (10 mL) was added and the phases were separated. The aqueous phase was extracted with further DCM (2 × 10 mL), and the combined organic phases were dried over anhyd Na$_2$SO$_4$, filtered and concentrated in vacuo to give a yellow gum (246.3 mg). Column chromatography (Al$_2$O$_3$, DCM/methanol mixtures) gave **26** (68.0 mg, 26% yield) as a white solid. The analytical sample was obtained by crystallization with EtOAc/pentane, mp: 178–179 °C. IR (ATR) ν: 3285, 2932, 2856, 1614, 1538, 1470, 1442, 1359, 1278, 1259, 1230, 1088, 1024, 1005, 968, 915, 865, 851, 804, 756, 648, 605, 570 cm^{-1}. ^1H NMR (500 MHz, $CDCl_3$) δ: 1.50–1.60 [complex signal, 6 H, 16(18)-H_2, 17-H_2], 1.91 [d, J = 12.5 Hz, 2H, 10(13)-H_b], 2.03 [d, J = 13.5 Hz, 2H, 6(12)-H_b], 2.12–2.22 [complex signal, 4H, 6(12)-H_a, 10(13)-H_a], 2.25 (d, J_{C-F} = 6.5 Hz, 2H, 8-H_2), 3.20–3.27 [complex signal, 6 H, 5(11)-H, 15(19)-H_2], 4.32 (s, 1H, NH), 7.07 [m, 2H, 1(4)-H], 7.11 [m, 2H, 3 (2)-H]. ^{13}C NMR (125.7 MHz, $CDCl_3$) δ: 24.4 (CH_2, C17), 25.6 [CH_2, C16(18)], 39.3 [CH_2, C6(12)], 39.6 [CH, d, $^3J_{C-F}$ = 13.3 Hz, C5(11)], 40.1 [CH_2, d, $^2J_{C-F}$ = 20.1 Hz, C10(13)], 44.9 [CH_2, C15(19)], 46.8 (CH_2, d, $^2J_{C-F}$ = 17.8 Hz, C8), 51.1 (C, d, $^3J_{C-F}$ = 11.4 Hz, C7), 95.4 (C, d, $^1J_{C-F}$ = 173.2 Hz, C9), 126.8 [CH, C2(3)], 128.1 [CH, C1(4)], 144.9 [d, C, C4a(C11a)], 156.3 (C, CO). GC-MS (EI), rt = 19.3 min, m/z (%); significant ions: 258 (17), 257 [$(C_{16}H_{16}FNO)^+$, 100], 215 (12), 170 (10), 159 (13), 155 (10), 141 (9), 129 (13), 128 (12), 115 (15). Anal. Calcd for $C_{21}H_{27}FN_2O$: C, 73.65; H, 7.95; N, 8.18. Calcd for $C_{21}H_{27}FN_2O\cdot0.1EtOAc$: C, 73.17; H, 7.98; N, 7.97. Found: C, 73.35; H, 8.06; N, 7.93.

4.1.17. *N*-(9-Methoxy-5,6,8,9,10,11-hexahydro-7H-5,9:7,11-dimethanobenzo[9]annulen-7-yl)piperidine-1-carboxamide, 27

To a solution of amine **9** (76.0 mg, 0.31 mmol) in DCM (3.5 mL) were added 1-piperidinecarbonyl chloride (0.04 mL, 0.33 mmol) and triethylamine (0.09 mL, 0.62 mmol) and the reaction mixture was stirred at room temperature overnight. Saturated aqueous $NaHCO_3$ solution (5 mL) was added and the phases were separated. The aqueous phase was extracted with further DCM (2 × 5 mL), and the combined organic phases were dried over anhyd Na_2SO_4, filtered and concentrated in vacuo to give a yellow gum (201.4 mg). Column chromatography (Al_2O_3, DCM/methanol mixtures) gave **27** (42.0 mg, 38% yield) as a white solid, mp 172–173 °C. IR (ATR) ν: 3293, 2926, 2850, 2820, 1616, 1540, 1491, 1441, 1409, 1383, 1360, 1344, 1265, 1256, 1231, 1151, 1080, 1064, 1045, 1025, 994, 984, 969, 914, 848, 756, 638, 602 cm^{-1}. ^1H NMR (500 MHz, $CDCl_3$) δ: 1.47–1.57 [complex signal, 6 H, 16 (18)-H_2, 17-H_2], 1.43 [d, J = 13.0 Hz, 2H, 10(13)-H_b], 1.96 [m, 2H, 10(13)-H_a], 2.08 (s, 2H, 8-H_2), 2.07 [d, J = 13.5 Hz, 2H, 6(12)-H_b], 2.14 [m, 2H, 6(12)-H_a], 3.18 [tt, J = 6.5 Hz, J' = 1.5 Hz, 2H, 5(11)-H], 3.23–3.27 [complex signal, 7 H, 15(19)-H, C9-OCH_3], 4.31 (s, 1H, NH), 7.05 [m, 2H, 1(4)-H], 7.09 [m, 2H, 3(2)-H]. ^{13}C NMR (125.7 MHz, $CDCl_3$) δ: 24.4 (CH_2, C17), 25.5 [CH_2, C16(18)], 38.3 [CH_2, C6(12)], 39.6 [CH_2, C10(13)], 39.9 [CH, C5(11)], 44.9 [CH_2, C15(19)], 45.4 (CH_2, C8), 48.2 (CH_3, OCH_3), 56.1 (C, C7), 74.8 (C, C9), 126.5 [CH, C2(3)], 128.0 [CH, C1(4)], 145.5 [d, C, C4a(C11a)], 156.5 (C, CO). GC-MS (EI), rt = 21.2 min, m/z (%); significant ions: 270 (18), 269 [$(C_{17}H_{19}NO_2)^+$, 100], 238 (36), 226 (12), 195 (15), 182 (20), 171 (22), 159 (32), 158 (91), 155 (35), 153 (15), 150 (17), 141 (20), 129 (26), 128 (30), 127 (13), 115 (32). Anal. Calcd for $C_{22}H_{30}N_2O_2$: C, 74.54; H, 8.53; N, 7.90. Calcd for $C_{22}H_{30}N_2O_2\cdot0.1CH_3OH$: C, 74.21; H, 8.57; N, 7.83. Found: C, 74.11; H, 8.54; N, 7.67.

4.2. Inhibition 11β-HSD1 assay

11β-HSD1 activity was determined in mixed sex, human liver microsomes (Celsis In-vitro Technologies) by measuring the conversion of 3H-cortisone to 3H-cortisol. Percentage inhibition was determined relative to a no inhibitor control. 5 μg of human liver microsomes was pre-incubated at 37 °C for 15 minutes with inhibitor and 1 mM NADPH in a final volume of 90 μl Krebs buffer. 10 μl of 200 nM 3H-cortisone was then added followed by incubation for at 37 °C for a further 30 min. The assay was terminated by rapid freezing on dry ice and 3H-cortisone to 3H-cortisol conversion determined in 50 μl of the defrosted reaction by capturing liberated 3H-cortisol on anti-cortisol (HyTest Ltd)-coated scintillation proximity assay beads (protein A-coated YSi, GE Healthcare).

4.3. Molecular modeling

Docking calculations were performed using Glide,[20] taking advantage of the X-ray structures of the murine (PDB ID 3LZ6)[18b] and human enzyme (PDB IDs 4BB6 and 4BB5)[23] 11ß-HSD1 enzymes in complex with inhibitors PF-877423, HD1 and HD2. Glide with the SP scoring function was used to perform the docking assays. Each molecule was energy minimized previously and the centroid of HD1 was used to generate the docking cavity by selecting all the residues located within 15 Å from the ligand. 100 poses were generated for each ligand and the best scored pose was selected for MD simulations. For each compound (**19**, **20** and PF-877423) three independent 50 ns MD simulations were run. Every complex was immersed in an octahedral box of TIP3P water molecules and sodium ions were added to neutralize the system.[24] A minimum distance of 12 Å between any atom of the protein and the box limits was used to define the size of the simulated system. The force field ff99SBildn[25] was used for the protein parameters and RESP charges at the HF/6-31G(d) level and the GAFF[26] force field were used to build the ligand and NADP parameters. The system was energy minimized following a three-step protocol. First, the hydrogens of the protein, the ligand and the cofactor were minimized. Second, the orientation of water molecules was optimized. Finally, a global minimization was run in which all the atoms were let free to move. At this point, the system was thermalized to 300 K in 4 steps of 50 ps each from an initial temperature of 100 K. The last snapshot from the thermalization procedure was used as starting point for MD simulations using the NPT ensemble, a 2 fs timestep, periodic boundary conditions and keeping frozen all the bonds implicating hydrogen atoms using SHAKE.[27] The $\log P_{o/w}$ values were determined from quantum mechanical calculations carried out at the B3LYP/6-31G(d) level in conjunction with the IEF/MST continuum solvation model, which was parametrized to describe the solvation of (bio)organic compounds in water and octanol.[22,28]

Acknowledgments

E. V. thanks the Institute of Biomedicine of the University of Barcelona (IBUB) for a PhD Grant. F. J. L. and S. V. thank financial support from *Ministerio de Economía y Competitividad* (Spain) (SAF2014-57094-R) and the *Generalitat de Catalunya* (2014-SGR-00052 and 2014-SGR-1189).

References and notes

1. (a) Landa, S. *Chem. Listy* **1933**, *27*, 415; (b) Landa, S. *Chem. Listy* **1933**, *27*, 443; (b) Fort, R. C., Jr.; von, R.; Schleyer, P. *Chem. Rev.* **1964**, *64*, 277; (c) Lamoureux, G.; Artavia, G. *Curr. Med. Chem.* **2010**, *17*, 2967.
2. (a) Wanka, L.; Iqbal, K.; Schreiner, P. R. *Chem. Rev.* **2013**, *113*, 3516; (b) Stockdale, T. P.; Williams, C. M. *Chem. Soc. Rev.* **2015**, *44*, 7737.
3. (a) Davies, W. L.; Grunert, R. R.; Haff, R. F.; McGahen, J. W.; Neumayer, E. M.; Paulshock, M.; Watts, J. C.; Wood, T. R.; Hermann, E. C.; Hoffmann, C. E. *Science* **1964**, *144*, 862; (b) Tsunoda, A.; Maassab, H. F.; Cochran, K. W.; Eveland, W. C. *Antimicrob. Agents Chemother. (1961–70)* **1965**, *5*, 553.
4. Danysz, W.; Parsons, C. G. *Br. J. Pharmacol.* **2012**, *167*, 324.
5. (a) Villhauer, E. B.; Brinkman, J. A.; Naderi, G. B.; Burkey, B. F.; Dunning, B. E.; Prasad, K.; Mangold, B. L.; Russell, M. E.; Hughes, T. E. *J. Med. Chem.* **2003**, *46*, 2774; (b) Augeri, D. J.; Robl, J. A.; Betebenner, D. A.; Magnin, D. R.; Khanna, A.; Robertson, J. G.; Wang, A.; Simpkins, L. M.; Taunk, P.; Huang, Q.; Han, S.-P.; Abboa-Offei, B.; Cap, M.; Xin, L.; Tao, L.; Tozzo, E.; Welzel, G. E.; Egan, D. M.; Marcinkeviciene, J.; Chang, S. Y.; Biller, S. A.; Kirby, M. S.; Parker, R. A.; Hamann, L. G. *J. Med. Chem.* **2005**, *48*, 5025.
6. (a) Anderson, A.; Walker, B. R. *Drugs* **2013**, *73*, 1385; (b) Scott, J. S.; Goldberg, F. W.; Turnbull, A. V. *J. Med. Chem.* **2014**, *57*, 4466; (c) Imig, J. D.; Hammock, B. D. *Nat. Rev. Drug Disc.* **2009**, *8*, 794; (d) Shen, H. C.; Hammock, B. D. *J. Med. Chem.* **2012**, *55*, 1789; (e) Duflot, T.; Roche, C.; Lamoureux, F.; Guerrot, D.; Bellien, J. *Expert Opin. Drug Discov.* **2014**, *9*, 229.

7. Fotsch, C.; Wang, M. *J. Med. Chem.* **2008**, *51*, 4851.
8. Wang, M. *Drug Dev. Res.* **2006**, *67*, 567.
9. Grundy, S. M.; Brewer, H. B.; Cleeman, J. I.; Smith, S. C.; Lenfant, C. *Circulation* **2004**, *109*, 433.
10. Valsamakis, G.; Anwar, A.; Tomlinson, J. W.; Shackleton, C. H. L.; McTernan, P. G.; Chetty, R.; Wood, P. J.; Banerjee, A. K.; Holder, G.; Barnett, A. H.; Stewart, P. M.; Kumar, S. *J. Clin. Endocrinol. Metab.* **2004**, *89*, 4755.
11. Scott, J. S.; Chooramun, J. 11β-Hydroxysteroid Dehydrogenase Type 1 (11β-HSD1) inhibitors in Development. In *New Therapeutic Strategies for Type 2 Diabetes*; Jones, R. M., Ed.; Small Molecule Approaches, RSC Drug Discovery Series No; Royal Society of Chemistry: Cambridge, 2012; Vol. 27, pp 109–141.
12. (a) Hosfield, D. J.; Wu, Y.; Skene, R. J.; Hilgers, M.; Jennings, A.; Snell, G. P.; Aertgeerts, K. *J. Biol. Chem.* **2005**, *280*, 4639; (b) Zhang, J.; Osslund, T. D.; Plant, M. H.; Clogston, C. L.; Nybo, R. E.; Xiong, F.; Delaney, J. M.; Jordan, S. R. *Biochemistry* **2005**, *44*, 6948; (c) Thomas, M. P.; Potter, B. V. L. *Future Med. Chem.* **2011**, *3*, 367.
13. Webster, S. P.; Pallin, T. D. *Expert Opin. Ther. Pat.* **2007**, *17*, 1407.
14. (a) Rubio, F. A.; Choma, N.; Fukuda, E. K. *J. Chromatogr.* **1989**, *497*, 147; (b) Su, H.; Boulton, D. W.; Barros, Anthony, Jr.; Wang, L.; Cao, K.; Bonacorsi, S. J., Jr.; Iyer, R. A.; Humphreys, W. G.; Christopher, L. J. *Drug Metab. Dispos.* **2012**, *40*, 1345.
15. (a) Gu, X.; Dragovic, J.; Koo, G. C.; Koprak, S. L.; Legrand, C.; Mundt, S. S.; Shah, K.; Springer, M. S.; Tan, E. Y.; Thieringer, R.; Hermanowski-Vosatka, A.; Zokian, H. J.; Balkovec, J. M.; Waddell, S. T. *Bioorg. Med. Chem. Lett.* **2005**, *15*, 5266; (b) Johansson, L.; Fotsch, C.; Bartberger, M. D.; Castro, V. M.; Chen, M.; Emery, M.; Gustafsson, S.; Hale, C.; Hickman, D.; Homan, E.; Jordan, S. R.; Komorowski, R.; Li, A.; McRae, K.; Moniz, G.; Matsumoto, G.; Orihuela, C.; Palm, G.; Veniant, M.; Wang, M.; Williams, M.; Zhang, J. *J. Med. Chem.* **2008**, *51*, 2933; (c) Véniant, M. M.; Hale, C.; Hungate, R. W.; Gahm, K.; Emery, M. G.; Jona, J.; Joseph, S.; Adams, J.; Hague, A.; Moniz, G.; Zhang, J.; Bartberger, M. D.; Li, V.; Syed, R.; Jordan, S.; Komorowski, R.; Chen, M. M.; Cupples, R.; Kim, K. W.; St Jean, D. J.; Johansson, L.; Henriksson, M. A.; Williams, M.; Vallgårda, J.; Fotsch, C.; Wang, M. *J. Med. Chem.* **2010**, *53*, 4481; (d) Maletic, M.; Leeman, A.; Szymonifka, M.; Mundt, S. S.; Zokian, H. J.; Shah, K.; Dragovic, J.; Lyons, K.; Thieringer, R.; Vosatka, A. H.; Balkovec, J.; Waddell, S. T. *Bioorg. Med. Chem. Lett.* **2011**, *21*, 2568; (e) Ye, X.-Y.; Chen, S. Y.; Nayeem, A.; Golla, R.; Seethala, R.; Wang, M.; Harper, T.; Sleczka, B. G.; He, B.; Gordon, D. A.; Robl, J. A. *Bioorg. Med. Chem. Lett.* **2011**, *21*, 6699; (f) Xia, G.; Liu, L.; Xue, M.; Liu, H.; Yu, J.; Li, P.; Chen, Q.; Xiong, B.; Liu, X.; Shen, J. *Mol. Cell. Endocrinol.* **2012**, *358*, 46; (g) Bauman, D. R.; Whitehead, A.; Contino, L. C.; Cui, J.; García-Calvo, M.; Gu, X.; Kevin, N.; Ma, X.; Pai, L.-Y.; Shah, K.; Shen, X.; Stribling, S.; Zokian, H. J.; Metzger, J.; Shevell, D. E.; Waddell, S. T. *Bioorg. Med. Chem. Lett.* **2013**, *23*, 3650–3653.
16. (a) Camps, P.; Duque, M. D.; Vázquez, S.; Naesens, L.; De Clercq, E.; Sureda, F. S.; López-Querol, M.; Camins, A.; Pallàs, M.; Prathalingam, S. R.; Kelly, J. M.; Romero, V.; Ivorra, D.; Cortés, D. *Bioorg. Med. Chem.* **2008**, *16*, 9925; (b) Duque, M. D.; Camps, P.; Profire, L.; Montaner, S.; Vázquez, S.; Sureda, F. S.; Mallol, J.; López-Querol, M.; Naesens, L.; De Clercq, E.; Prathalingam, S. R.; Kelly, J. M. *Bioorg. Med. Chem.* **2009**, *17*, 3198; (c) Duque, M. D.; Ma, C.; Torres, E.; Wang, J.; Naesens, L.; Juárez-Jiménez, J.; Camps, P.; Luque, F. J.; DeGrado, W. F.; Lamb, R. A.; Pinto, L. H.; Vázquez, S. *J. Med. Chem.* **2011**, *54*, 2646; (d) Rey-Carrizo, M.; Torres, E.; Ma, C.; Barniol-Xicota, M.; Wang, J.; Wu, Y.; Naesens, L.; DeGrado, W. F.; Lamb, R. A.; Pinto, L. H.; Vázquez, S. *J. Med. Chem.* **2013**, *56*, 9265; (e) Torres, E.; Leiva, R.; Gazzarrini, S.; Rey-Carrizo, M.; Frigolé-Vivas, M.; Moroni, A.; Naesens, L.; Vázquez, S. *ACS Med. Chem. Lett.* **2014**, *5*, 831; (f) Rey-Carrizo, M.; Barniol-Xicota, M.; Ma, C.; Frigolé-Vivas, M.; Torres, E.; Naesens, L.; Llabrés, S.; Juárez-Jiménez, J.; Luque, F. J.; DeGrado, W. F.; Lamb, R. A.; Pinto, L. H.; Vázquez, S. *J. Med. Chem.* **2014**, *57*, 5738; (g) Rey-Carrizo, M.; Gazzarrini, S.; Llabrés, S.; Frigolé-Vivas, M.; Juárez-Jiménez, J.; Font-Bardia, M.; Naesens, L.; Moroni, A.; Luque, F. J.; Vázquez, S. *Eur. J. Med. Chem.* **2015**, *96*, 318.
17. (a) Duque, M. D.; Camps, P.; Torres, E.; Valverde, E.; Sureda, F. X.; López-Querol, M.; Camins, A.; Prathalingam, S. R.; Kelly, J. M.; Vázquez, S. *Bioorg. Med. Chem.* **2010**, *18*, 46; (b) Torres, E.; Duque, M. D.; López-Querol, M.; Taylor, M. C.; Naesens, L.; Ma, C.; Pinto, L. H.; Sureda, F. X.; Kelly, J. M.; Vázquez, S. *Bioorg. Med. Chem.* **2012**, *20*, 942; (c) Valverde, E.; Sureda, F. X.; Vázquez, S. *Bioorg. Med. Chem.* **2014**, *22*, 2678.
18. (a) Richards, S.; Sorensen, B.; Jae, H.; Winn, M.; Chen, Y.; Wang, J.; Fung, S.; Monzon, K.; Frevert, E. U.; Jacobson, P.; Sham, H.; Link, J. T. *Bioorg. Med. Chem. Lett.* **2006**, *16*, 6241; (b) Cheng, H.; Hoffman, J.; Le, P.; Nair, S. K.; Cripps, S.; Matthews, J.; Smith, C.; Yang, M.; Kupchinsky, S.; Dress, K.; Edwards, M.; Cole, B.; Walters, E.; Loh, C.; Ermolieff, J.; Fanjul, A.; Bhat, G. B.; Herrera, J.; Pauly, T.; Hosea, N.; Paderes, G.; Rejto, P. *Bioorg. Med. Chem. Lett.* **2010**, *20*, 2897; (c) Tice, C. M.; Zhao, W.; Xu, Z.; Cacatian, S. T.; Simpson, R. D.; Ye, Y.-J.; Singh, S. B.; McKeever, B. M.; Lindblom, P.; Guo, J.; Krosky, P. M.; Kruk, B. A.; Berbaum, J.; Harrison, R. K.; Johnson, J. J.; Bukhtiyarov, Y.; Panemangalore, R.; Scott, B. B.; Zhao, Y.; Bruno, J. G.; Zhuang, L.; McGeehan, G. M.; He, W.; Claremon, D. A. *Bioorg. Med. Chem. Lett.* **2010**, *20*, 881.
19. Leiva, R.; Seira, C.; McBride, A.; Binnie, M.; Luque, F. J.; Bidon-Chanal, A.; Webster, S. P.; Vázquez, S. *Bioorg. Med. Chem. Lett.* **2015**, *25*, 4250.
20. Friesner, R. A.; Murphy, R. B.; Repasky, M. P.; Frye, L. L.; Greenwood, J. R.; Halgren, T. A.; Sanschagrin, P. C.; Mainz, D. T. *J. Med. Chem.* **2006**, *49*, 6177.
21. Gülden, M.; Mörchel, S.; Seibert, H. *Toxicol. In Vitro* **2001**, *15*, 233.
22. Curutchet, C.; Orozco, M.; Luque, F. J. *J. Comput. Chem.* **2001**, *22*, 1180.
23. Goldberg, F. W.; Leach, A. G.; Scott, J. S.; Snelson, W. L.; Groombridge, S. D.; Donald, C. S.; Bennett, S. N. L.; Bodin, C.; Morentin Gutierrez, P.; Gyte, A. C. *J. Med. Chem.* **2012**, *55*, 10652.
24. Jorgensen, W. L.; Chandrasekhar, J.; Madura, J. D.; Impey, R. W.; Klein, M. L. *J. Chem. Phys.* **1983**, *79*, 926.
25. (a) Hornak, V.; Abel, R.; Okur, A.; Strockbine, B.; Roitberg, A.; Simmerling, C. *Proteins* **2006**, *65*, 712; (b) Lindorff-Larsen, K.; Piana, S.; Palmo, K.; Maragakis, P.; Klepeis, J. L.; Dror, R. O.; Shaw, D. E. *Proteins* **2010**, *78*, 1950.
26. Wang, J.; Wolf, R. M.; Caldwell, J. W.; Kollman, P. A.; Case, D. A. *J. Comput. Chem.* **2004**, *25*, 1157.
27. Ryckaert, J.-P.; Ciccotti, G.; Berendsen, H. J. C. *J. Comput. Phys.* **1977**, *23*, 327.
28. (a) Soteras, I.; Curutchet, C.; Bidon-Chanal, A.; Orozco, M.; Luque, F. J. *J. Mol. Struct. Theochem.* **2005**, *727*, 29; (b) Kolar, M.; Fanfril, J.; Lepsik, M.; Fort, F.; Luque, F. J.; Hobza, P. *J. Phys. Chem. B* **2013**, *117*, 5950.

3.1.2 Artículo 2: *Novel 11 β -HSD1 inhibitors: C-1 versus C-2 substitution and effect of the introduction of an oxygen atom in the adamantane scaffold.*

Resumen

El grupo adamantano se encuentra en varios fármacos comercializados y en muchos inhibidores 11β-HSD1 en investigación. Curiosamente, todos los derivados de adamantano aprobados clínicamente tienen una substitución en C-1. En esta publicación se demuestra que, en una serie de isómeros de adamantano clasificados por parejas, es preferible la sustitución del adamantano en C-2 en vez de C-1 y es necesaria para aumentar la potencia de inhibición en11β-HSD1 humano. Además, la introducción de un átomo de oxígeno en la estructura de hidrocarburo del adamantano es perjudicial para la inhibición de 11β-HSD1. Los estudios de modelado molecular proporcionan una base para racionalizar estas características.

Bioorganic & Medicinal Chemistry Letters 25 (2015) 4250–4253

Contents lists available at ScienceDirect

Bioorganic & Medicinal Chemistry Letters

journal homepage: www.elsevier.com/locate/bmcl

Novel 11b-HSD1 inhibitors: C-1 versus C-2 substitution and effect of the introduction of an oxygen atom in the adamantane scaffold

Rosana Leiva [a], Constantí Seira [b], Andrew McBride [c], Margaret Binnie [c], F. Javier Luque [b], Axel Bidon-Chanal [b], Scott P. Webster [c], Santiago Vázquez [a,]

[a] Laboratori de Química Farmacèutica (Unitat Associada al CSIC), Facultat de Farmàcia, and Institute of Biomedicine (IBUB), Universitat de Barcelona, Av. Joan XXIII, s/n, Barcelona E-08028, Spain
[b] Departament de Fisicoquímica, Facultat de Farmàcia and Institute of Biomedicine (IBUB), Universitat de Barcelona, Av. Prat de la Riba, 171, 08921 Santa Coloma de Gramenet, Spain
[c] Endocrinology Unit, Centre for Cardiovascular Science, University of Edinburgh, Queen's Medical Research Institute, EH16 4TJ, United Kingdom

article info

Article history:
Received 6 July 2015
Revised 27 July 2015
Accepted 29 July 2015
Available online 5 August 2015

Keywords:
Adamantane
11b-HSD1 inhibitors
Drug discovery
Molecular modeling

abstract

The adamantane scaffold is found in several marketed drugs and in many investigational 11b-HSD1 inhibitors. Interestingly, all the clinically approved adamantane derivatives are C-1 substituted. We demonstrate that, in a series of paired adamantane isomers, substitution of the adamantane in C-2 is preferred over the substitution at C-1 and is necessary for potency at human 11b-HSD1. Furthermore, the introduction of an oxygen atom in the hydrocarbon scaffold of adamantane is deleterious to 11b-HSD1 inhibition. Molecular modeling studies provide a basis to rationalize these features.

© 2015 Elsevier Ltd. All rights reserved.

Adamantane is a very common building block in medicinal chemistry.[1] So far, seven adamantane derivatives have been introduced in clinical use for a variety of diseases and molecular targets (Fig. 1) and hundreds of derivatives have been tested against different targets.

Interestingly, the rapid inspection of the structures of the adamantane derivatives shown in Figure 1 reveals as a general trend that the polycyclic scaffold is substituted at the C-1 position. Of note, the anti-influenza A activity of amantadine is significantly higher than that of its isomer, 2-aminoadamantane.[2]

In recent years, more than 25 pharmaceutical companies have been working on the synthesis of 11b-hydroxysteroid dehydrogenase type 1 (11b-HSD1) inhibitors, as a potential new candidates for the treatment of type II diabetes and metabolic syndrome.[3] On the one hand, contrary to the aforementioned trend observed in clinically approved adamantanes, most of the 11b-HSD1 inhibitors evaluated are 2-adamantyl substituted derivatives (Fig. 2).[4,5] However, for these derivatives no comparison between the activities of compounds substituted at the C-1 and C-2 positions is available. On the other hand, a potential advantage of positioning the substituent at the 1-position is that one of the metabolically labile positions of the adamantane would be blocked. Also, for any given substituent, the theoretical c log P value of the 1-substituted analog is usually lower than that of the 2-substituted derivative.[6]

The synthesis and pharmacological evaluation of a series of 1-adamantyl amide 11b-HSD1 inhibitors has been previously reported by Webster et al.[7] Of note, inhibitors 1 and 2 were found to be equipotent compounds (Fig. 3). Later, Xia et al. reported that the C-2 substituted amide 3 was 20 times more potent than its 1-isomer, 4 (Fig. 3).[8]

Taking into account these seemingly contradictory results and the scarcity of data on 1-substituted adamantane derivatives evaluated as 11b-HSD1 inhibitors,[5] we decided to synthesize a small series of 1- and 2-adamantyl derivatives featuring fragments of proven inhibitors of 11b-HSD1 in order to compare their pharmacological behavior.

Moreover, considering that very few heteroadamantanes have been biologically tested as 11b-HSD1 inhibitors,[9] we also evaluated some 1- and 5-substituted 2-oxaadamantanes. The introduction of an oxygen atom in the scaffold increases the polar surface area and decreases the overall lipophilicity. Thus, if potency is retained, the lipophilic ligand efficiency, which is one of the most significant parameters that normalizes potency relative to lipophilicity, would increase.[10]

We started from known urea 5, an 11b-HSD1 inhibitor reported by Vitae.[11] In our microsomal assay, 5 was shown to be a submicromolar inhibitor of the human 11b-HSD1 enzyme

---

Corresponding author. Tel.: +34 934 024 533.
E-mail address: svazquez@ub.edu (S. Vázquez).

http://dx.doi.org/10.1016/j.bmcl.2015.07.097
0960-894X/© 2015 Elsevier Ltd. All rights reserved.

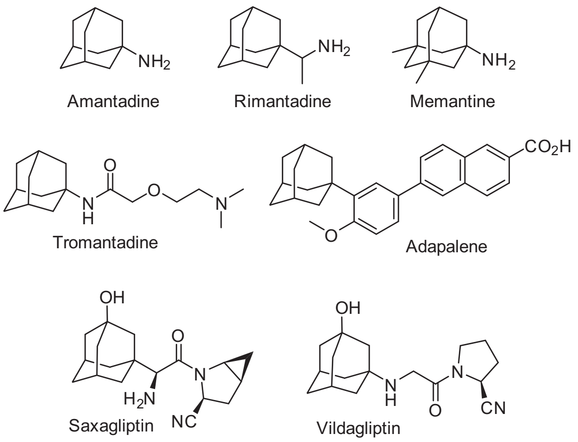

Figure 1. Clinically-approved adamantane derivatives. Amantadine, rimantadine and tromantadine are anti-virals, the first two are M2 channel blockers and are anti-Influenza drugs, and tromantadine inhibits herpex virus simplex replication; memantine is a NMDA receptor antagonist used in the treatment of Alzheimer's disease; adapalene inhibits keratinocyte differentiation and proliferation and is used for the treatment of acne; and saxagliptin and vildagliptin are DPP-IV inhibitors used to treat type 2 diabetes.

(IC_{50} = 0.87 μM). Table 1 shows the structures and the percentage of inhibition of human 11β-HSD1 at 10 μM of the novel compounds. The IC_{50} value of the more potent derivatives is also included.

All the compounds were synthesized in medium to high yields using standard chemistry from four known amines: amantadine (1-aminoadamantane), 2-aminoadamantane, 5-amino-2-oxaadamantane,[12] and 3-methyl-2-oxaadamantane-1-amine[13] (see details in Supplementary material). Briefly, the reaction of amantadine with 1-piperidinecarbonyl chloride in dichloromethane in the presence of triethylamine furnished, after column chromatography, urea **6** in 31% yield.[14] In the same way, starting from the known 3-methyl-2-oxaadamante-1-amine, urea **7** was obtained in 34% yield. We also synthesized amides **8** and **9** in high yields, by reaction of amantadine with 3,5-dichloro-4-aminobenzoic acid or cyclohexanecarboxylic acid, respectively.[15]

Surprisingly, in our microsomal assay ureas **6** and **7** and amide **8** did not inhibit the human 11β-HSD1 enzyme. Under the same conditions, amide **9** only inhibited 20% the enzyme activity. Oxaadamantanes **10** and **11** were also very poor inhibitors.

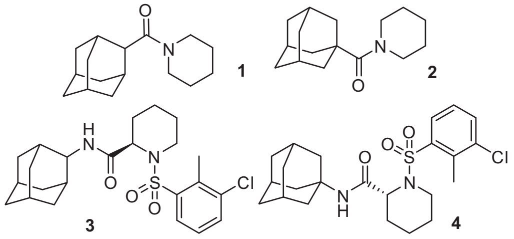

Figure 3. Structures of 11β-HSD1 inhibitors **1**–**4**.

Taking into account the aforementioned results and that the corresponding C-2 isomers of **8** and **9** had not been previously tested, we synthesized both amides from 2-aminoadamantane. By way of contrast with the lack of inhibitory activity of their C-1 isomers, amides **12** and **13** displayed potent, nanomolar inhibition. Also, in agreement with the previous trend observed in going from ureas **6** and **7** to their corresponding amides **9** and **10**, the novel amide **12** was more potent than our previous hit **5**. It was noteworthy that ring contraction from **12** to **14** led to a less potent inhibitor.

Overall, for the three pairs of isomers evaluated here, substitution in position 2 of the adamantyl scaffold consistently leads to more potent inhibitory activity of human 11β-HSD1.

The introduction of an oxygen atom in the adamantane does not improve the activity within the series of the C-1 substituted derivatives. As Ye et al. found, within a series of 2,2-disubstituted adamantanes, that the corresponding oxaadamantane analogs performed poorly,[9b] we have not evaluated oxaadamantane derivatives with the amino group attached to a methylene group of the polycyclic ring.[16]

In order to rationalize these results we combined docking studies with molecular dynamics simulations to examine the structural integrity of the binding of compounds **5**, **6**, and **12**. Let us note that the inhibitory activities of **5** and **6**, which only differ in the substitution at positions C1 and C2, vary from 87% (**5**) to 3% (**6**). On the other hand, compound **12** involves the replacement of the piperidine moiety present in **5** by the cyclohexyl one in **12**, leading to a moderate increase of the inhibitory activity from 87% (**5**) to 100% (**12**).

Compounds were docked in the binding cavity of human 11β-HSD1 using Glide.[17] In all cases the best scored poses mimicked the binding mode of PF-877423 (Fig. S1 in Supporting information), which is a potent adamantyl-based inhibitor against the human

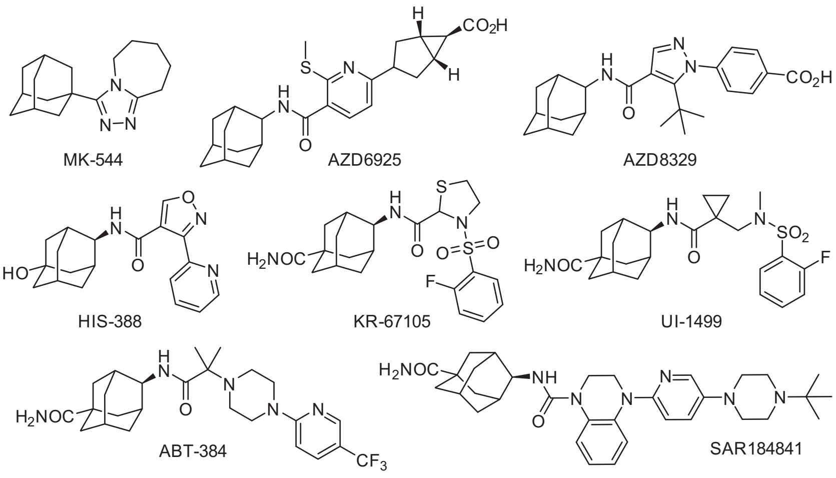

Figure 2. Selected adamantyl-based 11β-HSD1 inhibitors.

Table 1
Structures and human 11β-HSD1 inhibitory activities of compounds **5**–**14**

	Product	11β-hHSD1 inhibition at 10 μM[a]	11β-hHSD1IC$_{50}$ (nM)[a]
5	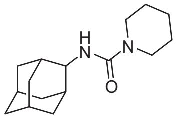	87	873
6	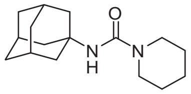	3	ND
7	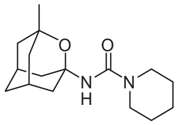	0	ND
8	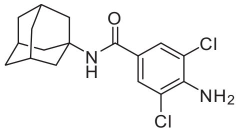	0	ND
9	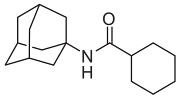	20	ND
10	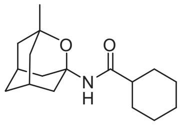	9	ND
11	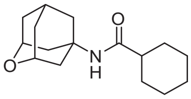	9	ND
12	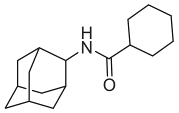	100	86
13	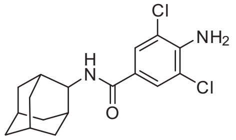	86	74
14	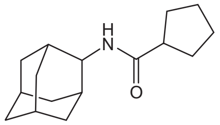	76	520

[a] 11β-HSD1 inhibition was determined in mixed sex, Human Liver Microsomes (Celsis In-vitro Technologies) by measuring the conversion of ^{3}H-cortisone to ^{3}H-cortisol in a cortisol-Scintillation Proximity Assay. Percentage inhibition was determined relative to a no inhibitor control.

enzyme ($K_i = 1.4$ nM).[18] Thus, all the compounds retained the hydrogen bond formed between the carbonyl oxygen of the amide/urea moiety with the hydroxyl group of Ser170 and the adamantyl cage filled a common site in the binding pocket.

Three independent 50 ns MD simulations were run for each ligand–receptor complex, and additional runs were performed for the complex with PF-877423, which was used as a reference system. All the simulations were stable except that of the complex with the C1-substituted compound **6**, since the ligand was released from the binding site in one simulation. Upon exclusion of this latter trajectory, the root-mean square deviation (RMSD) profiles were similar in all cases. Thus, the RMSD of the protein backbone varied from 1.5 to 2.2 Å, whereas the residues in the binding site showed a larger RMSD (2.5–3.7 Å) due to the enhanced flexibility of the loops that enclose the binding pocket.

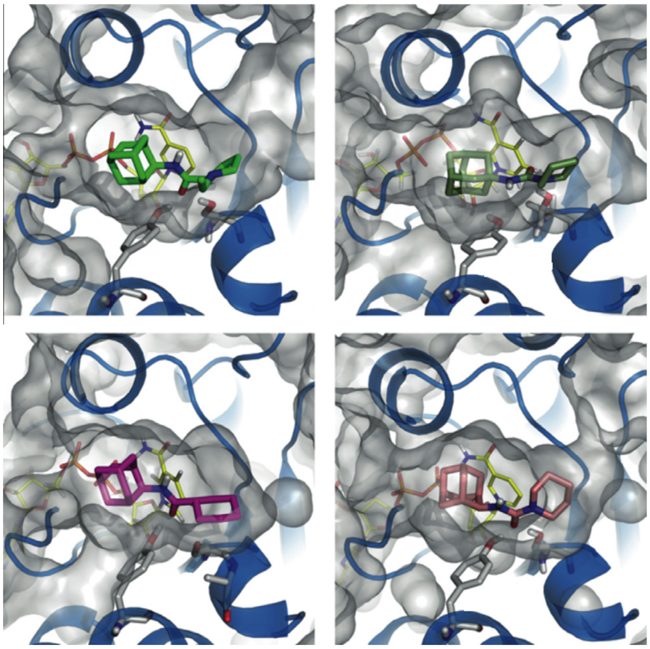

Figure 4. Last snapshot of a representative molecular dynamics simulation for the complexes between human 11β-HSD1 and compounds PF-877423 (top left), **6** (top right), **12** (bottom left) and **5** (bottom right). In all cases residues Tyr183 and Ser170, the NADP cofactor and the ligand are represented as sticks and only the polar hydrogens are shown. The shape of the binding cavity is shown as a white contour.

The hydrogen bond formed between the inhibitor and the hydroxyl group of Ser170 was retained in all cases (average distance of 2.8 Å). Often, an additional hydrogen bond with the hydroxyl unit of Tyr183 was transiently formed. Nevertheless, compound **6** consistently showed a higher root-mean square fluctuation (1.4 Å) compared to inhibitors **5** and **12** (RMSF of 0.8 Å), suggesting a poorer fit of the hydrophobic cage in the binding cavity due to the change in the substitution pattern from position C1 in **6** to position C2 in **5** and **12**. This reflects the larger steric hindrance of the adamantyl cage with the NADP nicotinamide ring arising from the C1-substitution, because C2-derived compounds are found to adopt a configuration where the C2-H unit is primarily oriented toward the nicotinamide ring (Fig. 4)

Finally, the moderate increase in the inhibitory activity of compound **12** relative to **5** may be ascribed to the enhanced hydrophobicity afforded by the cyclohexane unit, as noted in their respective *c*log*P* values of 4.5 and 3.6, determined from quantum mechanical IEF/MST continuum solvation calculations.[19] This trend agrees with similar findings reported for series of structurally related compounds.[20]

In conclusion, bearing in mind the aforementioned pharmacological results, it is clear that for potent 11β-HSD1 inhibitory activity, 2-substituted adamantanes are preferred over their corresponding 1-substituted counterpart. Also, the introduction of an oxygen atom in the polycyclic scaffold did not improve the activity (compare **9** vs **10** and **11**).

Acknowledgments

R.L. thanks the *Ministerio de Educación, Cultura y Deporte* for a PhD Grant (FPU program). We thank financial support from *Ministerio de Economía y Competitividad* (Project SAF2014-57094-R) and the *Generalitat de Catalunya* (Grants 2014-SGR-00052 and

2014-SGR-1189) and the *Consorci de Serveis Universitaris de Catalunya* for computational resources. F.J.L. acknowledges the support from ICREA Academia. We thank ACCIÓ (*Generalitat de Catalunya*) and CIDQO 2012 SL for financial support (*Programa Nuclis*, RD14-1-0057, SAFNAD).

Supplementary data

Supplementary data (experimental and computational procedures. NMR spectra for all the new compounds) associated with this article can be found, in the online version, at http://dx.doi.org/10.1016/j.bmcl.2015.07.097.

References and notes

1. (a) Lamoureux, G.; Artavia, G. *Curr. Med. Chem.* **2010**, *17*, 2967; (b) Liu, J.; Obando, D.; Liao, V.; Lifa, T.; Codd, R. *Eur. J. Med. Chem.* **1949**, *2011*, 46; (c) Wanka, L.; Iqbal, K.; Schreiner, P. R. *Chem. Rev.* **2013**, *113*, 3516.
2. Zoidis, G.; Kolocouris, N.; Foscolos, G. B.; Kolocouris, A.; Fytas, G.; Karayannis, P.; Padalko, E.; Neyts, J.; DeClercq, E. *Antiviral Chem. Chemother.* **2003**, *14*, 153; For another, non-related example, see: Lee, W.-G.; Lee, S.-D.; Cho, J.-H.; Jung, Y.; Kim, J.-H.; Hien, T. T.; Kang, K.-W.; Ko, H.; Kim, Y.-C. *J. Med. Chem.* **2012**, *55*, 3687.
3. (a) Scott, J. S.; Chooramun, J. 11β-Hydroxysteroid Dehydrogenase Type 1 (11β-HSD1) inhibitors in Development. In *New Therapeutic Strategies for Type 2 Diabetes*; Jones, R. M., Ed.; Small Molecule Approaches, RSC Drug Discovery Series No. 27; Royal Society of Chemistry: Cambridge, 2012; pp 109–141; (b) Gathercole, L. L.; Lavery, G. G.; Morgan, S. A.; Cooper, M. S.; Sinclair, A. J.; Tomlinson, J. W.; Stewart, P. M. *Endocrine Rev.* **2013**, *34*, 525; (c) Scott, J. S.; Goldberg, F. W.; Turnbull, A. V. *J. Med. Chem.* **2014**, *57*, 4466.
4. (a) Olson, S.; Aster, S. D.; Brown, K.; Carbin, L.; Graham, D. W.; Hermanowski-Vosatka, A.; LeGrand, C. B.; Mundt, S. S.; Robbins, M. A.; Schaeffer, J. M.; Slossberg, L. H.; Szymonifka, M. J.; Thieringer, R.; Wright, S. D.; Balkovec, J. M. *Bioorg. Med. Chem. Lett.* **2005**, *15*, 4359; (b) Sorensen, B.; Rohde, J.; Wang, J.; Fung, S.; Monzon, K.; Chiou, W.; Pan, L.; Deng, X.; Stolarik, D.; Frevert, E. U.; Jacobson, P.; Link, J. T. *Bioorg. Med. Chem. Lett.* **2006**, *16*, 5958; (c) Becker, C. L.; Engstrom, K. M.; Kerdesky, F. A.; Tolle, J. C.; Wagaw, S. H.; Wang, W. *Org. Process Res. Dev.* **2008**, *12*, 1114; (d) Scott, J. S.; Barton, P.; Bennett, S. N. L.; deSchoolmeester, J.; Godfrey, L.; Kilgour, E.; Mayers, R. M.; Packer, M. J.; Rees, A.; Schofield, P.; Selmi, N.; Swales, J. G.; Whittamore, P. R. O. *Med. Chem. Commun.* **2012**, *3*, 1263; (e) Scott, J. S.; deSchoolmeester, J.; Kilgour, E.; Mayers, R. M.; Packer, M. J.; Hargreaves, D.; Gerhardt, S.; Ogg, D. J.; Rees, A.; Selmi, N.; Stocker, A.; Swales, J. G.; Whittamore, P. R. O. *J. Med. Chem.* **2012**, *55*, 10136; (f) Venier, O.; Pascal, C.; Braun, A.; Namane, C.; Mougenot, P.; Crespin, O.; Pacquet, F.; Mougenot, C.; Monseau, C.; Onofri, B.; Dadji-Faïhun, R.; Leger, C.; Ben-Hassine, M.; Van-Pham, T.; Ragot, J.-L.; Philippo, C.; Farjot, G.; Noah, L.; Maniani, K.; Boutarfa, A.; Nicolaï, E.; Guillot, E.; Pruniaux, M.-P.; Güssregen, S.; Engel, C.; Coutant, A.-L.; de Miguel, B.; Castro, A. *Bioorg. Med. Chem. Lett.* **2013**, *23*, 2414; (g) Park, S. B.; Jung, W. H.; Kang, N. S.; Park, J. S.; Bae, G. H.; Kim, H. Y.; Rhee, S. D.; Kang, S. K.; Ahn, J. H.; Jeong, H. G.; Kim, K. Y. *Eur. J. Pharmacol.* **2013**, *721*, 70; (h) Okazaki, S.; Takahashi, T.; Iwamura, T.; Nakaki, J.; Sekiya, Y.; Yagi, M.; Kumagai, H.; Sato, M.; Sakami, S.; Nitta, A.; Kawai, K.; Kainoh, M. *J. Pharmacol. Exp. Ther.* **2014**, *351*, 181; (i) Byun, S. Y.; Shin, Y. J.; Nam, K. Y.; Hong, S. P.; Ahn, S. K. *Life Sci.* **2015**, *120*, 1.
5. For some examples of 1-substituted adamantane evaluated as 11β-HSD1 inhibitors see: (a) Olson, S.; Aster, S. D.; Brown, K.; Carbin, L.; Graham, D. W.; Hermanowski-Vosatka, A.; LeGrand, C. B.; Mundt, S. S.; Robbins, M. A.; Schaeffer, J. M.; Slossberg, L. H.; Szymonifka, M. J.; Thieringer, R.; Wright, S. D.; Balkovec, J. M. *Bioorg. Med. Chem. Lett.* **2005**, *15*, 4359; (b) Su, X.; Pradaux-Caggiano, F.; Thomas, M. P.; Szeto, M. W. Y.; Halem, H. A.; Culler, M. D.; Vicker, N.; Potter, B. V. L. *Chem. Med. Chem.* **2010**, *5*, 1026; (c) Su, X.; Vicker, N.; Thomas, M. P.; Pradaux-Caggiano, F.; Halem, H. A.; Culler, M. D.; Potter, B. V. L. *Chem. Med. Chem.* **2011**, *6*, 1439; (d) Su, X.; Pradaux-Caggiano, F.; Vicker, N.; Thomas, M. P.; Halem, H. A.; Culler, M. D.; Potter, B. V. L. *Chem. Med. Chem.* **2011**, *6*, 1616; (e) Wang, H.; Robl, J. A.; Hamann, L. G.; Simpkins, L.; Golla, R.; Li, Y.-X.; Seethala, R.; Zvyaga, T.; Gordon, D. A.; Li, J. J. *Bioorg. Med. Chem. Lett.* **2011**, *21*, 4146; (f) Kim, S. H.; Kwon, S. W.; Chu, S. Y.; Lee, J. H.; Narsaiah, B.; Kim, C. H.; Kang, S. K.; Kang, N. S.; Rhee, S. D.; Bae, M. A.; Ahn, S. H.; Ha, D. C.; Kim, K. Y.; Ahn, J. H. *Chem. Pharm. Bull.* **2011**, *59*, 46; (g) Su, X.; Halem, H. A.; Thomas, M. P.; Moutrille, C.; Culler, M. D.; Vicker, N.; Potter, B. V. L. *Bioorg. Med. Chem.* **2012**, *20*, 6394.
6. For example, the clogP of amide 2 (2.64) is 1 unit lower than that of amide 1 (3.68). Calculated using BioByte software: BioLoom 5.0 BioByte Co., Claremont, CA, USA. http://www.biobyte.com
7. Webster, S. P.; Ward, P.; Binnie, M.; Craigie, E.; McConnell, K. M. M.; Sooy, K.; Vinter, A.; Seckl, J. R.; Walker, B. R. *Bioorg. Med. Chem. Lett.* **2007**, *17*, 2838.
8. Xia, G.; Liu, L.; Liu, H.; Yu, J.; Xu, Z.; Chen, Q.; Ma, C.; Li, P.; Xiong, B.; Liu, X.; Shen, J. *Chem. Med. Chem.* **2013**, *8*, 577.
9. (a) Yeh, V. S. C.; Kurukulasuriya, R.; Madar, D.; Patel, J. R.; Fung, S.; Monzon, K.; Chiou, W.; Wang, J.; Jacobson, P.; Sham, H. L.; Link, J. T. *Bioorg. Med. Chem. Lett.* **2006**, *16*, 5408; (b) Ye, X.-Y.; Chen, S. Y.; Nayeem, A.; Golla, R.; Seethala, R.; Wang, M.; Harper, T.; Sleczka, B. G.; He, B.; Gordon, D. A.; Robl, J. A. *Bioorg. Med. Chem. Lett.* **2011**, *21*, 6699.
10. (a) Freeman-Cook, K. D.; Hoffman, R. L.; Johnson, T. W. *Future Med. Chem.* **2013**, *5*, 113; (b) Murray, C. W.; Erlanson, D. A.; Hopkins, A. L.; Keseru, G. M.; Leeson, P. D.; Rees, D. C.; Reynolds, C. H.; Richmond, N. J. *J. Med. Chem.* **2014**, *5*, 616.
11. Tice, C. M.; Zhao, W.; Xu, Z.; Cacatian, S. T.; Simpson, R. D.; Ye, Y.-J.; Singh, S. B.; McKeever, B. M.; Lindblom, P.; Guo, J.; Krosky, P. M.; Kruk, B. A.; Berbaum, J.; Harrison, R. K.; Johnson, J. J.; Bukhtiyarov, Y.; Panemangalore, R.; Scott, B. B.; Zhao, Y.; Bruno, J. G.; Zhuang, L.; McGeehan, G. M.; He, W.; Claremon, D. A. *Bioorg. Med. Chem. Lett.* **2010**, *20*, 881.
12. Duque, M. D.; Camps, P.; Profire, L.; Montaner, S.; Vázquez, S.; Sureda, F. S.; Mallol, J.; López-Querol, M.; Naesens, L.; De Clercq, E.; Prathalingam, S. R.; Kelly, J. M. *Bioorg. Med. Chem.* **2009**, *17*, 3198.
13. Leiva, R.; Gazzarrini, S.; Esplugas, R.; Moroni, A.; Naesens, L.; Sureda, F. X.; Vázquez, S. *Tetrahedron Lett.* **2015**, *56*, 1272.
14. Urea **6** had been synthesized previously using a Pd-catalyzed carbonylation reaction: Orito, K.; Miyazawa, M.; Nakamura, T.; Horibata, A.; Ushito, H.; Nagasaki, H.; Yuguchi, M.; Yamashita, S.; Yamazaki, T.; Tokuda, M. *J. Org. Chem.* **2006**, *71*, 5951.
15. The *N*-methyl derivative of **8** is reported to be a submicromolar inhibitor of 11β-HSD1. See, Richards, S.; Sorensen, B.; Jae, H.; Winn, M.; Chen, Y.; Wang, J.; Fung, S.; Monzon, K.; Frevert, E. U.; Jacobson, P.; Sham, H.; Link, J. T. *Bioorg. Med. Chem. Lett.* **2006**, *16*, 6241.
16. For further related 2,2-disubstituted adamantanes that led to the discovery of the clinical candidate BMS-816336 see: (a) Ye, X.-Y.; Yoon, D.; Chen, S. Y.; Nayeem, A.; Golla, R.; Seethala, R.; Wang, M.; Harper, T.; Sleczka, B. G.; Apedo, A.; Li, Y.-X.; He, B.; Kirby, M.; Gordon, D. A.; Robl, J. A. *Bioorg. Med. Chem. Lett.* **2014**, *24*, 654; (b) Ye, X.-Y.; Chen, S. Y.; Wu, S.; Yoon, D. S.; Wang, H.; Hong, Z.; Oconnor, S. P.; Li, J.; Li, J.; Walker, S.; Kennedy, L. J.; Apedo, A.; Nayeem, A.; Sheriff, S.; Morin, P.; Camac, D.; Harrity, T.; Zebo, R.; Taylor, J.; Morgan, N.; Ponticiello, R.; Golla, R.; Seethala, R.; Wang, M.; Harper, T.; Sleczka, B. G.; He, B.; Kirby, M.; DiMarco, J.; Scaringe, R.; Hanson, R. L.; Guo, Z.; Li, J.; Sun, J.-H.; Wong, M. K.; Chen, B.-C.; Haque, L.; Leahy, D. K.; Chan, C.; Li, Y.-X.; Zvyaga, T.; Hansen, L.; Patel, C.; Gordon, D. A.; Robl, J. A. *Chem. Abstr.* **2015**. 477592.
17. Friesner, R. A.; Murphy, R. B.; Repasky, M. P.; Frye, L. L.; Greenwood, J. R.; Halgren, T. A.; Sanschagrin, P. C.; Mainz, D. T. *J. Med. Chem.* **2006**, *49*, 6177.
18. Cheng, H.; Hoffman, J.; Le, P.; Nair, S. K.; Cripps, S.; Matthews, J.; Smith, C.; Yang, M.; Kupchinsky, S.; Dress, K.; Edwards, M.; Cole, B.; Walters, E.; Loh, C.; Ermolieff, J.; Fanjul, A.; Bhat, G. B.; Herrera, J.; Pauly, T.; Hosea, N.; Paderes, G.; Rejto, P. *Bioorg. Med. Chem. Lett.* **2010**, *20*, 2897.
19. (a) Curutchet, C.; Orozco, M.; Luque, F. J. *J. Comput. Chem.* **2001**, *22*, 1180; (b) Kolar, M.; Fanfril, J.; Lepsik, M.; Fort, F.; Luque, F. J.; Hobza, P. *J. Phys. Chem. B* **2013**, *117*, 5950.
20. Robb, G. R.; Boyd, S.; Davies, C. D.; Dossetter, A. G.; Goldberg, F. W.; Kemmitt, P. D.; Scott, J. S.; Swales, J. G. *Med. Chem. Commun.* **2015**, *6*, 926.

Supporting information

Novel 11β-HSD1 inhibitors: C-1 vs C-2 substitution and effect of the introduction of an oxygen atom in the adamantane scaffold

Rosana Leiva[a], Constantí Seira[b], Andrew McBride[c], Margaret Binnie[c], F. Javier Luque[b], Axel Bidon-Chanal[b], Scott P. Webster[c], and Santiago Vázquez[a]

[a] *Laboratori de Química Farmacèutica (Unitat Associada al CSIC), Facultat de Farmàcia, and Institute of Biomedicine (IBUB), Universitat de Barcelona, Av. Joan XXIII, s/n, Barcelona, E-08028, Spain*
[b] *Departament de Fisicoquímica, Facultat de Farmàcia and Institute of Biomedicine (IBUB), Universitat de Barcelona, Av. Prat de la Riba, 171, 08921 Santa Coloma de Gramenet, Spain*
[c] *Endocrinology Unit, Centre for Cardiovascular Science, University of Edinburgh, Queen's Medical Research Institute, EH16 4TJ, United Kingdom*

Table of content:

List of abbreviations S2

Chemical synthesis. General methods S3

Synthetic experimental procedures S4

Determination of the 11β-HSD1 inhibition S12

Computational methods S13

Figure S1. S15

^{1}H and ^{13}C NMR spectra of new compounds S16

List of abbreviations

ATR = Attenuated Total Reflectance

COSY = Correlation Spectroscopy

DCM = dichloromethane

EDC = 1-ethyl-3-(3-dimethylaminopropyl)carbodiimide

EtOAc = ethyl acetate

HOBT = 1-hydroxybenzotriazole

11β-HSD1 = 11β-HydroxySteroid Dehydrogenase type 1

HSQC = Heteronuclear Single Quantum Correlation

NMR = Nuclear Magnetic Resonance

RESP = Restrained Electrostatic Potential

TIP3P = Transferable Intermolecular Potential 3P

Chemical Synthesis. General Methods

Melting points were determined in open capillary tubes with a MFB 595010M Gallenkamp melting point apparatus. 400 MHz ^{1}H NMR and 100.6 MHz ^{13}C NMR spectra were recorded on a Varian Mercury 400 spectrometer. The chemical shifts are reported in ppm (δ scale) relative to internal tetramethylsilane, and coupling constants are reported in hertz (Hz). Assignments given for the NMR spectra of the new compounds is based on COSY ^{1}H/^{13}C (gHSQC sequence) experiments. IR spectra were run on a Perkin-Elmer Spectrum RX I spectrophotometer. Absorption values are expressed as wavenumbers (cm^{-1}). Column chromatography was performed on silica gel 60 Å (35-70 mesh, SDS, ref 2000027). Thin-layer chromatography was performed with aluminum-backed sheets with silica gel 60 F254 (Merck, ref 1.05554), and spots were visualized with UV light and 1% aqueous solution of $KMnO_4$. The analytical samples of all of the new compounds that were subjected to pharmacological evaluation possess a purity of >95%, as evidenced by results of their ^{1}H NMR spectra and elemental analyses.

Obtention of N-(2-adamantyl)piperidine-1-carboxamide (5)

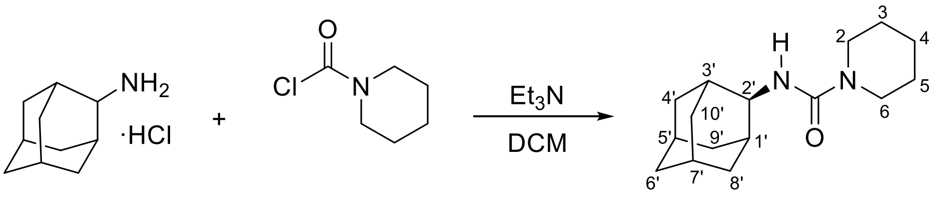

To a solution of 2-adamantanamine hydrochloride (300 mg, 1.6 mmol) in DCM (15 mL) were added 1-piperidinecarbonyl chloride (0.30 mL, 2.4 mmol) and triethylamine (0.8 mL, 6.4 mmol). The reaction mixture was stirred at room temperature overnight. To the resulting suspension was then added saturated aqueous $NaHCO_3$ solution (15 mL) and the phases were separated. The aqueous phase was extracted with further DCM (2 x 15 mL), and the organics were dried over anh. sodium sulphate, filtered and concentrated in *vacuo* to give a white yellowish solid (507 mg). Column chromatography (hexane/ethyl acetate mixture) gave **5** as a white solid (298 mg, 71% yield), mp 183-184 ºC. IR (ATR) ν: 753, 993, 1030, 1056, 1116, 1193, 1218, 1250, 1261, 1506, 1534, 1558, 1606, 1640, 2901, 2918, 3415 cm^{-1}. ^{1}H-NMR (400 MHz, $CDCl_3$) δ: 1.50-1.62 [c. s., 6 H, 4-H_2, 3(5)-H_2], 1.63 [m, 2 H, 8'(10')-H_a], 1.69-1.78 [c. s., 4 H, 8'(10')-H_b, 6'-H_2], 1.82 [c. s., 6 H, 5'-H, 7'-H, 4'(9')-H_2], 1.90 [m, 2 H, 1'(3')-H], 3.31 [c. s., 4 H, 2(6)-H_2], 3.93 (m, 1 H, 2'-H), 4.74 (d, J = 4.8 Hz, 1 H, NH). ^{13}C-NMR (100.5 MHz, $CDCl_3$) δ: 24.4 (CH_2, C4), 25.5 [CH_2, C3(5)], 27.2 (CH, C5' or C7'), 27.3 (CH, C7' or C5'), 32.1 [CH_2, C8'(10')], 32.4 [CH, C1'(3')], 37.2 [CH_2, C4'(9')], 37.6 (CH_2, C6'), 44.9 [CH_2, C2(6)], 54.0 (CH, C2'), 157.1 (C, CO). Calcd for $C_{17}H_{27}NO$: C 73.24, H 9.99, N 10.68. Found: C 73.22, H 10.27, N 10.71.

Obtention of N-(1-adamantyl)piperidine-1-carboxamide (6)

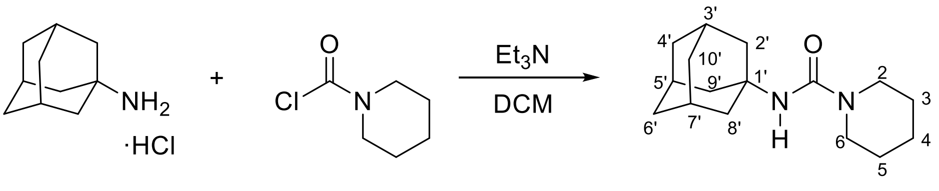

To a solution of 1-adamantanamine hydrochloride (300 mg, 1.6 mmol) in DCM (15 mL) were added 1-piperidinecarbonyl chloride (0.30 mL, 2.4 mmol) and triethylamine (0.8 mL, 6.4 mmol). The reaction mixture was stirred at room temperature overnight. To the resulting suspension was then added saturated aqueous $NaHCO_3$ solution (15 mL) and the phases were separated. The aqueous phase was extracted with further DCM (2 x 15 mL), and the organics were dried over anh. sodium sulphate, filtered and concentrated in *vacuo* to give a yellow solid (392 mg). Column chromatography (hexane/ethyl acetate mixture) gave **6** as a white solid (129 mg, 31% yield). The analytical sample was obtained by washing with pentane, mp 190-191 ºC. IR (ATR) ν: 756, 919, 982, 994, 1033, 1164, 1193, 1221, 1248, 1347, 1369, 1441, 1535, 1641, 2348, 2844, 2924, 3415 cm^{-1}. ^1H-NMR (400 MHz, $CDCl_3$) δ: 1.47-1.60 [c. s., 6 H, 3(5)-H_2, 4-H_2], 1.61-1.71 [c. s., 6 H, 4'(6')(10')-H_2], 1.94-2.00 [c. s., 6 H, 2'(8')(9')-H_2], 2.05 [m, 3 H, 3'(5')(7')-H], 3.24 (m, 4 H, 2(6)-H_2), 4.17 (b. s., 1 H, NH). ^{13}C-NMR (100.5 MHz, $CDCl_3$) δ: 24.4 (CH_2, C4), 25.6 [CH_2, C3(5)], 29.6 [CH, C3'(5')(7')], 36.5 [CH_2, C4'(6')(10')], 42.4 [CH_2, C2'(8')(9')], 44.9 [CH_2, C2(6)], 51.0 (C, C1'), 156.8 (C, CO). Calcd for $C_{17}H_{20}Cl_2N_2O$: C 73.24, H 9.99, N 10.68. Found: C 73.22, H 10.26, N 10.73.

Obtention of N-(3-methyl-2-oxaadamant-1-yl)piperidine-1-carboxamide (7)

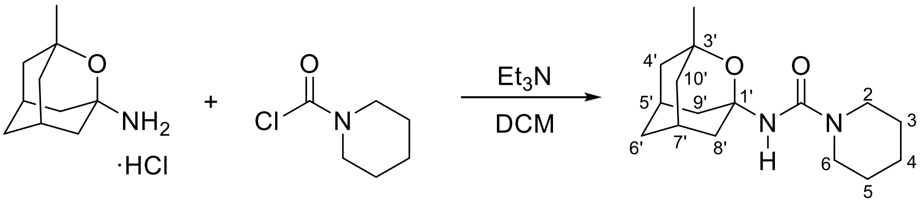

To a solution of (3-methyl-2-oxaadamant-1-yl)amine hydrochloride (137 mg, 0.7 mmol) in DCM (10 mL) were added 1-piperidinecarbonyl chloride (0.13 mL, 1 mmol) and triethylamine (0.34 mL, 2.7 mmol). The reaction mixture was stirred at room temperature overnight. To the resulting suspension was then added saturated aqueous $NaHCO_3$ solution (10 mL) and the phases were separated. The aqueous phase was extracted with further DCM (2 x 10 mL), and the organics were dried over anh. sodium sulphate, filtered and concentrated in *vacuo* to give an orange oil (374 mg). Column chromatography (hexane/ethyl acetate mixture) gave **7** as a white solid (64 mg, 34% yield), mp 116-117 ºC. IR (ATR) ν: 617, 672, 708, 764, 813, 852, 896, 922, 955, 964, 985, 995, 1037, 1067, 1144, 1166, 1195, 1220, 1253, 1349, 1374, 1392, 1443, 1538, 1632, 1643, 2847, 2922, 3322 cm^{-1}. ^1H-NMR (400 MHz, $CDCl_3$) δ: 1.13 (s, 3 H, CH_3-

C3’), 1.46-1.60 [c. s., 8 H, 4-H_2, 3(5)-H_2, 4’(10’)-H_a], 1.61-1.70 [c. s., 3 H, 6’-H_a, 4’(10’)-H_b], 1.72-1.80 (m, 1 H, 6’-H_b), 1.86 [dm, J = 11.6 Hz, 2 H, 8’(9’)-H_a], 2.25 [m, 2 H, 5’(7’)-H], 2.30 [dm, J = 11.6 Hz, 2H, 8’(9’)-H_b], 3.24 [c. s., 4 H, 2(6)-H_2), 4.63 (b. s., 1 H, NH). ^{13}C-NMR (100.5 MHz, $CDCl_3$) δ: 24.4 (CH_2, C4), 25.6 [CH_2, C3(5)], 28.7 [CH, C5’(7’)], 29.2 (CH_3, C3-CH_3), 33.9 (CH_2, C6’), 39.6 [CH_2, C8’(9’)], 41.0 [CH_2, C4’(10’)], 44.7 [CH_2, C2(6)], 73.0 (C, C3’), 83.3 (C, C1’), 155.5 (C, CO). Calcd for $C_{17}H_{27}NO$: C 69.03, H 9.41, N 10.06. Found: C 68.91, H 9.40, N 9.82.

Obtention of N-(1-adamantyl)-4-amino-3,5-dichlorobenzamide (8)

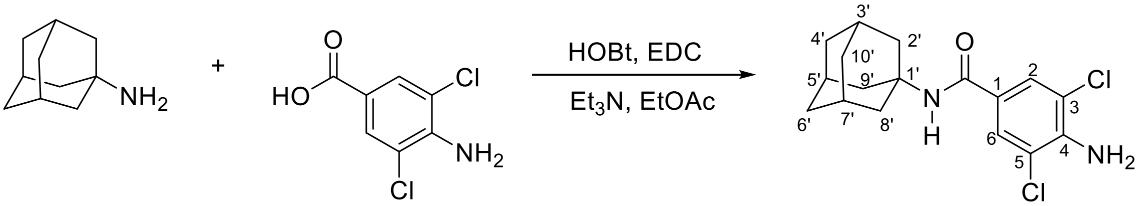

To a solution of 1-adamantanamine hydrochloride (207 mg, 1.1 mmol) in EtOAc (10 mL) were added 4-amino-3,5-dichlorobenzoic acid (206 mg, 1 mmol), HOBt (202.6 mg, 1.5 mmol), EDC (232 mg, 1.5 mmol) and triethylamine (0.6 mL, 4.4 mmol). The reaction mixture was stirred at room temperature for 22 hours. To the resulting suspension was then added water (20 mL) and the phases were separated. The organic phase was washed with saturated aqueous $NaHCO_3$ solution (15 mL) and brine (15 mL), dried over anh. sodium sulphate and filtered. Evaporation in *vacuo* of the organics gave **8** as a white yellowish solid (286 mg, 84% yield). The analytical sample was obtained by crystallization from ethyl acetate/pentane, mp 222-223 ºC. IR (ATR) ν: 648, 753, 799, 879, 907, 1027, 1053, 1087, 1107, 1250, 1306, 1321, 1483, 1533, 1569, 1600, 1638, 2353, 2844, 2901, 3381, 3729, 3832 cm^{-1}. ^{1}H-NMR (400 MHz, $CDCl_3$) δ: 1.65-1.76 [c. s., 6 H, 4’(6’)(10’)-H_2], 2.07-2.11 [c. s., 6 H, 2’(8’)(9’)-H_2], 2.11 [m, 3 H, 3’(5’)(7’)-H], 4.70 (b. s., 2 H, NH_2), 5.62 (b. s., 1 H, NH), 7.56 [s, 2 H, 2(6)-H_{Ar}]. ^{13}C-NMR (100.5 MHz, $CDCl_3$) δ: 29.5 [CH, C3’(5’)(7’)], 36.3 [CH_2, C4’(6’)(10’)], 41.6 [CH_2, C2’(8’)(9’)], 52.4 (C, C1’), 118.8 [C, C3(5)], 125.8 (C, C1), 126.6 [CH, C2(6)], 142.3 (C, C4), 164.2 (C, CO). Calcd for $C_{17}H_{20}Cl_2N_2O$: C 60.19, H 5.94, N 8.26. Found: C 60.32, H 6.09, N 8.32.

Obtention of N-(1-adamantyl)cyclohexanecarboxamide (9)

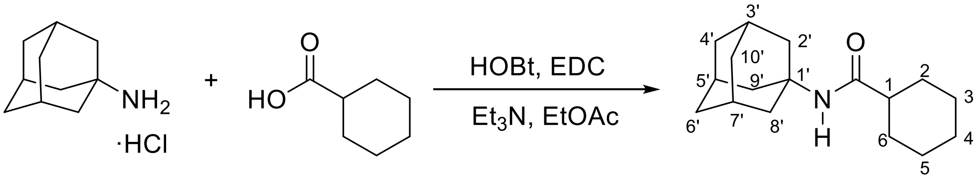

To a solution of 1-adamantanamine hydrochloride (207 mg, 1.1 mmol) in EtOAc (15 mL) were added cyclohexanecarboxylic acid (128 mg, 1 mmol), HOBt (203 mg, 1.5 mmol), EDC (232 mg, 1.5 mmol) and triethylamine (0.6 mL, 4.4 mmol). The reaction mixture was stirred at room temperature overnight. To the resulting suspension was then added water (15 mL) and the phases were separated. The organic phase was washed with saturated aqueous $NaHCO_3$ solution (15 mL) and brine (15 mL), dried over anh. sodium sulphate and filtered. Evaporation in *vacuo* of the organics gave **9** as a white solid (202 mg, 77% yield). The analytical sample was obtained by crystallization from ethyl acetate/pentane, mp 192-193 ºC. IR (ATR) ν: 665, 711, 762, 919, 950, 993, 1027, 1195, 1215, 1250, 1270, 1307, 1341, 1355, 1378, 1446, 1537, 1642, 2353, 2844, 2914, 3272, 3409 cm^{-1}. ^1H-NMR (400 MHz, $CDCl_3$) δ: 1.12-1.31 [c. s., 3 H, 3(5)-H_{ax} and 4-H_{ax}], 1.32-1.46 [c. s., 2 H, 2(6)-H_{ax}], 1.60-1.70 [c. s., 7 H, 4-H_{eq}, 4'(6')(10')-H_2], 1.72-1.82 [c. s., 4 H, 3(5)-H_{eq} and 2(6)-H_{eq}], 1.93 [tt, *J* = 11.6 Hz, *J'* = 3.6 Hz, 1 H, 1-H], 1.96-2.0 [c. s., 6 H, 2'(8')(9')-H_2], 2.05 [m, 3 H, 3'(5')(7')-H], 5.07 (b. s., 1 H, NH). ^{13}C-NMR (100.5 MHz, $CDCl_3$) δ: 25.8 [CH_2, C3(5) and C4], 29.4 [CH, C3'(5')(7')], 29.8 [CH_2, C2(6)], 36.4 [CH_2, C4'(6')(10')], 41.7 [CH_2, C2'(8')(9')], 46.4 (CH, C1), 51.4 (C, C1'), 175.4 (C, CO). Calcd for $C_{17}H_{27}NO$: C 78.11, H 10.41, N 5.36. Found: C 78.26, H 10.29, N 5.27.

Obtention of N-(3-methyl-2-oxaadamant-1-yl)cyclohexanecarboxamide (10)

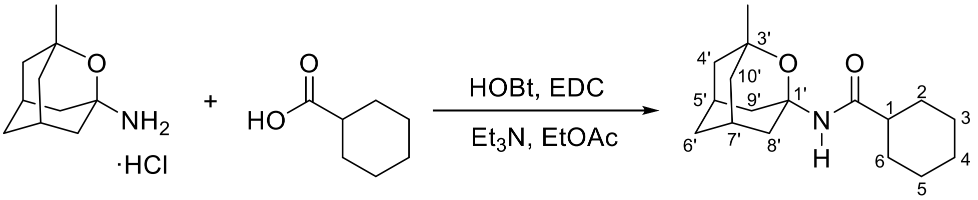

To a solution of (3-methyl-2-oxaadamant-1-yl)amine hydrochloride (120 mg, 0.6 mmol) in EtOAc (10 mL) were added cyclohexanecarboxylic acid (69 mg, 0.5 mmol), HOBt (111 mg, 0.8 mmol), EDC (127 mg, 0.8 mmol) and triethylamine

(0.3 mL, 2.4 mmol). The reaction mixture was stirred at room temperature overnight. To the resulting suspension was then added water (10 mL) and the phases were separated. The organic phase was washed with saturated aqueous $NaHCO_3$ solution (10 mL), brine (10 mL) and 2N HCl solution (2 x 10 mL), dried over anh. sodium sulphate and filtered. Evaporation in *vacuo* of the organics gave **10** as a white solid (59 mg, 39% yield), mp 101-102 ºC. IR (ATR) ν: 613, 642, 671, 714, 763, 797, 831, 890, 920, 953, 1000, 1037, 1074, 1100, 1146, 1204, 1217, 1255, 1302, 1319, 1338, 1374, 1445, 1540, 1662, 2850, 2918, 3316 cm^{-1}. ^1H-NMR (400 MHz, $CDCl_3$) δ: 1.12 (s, 3 H, C3'-CH_3), 1.15-1.29 [c. s., 3 H, 3(5)-H_{ax} and 4-H_{ax}], 1.38 [m, 2 H, 2(6)-H_{ax}], 1.51 [dm, *J* = 12.4 Hz, 2 H, 4'(10')-H_a], 1.60-1.88 [c. s., 11 H, 2(6)-H_{eq}, 3(5)-H_{eq}, 4-H_{eq}, 6'-H_2, 8'(9')-H_a, 4'(10')-H_b], 1.97 [tt, *J* = 11.6 Hz, *J'* = 3.6 Hz, 1 H, 1-H], 2.25 [m, 2 H, 5'(7')-H], 2.45 (dm, *J* = 12 Hz, 2 H, 8'(9')-H_b], 5.54 (b. s., 1 H, NH). ^{13}C-NMR (100.5 MHz, $CDCl_3$) δ: 25.71 [CH_2, C3(5)], 25.74 (CH_2, C4), 28.6 [CH, C5'(7')], 29.1 (CH_3, C3'-CH_3), 29.6 [CH_2, C2(6)], 33.6 (CH_2, C6'), 39.0 [CH_2, C8'(9')], 41.0 [CH_2, C4'(10')], 46.2 (CH, C1), 73.2 (C, C3'), 83.4 (C, C1'), 174.4 (C, CO). Calcd for $C_{17}H_{27}NO$: C 73.61, H 9.81, N 5.05. Found: C 73.45, H 10.01, N 5.15.

Obtention of N-(2-oxaadamant-5-yl)cyclohexanecarboxamide (11)

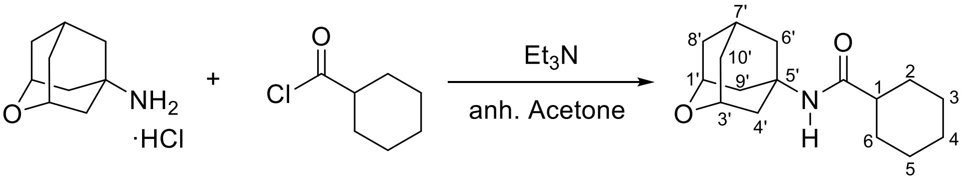

A solution of cyclohexanecarbonyl chloride (87 mg, 0.59 mmol) in anhydrous acetone (0.5 mL) was added to a solution of the 2-oxaadamantan-5-amine hydrochloride (86 mg, 0.49 mmol) and triethylamine in anhydrous acetone (0.5 mL). The reaction mixture was stirred at reflux for 3 hours. The residue was dissolved in DCM (5 mL) and 1N HCl solution (5 mL) and the phases were separated. The organic phase was washed with further 1N HCl solution (2 x 5 mL). The combined organic phases were dried, filtered and concentrated in *vacuo* to give RL-109 as a white solid (122 mg). Column chromatography (hexane/ethyl acetate mixture) gave **11** as a white solid (51 mg, 42% yield), mp 165-166 ºC. IR (ATR) ν: 675, 720, 733, 781, 803, 818, 847, 890, 924, 953, 972, 1002, 1015, 1073, 1106, 1144, 1190, 1217, 1249, 1273, 1315, 1347, 1357, 1438, 1548, 1639, 2847, 2899, 2933, 3073, 3267 cm-1. ^{1}H-NMR (400 MHz, $CDCl_3$) δ: 1.16-1.31 [c. s., 3 H, 3(5)-H_{ax} and 4-H_{ax}], 1.39 [m, 2 H, 2(6)-H_{ax}], 1.59 [dm, J = 12.4 Hz, 2 H, 8'(10')-H_a], 1.67 [m, 1 H, 4-H_{eq}], 1.74-1.86 [c. s., 4 H, 2(6)-H_{eq}, 3(5)-H_{eq}], 1.90-2.03 [c. s., 3 H, 1-H, 8'(10')-H_b], 2.06 (c. s., 4 H, 4'(9')-H_2], 2.18-2.22 (c. s., 2 H, 6'-H_2), 2.23 (m, 1 H, 7'-H), 4.17 (m, 2 H, 1'(3')-H), 5.13 (b. s., 1 H, NH). ^{13}C-NMR (100.5 MHz, $CDCl_3$) δ: 25.7 [CH_2, C3(5), C4], 27.3 (CH, C7'), 29.7 [CH_2, C2(6)], 34.9 [CH_2, C8'(10')], 39.7 (CH_2, C6'), 40.7 [CH_2, C4'(9')], 46.2 (CH, C1), 50.2 (C, C5'), 69.2 [CH, C1'(3')], 175.6 (C, CO). Calcd for $C_{16}H_{25}NO_2\cdot 0.2\ H_2O$: C 71.98, H 9.59, N 5.25. Found: C 72.02, H 9.58, N 5.15.

Obtention of N-(2-adamantyl)cyclohexanecarboxamide (12)

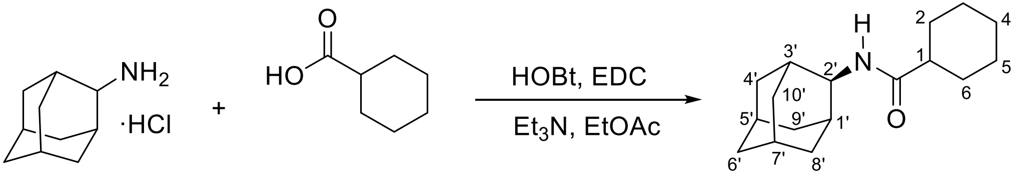

To a solution of 2-adamantanamine hydrochloride (207 mg, 1.1 mmol) in EtOAc (15 mL) were added cyclohexanecarboxylic acid (128 mg, 1 mmol), HOBt (203 mg, 1.5 mmol), EDC (232 mg, 1.5 mmol) and triethylamine (0.6 mL, 4.4 mmol). The reaction mixture was stirred at room temperature overnight. To the resulting suspension was then added water (15 mL) and the phases were separated. The organic phase was washed with saturated aqueous $NaHCO_3$ solution (15 mL) and brine (15 mL). The aqueous phase was extracted with further EtOAc (2 x 15 mL) and the organics were dried over anh. sodium sulphate and filtered. Evaporation in *vacuo* of the organics gave **12** as a white solid (184 mg, 71% yield). The analytical sample was obtained by crystallization from DCM/diethyl ether, mp 201-202 ºC. IR (ATR) ν: 659, 919, 979, 993, 1030, 1195, 1218, 1248, 1367, 1441, 1536, 1609, 1641, 2365, 2844, 2923, 3415 cm^{-1}. ^{1}H-NMR (400 MHz, $CDCl_3$) δ: 1.16-1.34 [c. s., 3 H, 3(5)-H_{ax} and 4-H_{ax}], 1.42 [m, 2 H, 2(6)-H_{ax}], 1.60-1.94 [c. s., 18 H, 2(6)-H_{eq}, 3(5)-H_{eq}, 1'(3')-H, 4'(9')-H_2, 5'(7')-H, 8'(10')-H_2, 6'-H_2], 2.08 (tt, *J* = 11.6 Hz, *J'* = 3.6 Hz, 1 H, 1-H), 4.02 (m, 1 H, 2'-H), 5.75 (b. s., 1 H, NH). ^{13}C-NMR (100.5 MHz, $CDCl_3$) δ: 25.8 [CH_2, C3(5) and C4], 27.1 (CH, C5' or C7'), 27.2 (CH, C7' or C5'), 29.8 [CH_2, C2(6)], 31.8 [CH_2, C8'(10')], 31.9 [CH, C1’(3’)], 37.1 [CH_2, C4’(9’)], 37.5 (CH_2, C6’), 45.8 (CH, C1), 52.7 (CH, C2’), 175.0 (C, CO). Calcd for $C_{17}H_{27}NO$: C 78.11, H 10.41, N 5.36. Found: C 78.23, H 10.52, N 5.30.

Obtention of N-(2-adamantyl)-4-amino-3,5-dichlorobenzamide (13)

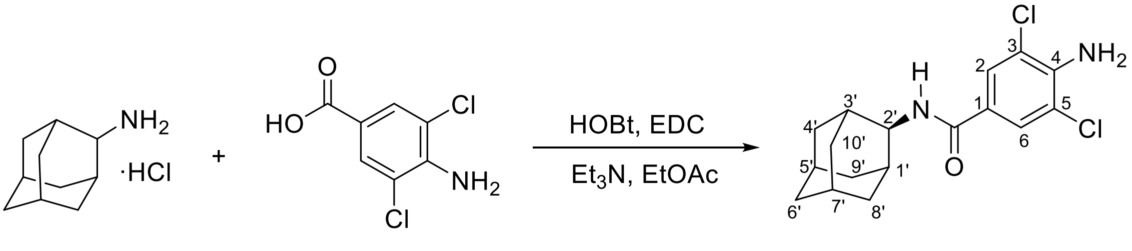

To a solution of 2-adamantanamine hydrochloride (413 mg, 2.2 mmol) in EtOAc (20 mL) were added 4-amino-3,5-dichlorobenzoic acid (412 mg, 2 mmol), HOBt (405 mg, 3 mmol), EDC (464.6 mg, 3 mmol) and triethylamine (1.2 mL, 8.8 mmol). The reaction mixture was stirred at room temperature for 22 hours. To the resulting suspension was then added water (40 mL) and the phases were separated. The organic phase was washed with saturated aqueous $NaHCO_3$ solution (30 mL) and brine (30 mL), dried over anh. sodium sulphate and filtered. Evaporation in *vacuo* of the organics gave **13** as a white yellowish solid (686 mg, quantitative yield). The analytical sample was obtained by crystallization from hot EtOAc, mp 173-174 ºC. IR (ATR) ν: 632, 655, 718, 760, 789, 817, 845, 894, 905, 945, 982, 1019, 1056, 1078, 1102, 1224, 1279, 1300, 1341, 1358, 1375, 1470, 1481, 1531, 1606, 2848, 2903, 3298, 3391, 3490 cm^{-1}. ^1H-NMR (400 MHz, $CDCl_3$) δ: 1.67-1.76 [m, 2 H, 8’(10’)-H_a], 1.77 (b. s., 2 H, 6’-H_2), 1.81-1.94 [c. s., 8 H, 8’(10’)-H_b, 4’(9’)-H_2, 5’(7’)-H], 2.01 [m, 2 H, 1’(3’)-H], 4.20 (dm, *J* = 7.2 Hz, 1 H, 2’-H), 4.74 (s, 2 H, NH_2), 6.23 (d, *J* = 7.2 Hz, 1 H, NH), 7.62 [s, 2 H, 2(6)-H_{Ar}]. ^{13}C-NMR (100.5 MHz, $CDCl_3$) δ: 27.1 (CH, C5’ or C7’), 27.2 (CH, C7’ or C5’), 31.9 [CH, C1’(3’)], 32.1 [CH_2, C8’(10’)], 37.1 [CH_2, C4’(9’)], 37.5 (CH_2, C6’), 53.8 (CH, C2’), 118.9 [C, C3(5)], 125.0 (C, C1), 126.7 [CH, C2(6)], 142.6 (C, C4), 164.3 (C, CO). Calcd for $C_{17}H_{27}NO$: C 60.19, H 5.94, N 8.26. Found: C 60.25, H 6.11, N 8.26.

Obtention of N-(2-adamantyl)cyclopentanecarboxamide (14)

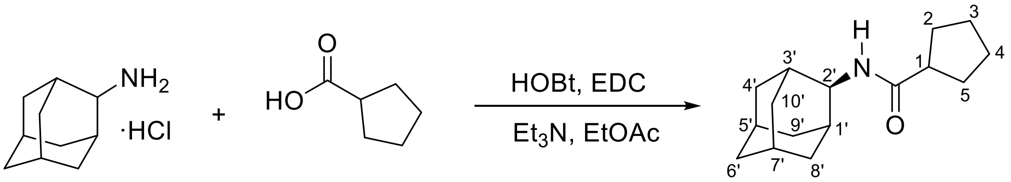

To a solution of 2-adamantanamine hydrochloride (207 mg, 1.1 mmol) in EtOAc (10 mL) were added cyclopentanecarboxylic acid (0.11 mL, 1 mmol), HOBt (202.6 mg, 1.5 mmol), EDC (232 mg, 1.5 mmol) and triethylamine (0.6 mL, 4.4 mmol). The reaction mixture was stirred at room temperature for 22 hours. To the resulting suspension was then added water (20 mL) and the phases were separated. The organic phase was washed with saturated aqueous $NaHCO_3$ solution (15 mL) and brine (15 mL), dried over anh. sodium sulphate and filtered. Evaporation in *vacuo* of the organics gave **14** as a white solid (227 mg, 92% yield). The analytical sample was obtained by crystallization from hot EtOAc (180 mg), mp 203-204 ºC. IR (ATR) ν: 665, 797, 819, 862, 930, 963, 981, 1058, 1098, 1116, 1145, 1228, 1271, 1306, 1387, 1444, 1471, 1537, 1633, 2847, 2901, 3312 cm^{-1}. ^1H-NMR (400 MHz, $CDCl_3$) δ: 1.54-1.60 [m, 2 H, 3(4)-H_a], 1.61-1.87 [c. s., 18 H, 4'(9')-H_2, 8'(10')-H_2, 2(5)-H_2, 5'-H, 7'-H, 6'- H_2, 3(4)-H_b], 1.90 [m, 2 H, 1'(3')-H], 2.53 (m, 1 H, 1-H), 4.04 (m, 1 H, 2'-H), 5.74 (b. s., 1 H, NH). ^{13}C-NMR (100.5 MHz, $CDCl_3$) δ: 25.9 [CH_2, C3(4)], 27.1 (CH, C5' or C7'), 27.2 (CH, C7' or C5'), 30.5 [CH_2, C2(5)], 31.9 [CH, C1'(3')], 32.0 [CH_2, C8'(10')], 37.1 [CH_2, C4'(9')], 37.5 (CH_2, C6'), 46.2 (CH, C1), 52.9 (CH, C2'), 175.2 (C, CO). Calcd for $C_{16}H_{25}NO\cdot0.1\ H_2O$: C 77.12, H 10.19, N 5.62. Found: C 77.05, H 10.16, N 5.52.

Determination of the 11β-HSD1 inhibition

11β-HSD1 activity was determined in mixed sex, Human Liver Microsomes (Celsis In-vitro Technologies) by measuring the conversion of ^{3}H-cortisone to ^{3}H-cortisol. Percentage inhibition was determined relative to a no inhibitor control. 5µg of Human Liver microsomes was pre-incubated at 37°C for 15 minutes with inhibitor and 1mM NADPH in a final volume of 90µl Krebs buffer. 10µl of 200nM ^{3}H-cortisone was then added followed by incubation for at 37°C for a further 30 minutes. The assay was terminated by rapid freezing on dry ice and ^{3}H-cortisone to ^{3}H-cortisol conversion determined in 50µl of the defrosted reaction by capturing liberated ^{3}H-cortisol on anti-cortisol (HyTest Ltd)-coated scintillation proximity assay beads (protein A-coated YSi, GE Healthcare).

Computational methods

Docking

Taking advantage of the X-ray structures of the murine 11ß-HSD1 (PDB ID 3LZ6)[1], and the human enzyme (PDB IDs 4BB6[2] and 4BB5[2]) in complex with the known inhibitors PF-877423, HD1 and HD2, docking experiments were run to find the most appropriate orientation of compounds **5**, **6** and **12** in the binding site of human 11ß-HSD1. The structures of the three complexes were used to restrict the position of the adamantyl amide group, and the protein coordinates were taken from X-ray structure 4BB6. NADP was also included in the docking experiment as it forms part of the binding site.
Glide[3] with the SP scoring function was used to perform the docking assays. Each molecule was energy minimized previously and the centroid of HD1 was used to generate the docking cavity by selecting all the residues located within 15 Å from the ligand. 100 poses were generated for each ligand and the best scored fulfilling the adamantly amide group position requirement was selected.

Molecular Dynamics

For each compound (**5**, **6**, **12** and PF-877423) three independent 50 ns molecular dynamic simulations were run starting from the ligand-enzyme generated from docking calculations. Every complex was immersed in an octahedral box of TIP3P[4] water molecules and sodium ions were added to neutralize the system. The box size was selected so that 12 Å was the minimum distance between any atom of the protein and the box limits. The force field *ff99SBildn*[5,6] was used for the protein parameters and RESP charges at the HF/6-31G(d) level and the *gaff*[7] force field were used to build the ligand and NADP parameters.

The system was energy minimized following a three-step protocol. First, the hydrogens of the protein, the ligand and the cofactor were minimized. Second, the orientation of water molecules was optimized. Finally, a global minimization was run in which all the atoms were let free to move. At this point, the system was thermalized to 300K in 4 steps of 50 ps each from an initial temperature of 100K. The last snapshot from the thermalization procedure was used as starting point for the molecular dynamic simulations that were run in the NVT ensemble using a 2 fs timestep, periodic boundary conditions and keeping frozen all the bonds implicating hydrogen atoms using SHAKE.[8]

1. Cheng, H.; Hoffman, J.; Le, P.; Nair, S.K.; Cripps, S.; Matthews, J.; Smith, C.; Yang, M.; Kupchinsky, S.; Dress, K.; Edwards, M.; Cole, B.; Walters, E.; Loh, C.; Ermolieff, J.; Fanjul, A.; Bhat, G.B.; Herrera, J.; Pauly, T.; Hosea, N.; Paderes, G.; Rejto, P. *Bioorg. Med. Chem. Lett.* **2010**, *20*, 2897.

2. Goldberg, F.W.; Leach, A.G.; Scott, J.S.; Snelson, W.L.; Groombridge, S.D.; Donald, C.S.; Bennett, S.N.L.; Bodin, C.; Morentin Gutierrez, P.; Gyte, A.C. *J. Med. Chem.* **2012**, *55*, 10652.

3. Friesner, R. A.; Banks, J. L.; Murphy, R. B.; Halgren, T. A.; Klicic, J. J.; Mainz, D. T.; Repasky, M. P.; Knoll, E. H.; Shaw, D. E.; Shelley, M.; Perry, J. K.; Francis, P.; Shenkin, P. S., *J. Med. Chem.*, **2004**, *47*, 1739

4. Jorgensen, W. L.; Chandrasekhar, J.; Madura, J. D.; Impey, R. W.; Klein, M. L. *J. Chem. Phys.*, **1983**, *79*, 926.

5. Hornak, V.; Abel, R.; Okur, A.; Strockbine, B.; Roitberg, A.; Simmerling, C. *Proteins* **2006**, *65*, 712.

6. Lindorff-Larsen, K.; Piana, S.; palmo, K.; Maragakis, P.; Klepeis, J. L.; Dror, R. O.; Shaw, D. E. *Proteins* **2010**, *78*, 1950.

7. Wang, J.; Wolf, R. M.; Caldwell, J. W.; Kollman, P. A.; Case, D. A. *J. Comp. Chem.*, **2004**, *25*, 1157

8. Ryckaert, J.-P.; Ciccotti, G.; Berendsen, H.J.C. *J. Comput. Phys.*, **1977**, *23*, 327.

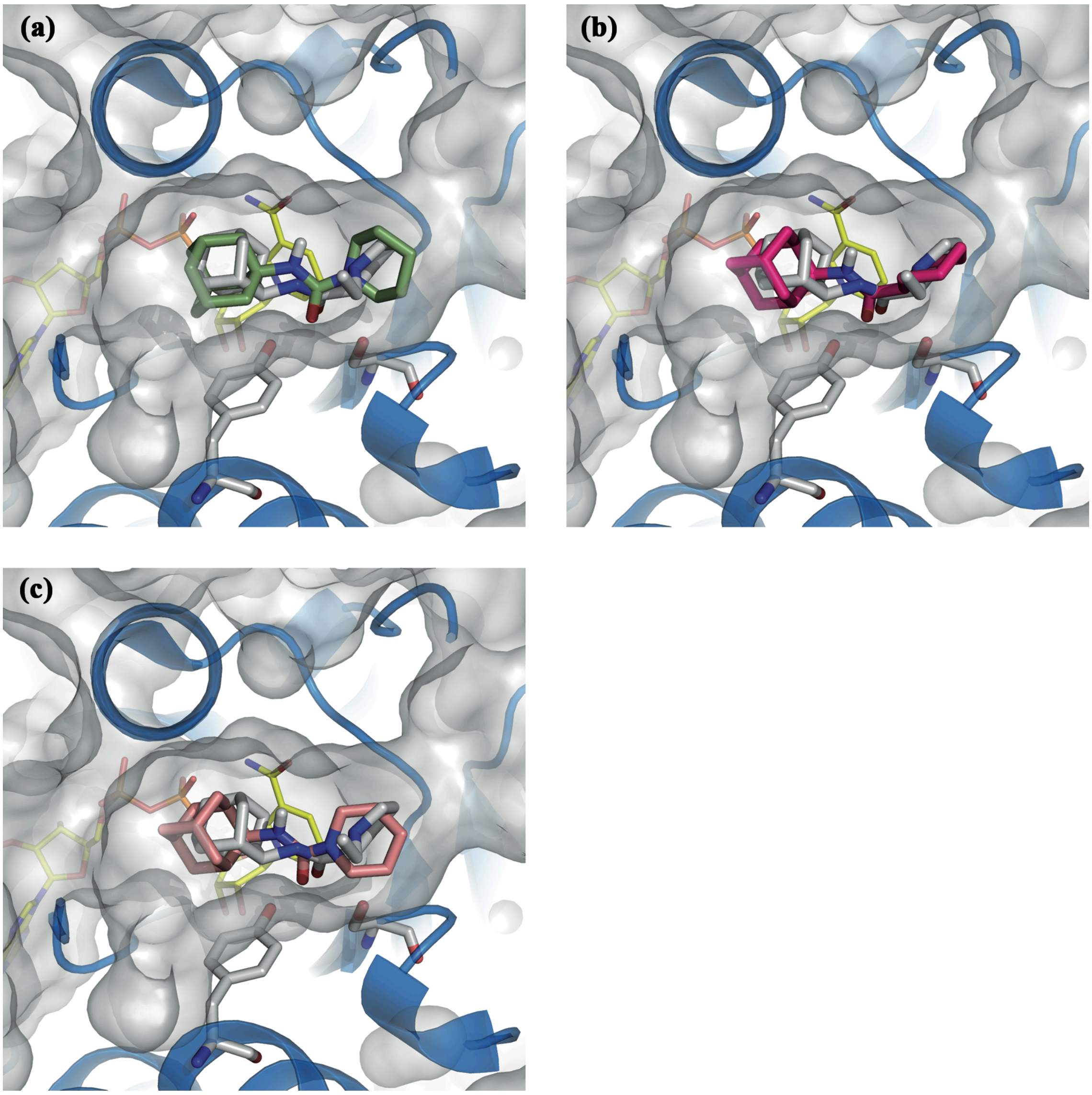

Figure S1. Best scoring complexes generated by docking for compounds **6** (a), **12** (b) and **5** (c) superposed to the crystallographic structure with PDB ID 3LZ6 containing the inhibitor PF-877423. The key residues Ser170 and Tyr183, NADP, PF-877423 and compounds **5**, **6** and **12** are shown as sticks. NADP carbons are colored in yellow, PF-877423 and the aminoacids carbons are colored in white. The secondary structure of the protein in the binding site region is ashown as blue cartoon and the surface of the protein as transparent white contour.

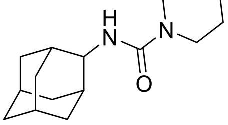
H
N
N
O

5

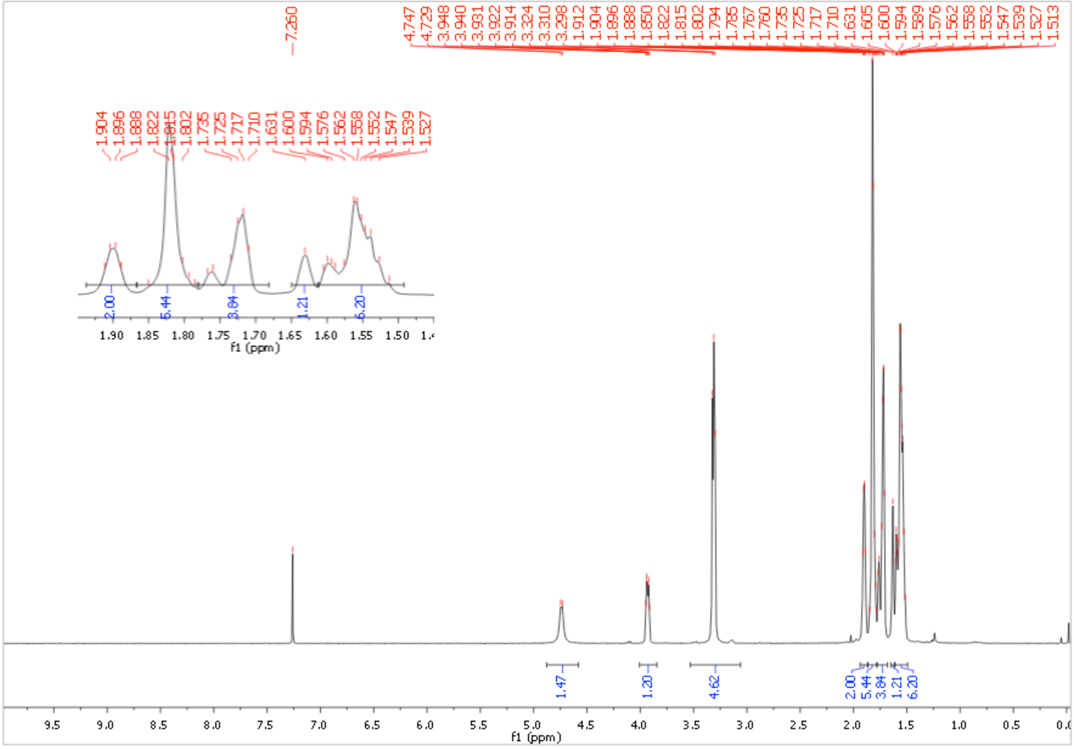
7.260
4.747
4.729
3.948
3.940
3.931
3.922
3.914
3.324
3.310
3.298
1.912
1.904
1.896
1.888
1.850
1.822
1.815
1.802
1.794
1.785
1.767
1.760
1.735
1.725
1.717
1.710
1.631
1.605
1.600
1.594
1.589
1.576
1.562
1.558
1.552
1.547
1.539
1.527
1.513
1.904
1.896
1.888
1.822
1.815
1.802
1.735
1.725
1.717
1.710
1.631
1.600
1.594
1.576
1.562
1.558
1.552
1.547
1.539
1.527
2.00
5.44
3.84
1.21
6.20
1.90 1.85 1.80 1.75 1.70 1.65 1.60 1.55 1.50 1.4
f1 (ppm)
1.47
1.20
4.62
2.00
5.44
3.84
1.21
6.20
9.5 9.0 8.5 8.0 7.5 7.0 6.5 6.0 5.5 5.0 4.5 4.0 3.5 3.0 2.5 2.0 1.5 1.0 0.5 0.0
f1 (ppm)

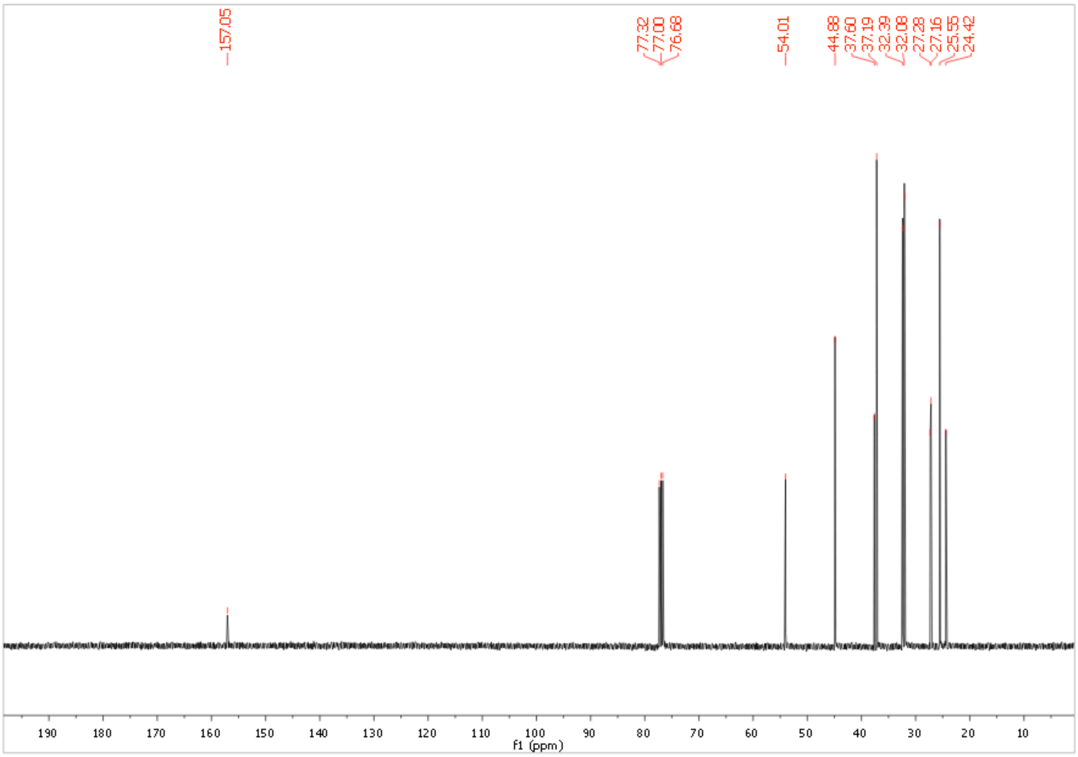
157.05
77.32
77.00
76.68
54.01
44.88
37.60
37.19
32.39
32.08
27.28
27.16
25.55
24.42
190 180 170 160 150 140 130 120 110 100 90 80 70 60 50 40 30 20 10
f1 (ppm)

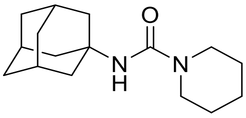
O
N
H
N

6

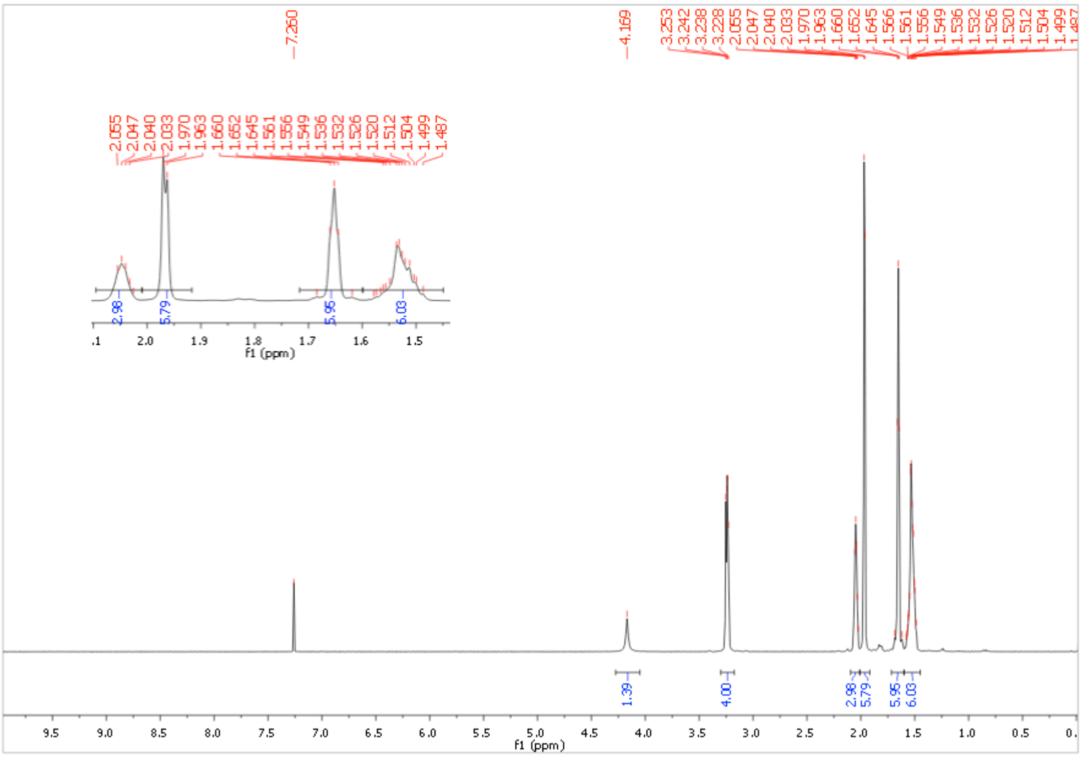
7.260
4.169
3.253
3.242
3.238
3.228
2.055
2.047
2.040
2.033
1.970
1.963
1.660
1.652
1.645
1.566
1.561
1.556
1.549
1.536
1.532
1.526
1.520
1.512
1.504
1.499
1.487
2.98
5.79
5.95
6.03
2.0
1.9
1.8
1.7
1.6
1.5
f1 (ppm)
1.39
4.00
9.5
9.0
8.5
8.0
7.5
7.0
6.5
6.0
5.5
5.0
4.5
4.0
3.5
3.0
2.5
2.0
1.5
1.0
0.5
f1 (ppm)

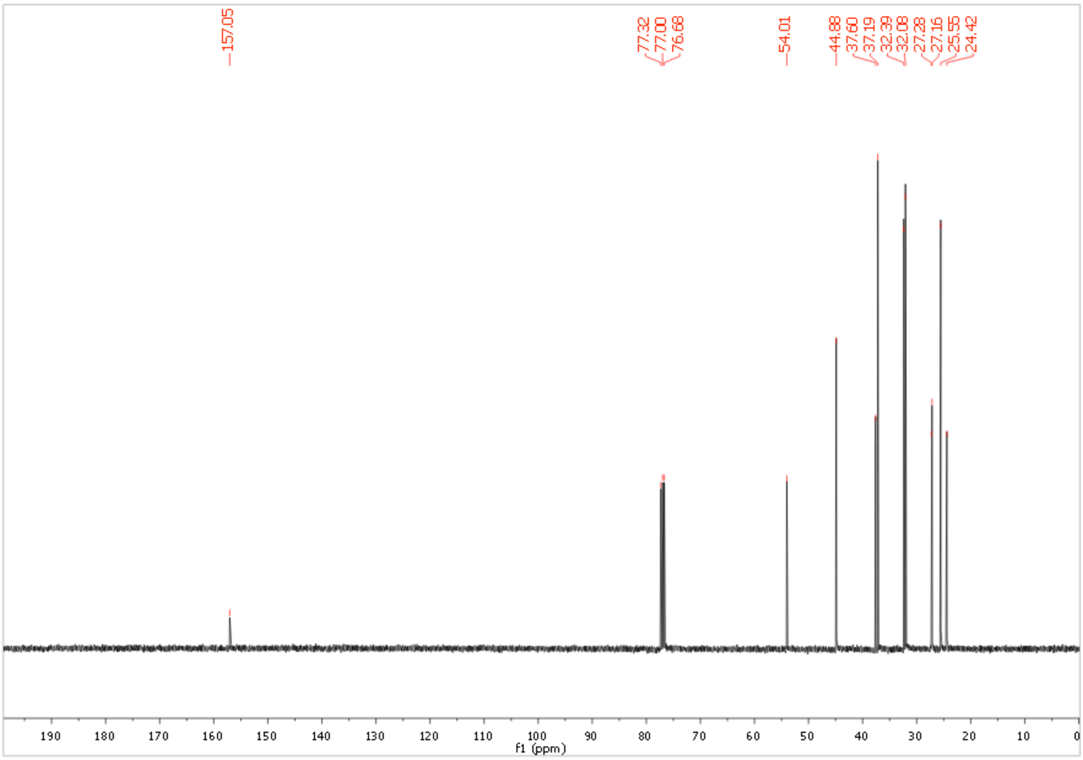
157.05
77.32
77.00
76.68
54.01
44.88
37.60
37.19
32.39
32.08
27.28
27.16
25.55
24.42
190
180
170
160
150
140
130
120
110
100
90
80
70
60
50
40
30
20
10
0
f1 (ppm)

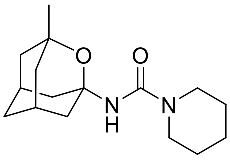
O
O
N
H
N

7

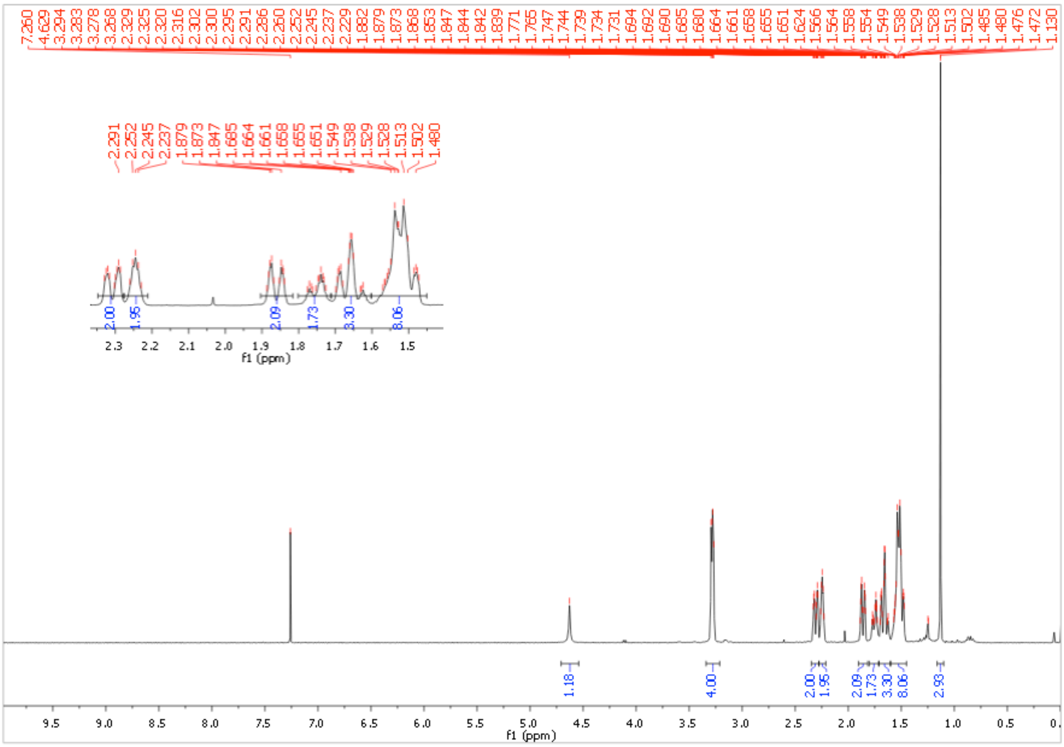
7.260
4.629
3.294
3.283
3.278
3.268
2.329
2.325
2.320
2.316
2.302
2.300
2.295
2.291
2.286
2.260
2.252
2.245
2.237
2.229
1.882
1.879
1.873
1.868
1.853
1.847
1.844
1.842
1.839
1.771
1.765
1.747
1.744
1.739
1.734
1.731
1.694
1.692
1.690
1.685
1.680
1.664
1.661
1.658
1.655
1.651
1.624
1.566
1.564
1.558
1.554
1.549
1.538
1.529
1.528
1.513
1.502
1.485
1.480
1.476
1.472
1.130
2.291
2.252
2.245
2.237
1.879
1.873
1.847
1.685
1.664
1.661
1.658
1.655
1.651
1.549
1.538
1.529
1.528
1.513
1.502
1.480
2.00
1.95
2.09
1.73
3.30
8.06
2.3
2.2
2.1
2.0
1.9
1.8
1.7
1.6
1.5
f1 (ppm)
1.18
4.00
2.00
1.95
2.09
1.73
3.30
8.06
2.93
9.5
9.0
8.5
8.0
7.5
7.0
6.5
6.0
5.5
5.0
4.5
4.0
3.5
3.0
2.5
2.0
1.5
1.0
0.5
0.
f1 (ppm)

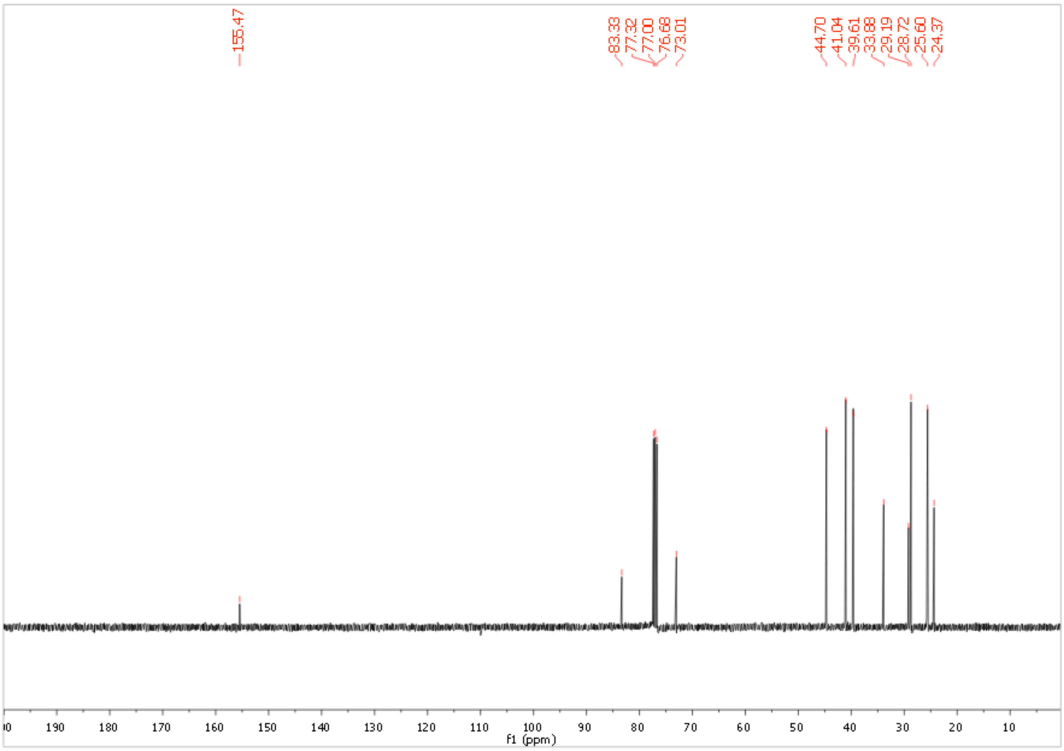
155.47
83.33
77.32
77.00
76.68
73.01
44.70
41.04
39.61
33.88
29.19
28.72
25.60
24.37
190
180
170
160
150
140
130
120
110
100
90
80
70
60
50
40
30
20
10
f1 (ppm)

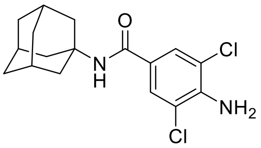
O
N
H
Cl
NH2
Cl

8

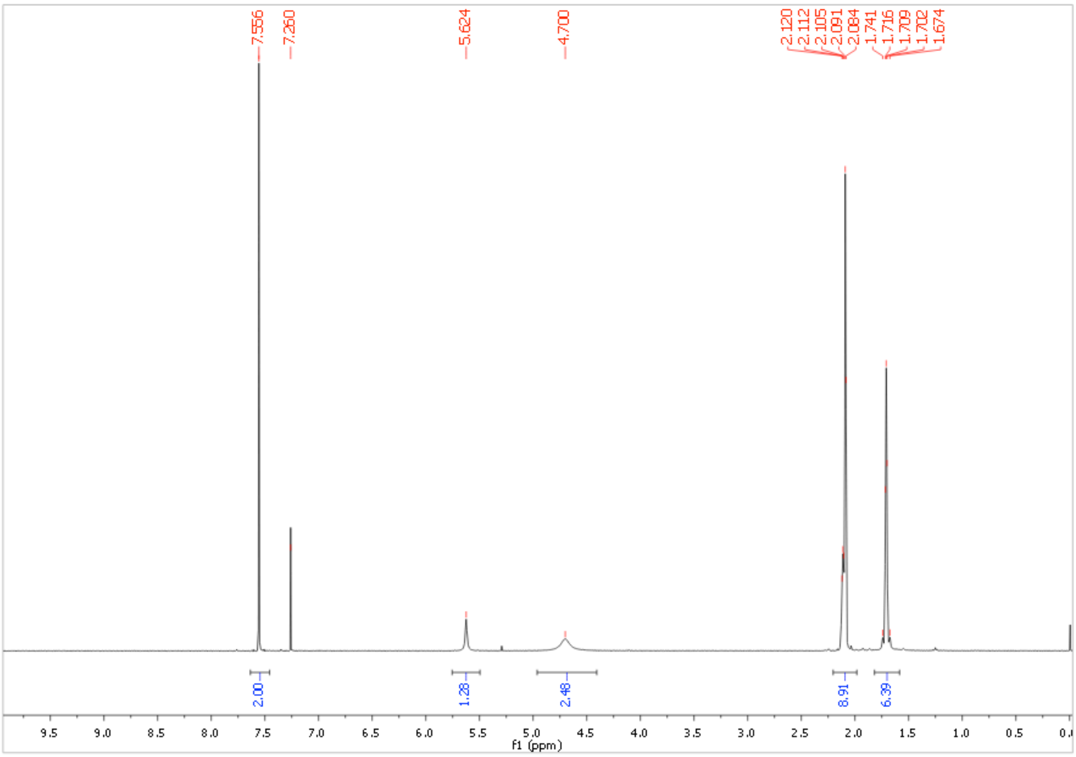
7.556
7.260
5.624
4.700
2.120
2.112
2.105
2.091
2.084
1.741
1.716
1.709
1.702
1.674
2.00
1.28
2.48
8.91
6.39
9.5
9.0
8.5
8.0
7.5
7.0
6.5
6.0
5.5
5.0
4.5
4.0
3.5
3.0
2.5
2.0
1.5
1.0
0.5
0.0
f1 (ppm)

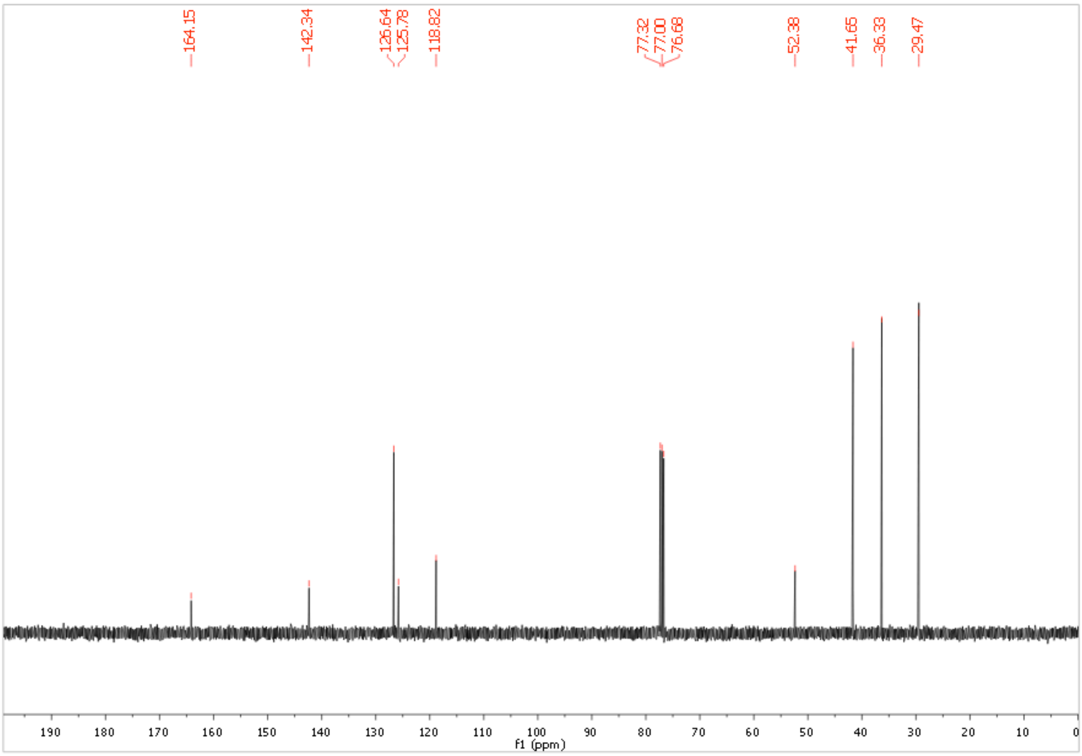
164.15
142.34
126.64
125.78
118.82
77.32
77.00
76.68
52.38
41.65
36.33
29.47
190
180
170
160
150
140
130
120
110
100
90
80
70
60
50
40
30
20
10
0
f1 (ppm)

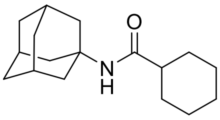
O
N
H

9

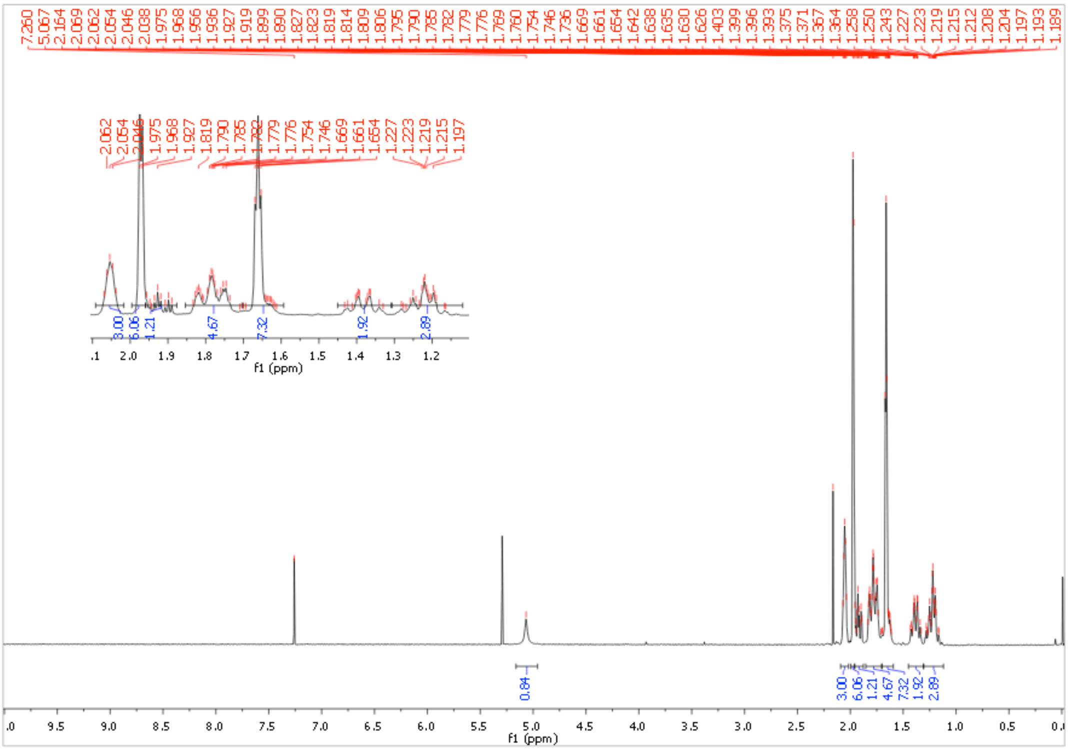
7.260
5.067
2.164
2.069
2.062
2.054
2.046
2.038
1.975
1.968
1.956
1.936
1.927
1.919
1.899
1.890
1.827
1.823
1.819
1.814
1.809
1.806
1.795
1.790
1.785
1.782
1.779
1.776
1.769
1.760
1.754
1.746
1.736
1.669
1.661
1.654
1.642
1.638
1.635
1.630
1.626
1.403
1.399
1.396
1.393
1.375
1.371
1.367
1.364
1.258
1.250
1.243
1.227
1.223
1.219
1.215
1.212
1.208
1.204
1.197
1.193
1.189
2.062
2.054
2.046
1.975
1.968
1.927
1.819
1.790
1.785
1.782
1.779
1.776
1.754
1.746
1.669
1.661
1.654
1.227
1.223
1.219
1.215
1.197
3.00
6.06
1.21
4.67
7.32
1.92
2.89
f1 (ppm)
0.84
3.00
6.06
1.21
4.67
7.32
1.92
2.89
f1 (ppm)

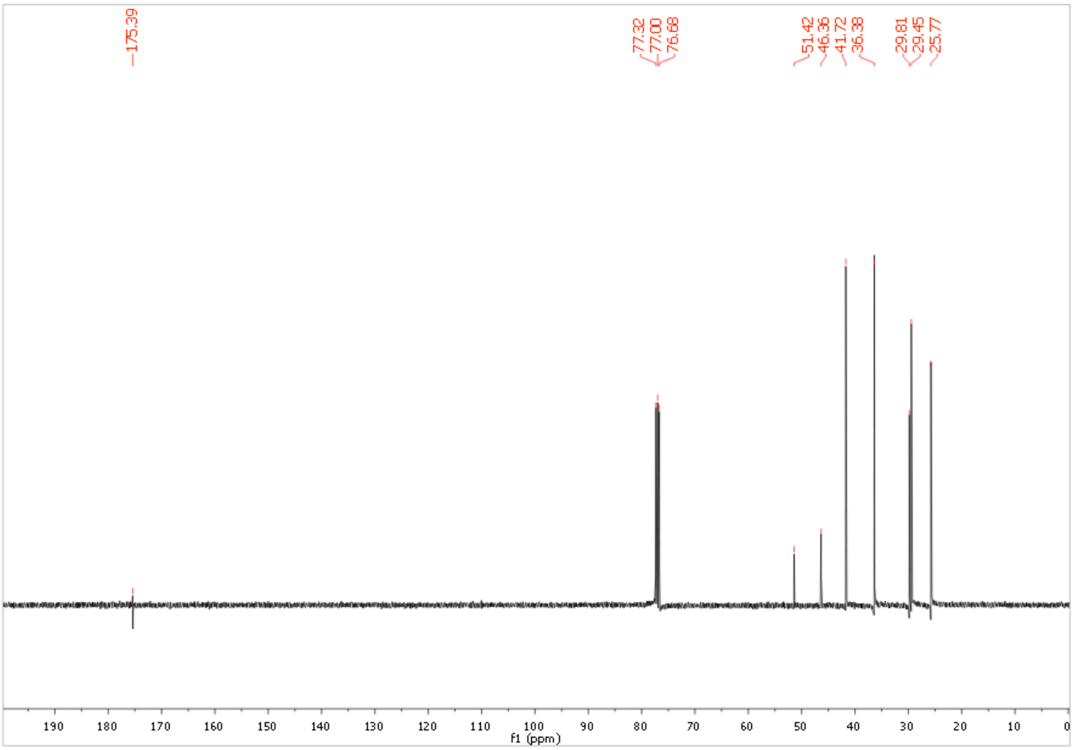
175.39
77.32
77.00
76.68
51.42
46.36
41.72
36.38
29.81
29.45
25.77
190
180
170
160
150
140
130
120
110
100
90
80
70
60
50
40
30
20
10
0
f1 (ppm)

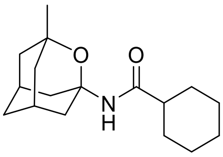
O
O
N
H

10

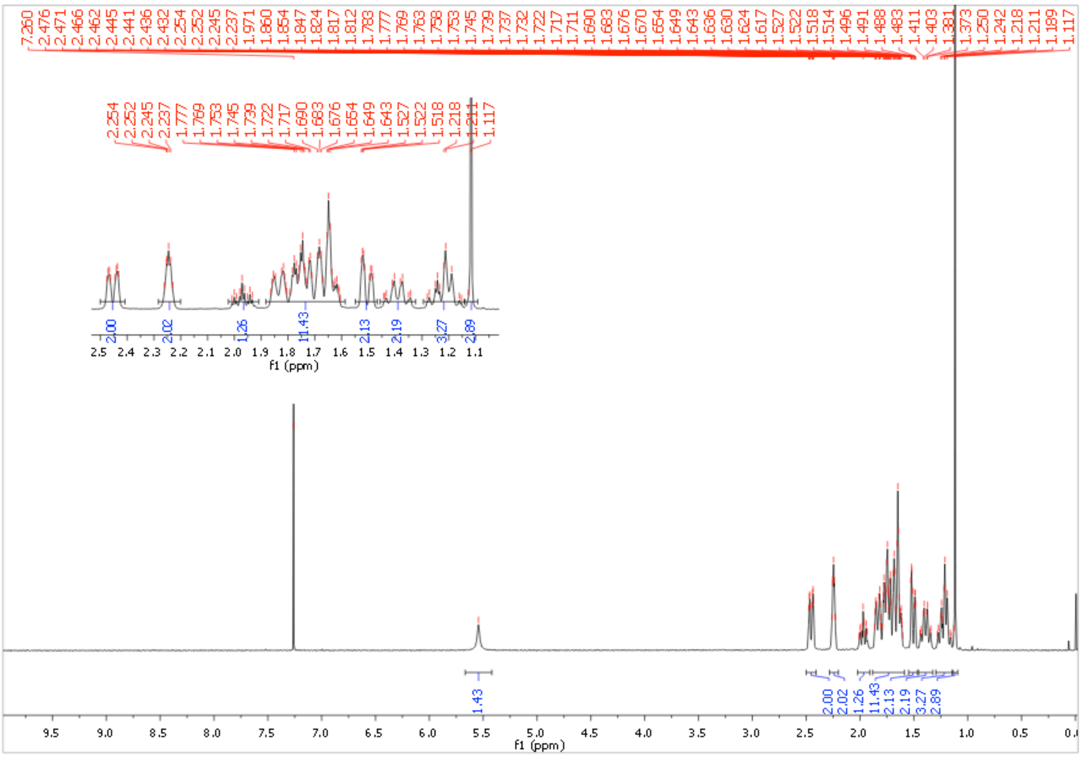
7.260
2.476
2.471
2.466
2.462
2.445
2.441
2.436
2.432
2.254
2.252
2.245
2.237
1.971
1.860
1.854
1.847
1.824
1.817
1.812
1.783
1.777
1.769
1.763
1.758
1.753
1.745
1.739
1.737
1.732
1.722
1.717
1.711
1.690
1.683
1.676
1.670
1.654
1.649
1.643
1.636
1.630
1.624
1.617
1.527
1.522
1.518
1.514
1.496
1.491
1.488
1.483
1.411
1.403
1.381
1.373
1.250
1.242
1.218
1.211
1.189
1.117
2.254
2.252
2.245
2.237
1.777
1.769
1.753
1.745
1.739
1.722
1.717
1.690
1.683
1.676
1.654
1.649
1.643
1.527
1.522
1.518
1.218
1.211
1.117
2.00
2.02
1.26
11.43
2.13
2.19
3.27
2.89
2.5 2.4 2.3 2.2 2.1 2.0 1.9 1.8 1.7 1.6 1.5 1.4 1.3 1.2 1.1
f1 (ppm)
1.43
2.00
2.02
1.26
11.43
2.13
2.19
3.27
2.89
9.5 9.0 8.5 8.0 7.5 7.0 6.5 6.0 5.5 5.0 4.5 4.0 3.5 3.0 2.5 2.0 1.5 1.0 0.5 0.
f1 (ppm)

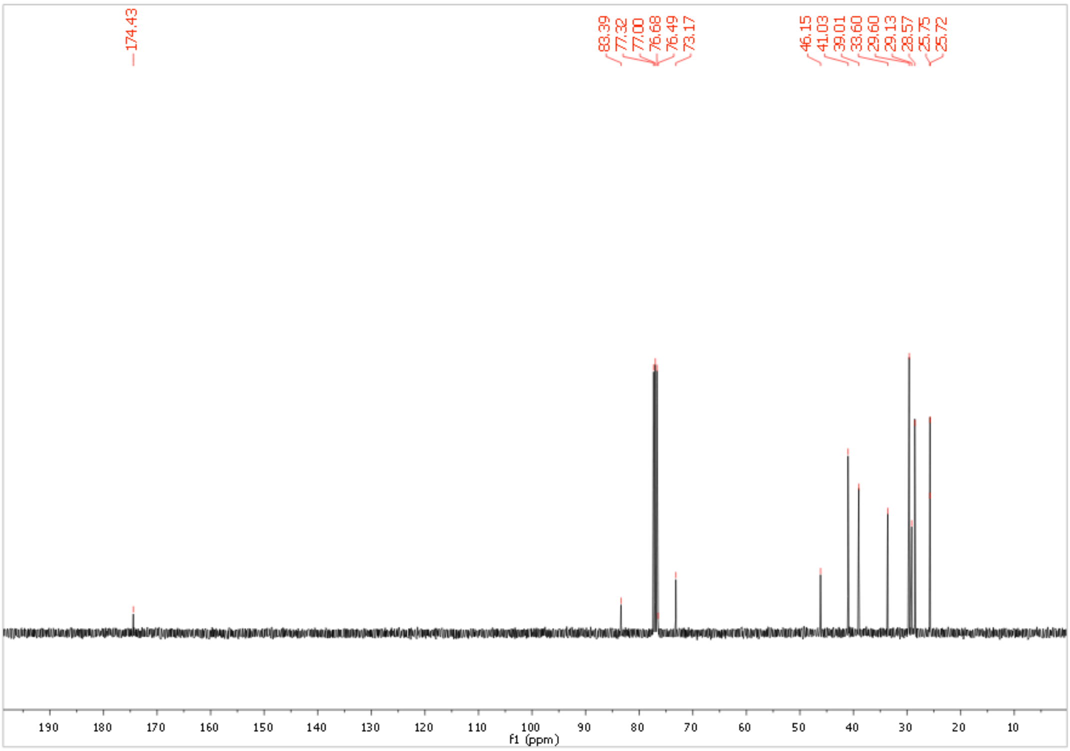
174.43
83.39
77.32
77.00
76.68
76.49
73.17
46.15
41.03
39.01
33.60
29.60
29.13
28.57
25.75
25.72
190 180 170 160 150 140 130 120 110 100 90 80 70 60 50 40 30 20 10
f1 (ppm)

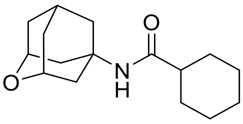

O
N
H
O

11

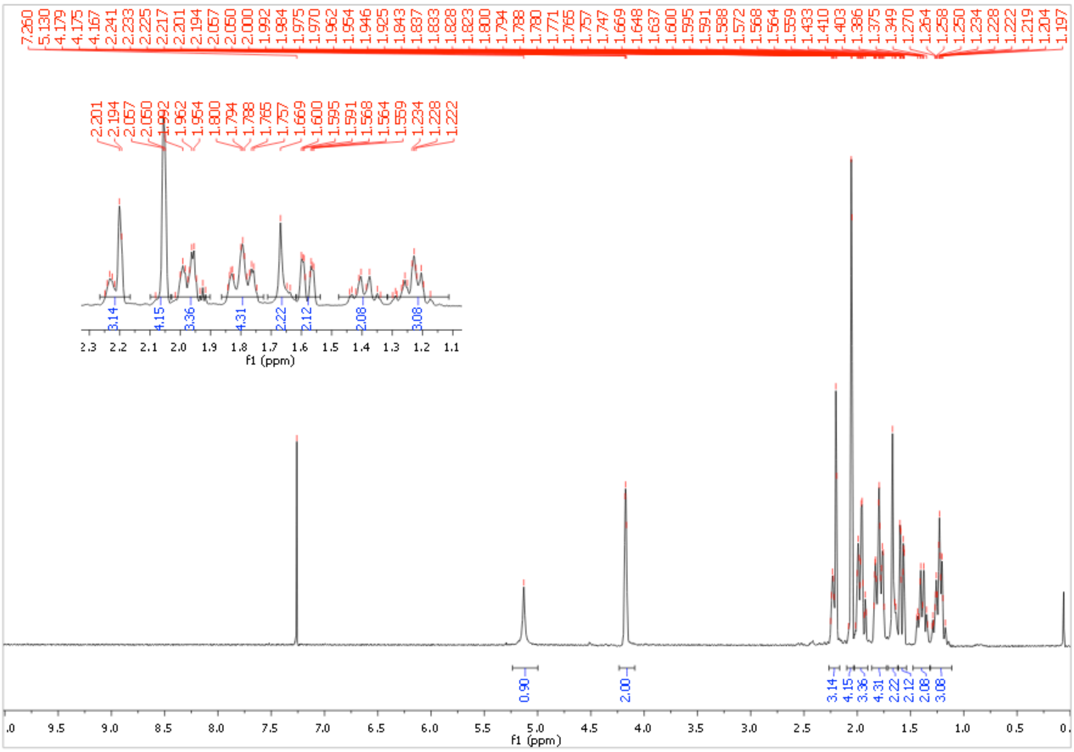

7.260
5.130
4.179
4.175
4.167
2.241
2.233
2.225
2.217
2.201
2.194
2.057
2.050
2.000
1.992
1.984
1.975
1.970
1.962
1.954
1.946
1.925
1.843
1.837
1.833
1.828
1.823
1.800
1.794
1.788
1.780
1.771
1.765
1.757
1.747
1.669
1.648
1.637
1.600
1.595
1.591
1.588
1.572
1.568
1.564
1.559
1.433
1.410
1.403
1.386
1.375
1.349
1.270
1.264
1.258
1.250
1.234
1.228
1.222
1.219
1.204
1.197
2.201
2.194
2.057
2.050
1.992
1.962
1.954
1.800
1.794
1.788
1.765
1.757
1.669
1.600
1.595
1.591
1.568
1.564
1.559
1.234
1.228
1.222
3.14
4.15
3.36
4.31
2.22
2.12
2.08
3.08
2.3 2.2 2.1 2.0 1.9 1.8 1.7 1.6 1.5 1.4 1.3 1.2 1.1
f1 (ppm)
0.90
2.00
3.14
4.15
3.36
4.31
2.22
2.12
2.08
3.08
.0 9.5 9.0 8.5 8.0 7.5 7.0 6.5 6.0 5.5 5.0 4.5 4.0 3.5 3.0 2.5 2.0 1.5 1.0 0.5 0.
f1 (ppm)

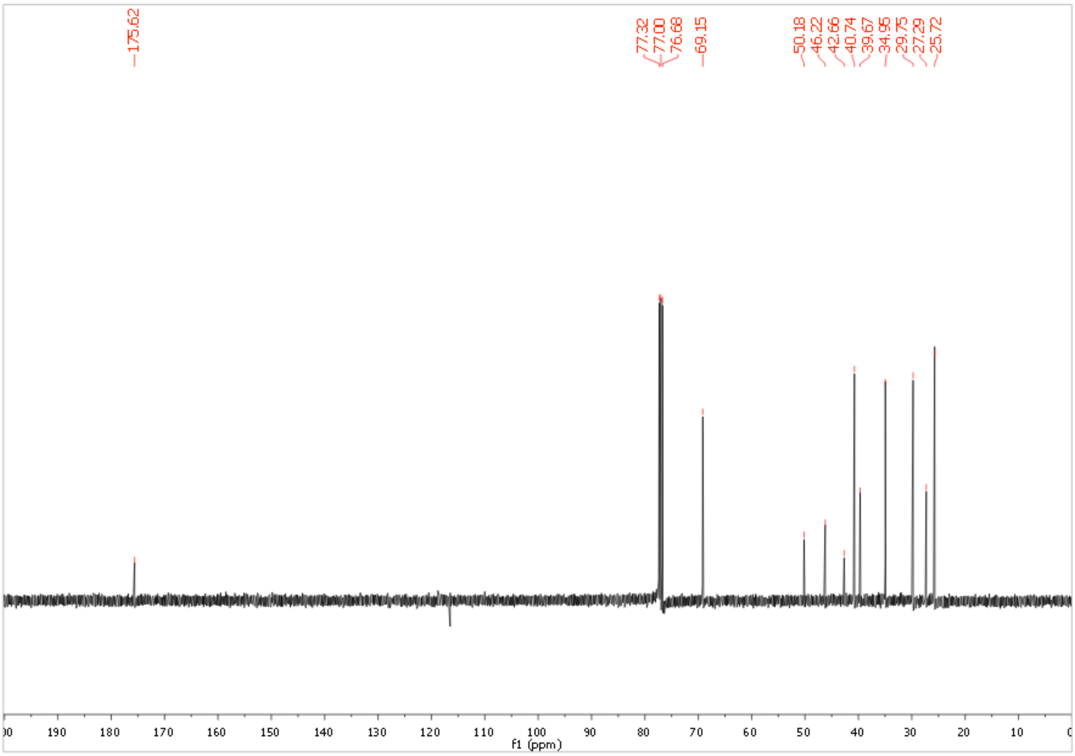

175.62
77.32
77.00
76.68
69.15
50.18
46.22
42.66
40.74
39.67
34.95
29.75
27.29
25.72
00 190 180 170 160 150 140 130 120 110 100 90 80 70 60 50 40 30 20 10 0
f1 (ppm)

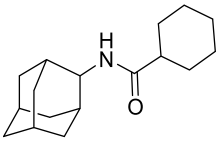
H
N
O

12

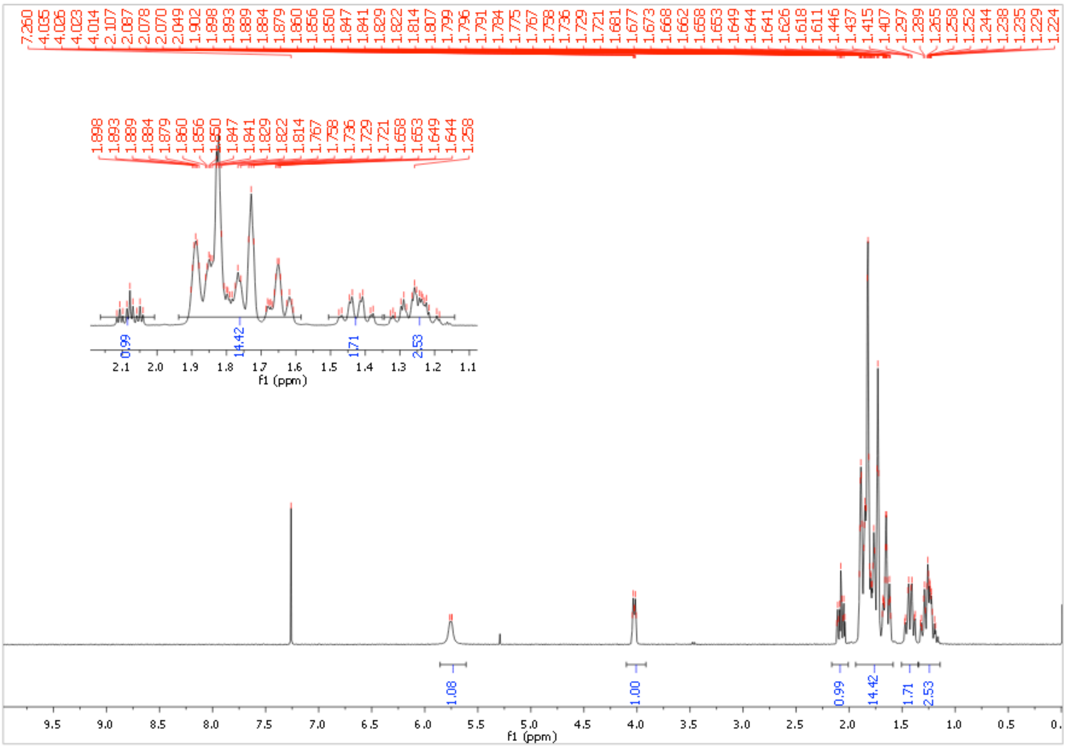
7.260
4.035
4.026
4.023
4.014
2.107
2.087
2.078
2.070
2.049
1.902
1.898
1.893
1.889
1.884
1.879
1.860
1.856
1.850
1.847
1.841
1.829
1.822
1.814
1.807
1.799
1.796
1.791
1.784
1.775
1.767
1.758
1.736
1.729
1.721
1.681
1.677
1.673
1.668
1.662
1.658
1.653
1.649
1.644
1.641
1.626
1.618
1.611
1.446
1.437
1.415
1.407
1.297
1.289
1.265
1.258
1.252
1.244
1.238
1.235
1.229
1.224
1.898
1.893
1.889
1.884
1.879
1.860
1.856
1.850
1.847
1.841
1.829
1.822
1.814
1.767
1.758
1.736
1.729
1.721
1.658
1.653
1.649
1.644
1.258
0.99
14.42
1.71
2.53
2.1
2.0
1.9
1.8
1.7
1.6
1.5
1.4
1.3
1.2
1.1
f1 (ppm)
1.08
1.00
0.99
14.42
1.71
2.53
9.5
9.0
8.5
8.0
7.5
7.0
6.5
6.0
5.5
5.0
4.5
4.0
3.5
3.0
2.5
2.0
1.5
1.0
0.5
0.
f1 (ppm)

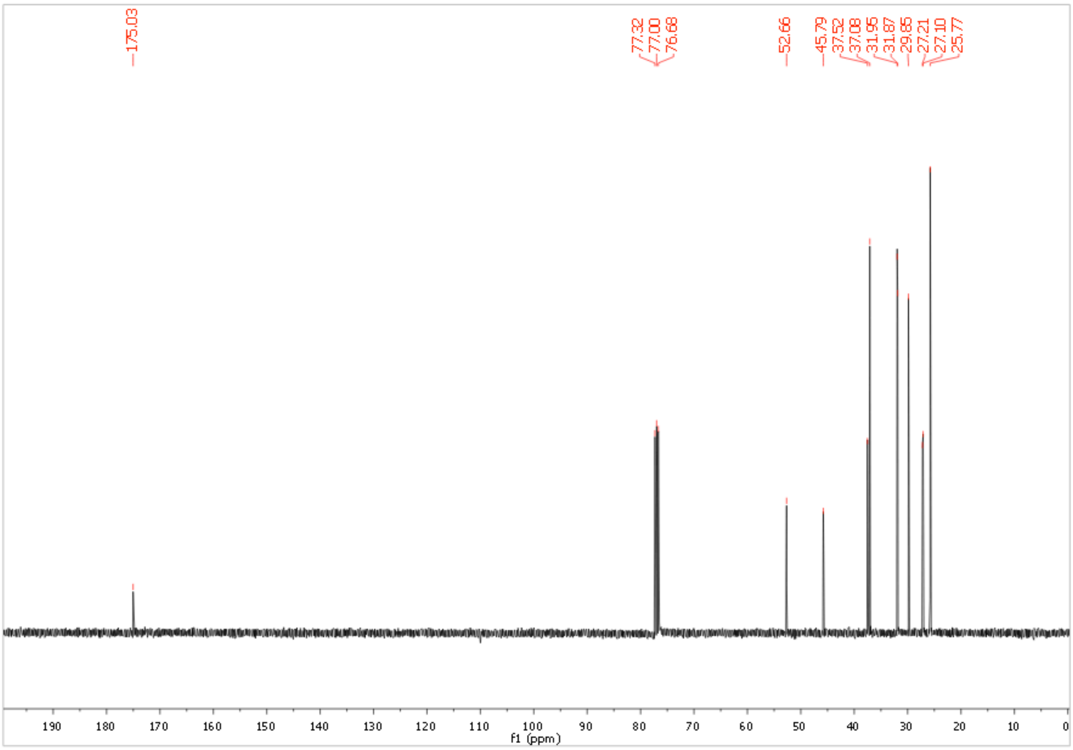
175.03
77.32
77.00
76.68
52.66
45.79
37.52
37.08
31.95
31.87
29.85
27.21
27.10
25.77
190
180
170
160
150
140
130
120
110
100
90
80
70
60
50
40
30
20
10
0
f1 (ppm)

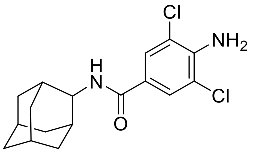
Cl
NH2
H
N
O
Cl

13

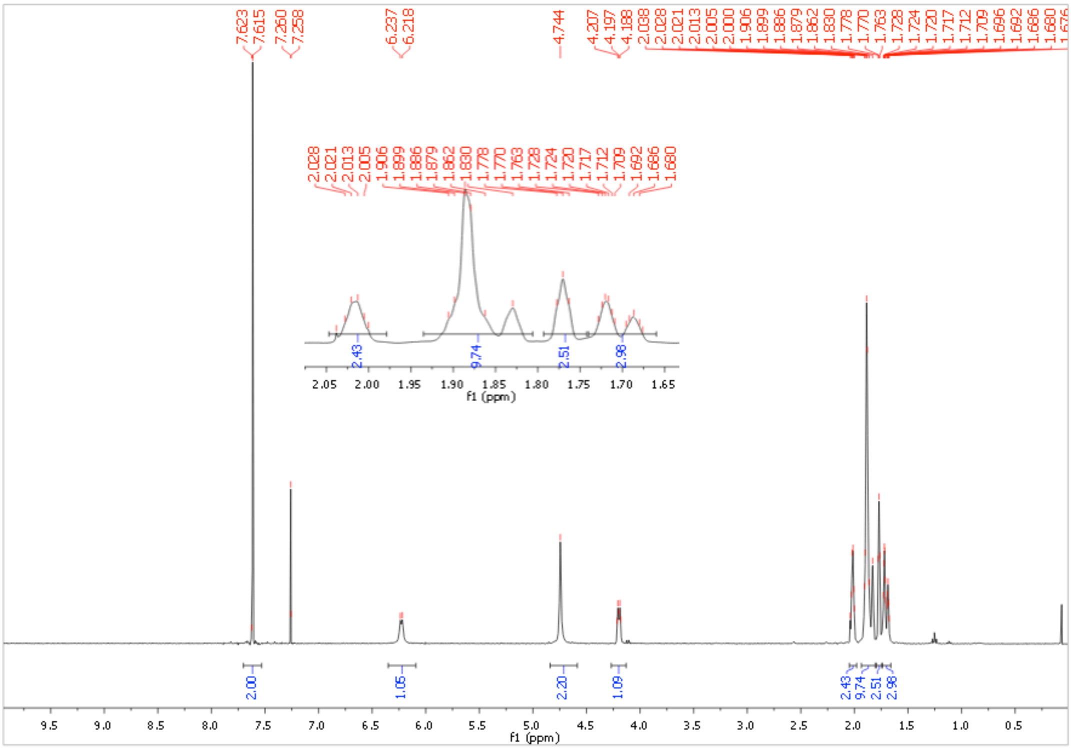
7.623
7.615
7.260
7.258
6.237
6.218
4.744
4.207
4.197
4.188
2.038
2.028
2.021
2.013
2.005
2.000
1.906
1.899
1.886
1.879
1.862
1.830
1.778
1.770
1.763
1.728
1.724
1.720
1.717
1.712
1.709
1.696
1.692
1.686
1.680
1.676
2.028
2.021
2.013
2.005
1.906
1.899
1.886
1.879
1.862
1.830
1.778
1.770
1.763
1.728
1.724
1.720
1.717
1.712
1.709
1.692
1.686
1.680
2.43
9.74
2.51
2.98
2.05
2.00
1.95
1.90
1.85
1.80
1.75
1.70
1.65
f1 (ppm)
2.00
1.05
2.20
1.09
2.43
9.74
2.51
2.98
9.5
9.0
8.5
8.0
7.5
7.0
6.5
6.0
5.5
5.0
4.5
4.0
3.5
3.0
2.5
2.0
1.5
1.0
0.5
f1 (ppm)

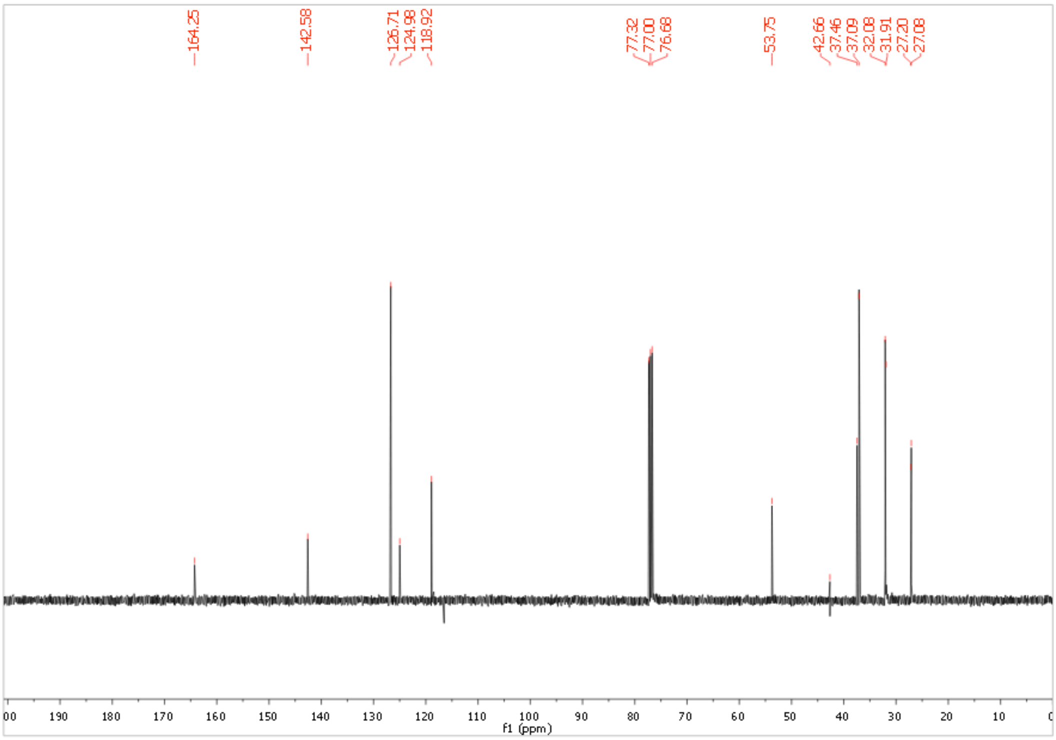
164.25
142.58
126.71
124.98
118.92
77.32
77.00
76.68
53.75
42.66
37.46
37.09
32.08
31.91
27.20
27.08
190
180
170
160
150
140
130
120
110
100
90
80
70
60
50
40
30
20
10
f1 (ppm)

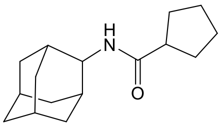
H
N
O

14

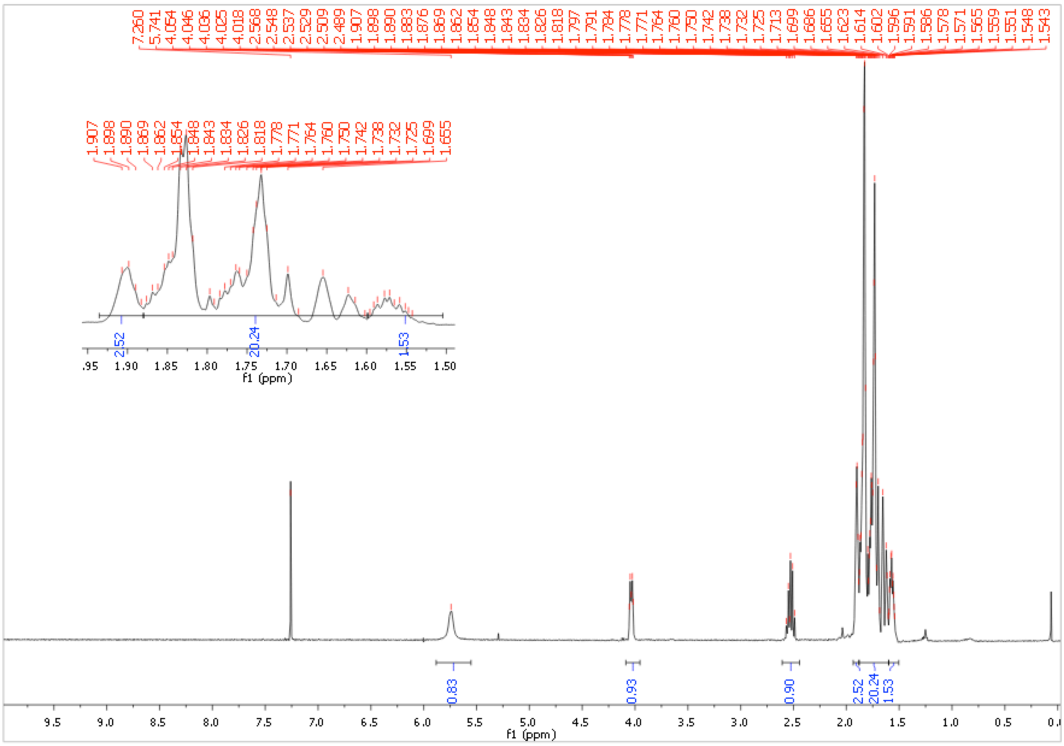
7.260
5.741
4.054
4.046
4.036
4.025
4.018
2.568
2.548
2.537
2.529
2.509
2.489
1.907
1.898
1.890
1.883
1.876
1.869
1.862
1.854
1.848
1.843
1.834
1.826
1.818
1.797
1.791
1.784
1.778
1.771
1.764
1.760
1.750
1.742
1.738
1.732
1.725
1.713
1.699
1.686
1.655
1.623
1.614
1.602
1.596
1.591
1.586
1.578
1.571
1.565
1.559
1.551
1.548
1.543
1.907
1.898
1.890
1.869
1.862
1.854
1.848
1.843
1.834
1.826
1.818
1.778
1.771
1.764
1.760
1.750
1.742
1.738
1.732
1.725
1.699
1.655
2.52
20.24
1.53
.95
1.90
1.85
1.80
1.75
1.70
1.65
1.60
1.55
1.50
f1 (ppm)
0.83
0.93
0.90
2.52
20.24
1.53
9.5
9.0
8.5
8.0
7.5
7.0
6.5
6.0
5.5
5.0
4.5
4.0
3.5
3.0
2.5
2.0
1.5
1.0
0.5
0.
f1 (ppm)

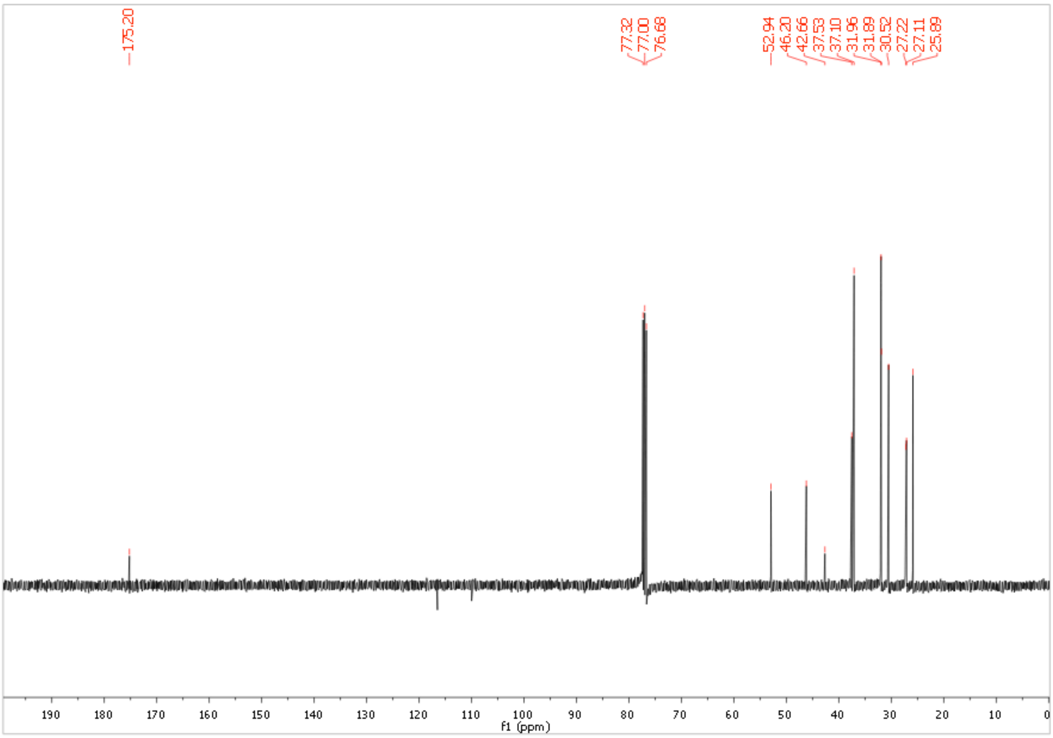
175.20
77.32
77.00
76.68
52.94
46.20
42.66
37.53
37.10
31.96
31.89
30.52
27.22
27.11
25.89
190
180
170
160
150
140
130
120
110
100
90
80
70
60
50
40
30
20
10
0
f1 (ppm)

3.1.3 Artículo 3: *Design, synthesis and in vivo study of novel pyrrolidine-based 11β-HSD1 inhibitors for age-related cognitive dysfunction*

Resumen

Los hallazgos recientes sugieren que el tratamiento con inhibidores de la 11β-HSD1 proporciona un enfoque novedoso para tratar las disfunciones cognitivas relacionadas con la edad, incluida la enfermedad de Alzheimer. En este trabajo, se comparan diferentes inhibidores potentes de 11β-HSD1 que presentan sustituyentes policíclicos basados en pirrolidina sin explorar. Un candidato seleccionado administrado a ratones SAMP8 de 12 meses de edad durante cuatro semanas evitó los déficits de memoria y mostró una acción neuroprotectora. Esta es la primera vez que se han estudiado los inhibidores de 11β-HSD1 en este modelo de ratón ampliamente utilizado de senescencia acelerada y enfermedad de Alzheimer de inicio tardío.

European Journal of Medicinal Chemistry 139 (2017) 412–428

Contents lists available at ScienceDirect

European Journal of Medicinal Chemistry

journal homepage: http://www.elsevier.com/locate/ejmech

Research paper

Design, synthesis and *in vivo* study of novel pyrrolidine-based 11β-HSD1 inhibitors for age-related cognitive dysfunction

Rosana Leiva [a], Christian Griñan-Ferré [b, c], Constantí Seira [d], Elena Valverde [a], Andrew McBride [e], Margaret Binnie [e], Belén Pérez [f], F. Javier Luque [d], Mercè Pallàs [b, c], Axel Bidon-Chanal [d], Scott P. Webster [e, *], Santiago Vázquez [a, **]

[a] *Laboratori de Química Farmacèutica (Unitat Associada al CSIC), Facultat de Farmàcia i Cienciès de l'Alimentació, and Institute of Biomedicine (IBUB), Universitat de Barcelona, Av. Joan XXIII 27-31, Barcelona E-08028, Spain*
[b] *Unitat de Farmacologia, Farmacognòsia i Terapèutica, Facultat de Farmàcia i Ciències de l'Alimentació i Institut de Neurociències, Universitat de Barcelona, Av. Joan XXIII, 27-31, 08028 Barcelona, Spain*
[c] *Biomedical Research Networking Center in Neurodegenerative Diseases (CIBERNED), Madrid, Spain*
[d] *Department of Nutrition, Food Science and Gastronomy, Faculty of Pharmacy and Institute of Biomedicine (IBUB), Universitat de Barcelona, Av. Prat de la Riba 171, Santa Coloma de Gramenet E-08921, Spain*
[e] *Centre for Cardiovascular Science, University of Edinburgh, Queen's Medical Research Institute, EH16 4TJ, United Kingdom*
[f] *Departament de Farmacologia, Terapèutica i Toxicologia, Universitat Autònoma de Barcelona, Bellaterra, Barcelona 08193, Spain*

ARTICLE INFO

Article history:
Received 25 June 2017
Received in revised form
30 July 2017
Accepted 2 August 2017
Available online 4 August 2017

Keywords:
Glucocorticoids
11β-HSD1 inhibitors
Drug design
Adamantane
Polycyclic substituents
Aged-related cognitive dysfunction
Alzheimer's disease
SAMP8 mouse

ABSTRACT

Recent findings suggest that treatment with 11β-HSD1 inhibitors provides a novel approach to deal with age-related cognitive dysfunctions, including Alzheimer's disease. In this work we report potent 11β-HSD1 inhibitors featuring unexplored pyrrolidine-based polycyclic substituents. A selected candidate administered to 12-month-old SAMP8 mice for four weeks prevented memory deficits and displayed a neuroprotective action. This is the first time that 11β-HSD1 inhibitors have been studied in this broadly-used mouse model of accelerated senescence and late-onset Alzheimer's disease.

© 2017 Elsevier Masson SAS. All rights reserved.

1. Introduction

Elevated glucocorticoids (GCs) exposure is widely accepted as a key factor in age-related cognitive decline in rodents and humans [1–3]. High levels of GCs have been found in elderly individuals who exhibit learning and memory impairments. GC levels correlate with greater hippocampal atrophy, a region of the brain that is crucial for memory formation [3]. In contrast, low GC levels achieved through neonatal programming or adrenalectomy with exogenous steroid replacement in rats results in the prevention of memory impairments with aging [4].

Growing evidence also suggests that excessive glucocorticoid activity may contribute to Alzheimer's disease (AD), since elevated levels of circulating cortisol in AD patients are associated with more rapid disease progression [5,6]. In a rodent model of AD, systemic administration of GCs led to increases in β-amyloid and tau pathology, the two major histopathologic hallmarks of AD, suggesting a relationship between elevated GC levels and AD pathology [7]. Overall, these data suggest that reducing GC levels in the brain may relieve cognitive dysfunction in both aging and AD.

As in other tissues, the presence of GCs in the brain is not only dependent on adrenal secretion and diffusion from the circulation but also on intracellular metabolism [8]. 11β-hydroxysteroid

---

* Corresponding author.
** Corresponding author.
E-mail addresses: scott.webster@ed.ac.uk (S.P. Webster), svazquez@ub.edu (S. Vázquez).

http://dx.doi.org/10.1016/j.ejmech.2017.08.003
0223-5234/© 2017 Elsevier Masson SAS. All rights reserved.

dehydrogenase type 1 (11β-HSD1) catalyzes the regeneration of active GCs (cortisol in humans, corticosterone in rodents) from their inactive forms (cortisone and 11-dehydrocorticosterone, respectively), providing a local amplification of GC action [9,10]. 11β-HSD1 is highly expressed in fundamental brain areas for cognition, such as the hippocampus, cortex and amygdala [11–13]. By contrast, the isoenzyme 11β-hydroxysteroid dehydrogenase type 2 (11β-HSD2), which catalyzes the opposite reaction, plays an important role during development, as expression of 11β-HSD2 is relevant in fetal brain and placenta, but it has very limited expression in the adult brain [14–16].

Recent studies have demonstrated that aged mice with cognitive deficits show increased 11β-HSD1 expression in the hippocampus and forebrain, and that overexpression of 11β-HSD1 leads to a similar premature memory decline [17]. Conversely, 11β-HSD1 knock-out mice and even heterozygous null mice performed better in different behavioural tests, which suggests resistance to cognitive decline due to a neuroprotective effect of 11β-HSD1 inhibition [18]. Accordingly, this protection correlates with loss of the age-associated rise in intrahippocampal corticosterone, insinuating a role for 11β-HSD1 in maintaining plasma corticosterone concentration [17]. Furthermore, acute and short-term treatments with 11β-HSD1 inhibitors have shown memory consolidation and improvements in cognitive function in aged mice and AD models [19–23]. Altogether, these findings suggest that 11β-HSD1 inhibitors provide a novel approach through a non-cholinergic mechanism to deal with these cognitive disorders.

In the present work, we report the results derived from a synthetic strategy, supported by molecular modeling studies, designed towards a novel family of potent 11β-HSD1 inhibitors, featuring unexplored pyrrolidine-based polycyclic substituents. The more potent compounds were characterized in terms of cellular potency, isoenzyme selectivity, human metabolic stability and predicted brain penetration to select a candidate for an *in vivo* study. For the first time in the context of 11β-HSD1 inhibitors, the Senescence Accelerated Mouse-Prone 8 (SAMP8) mice were used, as a naturally occurring mouse strain that displays a phenotype of accelerated aging as observed in AD and widely used as a robust rodent model of cognitive dysfunction [24,25].

2. Design, synthesis and *in vitro* evaluation of new inhibitors

Given that the 11β-HSD1 active site includes a hydrophobic pocket that can accommodate bulky lipophilic substituents, the introduction of a lipophilic group, such as adamantyl, has proven a successful strategy for the space filling of the cavity. Thus, several adamantyl-containing 11β-HSD1 inhibitors exhibit high affinity and potency and some of them (e.g. AZD8329 and ABT-384) have reached clinical trials (Fig. 1) [26–34]. Although the evaluation of alternative polycyclic hydrocarbons may offer further opportunities for optimizing the space filling of the hydrophobic cavity, the use of other polycyclic substituents featuring different size or shape has only been briefly scrutinized (e.g. AMG-221 and MK-0736) [35,36].

In the last few years, our research group has investigated new polycyclic substituents as surrogates of the adamantyl group, leading to inhibitors with promising results on multiple targets [37–45]. However, this strategy has not been successful yet in the case of human 11β-HSD1 inhibitors [46]. Very recently, we have found that the *N*-(2-adamantyl)amide derivatives **1** and **2** (Fig. 2), which are achiral analogues of PF-877423 (IC_{50} = 4 nM) [47], are potent inhibitors of 11β-HSD1 (IC_{50} = 86 and 74 nM, respectively) [48]. Interestingly, the corresponding urea analogue, **3**, was significantly less potent (IC_{50} = 873 nM) [48]. Taking into account the simplicity of these three right-hand side (RHS) units, here we initially selected these fragments for finding alternative polycyclic substituents able to successfully replace the adamantyl group in 11β-HSD1 inhibitors.

The design of new inhibitors was initially based on a structure-activity relationship (SAR) investigation we previously adopted [46]. The structure of the putative inhibitor was partitioned into two parts: the polycyclic substituent, a surrogate of adamantyl, and the carbocyclic or heterocyclic ring, linked by an amido or urea unit,

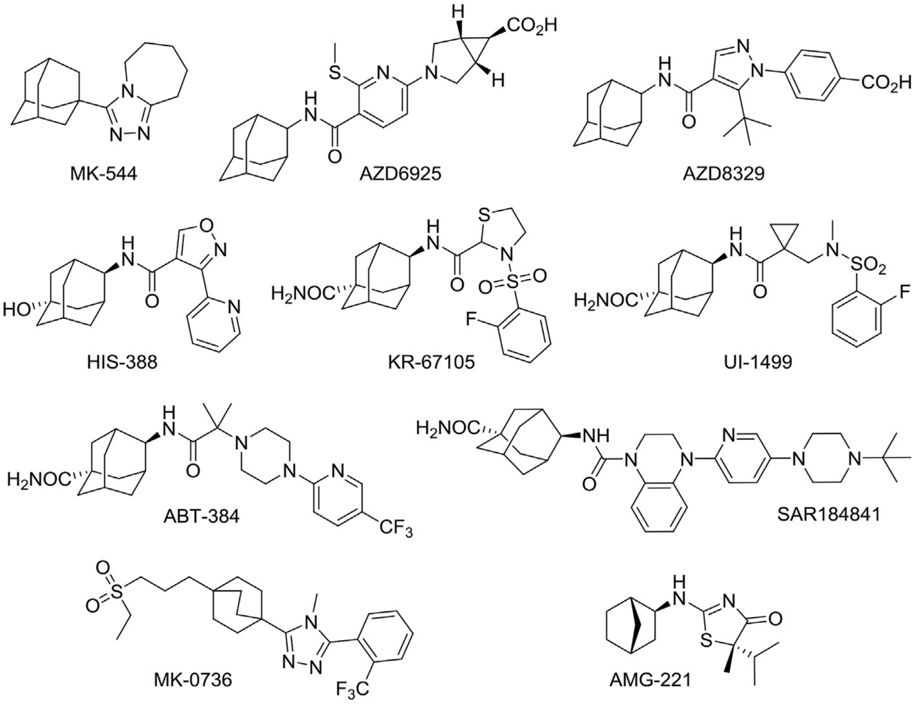

Fig. 1. Selected 11β-HSD1 inhibitors.

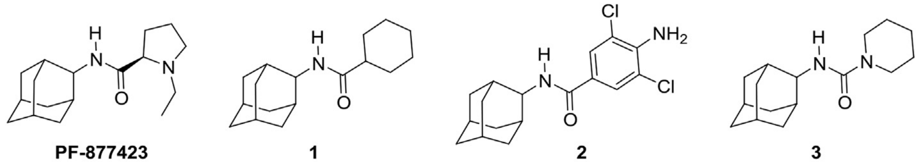

PF-877423 IC_{50} = 4 nM

1 IC_{50} = 86 nM

2 IC_{50} = 74 nM

3 IC_{50} = 873 nM

Fig. 2. PF-877423 and related inhibitors.

respectively. Since inspection of the available X-ray structures and preliminary docking studies (see below) indicated that the enzyme active site is large enough to accommodate a polycycle bigger than adamantane, we started our endeavour with previously synthesized amines **4**, **5** and **10**, three compounds that were successfully used to replace 1-adamantylamine in other targets (Scheme 1) [38]. These amines were then combined with a common RHS moiety to shed light on the effect of key structural features on the inhibitory action: i) primary *vs* secondary amine (e.g. **4** *vs* **10**), ii) distance between the polycyclic ring and the nitrogen atom (e.g. **4** *vs* **5**), iii) restraint of the conformational freedom (e.g. **5** *vs* **10**), and iv) by incorporating two double bonds in the polycycle, which might form additional interactions in the binding site (e.g. derivatives of **10** *vs* its reduced analogues). Amides **6** and **7** were prepared in high yields by reaction of cyclohexane acyl chloride with amines **4** and **5**, respectively. From amine **10**, using either cyclohexanecarboxylic acid or 4-amino-3,5-dichlorobenzoic acid in combination with 1-hydroxybenzotriazole (HOBt) and *N*-(3-dimethylaminopropyl)-*N′*-ethylcarbodiimide (EDC) amides **11** and **15** were synthesized in moderate yields. Ureas **8**, **9** and **13** were prepared from the required amine and *N*-chloroformylpiperidine in moderate to excellent yields. Finally, catalytic hydrogenation of **11**, **13** and **15** furnished **12**, **14** and **16**, respectively (Scheme 1).

A preliminary *in vitro* microsomal assay at 10 μM compound concentration was performed to assess if the synthesized compounds were able to inhibit human 11β-HSD1, and the IC_{50} values were determined for those compounds presenting an inhibition higher than 50% (Table 1).

The analysis of the inhibitory potencies disclosed some SAR. First, while amides **6** and **7** displayed poor inhibitory activity, derivatives **11** and **12**, featuring a pyrrolidine ring, showed low micromolar and submicromolar potency, respectively, reflecting a better fit within the hydrophobic pocket of the binding site. Second, replacement of the cyclohexyl ring of **12** by either a 1-piperidinyl substituent, as in **14**, or a 4-amino-3,5-dichlorophenyl group, as in **16**, retained the activity, further demonstrating that the adamantyl substituent may be replaced by other polycyclic groups. Third, no significant difference was found between the inhibitory

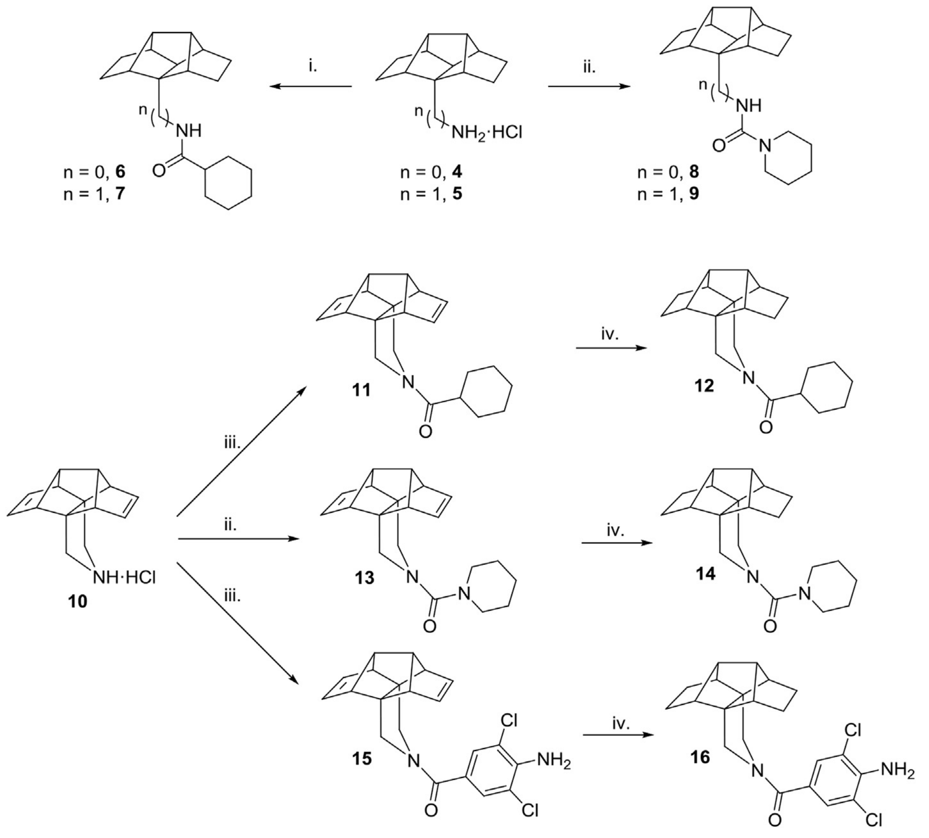

Scheme 1. Amines 4, 5 and 10, and amides and ureas derived thereof.

Reagents and conditions: (i) cyclohexanecarbonyl chloride, anh. acetone, reflux, 3 h, 95% yield for **6**; 78% yield for **7**; (ii) 1-piperidinecarbonyl chloride, Et_3N, DCM, rt, overnight, 54% yield for **8**; quant yield for **9**; 71% for **13**; (iii) cyclohexanecarboxylic acid for **11** or 4-amino-3,5-dichlorobenzoic acid for **15**, HOBt, EDC, Et_3N, EtOAc, rt, overnight, 42% yield for **11**; 47% yield for **15**; (iv) H_2, Pd/C, abs. EtOH, rt, 5 h for **12** and **16**, 3 h for **14**, 78% yield for **12**; 72% yield for **14**; 89% yield for **16**.

Table 1
11β-HSD1 inhibition by compounds **6**–**9**, **11**, **12** and **14**–**16**.[a,b]

Compound	hHSD1% inh at 10 μM	hHSD1 IC_{50} (μM)
6	41	ND
7	28	ND
8	50	ND
9	50	ND
11	95	1.08
12	100	0.29
14	100	0.32
15	98	2.77
16	98	0.41

[a] 11β-HSD1 inhibition was determined in mixed sex, human liver microsomes (Celsis In-vitro Technologies) by measuring the conversion of ^{3}H-cortisone to ^{3}H-cortisol in a cortisol-scintillation proximity assay.

[b] Percentage inhibition was determined relative to a control system in the absence of inhibitor (see Experimental section for further details). ND, not determined.

activity of **12** and **14**, and hence the replacement of the amide bridge by a urea within this particular polycycle does not seem to affect the potency. Finally, saturated hexacyclic pyrrolidines were more potent than their diene analogues (compare **12** *vs* **11** and **16** *vs* **15**). Overall, aliphatic amides **11** and **12** were slightly more potent than aromatic amides **15** and **16** (compare **11** *vs* **15** and **12** *vs* **16**).

Docking studies were combined with molecular dynamics (MD) simulations to shed light into the inhibitory potencies of selected compounds. The structural integrity of the simulated systems was supported by the stability of the positional root-mean square deviation of the residues that define the binding site and the ligand, especially for the most potent compounds (see Figs. S1-S3 in the Supplementary data file). A similar binding mode was found for compounds **8**, **12** and **14** (see Fig. 3). In all cases the carbonyl group of the ligand formed a stable hydrogen bond with Ser170 (distances ranging from 2.6 to 3.0 Å). However, the hydrogen bond of the ligand's carbonyl group with the hydroxyl group of Tyr183, which was retained during the setup of the simulated systems, exhibited larger fluctuations and was eventually disrupted during the trajectories. Docking calculations showed compounds **12** and **14** to have slightly better scores (−9.3 and −9.7 kcal/mol, respectively) than **6** (−8.4 kcal/mol) and **8** (−9.0 kcal/mol). The higher inhibitory potency of **12** and **14** may also be explained by the fused pyrrolidine ring, which should reduce the contribution of the conformational penalty to the binding affinity of these compounds compared to the more flexible compounds **6** and **8**. Although the results appear to support the ability of the size-expanded hydrophobic cage present in **12** and **14** to occupy the binding pocket, the lower inhibitory potency compared to **1** ($IC_{50} = 86$ nM; Fig. 2) suggests that the size of the polycyclic substituent in **12** and **14** may be close to the upper limit allowed for ligand binding without triggering significant structural distortions in the pocket.

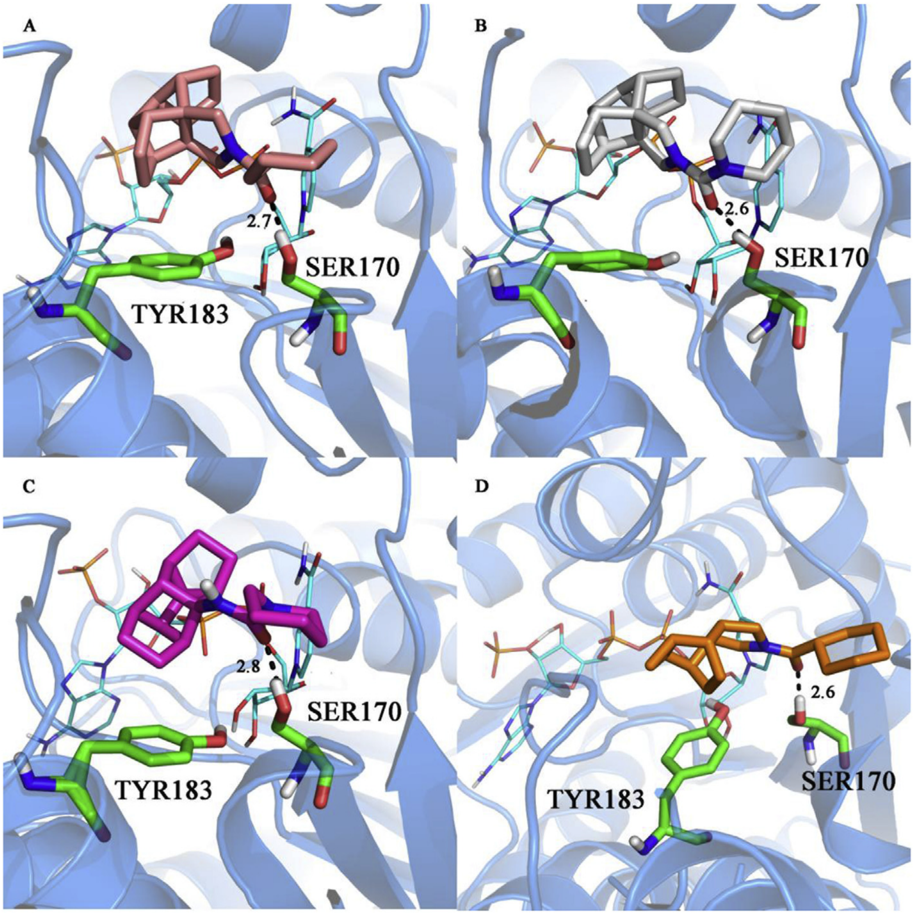

Fig. 3. Representative snapshot of the binding mode of compounds **12** (A), **14** (B), **8** (C), and **23** (D) to the human 11β-HSD1 enzyme as determined from the analysis of the MD simulations. The protein backbone is shown as blue carton, the NADP cofactor, residues Tyr183 and Ser170, and the ligands are shown as atom-coloured sticks. The hydrogen bond between the ligand and the hydroxyl group of Ser170 is shown as a dashed line. (For interpretation of the references to colour in this figure legend, the reader is referred to the web version of this article.)

Of note, the *N*-acylpyrrolidine motif contained in **11**, **12**, **15** and **16** has scarcely been explored in the context of the design of 11β-HSD1 inhibitors [49]. However, the pyrrolidine **10** is not an ideal starting compound for a medicinal chemistry program, as its synthesis is tedious and very low-yielding [38]. For this reason, we explored the synthesis of alternative, easily synthesized, pyrrolidine derivatives. To this end, we followed a polycyclic substituent optimization process in which the cyclohexyl was selected as the RHS of the molecule, due to its simplicity (i.e. achiral, easy access) and good performance with both adamantyl (**1**, $IC_{50} = 0.09$ μM) and hexacyclic substituents (**12**, $IC_{50} = 0.29$ μM). An array of 13 pyrrolidine-based polycyclic amides was prepared from cyclohexanecarboxylic acid, HOBt, EDC, and a series of previously synthesized amines (Fig. 4). Our aim was to obtain different pyrrolidine-based polycyclic compounds, some of them simplified analogues of the hexacyclic unit contained in **10** but with higher conformational freedom, in order to find the optimal size and shape to deliver more potent 11β-HSD1 inhibitors.

Following the aforementioned preliminary *in vitro* microsomal assay, the IC_{50} values were determined for compounds with an inhibitory activity higher than 50% at 10 μM (Table 2). In general, compounds containing smaller polycyclic rings (i.e. **17**–**23**) were one order of magnitude more potent than our initially best inhibitors **12**, **14** and **16**, and some of them were also more potent than the adamantyl derivative **1** ($IC_{50} = 0.09$ μM). The most potent inhibitors were **18**, **20**, **21**, **22** and **23** (IC_{50} values ranging from 0.02 to 0.03 μM). MD simulations of the enzyme complex with compound **23** confirmed the stability of the binding mode (see Fig. 3D and Fig. S4), which resembled the arrangement of compound **12**, and the formation of the hydrogen-bond interaction with Ser170 (average distance of 2.8 ± 0.3 Å). However, there was not a clear trend in terms of activity between the alkene/alkane pairs containing the same polycyclic ring system (compare **20** *vs* **21**, and **22** *vs* **23**). Thus, in the pair **18**/**19** the alkene derivative presented a slightly higher potency, but the bigger alkene derivatives **24** and **26** were significantly more potent than their alkane analogues **25** and **27** (IC_{50} = 1.49 μM *vs* 27% inhibition at 10 μM, and 0.04 μM *vs* 1.22 μM, respectively). Finally, the introduction of four methyl groups, either in an extended (**28**) or compact (**29**) arrangement, was highly deleterious to the inhibitory activity (compare **26** *vs* **28** and **29**). Overall, these findings reinforce the assumption that the hexacyclic substituent reaches the upper-limit size to fill the hydrophobic pocket of the binding site.

Table 2
11β-HSD1 inhibition by compounds **17**–**29**.[a,b]

Compound	hHSD1% inh at 10 μM	hHSD1 IC_{50} (μM)
17	85	0.05
18	89	0.02
19	92	0.09
20	96	0.03
21	95	0.02
22	100	0.02
23	100	0.03
24	83	1.49
25	27	ND
26	82	0.04
27	67	1.22
28	30	ND
29	42	ND

[a] 11β-HSD1 inhibition was determined in mixed sex, Human Liver Microsomes (Celsis In-vitro Technologies) by measuring the conversion of ^{3}H-cortisone to ^{3}H-cortisol in a cortisol-Scintillation Proximity Assay.

[b] Percentage inhibition was determined relative to a no inhibitor control (see Experimental section for further details). ND, not determined.

3. Biological profiling of the more potent 11β-HSD1 inhibitors

The more potent inhibitors obtained by this polycyclic substituent optimization process have clogP values between 2.68 and 3.99, more desirable than that of the adamantyl-containing analogue **1** (clogP = 4.65). These new compounds were characterized in terms of cellular potency, selectivity over 11β-HSD2, human metabolic stability and predicted brain permeability, in order to

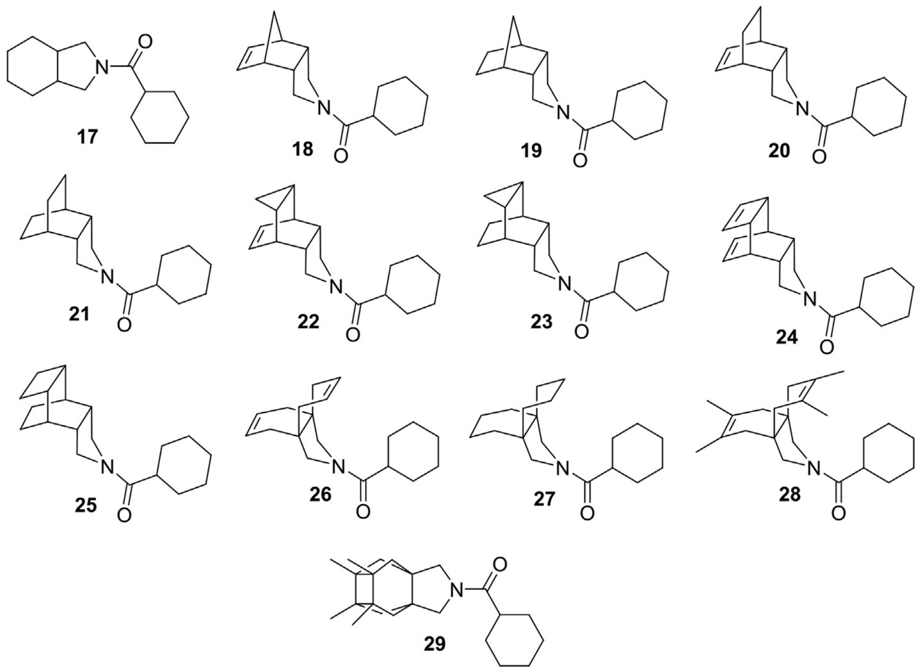

Fig. 4. Novel pyrrolidine-based polycyclic amides **17**–**29**.

select the best candidate to perform an *in vivo* study in a rodent model of cognitive dysfunction.

The cellular potency was assessed in Human Embryonic Kidney 293 (HEK293) cells stably transfected with the 11β-HSD1 gene. With the only exception of alkenes **18**, **20** and **26**, which showed a moderate inhibitory activity (55%, 64% and 64%, respectively), all compounds completely inhibited the enzyme at 10 μM (Table 3).

Selectivity over 11β-HSD2 is required for 11β-HSD1 inhibitors progressing into clinical trials since 11β-HSD2 inhibition in the kidney can lead to sodium retention and increased blood pressure *via* cortisol stimulation of mineralocorticoid receptors. However, for the purposes of our *in vivo* studiy of cognitive dysfunction in rodents, high selectivity *vs* 11β-HSD2 was not required. Notwithstanding, 11β-HSD2 inhibition was assessed in a cellular assay with HEK293 cells stably transfected with the 11β-HSD2 gene at 10, 1 and 0.1 μM in order to establish the selectivity of our compounds. Ideally, the 11β-HSD2 inhibition at 10 μM should be lower than 50% to consider a compound sufficiently selective toward 11β-HSD1. None of our compounds achieved this threshold but some slightly improved the poor selectivity of the adamantyl-containing analogue **1**, such as amide **22** (88% *vs* 69% inhibition at 10 μM, respectively, data not shown). Although **22** had an IC_{50} between 1 and 10 μM, so we cannot rigorously consider this compound to be selective against 11β-HSD1, its selectivity index was at least 50-fold compared to compounds **20** and **21,** which displayed selectivities less than 5-fold. Poor selectivity was observed for compounds **18**, **19** and **23**.

Microsomal stability was performed in human liver microsomes (HLM), which are widely used to determine the likely degree of primary metabolic clearance in the liver. Compounds **18**, **19** and **20** presented moderate microsomal stabilities between 36 and 60% of remaining parent compound after 30-min incubation, while amides **21** and **22** showed stabilities lower than 28%. Compound **23** displayed a high microsomal stability with 94% of remaining parent compound after the 30-min incubation period.

The active compounds in the 11β-HSD1 cellular assay (**19** and **21**–**23**) were further tested for predicted brain permeation using the widely used *in vitro* PAMPA-BBB model [50]. Unfortunately, the *in vitro* permeabilities (P_e) for compounds **21** and **22** could not be determined due to their lack of UV absorption. Whereas **19** showed an uncertain BBB permeation [CNS ± with $5.179 > P_e$ $(10^{-6}$ cm $s^{-1}) > 2.106]$, compound **23** had P_e clearly above the threshold established for a high blood-brain barrier (BBB) permeation ($P_e > 30 \times 10^{-6}$ cm s^{-1}).

4. *In vivo* study

Recent studies in rodents and humans with brain-penetrant 11β-HSD1 inhibitors have shown that they provide beneficial effects on the cognitive impairment associated with aging [13,18–23]. SAMP8 has been studied as a non-transgenic murine mouse model of accelerated senescence and late-onset AD [51,52]. These mice exhibit cognitive and emotional disturbances, probably due to early development of brain pathological hallmarks, such as oxidative stress (OS), inflammation, and activation of neuronal death pathways, which mainly affect cerebral cortex and hippocampus [24,53]. To date, this rodent model has not been used to test 11β-HSD1 inhibitors, being this work the first investigation of the effects of 11β-HSD1 pharmacological inhibition in SAMP8.

The *in vivo* study was performed with amide **23**, as this compound had low nanomolar potency against the murine 11β-HSD1 enzyme (mHSD1, $IC_{50} = 0.08$ μM), high cellular potency, high microsomal stability (both in human and mouse liver microsomes, 94 and 93%, respectively) and positive predicted brain penetration. A pharmacokinetic study of compound **23** was performed in order to assess its oral administration. Although its clearance seems to be rapid, the concentration levels at 30 min post-administration are five fold the IC_{50} (Table S1, Fig. S5 and Table S2). In addition, we could also measure compound concentration in brain tissue at 3 h post-administration (1.45 ng/mL), hint of *in vivo* BBB permeability. Then, compound **23** was administered to 12-month-old SAMP8 mice in drinking water during four weeks at a concentration of 105 mg/L (average body weight for 48-week-old mice is 25 g; fluid consumption is 5 mL, therefore the dose was 0.105 mg/mL x 5 mL/ 0.025 kg = 21 mg/kg). Compound **23** was dissolved in polyethylene glycol 400 (PEG400) and then diluted with water to a PEG400 final concentration of 2% (v/v) in drinking fluid. 2% PEG400 in water was given to the remaining mice in drinking fluid as a vehicle control.

Neuroprotective effects were investigated through a behavioural test, the novel object recognition test (NORT), as a common measure of cognition (short-term and long-term memory) [54], and biochemical analysis, which were made through Western blotting and quantitative real-time polymerase chain reaction (qPCR). Consistent with previous reports, we found that aged SAMP8 mice presented memory impairments in the NORT when compared to young animals [53]. Satisfactorily, treatment with **23** certainly prevented short-term and long-term memory deficits in SAMP8 mice (Fig. 5A).

Postsynaptic density 95 (PSD95) protein levels were evaluated

Table 3
Biological profiling of the most potent compounds.[a,b]

Compound	hHSD1 IC_{50} (μM)	HEK hHSD1% inh at 10 μM[c]	HEK hHSD2 inhibition at 10 μM or IC_{50} (μM)[c]	HLM % parent[d]	PAMPA-BBB P_e (10^{-6} cm s^{-1})[e,f]
1	0.09	100	88%	79	–
18	0.02	55	<0.1 μM	60	–
19	0.09	100	<0.1 μM	37	5.20 ± 0.1 (CNS±)
20	0.03	64	0.1–1 μM	44	–
21	0.02	100	0.1–1 μM	17	ND[g]
22	0.02	100	1-10 μM	27	ND
23	0.03	100	<0.1 μM	94	>30 (CNS+)
26	0.04	64	100%	–	–

[a] See Experimental section for further details.
[b] Percentage inhibition was determined relative to a no inhibitor control.
[c] HEK293 cells stably transfected with the full-length gene coding for human either 11β-HSD1 or 11β-HSD2 were used.
[d] The microsomal stability of each compound was determined using human liver microsomes.
[e] Permeability values from PAMPA-BBB assay. Values are expressed as the mean ± SD of three independent experiments. CNS+, predicted positive brain penetration.
[f] Calibration line between 0 and 30×10^{-6} cm s^{-1}.
[g] ND, not detected.

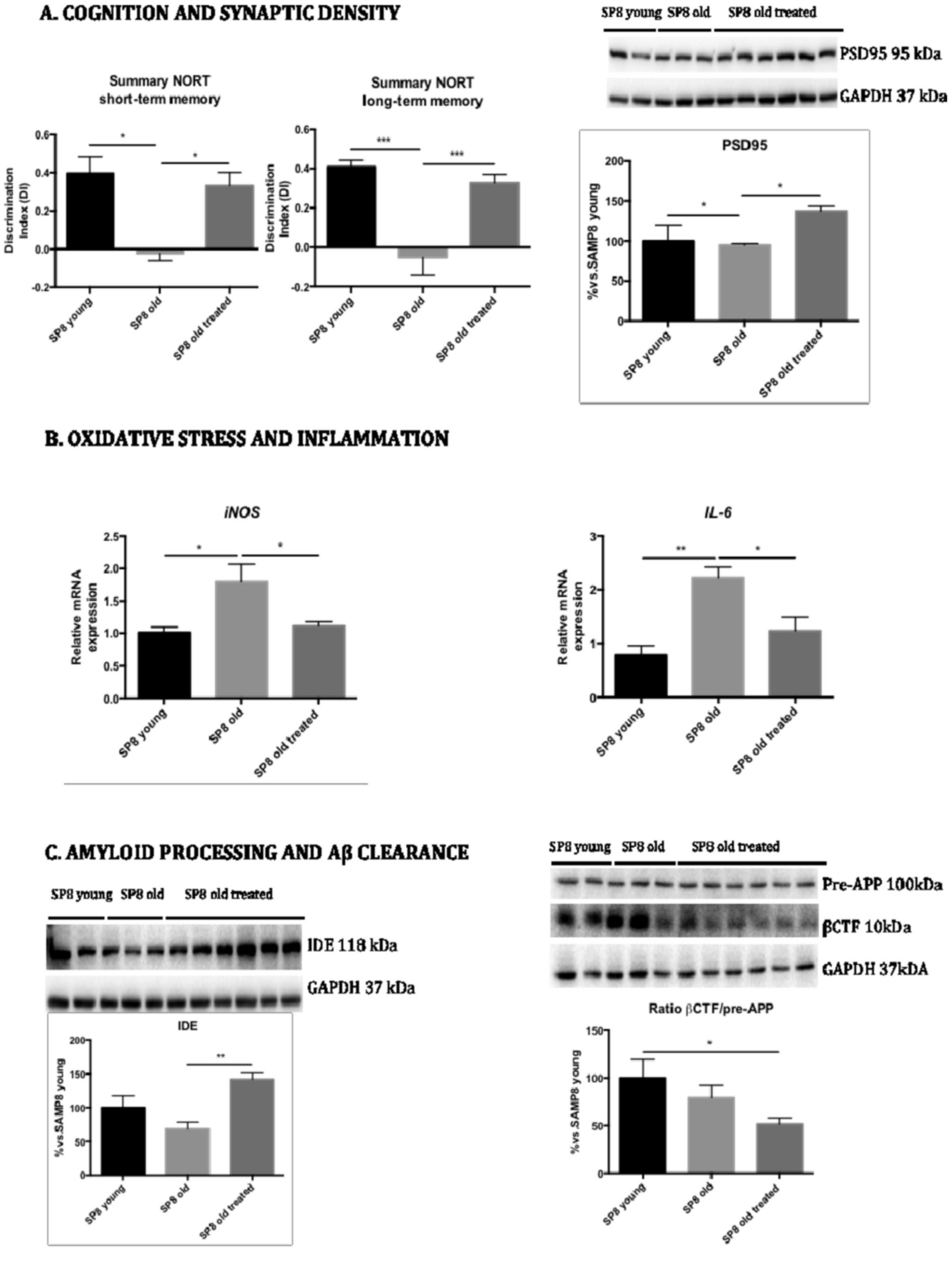
A. COGNITION AND SYNAPTIC DENSITY
Summary NORT short-term memory
Discrimination Index (DI)
0.6
0.4
0.2
0.0
-0.2
*
*
SP8 young
SP8 old
SP8 old treated
Summary NORT long-term memory
Discrimination Index (DI)
***
***
SP8 young
SP8 old
SP8 old treated
SP8 young
SP8 old
SP8 old treated
PSD95 95 kDa
GAPDH 37 kDa
PSD95
%vs.SAMP8 young
200
150
100
50
0
*
*
SP8 young
SP8 old
SP8 old treated
B. OXIDATIVE STRESS AND INFLAMMATION
iNOS
Relative mRNA expression
2.5
2.0
1.5
1.0
0.5
0.0
*
*
SP8 young
SP8 old
SP8 old treated
IL-6
Relative mRNA expression
3
2
1
0
**
*
SP8 young
SP8 old
SP8 old treated
C. AMYLOID PROCESSING AND Aβ CLEARANCE
SP8 young
SP8 old
SP8 old treated
IDE 118 kDa
GAPDH 37 kDa
IDE
%vs.SAMP8 young
200
150
100
50
0
**
SP8 young
SP8 old
SP8 old treated
SP8 young
SP8 old
SP8 old treated
Pre-APP 100kDa
βCTF 10kDa
GAPDH 37kDA
Ratio βCTF/pre-APP
%vs.SAMP8 young
150
100
50
0
*
SP8 young
SP8 old
SP8 old treated

as a measure of neuronal synapses, whereas gene expression for interleukin-6 (IL-6), which acts as a pro-inflammatory cytokine, and for inducible nitric oxide synthase (iNOS), an oxidative stress sensor that catalyzes the production of nitric oxide (NO), were also studied. Treatment with **23** prevented the reduction of PSD95 protein levels, while the oxidative stress and pro-inflammatory gene expression markers, such as iNOS and IL-6, were significantly decreased compared to untreated mice (Fig. 5A–B). These observations indicate a neuroprotective action of **23**, whereby reduced cognitive impairment in **23**-treated mice is mediated by a reduction of neuroinflammation and oxidative stress as confirmed by in the measurements of pro-inflammatory biomarkers (IL-6 and iNOS).

AD is characterized by the production and deposition of β-amyloid and it has been postulated that its reduction produces beneficial effects [55]. For these reasons, the effect of **23** in modifying amyloid processing pathways was also examined. No changes in amyloid beta A4 precursor (*Pre*APP), β-secretase 1 (*Bace1*), disintegrin and metalloproteinase 10 (*Adam 10*) gene expression levels were found (data not shown). Nevertheless, after treatment with **23**, we found a decrease of APP β-secretase C-terminal fragment (βCTF) protein levels without modification of those of *Pre*APP, together with an increase of the protein levels of insulin-degrading enzyme (IDE) (Fig. 1C), a zinc metalloprotease that degrades β-amyloid species. Several *in vitro* and *in vivo* studies have shown correlations between IDE, β-amyloid levels and AD [56].

In an attempt to elucidate the mechanisms underlying the beneficial effects of **23** and the relationship with cognitive amelioration in old SAMP8, we focused our study on amyloid processing and βCTF because of its implication in neurodegeneration and cognitive decline process in this strain [57]. Amide **23** did not alter the proamiloidogenic pathway in SAMP8, as demonstrated by the lack of effect on *Pre-APP*, *ADAM 10* or *Bace1* gene expression (see Fig. S6 in the Supplementary data file). However, the capacity of the brain to remove proamiloidogenic species by activation of specific proteases, such as IDE or neprilysine, appeared greatly increased in treated SAMP8 with higher protein levels of IDE than in control animals and consequently with substantially decreased βCTF protein levels. The results of the behavioural and biochemical studies in SAMP8 mice suggest that compound **23** acts centrally on 11β-HSD1.

Overall, behavioural tests and biochemical analyses confirmed a neuroprotective action of compound **23**, probably by reduction of inflammation and oxidative stress, as measured by reduction of IL-6 and iNOS.

5. Conclusions

We have found that adamantyl, widely used as a lipophilic substituent in 11β-HSD1 inhibitors, may successfully be replaced by other polycyclic hydrocarbons. The previously scarcely explored pyrrolidine-based polycyclic substituents presented here led to potent 11β-HSD1 inhibitors, and potentially these aliphatic ring-systems can serve as alternatives to adamantyl. Of note, the novel nanomolar inhibitors reported are achiral and easily synthesized in maximum four synthetic steps (compounds **19**, **21** and **23**) from commercially available starting materials. Biological profiling allowed us to select amide **23** for the first *in vivo* study in SAMP8 aiming to investigate the pharmacological effects of 11β-HSD1 inhibition in this model of cognitive dysfunction. In this study, prevention of cognitive impairment in aged SAMP8 after four-week treatment with **23** was demonstrated in comparison with control animals. The results provide further support for the neuroprotective effect of 11β-HSD1 inhibition, through reduction of neuroinflammation and oxidative stress, in cognitive decline related to the aging process. Due to the promising biological activity of **23**, further optimization is currently being carried out, with focus on modifying the RHS of the molecule to improve the selectivity and DMPK properties.

6. Experimental section

6.1. Chemistry

6.1.1. General

Melting points were determined in open capillary tubes with a MFB 595010M Gallenkamp. 400 MHz ^{1}H/100.6 MHz ^{13}C NMR spectra, and 500 MHz ^{1}H NMR spectra were recorded on Varian Mercury 400, and Varian Inova 500 spectrometers, respectively. The chemical shifts are reported in ppm (δ scale) relative to internal tetramethylsilane, and coupling constants are reported in Hertz (Hz). Assignments given for the NMR spectra of the new compounds have been carried out on the basis of DEPT, COSY ^{1}H/^{1}H (standard procedures), and COSY ^{1}H/^{13}C (gHSQC and gHMBC sequences) experiments. IR spectra were run on Perkin-Elmer Spectrum RX I spectrophotometer. Absorption values are expressed as wave-numbers (cm^{-1}); only significant absorption bands are given. High-resolution mass spectrometry (HRMS) analyses were performed with an LC/MSD TOF Agilent Technologies spectrometer. Column chromatography was performed either on silica gel 60 Å (35–70 mesh) or on aluminium oxide, neutral, 60 Å (50–200 μm, Brockmann I). Thin-layer chromatography was performed with aluminum-backed sheets with silica gel 60 F_{254} (Merck, ref 1.05554), and spots were visualized with UV light and 1% aqueous solution of $KMnO_4$. The analytical samples of all of the new compounds which were subjected to pharmacological evaluation possessed purity $\geq$95% as evidenced by their elemental analyses. The elemental analyses were carried out in a Flash 1112 series Thermofinnigan elemental microanalyzator (A5) to determine C, H and N.

6.1.2. General procedures for the synthesis of the compounds

6.1.2.1. General procedure A. A solution of cyclohexane acyl chloride (1.2 mmol) in anhydrous acetone was added to a solution of the amine hydrochloride (1 mmol) and triethylamine (2 mmol) in anhydrous acetone. The reaction mixture was stirred at 90° C for 3 h. The resulting residue was dissolved with DCM (20 mL) and washed with 1 M aqueous solution of HCl (4 × 25 mL), dried over anh. Na_2SO_4 and filtered. The evaporation *in vacuo* of the organics gave the desired product.

6.1.2.2. General procedure B. To a solution of the amine hydrochloride (1 mmol) in DCM (10 mL) were added 1-piperidinecarbonyl chloride (1.5 mmol) and triethylamine

Fig. 5. Results of *in vivo* study. 2A. -Cognition and synaptic density: -Left panel: Results. Discrimination index of Novel Object recognition test (NORT) obtained in young SAMP8, old SAMP8 and treated SAMP8, at 2 and 24 h -**Right Panel**: Representative Western blot (wb) for PSD95 and quantification. **2B. -Oxidative stress and inflammation: -Left Panel:** Oxidative stress gene expression iNOS. -**Right panel:** pro-inflammatory gene expression for IL-6. Gene exprexion levels were determined by real-time PCR. **2C. -Amyloid processing and β-CTF clearance: -Left panel:** Representative Western blot (wb) for IDE and quantification. **-Right panel:** Representative Western blot (wb) for Pre-APP and β-CTF and β-CTF/APP ratio quantification. For Western blot, bars represent mean ± standard error of the mean (SEM), and values are adjusted to 100% for levels SAMP8 young. For real-time PCR, mean ± SEM from five independent experiments performed in triplicate are represented. The One-Way ANOVA analysis and Tukey post hoc analysis were conducted. Statistical outliers (Grubbs' test) were removed from the analyses. *$p < 0.05$; **$p < 0.01$; ***$p < 0.001$.

(4 mmol). The reaction mixture was stirred at rt overnight. To the resulting mixture was added saturated aqueous solution of $NaHCO_3$ (10 mL) and the phases were separated. The aqueous layer was extracted with further DCM (2 × 10 mL). The organics were washed with 10% Na_2CO_3 solution (30 mL), dried over anh. Na_2SO_4, filtered and concentrated *in vacuo* to give the desired product.

6.1.2.3. General procedure C. To a solution of amine hydrochloride (1.1 mmol) in EtOAc (15 mL) were added the carboxylic acid (1 mmol), HOBt (1.5 mmol), EDC (1.5 mmol) and triethylamine (4 mmol) and the reaction mixture was stirred at rt overnight. To the resulting suspension was then added water (15 mL) and the phases were separated. The organic phase was washed with saturated aqueous $NaHCO_3$ solution (15 mL) and brine (15 mL), dried over anh. Na_2SO_4 and filtered. The organic layer was concentrated *in vacuo* to give the desired product.

6.1.2.4. General procedure D. A solution or suspension of the amide or urea (1 mmol) and 5 wt % palladium on carbon (50% in water, 10% of the weight) in absolute ethanol (ca 30 mL) was stirred at rt and atmospheric pressure under hydrogen for 3–72 h. The suspension was then filtered and the solids were washed with EtOH (10 mL). The solvents were removed *in vacuo* to give the desired reduced product.

*6.1.3. N-[Pentacyclo[6.4.0.0^{2,10}.0^{3,7}.0^{4,9}]dodec-8-yl] cyclohexanecarboxamide, (**6**)*

From cyclohexane acyl chloride (128 mg, 0.88 mmol) in anhydrous acetone (0.6 mL) and amine **4** [38] (152 mg, 0.72 mmol) and triethylamine (0.25 mL, 1.74 mmol) in anhydrous acetone (0.9 mL) and following the general procedure A, amide **6** (215 mg, 95% yield) was obtained as a yellow solid. The analytical sample was obtained by crystallization from EtOAc/pentane (164 mg), mp 228–229 °C; IR (ATR) ν: 580, 591, 604, 638, 663, 695, 722, 761, 824, 894, 933, 1143, 1194, 1221, 1277, 1304, 1336, 1386, 1448, 1547, 1639, 2851, 2923, 3271 cm^{-1}; ^1H NMR (400 MHz, $CDCl_3$) δ: 1.08 (t, *J* = 2.8 Hz, 1 H, 9′-H), 1.18–1.34 [complex signal, 3 H, 3(5)-H_{ax} and 4-H_{ax}], 1.39–1.55 [complex signal, 10 H, 5′(11′)-H_2, 6′(12′)-H_2 and 2(6)-H_{ax}], 1.66 (m, 1 H, 4-H_{eq}), 1.79 [m, 2 H, 3(5)-H_{eq}], 1.85 [m, 2 H, 2(6)-H_{eq}], 2.08 (tt, *J* = 11.6 Hz, *J*′ = 3.4 Hz, 1 H, 1-H), 2.13 [b. s., 2 H, 4′(10′)-H], 2.21 [m, 2 H, 2′(3′)-H], 2.81 [b. s., 2 H, 1′(7′)-H], 5.47 (s, 1 H, NH); ^{13}C NMR (100.5 MHz, $CDCl_3$) δ: 21.5 [CH_2, C5′(C11′)], 24.4 [CH_2, C6′(C12′)], 25.7 (CH_2, C4), 25.8 [CH_2, C3(5)], 30.1 [CH_2, C2(C6)], 45.8 (CH, C1), 46.9 [CH, C2′(3′)], 52.8 [CH, C4′(10′)], 53.4 [CH, C1′(7′)], 54.8 (CH, C9′), 65.4 (C, C8′), 176.7 (C, CO). Anal. Calcd for $C_{19}H_{27}NO$: C 79.95, H 9.54, N 4.91. Found: C 79.73, H 9.75, N 4.82.

*6.1.4. N-[[Pentacyclo[6.4.0.0^{2,10}.0^{3,7}.0^{4,9}]dodec-8-yl]methyl] cyclohexanecarboxamide, (**7**)*

From cyclohexane acyl chloride (119 mg, 0.81 mmol) in anhydrous acetone (0.6 mL) and amine **5** [38] (150 mg, 0.67 mmol) and triethylamine (0.23 mL, 1.62 mmol) in anhydrous acetone (0.8 mL) and following the general procedure A, amide **7** (155 mg, 78% yield) was obtained as a dark solid. The analytical sample was obtained by crystallization from EtOAc/pentane (77 mg), mp 148–149 °C; IR (ATR) ν: 576, 589, 604, 621, 660, 672, 711, 800, 894, 956, 979, 1037, 1106, 1123, 1180, 1213, 1252, 1298, 1314, 1380, 1435, 1443, 1550, 1633, 1659, 2855, 2928, 3299 cm^{-1}; ^1H NMR (400 MHz, $CDCl_3$) δ: 1.05 (b. s., 1 H, 9′-H), 1.17–1.33 [complex signal, 3 H, 3(5)-H_{ax} and 4-H_{ax}], 1.35–1.55 [complex signal, 8 H, 5′(11′)-$H_{exo\ or\ endo}$, 6′(12′)-H_2 and 2(6)-H_{ax}], 1.56–1.70 [complex signal, 3 H, 5′(11′)-$H_{endo\ or\ exo}$ and 4-H_{eq}], 1.74–1.87 [complex signal, 4 H, 2(6)-H_{eq} and 3(5)-H_{eq}], 1.98 [b. s., 2 H, 4′(10′)-H], 2.05 (tt, *J* = 11.6 Hz, *J*′ = 3.2 Hz, 1 H, 1-H), 2.13 [b. s., 2 H, 1′(7′)-H], 2.22 [m, 2 H, 2′(3′)-H], 3.38 [d, *J* = 5.6 Hz, 2 H, $NC\underline{H}_2$], 5.20 [b. s., 1H, NH]; ^{13}C NMR (100.5 MHz, $CDCl_3$) δ: 22.3 [CH_2, C5′(C11′)], 24.2 [CH_2, C6′(12′)], 25.7 (3 CH_2, C3, C4 and C5), 29.8 [CH_2, C2(6)], 36.9 (CH_2, $\underline{N}CH_2$), 42.7 (C, C8′), 45.7 (CH, C1), 47.9 [CH, C2′(3′)], 51.2 (CH, C9′), 53.1 [CH, C1′(7′)], 53.5 [CH, C4′(10′)], 175.6 (C, CO). Anal. Calcd for $C_{20}H_{29}NO\cdot0.15$ EtOAc: C 79.13, H 9.74, N 4.48. Found: C 79.03, H 9.88, N 4.52.

*6.1.5. N-[Pentacyclo[6.4.0.0^{2,10}.0^{3,7}.0^{4,9}]dodec-8-yl]piperidine-1-carboxamide, (**8**)*

From amine **4** [38] (100 mg, 0.47 mmol), 1-piperidinecarbonyl chloride (0.09 mL, 0.71 mmol) and triethylamine (0.23 mL, 1.88 mmol) in DCM (5 mL) and following the general procedure B, amide **8** (72 mg, 54% yield) was obtained as a white solid. The analytical sample was obtained by crystallization from hot EtOAc (22 mg), mp 225–226 °C; IR (ATR) ν: 700, 721, 734, 764, 794, 851, 866, 907, 954, 971, 1003, 1019, 1050, 1128, 1141, 1187, 1232, 1254, 1261, 1276, 1306, 1325, 1357, 1395, 1440, 1479, 1520, 1615, 2024, 2158, 2855, 2930, 3362 cm^{-1}; ^1H NMR (400 MHz, $CDCl_3$) δ: 0.99 (broad s, 1 H, 9′-H), 1.43–1.65 complex signal, 14 H, 5′(11′)-H_2, 6′(12′)-H_2, 3(5)-H_2 and 4-H_2], 2.13 [broad s, 2 H, 4′(10′)-H], 2.21 [broad s, 2 H, 2′(3′)-H], 2.78 [broad s, 2 H, 1′(7′)-H], 3.31 [m, 4 H, 2(6)-H_2], 4.53 (broad s, 1 H, NH); ^{13}C NMR (100.5 MHz, $CDCl_3$) δ: 21.5 [CH_2, C5′(11′)], 24.5 (CH_2, C4), 24.6 [CH_2, C6′(12′)], 25.6 [CH_2, C3(5)], 45.2 [CH_2, C2(6)], 46.8 [CH, C2′(3′)], 52.8 [CH, C4′(10′)], 53.6 [CH, C1′(7′)], 55.4 (CH, C9′), 65.8 (C, C8′), 157.4 (C, CO); HRMS-ESI + *m*/*z* $[M+H]^+$ calcd for $[C_{18}H_{26}N_2O + H]^+$: 287.2118, found: 287.2118.

*6.1.6. N-[[Pentacyclo[6.4.0.0^{2,10}.0^{3,7}.0^{4,9}]dodec-8-yl]methyl] piperidine-1-carboxamide, (**9**)*

From amine **5** [38] (96 mg, 0.42 mmol), 1-piperidinecarbonyl chloride (0.08 mL, 0.63 mmol) and triethylamine (0.21 mL, 1.68 mmol) in DCM (5 mL) and following the general procedure B, amide **9** (125 mg, quantitative yield) was obtained as a white solid. The analytical sample was obtained by crystallization from hot EtOAc (25 mg), mp 144–145 °C; IR (ATR) ν: 554, 572, 623, 637, 678, 734, 763, 851, 869, 900, 908, 945, 969, 992, 1023, 1107, 1155, 1232, 1253, 1261, 1340, 1397, 1438, 1451, 1475, 1524, 1614, 2018, 2158, 2842, 2860, 2930, 3378 cm^{-1}; ^1H NMR (400 MHz, $CDCl_3$) δ: 1.06 (broad s, 1 H, 9′-H), 1.40–1.70 [complex signal, 14 H, 5′(11′)-H_2, 6′(12′)-H_2, 3(5)-H_2 and 4-H_2], 2.00 [broad s, 2 H, 4′(10′)], 2.13 [broad s, 2 H, 1′(7′)-H], 2.22 [broad s, 2 H, 2′(3′)-H], 3.28 [m, 4 H, 2(6)-H_2], 3.37 (d, *J* = 5.2 Hz, 2 H, $NC\underline{H}_2$), 4.18 (broad s, 1H, NH); ^{13}C NMR (100.5 MHz, $CDCl_3$) δ: 22.4 [$\underline{C}H_2$, C5′(11′)], 24.3 [CH_2, C6′(12′)], 24.4 (CH_2, C4), 25.6 [CH_2, C3(5)], 38.6 (CH_2, $\underline{N}CH_2$), 44.5 (C, C8′), 45.0 [CH_2, C2(6)], 47.9 [CH, C2′(3′)], 51.2 (CH, $\underline{C}9$′), 53.1 [CH, C1′(7′)], 53.6 [CH, C4′(10′)], 157.8 (C, CO); HRMS-ESI + *m*/*z* $[M+H]^+$ calcd for $[C_{19}H_{29}N_2O + H]^+$: 301.2274, found: 301.2276.

*6.1.7. (3-Azahexacyclo[7.6.0.0^{1,5}.0^{5,12}.0^{6,10}.0^{11,15}]pentadeca-7,13-dien-3-yl)(cyclohexyl) methanone, (**11**)*

From amine **10** [38] (400 mg, 2.03 mmol), cyclohexanecarboxylic acid (237 mg, 1.85 mmol), HOBt (375 mg, 2.78 mmol), EDC (430 mg, 2.78 mmol) and triethylamine (0.570 mL, 4.07 mmol) in ethyl acetate (30 mL) and following the general procedure C, an orange oil (627 mg) was obtained. Column chromatography (Al_2O_3, DCM/methanol) gave amide **11** (260 mg, 42% yield) as a white solid. The analytical sample was obtained by crystallization from *tert*-butanol, mp 111–113 °C; IR (ATR) ν: 2961, 2930, 2853, 1630, 1443, 1425, 1347, 1305, 1223, 1194, 1138, 1067, 998, 897, 878, 830, 780, 749, 734, 696, 659, 646 cm^{-1}; ^1H NMR (500 MHz, $CDCl_3$) δ: 1.17–1.24 [complex signal, 3 H, 4′-H_{ax}, 3′(5′)-H_{ax}], 1.43 [complex signal, 2 H, 2′(6′)-H_{ax}], 1.60–1.66 [complex signal, 3 H, 2′(6′)-H_{eq}, 4′-H_{eq}], 1.75–1.78 [complex signal, 2 H, 3′(5′)-H_{eq}], 2.13 (tt, *J* = 12.0 Hz, *J*′ = 3.5 Hz, 1 H, 1′-H), 2.67 [m, 2 H, 10(11)-H], 2.98 [complex signal, 4 H, 6(12)-H, 9(15)-H], 3.18 (s, 2 H, 2-H_2 or

4-H_2), 3.19 (s, 2 H, 4-H_2 or 2-H_2), 6.00 [ddd, J = 6 Hz, J' = 3 Hz, J'' = 1.5 Hz, 2 H, 7(13)-H or 8(14)-H], 6.04 [ddd, J = 6 Hz, J' = 3 Hz, J'' = 1 Hz, 2 H, 8(14)-H or 7(13)-H]; ^{13}C NMR (125.7 MHz, $CDCl_3$) δ: 25.8 (CH_2, C4′), 25.9 [CH_2, C3′(5′)], 28.7 [CH_2, C2′(6′)], 42.5 (CH, C1′), 45.5 (CH_2, C2 or C4), 46.7 (CH_2, C4 or C2), 62.0 [CH, C6(12) and C9(15)], 62.8 [CH, C10(11)], 69.1 (C, C1 or C5), 70.8 (C, C5 or C1), 132.8 [CH, C7(13) or 8(14)], 134.1 [CH, C8(14) or C7(13)], 174.4 (C, CO); MS (EI), (rt = 25.4 min), *m/z* (%); significant ions: 308 (20), 307 ($M^{\cdot +}$, 83), 252 (16), 242 (25), 198 (17), 197 (100), 196 [$(C_{14}H_{14}N)^+$, 39], 182 (19), 181 (15), 180 (41), 179 (16), 168 (24), 167 (25), 166 (15), 165 (38), 156 (21), 153 (23), 152 (27), 132 (64), 131 (100), 130 (64), 128 (17), 118 (19), 117 (19), 115 (23), 91 (18), 83 [$(C_6H_{11})^+$, 85], 77 (15), 55 (72); HRMS-ESI + *m/z* $[M+H]^+$ calcd for $[C_{21}H_{25}NO + H]^+$: 308.2009, found: 308.2003.

6.1.8. (3-Azahexacyclo[7.6.0.0^{1,5}.0^{5,12}.0^{6,10}.0^{11,15}]pentadecane-3-yl)(cyclohexyl) methanone, (**12**)

From amide **11** (118 mg, 0.40 mmol) and Pd/C (13 mg) and following the general procedure D (5 h), amide **12** (94 mg, 78% yield) was obtained as a white solid. The analytical sample was obtained by crystallization from DCM/diethyl ether, mp 134–135 °C; IR (ATR) í: 2932, 2851, 1621, 1463, 1426, 1357, 1286, 1202, 1120, 1104, 1036, 1013, 969, 925, 886, 860, 825, 768, 732, 702, 657, 627 cm^{-1}; ^1H NMR (500 MHz, $CDCl_3$) δ: 1.25 [complex signal, 3 H, 4′-H_{ax}, 3′(5′)-H_{ax}], 1.48–1.57 [complex signal, 10 H, 7(13)-H_2, 8(14)-H_2, 17(21)-H_{ax}], 1.68 (m, 1 H, 4′-H_{eq}), 1.75–1.82 [complex signal, 4 H, 2′(6′)-H_{eq}, 3′(5′)-H_{eq}], 2.08 (broad signal, 4 H, 6(12)-H, 9(15)-H], 2.36 (tt, J = 12 Hz, J' = 3.5 Hz, 1 H, 1′-H), 2.41 [m, 2 H, 10(11)-H], 3.29 [s, 4 H, 2(4)-H_2]; ^{13}C NMR (125.7 MHz, $CDCl_3$) δ: 21.5 [CH_2, C7(13) or C8(14)], 21.8 [CH_2, C8(14) or C7(13)], 25.8 (CH_2, C4′), 25.9 [CH_2, C3′(5′)], 29.0 [CH_2, C2′(6′)], 40.7 (CH_2, C2 or C4), 42.0 (CH_2, C4 or C2), 42.9 (CH, C1′), 49.6 [CH, C10(11)], 55.0 [CH, C6(12) or C9(15)], 55.1 [CH, C9(15) or C6(12)], 57.5 (C, C1 or C5], 59.3 (C, C5 or C1], 175.1 (C, CO); MS (EI), (rt = 26.7 min), *m/z* (%); significant ions: 312 (23), 311 ($M^{\cdot +}$, 100), 270 (14), 257 (19), 256 (99), 243 (12), 228 [$(C_{15}H_{18}NO)^+$ 13], 202 (12), 201 (30), 184 (29), 129 (15), 128 (15), 91 (16), 83 [$(C_6H_{11})^+$, 24], 55 (25). Anal. Calcd for $C_{21}H_{29}NO$: C 80.98, H 9.39, N 4.50. Found: 80.76, H 9.61, N 4.33.

6.1.9. (3-Azahexacyclo[7.6.0.0^{1,5}.0^{5,12}.0^{6,10}.0^{11,15}]pentadeca-7,13-diene-3-yl)(piperidin-1-yl)methanone, (**13**)

From amine **10** [38] (400 mg, 2.03 mmol), 1-piperidinecarbonyl chloride (0.26 mL, 2.13 mmol) and triethylamine (0.56 mL, 4.06 mmol) in DCM and following the general procedure B amide **13** (443 mg, 71% yield) was obtained as a clear oil. Several attempts to crystallize this product met with failure. The product was used in the next step without further purification or characterization; MS (EI), (rt = 24.2 min), *m/z* (%); significant ions: 308 ($M^{\cdot +}$, 46), 196 [$(C_{14}H_{14}N)^+$, 17], 165 (14), 130 (15), 112 [$(C_6H_{10}NO)^+$, 100], 84 [$(C_5H_{10}N)^+$, 17], 69 (41).

6.1.10. (3-Azahexacyclo[7.6.0.0^{1,5}.0^{5,12}.0^{6,10}.0^{11,15}]pentadeca-3-yl)(piperidin-1-yl) methanone, (**14**)

From urea **13** (235 mg, 0.76 mmol) and Pd/C (24 mg) and following the general procedure D (3 h), urea **14** (171 mg, 72% yield) was obtained as a white solid, mp 124–126 °C; IR (ATR) ν: 3457, 3291, 2936, 2867, 2839, 1615, 1538, 1461, 1415, 1370, 1332, 1304, 1252, 1226, 1202, 1159, 1124, 1110, 1027, 991, 915, 882, 851, 767, 722, 632 cm^{-1}; ^1H NMR (500 MHz, $CDCl_3$) δ: 1.47–1.58 [complex signal, 14 H, 7(8,13,14)-H_2, 3′(5′)-H_2, 4′-H_2], 2.05 [m, 4 H, 6(9,12,15)-H], 2.38 [m, 2 H, 10(11)-H], 3.19 [m, 8 H, 2(4)-H_2, 2′(6′)-H_2]; ^{13}C NMR (125.7 MHz, $CDCl_3$) δ: 21.7 [CH_2, C7(8, 13, 14)], 24.8 (CH_2, C4′), 25.9 [CH_2, C3′(5′)], 43.3 [CH_2, C2(4)], 47.8 [CH_2, C16(20)], 49.6 [CH, C10(11)], 54.8 [CH, C6(9, 12, 15)], 58.8 [C, C1(5)], 163.3 (C, CO); MS (EI), (rt = 25.1 min), *m/z* (%); significant ions: 312 ($M^{\cdot +}$, 100), 201 (15), 200 [$(C_{14}H_{18}N)^+$, 82], 184 (33), 129 (36), 112 [$(C_6H_{10}NO)^+$, 54], 91 (16), 84 [$(C_5H_{10}N)^+$, 59], 69 (28). Anal. Calcd for $C_{20}H_{28}N_2O$: C 76.88, H 9.03, N 8.97. Found: 76.60, H 9.21, N 8.74.

6.1.11. (4-Amino-3,5-dichlorophenyl)(3-azahexacyclo[7.6.0.0^{1,5}.0^{5,12}.0^{6,10}.0^{11,15}]pentadeca-7,13-dien-3-yl)methanone, (**15**)

From amine **10** [38] (400 mg, 2.03 mmol), 4-amino-3,5-dichlorobenzoic acid (380 mg, 1.85 mmol), 1-hydroxybenzotriazole (HOBt) (375 mg, 2.78 mmol), 1-ethyl-3-(3-dimethylaminopropyl)carbodiimide (EDC) (430 mg, 2.78 mmol) and triethylamine (0.560 mL, 4.07 mmol) in EtOAc (30 mL) and DMF (2 mL) and following the general procedure C, a yellow solid (677 mg) was obtained. Column chromatography (Al_2O_3, DCM/methanol) furnished **15** (332 mg, 47% yield) as a white solid, mp 236–238 °C; IR (ATR) ν: 3449, 3306, 3250, 3204, 2954, 2867, 2150, 1597, 1538, 1501, 1456, 1410, 1384, 1342, 1316, 1295, 1244, 1225, 1192, 1054, 1002, 943, 896, 875, 791, 745, 733, 686, 667, 643 cm^{-1}; ^1H NMR (500 MHz, $CDCl_3$) δ: 2.61 [m, 2 H, 10(11)-H], 2.85 [broad s, 2 H, 6(12)-H or 9(15)-H], 2.94 [broad s, 2 H, 9(15)-H or 6(12)-H], 3.13 (broad s, 2 H, 2-H or 4-H), 3.33 (broad s, 2 H, 4-H or 2-H), 5.91 [m, 2 H, 7(13)-H or 8(14)-H], 6.03 [m, 2 H, 8(14)-H or 7(13)-H], 7.19 (s, 2 H, Ar-H); ^{13}C NMR (125.7 MHz, $CDCl_3$) δ: 45.5 (CH_2, C2 or C4), 49.9 (CH_2, C4 or C2), 61.8 [CH, C6(12), C9(15)], 62.7 [CH, C10(11)], 68.8 (C, C1 or C5), 71.0 (C, C5 or C1), 118.7 (C, Ar-C_{meta}), 126.7 (C, C_{ipso}), 127.1 (CH, Ar-C_{ortho}), 132.9 [CH, C7(13) or 8(14)], 133.9 [CH, C8(14) or C7(13)], 141.3 (C, Ar-C_{para}), 166.8 (C, CO); GC/MS (EI), (rt = 30.7 min), *m/z* (%); significant ions: 388 [$(C_{21}H_{18}^{37}Cl_2N_2O)^{\cdot +}$, 2], 386 [$(C_{21}H_{18}^{37}Cl^{35}ClN_2O)^{\cdot +}$, 12], 384 [$(C_{21}H_{18}^{35}Cl_2N_2O)^{\cdot +}$, 18], 192 [$(C_7H_4^{37}Cl_2NO)^+$, 10], 190 [$(C_7H_4^{37}Cl^{35}ClNO)^+$, 63], 188 [$(C_7H_4^{35}Cl_2NO)^+$, 100], 180 (12), 160 (12), 124 (16); HRMS-ESI + *m/z* $[M+H]^+$ calcd for $[C_{21}H_{18}Cl_2N_2O + H]^+$: 385.0869, found: 385.0875.

6.1.12. (4-Amino-3,5-dichlorophenyl) (3-azahexacyclo[7.6.0.0^{1,5}.0^{5,12}.0^{6,10}.0^{11,15}] pentadecan-3-yl)methanone, (**16**)

From amide **15** (200 mg, 0.78 mmol) and Pd/C (24 mg) and following the general procedure D (5 h) a yellow solid (207 mg) was obtained. Column chromatography (Al_2O_3, DCM/methanol) gave the desired amide **16** (180 mg, 89% yield) as a white solid, mp 243–244 °C; IR (ATR) ν: 3455, 3283, 3238, 3186, 2931, 2865, 1631, 1597, 1545, 1498, 1456, 1425, 1332, 1307, 1269, 1232, 1216, 1118, 1070, 1035, 944, 895, 789, 768, 745, 693, 647, 629 cm^{-1}; ^1H NMR (500 MHz, $CDCl_3$) δ: 1.43–1.60 [complex signal, 8 H, 7(13)-H_2, 8(14)-H_2], 2.04 [broad s, 2 H, 6(12)-H or 9(15)-H], 2.12 [broad s, 2 H, 9(15)-H or 6(12)-H], 2.41 [m, 2 H, 10(11)-H], 3.29 (s, 2 H, 2-H_2 or 4-H_2), 3.53 (s, 2 H, 4-H_2 or 2-H_2), 7.40 (s, 2 H, Ar-H); ^{13}C NMR (125.7 MHz, $CDCl_3$) δ: 21.5 [CH_2, C7(13) or C8(14)], 21.8 [CH_2, C8(14) or C7(13)], 40.8 (CH_2, C2 or C4), 45.5 (CH_2, C4 or C2), 49.6 [CH, C10(11)], 54.8 [broad CH, C6(12) and C9(15)], 57.9 (C, C1 or C5), 59.6 (C, C5 or C1), 118.8 (C, Ar-C_{meta}), 126.9 (C, C_{ipso}), 127.2 (CH, Ar-C_{ortho}), 141.4 (C, Ar-C_{para}), 167.0 (C, CO); MS (EI), (rt = 32.3 min), *m/z* (%); significant ions: 392 [$(C_{21}H_{22}^{37}Cl_2N_2O)^{\cdot +}$, 8], 390 [$(C_{21}H_{22}^{37}Cl^{35}ClN_2O)^{\cdot +}$, 42], 388 [$(C_{21}H_{22}^{35}Cl_2N_2O)^{\cdot +}$, 63], 200 (18), 192 [$(C_7H_4^{37}Cl_2NO)^+$, 11], 190 [$(C_7H_4^{37}Cl^{35}ClNO)^+$, 64], 188 [$(C_7H_4^{35}Cl_2NO)^+$, 100], 184 (33), 169 (13), 160 (12), 124 (13). Anal. Calcd for $C_{21}H_{22}Cl_2N_2O \cdot 0.50H_2O$: C 63.32, H 5.82, Cl 17.80, N 7.03. Found: C 63.23, H 5.71, Cl 17.82, N 6.77.

6.1.13. (Cyclohexyl)(octahydro-2*H*-isoindol-2-yl)methanone, (**17**)

From octahydro-1*H*-isoindole hydrochloride (300 mg, 2.40 mmol), cyclohexanecarboxylic acid (279 mg, 2.18 mmol), HOBt (442 mg, 3.27 mmol), EDC (506 mg, 3.27 mmol) and triethylamine (0.7 mL, 4.80 mmol) in EtOAc (10 mL) and following the general procedure C, **17** (458 mg, 89% yield) was obtained as a white solid. The analytical sample was obtained by crystallization from hot

EtOAc (82 mg), mp 67–68 °C; IR (ATR) ν: 734, 890, 973, 1073, 1113, 1136, 1173, 1184, 1307, 1341, 1358, 1443, 1481, 1622, 2851, 2873, 2917 cm^{-1}; ^{1}H NMR (400 MHz, $CDCl_3$) δ: 1.16–1.30 (complex signal, 3 H, 3-H_{ax}, 4-H_{ax} and 5-H_{ax}), 1.31–1.63 (complex signal, 10 H, 2-H_{ax}, 6-H_{ax}, 4′-H_2, 7′-H_2, 5′-H_2, 6′-H_2), 1.64–1.84 (complex signal, 5 H, 2-H_{eq}, 6-H_{eq}, 3-H_{eq}, 4-H_{eq} and 5-H_{eq}), 2.16 (m, 1 H, 3a'-H or 7a'-H), 2.24 (m, 1 H, 7a'-H or 3a'-H), 2.30 [tt, *J* = 11.6 Hz, *J*′ = 3.6 Hz, 1 H, 1-H], 3.31 (dd, *J* = 10.0 Hz, *J*′ = 6.0 Hz, 1 H, 1′-H_a or 3′-H_a), 3.36 (dd, *J* = 12.0 Hz, *J*′ = 6.6 Hz, 1 H, 3′-H_a or 1′-H_a), 3.40 (dd, *J* = 12.0 Hz, *J*′ = 7.8 Hz, 1 H, 3′-H_b or 1′-H_b), 3.45 (dd, *J* = 10.0 Hz, *J*′ = 7.0 Hz, 1 H, 1′-H_b or 3′-H_b); ^{13}C NMR (100.5 MHz, $CDCl_3$) δ: 22.5 (CH_2, C5′ or C6′), 22.8 (CH_2, C6′ or C5′), 25.73 (CH_2), 25.78 (CH_2), 25.80 (CH_2), 25.84 (CH_2) and 25.91 (CH_2) [C4′, C7′, C3, C4 and C5], 28.8 (CH_2, C2 or C6), 29.0 (CH_2, C6 or C2), 35.8 (CH, C3a′ or C7a'), 37.6 (CH, C7a′ or C3a'), 42.7 (CH, C1), 49.3 (CH_2, C1′ or C3′), 50.4 (CH_2, C3′ or C1′), 175.4 (C, CO). Anal. Calcd for $C_{15}H_{25}NO$: C 76.55, H 10.71, N 5.95. Found: 76.56, H 10.67, N 5.96.

*6.1.14. (4-Azatricyclo[5.2.1.0^{2,6}]dec-8-en-4-yl)(cyclohexyl) methanone, (**18**)*

From 4-azatricyclo[5.2.1.0^{2,6}]dec-8-ene hydrochloride [58] (240 mg, 1.40 mmol), cyclohexanecarboxylic acid (163 mg, 1.27 mmol), HOBt (258 mg, 1.91 mmol), EDC (296 mg, 1.91 mmol) and triethylamine (0.8 mL, 5.59 mmol) in EtOAc (8 mL) and following the general procedure C, amide **18** (304 mg, 97% yield) was obtained as a yellowish solid. Column chromatography (hexane/EtOAc) gave **18** as a white solid (209 mg), mp 77–78 °C; IR (ATR) ν: 702, 731, 761, 793, 897, 987, 1216, 1256, 1332, 1347, 1428, 1621, 2850, 2920 cm^{-1}; ^{1}H NMR (400 MHz, $CDCl_3$) δ: 1.12–1.29 (complex signal, 3 H, 3-H_{ax}, 4-H_{ax} and 5-H_{ax}), 1.36–1.51 (complex signal, 3 H, 2-H_{ax}, 6-H_{ax} and 10′-H_a], 1.54 (dt, *J* = 8.4 Hz, *J*′ = 1.6 Hz, 1 H, 10′-H_b), 1.60–1.70 [complex signal, 3 H, 2-H_{eq}, 6-H_{eq} and 4-H_{eq}), 1.71–1.84 (complex signal, 2 H, 3-H_{eq} and 5-H_{eq}), 2.16 (tt, *J* = 11.6 Hz, *J*′ = 3.6 Hz, 1 H, 1-H), 2.82–3.00 (complex signal, 4 H, 1′-H, 7′-H, 2′-H and 6′-H), 3.10 (dd, *J* = 10.8 Hz, *J*′ = 3.6 Hz, 1 H, 3′-H_a or 5′- H_a), 3.21 (dd, *J* = 13.5 Hz, *J*′ = 3.6 Hz, 1 H, 5′-H_a or 3′- H_a), 3.29 (dd, *J* = 13.5 Hz, *J*′ = 9.2 Hz, 1 H, 5′-H_b or 3′- H_b), 3.43 (dd, *J* = 10.8 Hz, *J*′ = 9.2 Hz, 1 H, 3′-H_b or 5′- H_b), 6.14 (dd, *J* = 6.0 Hz, *J*′ = 3.2 Hz, 1 H, 8′-H or 9′-H), 6.19 (dd, *J* = 6.0 Hz, *J*′ = 3.2 Hz, 1 H, 9′-H or 8′-H); ^{13}C NMR (100.5 MHz, $CDCl_3$) δ: 25.8 [CH_2, C3(5)], 25.9 (CH_2, C4), 28.69 (CH_2, C2 or C6), 28.71 (CH_2, C6 or C2), 42.7 (CH, C1), 43.8 (CH, C2′ or C6′), 45.9 (CH, C6′ or C2′), 46.66 (CH, C1′ or C7′), 46.70 (CH, C7′ or C1′), 48.0 (CH_2, C3′ or C5′), 48.8 (CH_2, C5′ or C3′), 51.9 (CH_2, C10′), 134.7 (CH, C8′ or C9′), 136.1 (CH, C9′ or C8′), 173.9 (C, CO). Anal. Calcd for $C_{16}H_{23}NO$: C 78.32, H 9.45, N 5.71. Found: 78.03, H 9.41, N 5.58.

*6.1.15. (4-Azatricyclo[5.2.1.0^{2,6}]dec-4-yl)(cyclohexyl)methanone, (**19**)*

From amide **18** (177 mg) and Pd/C (36 mg) and following the general procedure D (18 h), amide **19** (156 mg, 88% yield) was obtained as a white solid, mp 83–84 °C; IR (ATR) ν: 611, 625, 642, 886, 1002, 1133, 1170, 1187, 1204, 1218, 1290, 1327, 1344, 1357, 1425, 1446, 1623, 2871, 2936, 2945 cm^{-1}; ^{1}H NMR (400 MHz, $CDCl_3$) δ: 1.20–1.94 (complex signal, 16 H, 3-H_2, 4-H_2, 5-H_2, 2-H_2, 6-H_2, 8′-H_2, 9′-H_2 and 10′-H_2), 2.18–2.27 (complex signal, 2 H, 1′-H and 7′-H), 2.37 (tt, *J* = 11.6 Hz, *J*′ = 3.2 Hz, 1 H, 1-H), 2.52 (m, 1 H, 2′-H or 6′-H), 2.60 (m, 1 H, 6′-H or 2′-H), 3.03 (dd, *J* = 13.2 Hz, *J*′ = 8.4 Hz, 1 H, 3′-H_a or 5′- H_a), 3.26 (dd, *J* = 11.6 Hz, *J*′ = 7.6 Hz, 1 H, 5′-H_a or 3′- H_a), 3.57 (dd, *J* = 11.6 Hz, *J*′ = 1.6 Hz, 1 H, 5′-H_b or 3′- H_b), 3.84 (dd, *J* = 13.2 Hz, *J*′ = 1.6 Hz, 1 H, 3′-H_b or 5′- H_b); ^{13}C NMR (100.5 MHz, $CDCl_3$) δ: 22.1 (CH_2, C8′ or C9′), 22.8 (CH_2, C9′ or C8′), 25.79 (CH_2), 25.86 (CH_2) and 25.88 (CH_2) (C3, C4 and C5), 28.87 (CH_2, C2 or C6), 28.89 (CH_2, C6 or C2), 41.2 (CH, C1′ or C7′), 41.4 (CH, C7′ or C1′), 42.0 (CH_2, C2′ or C6′), 42.1 (CH_2, C10′), 42.9 (CH, C1), 44.0 (CH_2, C6′ or C2′), 45.7 (CH_2, C3′ or C5′), 46.9 (CH_2, C5′ or C3′), 174.4 (C, CO). Anal. Calcd for $C_{16}H_{25}NO$: 77.68, H 10.19, N 5.66. Found: C 77.55, H 10.05, N 5.54.

*6.1.16. (4-Azatricyclo[5.2.2.0^{2,6}]undec-8-en-4-yl)(cyclohexyl) methanone, (**20**)*

From 4-azatricyclo[5.2.2.0^{2,6}]undec-8-ene hydrochloride [59] (300 mg, 1.62 mmol), cyclohexanecarboxylic acid (188 mg, 1.47 mmol), HOBt (300 mg, 2.21 mmol), EDC (342 mg, 2.21 mmol) and triethylamine (0.9 mL, 6.47 mmol) in EtOAc (10 mL) and following the general procedure C, amide **20** (323 mg, 85% yield) was obtained as a yellowish solid. Column chromatography (hexane/EtOAc) gave **20** as a white solid (205 mg), mp 86–87 °C; IR (ATR) ν: 703, 715, 849, 887, 986, 1044, 1132, 1165, 1216, 1239, 1307, 1347, 1357, 1375, 1431, 1625, 2850, 2921, 3037 cm^{-1}; ^{1}H NMR (400 MHz, $CDCl_3$) δ: 1.15–1.34 (complex signal, 5 H, 10′-H_a, 11′-H_a, 3-H_{ax}, 4-H_{ax} and 5-H_{ax}), 1.37–1.54 (complex signal, 4 H, 2-H_{ax}, 6-H_{ax}, 10′-H_b, 11′-H_b), 1.58–1.86 (complex signal, 5 H, 2-H_{eq}, 6-H_{eq}, 3-H_{eq}, 4-H_{eq} and 5-H_{eq}), 2.23 (tt, *J* = 11.6 Hz, *J*′ = 3.6 Hz, 1 H, 1-H), 2.42 (m, 1 H, 2′-H or 6′-H), 2.51–2.61 (complex signal, 3 H, 1′-H, 7′-H, 6′-H or 2′-H), 3.09 (d, *J* = 12.8 Hz, 1 H, 3′-H_a or 5′-H_a), 3.11 (d, *J* = 12.4 Hz, 1 H, 5′-H_a and 3′-H_a), 3.62 (dd, *J* = 12.4 Hz, *J*′ = 9.2 Hz, 1 H, 5′-H_b or 3′-H_b), 3.65 (dd, *J* = 12.8 Hz, *J*′ = 9.6 Hz, 1 H, 3′-H_b and 5′-H_b), 6.15–6.26 (complex signal, 2 H, 8′-H and 9′-H); ^{13}C NMR (100.5 MHz, $CDCl_3$) δ: 24.2 (CH_2, C10′ or C11′), 24.3 (CH_2, C11′ or C10′), 25.81 (CH_2), 25.84 (CH_2) and 25.9 (CH_2) [C3, C4 and C5], 28.7 (CH_2, C2 or C6), 28.8 (CH_2, C6 or C2), 34.1 (CH, C1′ and C7′), 41.9 (CH, C2′ or C6′), 42.6 (CH, C1), 44.0 (CH, C6′ or C2′), 50.8 (CH_2, C3′ or C5′), 51.6 (CH_2, C5′ or C3′), 132.9 (CH, C8′ or C9′), 134.3 (CH, C9′ or C8′), 173.9 (C, CO). Anal. Calcd for $C_{17}H_{25}NO$: C 78.72, 9.71, N 5.40. Found: C 78.82, H 9.71, N 5.30.

*6.1.17. (4-Azatricyclo[5.2.2.0^{2,6}]undec-4-yl)(cyclohexyl)methanone, (**21**)*

From amide **20** (165 mg) and Pd/C (33 mg) and following the general procedure D (18 h) amide **21** (151 mg, 91% yield) was obtained as a white solid, mp 78–79 °C; IR (ATR) ν: 622, 725, 868, 976, 1138, 1173, 1204, 1346, 1429, 1443, 1622, 2861, 2901, 2923 cm^{-1}; ^{1}H NMR (400 MHz, $CDCl_3$) δ: 1.18–1.42 (complex signal, 5 H, 3-H_{ax}, 4-H_{ax}, 5-H_{ax}, 8′-H_a and 9′-H_a), 1.44–1.90 (complex signal, 15 H, 3-H_{eq}, 4-H_{eq}, 5-H_{eq}, 2-H_2, 6-H_2, 1′-H, 7′-H, 8′-H_b, 9′-H_b, 10′-H_2 and 11′-H_2), 2.33 (m, 1 H, 2′-H or 6′-H), 2.37 (tt, *J* = 11.2 Hz, *J*′ = 3.4 Hz, 1 H, 1-H), 2.43 (m, 1 H, 6′-H and 2′-H), 3.44–3.65 (complex signal, 4 H, 3′-H_2 and 5′-H_2); ^{13}C NMR (100.5 MHz, $CDCl_3$) δ: 19.8 (CH_2, C9′ or C8′), 20.1 (CH_2, C8′ or C9′), 25.7 (CH, C1′ and C7′), 25.81 (CH_2), 25.86 (CH_2) and 25.91 (CH_2) (C3, C4 and C5), 27.8 (CH_2, C11′ or C10′), 28.0 (CH_2, C10′ or C11′), 28.86 (CH_2, C2 or C6), 28.92 (CH_2, C6 or C2), 37.8 (CH_2, C2′ or C6′), 40.0 (CH_2, C6′ or C2′), 42.8 (CH, C1), 49.1 (CH_2, C3′ or C5′), 49.9 (CH_2, C5′ or C3′), 174.3 (C, CO). Anal. Calcd for $C_{17}H_{27}NO$: C 78.11, H 10.41, N 5.36. Found: C 78.14, H 10.35, N 5.14.

*6.1.18. (4-Azatetracyclo[5.3.2.0^{2,6}.0^{8,10}]dodec-11-en-4-yl)(cyclohexyl)methanone, (**22**)*

From 4-azatetracyclo[5.3.2.0^{2,6}.0^{8,10}]dodec-11-ene hydrochloride [40] (2.06 g, 10.6 mmol), cyclohexanecarboxylic acid (1.24 g, 9.67 mmol), HOBt (1.96 g, 14.5 mmol), EDC (2.25 g, 14.5 mmol) and triethylamine (5.9 mL, 42.5 mmol) in EtOAc (150 mL) and following the general procedure C, amide **22** (2.43 g, 94% yield) was obtained as a yellowish solid. The analytical sample was obtained by crystallization from hot EtOAc (2.04 g), mp 96–97 °C; IR (ATR) ν: 560, 570, 587, 696, 718, 741, 767, 812, 829, 847, 894, 915, 942, 963, 991, 1036, 1089, 1134, 1167, 1209, 1217, 1242, 1272, 1299, 1361, 1380, 1432, 1624, 2849, 2925, 3002, 3040 cm^{-1}; ^{1}H NMR (400 MHz, $CDCl_3$) δ: 0.12–0.16 (complex signal, 2 H, 9′-H_2), 0.86–0.96 (complex signal, 2 H, 8′-H and 10′-H), 1.14–1.29 (complex signal, 3 H, 3-H_{ax}, 4-H_{ax}

and 5-H_{ax}), 1.36–1.53 (complex signal, 2 H, 2-H_{ax} and 6-H_{ax}), 1.60–1.70 (complex signal, 3 H, 2-H_{eq}, 4-H_{eq} and 6-H_{eq}), 1.72–1.80 (complex signal, 2 H, 3-H_{eq} and 5-H_{eq}), 2.21 (tt, *J* = 11.6 Hz, *J'* = 3.4 Hz, 1 H, 1-H), 2.55 (dm, *J* = 12.8 Hz, 1 H, 2′-H or 6′-H), 2.67 (dm, *J* = 12.8 Hz, 1 H, 6′-H or 2′-H), 2.81–2.87 (complex signal, 2 H, 1′-H and 7′-H), 3.12 (dd, *J* = 11.0 Hz, *J'* = 5.0 Hz, 1 H, 3′-H_a or 5′-H_a), 3.15 (dd, *J* = 13.2 Hz, *J'* = 5.6 Hz, 1 H, 5′-H_a or 3′-H_a), 3.55 (t, *J* = 10.0 Hz, 1 H, 5′-H_b or 3′-H_b), 3.58 (t, *J* = 8.8 Hz, 1 H, 3′-H_b or 5′-H_b), 5.73 (ddd, *J* = 14.4 Hz, *J'* = 8.4 Hz, *J"* = 2.0 Hz, 1 H, 11′-H or 12′-H], 5.77 (ddd, *J* = 14.4 Hz, *J'* = 8.4 Hz, *J"* = 2.0 Hz, 1 H, 12′-H or 11′-H]; ^{13}C NMR (100.5 MHz, $CDCl_3$) δ: 4.1 (CH_2, C9′), 10.0 (CH, C8′ or C10′), 10.2 (CH, C10′ or C8′), 25.80 (CH_2), 25.83 (CH_2) and 25.9 (CH_2) [C3, C4 and C5], 28.7 (CH_2, C2 or C6), 28.8 (CH_2, C6 or C2), 35.6 (CH, C1′ or C7′), 35.7 (CH, 7′ or C1′), 42.6, (CH, C1), 42.7 (CH, C2′ or C6′), 44.8 (CH, C6′ or C2′), 49.6 (CH_2, C3′ or C5′), 50.6 (CH_2, C5′ or C3′), 128.1 (CH, C11′ or C12′), 129.6 (CH, C12′ or C11′), 174.1 (C, CO). Anal. Calcd for $C_{18}H_{25}NO$: C 79.66, H 9.29, N 5.16. Found: C 79.64, H 9.24, N 5.21.

*6.1.19. (4-Azatetracyclo[5.3.2.0^{2,6}.0^{8,10}]dodec-4-yl)(cyclohexyl) methanone, (**23**)*

From **22** (500 mg) and Pd/C (100 mg) and following the general procedure D (72 h) amide **23** (426 mg, 83% yield) was obtained as a white solid, mp 74–75 °C; IR (ATR) ν: 651, 679, 707, 729, 748, 789, 805, 826, 839, 865, 885, 950, 961, 988, 1016, 1030, 1082, 1113, 1133, 1171, 1205, 1213, 1234, 1264, 1295, 1325, 1346, 1358, 1427, 1471, 1486, 1623, 2846, 2897, 2928, 3009, cm^{-1}; ^{1}H NMR (400 MHz, $CDCl_3$) δ: 0.45 (dt, *J* = 6.0 Hz, *J'* = 8.0 Hz, 1 H, 9′-H_a), 0.78 (m, *J* = 6.0 Hz, *J'* = 3.6 Hz, 1 H, 9′-H_b), 0.90–0.96 (complex signal, 2 H, 8′-H and 10′-H), 1.00–1.14 (complex signal, 2 H, 11′-H_{ax} and 12′-H_{ax}), 1.17–1.34 [complex signal, 5 H, 11′-H_{eq}, 12′-H_{eq}, 3-H_{ax}, 4-H_{ax} and 5-H_{ax}], 1.42–1.61 (complex signal, 2 H, 2-H_{ax} and 6-H_{ax}), 1.67 (m, 1 H, 4′-H_{eq}), 1.69–1.83 (complex signal, 4 H, 3-H_{eq}, 4-$H_{eq,}$ 5-H_{eq}, 6-H_{eq}), 1.84–1.91 (complex signal, 2 H, 1′-H and 7′-H), 2.38 [tt, *J* = 11.6 Hz, *J'* = 3.6 Hz, 1 H, 1-H], 2.50 (dm, *J* = 12.8 Hz, 1 H, 2′-H or 6′-H), 2.55 (dm, *J* = 12.8 Hz, 1 H, 6′-H or 2′-H), 3.32 (dd, *J* = 12.8 Hz, *J'* = 8.8 Hz, 1 H, 3′-H_a or 5′-H_a), 3.52 (m, 2 H, 5′-H_2 or 3′-H_2), 3.76 (dd, *J* = 12.8 Hz, *J'* = 3.0 Hz, 1 H, 3′-H_b or 5′-H_b); ^{13}C NMR (100.5 MHz, $CDCl_3$) δ: 4.7 (CH_2, C9′), 14.9 (CH, C8′ or C10′), 15.1 (CH, C10′ or C8′), 17.3 (CH_2, C11′ or C12′), 17.9 (CH_2, C12′ or C11′), 25.8 (CH_2, C4), 25.9 [CH_2, C3(5)], 28.87 (CH_2, C2 or C6), 28.92 (CH_2, C6 or C2), 29.0 (CH, C1′ or C7′), 29.4 (CH, C7′ or C1′), 38.4 (CH, C2′ or C6′), 40.5, (CH, C6′ or C2′), 42.7 (CH, C1), 48.1 (CH, C3′ or C5′), 49.3 (CH_2, C5′ or C3′), 174.4 (C, CO). Anal. Calcd for $C_{18}H_{27}NO$: C 79.07, H 9.95, N 5.12. Found: 79.15, H 9.88, N 5.29.

*6.1.20. (4-Azatetracyclo[5.4.2.0^{2,6}.0^{8,11}]trideca-9,12-dien-4-yl)(cyclohexyl) methanone, (**24**)*

From 4-azatetracyclo[5.4.2.0^{2,6}.0^{8,11}]trideca-9,12-diene hydrochloride [40] (139 mg, 0.66 mmol), cyclohexanecarboxylic acid (77 mg, 0.60 mmol), HOBt (122 mg, 0.90 mmol), EDC (139 mg, 0.90 mmol) and triethylamine (0.4 mL, 2.64 mmol) in EtOAc (6 mL) and following the general procedure C, amide **24** (151 mg, 80% yield) was obtained as a yellowish solid. The analytical sample was obtained by crystallization from hot EtOAc (97 mg), mp 120–121 °C; IR (ATR) ν: 730, 760 788, 808, 967, 994, 1173, 1187, 1214, 1235, 1294, 1361, 1442, 1463, 1617, 2860, 2901, 2922 cm^{-1}; ^{1}H NMR (400 MHz, $CDCl_3$) δ: 1.15–1.30 [complex signal, 3 H, 3-H_{ax}, 4-H_{ax} and 5-H_{ax}], 1.38–1.54 [complex signal, 2 H, 2-H_{ax} and 6-H_{ax}], 1.60–1.72 (complex signal, 3 H, 2-H_{eq}, 4-H_{eq} and 6-H_{eq}), 1.73–1.82 (complex signal, 2 H, 3-H_{eq} and 5-H_{eq}), 2.24 [tt, *J* = 11.6 Hz, *J'* = 3.6 Hz, 1 H, 1-H], 2.37 (tdd, *J* = 9.6 Hz, *J'* = 5.8 Hz, *J"* = 2.8 Hz, 1 H, 2′-H or 6′-H), 2.50 (tdd, *J* = 8.8 Hz, *J'* = 5.6 Hz, *J"* = 2.8 Hz, 1 H, 6′-H or 2′-H), 2.60–2.66 (complex signal, 2 H, 1′-H and 7′-H), 2.67–2.70 (complex signal, 2 H, 8′-H and 11′-H), 3.17–3.24 (complex signal, 2 H, 3′-H_a and 5′-H_a), 3.63–3.73 (complex signal, 2 H, 3′-H_b and 5′-H_b), 5.84–5.87 (complex signal, 2 H, 9′-H and 10′-H), 5.89–5.99 (complex signal, 2 H, 12′-H and 13′-H); ^{13}C NMR (100.5 MHz, $CDCl_3$) δ: 25.81 (CH_2), 25.84 (CH_2) and 25.9 (CH_2) (C3, C4 and C5), 28.7 (CH_2, C2 or C6), 28.8 (CH_2, C6 or C2), 39.36 (CH, C1′ or C7′), 39.37 (CH, C7′ or C1′), 41.1 (CH, C2′ or C6′), 42.6 (CH, C1), 43.2 (CH, C6′ or C2′), 44.9 (CH, C8′ or C11′), 45.1 (CH, C11′ or C8′), 50.7 (CH_2, C3′ or C5′), 51.5 (CH_2, C5′ or C3′), 129.0 (CH, C12′ or C13′), 130.3 (CH, C13′ or C12′), 137.7 (CH, C9′ or C10′), 138.0 (CH, C10′ or C9′), 174.0 (C, CO). Anal. Calcd for $C_{19}H_{25}NO$: C 80.52, H 8.89, N 4.94. Found: 80.31, H 8.81, N 4.97.

*6.1.21. (4-Azatetracyclo[5.4.2.0^{2,6}.0^{8,11}]tridec-4-yl)(cyclohexyl) methanone, (**25**)*

From 4-azatetracyclo[5.4.2.0^{2,6}.0^{8,11}]tridecane hydrochloride [40] (235 mg, 1.10 mmol), cyclohexanecarboxylic acid (128 mg, 1.0 mmol), HOBt (203 mg, 1.50 mmol), EDC (232 mg, 1.50 mmol) and triethylamine (0.6 mL, 4.40 mmol) in EtOAc (10 mL) and following the general procedure C, amide **25** (253 mg, 80% yield) was obtained as a yellowish solid. The analytical sample was obtained by crystallization from hot EtOAc (110 mg), mp 115–116 °C; IR (ATR) ν: 658, 731, 887, 988, 1133, 1172, 1204, 1236, 1357, 1434, 1440, 1621, 2908, 2925 cm^{-1}; ^{1}H NMR (400 MHz, $CDCl_3$) δ: 1.18–1.34 (complex signal, 3 H, 3-H_{ax}, 4-H_{ax} and 5-H_{ax}), 1.42–1.62 (complex signal, 6 H, 1′-H, 7′-H, 2-H_{ax}, 6-H_{ax}, 12′-H_a and 13′-H_a), 1.64–1.92 (complex signal, 7 H, 2-H_{eq}, 6-H_{eq}, 3-H_{eq}, 4-H_{eq}, 5-H_{eq}, 12′-H_b and 13′-H_b), 2.02–2.20 (complex signal, 5 H, 2′-H or 6′-H, 9′-H_a, 9′-H_b, 10′-H_a and 10′-H_b), 2.27 (m, 1 H, 6′-H or 2′-H), 2.34–2.44 (complex signal, 3 H, 1-H, 8′-H and 11′-H), 3.48–3.70 (complex signal, 4 H, 3′-H_2 and 5′-H_2); ^{13}C NMR (100.5 MHz, $CDCl_3$) δ: 15.0 (CH_2, C12′ or C13′), 15.3 (CH_2, C13′ or C12′), 20.8 [CH_2, C9′(10′)], 25.82 (CH_2), 25.88 (CH_2) and 25.92 (CH_2) (C3, C4 and C5), 28.88 (CH_2, C2 or C6), 28.95 (CH_2, C6 or C2), 31.2 (CH, C1′ or C7′), 31.5 (CH, C7′ or C1′), 36.37 (CH, C8′ or C11′), 36.44 (CH, C11′ or C8′), 37.4 (CH, C2′ or C6′), 39.5 (CH, C6′ or C2′), 42.8 (CH, C1), 48.8 (CH_2, C3′ or C5′), 49.7 (CH_2, C5′ or C3′), 174.4 (C, CO). Anal. Calcd for $C_{19}H_{29}NO$: C 79.39, H 10.17, N 4.87. Found: C 79.20, H 10.30, N 4.72.

*6.1.22. (12-Azatricyclo[4.4.3.0^{1,6}]trideca-3,8-dien-12-yl)(cyclohexyl)methanone, (**26**)*

From 12-azatricyclo[4.4.3.0^{1,6}]trideca-3,8-diene hydrochloride [41] (150 mg, 0.71 mmol), cyclohexanecarboxylic acid (82 mg, 0.64 mmol), HOBt (131 mg, 0.97 mmol), EDC (150 mg, 0.97 mmol) and triethylamine (0.4 mL, 2.82 mmol) in EtOAc (6 mL) and following general procedure C, amide **26** (185 mg, 92% yield) was obtained as a yellowish solid. The analytical sample was obtained by crystallization from hot EtOAc (106 mg), mp 116–117 °C; IR (ATR) ν: 605, 676, 739, 813, 865, 1004, 1187, 1207, 1224, 1332, 1347, 1427, 1629, 2858, 2918 cm^{-1}; ^{1}H NMR (400 MHz, $CDCl_3$) δ: 1.16–1.31 (complex signal, 3 H, 3(5)-H_{ax} and 4-H_{ax}), 1.51 [m, 2 H, 2(6)-H_{ax}], 1.62–1.84 [complex signal, 5 H, 2(6)-H_{eq}, 3(5)-H_{eq} and 4-H_{eq}], 1.92–2.10 [complex signal, 8 H, 2′(10′)-H_2 and 5′(7′)-H_2], 2.29 [tt, *J* = 11.6 Hz, *J'* = 3.6 Hz, 1 H, 1-H], 3.35–3.37 (complex signal, 4 H, 3′-H_a, 3′-H_b, 5′-H_a and 5′-H_b), 5.48–5.57 [complex signal, 4 H, 3′(9′)-H and 4′(8′)-H]; ^{13}C NMR (100.5 MHz, $CDCl_3$) δ: 25.8 (CH_2, C4), 25.9 [CH_2, C3(5)], 28.9 [CH_2, C2(6)], 32.1 [CH_2, C2′(10′) or C5′(7′)], 32.2 [CH_2, C5′(7′) or C2′(10′)], 37.3 (C, C1′ or C6′), 39.2 (C, C6′ or C1′), 42.6 (CH, C1), 55.3 (CH_2, C11′ or C13′), 56.1 (CH_2, C13′ or C11′), 123.3 (CH, C3′ and C9′), 123.9 (CH, C4′ and C8′), 176.3 (C, CO); HRMS-ESI + *m/z* $[M+H]^+$ calcd for $[C_{19}H_{27}NO + H]^+$: 286.2165, found: 286.2176.

*6.1.23. (12-Azatricyclo[4.4.3.0^{1,6}]tridec-12-yl)(cyclohexyl) methanone, (**27**)*

From **26** (362 mg) and Pd/C (72 mg) and following the general procedure D (24 h), amide **27** (330 mg, 90% yield) was obtained as a white solid. The analytical sample was obtained by crystallization from hot EtOAc (178 mg), mp 160–161 °C; IR (ATR) ν: 670, 764, 874, 891, 976, 1157, 1290, 1343, 1360, 1435, 1623, 1635, 2850, 2907, 2921 cm^{-1}; ^{1}H NMR (400 MHz, $CDCl_3$) δ: 1.18–1.29 [complex signal, 3 H, 3(5)-H_{ax} and 4-H_{ax}], 1.31–1.62 [complex signal, 18 H, 2′(6)-H_{ax}, 3′(9′)-H_2, 4′(8′)-H_2, 5′(7′)-H_2, 10′(13′)-H_2], 1.64–1.84 [complex signal, 5 H, 2(6)-H_{eq}, 3(5)-H_{eq} and 4-H_{eq}], 2.30 [tt, J = 11.6 Hz, J' = 3.6 Hz, 1 H, 1-H], 2.70–3.90 (complex signal, 4 H, 3′-H_2 and 5′-H_2); ^{13}C NMR (100.5 MHz, $CDCl_3$) δ: 21.6 [CH_2, C3′(9′) or C4′(8′)], 21.8 [CH_2, C4′(8′) or C3′(9′)], 25.8 (CH_2, C4), 25.9 [CH_2, C3(5)], 28.9 [CH_2, C2(6)], 39.8 (C, C1′ and C6′), 41.7 [CH_2, C2′(10′) and C5′(7′)], 42.6 (CH, C1), 55.1 (CH_2, C11′ or C13′), 55.8 (CH_2, C13′ or C11′), 176.0 (C, CO). Anal. Calcd for $C_{19}H_{31}NO$: C 78.84, H 10.80, N 4.84. Found: 78.83, H 10.74, N 4.75.

6.1.24. *(3,4,8,9-Tetramethyl-12-azatricyclo[4.4.3.0^{1,6}]trideca-3,8-dien-12-yl) (cyclohexyl)methanone, (**28**)*

From 3,4,8,9-tetramethyl-12-azatricyclo[4.4.3.0^{1,6}]trideca-3,8-diene hydrochloride [41] (136 mg, 0.51 mmol), cyclohexanecarboxylic acid (62 mg, 0.48 mmol), HOBt (111 mg, 0.82 mmol), EDC (127 mg, 0.82 mmol) and triethylamine (0.3 mL, 2.38 mmol) in EtOAc (6 mL) and following the general procedure C, amide **28** (138 mg, 79% yield) was obtained as a yellowish solid. Column chromatography (hexane/EtOAc) gave **28** as a white solid (74 mg), mp 162–163 °C; IR (ATR) ν: 748, 785, 848, 973, 1118, 1358, 1434, 1441, 1603, 1613, 2861, 2931 cm^{-1}; ^{1}H NMR (400 MHz, $CDCl_3$) δ: 1.40–1.1.54 [complex signal, 3 H, 3(5)-H_{ax} and 4-H_{ax}], 1.56 (s, 12 H, CH_3), 1.62–1.98 [complex signal, 15 H, 3(5)-H_{eq}, 4-H_{eq}, 2-H_2, 6-H_2, 2′(10′)-H_2, 5′(7′)-H_2], 2.28 (tt, 1 H, J = 11.6 Hz, J' = 3.2 Hz, 1 H, 1-H), 3.28–3.34 (complex signal, 4 H, 11′-H_2 and 13′-H_2); ^{13}C NMR (100.5 MHz, $CDCl_3$) δ: 18.68 [CH_3, $H_3\underline{C}$-C3′(9′) or $H_3\underline{C}$-C4′(8′)], 18.71 [CH_3, $H_3\underline{C}$-C4′(8′) or $H_3\underline{C}$-C3′(9′)], 25.8 (CH_2, C4), 25.9 [CH_2, C3(5)], 28.9 [CH_2, C2(6)], 38.6 (CH_2, C1′ or C6′), 38.7 [CH_2, C2′(10′) or C5′(7′)], 38.8 [CH_2, C5′(7′) or C2′(10′)], 40.4 (CH_2, C6′ or C1′), 42.6 (CH, C1), 55.5 (CH_2, C11′ or C13′), 56.4 (CH_2, C13′ or C11′), 121.6 [C, C3′(9′) or C4′(8′)], 122.2 (C, C4′(8′) or C3′(9′)], 176.4 (C, CO); HRMS-ESI + m/z $[M+H]^+$ calcd for $[C_{23}H_{36}NO + H]^+$: 342.2791, found: 342.2793.

6.1.25. *(7,8,9,10-Tetramethyl-3-azapentacyclo[7.2.1.1^{5,8}.0^{1,5}.0^{7,10}] tridec-3-yl) (cyclohexyl) methanone, (**29**)*

From 7,8,9,10-tetramethyl-3-azapentacyclo[7.2.1.1^{5,8}.0^{1,5}.0^{7,10}] tridecane hydrochloride [40] (145 mg, 0.54 mmol), cyclohexanecarboxylic acid (67 mg, 0.52 mmol), HOBt (105 mg, 0.78 mmol), EDC (121 mg, 0.78 mmol) and triethylamine (0.3 mL, 2.29 mmol) in EtOAc (6 mL) and following the general procedure C, amide **29** (143 mg, 78% yield) was obtained as a yellowish solid. Column chromatography (hexane/EtOAc) gave **29** as a white solid (101 mg), mp 100–101 °C; IR (ATR) ν: 636, 747, 791, 829, 866, 891, 977, 1026, 1083, 1124, 1207, 1243, 1266, 1346, 1382, 1442, 1625, 2857, 2925 cm^{-1}; ^{1}H NMR (400 MHz, $CDCl_3$) δ: 0.84 [dd, J = 10.8 Hz, J' = 4.8 Hz, 4 H, 6′(13′)-H_2 or 11′(12′)-H_2], 0.93 (d, J = 3.6 Hz, 12 H, 7′(8′)-$C\underline{H}_3$ and 9′(10′)-$C\underline{H}_3$], 1.18–1.34 [complex signal, 3 H, 3(5)-H_{ax} and 4-H_{ax}], 1.52 (m, 2 H, 2(6)-H_{ax}), 1.64–1.84 [complex signal, 9 H, 3(5)-H_{eq}, 4-H_{eq}, 2(6)-H_{ax} and 11′(12′)-H_2 or 6′(13′)-H_2], 2.35 (tt, 1 H, J = 11.6 Hz, J' = 3.2 Hz, 1 H, 1-H), 3.59 (d, J = 15.6 Hz, 4 H, 2′-H_2 and 4′-H_2); ^{13}C NMR (100.5 MHz, $CDCl_3$) δ: 15.5 [CH_3, $H_3\underline{C}$-C7′(8′) or $H_3\underline{C}$-C9′(10′)], 15.6 [CH_3, $H_3\underline{C}$-C9′(10′) or $H_3\underline{C}$-C7′(8′)], 25.8 (CH_2, C4), 25.9 [CH_2, C3(5)], 29.0 [CH_2, C2(6)], 42.4 (CH, C1), 42,9 [CH_2, C6′(13′) or C11′(12′)], 43.0 [CH_2, C11′(12′) or C6′(13′)], 45.3 [C, C7′(8′) or C9′(10′)], 45.4 [C, C9′(10′) or C7′(8′)], 47.0 (C, C1′ or C5′), 48.9 (C, C5′ or C1′), 51.6 [CH_2, C2′ or C4’], 53.1 [CH_2, C4′ or C2’], 174.6 (C, CO). Anal. Calcd for $C_{23}H_{35}NO$: C 80.88, H 10.33, N 4.10. Found: 80.97, H 10.27, N 4.00.

6.2. *Molecular modeling*

Docking calculations were carried out using Glide [60], with the X-ray structure of human enzyme 4BB6 [61]. The geometry of each ligand was energy minimized and the centroid of the inhibitor cocrystalised in 4BB6 was used to generate the docking cavity by selecting all the residues located within 20 Å from the ligand. Between 70 and 100 poses were generated for each ligand, and the best-scored poses (and the expected arrangement within the binding pocket) were chosen as starting structures for MD simulations.

For each ligand-protein complex two independent 50ns MD simulations were run to check the consistency of the binding mode. To this end, the ligand-protein complex was immersed in an octahedral box of TIP3P [62] water molecules and sodium ions were added to neutralize the system. The force field ff99SBildn [63,64] was used for the protein parameters, and RESP charges at the HF/6-31G (d) together with the gaff [65] force field were used to for the ligand and NADP parameters. All systems were refined using a three-step energy minimization procedure (involving first hydrogen atoms, then water molecules, and finally the whole system) and a six-step equilibration (heating the system from 0 K to 300 K in 6 steps of 20 ps, the first, 50 ps the next four, and 5 ns the last one).

6.3. *Human 11β-HSD1 in vitro enzyme inhibition assay*

11β-HSD1 activity was determined in mixed sex, human liver microsomes (Celsis In-vitro Technologies) by measuring the conversion of ^{3}H-cortisone to ^{3}H-cortisol. Percentage inhibition was determined relative to a no inhibitor control. 5 μg of human liver microsomes were pre-incubated at 37 °C for 15 min with inhibitor and 1 mM NADPH in a final volume of 90 μL Krebs buffer. 10 μL of 200 nM ^{3}H-cortisone was then added followed by incubation at 37 °C for a further 30 min. The assay was terminated by rapid freezing on dry ice and ^{3}H-cortisone to ^{3}H-cortisol conversion determined in 50 μL of the defrosted reaction by capturing liberated ^{3}H-cortisol on anti-cortisol (HyTest Ltd)-coated scintillation proximity assay beads (protein A-coated YSi, GE Healthcare). A nanomolar 11β-HSD1 inhibitor, UE2316, was added as a positive control within in each set of assays. IC_{50} values for UE2316 were within the normal range across each test occasion [66].

6.4. *Mouse 11β-HSD1 in vitro enzyme inhibition assay*

11β-HSD1 activity was determined in pooled mouse (CD-1) liver microsomes (Celsis In-vitro Technologies) by measuring the conversion of cortisone to cortisol by LC/MS. Percentage inhibition was determined relative to a no inhibitor control. 5 μg of mouse liver microsomes were pre-incubated at 37 °C for 15 min with inhibitor and 1 mM NADPH in a final volume of 90 μL Krebs buffer. 10 μL of 2 μM cortisone was then added followed by incubation at 37 °C for a further 30 min. The assay was terminated by rapid freezing on dry ice and subsequent extraction with acetonitrile on thawing. Samples dried down under nitrogen at 65 °C and solubilised in 100 μL 70:30 H_2O:ACN and removed to a 96-well V-bottomed plate for LC/MS analysis. Separation was carried out on a sunfire 150 × 2.1 mm, 3.5 μM column using a H_2O:ACN gradient profile. Typical retention times were 2.71 min for cortisol and 2.80 min for cortisone. The peak area was calculated and the concentration of each compound determined from the calibration curve.

6.5. *Microsomal stability assay*

The microsomal stability of each compound was determined using either human or mouse liver microsomes (Celsis In-vitro Technologies). Microsomes were thawed and diluted to a concentration of 2 mg/mL in 50 mM $NaPO_4$ buffer pH 7.4. Each compound was diluted in 4 mM NADPH (made in the phosphate buffer above) to a concentration of 10 μM. Two identical incubation plates were prepared to act as a 0 min and a 30 min time point assay. 30 μL of each compound dilution was added in duplicate to the wells of a U-bottom 96-well plate and warmed at 37 °C for approximately 5 min. Verapamil, lidocaine and propranolol at 10 μM concentration were utilized as reference compounds in this experiment. Microsomes were also pre-warmed at 37 °C before the addition of 30 μL to each well of the plate resulting in a final concentration of 1 mg/mL. The reaction was terminated at the appropriate time point (0 or 30 min) by addition of 60 μL of ice-cold 0.3 M trichloroacetic acid (TCA) per well. The plates were centrifuged for 10 min at 112 x *g* and the supernatant fraction transferred to a fresh U-bottom 96-well plate. Plates were sealed and frozen at −20 °C prior to MS analysis. LC-MS/MS was used to quantify the peak area response of each compound before and after incubation with liver microsomes using MS tune settings established and validated for each compound. These peak intensity measurements were used to calculate the % remaining after incubation with microsomes for each hit compound.

6.6. *Cellular 11β-HSD1 enzyme inhibition assay*

The cellular 11β-HSD1 enzyme inhibition assay was performed using HEK293 cells stably transfected with the human 11β-HSD1 gene. Cells were incubated with substrate (cortisone) and product (cortisol) was determined by LC/MS. Cells were plated at 2×10^4 cells/well in a 96-well poly-D-lysine coated tissue culture microplate (Greiner Bio-one) and incubated overnight at 37 °C in 5% CO_2 95% O_2. Compounds to be tested were solubilised in 100% DMSO at 10 mM and serially diluted in water and 10% DMSO to final concentration of 10 μM in 10% DMSO. 10 μL of each test dilution and 10 μL of 10% DMSO (for low and high control) were dispensed into the well of a new 96-well microplate (Greiner Bio-one). Medium was removed from the cell assay plate and 100 μL of DMEM solution (containing 1% penicillin, 1% streptomycin and 300 nM cortisone) added to each well. Cells were incubated for 2 h at 37 °C in 5% CO_2 95% O_2. Following incubation, medium was removed from each well into an eppendorf containing 500 μL of ethyl acetate, mixed by vortex and incubated at rt for 5 min. A calibration curve of known concentrations of cortisol in assay medium was also set up and added to 500 μL of ethyl acetate, vortexed and incubated as above. The supernatant of each eppendorf was removed to a 96-deep-well plate and dried down under liquid nitrogen at 65 °C. Each well was solubilised in 100 μL 70:30 H_2O:ACN and removed to a 96-well V-bottomed plate for LC/MS analysis. Separation was carried out on a sunfire 150 × 2.1 mm, 3.5 μM column using a H_2O:ACN gradient profile. Typical retention times were 2.71 min for cortisol and 2.8 min for cortisone. The peak area was calculated and the concentration of each compound determined from the calibration curve.

6.7. *Cellular 11β-HSD2 enzyme inhibition assay*

For measurement of inhibition of 11β-HSD2, HEK293 cells stably transfected with the full-length gene coding for human 11β-HSD2 were used. The protocol was the same as for the cellular 11β-HSD1 enzyme inhibition assay, only changing the substrate, this time cortisol, and the concentrations of the tested compounds, 10, 1 and 0.1 μM.

6.8. *Parallel Artificial Membrane Permeation Assays- Blood-Brain Barrier (PAMPA-BBB)*

To evaluate the brain penetration of the different compounds, a parallel artificial membrane permeation assay for blood-brain barrier was used, following the method described by Di [50]. The *in vitro* permeability (P_e) of fourteen commercial drugs through lipid extract of porcine brain membrane together with the test compounds were determined. Commercial drugs and assayed compounds were tested using a mixture of PBS:EtOH (70:30). Assay validation was made by comparing the experimental permeability with the reported values of the commercial drugs by bibliography and lineal correlation between experimental and reported permeability of the fourteen commercial drugs using the parallel artificial membrane permeation assay was evaluated ($y = 1.5366x - 0.9672$; $R_2 = 0.9382$). From this equation and taking into account the limits established by Di et al. for BBB permeation [50], we established the ranges of permeability as compounds of high BBB permeation (CNS +): P_e (10^{-6} cm s^{-1}) > 5.179; compounds of low BBB permeation (CNS −): P_e (10^{-6} cm s^{-1}) < 2.106 and compounds of uncertain BBB permeation (CNS ±): 5.179 > P_e (10^{-6} cm s^{-1}) > 2.106.

6.9. *Pharmacokinetic study*

All the animal experiments were performed according to the protocols approved by the Animal Experimentation Ethical Committee of Universitat Autònoma de Barcelona and by the Animal Experimentation Commission of the Generalitat de Catalunya (Catalan Government). Male CD-1 mice (20–25 g) purchased from Envigo Laboratories were used. Compound **23** was dissolved in cyclodextrin 10% at 3 mg/mL to give a clear solution. After oral administration (21 mg/kg, 10 mL/kg), blood (0.6 mL) was collected from cava vein using a syringe (23G needle) rinsed with 5% EDTA(K2) at 0, 0.5, 1, 3, 5 and 24 (3 animals/point). Each blood sample was immediately transferred to a tube containing 40 μL of water with 5% EDTA. Blood samples were centrifuged at 10000 g for 5 min and plasma samples were stored at −20 °C until analysis of compound concentration by UPLC-MS/MS. Brains were transcardially perfused with 10 mL of saline, removed, frozen in liquid N_2 and stored at −80 °C until analysis of the compound concentration by UPLC-MS/MS.

6.10. *In vivo study*

6.10.1. *Animals*

SAMP8 mice 12 months old (n = 12) were randomized in 2 experimental groups (control, n = 4; treated, n = 8), and additional group 2 months old (n = 4) were planned as a young population. Mice were used with free access to food and water, under standard temperature conditions (22 ± 2 °C) and 12-h:12-h light-dark cycles (300 lx/0 lx). Compound **23** was administered dissolved in tap water and PEG400 (2% final concentration) yielding a dose of 21 mpk for 4 weeks. The dose was selected based on the IC_{50} value of **23** and our previous expertise in *in vivo* studies with other 11β-HSD1 inhibitors [20,21]. To maintain the correct dose along the treatment period, once a week the weight of the animals and the quantity of water that they drank were measured. Therefore, we adjusted the concentration (mg/mL) of the compound **23** in the drink bottle to achieve the correct dose of compound (mpk) to be administered to mice. Studies were performed in accordance with the institutional guidelines for the care and use of laboratory animals established by the Ethical Committee for Animal Experimentation at the University of Barcelona.

6.10.2. Novel Object Recognition Test (NORT)

The test was conducted in a 90-degree, two-arm, 25-cm-long, 20-cm-high maze. Light intensity in the middle of the field was 30 lux. The objects to be discriminated were plastic figures (object A, 5.25-cm-high, and object B, 4.75-cm-high). First, mice were individually habituated to the apparatus for 10 min per day during 3 days. On day 4, they were submitted to a 10-min acquisition trial (first trial), during which they were placed in the maze in the presence of two identical novel objects (A + A or B + B) placed at the end of each arm. A 10-min retention trial (second trial) occurred 2 h (short term memory) or 24 h (long term memory) later. During this second trial, objects A and B were placed in the maze, and the times that the animal took to explore the new object (tn) and the old object (to) were recorded. A Discrimination index (DI) was defined as (tn-to)/(tn + to). In order to avoid object preference biases, objects A and B were counterbalanced so that one half of the animals in each experimental group were first exposed to object A and then to object B, whereas the other one half first saw object B and then object A was presented. The maze, the surface, and the objects were cleaned with 96° ethanol between the animals' trials so as to eliminate olfactory cues.

6.10.3. Brain isolation and western blot analysis

Mice were euthanized 1 day after the last NORT trial was conducted, and brain quickly removed from the skull. Hippocampus were dissected and frozen in powdered dry ice and maintained at −80 °C for further use. Tissue samples were homogenized in lysis buffer containing phosphatase and protease inhibitors (Cocktail II, Sigma), and cytosol and nuclear fractions were obtained as described elsewhere. Protein concentration was determined by the Bradford method. 20 µg of protein were separated by Sodium dodecyl sulfate-Polyacrylamide gel electrophoresis (SDS-PAGE) (8–15%) and transferred onto Polyvinylidene diflouride (PVDF) membranes (Millipore). The membranes were blocked in 5% non-fat milk in Tris-buffered saline containing 0.1% Tween 20 (TBS-T) for 1 h at rt, followed by overnight incubation at 4 °C with primary antibodies against PSD95 (1:1,000, ab18258/Abcam), IDE (1:1,000, ab32216/Abcam) and APP C-Terminal Fragment (1:1,000, C1/6.1/Covance) diluted in TBS-T and 5% bovine serum albumin (BSA). GAPDH (1:2,000, Millipore) was used as a control protein charge. Membranes were then washed and incubated with secondary antibodies for 1 h at rt. Immunoreactive proteins were visualized utilizing an Enhanced chemiluminescence-based detection kit (ECL kit; Millipore) and digital images were acquired employing a ChemiDoc XRS + System (BioRad). Band intensities were quantified by densitometric analysis using Image Lab software (BioRad) and values were normalized to GAPDH.

6.10.4. RNA extraction and gene expression determination

Total RNA isolation was carried out by means of Trizol reagent following the manufacturer's instructions. RNA content in the samples was measured at 260 nm, and sample purity was determined by the A260/280 ratio in a NanoDrop™ ND-1000 (Thermo Scientific). Samples were also tested in an Agilent 2100B Bioanalyzer (Agilent Technologies) to determine the RNA integrity number. Reverse transcription-Polymerase chain reaction (RT-PCR) was performed as follows: 2 µg of messenger RNA (mRNA) was reverse-transcribed using the High Capacity complementary DNA (cDNA) Reverse Transcription kit (Applied Biosystems). Real-time quantitative PCR (qPCR) was utilized to quantify the mRNA expression of inflammatory genes Interleukin 6 (*IL-6*) and inducible nitric oxide synthase (*iNOS*). Normalization of expression levels was performed with *Actin* for SYBER Green. The primers were as follows: for *IL-6*, forward 5′-ATCCAGTTGCCTTCTTGGGACTGA-3′ and reverse 5′-TAAGCCTCCGACTTGTGAAGTGGT-3′, for *iNOS*, forward 5′- GGCAGCCTGTGAGACCTTTG-3′ and reverse 5′-GAAGCGTTTCGGGATCTGAA-3′, for *Actin*, forward 5′-CAACGAGCGGTTCCGAT-3′ and reverse 5′-GCCACAGGTTCCATACCCA-3'.

Real-time PCR was performed on the Step One Plus Detection System (Applied Biosystems) employing the SYBR Green PCR Master Mix (Applied Biosystems). Each reaction mixture contained 7.5 µL of cDNA, whose concentration was 2 µg/µL, 0.75 µL of each primer (whose concentration was 100 nM), and 7.5 µL of SYBR Green PCR Master Mix (2X).

Data were analysed utilizing the comparative Cycle threshold (Ct) method (ΔΔCt), where the actin transcript level was utilized to normalize differences in sample loading and preparation. Each sample (n = 4–8) was analysed in triplicate, and the results represented the n-fold difference of transcript levels among different samples.

6.10.5. Data analysis

Data are expressed as the mean ± Standard Error of the Mean (SEM). Data analysis was conducted using GraphPad Prism® ver. 6 statistical software. Means were compared with one-way Analysis of Variance (ANOVA) and Tukey post hoc analysis.

Acknowledgements

We thank financial support from *Ministerio de Economía y Competitividad* and FEDER (Projects SAF2014-57094-R and SAF2016-77703-C2-1-R) and the *Generalitat de Catalunya* (grants 2014-SGR-00052 and 2014-SGR-1189) and the *Consorci de Serveis Universitaris de Catalunya* for computational resources. R. L. thanks the Spanish *Ministerio de Educación Cultura y Deporte* for a PhD Grant (FPU program, FPU13/05657) and the *Fundació Universitària Agustí Pedro i Pons* for a Travel Grant. E. V. thanks the Institute of Biomedicine of the University of Barcelona (IBUB) for a PhD Grant. F. J. L. acknowledges the support from ICREA Academia. We thank ACCIÓ (*Generalitat de Catalunya*) and CIDQO 2012 SL for financial support (*Programa Nuclis*, RD14-1-0057, SAFNAD).

Appendix A. Supplementary data

Supplementary data related to this article can be found at http://dx.doi.org/10.1016/j.ejmech.2017.08.003.

References

[1] M.J. Meaney, D. O'Donnell, W. Rowe, B. Tannenbaum, A. Steverman, M. Walker, N.P.V. Nair, S. Lupien, Individual differences in hypothalamic-pituitary-adrenal activity in later life and hippocampal aging, Exp. Gerontol. 30 (1995) 229–251.

[2] J.L. Yau, T. Olsson, R.G. Morris, M.J. Meaney, J.R. Seckl, Glucocorticoids, hippocampal corticosteroid receptor gene expression and antidepressant treatment: relationship with spatial learning in young and aged rats, Neuroscience 66 (1995) 571–581.

[3] S.J. Lupien, M. de Leon, S. de Santi, A. Convit, C. Tarshish, N.P.V. Nair, M. Thakur, B.S. McEwen, R.L. Hauger, M.J. Meaney, Cortisol levels during human aging predict hippocampal atrophy and memory deficits, Nat. Neurosci. 1 (1998) 69–73.

[4] R.M. Reynolds, Glucocorticoid excess and the developmental origins of disease: two decades of testing the hypothesis, Psychoneuroendocrinology 38 (2013) 1–11.

[5] E.R. Peskind, C.W. Wilkinson, E.C. Petrie, G.D. Schellenberg, M.A. Raskind, Increased CSF cortisol in AD is a function of APOE genotype, Neurology 56 (2001) 1094–1098.

[6] J.G. Cernansky, H. Dong, A.M. Fagan, L. Wang, C. Xiong, D.M. Holtzman, J.C. Morris, Plasma cortisol and progression of dementia in subjects with Alzheimer-type dementia, Am. J. Psychiatry 163 (2006) 2164–2169.

[7] K.N. Green, L.M. Billings, B. Roozendaal, J.L. McGaugh, F.M. LaFerla, Glucocorticoids increase amyloid-β and tau pathology in a mouse model of Alzheimer's disease, J. Neurosci. 26 (2006) 9047–9056.

[8] M.C. Holmes, J.L. Yau, Y. Kotelevtsev, J.J. Mullins, J.R. Seckl, 11 beta- hydroxysteroid dehydrogenases in the brain: two enzymes two roles, Ann. N.Y. Acad. Sci. 1007 (2003) 357–366.

[9] M.C. Holmes, J.R. Seckl, The role of 11 beta-hydroxysteroid dehydrogenases in the brain, Mol. Cell. Endocrinol. 248 (2006) 9–14.

[10] C.S. Wyrwoll, M.C. Holmes, J.R. Seckl, 11β-Hydroxysteroid dehydrogenases and the brain: from zero to hero, a decade of progress, Front. Neuroendocrinol. 32 (2011) 265–286.

[11] M.-P. Moisan, J.R. Seckl, C.R.W. Edwards, 11β-hydroxysteroid dehydrogenase bioactivity and messenger RNA expression in rat forebrain: localization in hypothalamus, hippocampus and cortex, Endocrinology 127 (1990) 1450–1455.

[12] G. Pelletier, V. Luu-The, S. Li, G. Bujold, F. Labrie, Localization and glucocorticoid regulation of 11beta-hydroxysteroid dehydrogenase type 1 mRNA in the male mouse forebrain, Neuroscience 145 (2007) 110–115.

[13] T.C. Sandeep, J.L. Yau, A.M. MacLullich, J. Noble, I.J. Deary, B.R. Walker, J.R. Seckl, 11Beta-hydroxysteroid dehydrogenase inhibition improves cognitive function in healthy elderly men and type 2 diabetics, Proc. Natl. Acad. Sci. U. S. A. 101 (2004) 6734–6739.

[14] R.W. Brown, R. Diaz, A.C. Robson, Y.V. Kotelevtsev, J.J. Mullins, M.H. Kaufman, J.R. Seckl, The ontogeny of 11 beta-hydroxysteroid dehydrogenase type 2 and mineralocorticoid receptor gene expression reveal intricate control of glucocorticoid action in development, Endocrinology 137 (1996) 794–797.

[15] R.W. Brown, Y. Kotolevtsev, C. Leckie, R.S. Lindsay, V. Lyons, P. Murad, J.J. Mullins, K.E. Chapman, C.R.W. Edwards, J.R. Seckl, Isolation and cloning of human placental 11β-hydroxysteroid dehydrogenase-2 cDNA, Biochem. J. 313 (1996) 1007–1017.

[16] C. Wyrwoll, M. Keith, J. Noble, P.L. Stevenson, V. Bomball, S. Crombie, L.C. Evans, M.A. Bailey, E. Wood, J.R. Seckl, M.C. Holmes, Fetal brain 11β-hydroxysteroid dehydrogenase type 2 selectively determines programming of adult depressive-like behaviors and cognitive function, but not anxiety behaviors in male mice, Psychoneuroendocrinology 59 (2015) 59–70.

[17] M.C. Holmes, R.N. Carter, J. Noble, S. Chitnis, A. Dutia, J.M. Paterson, J.J. Mullins, J.R. Seckl, J.L. Yau, 11β-hydroxysteroid dehydrogenase type 1 expression is increased in the aged mouse hippocampus and parietal cortex and causes memory impairments, J. Neurosci. 30 (2010) 6916–6920.

[18] J.L. Yau, J. Noble, C.J. Kenyon, C. Hibberd, Y. Kotelevtsev, J.J. Mullins, J.R. Seckl, Lack of tissue glucocorticoid reactivation in 11beta-hydroxysteroid dehydrogenase type 1 knockout mice ameliorates age-related learning impairments, Proc. Natl. Acad. Sci. U. S. A. 98 (2001) 4716–4721.

[19] K. Sooy, S.P. Webster, J. Noble, M. Binnie, B.R. Walker, J.R. Seckl, J.L.W. Yau, Partial deficiency or short-term inhibition of 11β-hydroxysteroid dehydrogenase type 1 improves cognitive function in aging mice, J. Neurosci. 30 (2010) 13867–13872.

[20] N. Wheelan, S.P. Webster, C.J. Kenyon, S. Caughey, B.R. Walker, M.C. Holmes, J.R. Seckl, J.L.W. Yau, Short-term inhibition of 11β-hydroxysteroid dehydrogenase type 1 reversibly improves spatial memory but persistently impairs contextual fear memory in aged mice, Neuropharmacol 91 (2015) 71–76.

[21] K. Sooy, J. Noble, A. McBride, M. Binnie, J.L.W. Yau, J.R. Seck, B.R. Walker, S.P. Webster, Cognitive and disease-modifying effects of 11β-hydroxysteroid dehydrogenase type 1 inhibition in male Tg2576 mice, a model of Alzheimer's Disease, Endocrinology 156 (2015) 4592–4603.

[22] E.G. Mohler, K.E. Browman, V.A. Roderwald, E.A. Cronin, S. Markosyan, R.S. Bitner, M.I. Strakhova, K.U. Drescher, W. Hornberger, J.J. Rohde, M.E. Brune, P.B. Jacobson, L.E. Rueter, Acute inhibition of 11β-hydroxysteroid dehydrogenase type-1 improves memory in rodent models of cognition, J. Neurosci. 31 (2011) 5406–5413.

[23] J.L.W. Yau, J.R. Seckl, Local amplification of glucocorticoids in the aging brain and impaired spatial memory, Front. Aging Neurosci. 4 (2012) 24.

[24] J.E. Morley, S.A. Farr, V.B. Kumar, H.J. Armbrecht, The SAMP8 mouse: a model to develop therapeutic interventions for Alzheimer's disease, Curr. Pharm. Des. 18 (2012) 1123–1130.

[25] J.E. Morley, H.J. Armbrecht, S.A. Farr, V.B. Kumar, The senescence accelerated mouse (SAMP8) as a model for oxidative stress and Alzheimer's disease, Biochim. Biophys. Acta 1822 (2012) 650–656.

[26] S. Olson, S.D. Aster, K. Brown, L. Carbin, D.W. Graham, A. Hermanowski-Vosatka, C.B. LeGrand, S.S. Mundt, M.A. Robbins, J.M. Schaeffer, L.H. Slossberg, M.J. Szymonifka, R. Thieringer, S.D. Wright, J.M. Balkovec, Adamantyl triazoles as selective inhibitors of 11beta-hydroxysteroid dehydrogenase type 1, Bioorg. Med. Chem. Lett. 15 (2005) 4359–4362.

[27] B. Sorensen, J. Rohde, J. Wang, S. Fung, K. Monzon, W. Chiou, L. Pan, X. Deng, D. Stolarik, E.U. Frevert, P. Jacobson, J.T. Link, Adamantane 11-beta-HSD-1 inhibitors: application of an isocyanide multicomponent reaction, Bioorg. Med. Chem. Lett. 16 (2006) 5958–5962.

[28] C.L. Becker, K.M. Engstrom, F.A. Kerdesky, J.C. Tolle, S.H. Wagaw, W. Wang, A convergent process for the preparation of adamantane 11b-HSD1 inhibitors, Org. Process Res. Dev. 12 (2008) 1114–1118.

[29] J.S. Scott, P. Barton, S.N.L. Bennett, J. deSchoolmeester, L. Godfrey, E. Kilgour, R.M. Mayers, M.J. Packer, A. Rees, P. Schofield, N. Selmi, J.G. Swales, P.R.O. Whittamore, Reduction of acyl glucuronidation in a series of acidic 11beta-hydroxysteroid dehydrogenase type 1 (11beta-HSD1) inhibitors: the discovery of AZD6925, Med. Chem. Commun. 3 (2012) 1264–1269.

[30] J.S. Scott, J. deSchoolmeester, E. Kilgour, R.M. Mayers, M.J. Packer, D. Hargreaves, S. Gerhardt, D.J. Ogg, A. Rees, N. Selmi, A. Stocker, J.G. Swales, P.R.O. Whittamore, Novel acidic 11β-hydroxysteroid dehydrogenase type 1 (11β-HSD1) inhibitor with reduced acyl glucuronide liability: the discovery of 4-[4-(2-adamantylcarbamoyl)-5-tert-butyl-pyrazol-1-yl]benzoic acid (AZD8329), J. Med. Chem. 55 (2012) 10136–10147.

[31] O. Venier, C. Pascal, A. Braun, C. Namane, P. Mougenot, O. Crespin, F. Pacquet, C. Mougenot, C. Monseau, B. Onofri, R. Dadji-Faïhun, C. Leger, M. Ben-Hassine, T. Van-Pham, J.-L. Ragot, C. Philippo, G. Farjot, L. Noah, K. Maniani, A. Boutarfa, E. Nicolaï, E. Guillot, M.-P. Pruniaux, S. Güssregen, C. Engel, A.-L. Coutant, B. de Miguel, A. Castro, Discovery of SAR184841, a potent and long-lasting inhibitor of 11β-hydroxysteroid dehydrogenase type 1, active in a physiopathological animal model of T2D, Bioorg. Med. Chem. Lett. 23 (2013) 2414–2421.

[32] S.B. Park, W.H. Jung, N.S. Kang, J.S. Park, G.H. Bae, H.Y. Kim, S.D. Rhee, S.K. Kang, J.H. Ahn, H.G. Jeong, K.Y. Kim, Anti-diabetic and anti-inflammatory effect of a novel selective 11β-HSD1 inhibitor in the diet-induced obese mice, Eur. J. Pharmacol. 721 (2013) 70–79.

[33] S. Okazaki, T. Takahashi, T. Iwamura, J. Nakaki, Y. Sekiya, M. Yagi, H. Kumagai, M. Sato, S. Sakami, A. Nitta, K. Kawai, M. Kainoh, HIS-388, a novel orally active and long-acting 11β-hydroxysteroid dehydrogenase type 1 inhibitor, ameliorates insulin sensitivity and glucose intolerance in diet-induced obesity and nongenetic type 2 diabetic murine models, J. Pharmacol. Exp. Ther. 351 (2014) 181–189.

[34] S.Y. Byun, Y.J. Shin, K.Y. Nam, S.P. Hong, S.K. Ahn, A novel highly potent and selective 11β-hydroxysteroid dehydrogenase type 1 inhibitor, UI-1499, Life Sci. 120 (2015) 1–7.

[35] J.P. Gibbs, M.G. Emery, I. McCaffery, B. Smith, M.A. Gibbs, A. Akrami, J. Rossi, K. Paweletz, M.R. Gastonguay, E. Bautista, M. Wang, R. Perfetti, O. Daniels, Population pharmacokinetic/pharmacodynamic model of subcutaneous adipose 11β-hydroxysteroid dehydrogenase type 1 (11β-HSD1) activity after oral administration of AMG 221, a selective 11β-HSD1 inhibitor, J. Clin. Pharmacol. 51 (2011) 830–841.

[36] S. Shah, A. Hermanowski-Vosatka, K. Gibson, R.A. Ruck, G. Jia, J. Zhang, P.M.T. Hwang, N.W. Ryan, R.B. Langdon, P.U. Feig, Efficacy and safety of the selective 11β-HSD1 inhibitors MK-0736 and MK-0916 in overweight and obese patients with hypertension, J. Am. Soc. Hypertens. 5 (2011) 166–176.

[37] M.D. Duque, P. Camps, L. Profire, S. Montaner, S. Vázquez, F.X. Sureda, J. Mallol, M. López-Querol, L. Naesens, E. De Clercq, S.R. Prathalingam, J.M. Kelly, Synthesis and pharmacological evaluation of (2-oxaadamantan-1-yl)amines, Bioorg. Med. Chem. 17 (2009) 3198–3206.

[38] M.D. Duque, C. Ma, E. Torres, J. Wang, L. Naesens, J. Juárez-Jiménez, P. Camps, F.J. Luque, W.F. DeGrado, R.A. Lamb, L.H. Pinto, S. Vázquez, Exploring the size limit of templates for inhibitors of the M2 ion channel of influenza A virus, J. Med. Chem. 54 (2011) 2646–2657.

[39] M. Rey-Carrizo, E. Torres, C. Ma, M. Barniol-Xicota, J. Wang, Y. Wu, L. Naesens, W.F. Degrado, R.A. Lamb, L.H. Pinto, S. Vázquez, 3-Azatetracyclo$[5.2.1.1^{5,8}.0^{1,5}]$undecane derivatives: from wild-type inhibitors of the M2 ion channel of influenza A virus to derivatives with potent activity against the V27A mutant, J. Med. Chem. 56 (2013) 9265–9274.

[40] M. Rey-Carrizo, M. Barniol-Xicota, C. Ma, M. Frigolé-Vivas, E. Torres, L. Naesens, S. Llabrés, J. Juárez-Jiménez, F.J. Luque, W.F. Degrado, R.A. Lamb, L.H. Pinto, S. Vázquez, Easily accessible polycyclic amines that inhibit the wild-type and amantadine-resistant mutants of the M2 channel of the influenza A virus, J. Med. Chem. 57 (2014) 5738–5747.

[41] E. Torres, R. Leiva, S. Gazzarrini, M. Rey-Carrizo, M. Frigolé-Vivas, A. Moroni, L. Naesens, S. Vázquez, Azapropellanes with anti-influenza a virus activity, ACS Med. Chem. Lett. 5 (2014) 831–836.

[42] R. Leiva, S. Gazzarrini, R. Esplugas, A. Moroni, L. Naesens, F.X. Sureda, S. Vázquez, Ritter reaction-mediated syntheses of 2-oxaadamantan-5-amine, a novel amantadine analog, Tetrahedron Lett. 56 (2015) 1272–1275.

[43] M.D. Duque, P. Camps, E. Torres, E. Valverde, F.X. Sureda, M. López-Querol, A. Camins, S.R. Prathalingam, J.M. Kelly, S. Vázquez, New oxapolycyclic cage amines with NMDA receptor antagonist and trypanocidal activities, Bioorg. Med. Chem. 18 (2010) 46–57.

[44] E. Torres, M.D. Duque, M. López-Querol, M.C. Taylor, L. Naesens, C. Ma, L.H. Pinto, F.X. Sureda, J.M. Kelly, S. Vázquez, Synthesis of benzopolycyclic cage amines: NMDA receptor antagonist, trypanocidal and antiviral activities, Bioorg. Med. Chem. 20 (2012) 942–948.

[45] E. Valverde, F.X. Sureda, S. Vázquez, Novel benzopolyclic amines with NMDA receptor antagonist activity, Bioorg. Med. Chem. 22 (2014) 2678–2683.

[46] E. Valverde, C. Seira, A. McBride, M. Binnie, F.J. Luque, S.P. Webster, A. Bidon-Chanal, S. Vázquez, Searching for novel applications of the benzohomoadamantane scaffold in medicinal chemistry: synthesis of novel 11β-HSD1 inhibitors, Bioorg. Med. Chem. 23 (2015) 7607–7617.

[47] H. Cheng, J. Hoffman, P. Le, S.K. Nair, S. Cripps, J. Matthews, C. Smith, M. Yang, S. Kupchinsky, K. Dress, M. Edwards, B. Cole, E. Walters, C. Loh, J. Ermolieff, A. Fanjul, G.B. Bhat, J. Herrera, T. Pauly, N. Hosea, G. Paderes, P. Rejto, The development and SAR of pyrrolidine carboxamide 11β-HSD1 inhibitors, Bioorg. Med. Chem. Lett. 20 (2010) 2897–2902.

[48] R. Leiva, C. Seira, A. McBride, M. Binnie, A. Bidon-Chanal, F.J. Luque, S.P. Webster, S. Vázquez, Novel 11β-HSD1 inhibitors: effects of the C-1 vs C2-substitution and of the introduction of an oxygen atom in the adamantane scaffold, Bioorg. Med. Chem. Lett. 25 (2015) 4250–4253.

[49] During the writing of this manuscript it has been reported the discovery and the results of Phase 1 clinical trials of UE2343, a brain-penetrant 11β-HSD1 inhibitor featuring a pyrrolidine unit embedded in a tropane core. The compound is being developed by Actinogen Medical for the treatment of Alzheimer's disease. See, S.P. Webster, A. McBride, M. Binnie, K. Sooy, J.R. Seckl, R. Andrew, T.D. Pallin, H.J. Hunt, T.R. Perrior, V.S. Ruffles, J.W. Ketelbey, A. Boyd, B.R. Walker, Selection and early clinical evaluation of the brain-penetrant 11β-hydroxysteroid dehydrogenase type 1 (11β-HSD1) inhibitor

UE2343 (XanamemTM), British J. Pharmacol. 174 (2017) 396–408.

[50] L. Di, E.H. Kerns, K. Fan, O.J. McConnell, G.T. Carter, High throughput artificial membrane permeability assay for blood-brain barrier, Eur. J. Med. Chem. 38 (2003) 223–232.

[51] T. Takeda, Senescence-accelerated mouse (SAM) with special references to neurodegeneration models, SAMP8 and SAMP10 mice, Neurochem. Res. 34 (2009) 639–659.

[52] M. Pallàs, Senescence-accelerated mice P8: a tool to study brain aging and Alzheimer's disease in a Mouse Model, ISRN Cell Biol. (2012) 917167.

[53] C. Griñan-Ferré, V. Palomera-Ávalos, D. Puigoriol-Illamola, A. Camins, D. Porquet, V. Plá, F. Aguado, M. Pallàs, Behaviour and cognitive changes correlated with hippocampal neuroinflammaging and neuronal markers in female SAMP8, a model of accelerated senescence, Exp. Gerontol. 80 (2016) 57–69.

[54] M. Antunes, G. Biala, The novel object recognition memory: neurobiology, test procedure, and its modifications, Cogn. Process. 13 (2012) 93–110.

[55] M.P. Murphy, H. LeVine III, Alzheimer's disease and the amyloid-beta peptide, J. Alzheimers Dis. 19 (2010) 311–323.

[56] M. Kim, L.B. Hersh, M.A. Leissring, M. Ingelsson, T. Matsui, W. Farris, A. Lu, B.T. Hyman, D.J. Selkoe, L. Bertram, R.E. Tanzi, Decreased catalytic activity of the insulin-degrading enzyme in chromosome 10-linked Alzheimer Disease families, J. Biol. Chem. 282 (2007) 7825–7832.

[57] J.E. Morley, S.A. Farr, J.F. Flood, Antibody to amyloid beta protein alleviates impaired acquisition, retention, and memory processing in SAMP8 mice, Neurobiol. Learn. Mem. 78 (2002) 125–138.

[58] C.F. Culberson, P. Wilder Jr., The synthesis of 2-aza-1,2-dihydrodicyclopentadienes, J. Org. Chem. 25 (1960) 1358–1362.

[59] M. Fumimoto, K. Okabe, Nouvelle méthode de synthése des dérivés d'ethano-4,7 polyhydroisoindoline, Chem. Pharm. Bull. 10 (1962) 714–718.

[60] R.A. Friesner, R.B. Murphy, M.P. Repasky, L.L. Frye, J.R. Greenwood, T.A. Halgren, P.C. Sanschagrin, D.T. Mainz, Extra precision Glide: docking and scoring incorporating a model of hydrophobic enclosure for protein-ligand complexes, J. Med. Chem. 49 (2006) 6177–6196.

[61] F.W. Goldberg, A.G. Leach, J.S. Scott, W.L. Snelson, S.D. Groombridge, C.S. Donald, S.N.L. Bennett, C. Bodin, P.M. Gutierrez, A.C. Gyte, Free-Wilson and structural approaches to co-optimising human and rodent isoform potency for 11β-hydroxysteroid dehydrogenase type 1 (11β-HSD1) inhibitors, J. Med. Chem. 55 (2012) 10652–10661.

[62] W.L. Jorgensen, J. Chandrasekhar, J.D. Madura, R.W. Impey, M.L. Klein, Comparison of simple potential functions for simulating liquid water, J. Chem. Phys. 79 (1983) 926–935.

[63] V. Hornak, R. Abel, A. Okur, B. Strockbine, A. Roitberg, C. Simmerling, Comparison of multiple Amber force fields and development of improved protein backbone parameters, Proteins 65 (2006) 712–725.

[64] K. Lindorff-Larsen, S. Piana, K. Palmo, P. Maragakis, J.L. Klepeis, R.O. Dror, D.E. Shaw, Improved side-chain torsion potentials for the Amber ff99SB force field, Proteins 78 (2010) 1950–1958.

[65] J. Wang, R.M. Wolf, J.W. Caldwell, P.A. Kollman, D.A. Case, Development and testing of a general force field, J. Comp. Chem. 25 (2004) 1157–1174.

[66] J.L.W. Yau, N. Wheelan, J. Noble, B.R. Walker, S.P. Webster, C.J. Kenyon, M. Ludwig, J.R. Seckl, Intrahippocampal glucocorticoids generated by 11β-HSD1 affect memory in aged mice, Neurobiol. Aging 36 (2015) 334–343.

SUPPLEMENTARY MATERIAL FOR

Design, synthesis and *in vivo* study of novel pyrrolidine-based 11β-HSD1 inhibitors for age-related cognitive dysfunction

Rosana Leiva[1], Christian Griñan-Ferré[2], Constantí Seira[3], Elena Valverde[1], Andrew McBride[4], Margaret Binnie[4], Belén Pérez[5], F. Javier Luque[3], Mercè Pallàs[2], Axel Bidon-Chanal[3], Scott P. Webster[,4], and Santiago Vázquez*[*,1]*

[1]*Laboratori de Química Farmacèutica (Unitat Associada al CSIC), Facultat de Farmàcia i Institut de Biomedicina (IBUB), Universitat de Barcelona, Av. Joan XXIII, 27-31, 08028 Barcelona, Spain.*

[2]*Unitat de Farmacologia, Farmacognòsia i Terapèutica, Facultat de Farmàcia i Institut de Neurociències, Universitat de Barcelona, Av. Joan XXIII, 27-31, 08028 Barcelona, Spain.*

[3]*Department of Nutrition, Food Science and Gastronomy, Faculty of Pharmacy and Institute of Biomedicine (IBUB), University of Barcelona, Av. Prat de la Riba, 171, 08921 Santa Coloma de Gramenet, Spain.*

[4]*Centre for Cardiovascular Science, University of Edinburgh, Queen's Medical Research Institute, EH16 4TJ, United Kingdom.*

[5]*Departament de Farmacologia, Terapèutica i Toxicologia, Universitat Autònoma de Barcelona, 08193 Bellaterra, Barcelona, Spain.*

Table of contents

Figure S1 Page S3

Figure S2 Page S3

Figure S3 Page S4

Figure S4 Page S4

Table S1 Page S5

Figure S5 Page S5

Table S2 Page S6

Figure S6 Page S7

^{1}H and ^{13}C NMR spectra of new compounds Page S8

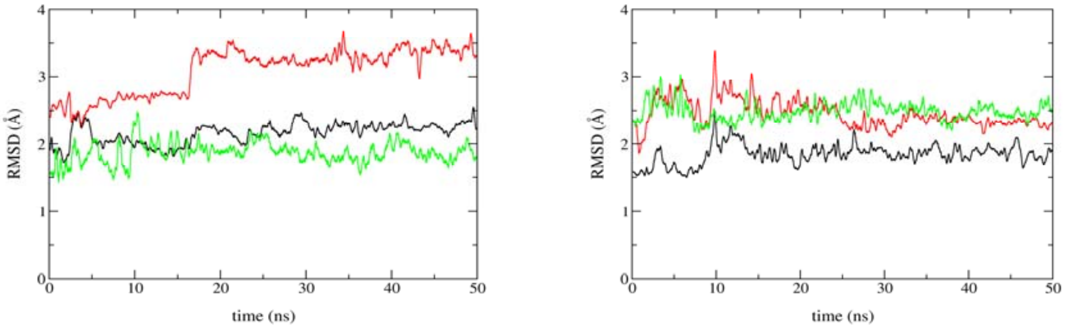

Figure S1. Representation of the root-mean square deviation (RMSD; Å) along the simulation time (ns) for the two independent MD simulations run for the complex between 11β-HSD1 and compound **12**. The RMSD was determined for the backbone atoms of the whole protein (black), the heavy atoms of the residues in the binding site (red), and the ligand (green).

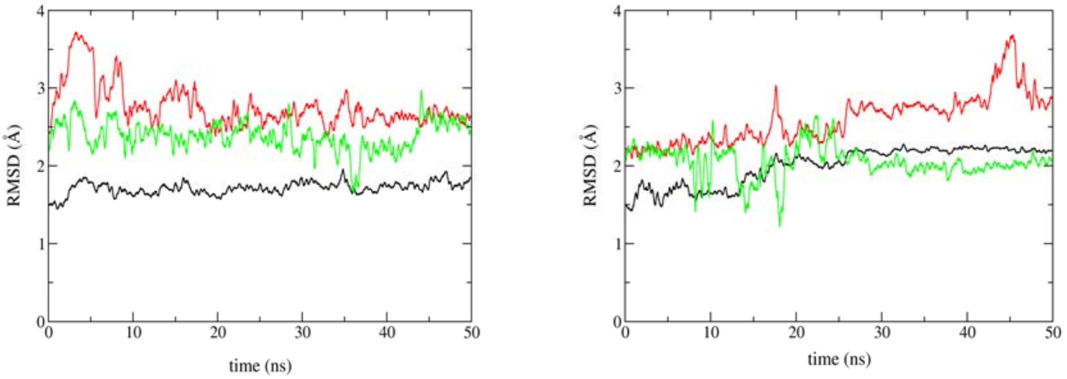

Figure S2. Representation of the root-mean square deviation (RMSD; Å) along the simulation time (ns) for the two independent MD simulations run for the complex between 11β-HSD1 and compound **14**. The RMSD was determined for the backbone atoms of the whole protein (black), the heavy atoms of the residues in the binding site (red), and the ligand (green).

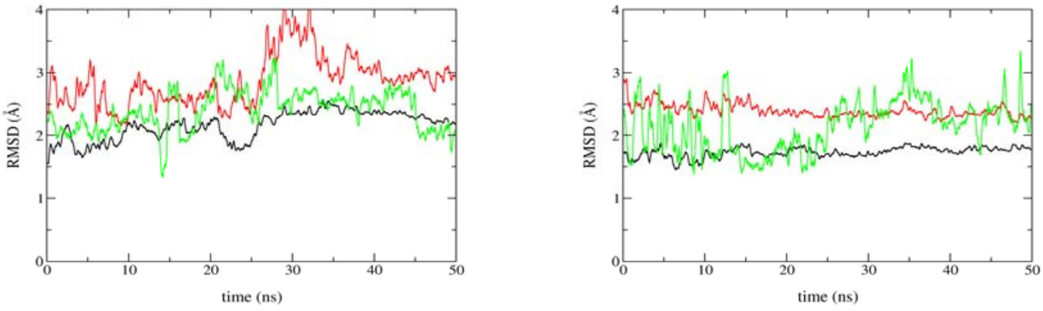

Figure S3. Representation of the root-mean square deviation (RMSD; Å) along the simulation time (ns) for the two independent MD simulations run for the complex between 11β-HSD1 and compound **8**. The RMSD was determined for the backbone atoms of the whole protein (black), the heavy atoms of the residues in the binding site (red), and the ligand (green).

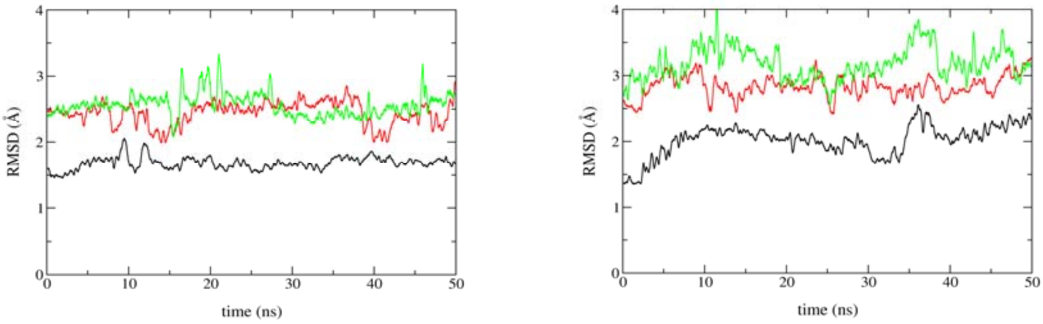

Figure S4. Representation of the root-mean square deviation (RMSD; Å) along the simulation time (ns) for the two independent MD simulations run for the complex between 11β-HSD1 and compound **23**. The RMSD was determined for the backbone atoms of the whole protein (black), the heavy atoms of the residues in the binding site (red), and the ligand (green).

23 PO 21 mg/kg				
Time	**ID**	**Total concentration (ng/mL)**	**Mean (ng/mL)**	**SD (ng/mL)**
0h	Mouse 31 Mouse 32 Mouse 33	0 0 0	0	0
0.5h	Mouse 1 Mouse 2 Mouse 3	47.05 32.05 54.65	44.58	11.50
1h	Mouse 4 Mouse 5 Mouse 6	10.13 6.01 14.65	10.26	4.32
3h	Mouse 7 Mouse 8 Mouse 9	3.73 0.97 1.67	2.12	1.43
5h	Mouse 10 Mouse 11 Mouse 12	0.10 0.15 0.60	0.28	0.28
24h	Mouse 13 Mouse 14 Mouse 15	0.00 0.00 0.00	0.00	0.00

Table S1. Concentrations of **23** in mouse plasma at different times after oral administration at 21 mg/kg.

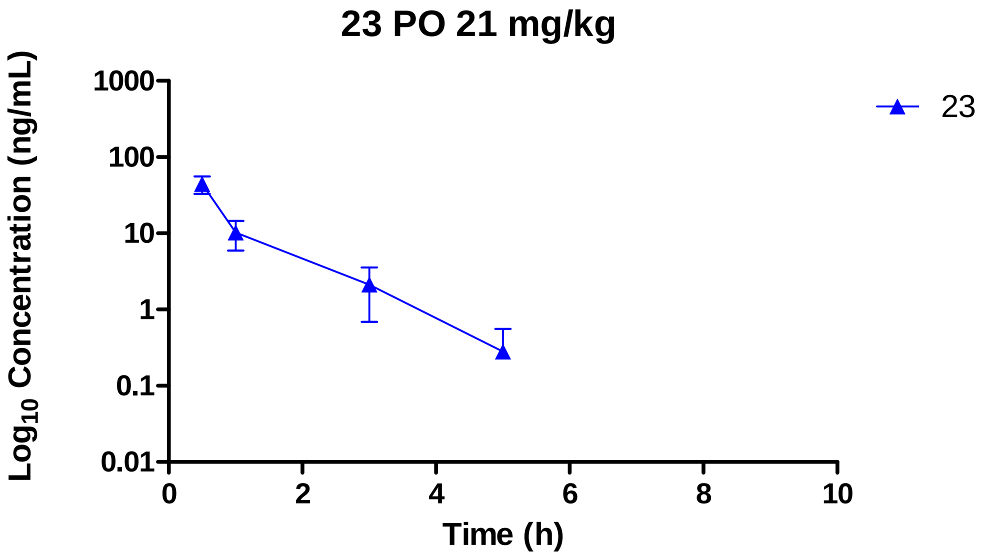

Figure S5. Concentration ($\log_{10}$) *vs* time for oral administration at 21 mg/kg of **23**.

Parameter	Units	Estimate
Lambda_z	1/h	0.899
HL_Lambda_z	h	0.771
Tmax	h	0.500
Cmax	ng/mL	44.583
Cmax_D	kg*ng/mL/mg	2.123
AUClast	h*ng/mL	39.721
AUCINF_obs	h*ng/mL	40.036
AUCINF_D_obs	h*kg*ng/mL/mg	1.906
AUC_%Extrap_obs	%	0.787
Vz_F_obs	L/kg	583.499
Cl_F_obs	L/h/kg	524.522

Table S2. Pharmacokinetic parameters of the pharmacokinetic study calculated by a Non Compartimental Analysis with Phoenix 7.0 Winnolin software.

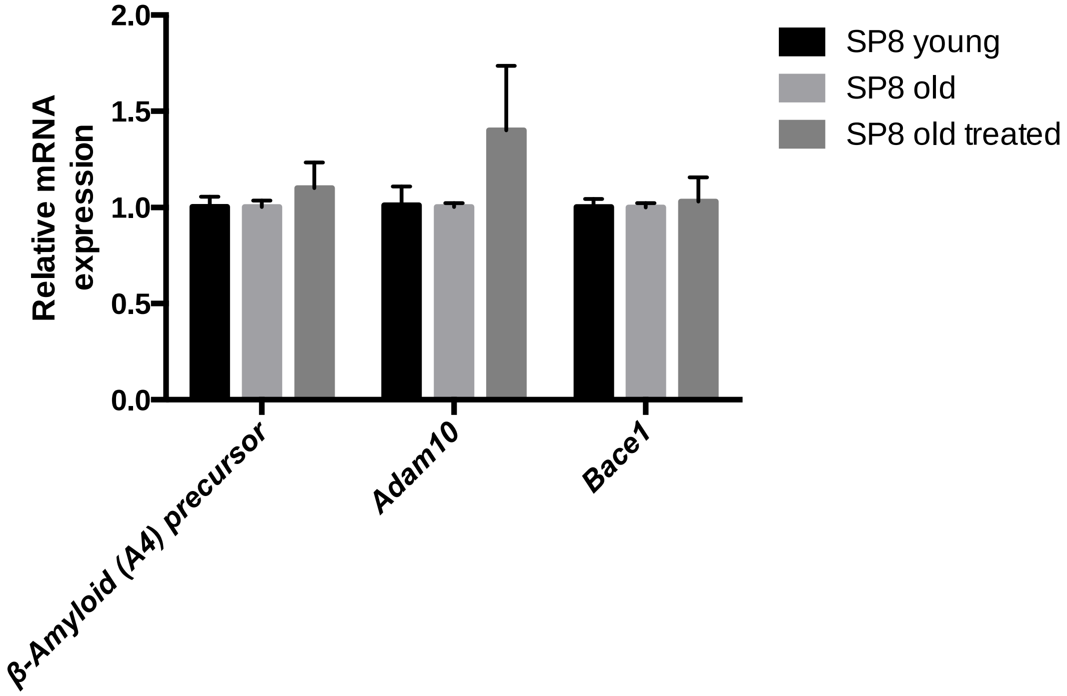

Figure S6. Lack of effects of amide **23** (at 21 mg/kg) on Pre-APP, Adam10 or Bace1 gene expression.

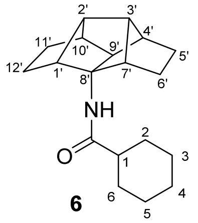
2'
3'
11'
10'
9'
4'
5'
12'
1'
8'
7'
6'
NH
O
1
2
3
4
5
6

6

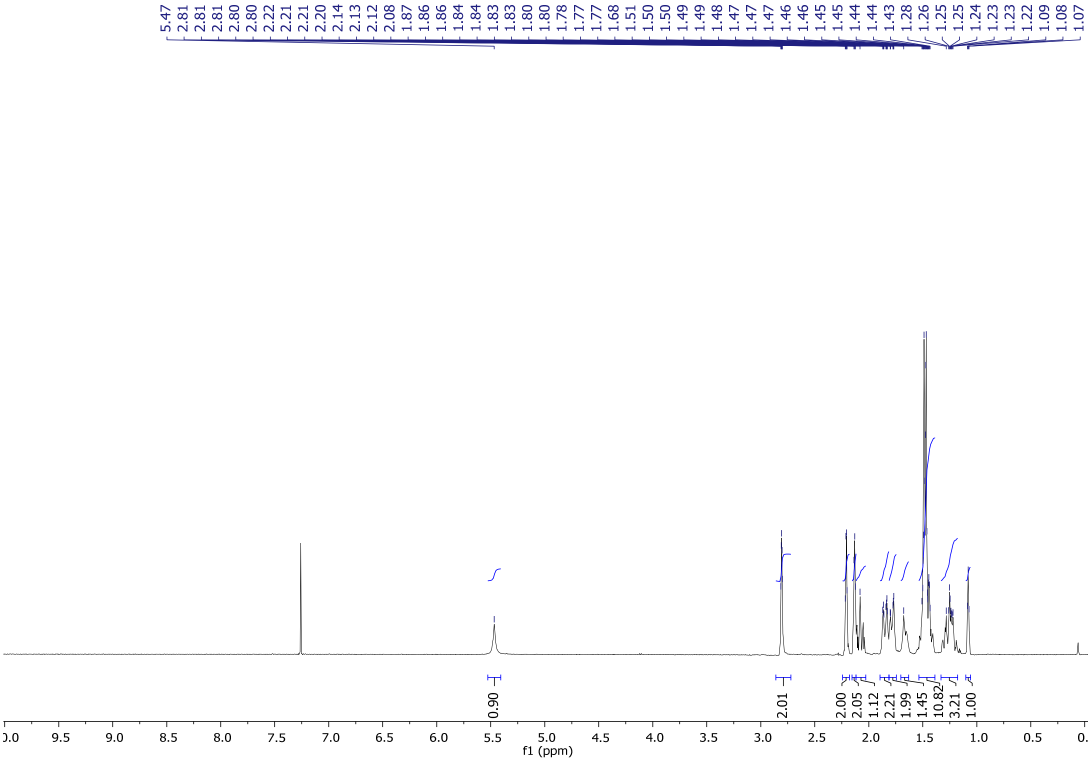
5.47
2.81
2.81
2.81
2.80
2.80
2.22
2.21
2.21
2.20
2.14
2.13
2.12
2.08
1.87
1.86
1.86
1.84
1.84
1.83
1.83
1.80
1.80
1.78
1.77
1.77
1.68
1.51
1.50
1.50
1.49
1.49
1.48
1.47
1.47
1.47
1.46
1.46
1.45
1.45
1.44
1.44
1.43
1.43
1.28
1.26
1.25
1.25
1.24
1.23
1.23
1.23
1.22
1.09
1.08
1.07
0.90
2.01
2.00
2.05
1.12
2.21
1.99
1.45
10.82
3.21
1.00
10.0
9.5
9.0
8.5
8.0
7.5
7.0
6.5
6.0
5.5
5.0
4.5
4.0
3.5
3.0
2.5
2.0
1.5
1.0
0.5
0.
f1 (ppm)

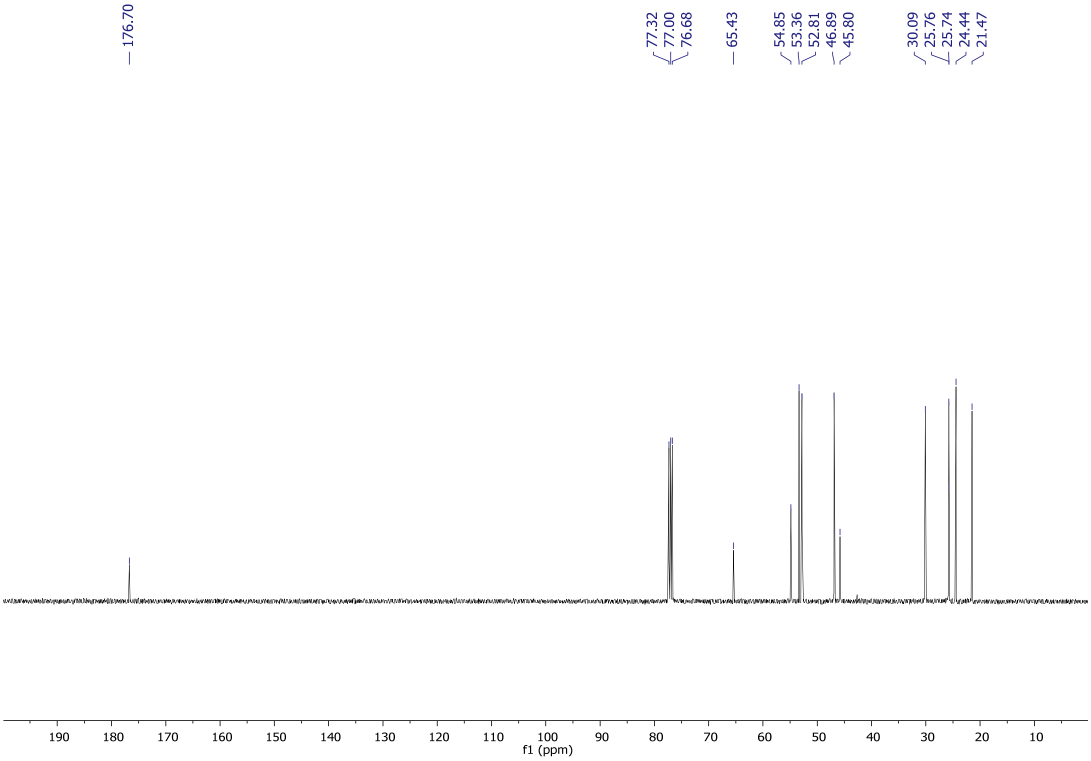
176.70
77.32
77.00
76.68
65.43
54.85
53.36
52.81
46.89
45.80
30.09
25.76
25.74
24.44
21.47
190
180
170
160
150
140
130
120
110
100
90
80
70
60
50
40
30
20
10
f1 (ppm)

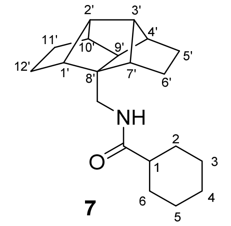
2'
3'
11'
10'
9'
4'
5'
12'
1'
8'
7'
6'
NH
O
1
2
3
4
5
6

7

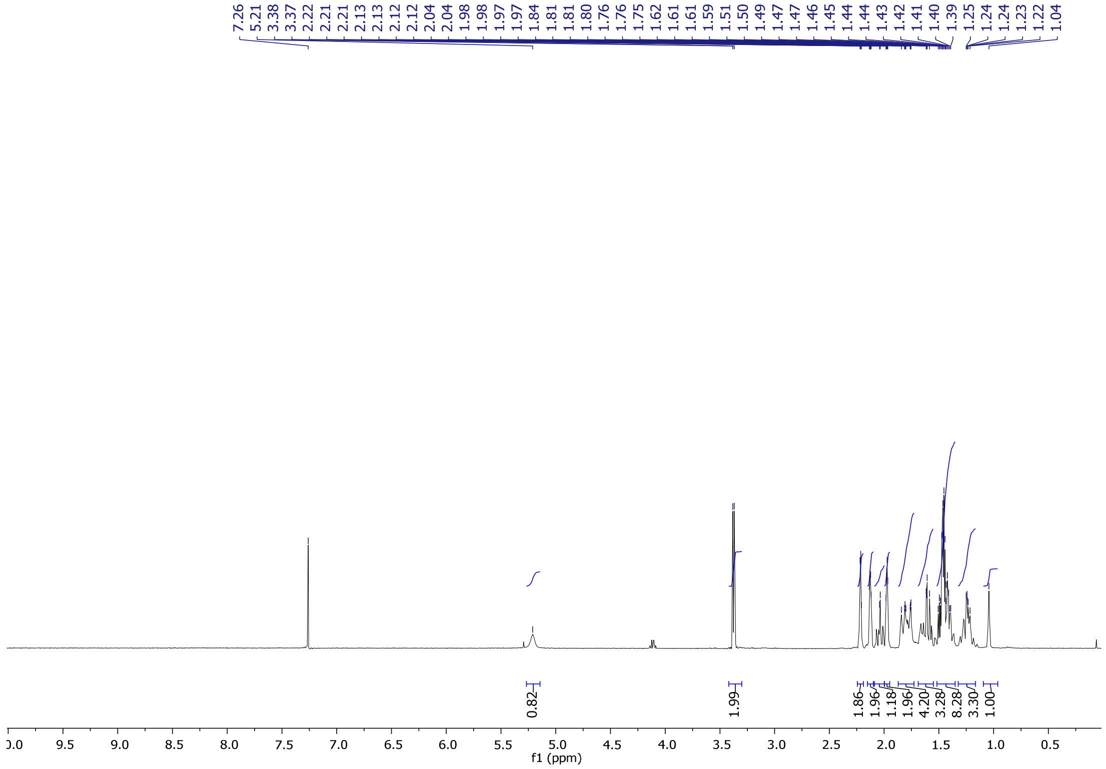
7.26
5.21
3.38
3.37
2.22
2.21
2.21
2.13
2.12
2.12
2.04
2.04
1.98
1.97
1.97
1.84
1.81
1.81
1.80
1.76
1.75
1.62
1.61
1.61
1.59
1.51
1.50
1.49
1.47
1.46
1.45
1.44
1.44
1.43
1.42
1.41
1.40
1.39
1.25
1.24
1.24
1.23
1.22
1.04
0.82
1.99
1.86
1.96
1.18
1.96
4.20
3.28
8.28
3.30
1.00
9.5
9.0
8.5
8.0
7.5
7.0
6.5
6.0
5.5
5.0
4.5
4.0
3.5
3.0
2.5
2.0
1.5
1.0
0.5
f1 (ppm)

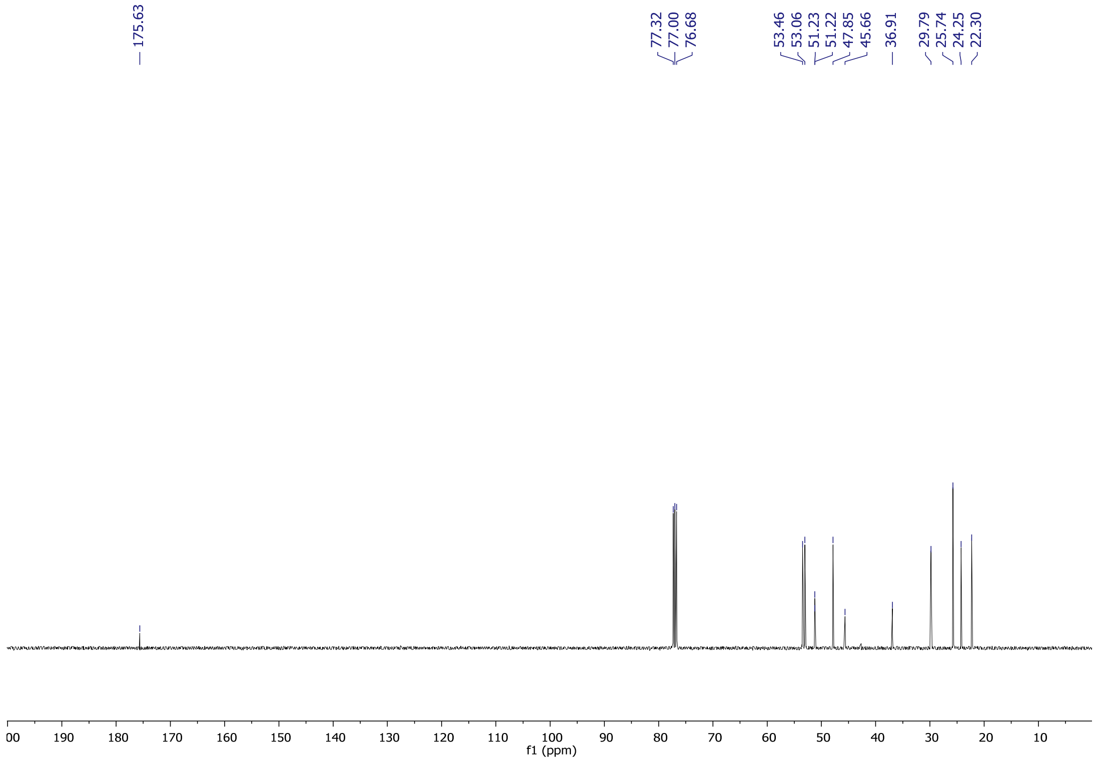
175.63
77.32
77.00
76.68
53.46
53.06
51.23
51.22
47.85
45.66
36.91
29.79
25.74
24.25
22.30
190
180
170
160
150
140
130
120
110
100
90
80
70
60
50
40
30
20
10
f1 (ppm)

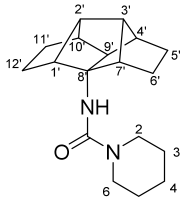
2'
3'
4'
11'
10'
9'
5'
12'
1'
8'
7'
6'
NH
2
O
N
3
4
6
5

8

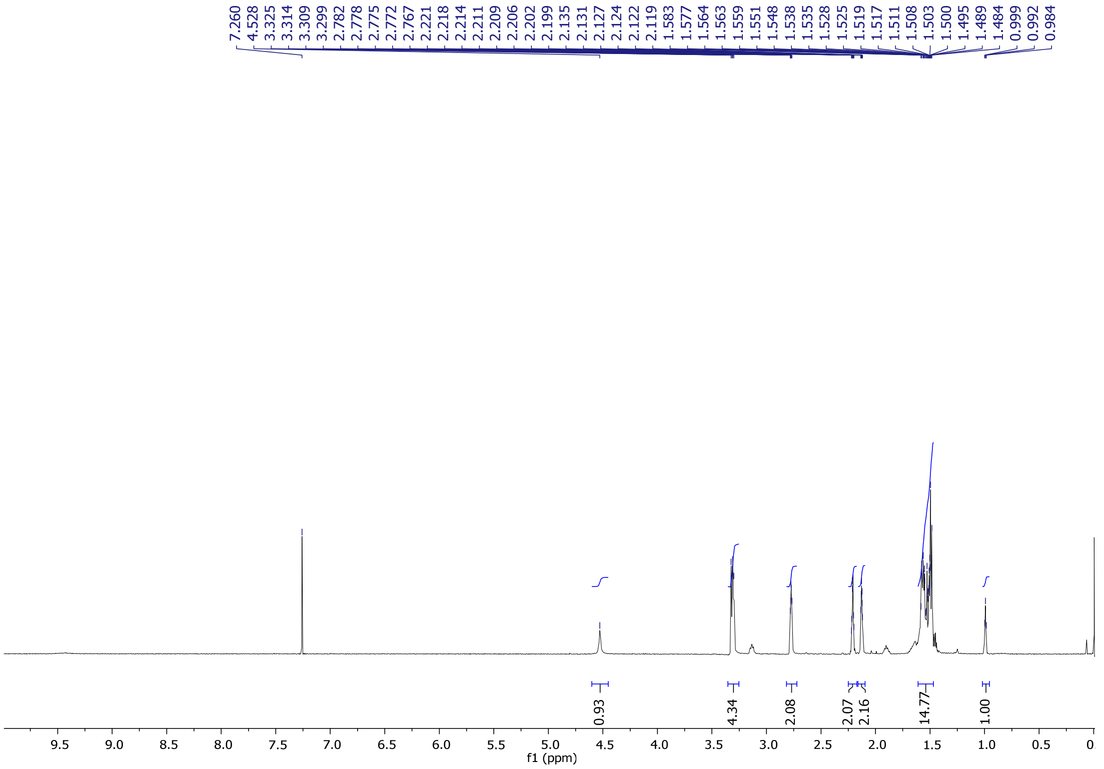
7.260
4.528
3.325
3.314
3.309
3.299
2.782
2.778
2.775
2.772
2.767
2.221
2.218
2.214
2.211
2.209
2.206
2.202
2.199
2.135
2.131
2.127
2.124
2.122
2.119
1.583
1.577
1.564
1.563
1.559
1.551
1.548
1.538
1.535
1.528
1.525
1.519
1.517
1.511
1.508
1.503
1.500
1.495
1.489
1.484
0.999
0.992
0.984
0.93
4.34
2.08
2.07
2.16
14.77
1.00
9.5
9.0
8.5
8.0
7.5
7.0
6.5
6.0
5.5
5.0
4.5
4.0
3.5
3.0
2.5
2.0
1.5
1.0
0.5
0
f1 (ppm)

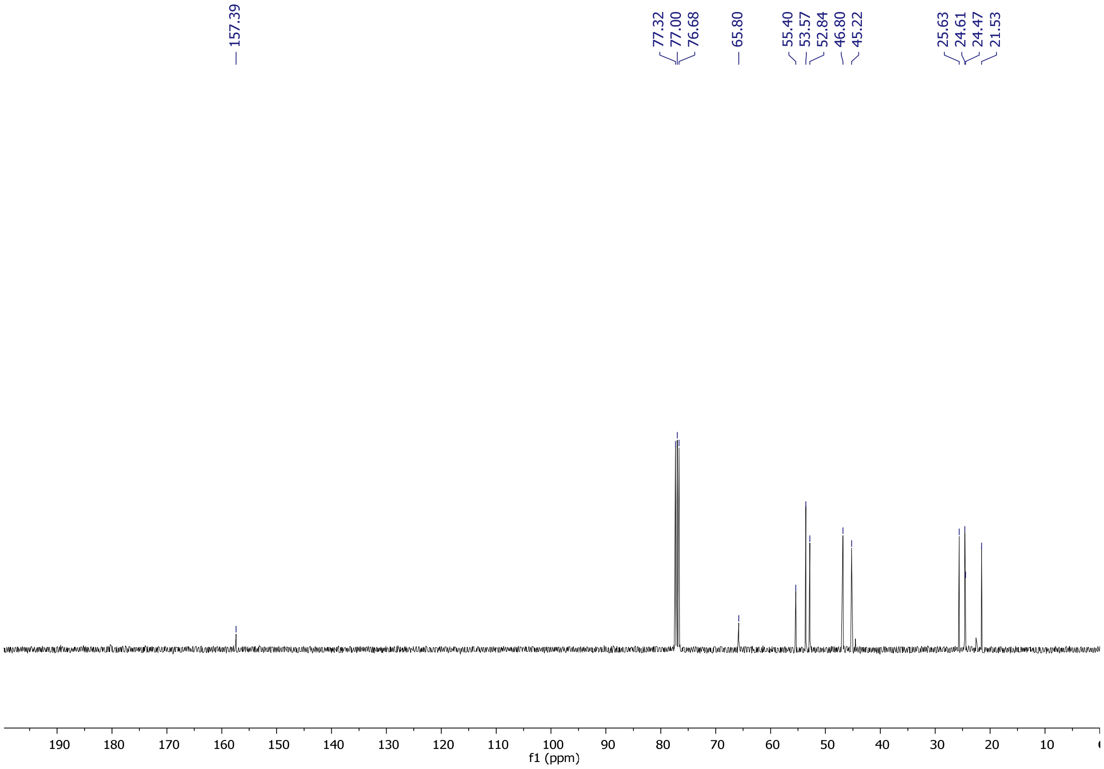
157.39
77.32
77.00
76.68
65.80
55.40
53.57
52.84
46.80
45.22
25.63
24.61
24.47
21.53
190
180
170
160
150
140
130
120
110
100
90
80
70
60
50
40
30
20
10
f1 (ppm)

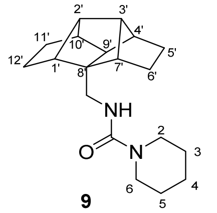
2'
3'
11'
4'
10'
9'
5'
12'
1'
8'
7'
6'
NH
2
O
N
3
6
4
5

9

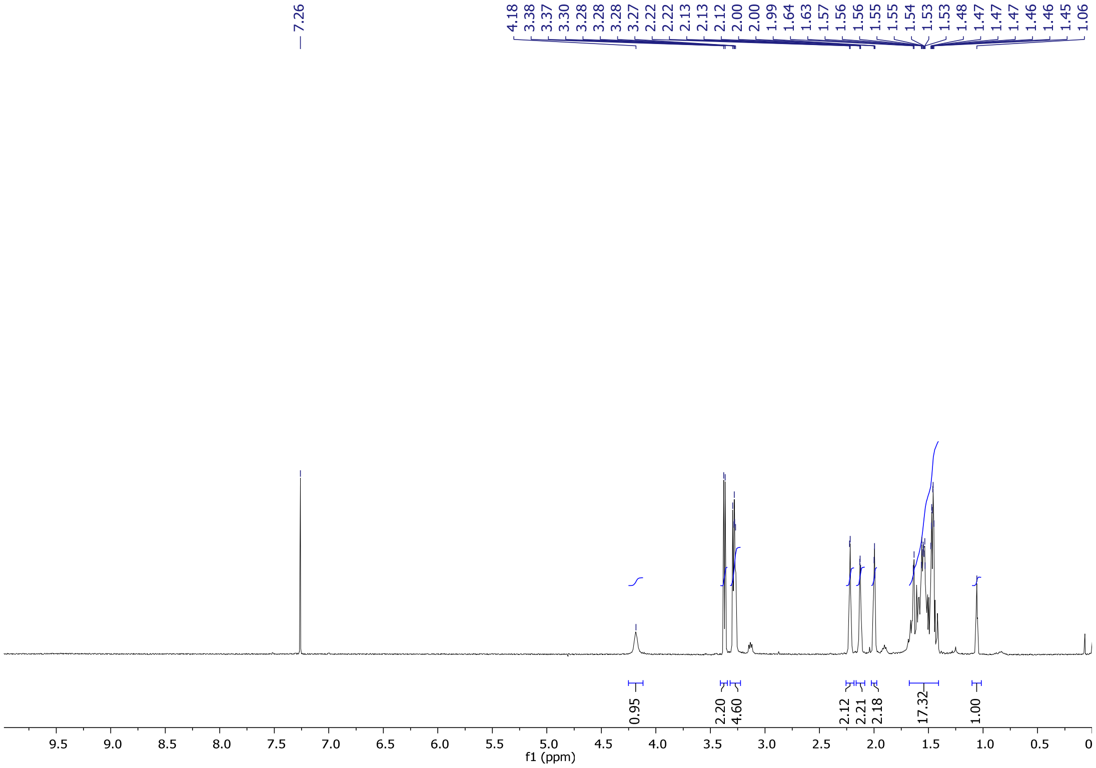
7.26
4.18
3.38
3.37
3.30
3.28
3.28
3.28
3.27
2.22
2.22
2.13
2.13
2.12
2.00
2.00
1.99
1.64
1.63
1.57
1.56
1.55
1.55
1.54
1.53
1.53
1.48
1.47
1.47
1.46
1.45
1.06
0.95
2.20
4.60
2.12
2.21
2.18
17.32
1.00
9.5
9.0
8.5
8.0
7.5
7.0
6.5
6.0
5.5
5.0
4.5
4.0
3.5
3.0
2.5
2.0
1.5
1.0
0.5
0
f1 (ppm)

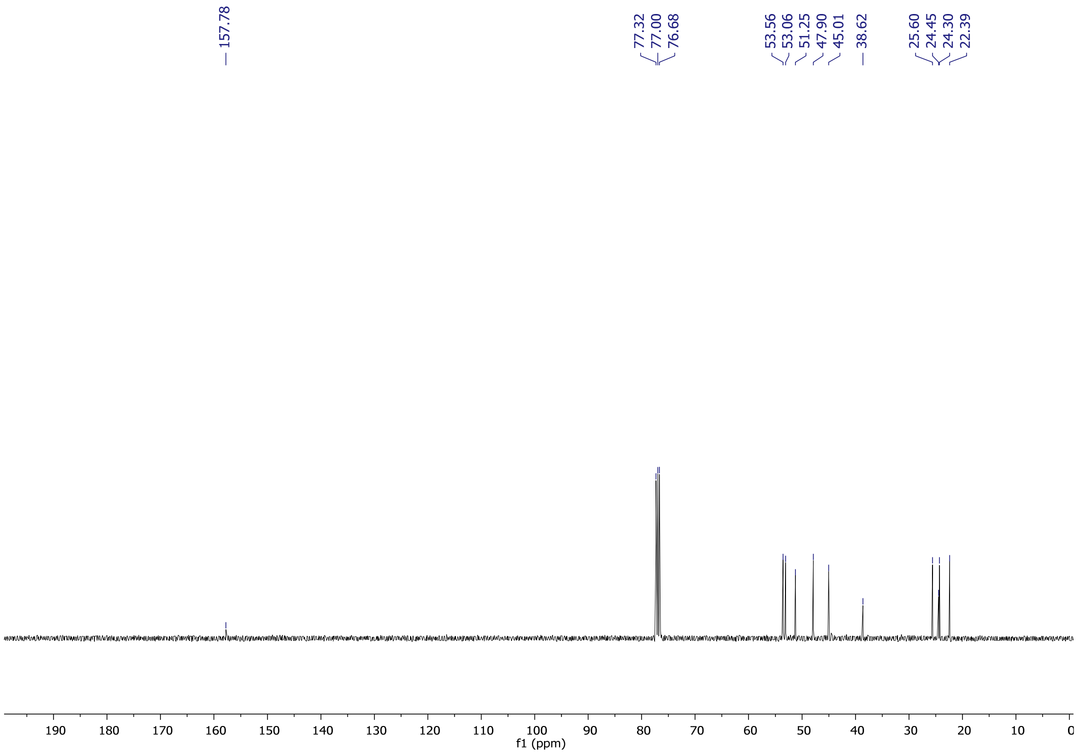
157.78
77.32
77.00
76.68
53.56
53.06
51.25
47.90
45.01
38.62
25.60
24.45
24.30
22.39
190
180
170
160
150
140
130
120
110
100
90
80
70
60
50
40
30
20
10
0
f1 (ppm)

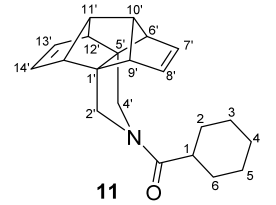
11'
10'
13'
6'
7'
12'
5'
14'
9'
8'
1'
4'
2'
N
2
3
4
1
5
6
O

11

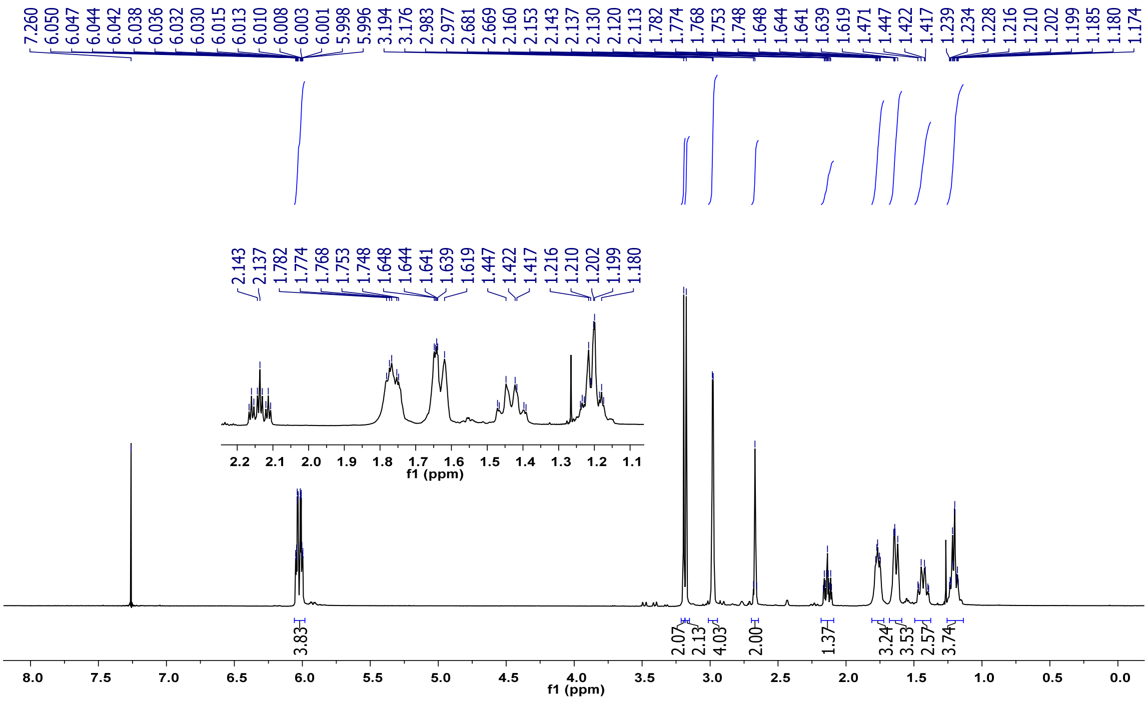
7.260
6.050
6.047
6.044
6.042
6.038
6.036
6.032
6.030
6.015
6.013
6.010
6.008
6.003
6.001
5.998
5.996
3.194
3.176
2.983
2.977
2.681
2.669
2.160
2.153
2.143
2.137
2.130
2.120
2.113
1.782
1.774
1.768
1.753
1.748
1.648
1.644
1.641
1.639
1.619
1.471
1.447
1.422
1.417
1.239
1.234
1.228
1.216
1.210
1.202
1.199
1.185
1.180
1.174
2.143
2.137
1.782
1.774
1.768
1.753
1.748
1.648
1.644
1.641
1.639
1.619
1.447
1.422
1.417
1.216
1.210
1.202
1.199
1.180
2.2
2.1
2.0
1.9
1.8
1.7
1.6
1.5
1.4
1.3
1.2
1.1
f1 (ppm)
3.83
2.07
2.13
4.03
2.00
1.37
3.24
3.53
2.57
3.74
8.0
7.5
7.0
6.5
6.0
5.5
5.0
4.5
4.0
3.5
3.0
2.5
2.0
1.5
1.0
0.5
0.0
f1 (ppm)

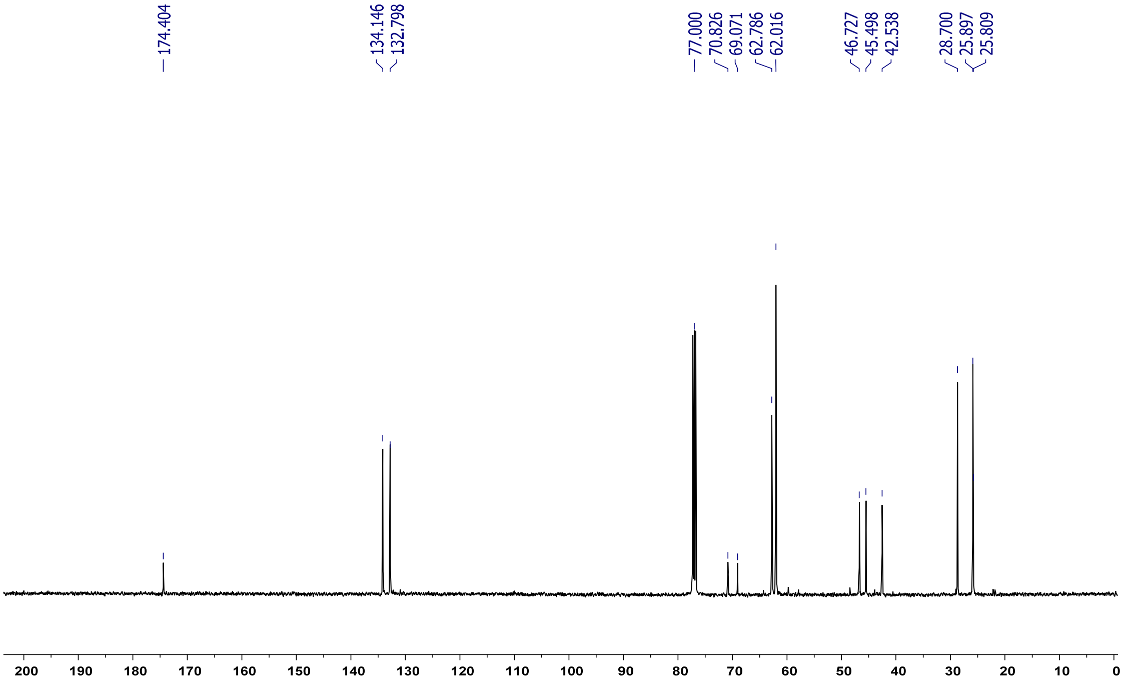
174.404
134.146
132.798
77.000
70.826
69.071
62.786
62.016
46.727
45.498
42.538
28.700
25.897
25.809
200
190
180
170
160
150
140
130
120
110
100
90
80
70
60
50
40
30
20
10
0

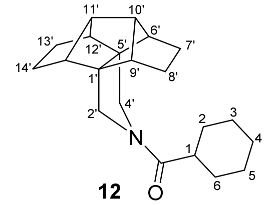
11'
10'
13'
6'
12'
5'
7'
14'
1'
9'
8'
4'
2'
2
3
N
1
4
5
6
O

12

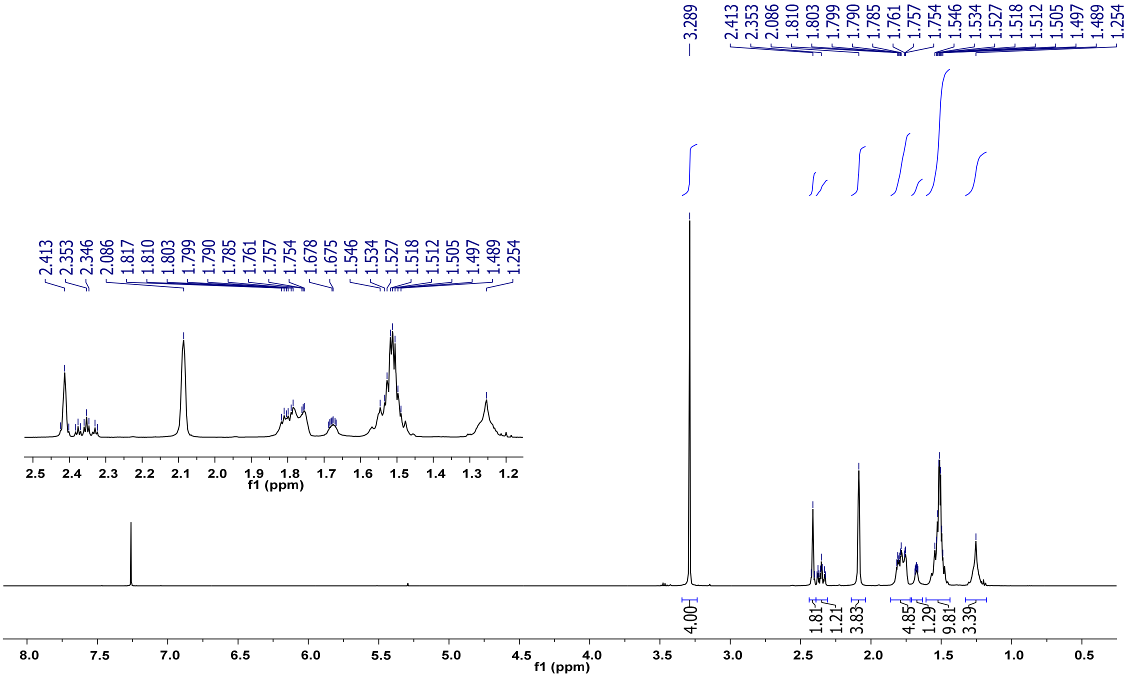
3.289
2.413
2.353
2.086
1.810
1.803
1.799
1.790
1.785
1.761
1.757
1.754
1.546
1.534
1.527
1.518
1.512
1.505
1.497
1.489
1.254
2.413
2.353
2.346
2.086
1.817
1.810
1.803
1.799
1.790
1.785
1.761
1.757
1.754
1.678
1.675
1.546
1.534
1.527
1.518
1.512
1.505
1.497
1.489
1.254
2.5
2.4
2.3
2.2
2.1
2.0
1.9
1.8
1.7
1.6
1.5
1.4
1.3
1.2
f1 (ppm)
4.00
1.81
1.21
3.83
4.85
1.29
9.81
3.39
8.0
7.5
7.0
6.5
6.0
5.5
5.0
4.5
4.0
3.5
3.0
2.5
2.0
1.5
1.0
0.5
f1 (ppm)

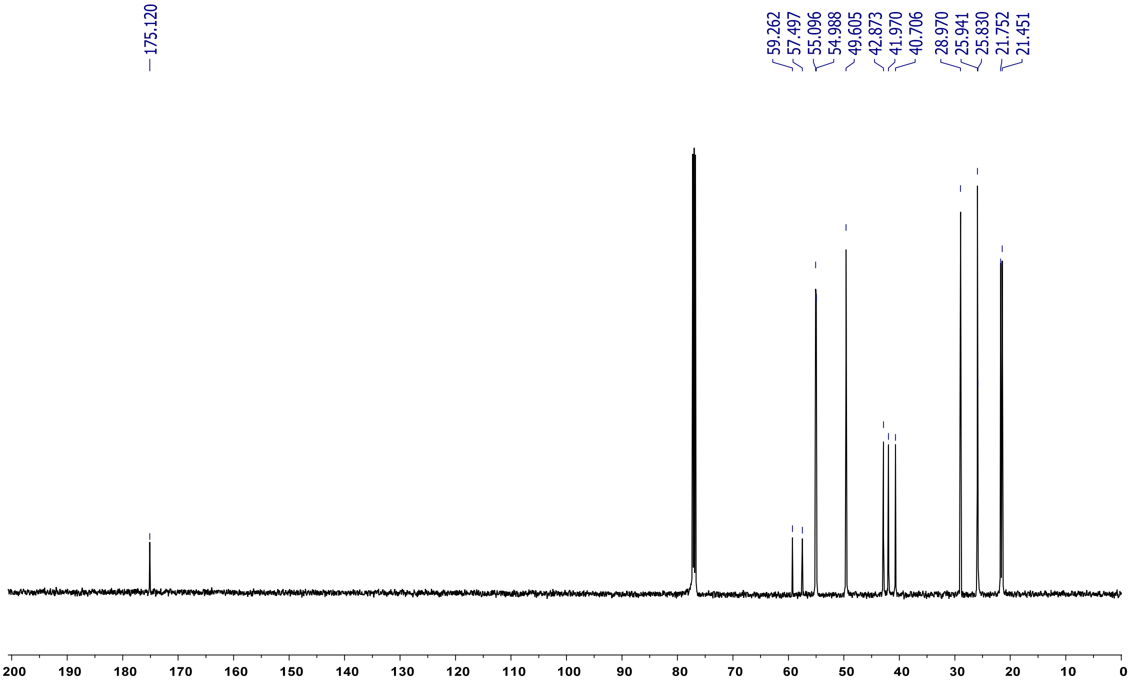
175.120
59.262
57.497
55.096
54.988
49.605
42.873
41.970
40.706
28.970
25.941
25.830
21.752
21.451
200
190
180
170
160
150
140
130
120
110
100
90
80
70
60
50
40
30
20
10
0

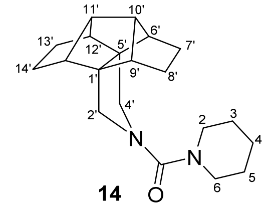
11'
10'
6'
13'
12'
5'
7'
14'
9'
1'
8'
4'
2'
N
2
3
4
N
5
6
O

14

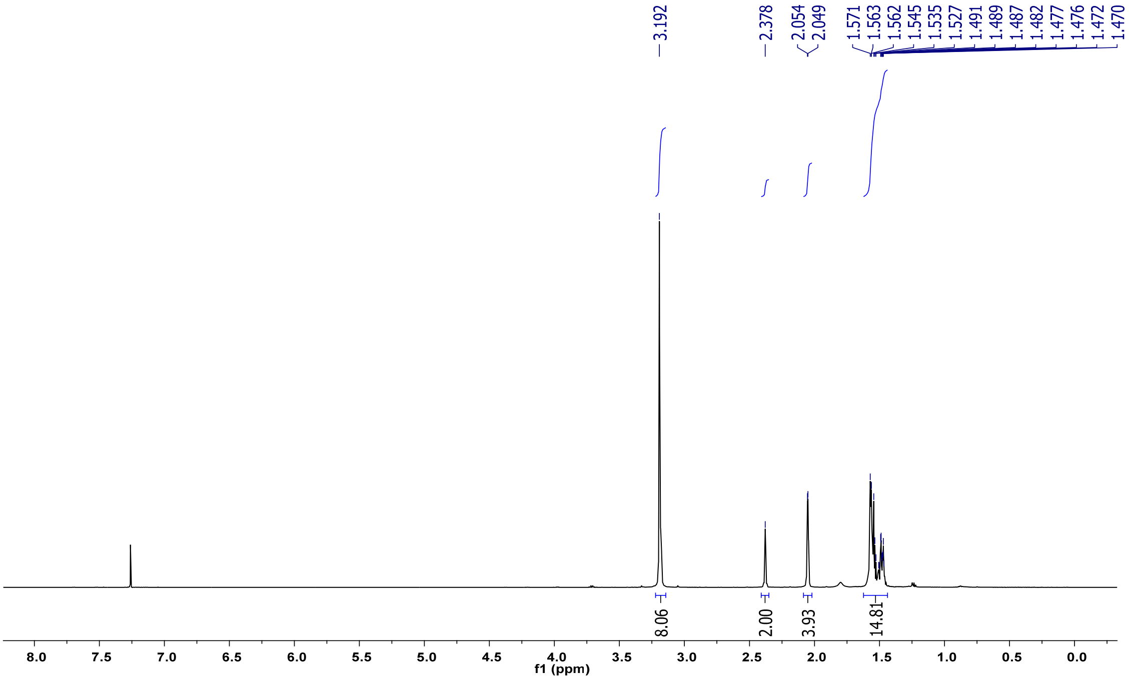
3.192
2.378
2.054
2.049
1.571
1.563
1.562
1.545
1.535
1.527
1.491
1.489
1.487
1.482
1.477
1.476
1.472
1.470
8.06
2.00
3.93
14.81
8.0
7.5
7.0
6.5
6.0
5.5
5.0
4.5
4.0
3.5
3.0
2.5
2.0
1.5
1.0
0.5
0.0
f1 (ppm)

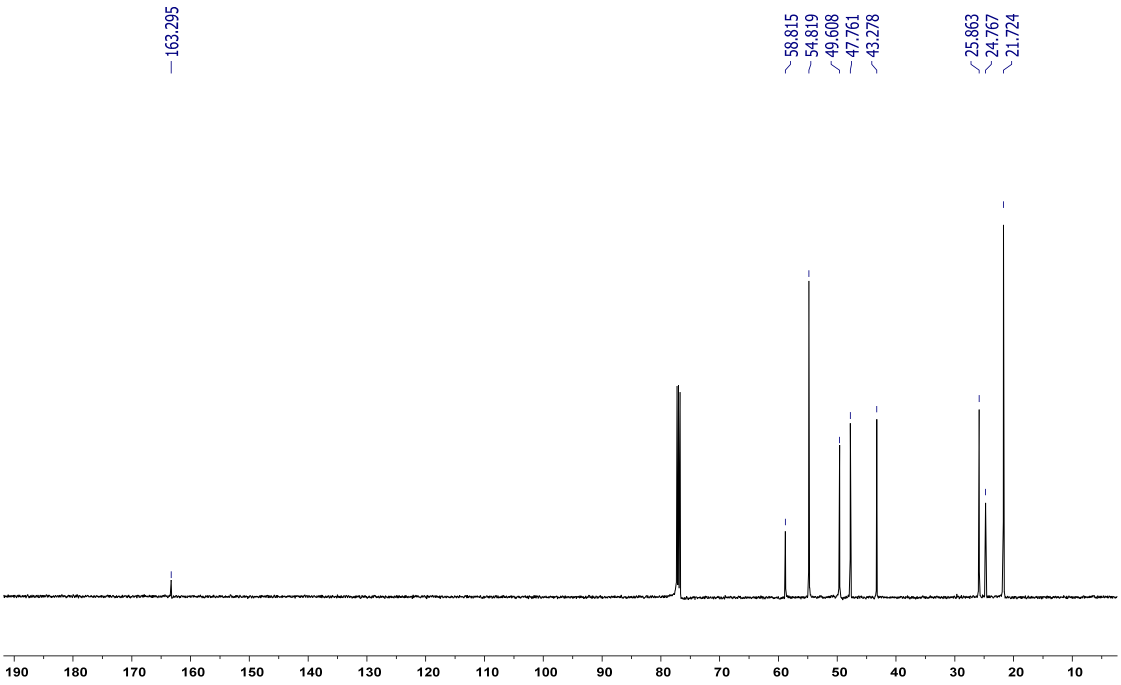
163.295
58.815
54.819
49.608
47.761
43.278
25.863
24.767
21.724
190
180
170
160
150
140
130
120
110
100
90
80
70
60
50
40
30
20
10

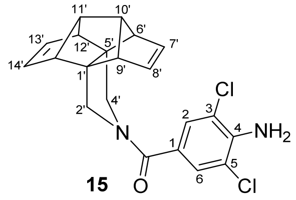
11'
10'
13'
6'
12'
5'
7'
14'
1'
9'
8'
Cl
4'
2'
3
2
4
NH2
N
1
5
6
O
Cl

15

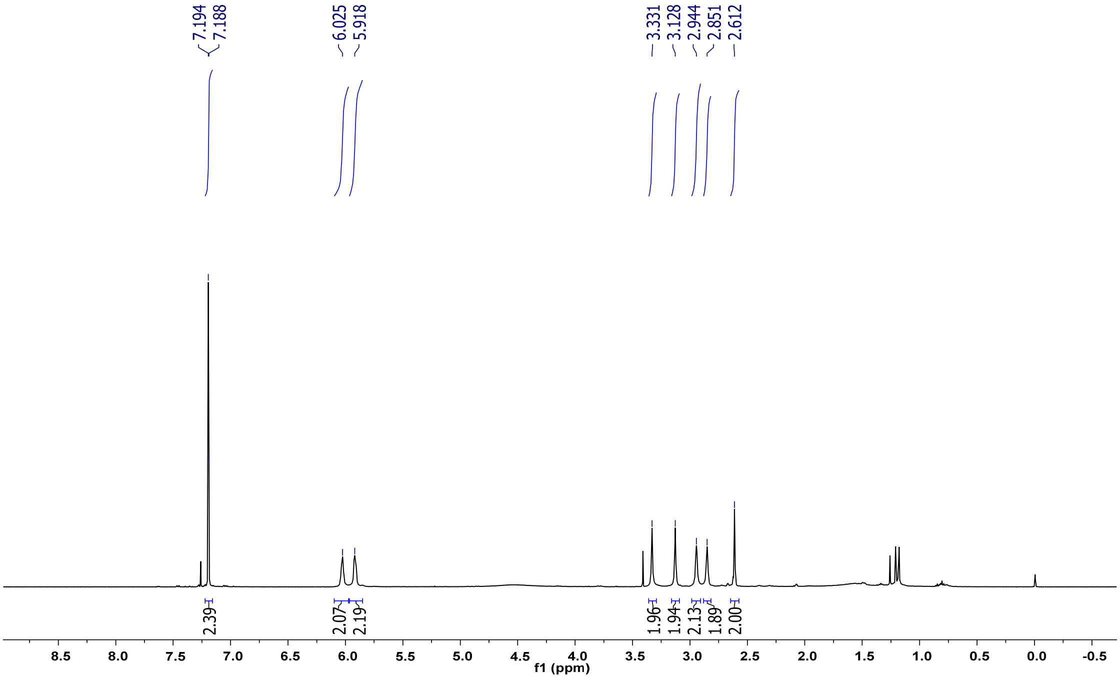
7.194
7.188
6.025
5.918
3.331
3.128
2.944
2.851
2.612
2.39
2.07
2.19
1.96
1.94
2.13
1.89
2.00
8.5
8.0
7.5
7.0
6.5
6.0
5.5
5.0
4.5
4.0
3.5
3.0
2.5
2.0
1.5
1.0
0.5
0.0
-0.5
f1 (ppm)

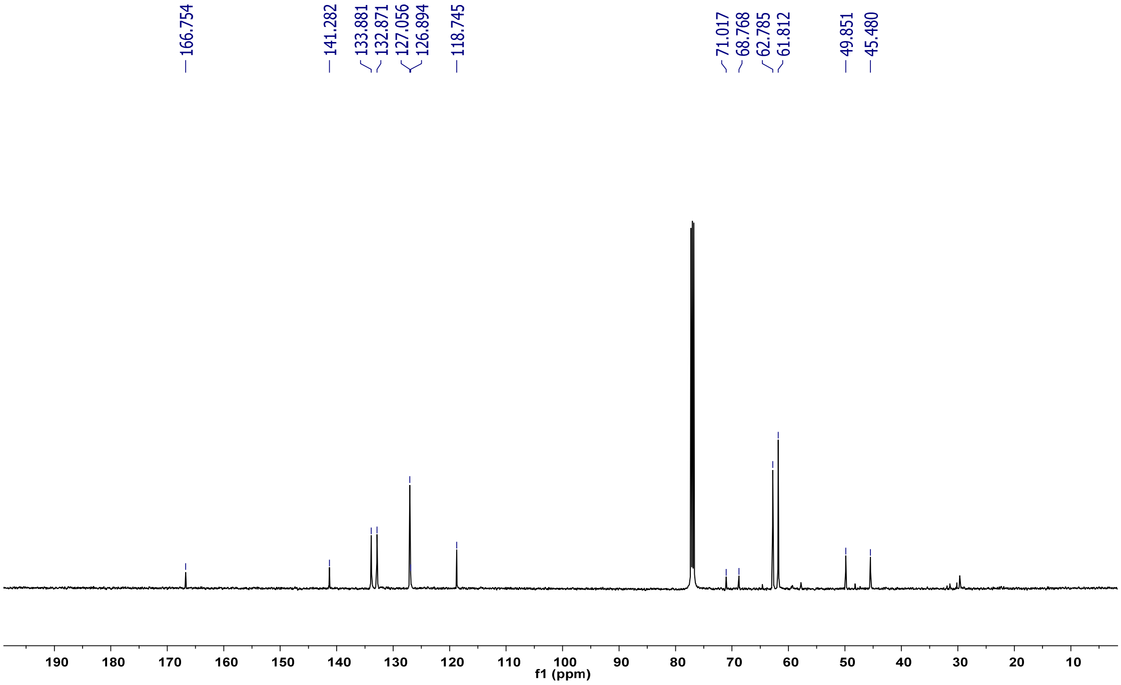
166.754
141.282
133.881
132.871
127.056
126.894
118.745
71.017
68.768
62.785
61.812
49.851
45.480
190
180
170
160
150
140
130
120
110
100
90
80
70
60
50
40
30
20
10
f1 (ppm)

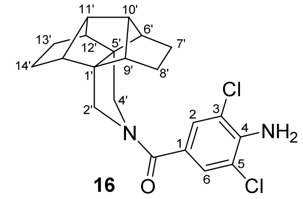
11'
10'
6'
13'
12'
5'
7'
14'
9'
1'
8'
Cl
4'
2'
2
3
N
4
NH2
1
5
6
O
Cl

16

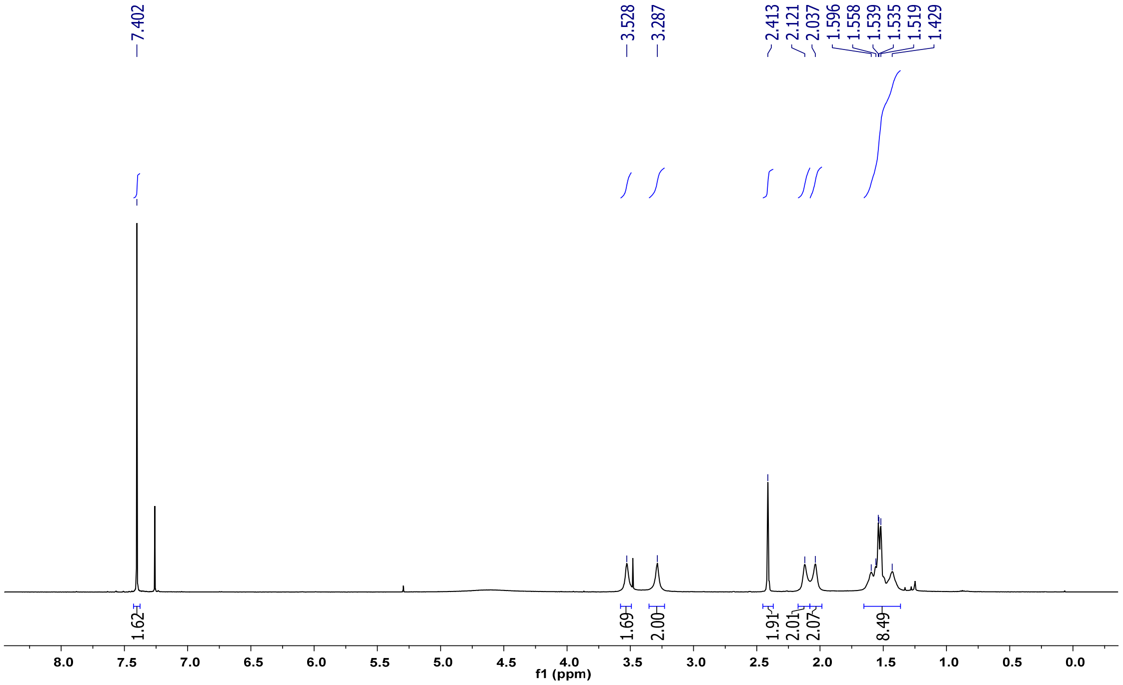
7.402
3.528
3.287
2.413
2.121
2.037
1.596
1.558
1.539
1.535
1.519
1.429
1.62
1.69
2.00
1.91
2.01
2.07
8.49
8.0
7.5
7.0
6.5
6.0
5.5
5.0
4.5
4.0
3.5
3.0
2.5
2.0
1.5
1.0
0.5
0.0
f1 (ppm)

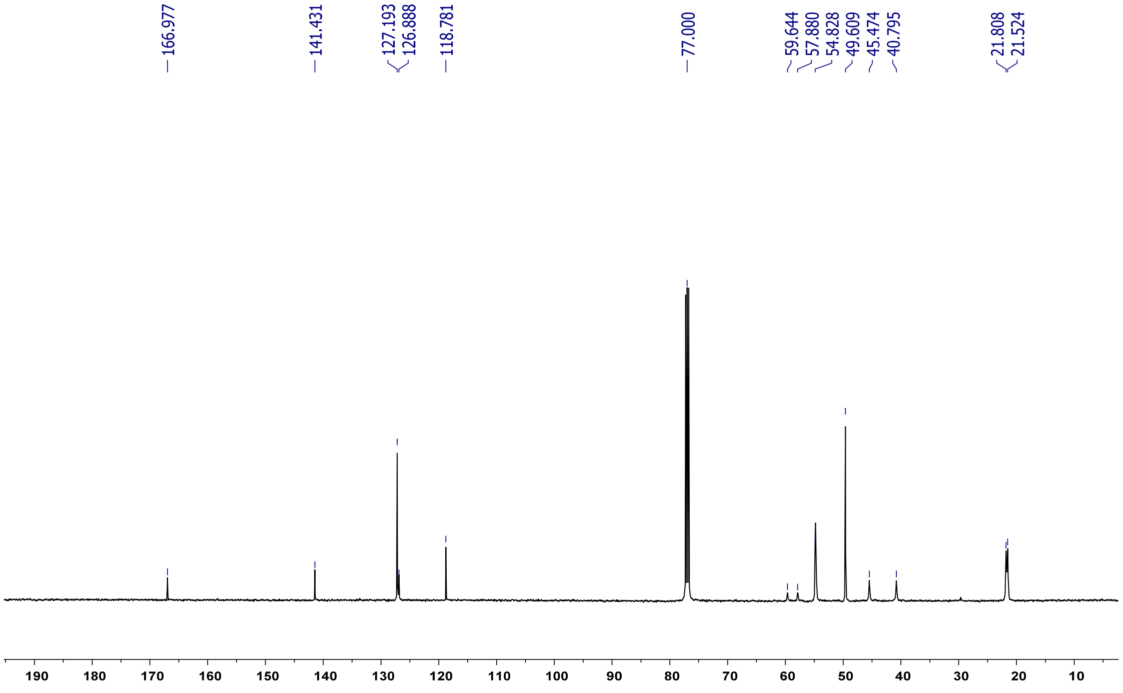
166.977
141.431
127.193
126.888
118.781
77.000
59.644
57.880
54.828
49.609
45.474
40.795
21.808
21.524
190
180
170
160
150
140
130
120
110
100
90
80
70
60
50
40
30
20
10

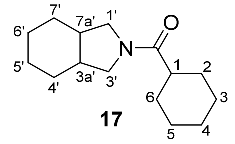
7'
7a'
1'
O
6'
N
5'
1
2
3a'
3'
4'
6
3
5
4

17

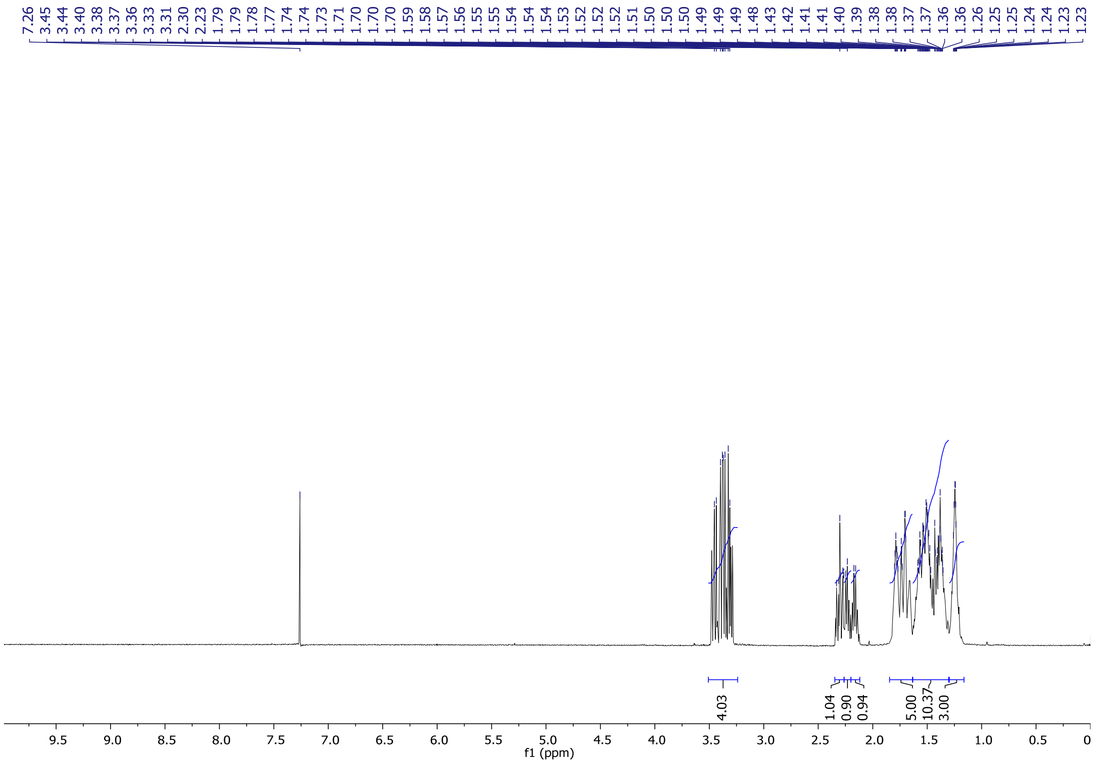
7.26
3.45
3.44
3.40
3.38
3.37
3.36
3.33
3.31
2.30
2.23
1.79
1.79
1.78
1.77
1.74
1.74
1.73
1.71
1.70
1.70
1.70
1.59
1.58
1.57
1.56
1.55
1.55
1.54
1.54
1.54
1.53
1.52
1.52
1.52
1.51
1.50
1.50
1.50
1.49
1.49
1.49
1.48
1.43
1.42
1.41
1.41
1.40
1.39
1.38
1.38
1.37
1.37
1.36
1.36
1.26
1.25
1.25
1.24
1.24
1.23
1.23
4.03
1.04
0.90
0.94
5.00
10.37
3.00
9.5
9.0
8.5
8.0
7.5
7.0
6.5
6.0
5.5
5.0
4.5
4.0
3.5
3.0
2.5
2.0
1.5
1.0
0.5
0
f1 (ppm)

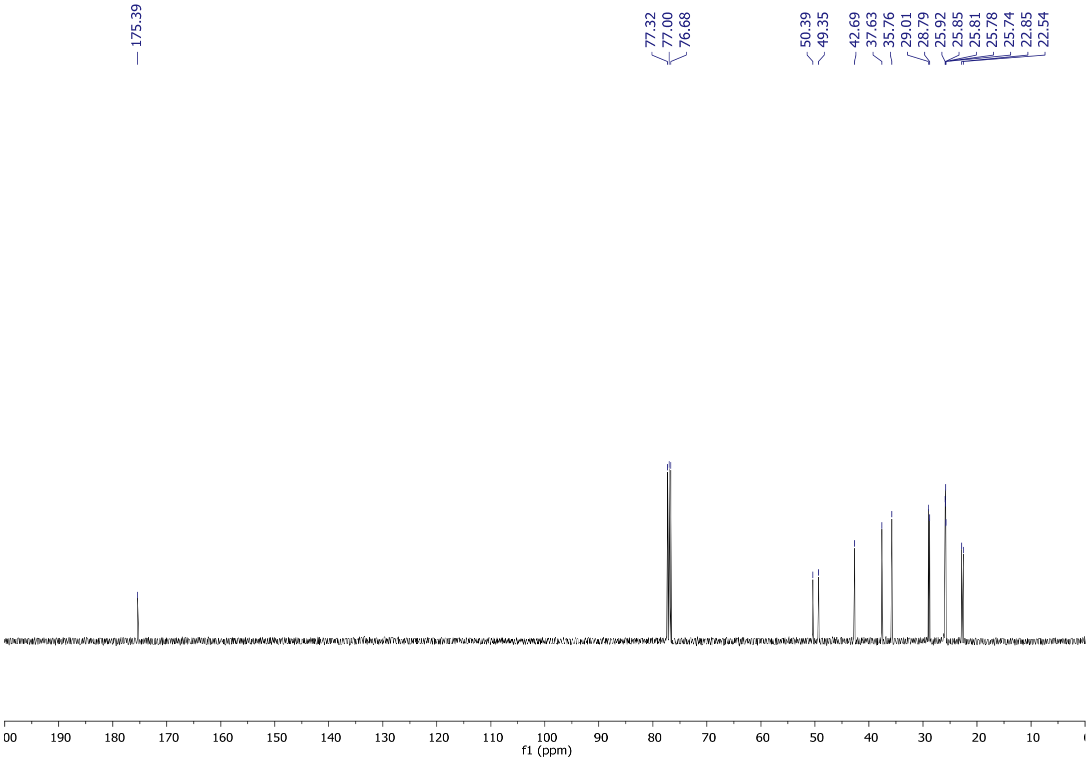
175.39
77.32
77.00
76.68
50.39
49.35
42.69
37.63
35.76
29.01
28.79
25.92
25.85
25.81
25.78
25.74
22.85
22.54
00
190
180
170
160
150
140
130
120
110
100
90
80
70
60
50
40
30
20
10
f1 (ppm)

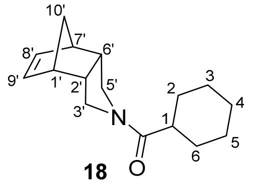
10'
7'
6'
8'
9'
1'
2'
5'
3'
N
1
2
3
4
5
6
O

18

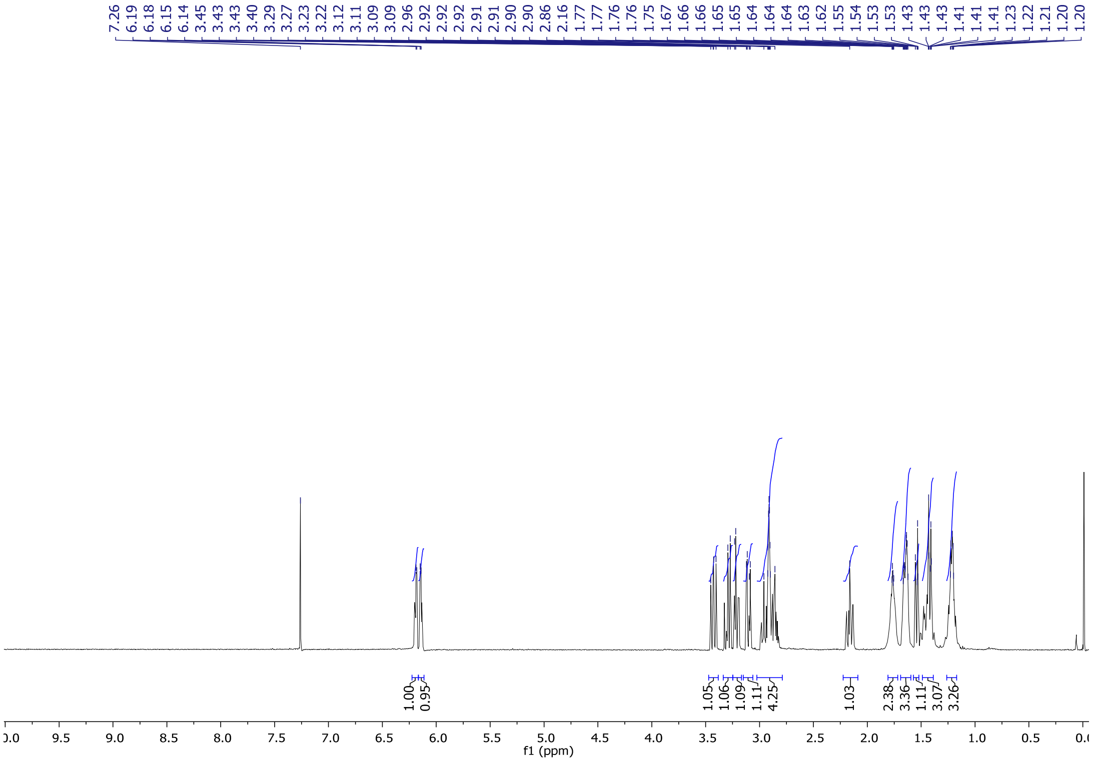
7.26
6.19
6.18
6.15
6.14
3.45
3.43
3.43
3.40
3.29
3.27
3.23
3.22
3.12
3.11
3.09
2.96
2.92
2.92
2.92
2.91
2.91
2.90
2.90
2.86
2.16
1.77
1.77
1.76
1.76
1.75
1.67
1.66
1.66
1.65
1.65
1.64
1.64
1.64
1.63
1.62
1.55
1.54
1.53
1.53
1.43
1.43
1.43
1.41
1.41
1.41
1.23
1.22
1.21
1.20
1.20
1.00
0.95
1.05
1.06
1.09
1.11
4.25
1.03
2.38
3.36
1.11
3.07
3.26
10.0
9.5
9.0
8.5
8.0
7.5
7.0
6.5
6.0
5.5
5.0
4.5
4.0
3.5
3.0
2.5
2.0
1.5
1.0
0.5
0.0
f1 (ppm)

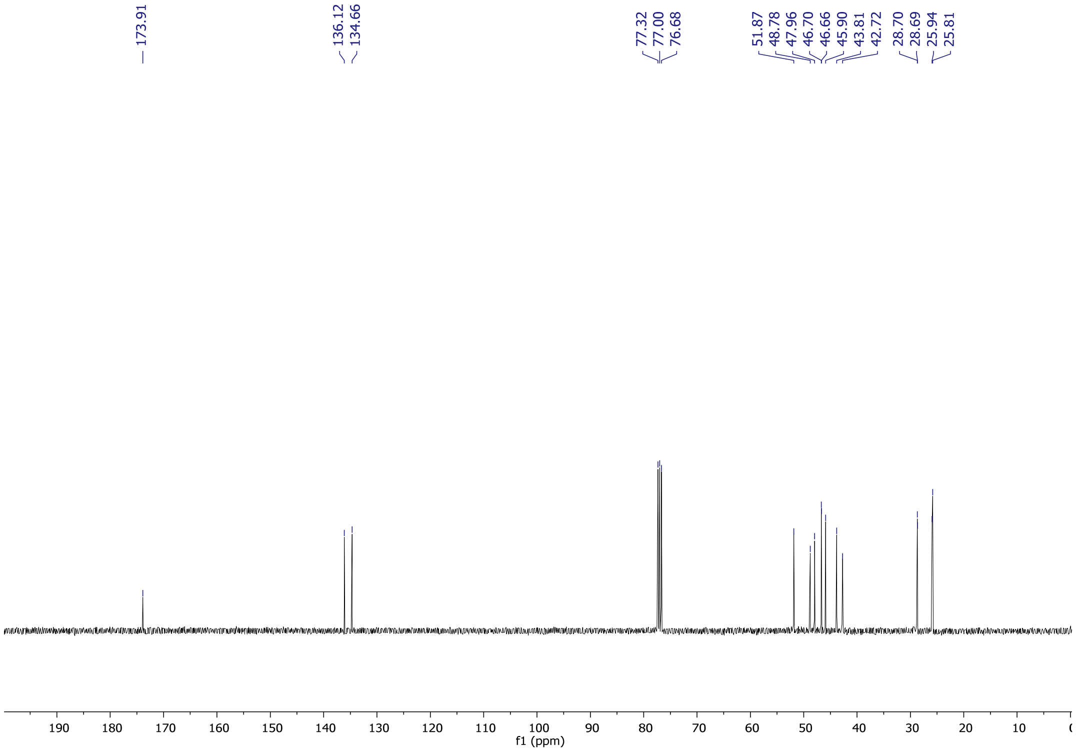
173.91
136.12
134.66
77.32
77.00
76.68
51.87
48.78
47.96
46.70
46.66
45.90
43.81
42.72
28.70
28.69
25.94
25.81
190
180
170
160
150
140
130
120
110
100
90
80
70
60
50
40
30
20
10
0
f1 (ppm)

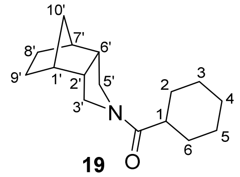
10'
7'
8'
6'
9'
1'
2'
5'
3'
N
1
2
3
4
5
6
O

19

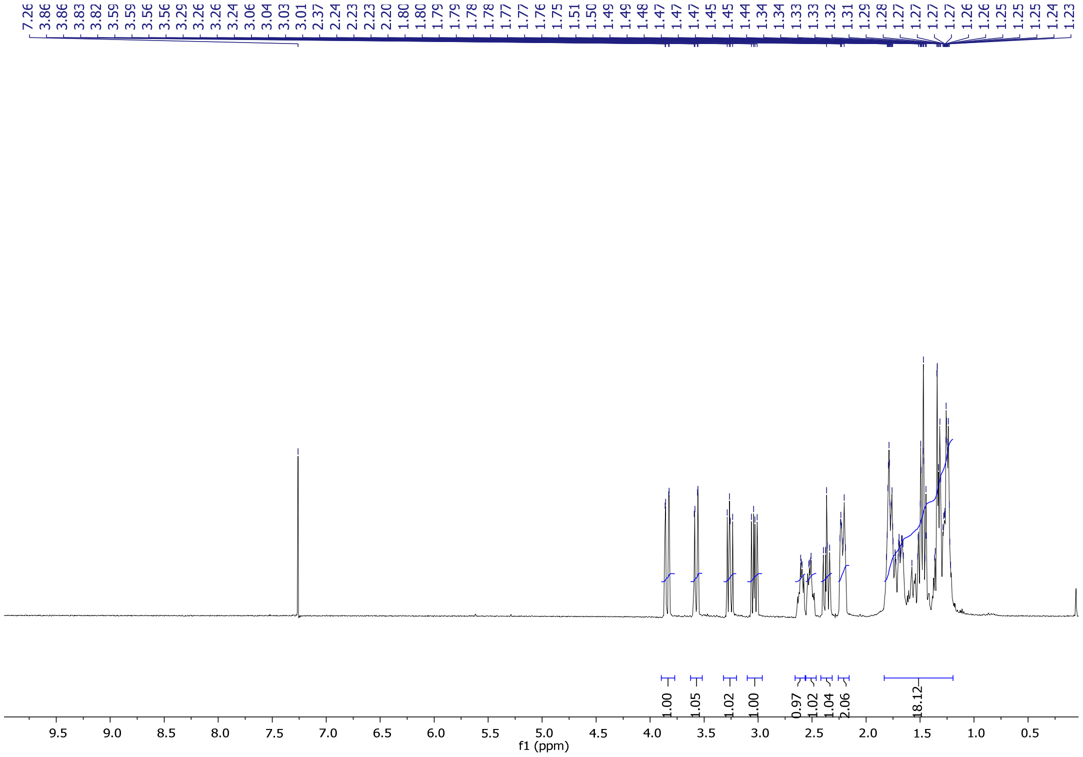
7.26
3.86
3.86
3.83
3.82
3.59
3.59
3.56
3.56
3.29
3.26
3.26
3.24
3.06
3.04
3.03
3.01
2.37
2.24
2.23
2.23
2.20
1.80
1.80
1.79
1.79
1.78
1.78
1.77
1.77
1.76
1.75
1.51
1.50
1.49
1.49
1.48
1.47
1.47
1.47
1.45
1.45
1.44
1.34
1.34
1.33
1.33
1.32
1.31
1.29
1.28
1.27
1.27
1.27
1.27
1.27
1.26
1.26
1.25
1.25
1.24
1.23
1.00
1.05
1.02
1.00
0.97
1.02
1.04
2.06
18.12
9.5
9.0
8.5
8.0
7.5
7.0
6.5
6.0
5.5
5.0
4.5
4.0
3.5
3.0
2.5
2.0
1.5
1.0
0.5
f1 (ppm)

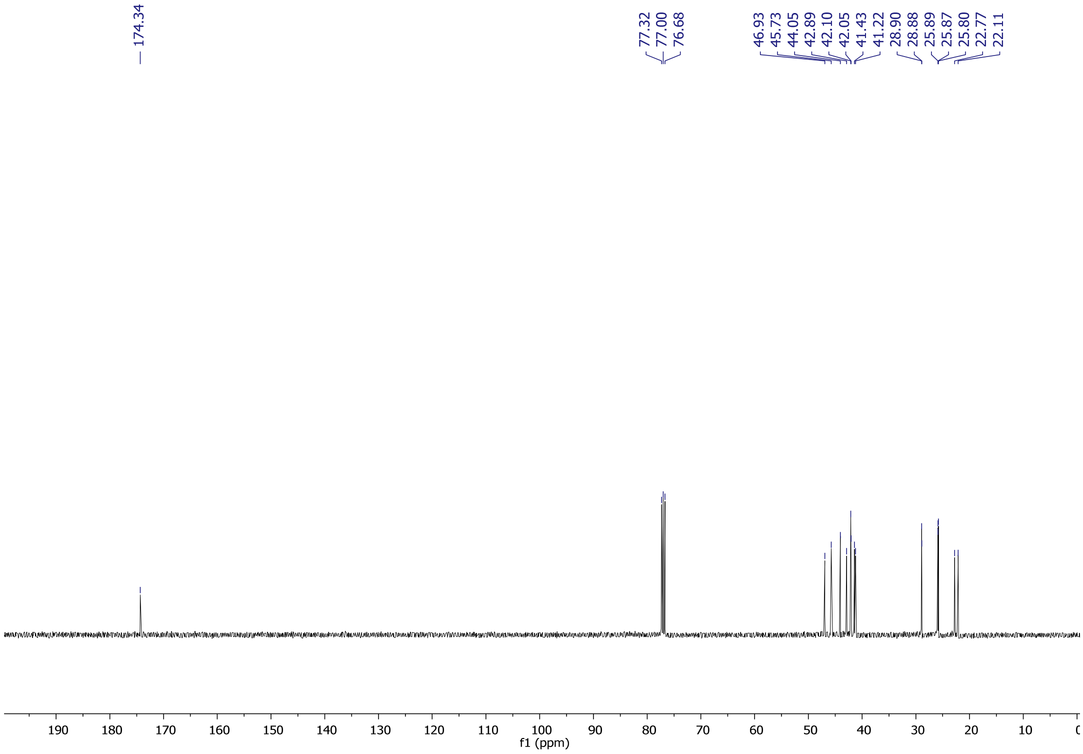
174.34
77.32
77.00
76.68
46.93
45.73
44.05
42.89
42.10
42.05
41.43
41.22
28.90
28.88
25.89
25.87
25.80
22.77
22.11
190
180
170
160
150
140
130
120
110
100
90
80
70
60
50
40
30
20
10
0
f1 (ppm)

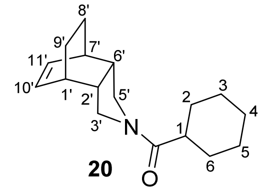
8'
9'
7'
6'
11'
10'
1'
2'
5'
3'
N
2
3
4
1
5
6
O

20

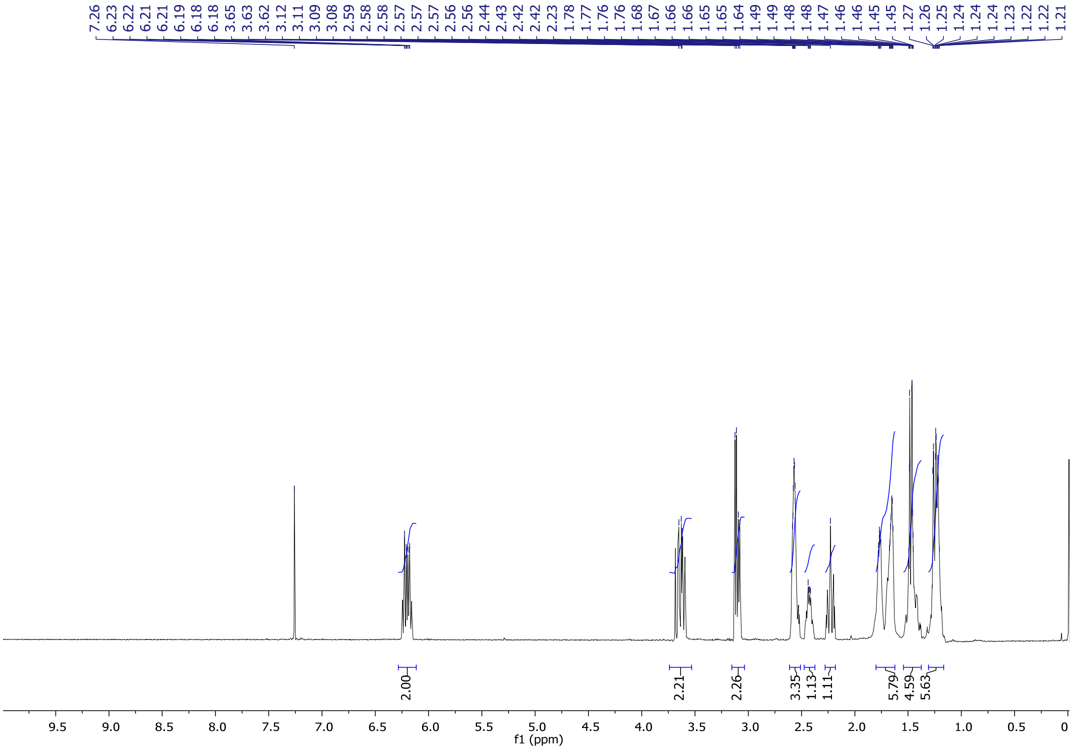
7.26
6.23
6.22
6.21
6.21
6.19
6.18
6.18
3.65
3.63
3.62
3.12
3.11
3.09
3.08
2.59
2.58
2.58
2.57
2.57
2.57
2.56
2.56
2.44
2.43
2.42
2.42
2.23
1.78
1.77
1.76
1.76
1.68
1.67
1.66
1.66
1.65
1.65
1.64
1.49
1.49
1.48
1.48
1.47
1.46
1.46
1.45
1.45
1.27
1.26
1.25
1.24
1.24
1.24
1.23
1.22
1.22
1.21
2.00
2.21
2.26
3.35
1.13
1.11
5.79
4.59
5.63
9.5
9.0
8.5
8.0
7.5
7.0
6.5
6.0
5.5
5.0
4.5
4.0
3.5
3.0
2.5
2.0
1.5
1.0
0.5
0
f1 (ppm)

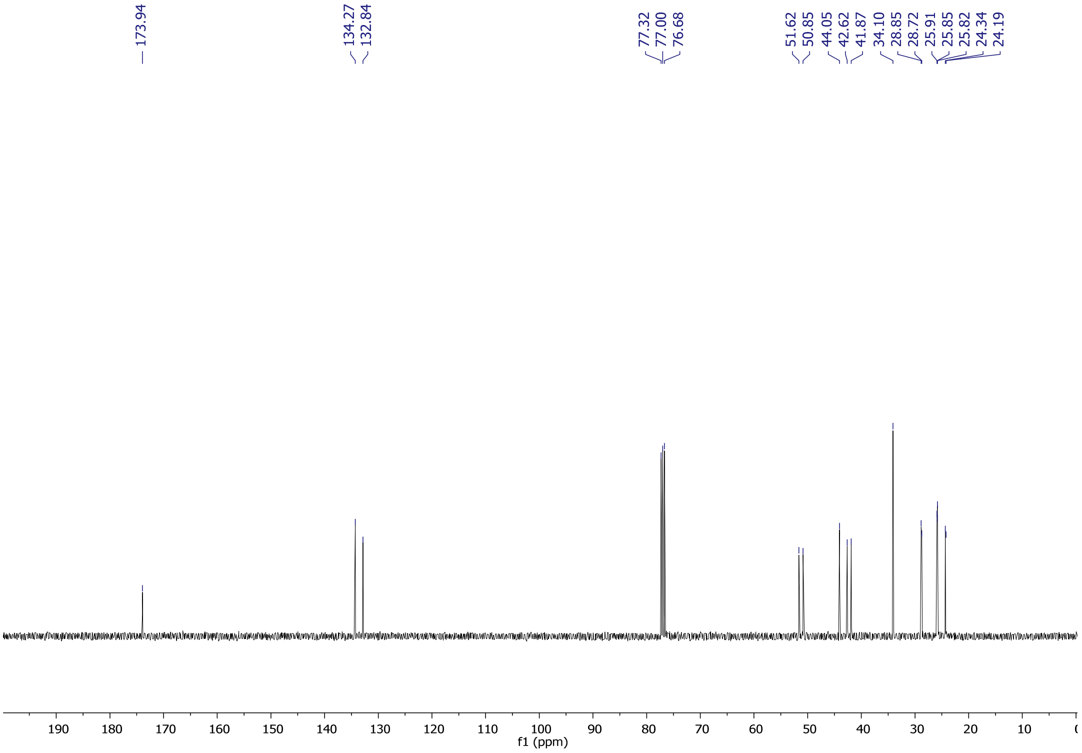
173.94
134.27
132.84
77.32
77.00
76.68
51.62
50.85
44.05
42.62
41.87
34.10
28.85
28.72
25.91
25.85
25.82
24.34
24.19
190
180
170
160
150
140
130
120
110
100
90
80
70
60
50
40
30
20
10
f1 (ppm)

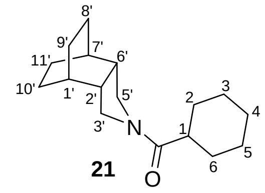
8'
9'
7'
11'
6'
10'
1'
2'
5'
3
2
4
1
3'
N
5
6
O

21

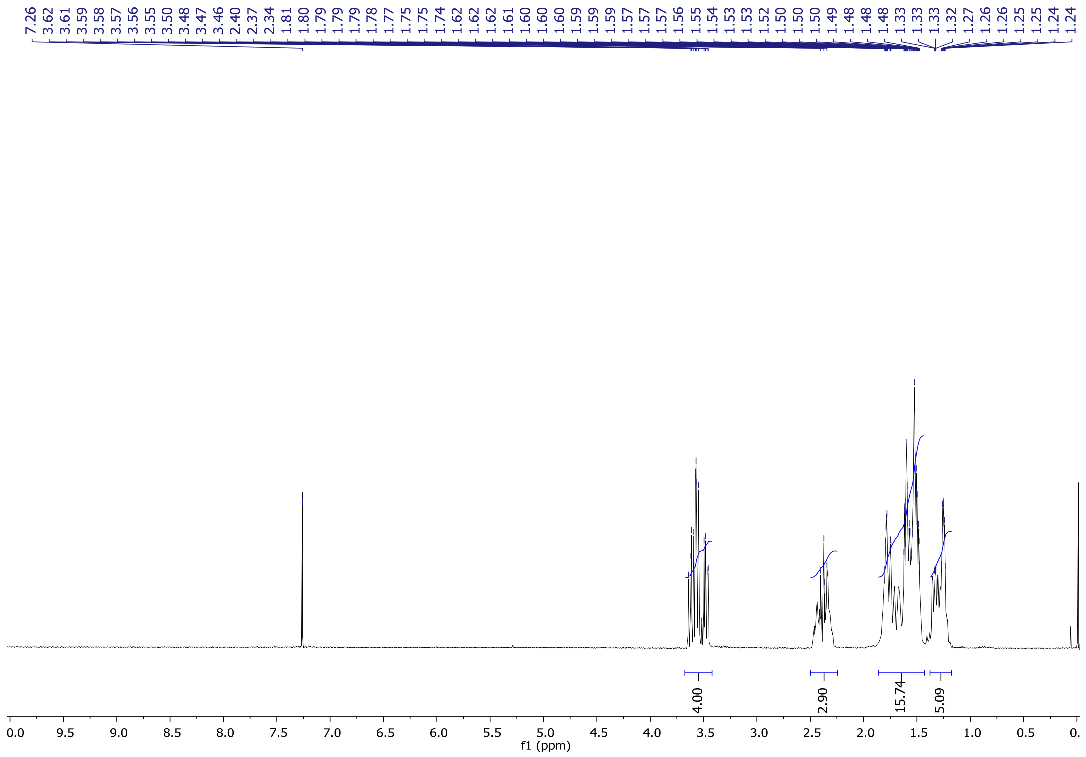
7.26
3.62
3.61
3.59
3.58
3.57
3.56
3.55
3.50
3.48
3.47
3.46
2.40
2.37
2.34
1.81
1.80
1.79
1.79
1.79
1.78
1.77
1.75
1.75
1.74
1.62
1.62
1.62
1.61
1.60
1.60
1.60
1.59
1.59
1.59
1.57
1.57
1.57
1.56
1.55
1.54
1.53
1.53
1.52
1.50
1.50
1.50
1.49
1.48
1.48
1.48
1.33
1.33
1.33
1.33
1.32
1.27
1.26
1.26
1.25
1.25
1.24
1.24
4.00
2.90
15.74
5.09
0.0
9.5
9.0
8.5
8.0
7.5
7.0
6.5
6.0
5.5
5.0
4.5
4.0
3.5
3.0
2.5
2.0
1.5
1.0
0.5
0.
f1 (ppm)

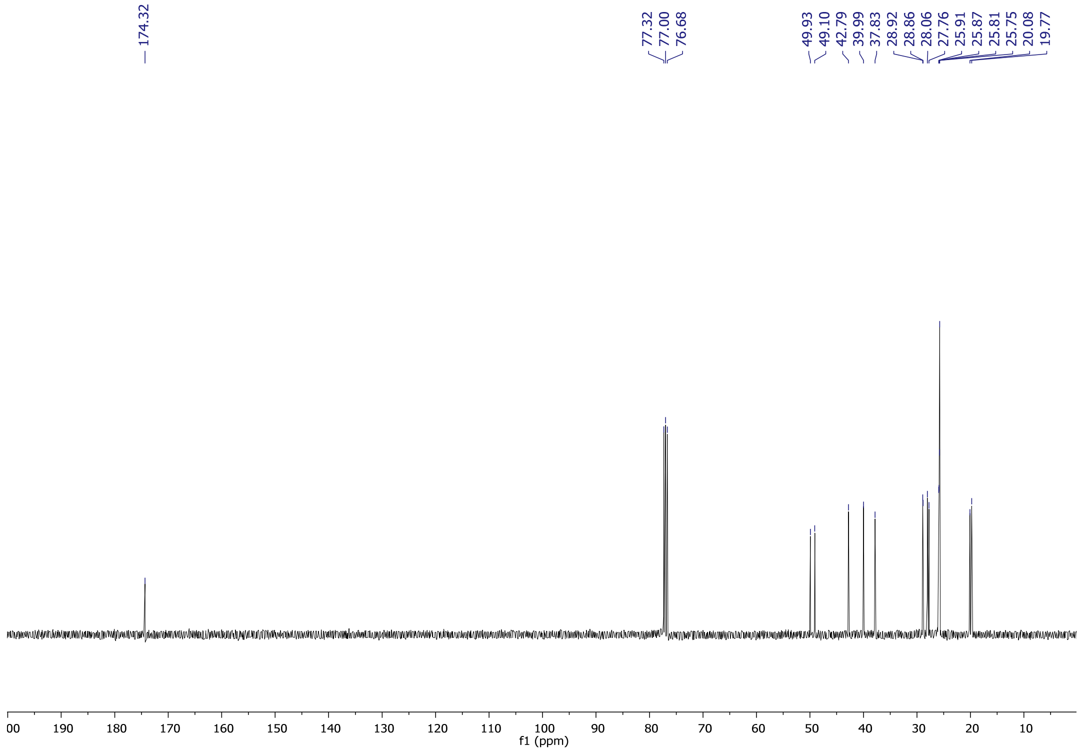
174.32
77.32
77.00
76.68
49.93
49.10
42.79
39.99
37.83
28.92
28.86
28.06
27.76
25.91
25.87
25.81
25.75
20.08
19.77
00
190
180
170
160
150
140
130
120
110
100
90
80
70
60
50
40
30
20
10
f1 (ppm)

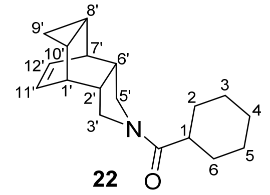
8'
9'
10'
7'
6'
12'
11'
1'
2'
5'
3'
N
2
3
4
1
5
6
O

22

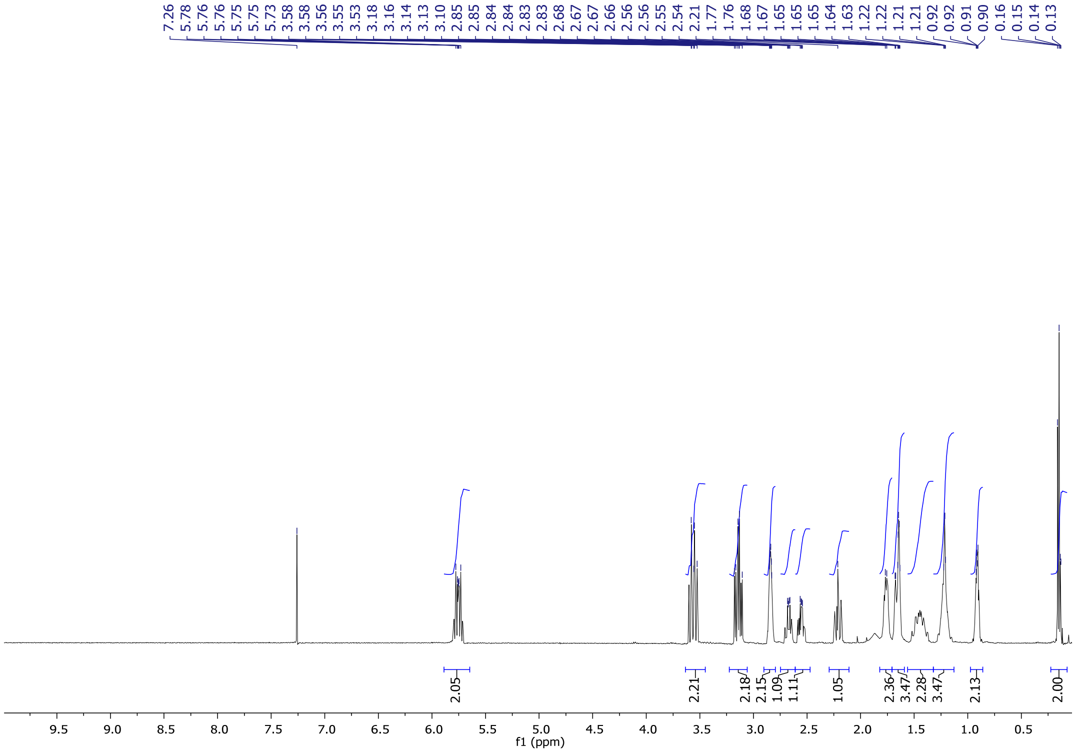
7.26
5.78
5.76
5.76
5.75
5.75
5.73
3.58
3.58
3.56
3.55
3.53
3.18
3.16
3.14
3.13
3.10
2.85
2.85
2.84
2.84
2.83
2.83
2.68
2.67
2.67
2.66
2.56
2.56
2.55
2.54
2.21
1.77
1.76
1.68
1.67
1.65
1.65
1.65
1.64
1.63
1.22
1.22
1.21
1.21
0.92
0.92
0.91
0.90
0.16
0.15
0.14
0.13
2.05
2.21
2.18
2.15
1.09
1.11
1.05
2.36
3.47
2.28
3.47
2.13
2.00
9.5
9.0
8.5
8.0
7.5
7.0
6.5
6.0
5.5
5.0
4.5
4.0
3.5
3.0
2.5
2.0
1.5
1.0
0.5
f1 (ppm)

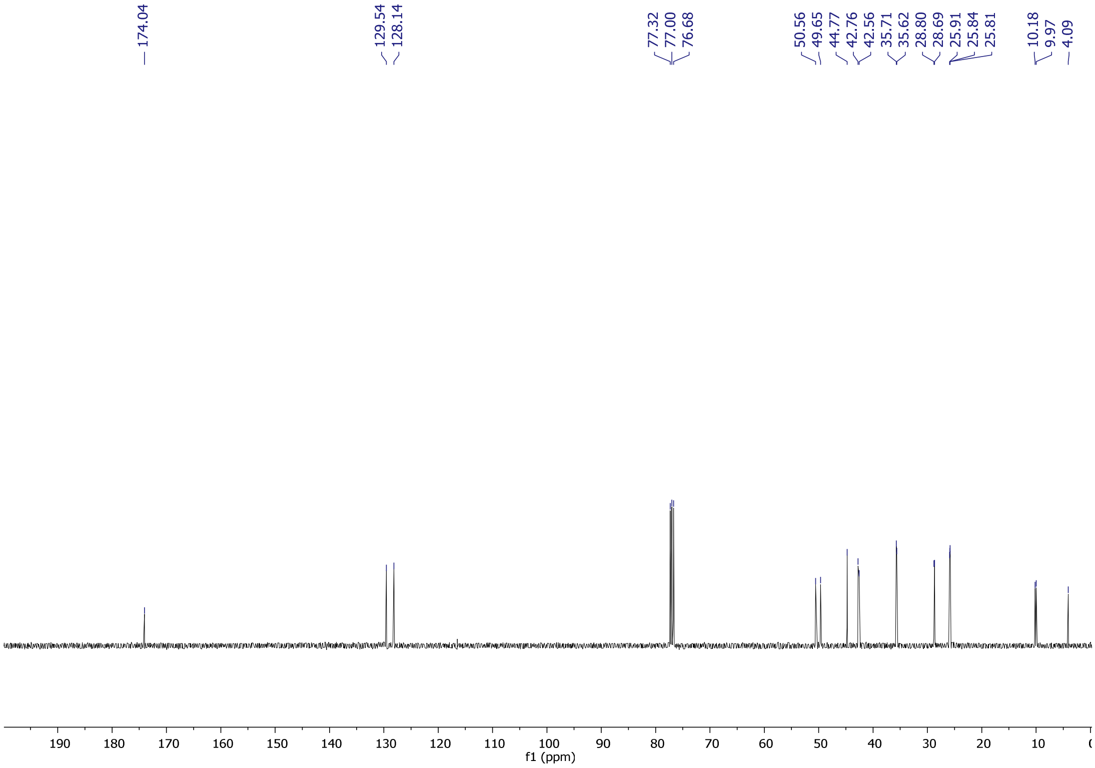
174.04
129.54
128.14
77.32
77.00
76.68
50.56
49.65
44.77
42.76
42.56
35.71
35.62
28.80
28.69
25.91
25.84
25.81
10.18
9.97
4.09
190
180
170
160
150
140
130
120
110
100
90
80
70
60
50
40
30
20
10
f1 (ppm)

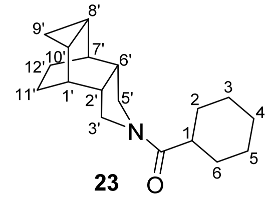
8'
9'
10'
7'
6'
12'
11'
1'
2'
5'
3'
N
1
2
3
4
5
6
O

23

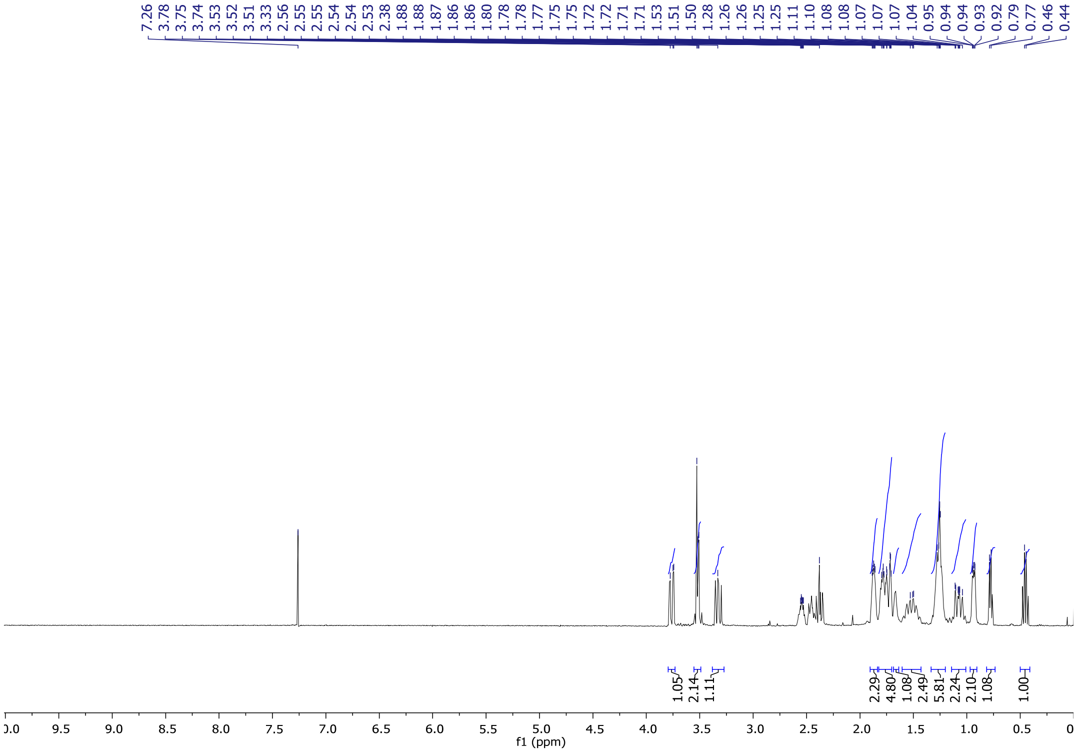
7.26
3.78
3.75
3.74
3.53
3.52
3.51
3.33
2.56
2.55
2.54
2.54
2.53
2.38
1.88
1.88
1.87
1.86
1.86
1.80
1.78
1.78
1.77
1.75
1.75
1.72
1.72
1.71
1.71
1.53
1.51
1.50
1.28
1.26
1.26
1.25
1.11
1.10
1.08
1.08
1.07
1.07
1.07
1.04
0.95
0.94
0.94
0.93
0.92
0.79
0.77
0.46
0.44
1.05
2.14
1.11
2.29
4.80
1.08
2.49
5.81
2.24
2.10
1.08
1.00
0.0
9.5
9.0
8.5
8.0
7.5
7.0
6.5
6.0
5.5
5.0
4.5
4.0
3.5
3.0
2.5
2.0
1.5
1.0
0.5
0
f1 (ppm)

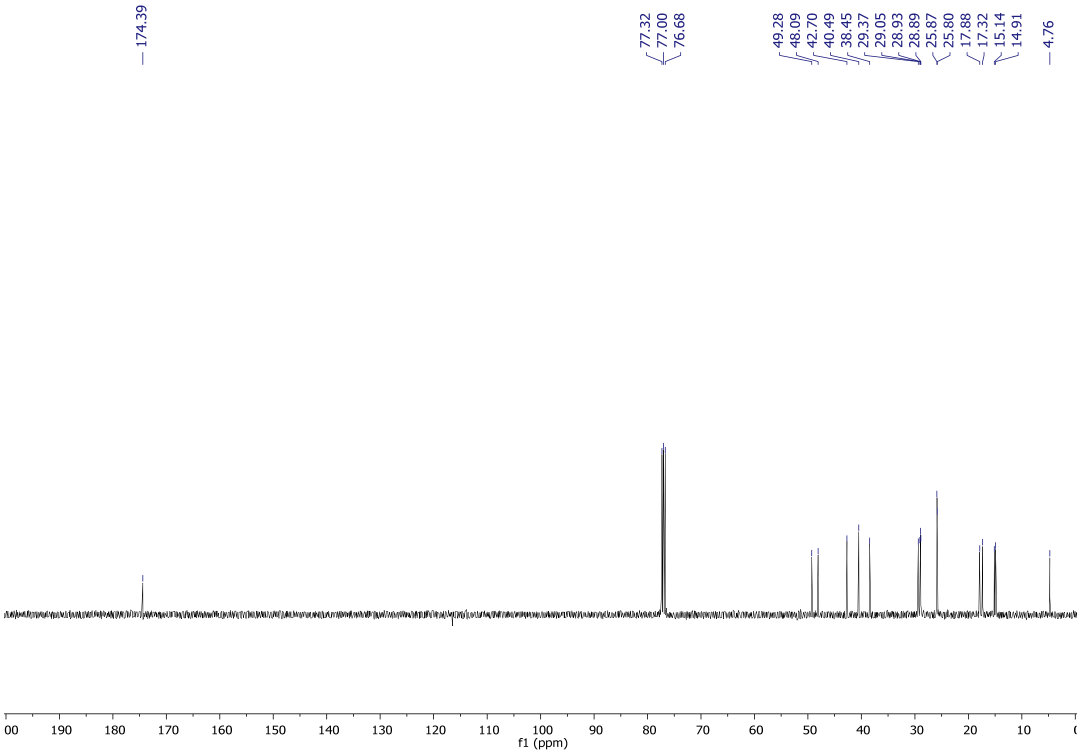
174.39
77.32
77.00
76.68
49.28
48.09
42.70
40.49
38.45
29.37
29.05
28.93
28.89
25.87
25.80
17.88
17.32
15.14
14.91
4.76
00
190
180
170
160
150
140
130
120
110
100
90
80
70
60
50
40
30
20
10
f1 (ppm)

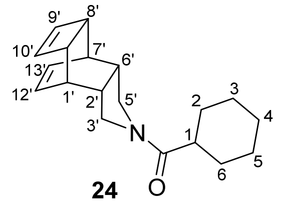
9'
8'
10'
7'
13'
6'
12'
1'
2'
5'
3'
N
1
2
3
4
5
6
O

24

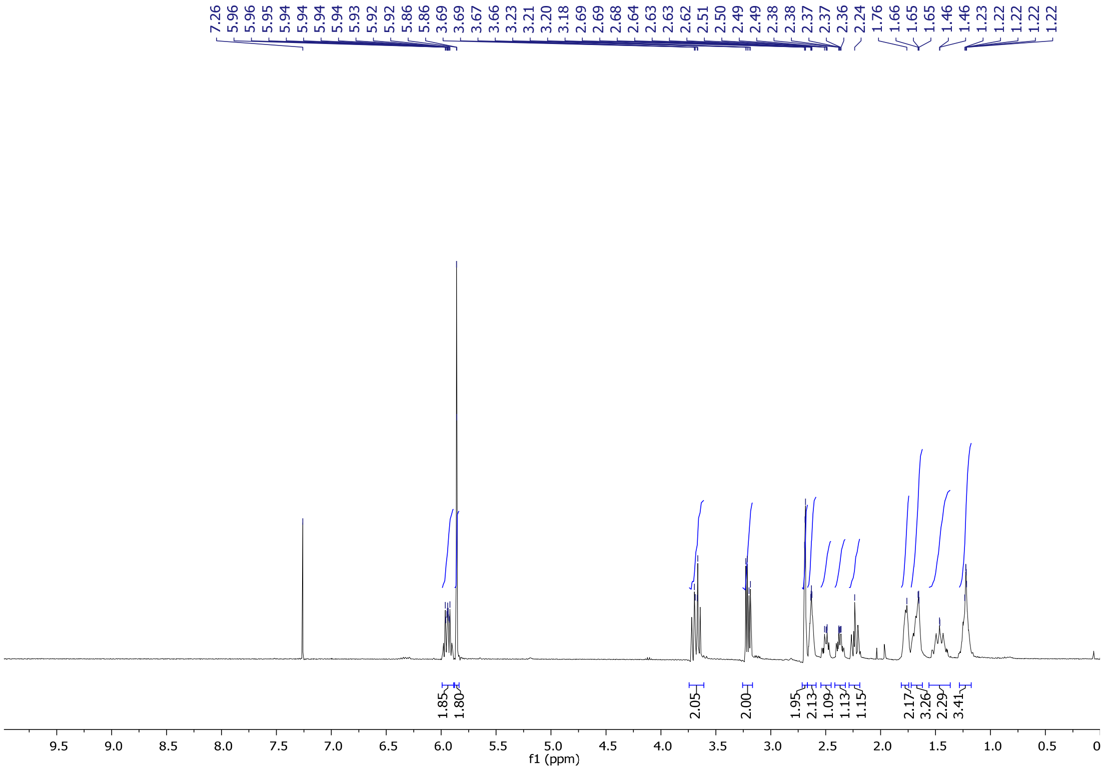
7.26
5.96
5.96
5.95
5.94
5.94
5.94
5.94
5.93
5.92
5.92
5.86
5.86
3.69
3.69
3.67
3.66
3.23
3.21
3.20
3.18
2.69
2.69
2.68
2.64
2.63
2.63
2.62
2.51
2.50
2.49
2.49
2.38
2.38
2.37
2.37
2.36
2.24
1.76
1.66
1.65
1.65
1.46
1.46
1.23
1.22
1.22
1.22
1.22
1.85
1.80
2.05
2.00
1.95
2.13
1.09
1.13
1.15
2.17
3.26
2.29
3.41
9.5
9.0
8.5
8.0
7.5
7.0
6.5
6.0
5.5
5.0
4.5
4.0
3.5
3.0
2.5
2.0
1.5
1.0
0.5
0
f1 (ppm)

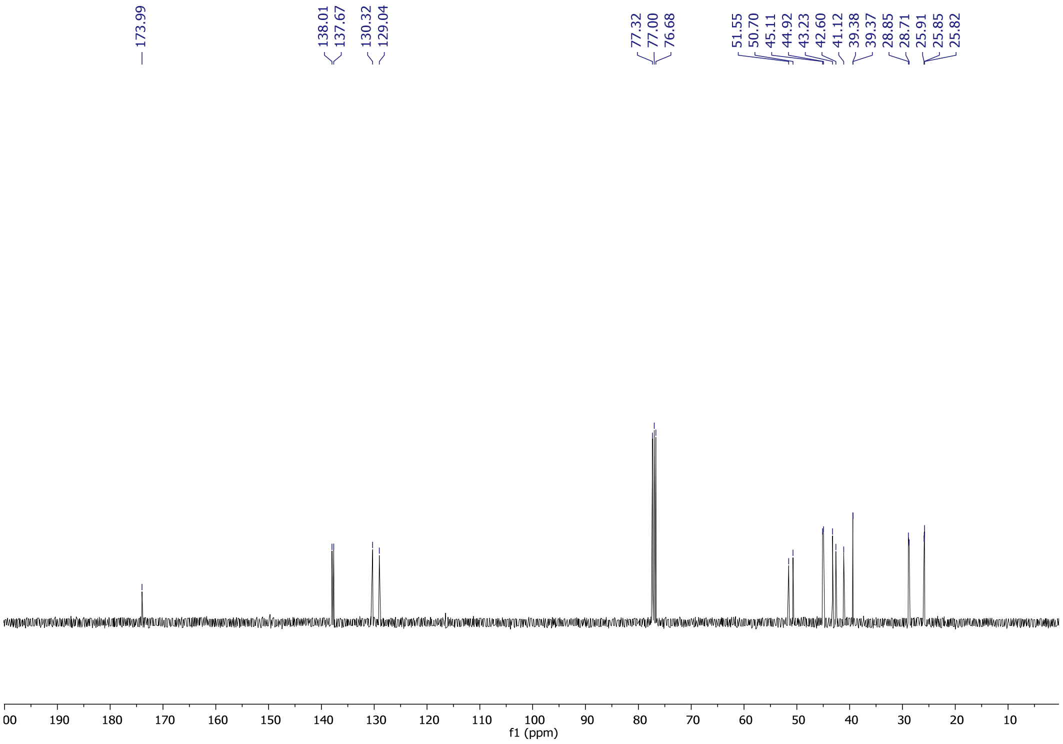
173.99
138.01
137.67
130.32
129.04
77.32
77.00
76.68
51.55
50.70
45.11
44.92
43.23
42.60
41.12
39.38
39.37
28.85
28.71
25.91
25.85
25.82
00
190
180
170
160
150
140
130
120
110
100
90
80
70
60
50
40
30
20
10
f1 (ppm)

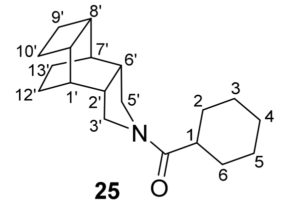
9'
8'
10'
7'
13'
6'
12'
1'
2'
5'
3'
N
1
2
3
4
5
6
O

25

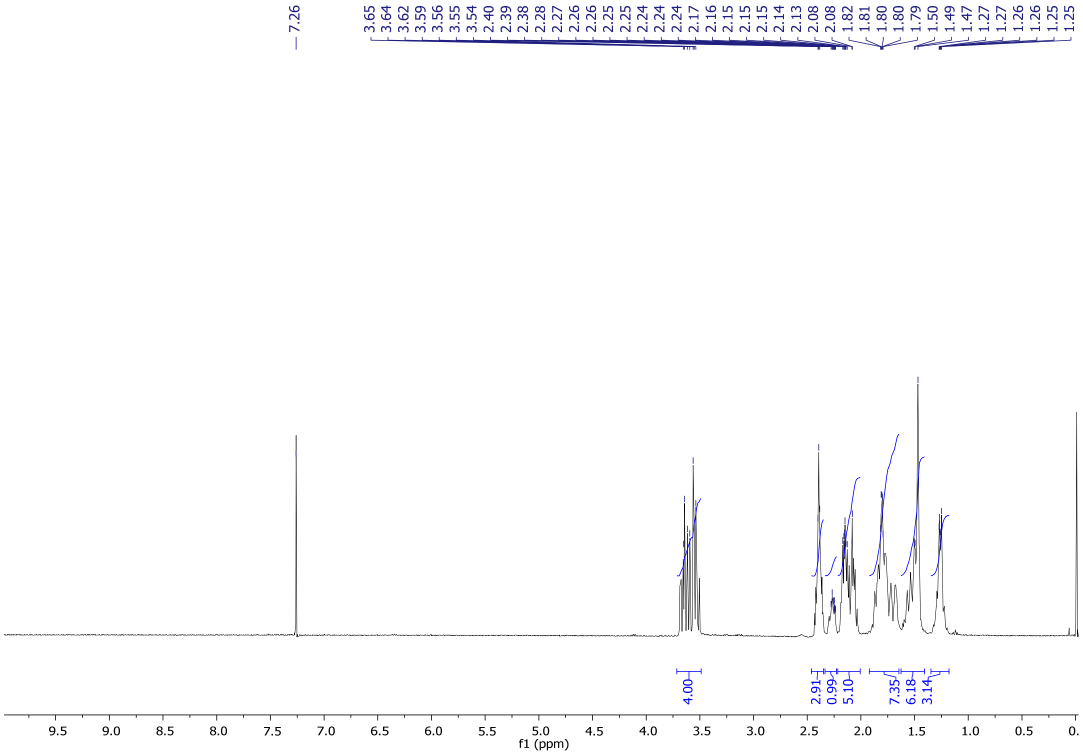
7.26
3.65
3.64
3.62
3.59
3.56
3.55
3.54
2.40
2.39
2.38
2.28
2.27
2.26
2.25
2.25
2.24
2.24
2.24
2.17
2.16
2.15
2.15
2.15
2.14
2.13
2.08
2.08
1.82
1.81
1.80
1.80
1.79
1.50
1.49
1.47
1.27
1.27
1.26
1.25
1.25
4.00
2.91
0.99
5.10
7.35
6.18
3.14
9.5
9.0
8.5
8.0
7.5
7.0
6.5
6.0
5.5
5.0
4.5
4.0
3.5
3.0
2.5
2.0
1.5
1.0
0.5
0.
f1 (ppm)

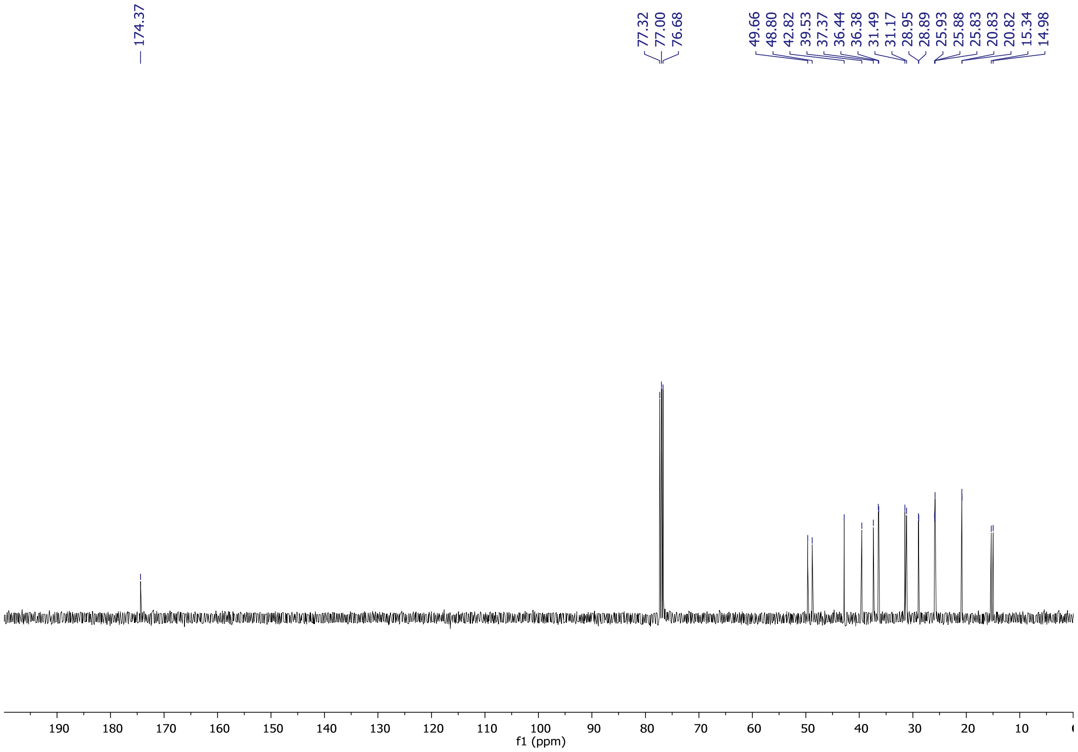
174.37
77.32
77.00
76.68
49.66
48.80
42.82
39.53
37.37
36.44
36.38
31.49
31.17
28.95
28.89
25.93
25.88
25.83
20.83
20.82
15.34
14.98
190
180
170
160
150
140
130
120
110
100
90
80
70
60
50
40
30
20
10
f1 (ppm)

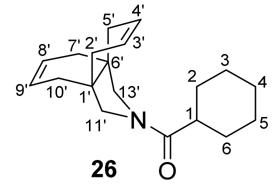
4'
5'
3'
8'
7'
2'
6'
3
2
4
9'
10'
1'
13'
1
11'
N
5
6
O

26

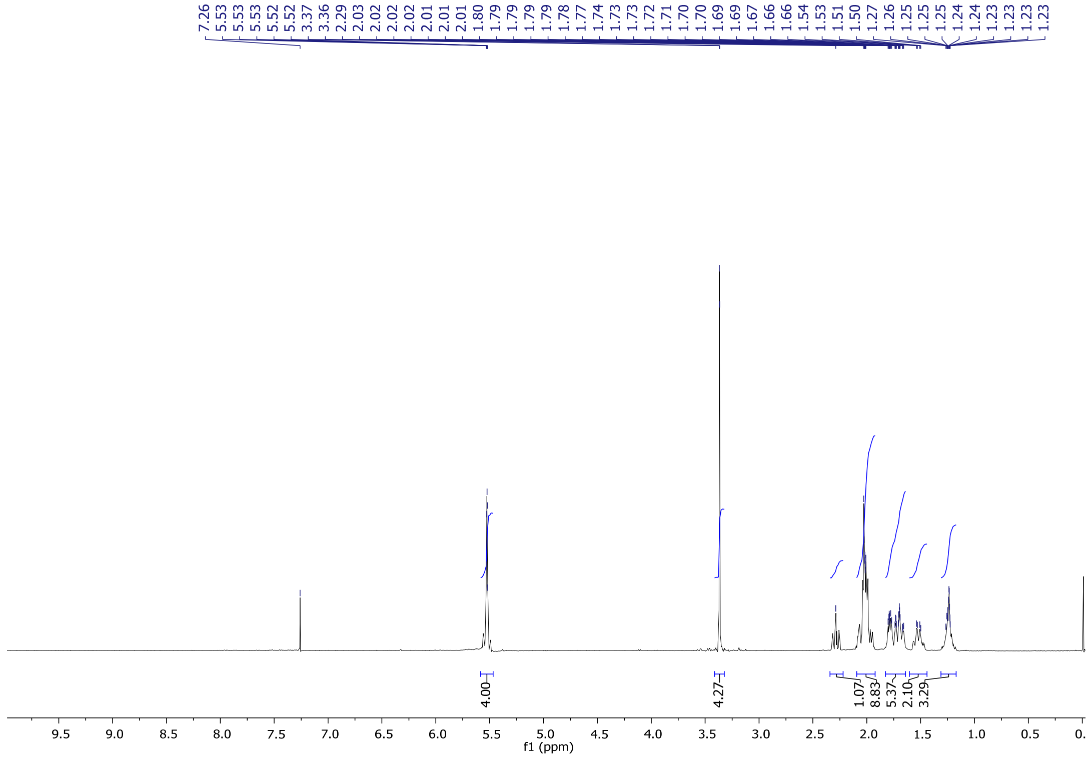
7.26
5.53
5.53
5.53
5.52
5.52
3.37
3.36
2.29
2.03
2.02
2.02
2.02
2.01
2.01
2.01
1.80
1.79
1.79
1.79
1.79
1.78
1.77
1.74
1.73
1.73
1.72
1.71
1.70
1.70
1.69
1.67
1.66
1.66
1.54
1.53
1.51
1.50
1.27
1.26
1.25
1.25
1.25
1.24
1.24
1.23
1.23
1.23
1.23
4.00
4.27
1.07
8.83
5.37
2.10
3.29
9.5
9.0
8.5
8.0
7.5
7.0
6.5
6.0
5.5
5.0
4.5
4.0
3.5
3.0
2.5
2.0
1.5
1.0
0.5
0.
f1 (ppm)

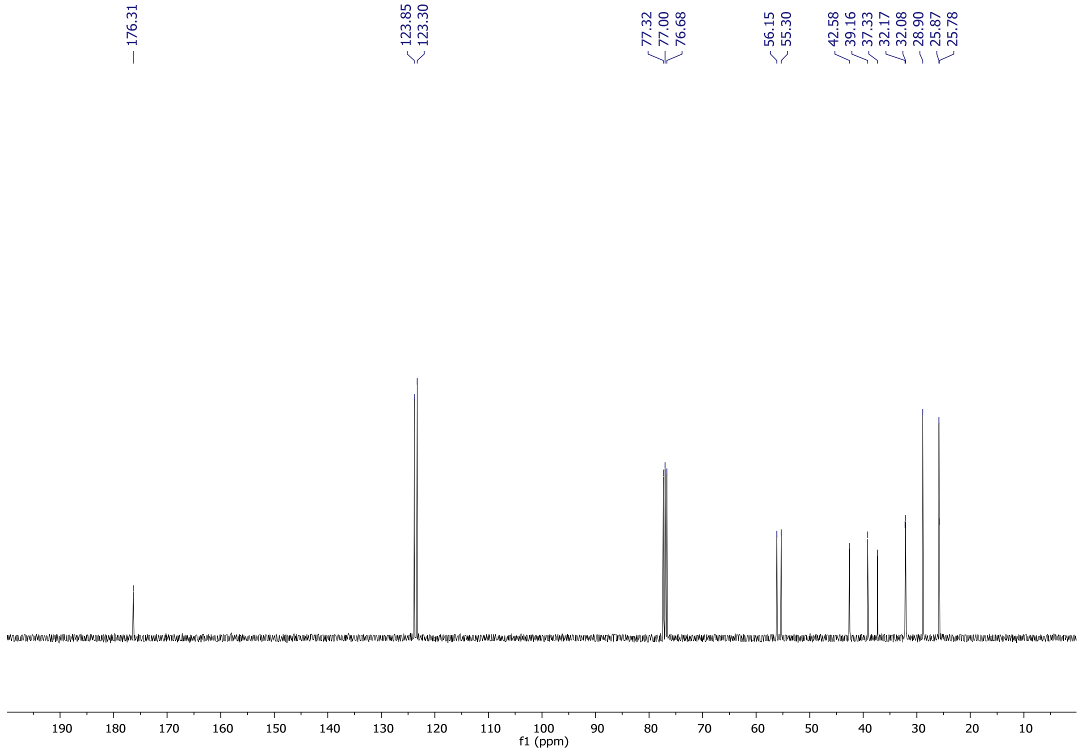
176.31
123.85
123.30
77.32
77.00
76.68
56.15
55.30
42.58
39.16
37.33
32.17
32.08
28.90
25.87
25.78
190
180
170
160
150
140
130
120
110
100
90
80
70
60
50
40
30
20
10
f1 (ppm)

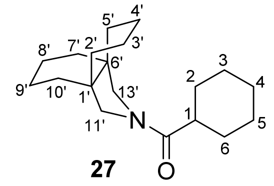
4'
5'
3'
8'
7'
2'
6'
3
2
4
9'
10'
1'
13'
1
11'
N
5
6
O

27

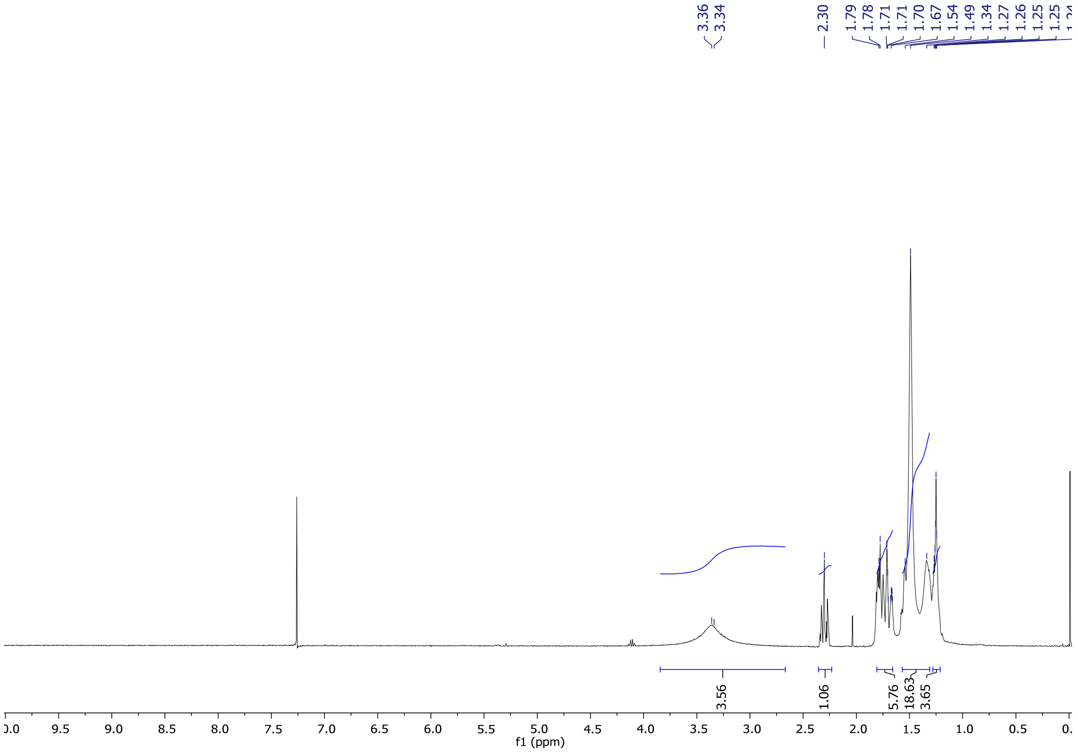
3.36
3.34
2.30
1.79
1.78
1.71
1.71
1.70
1.67
1.54
1.49
1.34
1.27
1.26
1.25
1.25
3.56
1.06
5.76
18.63
3.65
0.0
9.5
9.0
8.5
8.0
7.5
7.0
6.5
6.0
5.5
5.0
4.5
4.0
3.5
3.0
2.5
2.0
1.5
1.0
0.5
0.
f1 (ppm)

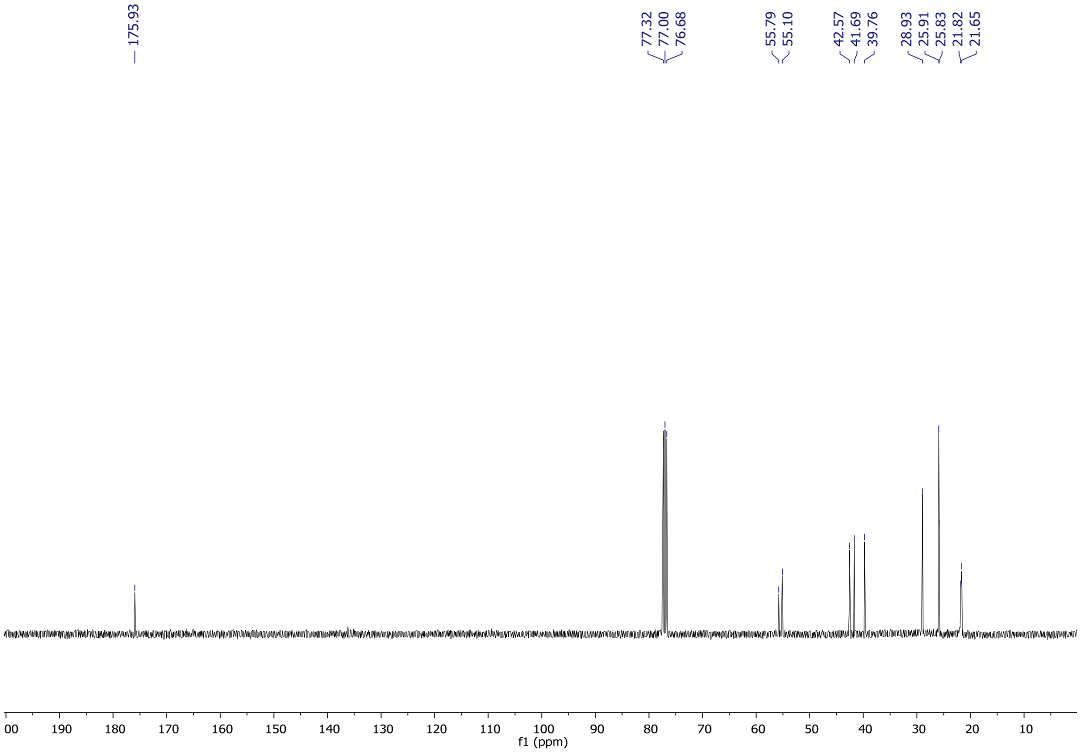
175.93
77.32
77.00
76.68
55.79
55.10
42.57
41.69
39.76
28.93
25.91
25.83
21.82
21.65
00
190
180
170
160
150
140
130
120
110
100
90
80
70
60
50
40
30
20
10
f1 (ppm)

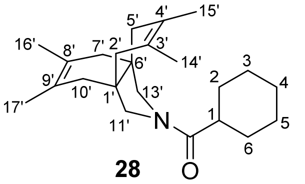
16'
8'
7'
2'
5'
4'
15'
3'
14'
6'
9'
10'
1'
13'
17'
11'
N
1
2
3
4
5
6
O

28

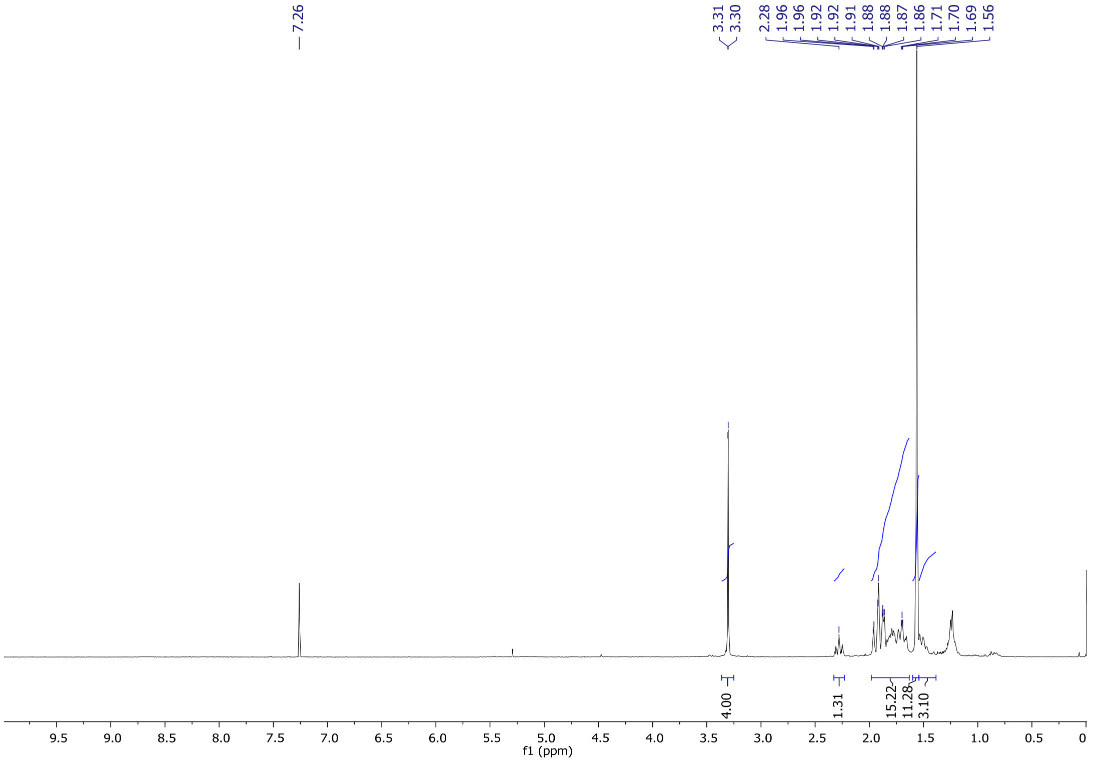
7.26
3.31
3.30
2.28
1.96
1.96
1.92
1.92
1.91
1.88
1.88
1.87
1.86
1.71
1.70
1.69
1.56
4.00
1.31
15.22
11.28
3.10
9.5
9.0
8.5
8.0
7.5
7.0
6.5
6.0
5.5
5.0
4.5
4.0
3.5
3.0
2.5
2.0
1.5
1.0
0.5
0
f1 (ppm)

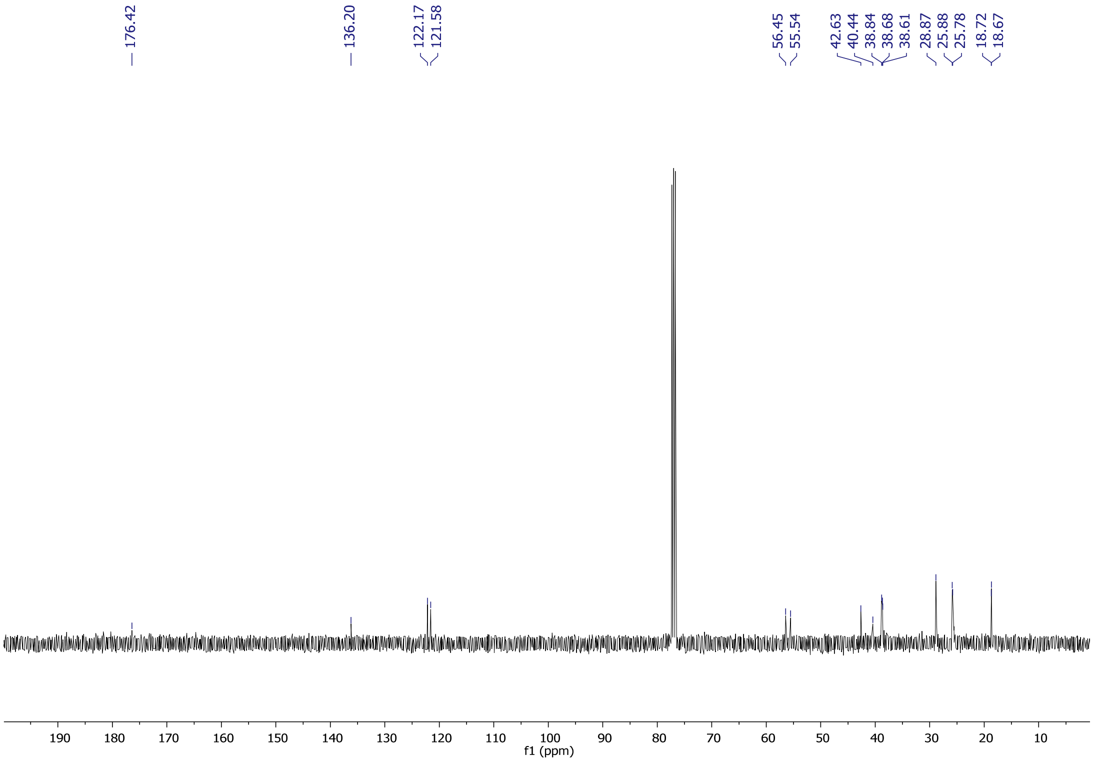
176.42
136.20
122.17
121.58
56.45
55.54
42.63
40.44
38.84
38.68
38.61
28.87
25.88
25.78
18.72
18.67
190
180
170
160
150
140
130
120
110
100
90
80
70
60
50
40
30
20
10
f1 (ppm)

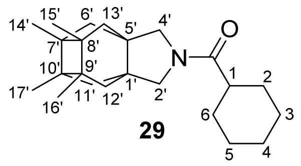
15'
6'
13'
14'
5'
4'
O
7'
8'
N
10'
9'
1
2
17'
11'
12'
1'
2'
16'
6
3
5
4

29

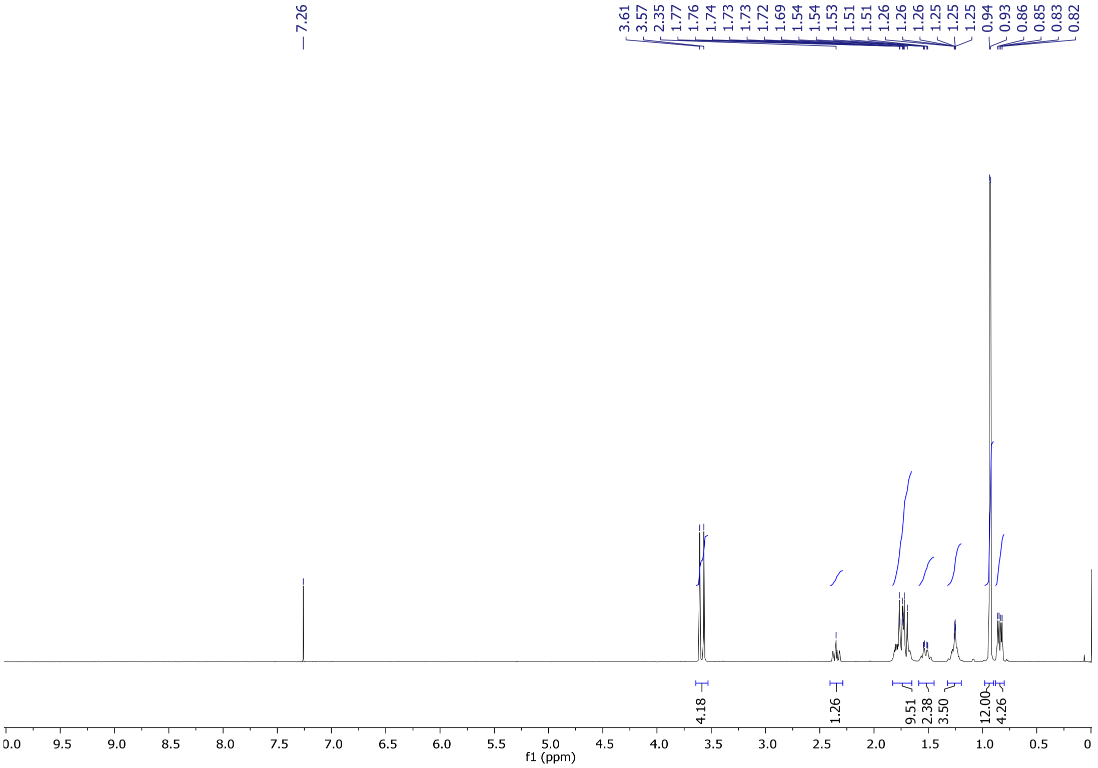
7.26
3.61
3.57
2.35
1.77
1.76
1.74
1.73
1.73
1.72
1.69
1.54
1.54
1.53
1.51
1.51
1.26
1.26
1.26
1.25
1.25
1.25
0.94
0.93
0.86
0.85
0.83
0.82
4.18
1.26
9.51
2.38
3.50
12.00
4.26
0.0
9.5
9.0
8.5
8.0
7.5
7.0
6.5
6.0
5.5
5.0
4.5
4.0
3.5
3.0
2.5
2.0
1.5
1.0
0.5
0
f1 (ppm)

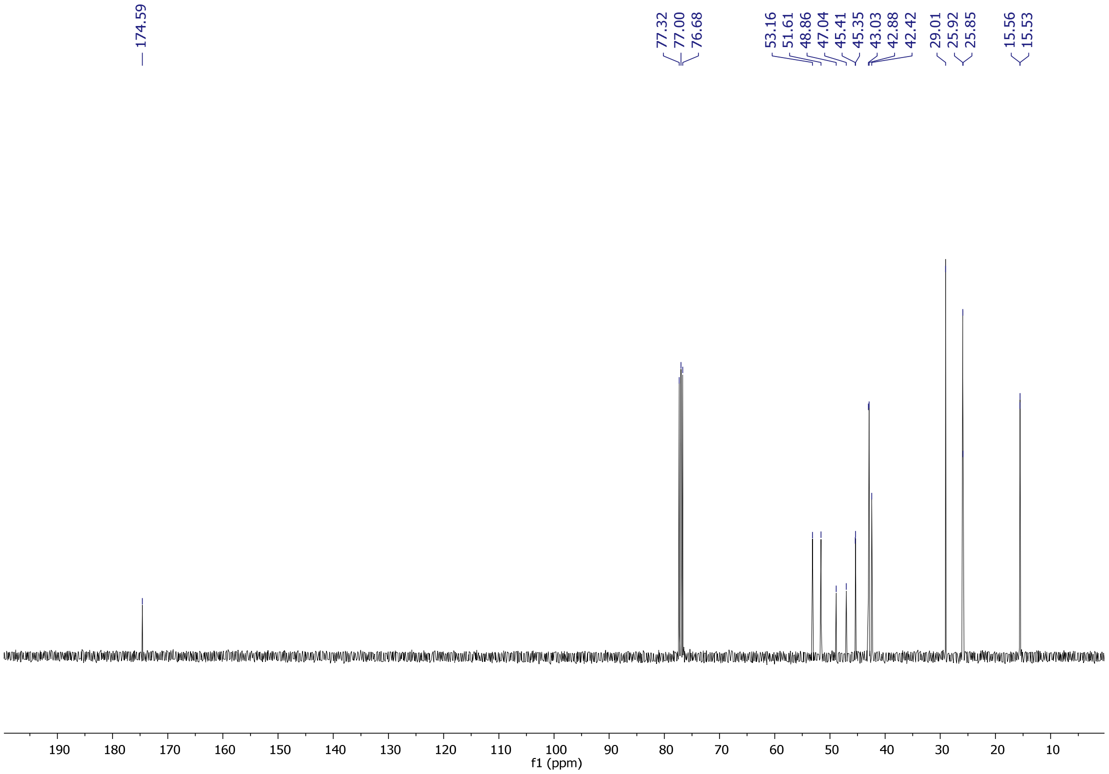
174.59
77.32
77.00
76.68
53.16
51.61
48.86
47.04
45.41
45.35
43.03
42.88
42.42
29.01
25.92
25.85
15.56
15.53
190
180
170
160
150
140
130
120
110
100
90
80
70
60
50
40
30
20
10
f1 (ppm)

3.1.4 Artículo 4: *Rational design in the discovery of novel N-acylpyrrolidine-based 11β-HSD1 inhibitors.*

Resumen

El diseño del fármacos basado en la estructura se ha utilizado para obtener información sobre la actividad de los inhibidores potentes de 11β-HSD1 que contienen la estructura de N-acilpirrolidina previamente descrita. Con este fin, se ha construido un modelo de farmacóforo 3D-QSAR utilizando un conjunto de descriptores hidrofóbicos que utilizan los datos de las estructuras de rayos X disponibles. A partir de de esta información, se describieron una serie de nuevos compuestos como inhibidores potenciales de 11β-HSD1, que se sometieron a síntesis y evaluación farmacológica.

Rational design in the discovery of novel *N*-acylpyrrolidine-based 11β-HSD1 inhibitors

Constantí Seira[1], *Rosana Leiva*[2], *Andrew McBride*[3], *Margaret Binnie*[3], *F. Javier Luque*[1], , *Scott P. Webster*[3], *Axel Bidon-Chanal*[*,1]*and Santiago Vázquez*[*,2] ,

[1]Department of Nutrition, Food Science and Gastronomy, Facultat de Farmàcia i Ciències de l'Alimentació, Institute of Biomedicine (IBUB) and Institute of Theoretical and Computational Chemistry (IQTCUB), Universitat de Barcelona, Av. Prat de la Riba, 171, 08921 Santa Coloma de Gramenet, Spain

[2]Laboratori de Química Farmacèutica (Unitat Associada al CSIC), Facultat de Farmàcia i Ciències de l'Alimentació and Institut of Biomedicine (IBUB), Universitat de Barcelona, Av. Joan XXIII, 27-31, 08028 Barcelona, Spain.

[3]Centre for Cardiovascular Science, University of Edinburgh, Queen's Medical Research Institute, EH16 4TJ, United Kingdom.

Abstract:

Structure-based drug design has been used to gain insight into the activity of potent 11β-HSD1 inhibitors containing the previously reported *N*-acylpyrrolidine structure. To this end, a 3D-QSAR pharmacophore model has been built up using a set of hydrophobic descriptors taking advantage of the available X-ray structural data. On the basis of this information, a series of novel compounds were descripted as potential inhibitors of 11β-HSD1, which were subjected to synthesis and pharmacological evaluation. In particular, biaryl derivatives **11** and **17** have ben identified as low nanomolar inhibitors with greater metabolic stabilities than the earlier hit dichloroaniline **7**, although better selectivity over the isoenzyme 11β-HSD2 remains to be achieved.

Keywords:

Glucocorticoids, 11β-HSD1 inhibitors, rational drug design, polycyclic substituents.

1. Introduction

Cushing's syndrome is caused by increased circulating levels of cortisol, the glucocorticoid (GC) hormone. The elevated and sustained cortisol level causes the characteristic clinical symptomatology, namely central obesity, hyperglycaemia, dyslipidaemia and hypertension by its action in key metabolic tissues, and depression and cognitive impairments by acting in the CNS.[1] These findings, in conjunction with mechanistic investigations, suggest that elevated cortisol seems to be key in metabolic syndrome and age-related diseases such as cognitive decline.[2-5]

11β-Hydroxysteroid dehydrogenase (11β-HSD) enzymes are responsible for the interconversion of cortisone and cortisol (or 11-dehydrocorticosterone and corticosterone in rodents, respectively) in target tissues, being an enzymatic barrier gating GC access to intra-cellular receptors.[6,7] 11β-HSD presents two isoforms: 11β-HSD1 and HSD2. The former is characterized by a predominantly reductase activity, and is present in liver, adipose tissue, hippocampus and brain cortex, where it regenerates the active cortisol from cortisone. In contrast, 11β-HSD2 is found in mineralocorticoid tissues such as kidney, with an oxidative activity on cortisol to inactivate it to cortisone, protecting by this way mineralocorticoid receptors from GC activation.[8]

The expected promising effects have been found both in metabolic and cognitive disorders in numerous studies using 11β-HSD1 knockout mice. Global knockout of 11β-HSD1 causes enhanced hepatic insulin sensitivity and reduced gluconeogenesis and glycogenolysis, indicating a potential use of 11β-HSD1 inhibitors for type 2 diabetes.[9] These same mice also present low serum triglycerides and increased HDL cholesterol and apo-lipoprotein A1 levels, suggesting a positive effect of 11β-HSD1 inhibition in atherosclerosis prevention.[10] Furthermore, 11β-HSD1 knockout mice are also protected against age-related cognitive impairment, encouraging the use of these inhibitors in cognitive dysfunction-related diseases, such as Alzheimer's disease.[11]

Very encouraging results have also been obtained in several *in vitro* and *in vivo* models of both cognitive and metabolic disorder using a variety of 11β-HSD1 inhibitors.[12] Notwithstanding, the efficacy of 11β-HSD1 inhibitors in clinics has still to be proven since no compounds have progressed beyond phase II, with insufficient efficacy being the main cause of attrition. Regarding metabolic indications, the failure to achieve primary efficacy endpoints such as glycaemic control or blood pressure were disappointing.[13] Although Abbott's compound ABT-384 failed in demonstrating efficacy in phase II clinical trial,[14] central 11β-HSD1 inhibition seems a promising approach to deal with cognitive dysfunction associated with AD, since sub-maximal inhibition of the target in the brain seems to be capable of reversing memory impairment in ageing and AD.[15] Indeed, inhibitors from Actinogen Medical (UE2343) and Astellas (ASP3662) are still in active development, both of them in phase II trials, in relation to age-associated cognitive impairment and AD.[15,16]

2. Previous work

We have previously described novel series of 11β-HSD1 inhibitors featuring polycyclic *N*-acylpyrrolidines. Our first efforts were focused on the optimization of the polycylic substituent to replace the adamantyl nucleus broadly used in 11β-HSD1 inhibitors.[17] After working on the polycylic group and finding potent enzyme inhibitors (**1-6**) (Figure 1), we moved forward to explore the right-hand side (RHS) substituent of the molecule in order to improve selectivity and DMPK properties maintaining the potency. This work motivated us to explore the structure-activity relationships (SAR) of our molecules, leading to the discovery of new nanomolar inhibitors containing the 4-azapentacyclo[5.3.2.$0^{2,6}$.$0^{8,10}$]dodec-11-ene polycycle (**7** and **8**).[18]

The replacement of the cyclohexyl moiety of compound **6** by a phenyl group was detrimental for the potency (**6**, IC_{50} = 29 nM *vs* **9**, 546 nM); however, the introduction of a previously reported substitution pattern on the aryl unit delivered again a low nanomolar inhibitor (**7**, IC_{50} = 45 nM). Despite the potent inhibitory activity of **7**, its low metabolic stability (13% remaining compound after 30-min incubation with human liver microsomes, HLM), the sub-optimal selectivity over 11β-HSD2 (71% inhibition at 1 μM) and the aromatic amine as a structural alert of mutagenicity –even though the *ortho*-di-substitution is expected to hinder its metabolic activation– made this compound not an ideal lead for our medicinal chemistry program.

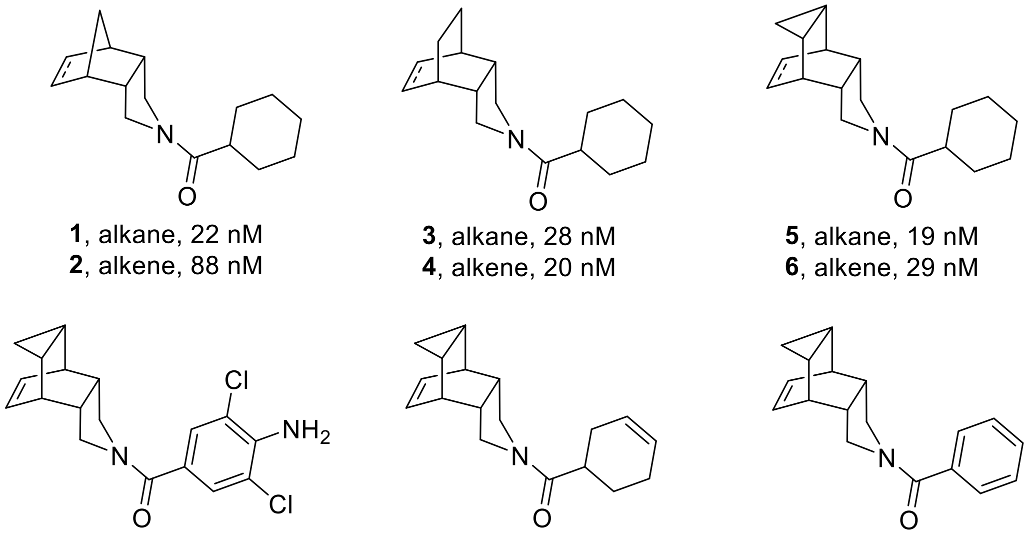

1, alkane, 22 nM
2, alkene, 88 nM

3, alkane, 28 nM
4, alkene, 20 nM

5, alkane, 19 nM
6, alkene, 29 nM

7, 45 nM

8, 56 nM

9, 546 nM

Figure 1. Previous 11β-HSD1 inhibitors reported by the group with their IC_{50} values.[17,18]

3. Design of new inhibitors

In light of these findings, we focused our efforts on a rational design of new substitution patterns of this RHS aryl group in order to establish additional interactions in the binding site that would deliver more potent and selective inhibitors using docking coupled to molecular dynamics simulations. The aim of this work was to identify a 3D-QSAR pharmacophore model taking advantage of the available X-ray data. To this end, we have used a CoMFA analysis using two distinct sets of descriptors that rely on the use of hydrophobic descriptors reported recently by Ginex at al.[19] The former set, denoted H1 in the following, corresponds to the combination of the electrostatic component of the octanol/water partition coefficient (log P) and the third power of the atomic radii, which were used to examine the features of the electrostatic and steric fields. In the second set, denoted H2, the atomic radii are replaced by the cavitation contribution to the logP (see ref. 19 for details).

The pharmacophore model was determined using the PharmQSAR software.[21] To this end, a dataset of 48 compounds, which were partitioned into training (41) and test (7) subsets, was selected taking into account the availability of the known binding mode to the 11β-HSD1 enzyme (PDN entries 3D5Q, 3CH6, 4C7J, 4HFR),[22] and the diversity of chemical scaffolds. The hydrophobic contribution of atoms were derived from the solvation free energies in water and *n*-octanol, using the quantum mechanical IEF-

PCM/MST solvation model parametrized at the B3LYP/6-31G(d) level.[20] The solvation free energies were then combined to generate the atomic contributions to the electrostatic and cavitation components of logP. The alignment of the 41 compounds that form the training set is shown in Figure 2, which shows the challenging question of deriving a pharmacophore model taking into account the diverse subpockets filled by the inhibitors in the training set.

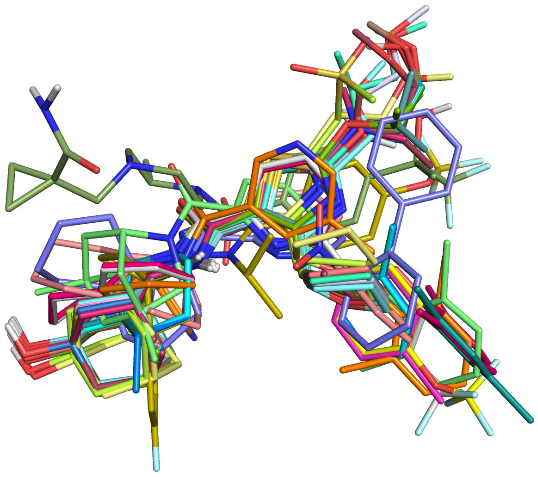

Figure 2. Alignment of the compounds in the training set.

Figure 2 shows the comparison of the experimental and predicted inhibitory potencies for the training and test subsets. The statistical parameters of the model are shown in Table 1, and the representation of the experimental versus predicted inhibitory activities is shown in Figure 3. The two sets of hydrophobic descriptors provide qualitatively similar results, with Pearson correlation coefficients of 0.82 (H1) and 0.86 (H2) for the training set. lower values are obtained for the test set, even though this also reflects the reduced range of pIC50 values (close to 1.5 units) corresponding to these compounds. The leave-out-out validation lead to q^2 values close to 0.56 (Table 3), and the error is estimated to be close to 0.44. Finally, the electrostatic and nonelectrostatic terms have a more balanced contribution to the 3D-QSAR model than in the case of the H1 model, where the steric term has a larger contribution compared to the electrostatic one.

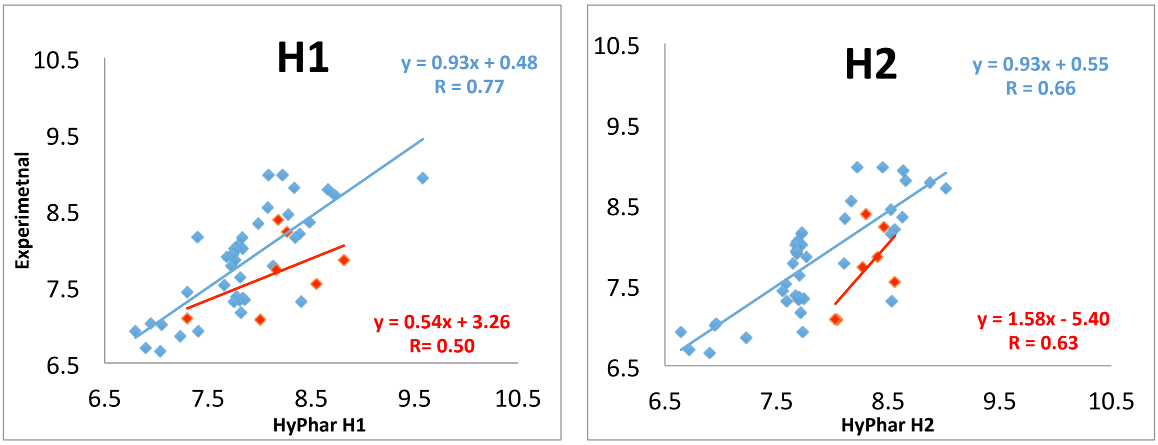

Figure 3. Comparison of the results obtained from standard COMFA models (data taken from refs. (20,22-24) and the MST-based hydrophobic H1(A) and H2(B) models. Compounds of training/test are showing in blue/red respectively.

Set of 41 compounds	H1	H2
r	0.82	0.86
r^2	0.67	0.74
q^2	0.57	0.54
S_{press}	0.43	0.45
Number of Components (NC)	2	2
ELECTROSTATIC FIELD (%)	38.4%	57.3%
NON ELECTROSTATIC FIELD (%)	61.6%	42.7%

Table 1. Summary of statistical parameters obtained from HyPhar models derived from the QM-MST based hydrophobic descriptors (models H1 -H4).

In conjunction with docking and molecular dynamics simulation, this information was used to explore novel scaffolds against this target, which were subsequently synthesized and evaluated pharmacologically. Our endeavor started with the search of different crystalized 11β-HSD1 potent inhibitors and its superposition with the docking generated complex of our (best) hit, compound **7**. For each case, visual inspection of the superposed ligands led to a ligand inspired new compound that was proposed also taking into account its synthetic accessibility. A docking experiment was carried out with each proposed ligand in order to build a ligand–receptor complex for each of them.

In every case, the best prediction was selected as the highest scored pose where the ligand preserved the orientation of compound **7** and the hydrogen bond interaction with the crucial residues Ser170 and/or Tyr183. Afterwards, at least three independent 50 ns molecular dynamics (MD) simulations were run to obtain a relaxed structure of the selected docking pose in the binding site. The MD run for compound **7** was used as a reference system to compare with the different proposals. The root-mean square deviation (RMSD) profiles were similar in all cases. Thus, the RMSD of the protein backbone varied from 1.35–2.0 Å, whereas the residues in the binding site showed a larger RMSD (2.05 to 2.60 Å) due to the enhanced flexibility of the loops that surround it. The proximity of the binding site to the C-terminal endpoint of the protein has also an influence in its instability in both chains[23].

In the first case, compound **7** was superposed to the 3D5Q crystal ligand featuring a trifluoromethoxy group on its RHS phenyl moiety (Table 1).[24] The scores obtained for both molecules in the docking experiment were similar (-8.72 and -8.67, respectively). The proposed substitution pattern inspired in this crystal ligand was a methoxy group in *para* position to replace the amino group and maintaining one chloro substituent in order to fill a small hydrophobic cavity present in the binding site (residues Leu152, Gly197, Leu198, Val212, Met214). The score for this new compound **10** was the same as for the crystal ligand (-8.67), so we expected a similar potency. The binding mode was also the usual with the central amide carbonyl group making a hydrogen bond interaction with the hydroxyl groups of Ser170 and Tyr183. The binding pose obtained with the docking experiment was taken as the starting point to run three independent 50 ns unrestrained MD simulations of the enzyme complex with compound **10**. The ligand was placed in both chains of the crystal structure and the obtained trajectories confirmed the stability of the binding mode in the standard V-shaped conformation. However, due to the enhanced flexibility of the loops and the C-terminal part, the ligand was kept in both binding sites throughout the whole simulation only in one trajectory. For the cases where the ligand was kept in the binding site, the mean hydrogen bond distances with the critical residue Ser170 were 2.89 Å, 3.69 Å and 2.76 Å respectively.

In the second case, we did not observe a significant difference between the scores of the 3CH6 crystal ligand and our compound **7** (-10.90 *vs* -10.20).[20] Our proposal was compound **11**, mimicking the biaryl structure of the crystal ligand but substituting the methyl group in *para* position by a hydroxyl group to interact through a hydrogen bond with Pro178. Docking calculations corroborated our expectations predicting a higher score for **11** (-12.08). Again, three independent 50 ns unrestrained MD simulations were run with the ligand placed in both chains of the crystal structure. In this case, the ligand was kept in the binding site of the chain B in all the cases, however it was only stable in one of the trajectories for the chain A. In the cases where the ligand was kept in the binding site, the mean hydrogen bond distances of the central amide carbonyl group with the side chain of Ser170 were 2.81 Å, 3.51 Å, 3.54 Å and 2.69 Å.

The next case was using the 4C7J crystal ligand to superpose our compound **7** on it.[25] After docking calculations, the score obtained for the crystal ligand was similar to the calculated for **7** (-10.71 and -10.17, respectively), despite of the additional interaction of the hydroxyl group of the ethylene chain with the side chain of Asp259. The proposed new compound, **12**, replicating the lateral chain of the crystal ligand, presented an even higher score (-11.13) in the docking and a good consistency of the binding mode in the three independent 50 ns unrestrained MD simulation runs. In this case, the mean hydrogen bond distances of the central amide carbonyl group with the hydroxyl group of Ser170 for those simulations in which the ligand was kept in the binding site were 2.66 Å, 2.73 Å and 3.54 Å.

In the last case, the superposition of **7** with the crystal ligand of 4HFR was suitable.[26] Again, the crystal ligand showed a higher docking score than **7** (-10.65 *vs* -10.39) and established an additional interaction between the carboxylic acid moiety and the amide group of Leu217. Our proposal was to reproduce the two-ring structure of the crystal ligand with a different final hydrogen bond donor to seek the interaction with Asp259. The proposed compound **13** presented a high score (-11.49) in the docking calculations although this predicted additional interaction between the amino group of the distal amide and the Asp259 was not observed in the docking calculations without losing the principal interactions of the central amide carbonyl group. Furthermore, the ligand was kept in the binding site only in two simulations with mean hydrogen bond distances between the central amide carbonyl group and the side chain hydroxyl group of Ser170 of 2.91 Å and 2.95 Å.

Crystal	**Compound**	**Score**
3D5Q	**7**	-8.72
	Crystal ligand[24] 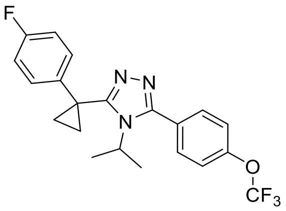	-8.67
	Proposed compound **10** 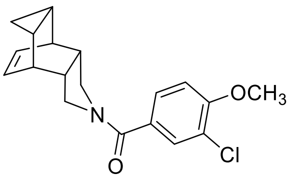	-8.67
3CH6	**7**	-10.20
	Crystal ligand[22] 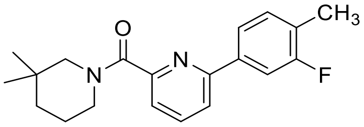	-10.90
	Proposed compound **11** 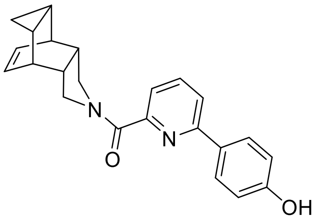	-12.08
4C7J	**7**	-10.17
	Crystal ligand[25] 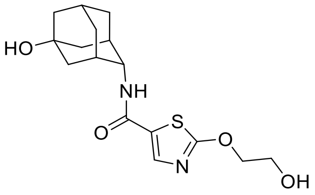	-10.71
	Proposed compound **12** 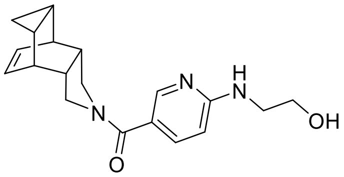	-11.13
4HFR	**7**	-10.39

Crystal ligand[26] 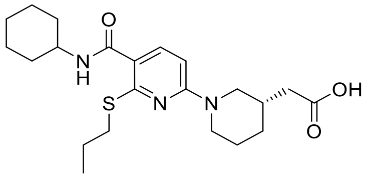	-10.65
Proposed compound **13** 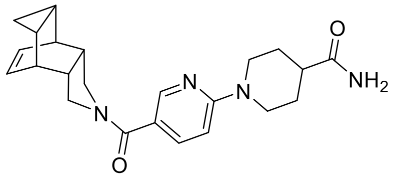	-11.49

Table 2. Reference crystal ligands, new designed compounds and their docking scores.

4. Synthesis

The novel compounds were synthesized according to the Scheme 1. Compound **10** was obtained in quantitative yield from the coupling reaction between 4-azapentacyclo[5.3.2.$0^{2,6}$.$0^{8,10}$]dodec-11-ene hydrochloride,[27] **14**, and 3-chloro-4-methoxybenzoic acid using 1-hydroxybenzotriazole (HOBt) and *N*-(3-dimethylaminopropyl)-*N'*-ethylcarbodiimide (EDC). For the preparation of compound **11**, was first necessary the synthesis of the 6-bromopyridin-2-yl-cointaining intermediate **15** using the previous methodology for the amide formation, followed by a Suzuki-Miyaura cross-coupling with 4-hydroxyphenylboronic acid which proceeded with moderate yield. Finally, compounds **12** and **13** were obtained by a nucleophilic aromatic substitution using the chloropyridine derivative **16** previously described by our group as the starting material.[18] Amide **16** was dissolved in ethanolamine and heated at 120 ºC for 24 hours to give compound **12** in moderate yield. Besides, compound **13** was obtained in high yield heating a solution of the starting material **16**, piperidine-4-carboxamide and potassium carbonate in DMF at 90 ºC for 2 days.

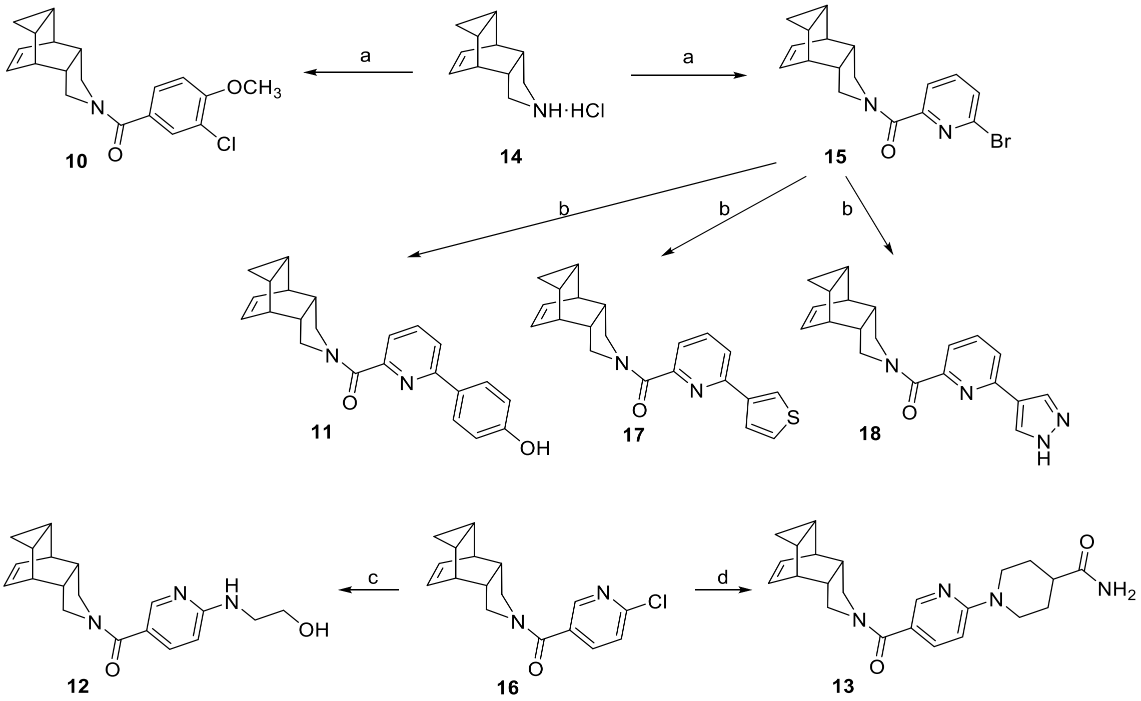

Scheme 1. **Syntheses of compound 10-14 and 16-17**. a) HOBt, EDC, Et_3N, EtOAc, rt, 24 h, 3-chloro-4-methoxybenzoic acid for **10** (quant. yield), 6-bromopyridine-2-carboxylic acid for **15** (73% yield). b) $Pd(Ph_3)_4$, K_2CO_3, dioxane, water, 4-hydroxyphenylboronic acid for **11** (59% yield), thiophene-3-boronic acid for **17** (79% yield), 1*H*-pirazole-4-boronic acid for **18** (28% yield). c) Ethanolamine, 120 ºC, 24 h, 61% yield. d) 4-piperidinecarboxamide, DMF, 90 ºC, 2 d, 85% yield.

5. Pharmacological evaluation

Target compounds **10-13** together with the intermediate amide **15** were tested to determine their human 11β-HSD1 inhibitory activity using a microsomal assay as the preliminary screen. Compounds, **12** and **13** presented 20% and 21% inhibition at 10 μM concentration, respectively, so they were not further examined to get their IC_{50} values. However, **11** and **15** presented high inhibition of the enzyme, exhibiting diverse potencies. The bromopyridine analog, **15**, presented a submicromolar value (200 nM). The IC_{50} value of the biaryl **11** (14 nM) was lower than that of our early hit dichloroaniline **7** (45 nM) (Table 2).

As compounds **12** and **13** showed poor inhibition, one may hypothesize that we could not obtain the designed compounds interacting with the Asp259 that was expected to deliver more potent compounds. However, we cannot feel confident with this statement since the performed assay uses a cellular fraction (HLM) instead of the purified enzyme, which introduces more factors to consider besides the mere interaction between the ligand and the target protein.

The most potent compounds **10**, **11** and **15** were further evaluated in terms of cellular potency and selectivity over 11β-HSD2.

Cellular potency was assessed using Human Embryonic Kidney 293 (HEK293) cells stably transfected with the 11β-HSD1 gene. Results for compounds **11** and **15** were in line with those derived from the microsomal assay (cellular IC_{50} = 2 and 208 nM, respectively). Compound **10** showed in cells an IC_{50} of 82 nM.

Selectivity over 11β-HSD2 was also assessed in a cell-based assay using HEK293 stably transfected with the 11β-HSD2 gene. Regretfully, none of the tested compounds improved the selectivity of **7**, since they presented moderate to high inhibition of the isoenzyme at 10 and 1 μM concentration.

Since compound **11** was the most promising inhibitor in terms of potency against the target enzyme, we envisage the preparation of few biaryl analogs in order to explore the SAR of these compounds. To this end, the pyridinyl-containing polycyclic *N*-acylpyrrolidine structure was kept unchanged, and the aromatic group was varied. Doing so we synthesized the 3-thienyl and 1*H*-4-pirazolyl analogs, **17** and **18**, using the Suzuki-Miyaura cross-coupling as previously applied for the preparation of compound **11** (Scheme 1). These new compounds were tested for 11β-HSD1 inhibitory activity both in HLM and HEK cells, being the 3-thiophenyl derivative one order of magnitude more potent than the 1*H*-4-pirazolyl analog (cellular IC_{50} = 28 *vs* 344 nM, respectively).

Diminished activity *vs* the murine enzyme was not desirable since the mouse was our most accessible *in vivo* animal model to further study these inhibitors. Thus, these biaryl inhibitors were assayed for their mouse 11β-HSD1 inhibitory activity in murine liver microsomes (MLM). Surprisingly, substituent effects on the inhibitory activity of the murine 11β-HSD1 were more pronounced than on the human enzyme. The promising phenol-containing derivative, **11**, displayed almost no 11β-HSD1 inhibition with an IC_{50} in the high micromolar range (77.75 μM). By contrast, compound **18** that had displayed a modest submicromolar IC_{50} in the human enzyme was the most potent inhibitor against the murine 11β-HSD1 (IC_{50} = 84 nM), while the 3-thienyl derivative, **17**, presented a potency in between the other two biaryl analogs (IC_{50} = 774 nM).

Finally, their metabolic stability was also measured using both human and mouse liver microsomes. Not surprisingly, the three compounds were more stable in HLM than in MLM. Compared with the microsomal stability of our earlier hit compound **7** (13%

remaining compound after 30-min incubation in HLM), the new biaryl derivatives were far more stable, presenting good to excellent stabilities (77, 93 and 100% for **11**, **18** and **17**, respectively).

Cp	hHSD1 IC_{50} (nM)	HEK hHSD1 IC_{50} (nM)[c]	HEK hHSD2 % inh at 10 and 1 μM[c]	mHSD1 IC_{50} (nM)	HLM % parent[d]	MLM % parent[d]
7	45	ND	86% 71%	ND	13%	ND
10	ND	82	94% 88%	ND	ND	ND
11	14	2	96% 92%	77750	77%	47%
15	200	208	81% 64%	ND	ND	ND
17	39	28	96% 92%	774	100%	37%
18	333	344	91% 83%	84	93%	23%

Table 3. *In vitro* biological profiling of the new 11β-HSD1 inhibitors. [a,b]

[a] See Experimental section for further details. [b] Percentage inhibition was determined relative to a no inhibitor control. [c] HEK293 cells stably transfected with the full-length gene coding for human either 11β-HSD1 or 11β-HSD2 were used. [d] The microsomal stability of each compound was determined using either human or mouse liver microsomes. ND, not determined.

6. Conclusions

We have reported the rational design, synthesis and pharmacological evaluation of novel 11β-HSD1 inhibitors featuring a polycyclic *N*-acylpyrrolidine previously described by our group. The designed compounds inspired in reported inhibitors crystalized in complex with the enzyme delivered potent compounds against the human

11β-HSD1. Particularly interesting were the biaryl derivatives, that were further characterized, with the phenol-containing analog, **11**, being the most active compound in the human enzyme with a low nanomolar IC_{50}, despite not corresponding with a potent murine activity. The polarity of the compounds conferred them a higher microsomal stability in HLM, one parameter aimed to be improved in our early hit compound **7**. Unfortunately, the additional substituents introduced to establish potential interactions and to provide selectivity over 11β-HSD2 were not successful, presenting all the compounds undesirable high inhibition at micromolar concentrations. This selectivity issue should be further addressed before moving forward to *in vivo* efficacy studies.

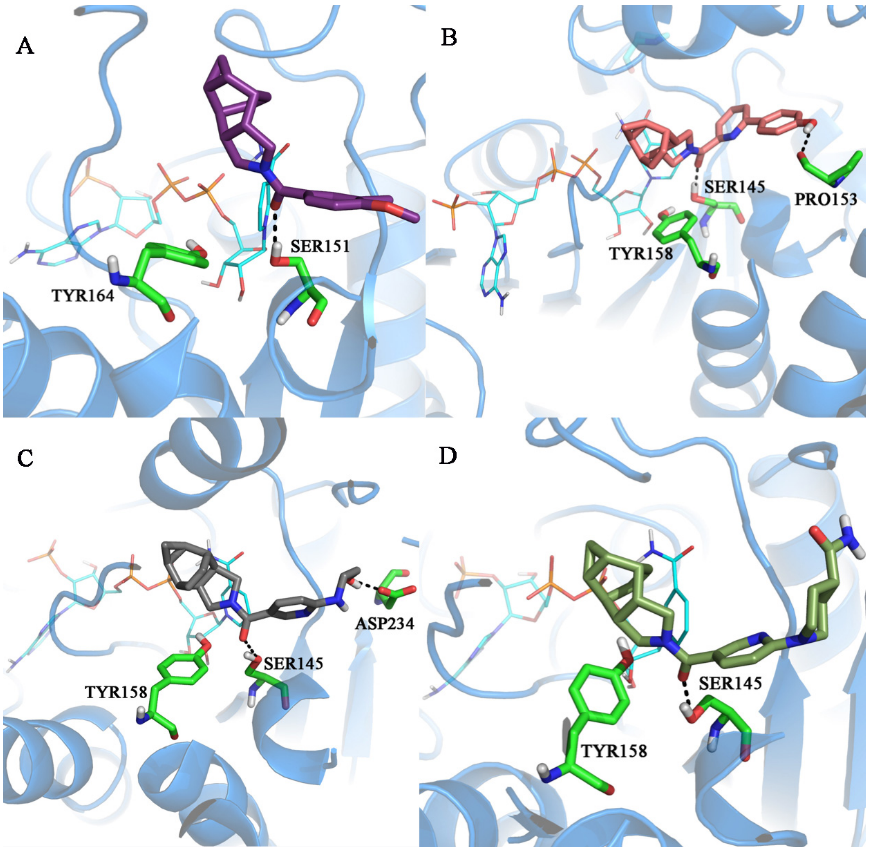

Figure 4. Representative snapshot of the binding mode of compounds 10 (A), 11 (B), 12 (C), and 13 (D) to the human 11β-HSD1 enzyme as determined from the analysis of the MD simulations. The protein backbone is shown as blue carton, the NADP cofactor, residues Tyr183 and Ser170, and the ligands are shown as atom-coloured sticks. The hydrogen bond between the ligand and the hydroxyl group of Ser170 is shown as a

dashed line. (For interpretation of the references to colour in this figure legend, the reader is referred to the web version of this article.)

7. Experimental section

7.1. Computational methods

For the comparative analysis of this work we have used 41 compounds, 3 of them taken of the X-ray structures in the pdb.org website and the remaining 38 from the literature.[20,22,23,24]

We adopted the same distinction between training and test sets of compounds adopted in the reference works taken from the literature.[17,28,29] Finally, since a correct molecular alignment is of utmost importance for the derivation of 3D-QSAR models.

Docking calculations were performed using Glide,[30] with the X-ray structures of the human enzymes with PDB ID: 3D5Q, 3CH6, 4C7J and 4HFR.[31] The geometry of each ligand was energy minimized and the centroids of the inhibitors cocrystalized in each of them were used to generate the docking cavity by selecting all the residues located within 20 Å from the ligand. 100 poses were generated for each ligand, and the best-scored poses fitting the expected arrangement within the binding pocket were chosen as starting structures for MD simulations.

For each ligand-protein complex three independent 50 ns MD simulations were run to check the consistency of the binding mode. To this end, the ligand-protein complex was located inside an octahedral box of TIP3P[32] water molecules and sodium ions were added to neutralize the system. The force field ff99SBildn[33,34] was used for the protein parameters, and RESP charges at the HF/6-31G (d) together with the gaff[35] force field were used to generate the ligand and the NADP parameters. All systems were refined through a three-step energy minimization procedure (entailing first hydrogen atoms, water molecules, and finally the entire system) and a six-step equilibration (heating the system from 0 K to 300 K in 6 steps of 20 ps, the first, 50 ps the next four, and 5 ns the last one). The resulting structures were used as initial structures for MD production runs.

7.2. Chemistry

7.2.1. General Methods.

Melting points were determined in open capillary tubes with a MFB 595010M Gallenkamp. 400 MHz ^{1}H/100.6 MHz ^{13}C NMR spectra were recorded on a Varian Mercury 400 spectrometer. The chemical shifts are reported in ppm (δ scale) relative to internal tetramethylsilane, and coupling constants are reported in Hertz (Hz). Assignments given for the NMR spectra of the new compounds have been carried out on the basis of COSY $^1H/^{13}C$ (gHSQC sequences) experiments. IR spectra were run on Perkin-Elmer Spectrum RX I spectrophotometer. Absorption values are expressed as wave-numbers (cm^{-1}); only significant absorption bands are given. High-resolution mass spectrometry (HRMS) analyses were performed with an LC/MSD TOF Agilent Technologies spectrometer. Column chromatography was performed either on silica gel 60 Å (35–70 mesh) or on aluminium oxide, neutral, 60 Å (50-200 μm, Brockmann I). Thin-layer chromatography was performed with aluminum-backed sheets with silica gel 60 F_{254} (Merck, ref 1.05554), and spots were visualized with UV light and 1% aqueous solution of $KMnO_4$. The elemental analysis of compound **15** was carried out in a Flash 1112 series Thermofinnigan elemental microanalyzator (A5) to determine C, H and N. HPLC/MS were determined with a HPLC Thermo Ultimate 3000SD (Thermo Scientific Dionex) coupled to a photodiode array detector DAD-3000 (Thermo Scientific Dionex) and mass spectrometer LTQ XL ESI-ion trap (Thermo Scientific) with Xcalibur v2.2 acquisition software (Thermo Scientific) (HPLC-PDA-MS). 5 μL of sample 0.5 mg/mL in methanol were injected, using a ZORBAX Extend-C18 3.5 um 2.1x50 mm column at 30 °C. The mobile phase was a mixture of A = formic acid 0.05% in water and B = formic acid 0.05% in acetonitrile with the method described as follows: flow 0.6 mL/min, 5%B-95%A 3 min, 100%B 4 min, 95%B-5%A 8 min. Purity is given as % of absorvance at 254 nm; UV-Vis spectra were collected every 0.2 s between 650 and 275 nm; data from mass spectra were analysed by electrospray ionization in positive mode every 0.3 s between 50 and 1000 Da.

*7.2.2. (4-azatetracyclo[5.3.2.0^{2,6}.0^{8,10}]dodec-11-en-4-yl)(3-chloro-4-methoxyphenyl) methanone, (**10**).*

To a solution of 4-azapentacyclo[5.3.2.0^{2,6}.0^{8,10}]dodec-11-ene hydrochloride (200 mg, 1.03 mmol) in EtOAc (10 mL) were added 3-chloro-4-methoxybenzoic acid (176 mg, 0.94 mmol), HOBt (190 mg, 1.41 mmol), EDC (218 g, 1.41 mmol) and triethylamine (0.6 mL, 4.14 mmol). The reaction mixture was stirred at room temperature overnight. To the resulting suspension was then added water (10 mL) and the phases were separated. The organic phase was washed with saturated aqueous $NaHCO_3$ solution (10 mL) and brine (10 mL), dried over anh. Na_2SO_4 and filtered. Evaporation in *vacuo* of the organics gave **10** as an orange semisolid (329 mg, quantitative yield). IR (ATR) ν:

615, 651, 692, 708, 754, 814, 835, 850, 891, 915, 946, 1018, 1059, 1095, 1142, 1183, 1232, 1256, 1294, 1349, 1387, 1418, 1501, 1560, 1599, 1617, 2868, 2925, 3002 cm^{-1}. ^{1}H-NMR (400 MHz, $CDCl_3$) δ: 0.10-0.18 (complex signal, 2 H, 9’-H_2), 0.82-0.98 (complex signal, 2 H, 8’-H and 10’-H), 2.54-2.64 (complex signal, 2 H, 2’-H and 6’-H), 2.74 (m, 1 H, 1’-H or 7’-H), 2.90 (m, 1 H, 7’-H or 1’-H), 3.12 (broad d, *J* = 11.2 Hz, 1 H, 5’-H_a or 3’-H_a), 3.45 (broad d, *J* = 11.2 Hz, 1 H, 3’-H_a or 5’-H_a), 3.54 (m, 1 H, 5’-H_b or 3’-H_b), 3.71 (m, 1 H, 3’-H_b or 5’-H_b), 3.91 (s, 3 H, OCH_3), 5.69 (m, 1 H, 11’-H or 12’-H), 5.85 (m, 1 H, 12’-H or 11’-H), 6.90 (d, *J* = 8.8 Hz, 1 H, 5-H), 7.31 (dd, *J* = 8.8 Hz, *J’* = 2.4 Hz, 1 H, 6-H), 7.45 (d, *J* = 2.4 Hz, 1 H, 2-H). ^{13}C-NMR (100.5 MHz, $CDCl_3$) δ: 3.9 (CH_2, C9’), 9.9 (CH, C8’ or C10’), 10.1 (CH, C10’ or C8’), 35.5 (CH, C1’ and C7’), 42.7 (CH, C2’ or C6’), 44.9 (CH, C6’ or C2’), 49.5 (CH_2, C3’ or C5’), 53.5 (CH_2, C5’ or C3’), 56.2 (CH_3, OCH_3), 111.3 (CH, C5), 122.1 (C, C3), 127.1 (CH, C6), 128.2 (CH, C11’ or C12’), 129.25 (CH, C12’ or C11’), 129.31 (CH, C2), 130.3 (C, C1), 155.9 (C, C4), 167.2 (C, CO). HPLC-PDA-MS: RT = 3.63 min; λ_{max} = 209 nm; purity 98.5% (254 nm). HRMS-ESI+ m/z $[M+H]^+$: Calcd for $[C_{19}H_{20}ClNO_2+H]^+$: 330.1255, found: 330.1251.

*7.2.3. (4-azatetracyclo[5.3.2.0^{2,6}.0^{8,10}]dodec-11-en-4-yl)[6-(4-hydroxyphenyl)pyridin-2-yl] methanone, (**11**).*

A mixture of **15** (300 mg, 0.87 mmol), 4-hydroxyphenylboronic acid (132 mg, 0.96 mmol), tetrakis(triphenylphosphine)palladium(0) (10 mg, 0.009 mmol) and K_2CO_3 (240 mg, 1.74 mmol) in 1,4-dioxane (3 mL) and H_2O (1.5 mL) was heated at 100 ºC for 2 h. EtOAc (10 mL) was added and then washed with H_2O (10 mL). The aqueous phase was extracted with further EtOAc (10 mL). The organics were dried over anh. Na_2SO_4, filtered and evaporated in *vacuo* to give a brownish solid (461 mg). Column chromatography (Hexane/Ethyl acetate mixture) gave **11** as a white solid (184 mg, 59% yield), mp 221-222 ºC. IR (ATR) ν: 630, 654, 711, 754, 822, 840, 915, 946, 992, 1039, 1085, 1103, 1173, 1230, 1276, 1297, 1346, 1380, 1400, 1429, 1460, 1516, 1558, 1586, 1604, 2930, 3002, 3126 cm^{-1}. ^{1}H-NMR (400 MHz, $CDCl_3$) δ: 0.10-0.20 (complex signal, 2 H, 9’-H_2), 0.84-0.98 (complex signal, 2 H, 8’-H and 10’-H), 2.58-2.74 (complex signal, 2 H, 2’-H and 6’-H), 2.77 (m, 1 H, 1’-H or 7’-H), 2.93 (m, 1 H, 7’-H or 1’-H), 3.47 (dd, *J* = 12.4 Hz, *J’* = 4.0 Hz, 1 H, 5’-H_a or 3’-H_a), 3.54 (dd, *J* = 13.2 Hz, *J’* = 4.0 Hz, 1 H, 3’-H_a or 5’-H_a), 3.83 (dd, *J* = 13.2 Hz, *J’* = 8.6 Hz, 1 H, 3’-H_b or 5’-H_b), 3.97 (dd, *J* = 12.4 Hz, *J’* = 8.6 Hz, 1 H, 5’-H_b or 3’-H_b), 5.73 (m, 1 H, 11’-H or 12’-H), 5.85 (m, 1 H, 12’-H or 11’-H), 6.94 [dm, *J* = 8.6 Hz, 2 H, 3’’(5’’)-H], 7.56 (dd, *J* = 8.0, *J’* = 0.8 Hz, 1 H, 5-H), 7.63 (dd, *J* = 8.4 Hz, *J’* = 0.8 Hz, 1 H, 3-H), 7.74 (dd, *J* = 8.4 Hz, *J’* = 8.0 Hz, 1 H, 4-H), 7.83 [dm, *J* = 8.6 Hz, 2 H, 2’’(6’’)-H], 7.91 (broad singlet, 1 H, OH). ^{13}C-NMR (100.5 MHz, $CDCl_3$) δ: 4.0 (CH_2, C9’), 10.0 (CH, C8’ or C10’), 10.2 (CH, C10’ or C8’), 35.6 (CH, C1’ and C7’), 42.4 (CH, C2’ or C6’), 45.1 (CH, C6’ or C2’), 50.6 (CH_2, C3’ or C5’), 53.2 (CH_2, C5’ or C3’), 115.9 [CH, C3’’(5’’)], 120.2 (CH, C3), 120.9 (CH, C5), 128.2 [CH, C2’’(6’’)], 128.6 (CH, C11’ or C12’), 129.1 (CH, C12’ or C11’), 130.5 (C, C1’’), 137.5 (CH, C4), 153.7 (C, C6), 155.7 (C, C2), 158.0 (C, C4’’), 166.4 (C, CO). HPLC-PDA-MS: RT = 3.28 min; λ_{max} = 215, 269, 287 nm; purity > 99.5% (254 nm). HRMS-ESI+ m/z $[M+H]^+$: Calcd for $[C_{23}H_{22}N_2O_2+H]^+$: 359.1754, found: 359.1750.

7.2.4 *(4-azatetracyclo[5.3.2.$0^{2,6}$.$0^{8,10}$]dodec-11-en-4-yl)[6-((2-hydroxyethyl)amino) pyridine-3-yl]methanone, (**12**).*

A mixture of **16** (100 mg, 0.33 mmol) and ethanolamine (0.36 mL, 6 mmol) was heated at 120 ºC for 24 h. Water (10 mL) and EtOAc (10 mL) were added and the phases were separated. The organic phase was dried over anh. Na_2SO_4, filtered and evaporated in *vacuo* to give an orange oil (65 mg). Crystalization from hot EtOAc gave **12** as a yellowish solid (59 mg, 55% yield), mp 87-88 ºC. IR (ATR) ν: 636, 716, 731, 767, 811, 832, 909, 943, 984, 1010, 1044, 1070, 1150, 1232, 1274, 1302, 1343, 1423, 1460, 1488, 1527, 1591, 1612, 2868, 2914, 3002, 3064, 3136, 3271 cm^{-1}. ^{1}H-NMR (400 MHz, $CDCl_3$) δ: 0.10-0.22 (complex signal, 2 H, 9’-H_2), 0.84-1.00 (complex signal, 2 H, 8’-H and 10’-H), 2.51-2.65 (complex signal, 2 H, 2’-H and 6’-H), 2.76 (m, 1 H, 1’-H or 7’-H), 2.88 (m, 1 H, 7’-H or 1’-H), 3.22 (m, 1 H, 5’-H_a or 3’-H_a), 3.34-3.53 (complex signal, 2 H, 3’-H_a or 5’-H_a), 3.48 (m, 1 H, 1’’-H_2), 3.61 (m, 1 H, 5’-H_b or 3’-H_b), 3.69 (m, 1 H, 3’-H_b or 5’-H_b), 3.77 (t, *J* = 4.6 Hz, 2 H, 2’’-H_2), 5.36 (m, 1 H, NH), 5.68 (m, 1 H, 11’-H or 12’-H), 5.82 (m, 1 H, 12’-H or 11’-H), 6.35 (d, *J* = 8.6 Hz, 1 H, 5-H), 7.51 (d, *J* = 8.6 Hz, 1 H, 4-H), 8.14 (s, 1 H, 2-H). ^{13}C-NMR (100.5 MHz, $CDCl_3$) δ: 3.9 (CH_2, C9’), 9.99 (CH, C8’ or C10’), 10.01 (CH, C10’ or C8’), 35.5 (CH, C1’ and C7’), 42.6 (CH, C2’ or C6’), 44.9 (CH, C6’ or C2’ and C1’’), 49.5 (CH_2, C3’ or C5’), 53.6 (CH_2, C5’ or C3’), 62.8 (CH_2, C2’’), 107.6 (CH, C5), 121.6 (C, C3), 128.2 (CH, C11’ or C12’), 129.2 (CH, C12’ or C11’), 137.2 (CH, C4), 147.1 (CH, C2), 159.3 (C, C6), 167.1 (C, CO). HPLC-PDA-MS: RT = 2.27 min; λ_{max} = 196, 258, 312 nm; purity 96.1% (254 nm). HRMS-ESI+ m/z $[M+H]^+$: Calcd for $[C_{19}H_{23}N_3O_2+H]^+$: 326.1863, found: 326.1867.

*7.2.5. 1-[[5-(4-azatetracyclo[5.3.2.0^{2,6}.0^{8,10}] dodec-11-en-4-yl)carbonyl]pyridin-2-yl] piperidine-4-carboxamide, (**13**).*

To a solution of **16** (100 mg, 0.33 mmol) and 4-piperidinecarboxamide (85 mg, 0.66 mmol) in DMF (0.5 mL) was added solid K_2CO_3 (82 mg, 0.59 mmol). The resulting suspension was stirred at 120 ºC for 48 hours. Water (5 mL) and DCM (5 mL) were added and the phases were separated. The aqueous phase was then extracted with further DCM (2 x 5 mL). The organics were dried over anh. Na_2SO_4, filtered and evaporated in *vacuo* to give **13** as a yellowish solid (110 mg, 85% yield), mp 162-163 ºC. IR (ATR) ν: 630, 692, 723, 773, 811, 845, 943, 982, 1010, 1028, 1041, 1095, 1129, 1178, 1219, 1238, 1312, 1351, 1367, 1408, 1431, 1501, 1540, 1584, 1599, 1687, 1736, 2919, 3152, 3307 cm^{-1}. ^{1}H-NMR (400 MHz, $CDCl_3$) δ: 0.10-0.20 (complex signal, 2 H, 9''-H_2), 0.84-1.00 (complex signal, 2 H, 8''-H and 10''-H), 1.72 [m, 2 H, 3(5)-H_{ax}], 1.92 [m, 2 H, 3(5)-H_{eq}], 2.39 (m, 1 H, 2''-H or 6''-H), 2.59 (m, 1 H, 6''-H or 2''-H), 2.75 (m, 1 H, 1''-H or 7''-H), 2.82-2.98 [complex signal, 3 H, 7''-H or 1''-H and 2(6)-H_{ax}], 3.24 (m, 1 H, 5''-H_a or 3''-H_a), 3.46 (m, 1 H, 5''-H_b or 3''-H_b), 3.56-3.80 (complex signal, 2 H, 3''-H_a or 5''-H_a and 3''-H_b or 5''-H_b), 4.35 [dm, *J* = 12.8 Hz, 2 H, 2(6)-H_{eq}], 5.55-6.00 (complex signal, 4 H, 11'-H, 12'-H and NH_2), 6.60 (d, *J* = 9.0 Hz, 1 H, 3'-H), 7.59 (d, *J* = 9.0 Hz, 1 H, 4'-H), 8.26 (s, 1 H, 6'-H). ^{13}C-NMR (100.5 MHz, $CDCl_3$) δ: 3.9 (CH_2, C9''), 10.1 (broad singlet, CH, C8'' and C10''), 28.2 [CH_2, C3(5)], 35.5 (CH, C1'' and C7''), 42.6 (CH, C2'' and C6''), 44.6 [CH_2, C2(6)], 45.0 (CH, C4), 49.6 (CH_2, C3'' or C5''), 53.6 (CH_2, C5'' or C3''), 105.8 (CH, C3'), 121.3 (C, C5'), 128.2 (CH, C11'' or C12''), 129.2 (CH, C12'' or C11''), 137.3 (CH, C4'), 147.5 (CH, C6'), 159.1 (C, C2'), 167.2 (C, CO), 176.9 (C, $CONH_2$). HPLC-PDA-MS: RT = 2.49 min; λ_{max} = 195, 268, 318 nm; purity 95.3% (254 nm). HRMS-ESI+ m/z $[M+H]^+$: Calcd for $[C_{23}H_{28}N_4O_2+H]^+$: 393.2285, found: 393.2285.

*7.2.6. (4-azatetracyclo[5.3.2.0^{2,6}.0^{8,10}]dodec-11-en-4-yl)(6-bromopyridin-2-yl) methanone, (**15**).*

To a solution of 4-azapentacyclo[5.3.2.0^{2,6}.0^{8,10}]dodec-11-ene hydrochloride (200 mg, 1.03 mmol) in EtOAc (10 mL) were added 6-bromopyridine-2-carboxylic acid (190 mg, 0.94 mmol), HOBt (190 mg, 1.41 mmol), EDC (218 g, 1.41 mmol) and triethylamine (0.6 mL, 4.14 mmol). The reaction mixture was stirred at room temperature overnight. To the resulting suspension was then added water (10 mL) and the phases were separated. The organic phase was washed with saturated aqueous $NaHCO_3$ solution (10 mL) and brine (10 mL), dried over anh. Na_2SO_4 and filtered. Evaporation in *vacuo* of the organics gave **15** as a white solid (235 mg, 73% yield), mp 185-186 ºC. IR (ATR) ν: 643, 659, 705, 734, 762, 814, 827, 850, 912, 935, 984, 1044, 1080, 1119, 1165, 1199, 1225, 1245, 1274, 1305, 1341, 1392, 1405, 1454, 1545, 1576, 1617, 2857, 2925, 3002, 3043, 3059 cm^{-1}. ^{1}H-NMR (400 MHz, $CDCl_3$) δ: 0.11-0.19 (complex signal, 2 H, 9'-H_2), 0.86-0.98 (complex signal, 2 H, 8'-H and 10'-H), 2.61 (m, 1 H, 2'-H or 6'-H), 2.68 (m, 1 H, 6'-H or 2'-H), 2.81 (m, 1 H, 1'-H or 7'-H), 2.91 (m, 1 H, 7'-H or 1'-H), 3.34 (dd, J = 12.2 Hz, J' = 5.2 Hz, 1 H, 5'-H_a or 3'-H_a), 3.42 (dd, J = 13.2 Hz, J' = 5.2 Hz, 1 H, 3'-H_a or 5'-H_a), 3.77 (dd, J = 13.2 Hz, J' = 9.2 Hz, 1 H, 3'-H_b or 5'-H_b), 3.92 (dd, J = 12.2 Hz, J' = 9.2 Hz, 1 H, 5'-H_b or 3'-H_b), 5.72 (m, 1 H, 11'-H or 12'-H), 5.82 (m, 1 H, 12'-H or 11'-H), 7.50 (dd, J = 8.0 Hz, J' = 1.0 Hz, 1 H, 5-H), 7.62 (dd, $J = J'$ = 8.0 Hz, 1 H, 4-H), 7.72 (dd, J = 8.0 Hz, J' = 1.0 Hz, 1 H, 3-H). ^{13}C-NMR (100.5 MHz, $CDCl_3$) δ: 4.1 (CH_2, C9'), 10.0 (CH, C8' or C10'), 10.2 (CH, C10' or C8'), 35.52 (CH, C1' or C7'), 35.54 (CH, C7' or C1'), 42.3 (CH, C2' or C6'), 45.2 (CH, C6' or C2'), 50.6 (CH_2, C3' or C5'), 52.8 (CH_2, C5' or C3'), 122.7 (CH, C3), 128.7 (CH, C11' or C12'), 129.0 (CH, C5), 129.1 (CH, C12' or C11'), 139.1 (CH, C4), 140.1 (C, C6), 155.2 (C, C2), 163.8 (C, CO). Anal. Calcd for $C_{17}H_{17}BrN_2O$: C, 59.14; H, 4.96; N, 8.11. Found: C, 59.31; H, 4.92; N, 7.87.

*7.2.7. (4-azatetracyclo[5.3.2.0^{2,6}.0^{8,10}]dodec-11-en-4-yl)[6-(thien-3-yl)pyridin-2-yl] methanone, (**17**).*

A mixture of **15** (230 mg, 0.67 mmol), 3-thiopheneboronic acid (93 mg, 0.73 mmol), tetrakis(triphenylphosphine)palladium(0) (8 mg, 0.007 mmol) and K_2CO_3 (185 mg, 1.34 mmol) in 1,4-dioxane (2.3 mL) and H_2O (1.2 mL) was heated at 100 ºC for 2 h. EtOAc (10 mL) was added and then washed with H_2O (10 mL). The aqueous phase was extracted with further EtOAc (10 mL). The organics were dried over anh. Na_2SO_4, filtered and evaporated in *vacuo* to give a brownish semisolid (238 mg). Column chromatography (Hexane/Ethyl acetate mixture) gave **17** as a brownish semisolid (184 mg, 79% yield), mp 48-49 ºC. IR (ATR) ν: 615, 646, 703, 716, 752, 791, 829, 845, 863, 915, 948, 987, 1036, 1095, 1178, 1235, 1274, 1343, 1418, 1431, 1460, 1566, 1581, 1617, 2000, 2051, 2175, 2325, 2868, 2919, 2997 cm^{-1}. ^{1}H-NMR (400 MHz, $CDCl_3$) δ: 0.11-0.20 (complex signal, 2 H, 9'-H_2), 0.86-1.00 (complex signal, 2 H, 8'-H and 10'-H), 2.59-2.74 (complex signal, 2 H, 2'-H and 6'-H), 2.79 (m, 1 H, 7'-H or 1'-H), 2.93 (m, 1 H, 1'-H or 7'-H), 3.43-3.57 (complex signal, 2 H, 3'-H_a and 5'-H_a), 3.81 (dd, J = 13.0 Hz, J' = 8.6 Hz, 1 H, 3'-H_b or 5'-H_b), 4.01 (dd, J = 11.8 Hz, J' = 8.2 Hz, 1 H, 5'-H_b or 3'-H_b), 5.74 (m, 1 H, 11'-H or 12'-H), 5.86 (m, 1 H, 12'-H or 11'-H), 7.40 (dd, J

= 5.2 Hz, *J'* = 3.2 Hz, 1 H, 4''-H), 7.61-7.68 (complex signal, 3 H, 5-H, 3-H and 5''-H), 7.77 (dd, *J* = 8.0 Hz, *J'* = 7.6 Hz, 1 H, 4-H), 7.89 (dd, *J* = 3.2 Hz, *J'* = 1.4 Hz, 1 H, 2''-H). ^{13}C-NMR (100.5 MHz, $CDCl_3$) δ: 4.0 (CH_2, C9'), 10.0 (CH, C8' or C10'), 10.2 (CH, C10' or C8'), 35.6 (CH, C1' or C7'), 35.7 (CH, C7' or C1'), 42.4 (CH, C2' or C6'), 45.3 (CH, C6' or C2'), 50.5 (CH_2, C3' or C5'), 53.0 (CH_2, C5' or C3'), 120.7 (CH, C3), 121.9 (CH, C5), 123.8 (CH, C2''), 126.2 (CH, C4''), 126.4 (CH, C5''), 128.6 (CH, C11' or C12'), 129.1 (CH, C12' or C11'), 137.5 (CH, C4), 141.8 (C, C3''), 151.5 (C, C6), 154.3 (C, C2), 165.5 (C, CO). HPLC-PDA-MS: RT = 3.78 min; λ_{max} = 218, 259 nm; purity 99.3%. HRMS-ESI+ m/z $[M+H]^+$: Calcd for $[C_{21}H_{20}N_2OS+H]^+$: 349.1369, found: 349.1374.

*7.2.8. (4-azatetracyclo[5.3.2.0^{2,6}.0^{8,10}]dodec-11-en-4-yl)[6-(1H-pyrazol-4-yl)pyridin-2-yl]methanone, (**18**).*

A mixture of **15** (285 mg, 0.83 mmol), 1*H*-pirazole-4-boronic acid (102 mg, 0.91 mmol), tetrakis(triphenylphosphine)palladium(0) (9 mg, 0.008 mmol) and K_2CO_3 (229 mg, 1.66 mmol) in 1,4-dioxane (2.8 mL) and H_2O (1.4 mL) was heated at 100 ºC for 2 h. EtOAc (10 mL) was added and then washed with H_2O (10 mL). The aqueous phase was extracted with further EtOAc (10 mL). The organics were dried over anh. Na_2SO_4, filtered and evaporated in *vacuo* to give a brown solid (300 mg). Column chromatography (Hexane/Ethyl acetate mixture) gave **18** as a brownish solid (78 mg, 28% yield), mp 164-165 ºC. IR (ATR) ν: 623, 646, 708, 729, 762, 809, 845, 868, 928, 974, 1026, 1041, 1085, 1145, 1176, 1219, 1238, 1276, 1307, 1336, 1367, 1377, 1413, 1431, 1460, 1558, 1581, 1917, 1940, 1987, 2935, 3162 cm^{-1}.^{1}H-NMR (400 MHz, $CDCl_3$) δ: 0.10-0.21 (complex signal, 2 H, 9'-H_2), 0.84-1.00 (complex signal, 2 H, 8'-H and 10'-H), 2.58-2.72 (complex signal, 2 H, 2'-H and 6'-H), 2.77 (m, 1 H, 1'-H or 7'-H), 2.92 (m, 1 H, 7'-H or 1'-H), 3.40-3.54 (complex signal, 2 H, 3'-H_a and 5'-H_a), 3.82 (dd, *J* = 13.0 Hz, *J'* = 8.6 Hz, 1 H, 3'-H_b or 5'-H_b), 3.94 (dd, *J* = 12.2 Hz, *J'* = 8.6 Hz, 1 H, 5'-H_b or 3'-H_b), 5.73 (m, 1 H, 11'-H or 12'-H), 5.84 (m, 1 H, 12'-H or 11'-H), 7.47 (d, *J* = 8.0 Hz, 1 H, 3-H), 7.54 (d, *J* = 7.4 Hz, 5-H), 7.72 (dd, *J* = 8.0 Hz, *J'* = 7.4 Hz, 1 H, 4-H), 8.09 (s, 2 H, 3''-H and 5''-H). ^{13}C-NMR (100.5 MHz, $CDCl_3$) δ: 4.0 (CH_2, C9'), 10.0 (CH, C8' or C10'), 10.2 (CH, C10' or C8'), 35.58 (CH, C1' or C7'), 35.62 (CH, C7' or C1'), 42.4 (CH, C2' or C6'), 45.2 (CH, C6' or C2'), 50.5 (CH_2, C3' or C5'), 53.0 (CH_2, C5' or C3'), 120.2 (CH, C3), 121.0 (CH, C5), 122.7 (C, C4''), 128.6 (CH, C11' or C12'), 129.1 (CH, C12' or C11'), 132.5 (broad singlet, CH, C3'' and C5''), 137.4 (CH, C4), 150.4 (C, C6), 154.3 (C, C2), 165.9 (C, CO). HPLC-PDA-MS:

RT = 2.90 min; λ_{max} = 196, 253, 292 nm; purity 99.4% (254 nm). HRMS-ESI+ m/z $[M+H]^+$: Calcd for $[C_{20}H_{20}N_4O+H]^+$: 333.1710, found: 333.1716.

7.3. 11β-HSD1 *in vitro* Enzyme Inhibition Assay

11β-HSD1 activity was determined in mixed sex, human or murine liver microsomes (Celsis In-vitro Technologies) by measuring the conversion of cortisone to cortisol by LC/MS. Percentage inhibition was determined relative to a no inhibitor control. 5 µg of human liver microsomes were pre-incubated at 37°C for 15 min with inhibitor and 1 mM NADPH in a final volume of 90 µL Krebs buffer. 10 µL of 2 µM cortisone was then added followed by incubation at 37°C for a further 30 min. The assay was terminated by rapid freezing on dry ice and subsequent extraction with acetonitrile on thawing. Samples dried down under nitrogen at 65ºC and solubilised in 100 µl 70:30 H_2O:ACN and removed to a 96-well V-bottomed plate for LC/MS analysis. Separation was carried out on a sunfire 150 x 2.1 mm, 3.5 µM column using a H_2O:ACN gradient profile. Typical retention times were 2.71 min for cortisol and 2.80 min for cortisone. The peak area was calculated and the concentration of each compound determined from the calibration curve.

7.4. Cellular 11β-HSD1 Enzyme Inhibition Assay

The cellular 11β-HSD1 enzyme inhibition assay was performed using HEK293 cells stably transfected with the human 11β-HSD1 gene. Cells were incubated with substrate (cortisone) and product (cortisol) was determined by LC/MS. Cells were plated at 2×10^4 cells/well in a 96-well poly-D-lysine coated tissue culture microplate (Greiner Bio-one) and incubated overnight at 37ºC in 5% CO_2 95% O_2. Compounds to be tested were solubilized in 100% DMSO at 10 mM and serially diluted in water and 10% DMSO to final concentration of 10 µM in 10% DMSO. 10 µL of each test dilution and 10 µL of 10% DMSO (for low and high control) were dispensed into the well of a new 96-well microplate (Greiner Bio-one). Medium was removed from the cell assay plate and 100 µL of DMEM solution (containing 1% penicillin, 1% streptomycin and 300 nM cortisone) added to each well. Cells were incubated for 2 h at 37 ºC in 5% CO_2 95% O_2. Following incubation, medium was removed from each well into an eppendorf containing 500 µL of ethyl acetate, mixed by vortex and incubated at rt for 5 min. A calibration curve of known concentrations of cortisol in assay medium was also set up and added to 500 µL of ethyl acetate, vortexed and incubated as above. The supernatant of each eppendorf was removed to a 96-deep-well plate and dried down under liquid nitrogen at 65ºC. Each well was solubilised in 100 µL 70:30 H_2O:ACN and removed to a 96-well V-bottomed plate for LC/MS analysis. Separation was carried out on a sunfire 150 x 2.1 mm, 3.5 µM column using a H_2O:ACN gradient profile. Typical retention times were 2.71 min for cortisol and 2.80 min for cortisone. The peak area was calculated and the concentration of each compound determined from the calibration curve.

7.5. Cellular 11β-HSD2 Enzyme Inhibition Assay

For measurement of inhibition of 11β-HSD2, HEK293 cells stably transfected with the full-length gene coding for human 11β-HSD2 were used. The protocol was the same as for the cellular 11β-HSD1 enzyme inhibition assay, only changing the substrate, this time cortisol, and the concentrations of the tested compounds, 10 and 1 µM.

7.6. Microsomal Stability Assay

The microsomal stability of each compound was determined using either human or mouse liver microsomes (Celsis In-vitro Technologies). Microsomes were thawed and diluted to a concentration of 2 mg/mL in 50 mM $NaPO_4$ buffer pH 7.4. Each compound was diluted in 4 mM NADPH (made in the phosphate buffer above) to a concentration of 10 µM. Two identical incubation plates were prepared to act as a 0 minute and a 30 minute time point assay. 30 µL of each compound dilution was added in duplicate to the wells of a U-bottom 96-well plate and warmed at 37ºC for approximately 5 min. Verapamil, lidocaine and propranolol at 10 µM concentration were utilised as reference compounds in this experiment. Microsomes were also pre-warmed at 37ºC before the addition of 30 µL to each well of the plate resulting in a final concentration of 1 mg/mL. The reaction was terminated at the appropriate time point (0 or 30 min) by addition of 60 µL of ice-cold 0.3 M trichloroacetic acid (TCA) per well. The plates were centrifuged for 10 min at 112 x g and the supernatant fraction transferred to a fresh U-bottom 96-well plate. Plates were sealed and frozen at -20ºC prior to MS analysis. LC-MS/MS was used to quantify the peak area response of each compound before and after incubation with human liver microsomes using MS tune settings established and validated for each compound. These peak intensity measurements were used to calculate the % remaining after incubation with human microsomes for each hit compound.

Acknowledgements

We thank financial support from *Ministerio de Economía y Competitividad* and FEDER (Project SAF2014-57094-R) and the *Generalitat de Catalunya* (grants 2014-SGR-00052 and 2014-SGR-1189) and the *Consorci de Serveis Universitaris de Catalunya* for computational resources. R. L. thanks the Spanish *Ministerio de Educación Cultura y Deporte* for a PhD Grant (FPU program). F. J. L. acknowledges the support from ICREA Academia. We thank ACCIÓ (*Generalitat de Catalunya*) and CIDQO 2012 SL for financial support (*Programa Nuclis*, RD14-1-0057, SAFNAD).

References

1. Arnaldi, G.; Angeli, A.; Atkinson, A. P.; Bertagna, X.; Cavagnini, F.; Chrousos, G. P.; Fava, G. A.; Findling, J. W.; Gaillard, R. C.; Grossman, A. B.; Kola, B.; Lacroix, A.; Mancini, T.; Mantero, F.; Newell-Price, J.; Nieman, L. K.; Sonino, N.; Vance, M. L.; Giustina, A.; Boscaro, M. *J. Clin. Endocrinol. Metab.* **2003**, *88,* 5593-5602.
2. Walker, B. R. *Eur. J. Endocrinol.* **2007**, *157*, 545-559.
3. Van Raalte, D. H.; Ouwens, D. M.; Diamant, M. *Eur. J. Clin. Invest.* **2009**, *39*, 81-93.
4. Swabb, D. F.; Bao, A. M.; Lucassen, P. J. *Ageing Res. Rev.* 2005, 4, 141-194.
5. Meaney, M. J.; O'Donnell, D.; Rowe, W. *Exp. Gerontol.* 1995, 30, 229-251.
6. Seckl, J. R.; Walker, B. R. *Endocrinology* **2001**, *142*, 1371-1376.
7. Morton, N. M.; Seckl, J. R. *Front. Horm. Res.* **2008**, *36*, 146-164.
8. Brown, R. W.; Chapman, K. E.; Edwards, C. R.; Seckl, J. R. *Endocrinology* **1993**, *132*, 2614–2621.
9. Kotelevtsev, Y.; Holmes, M. C.; Burdell, A.; Houston, P. M.; Schmoll, D.; Jamieson, P.; Best, R.; Brown, R.; Edwards, C. R. W.; Seckl, J. R.; Mullins, J. J. *Proc. Natl. Acad. Sci. U.S.A.* **1997**, *94*, 14924-14929.
10. Morton, N. M.; Holmes, M. C.; Fievet, C.; Staels, B.; Tailleux, A.; Mullins, J. J. *J. Biol. Chem.* **2001**, *276*, 41293-41300.

11. Yau, J. L. W.; Noble, J.; Kenyon, C. J.; Hibberd, C.; Kotelevstev, Y.; Mullins, J. J.; Seckl, J. R. *Proc. Natl. Acad. Sci. U.S.A.* **2001**, *98*, 4716-4721.
12. Scott, J. S.; Goldberg, F. W.; Turnbull, A. V. *J. Med. Chem.* **2014**, *57*, 4466–4486.
13. Feig, P. U.; Shah, S.; Hermanowski-Vosatka, A.; Plotkin, D.; Springer, M. S.; Donahue, S.; Thach, C.; Klein, E. J.; Lai, E.; Kaufman, K. D. *Diabetes, Obesity Metab*. **2011**, *13*, 498–504.
14. Marek, G. J.; Katz, D. A.; Meier, A.; Greco, N.; Zhang, W.; Liu, W.; Lenz, R. A. *Alzheimers Dement*. **2014**, *10*, (5 Suppl), S364-S373.
15. Webster, S. P.; McBride, A.; Binnie, M.; Sooy, K.; Seckl, J. R.; Andrew, R.; Pallin, T. D.; Hunt, H. J.; Perrior, T. R.; Ruffles, V. S.; Ketelbey, J. W.; Boyd, A.; Walker, B. R. *British J. Pharmacol*. **2017**, *174*, 396-408.
16. https://www.astellas.com/en/ir/library/medical.html. Accessed June 2017.
17. Leiva, R.; Griñan-Ferré, C.; Seira, C.; Valverde, E.; McBride, A.; Binnie, M.; Pérez, B.; Luque, F. J.; Pallàs, M.; Bidon-Chanal, A.; Webster, S. P.; Vázquez, S. *Eur. J. Med. Chem*. **2017**, *139*, 412-428.
18. Leiva, R.; McBride, A.; Binnie, M.; Webster, S. P.; Vázquez, S. *Molecules* **2018**, *23* (3), 1–14.
19. Ginex, T.; Muñoz-Muriedas, J.; Herrero, E.; Gibert, E.; Cozzini, P.; Luque, F. J. *J. Comput. Chem.* **2016**, *37* (13), 1147–1162.
20. Curutehet, C.; Bidon-Chanal, A.; Soteras, I.; Orozco, M.; Luque, F. J. *J. Phys. Chem. B* **2005**, *109* (8), 3565–3574.
21. PharmQSAR; Pharmacelera; Barcelona; **2015**
22. Wang, H.; Ruan, Z.; Li, J. J.; Simpkins, L. M.; Smirk, R. A.; Wu, S. C.; Hutchins, R. D.; Nirschl, D. S.; Kirk, K. V.; Cooper, C. B.; Sutton, J. C.; Ma, Z.; Golla, R.; Seethala, R.; Salyan, M. E. K.; Nayeem, A.; Krystek Jr., S. R.; Sheriff, S.; Camc, D. M.; Morin, P. E.; Carpenter, B.; Robl, J. A.; Zahler, R.; Gordon, D. A.; Hamann, L. G. *Bioorg. Med. Chem. Lett.* **2008**, *18*, 3168-3172.
23. Liang, J.; Naveed, H.; Jimenez-Morales, D.; Adamian, L., & Lin, M. *Biochim. Biophys. Acta* **2012**, *1818*, 927–941.
24. Tu, H.; Powers, J. P.; Liu, J.; Ursu, S.; Sudom, A.; Yan, X.; Xu, H.; Meininger, D.; DeGraffenreid, M.; He, X.; Jaen, J. C.; Sun, D.; Labelle, M.; Yamamoto, H.; Shan, B.; Walker, N. P. C.; Wang, Z. *Bioorg. Med. Chem.* **2008**, *16*, 8922-8931.

25. Goldberg, F. W.; Dossetter, A. G.; Scott, J. S.; Robb, G. R.; Boyd, S.; Groombridge, S. D.; Kemmitt, P. D.; Sjögren, T.; Moretin Gutiérrez, P.; deSchoolmeester, J.; Swales, J. G.; Turnbull, A. V.; Wild, M. J. *J. Med. Chem.* **2014**, *57*, 970-986.
26. Scott, J. S.; Bowker, S. S.; deSchoolmeester, J.; Gerhardt, S.; Hargreaves, D.; Kilgour, E.; Lloyd, A.; Mayers, R. M.; McCoull, W.; Newcombe, N. J.; Ogg, D.; Packer, M. J.; Rees, A.; Revill, J.; Schofield, P.; Selmi, N.; Swales, J. G.; Whittamore, P. R. O. *J. Med. Chem.* **2012**, 55, 5951-5964.
27. Rey-Carrizo, M.; Barniol-Xicota, M.; Ma, C.; Frigolé-Vivas, M.; Torres, E.; Naesens, L.; Llabrés, S.; Juárez-Jiménez, J.; Luque, F. J.; DeGrado, W. F.; Lamb, R. A.; Pinto, L. H.; Vázquez, S. *J. Med. Chem.* **2014**, *57*, 5738–5747.
28. Valverde, E.; Seira, C.; McBride, A.; Binnie, M.; Luque, F. J.; Webster, S. P.; Bidon-Chanal, A.; Vázquez, S. Searching for novel applications of the benzohomoadamantane scaffold in medicinal chemistry: Synthesis of novel 11β-HSD1 inhibitors. *Bioorganic Med. Chem*. **2015**, 23 (24), 7607–7617.
29. Leiva, R.; Seira, C.; McBride, A.; Binnie, M.; Luque, F. J.; Bidon-Chanal, A.; Webster, S. P.; Vázquez, S. Novel 11β-HSD1 inhibitors: C-1 versus C-2 substitution and effect of the introduction of an oxygen atom in the adamantane scaffold. Bioorganic *Med. Chem. Lett*. **2015**, 25 (19), 4250–4253.
30. Friesner, R. A.; Murphy, R. B.; Repasky, M. P.; Frye, L. L.; Greenwood, J. R.; Halgren, T. A.; Sanschagrin, P. C.; Mainz, D. T. *J. Med. Chem.* **2006**, *49*, 6177–6196.
31. Goldberg, F. W.; Leach, A. G.; Scott, J. S.; Snelson, W. L.; Groombridge, S. D.; Donald, C. S.; Bennett, S. N. L.; Bodin, C.; Gutierrez, P. M.; Gyte, A. C. *J. Med. Chem.* **2012**, *55*, 10652–10661.
32. Jorgensen, W. L.; Chandrasekhar, J.; Madura, J. D.; Impey, R. W.; Klein, M. L. *J. Chem. Phys.* **1983**, *79*, 926–935.
33. Hornak, V.; Abel, R.; Okur, A.; Strockbine, B.; Roitberg, A.; Simmerling, C. *Proteins* **2006**, *65*, 712–725.
34. Lindorff-Larsen, K.;Piana, S.; Palmo, K.; Maragakis, P.; Klepeis, J. L.; Dror, R. O.; Shaw, D. E. *Proteins* **2010**, *78*, 1950–1958.
35. Wang, J.; Wolf, R. M.; Caldwell, J. W.; Kollman, P. A.; Case, D. A. *J. Comput. Chem.* **2004**, *25*, 1157–1174.

3.2.1 Artículo 5: *Understanding the kinetics of ligand binding to globins with molecular dynamics simulations: the necessity of multiple state models*

Los cambios conformacionales de los residuos y los procesos de migración de la cavidad interna desempeñan un papel clave en la regulación de la cinética de la migración del ligando y los eventos de unión en globinas. Las simulaciones de dinámica molecular han demostrado su valor en el estudio de estos procesos en diferentes hemoglobinas, pero la derivación de los datos cinéticos exige el uso de técnicas más complejas como métodos mejorados de dinámica molecular de muestreo. Esta revisión discute las diferentes metodologías que se aplican actualmente para estudiar el proceso de migración del ligando en globins y resaltar aquellas especialmente desarrolladas para derivar datos cinéticos.

Drug Discovery Today: Technologies

Vol. 17, 2015

Editors-in-Chief
Kelvin Lam – Simplex Pharma Advisors, Inc., Boston, MA, USA
Henk Timmerman – Vrije Universiteit, The Netherlands

The role of binding kinetics in drug discovery

Understanding the kinetics of ligand binding to globins with molecular dynamics simulations: the necessity of multiple state models

Carolina Estarellas Martin, Constantí Seira Castan, F. Javier Luque Garriga, Axel Bidon-Chanal Badia*

Departament de Fisicoquímica and Institut de Biomedicina (IBUB), Facultat de Farmàcia, Universitat de Barcelona, Campus de l'Alimentació de Torribera, Santa Coloma de Gramenet, Spain

Residue conformational changes and internal cavity migration processes play a key role in regulating the kinetics of ligand migration and binding events in globins. Molecular dynamics simulations have demonstrated their value in the study of these processes in different haemoglobins, but derivation of kinetic data demands the use of more complex techniques like enhanced sampling molecular dynamics methods. This review discusses the different methodologies that are currently applied to study the ligand migration process in globins and highlight those specially developed to derive kinetic data.

Section editors:
Xavier Barril – Facultat de Farmacia, Universitat de Barcelona, Spain;
Helena Danielsson – Uppsala University, Uppsala, Sweden.

Introduction

Modulated by factors like the nature of residues surrounding the haem-binding cavity, the presence of several ligand docking sites and even tunnels, the intrinsic motions of the protein and the ligand reactivity towards the haem iron, the kinetics of ligand binding to globins usually involves complex reaction mechanisms encoding multiple protein-ligand complexes along the migration pathway rather than a two state model where only bound and unbound configurations are taken into account [1–4]. Except for the bond formation/breaking event that would require a quantum mechanical description of the atoms, molecular dynamics (MD) simulations can provide valuable information on the aforementioned factors as this computational tool allows tracking residue conformational changes, loop movements and helix displacements or even large scale structural changes [5]. Here we review MD-based techniques that provide valuable information to describe ligand-binding events in globins and enable to establish links between structure, kinetics, and function.

Globins

Since the first three dimensional structure of myoglobin (Mb) was characterised by X-ray crystallography in 1958 [6], more than 350 structures of Mb have been deposited in the Protein Data Bank (http://www.rcsb.org) with different haem-bound ligands like carbon monoxide, oxygen, cyanide, imidazole, among others. Although different techniques have been used to obtain these structures (X-ray crystallography, neutron diffraction or NMR), the differences between them are limited

---

Corresponding author: A. Bidon-Chanal Badia (abidonchanalb@ub.edu)

1740-6749/$ © 2015 Elsevier Ltd. All rights reserved. http://dx.doi.org/10.1016/j.ddtec.2015.09.002

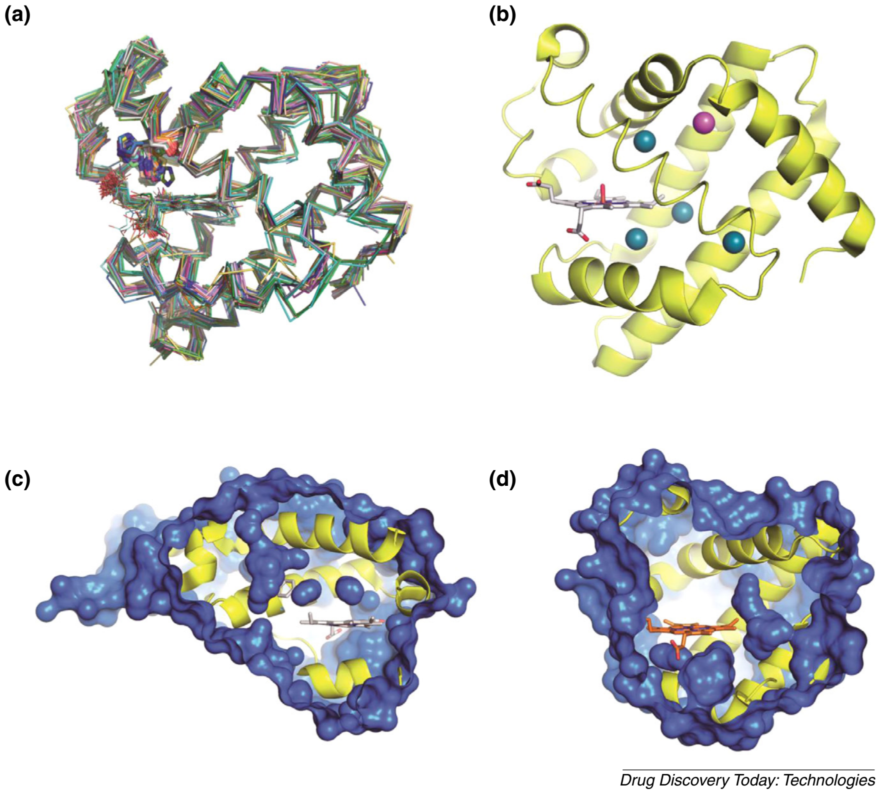

Figure 1. Factors that modulate ligand migration in different haemoglobins. **(a)** Superposition of the 350 structures of Mb found in the PDB showing the different conformational arrangements adopted by HisE7. **(b)** Xe binding cavities found in myoglobin under 7 bar pressure (pale green) and 30 bar (pale green plus the pink sphere). **(c)** Surface representation of trHbN from *M. tuberculosis* showing the long tunnel pathway blocked by PheE15. **(d)** Surface representation of *C. Lacteus* mini-Hb showing the continuous tunnel that connects the haem-binding site with the solvent.

to some side-chain orientations and none of the structures present large helix displacements with respect to others (Fig. 1). Overall, Mb displays a well-defined spatial helical arrangement, which follows the classic 3/3-globin fold, its 3D structure seems to be tightly shaped and small ligands of different nature are capable to reach the haem cavity without apparently perturbing its global structure. Nevertheless, this static picture hides a complex network of internal motions relevant for the biological role of oxygen storage and transport.

Interestingly, soaking experiments with xenon showed the existence of four internal cavities (called Xe1, Xe2, Xe3 and Xe4) in Mb, other than the distal pocket (DP), able to host Xe atoms inside (Fig. 1) [7]. In the crystal structure, the cavities looked disconnected between them due to the surrounding amino acid side-chains. However, recent time-resolved X-ray crystallography experiments have revealed that a photolysed ligand can migrate through the protein matrix and sample the different cavities [8–13]. Apparently, the connection between them turned out to be facilitated by the readjustment of side-chains due to thermal fluctuations that are seemingly hindered in the X-ray structures.

From the structural analysis, the only apparent clear connection between the solvent and the haem cavity seemed to be the so-called HisE7 gate, as it was described by Perutz 40 years ago with the analysis of the first Mb X-ray crystal structure [14]. Mutation of this residue clearly alters the kinetic parameters of ligand binding by modifying the kinetic constants for ligand association (k_{on}) and/or dissociation (k_{off}) [15,16]. Its replacement with a smaller residue like alanine or glycine increased the association rate constant, while introducing a much bulkier residue like tryptophan significantly reduced it. Even though the migration through inner cavities was found possible, the ligand entry/exit through a different pathway other than the HisE7 gate has received little experimental evidence.

What was learned with the study of Mb is partly transferable to other globins. Some of them also present gating residues, like the nonsymbiotic haemoglobin AHb1 from *Arabidopsis thaliana*, or the truncated haemoglobin N (trHbN) from *Mycobacterium tuberculosis*, while others present tunnel systems free of any blocking residues, like the *Cerebratulus lacteus* mini-haemoglobin (mini-Hb) (Fig. 1) [17–20]. The presence of small pockets where a small gaseous ligand can migrate once it is photolysed from the haem has been reported also for other globins like neuroglobin or cytoglobin (Cygb), as well as that thermal fluctuations modulate the accessibility of these cavities [21,22]. These topological features can be remarkably important to describe properly the ligand binding kinetics, which is also determined by the intrinsic reactivity of the ligand towards the haem iron.

All the aforementioned factors need to be taken into account to explain the different ligand migration and binding kinetics among globins. Here, we limit ourselves to the analysis of the ligand migration through the protein matrix, excluding the quantum mechanical analysis of the ligand–iron interaction [23]. Hence, attention will be paid to a variety of techniques that take advantage of MD simulations to examine the migration of ligands.

Ligand migration pathways

Two major types of strategies can be carried out to find ligand migration pathways in globins with the help of MD simulations and to estimate the energetics of ligand migration through the protein matrix. The main difference between them is that the ligand is present or not within the simulated system during the MD.

Ligand-independent techniques

The strategies enclosed in this category rely on the post-processing of MD trajectories of a protein without the ligand of interest in the simulated system. Assuming that the ligand interacts weakly with the protein, it can be generally accepted that the conformational space explored during an MD trajectory of the protein without the ligand does not differ from the configurational ensemble accessible to the ligand-bound protein.

Implicit Ligand Sampling (ILS)

Developed by Cohen and co-workers [24], the method computes the interaction free energy of a ligand with a protein as the Boltzmann-weighted average interaction energy of a series of selected snapshots from a MD trajectory of the protein. To this end, a grid of points around a region of interest is built and the interaction energy between the ligand (located at a given grid point) and the surrounding atoms is computed for the whole set of snapshots. To account for the multiple possible orientations of the ligand at each grid point, one can choose how many ligand orientations have to be taken into account. The final result is a three-dimensional map of the potential of mean force of placing a ligand in the points of the predefined grid. The method has been used to characterise diatomic ligand docking sites and migration pathways in Mb, *M. tuberculosis* trHbN and *Methanosarcina acetivorans* protoglobin, among others [25,26].

Ligand-dependent techniques

Locally Enhanced Sampling (LES)

First introduced by Elber and Karplus in 1990 to study CO migration inside myoglobin [27], it has been widely used to find ligand migration pathways in a variety of globins. The method is intended to compensate for the lack of sampling due to the limited length of MD simulations by adding simultaneously multiple ligand copies to the system. These copies move independently from each other exploring different regions of the simulated system at the same time, increasing the statistical sampling in comparison with a normal MD trajectory of the same length. Each copy of the ligand interacts with the protein with a scaling factor of 1/*N*, being *N* the number of copies. This way, the protein feels an average field generated by the multiple copies of the ligand. Only if all the copies occupy the same coordinates, the energy corresponds to that of the real system. By running only one LES MD simulation it is possible to detect ligand migration pathways, as well as to identify the most used ones. The strategy has been successfully used by different groups to explore the ligand migration pathways and to identify ligand-docking sites inside the protein matrix in a variety of globins, like Mb, Cygb, or different types of truncated haemoglobins, however, it does not provide a detailed energetic description of the pathways used by the ligand [27–29].

Multiple Steered Molecular Dynamics

An effective strategy that has been applied to the study of different truncated haemoglobins, like *M. tuberculosis* trHbN and trHbO, *Bacillus subtilis* trHbO or *C. lacteus* mini-Hb, to obtain the free energy profiles through pathways that drive the ligand from the solvent to the haem binding site is the Multiple Steered Molecular Dynamics method (MSMD) [30–33]. In this framework, the free energy profile for a ligand migration through a delimited pathway inside the protein matrix can be obtained by pushing or pulling the ligand to/from the haem binding site using steered MD. To this end, the ligand is placed in a local minimum along the selected pathway and a guiding force is applied to move the ligand along it. Repeating the process many times and obtaining the irreversible work of the process for each independent run, it is possible to obtain the free energy of the ligand migration process using the Jarzynski equality [34] with the exponential average of the work accumulated in each trajectory. A complete energetic profile for the ligand migration process through a determined pathway is obtained, making easy the detection of bottlenecks, docking sites, and energy barriers.

Finally, a mention should be made of PELE (Protein Energy Landscape Exploration) [35], a Monte Carlo based approach in which the ligand is pushed towards the binding site or outside of it concurrently allowing for the exploration of amino acids side chain's orientations. The method has been successfully applied to study the migration process of carbon monoxide in human haemoglobin and in the truncated haemoglobin-II from *M. tuberculosis* [36,37].

Extracting kinetic rate constants from MD

The growing processing power of supercomputers and the introduction, more recently, of Graphics Processing Units (GPUs) devoted to run molecular modelling codes, have lead to a dramatic increase in the time length of MD simulations from tens to hundreds or thousands of nanoseconds, nowadays usually achieving microsecond time scale simulation lengths and in some cases up to milliseconds. As a consequence, it is now possible to study fast and local motions in proteins with MD simulations, and even longer processes like the formation of protein ligand complexes or ligand migration through proteins. However, although longer MD trajectories are now accessible, a good sampling of all the possible ligand migration pathways using normal MD simulations is still computationally very expensive due to the need to collect a representative ensemble. Therefore, in the recent years a lot of work has been directed to the development of new techniques coupled to MD simulations to obtain thermodynamic and kinetic data of biological processes by combining the information obtained from multiple MD simulations or with non-equilibrium methods to enhance sampling during MD.

Multiple MD strategy

A possible strategy to obtain a scheme of the kinetic mechanism implicated in the ligand migration from/to the haem is to accumulate trajectories of ligand entry/exit from/to the protein matrix. This approach, for example, has been used to study the binding kinetics of different diatomic ligands to Mb with credited success. Ruscio *et al.* [38] initially applied this strategy to identify the ligand migration pathways between the solvent and the binding site. The study consisted in running MD simulations of Mb with CO molecules either located inside the binding cavity or in the solvent. They run a total of 68 trajectories for the wild-type protein and 9 for the V68F mutant, each of 90 ns and accumulating a total simulation time of 7 μs. By tracking the trajectory of CO through the protein matrix and to the solvent, the preferred entry/exit pathways could be identified. Furthermore, with this methodology they obtained the kinetic constants for ligand rebinding and exit with remarkable agreement to the experimental values reported before. The estimated rate constants for ligand rebinding and ligand exit were 0.3 $\mu\text{s}\,\text{M}^{-1}$ and 113 ns^{-1}, very close to the reported association rate constant of 0.5 $\mu\text{s}\,\text{M}^{-1}$ [39] and the binding pocket escape rate of 190 ns^{-1} obtained with time resolved crystallography measurements [10,11].

Anselmi and co-workers [40] applied a similar strategy to study the kinetics of ligand migration through Mb. In this case, they run 32 independent MD simulations of 25 ns each starting with the CO molecule in the DP as if it had been photolysed. They obtained a model for the kinetics mechanism of ligand migration through the internal cavities and provided kinetic constants for the cavity hoping events. In a subsequent work, Abramo *et al.* [41] obtained a full kinetic description of CO migration and binding to Mb with a similar strategy. Here, they combined MD simulations to follow the ligand migration through the protein with the Perturbed Matrix Method to obtain the binding–unbinding reaction kinetics.

In this context, an especially useful technique to study dynamical processes in which a system transits between discrete states through multiple pathways is Transition Network Analysis, also referred as Markov state modelling. Considering a ligand migration process as the result of multiple transitions between docking sites inside the protein matrix in its way towards the solvent, transition matrices may be constructed from the time evolution of ligand density distributions in the docking sites. The elements of the transition matrix provide the transition probability for any two states of the system within a certain amount of time. To this end, one needs to count the number of transitions between two states that occur within an arbitrary amount of time and construct transition count matrices. Finally, time constants associated with population decays for the docking sites can be obtained by adjusting the population decay profiles to exponential decay functions.

Meuwly and co-workers [42] have applied this method to study the ligand migration process in trHbN. Thus, they run 24 independent molecular dynamics simulations of the oxy form of trHbN with free NO inside the protein matrix. The ligand was placed in the distal pocket or in one of the five xenon-binding site pockets and 4 replicates were run for each system. A time-resolved connectivity network between the ligand docking sites and population decay time constants were obtained in reasonably good agreement with experimental measurements.

Enhanced sampling techniques

A widely used approach to obtain good sampling of transition events consists in introducing a bias in the MD simulation to enhance the sampling of the conformational space. For example, in metadynamics energy penalties in the form of positive Gaussians are added to the energy landscape of the system to force exploration of unexplored regions and prevent the system to go back to the already sampled ones [43]. Inspired in metadynamics, a different approach was introduced with the Temperature Accelerated Molecular Dynamics (TAMD), where enhanced sampling is achieved by introducing an artificial high temperature for a system of selected collective variables for which extra sampling is needed [44]. Applications of this method have demonstrated its validity to obtain kinetic information of ligand migration in globin systems with calculated values for the rate constants in the same order as the experimentally measured when coupled to Markovian models.

Table 1. Technologies comparison

	ILS	LES MD	MSMD	Multiple MD	TAMD
Description	Grid based free energy computation method to detect pathways	Pathway detection with multiple non-interacting copies MD	Non equilibrium free energy computation of the ligand migration process along a reaction coordinate	Pathway detection through multiple MD simulations of the ligand-protein system	Enhanced sampling MD pathway detection
Advantage	Fast and computationally cheap	Low cost inclusion of the ligand in the simulated system	Full energetic description of ligand migration along a pathway	Equilibrium method that provides direct information on the ligand migration process	Efficient sampling of migration pathways
Limitation	Ligand induced changes are not taken into account	Biased energetic description of the system	Computationally expensive	Computationally expensive Limited sampling	No direct calculation of free energy

Recently, Yu *et al.* [45] provided a full kinetic picture of CO migration out of, inside, and into Mb by reconstructing the kinetic network between docking sites and to the solvent from independent restrained MD simulations and a particular implementation of the Transition-Path Theory. Here, 30 independent TAMD simulations were used to explore the ligand-accessible regions inside Mb and all escape pathways. Selecting a discrete number of CO positions from these simulations, restrained MD trajectories were generated to obtain the mean force for a CO molecule at each preselected point and from that, the global free energy surface was reconstructed as an expansion in Gaussian radial basis functions. Minimum Free-Energy Pathways were derived with the zero-temperature string method and discrete points along these pathways, following a Voronoi tessellation scheme [46], were selected to run Markovian milestoning simulations. With this new recently introduced methodology, the authors obtained kinetic rate constants that were in near-quantitative agreement with those derived from geminate recombination experiments. Furthermore, ligand escape from the protein matrix was determined to occur mainly through the HisE7 gate, thus reconciling simulations with experiments.

Conclusions

Advances in experimental techniques like time resolved X-ray crystallography or laser flash-photolysis and also in computational methods have evidenced the complex internal cavity migration systems in different types of haemoglobins, demonstrating that the migration process is complex and its full understanding requires a very accurate description of all the intermediate states and the use of multiple state models. Different pathway detection methods, summarised in Table 1, have been developed that take advantage of the increased processing power of supercomputers and GPUs, facilitating the task of identification and energetic description of possible ligand migration pathways. Remarkable agreement with experimental findings have been achieved with respect to the identification of docking sites inside the protein matrix or identification of key controlling residues in the pathway. However, one of the major difficulties of these studies has been the derivation of kinetic data, as it requires a detailed exploration of all the possible state transitions within a ligand migration pathway. With recent advances in enhanced sampling MD methods coupled to Markovian state modelling techniques in different formulations, time constants as well as kinetic rate constants have been obtained with close agreement to experimentally measured values, demonstrating the usefulness of Markovian descriptions to rationalise molecular events with random transitions between states. The lessons learned from the study of ligand migration and binding to globins can be perfectly transferred to more complex systems like the formation of drug-protein complexes, where the existence of long-lived metastable states is needed to describe the kinetics of the overall binding process [47].

Conflict of interest

The authors have no conflict of interest to declare.

Acknowledgements

Authors thank financial support from Ministerio de Economía y Competitividad (SAF2014-57094-R) and the Generalitat de Catalunya (2014-SGR-1189). Carolina Estarellas thanks the Spanish Ministerio de Ecomonía y Competitivdad for the postdoctoral fellowship (FPD-2013-15572). F. Javier Luque acknowledges support from ICREA Academia.

References

[1] Nelson DL, Cox MM, editors. Lehninger principles of biochemistry. sixth edition, W.H. Freeman; 2012.
[2] Vinogradov SN, Hoogewijs D, Bailly X, Arredondo-Peter R, Gough J, Dewilde S, et al. A phylogenomic profile of globins. BMC Evol Biol 2006;6:31.
[3] Abbruzzetti S, Spyrakis F, Bidon-Chanal A, Luque FJ, Viapiani C. Ligand migration through hemeprotein cavities: insights from laser flash photolysis and molecular dynamics simulations. Phys Chem Chem Phys 2013;15:10686–701.

[4] Bocahut A, Bernad S, Sebban P, Sacquin-Mora S. Frontier residues lining globin internal cavities present specific mechanical properties. J Am Chem Soc 2011;133:8753–61.

[5] Spyrakis F, Bidon-Chanal A, Barril X, Luque FJ. Protein flexibility and ligand recognition: challenges for molecular modeling. Curr Top Med Chem 2011;11:192–210.

[6] Kendrew JC, Bodo G, Dintzis HM, Parrish RG, Wyckoff H. A three-dimensional model of the myoglobin molecule obtained by X-ray analysis. Nature 1958;181:662–6.

[7] Tilton RF, Kuntz Jr ID, Petsko GA. Cavities in proteins: structure of a metmyoglobin xenon complex solved to 1.9 Å,. Biochemistry 1984;23:2849–57.

[8] Srajer V. Photolysis of the carbon monoxide complex of myoglobin: nanosecond time-resolved crystallography. Science 1996;274:1726–9.

[9] Ostermann A, et al. Ligand binding and conformational motions in myoglobin. Nature 2000;404:205–8.

[10] Schotte F, Lim M, Jackson TA, Smirnov AV, Soman J, Olson JS, et al. Watching a protein as it functions with 150-ps time-resolved X-ray crystallography. Science 2003;300:1944–7.

[11] Schotte F, Soman J, Olson JS, Wulff M, Anfinrud PA. Picosecond time-resolved X-ray crystallography: probing protein function in real time. Struct Biol 2004;147:235–46.

[12] Hummer G, Schotte F, Anfinrud PA. Unveiling functional protein motions with picosecond X-ray crystallography and molecular dynamics simulations. Proc Natl Acad Sci USA 2004;101:15330–34.

[13] Bourgeois D, Vallone B, Arcovito A, Sciara G, Schotte F, Anfinrud PA, et al. Extended subnanosecond structural dynamics of myoglobin revealed by Laue crystallography. Proc Natl Acad Sci USA 2006;103:4924–9.

[14] Perutz MF, Mathews FS. An X-ray study of azide methaemoglobin. J Mol Biol 1966;132:343–68.

[15] Tian WD, Sage JT, Champion PM. Investigations of ligand association and dissociation rates in the open and closed states of myoglobin. JMol Biol 1993;233:155–66.

[16] Olson JS, Soman J, Philips GN. Ligand pathways in myoglobin: a review of Trp cavity mutations. IUBMB Life 2007;59:552–62.

[17] Spyrakis F, Faggiano S, Abruzzetti S, Dominici P, Cacciatori E, Astegno A, et al. Histidine E7 dynamics modulates ligand exchange between distal pocket and solvent in AHb1 from *Arabidopsis thaliana*. J Phys Chem B 2011;115:4138–46.

[18] Milani M, Pesce A, Ouellet Y, Ascenzi P, Guertin M, Bolognesi M. Mycobacterium tuberculosis hemoglobin N displays a protein tunnel suited for O_2 diffusion to the heme. EMBO J 2001;20:3902–9.

[19] Oliveira A, Pesce A, Yannick Ouellet P, Ascenzi M, Guertin M, Bolognesi. Role of PheE15 gate in ligand entry and nitric oxide detoxification function of *Mycobacterium tuberculosis* truncated hemoglobin N. PLoS One 2012;7:e49291.

[20] Pesce A, Nardini M, Dewilde S, Capece L, Martí MA, Congia S, et al. Ligand migration in the apolar tunnel of *Cerebratulus lacteus* mini-hemoglobin. J Biol Chem 2011;286:5347–58.

[21] Gabba M, Abruzzetti S, Spyrakis F, Forti F, Bruno S, Mozzarelli A, et al. CO rebinding kinetics and molecular dynamics simulations highlight dynamic regulation of internal cavities in human cytoglobin. PloS One 2013;8:e49770.

[22] Abbruzzetti S, Faggiano S, Bruno S, Spyrakis F, Mozzarelli A, Dewilde S, et al. Ligand migration through the internal hydrophobic cavities in human neuroglobin. Proc Natl Acad Sci USA 2009;106:18984–89.

[23] Capece L, Boechi L, Perissinotti LL, Arroyo-Mañez P, Bikiel DE, et al. Small ligand–globin interactions: reviewing lessons derived from computer simulation. BBA-Proteins Proteom 2013;1834:1722–38.

[24] Cohen J, Olsen KW, Schulten K. Finding gas migration pathways in proteins using implicit ligand sampling. Meth Enzym 2008;437:439–57.

[25] Lama A, Pawaria S, Bidon-Chanal A, Anand A, Gelpí JL, Arya S, et al. Role of pre-A motif in nitric oxide scavenging by truncated hemoglobin, HbN, of *Mycobacterium tuberculosis*. J Biol Chem 2009;284:14457–68.

[26] Forti F, et al. Ligand migration in *Methanosarcina acetivorans* protoglobin: effects of ligand binding and dimeric assembly. J Phys Chem B 2011;115:13771–80.

[27] Elber R, Karplus M. Enhanced sampling in moleculardynamics – use of the time-dependent hartree approximation for a simulation of carbon-monoxide diffusion through myoglobin. J Am Chem Soc 1990;112: 9161–75.

[28] Orlowski S, Nowak W. Locally enhanced sampling molecular dynamics study of the dioxygen transport in human cytoglobin. J Mol Model 2007;13:715–23.

[29] Heroux MS, Mohan AD, Olsen KW. Ligand migration in the truncated hemoglobin of *Mycobacterium tuberculosis*. IUBMB Life 2011;63:214–20.

[30] Bidon-Chanal A, Martí MA, Crespo A, Milani M, Orozco M, Bolognesi M, et al. Ligand-induced dynamical regulation of NO conversion in *Mycobacterium tuberculosis* truncated hemoglobin-N. Proteins Struct Funct Bioinform 2006;64:457–64.

[31] Boechi L, Martí MA, Milani M, Bolognesi M, Luque FJ, Estrin DA. Structural determinants of ligand migration in *Mycobacterium tuberculosis* truncated hemoglobin O. Proteins Struct Funct Bioinform 2008;73:372–9.

[32] Boechi L, Arroyo Mañez P, Luque FJ, Marti MA, Estrin DA. Unraveling the molecular basis for ligand binding in truncated hemoglobins: the trHbO *Bacillus subtilis* case. Proteins Struct Funct Bioinform 2010;78:962–70.

[33] Marti MA. Two distinct heme distal site states define *Cerebratulus lacteus* mini-hemoglobin oxygen affinity. Proteins Struct Funct Bioinform 2006;62:641–8.

[34] Jarzynski C. Nonequilibrium equality for free energy differences. Phys Rev Lett 1997;78:2690.

[35] Borrelli KW, Vitalis A, Alcantara R, Guallar V. PELE: Protein Energy Landscape Exploration. A novel Monte Carlo based technique. J Chem Theory Comput 2005;1:1304–11.

[36] Guallar V, Lu C, Borrelli K, Egwa T, Yeh SR. Ligand migration in the truncated hemoglobin-II from *Mycobacterium tuberculosis*. The role of G8 tryptophan. J Biol Chem 2009;284:3106–16.

[37] Lucas F, Guallar V. An atomistic view on human hemoglobin carbon monoxide migration. Biophys J 2012;102:887–96.

[38] Ruscio JZ. Atomic level computational identification of ligand migration pathways between solvent and binding site in myoglobin. Proc Natl Acad Sci USA 2008;105:9204–9.

[39] Olson JS, Phillips Jr GN. Kinetic pathways and barriers for ligand binding to myoglobin. J Biol Chem 1996;271:17593–96.

[40] Anselmi M, Di Nola A, Amadei A. The kinetics of ligand migration in crystallized myoglobin as revealed by molecular dynamics simulations. Biophys J 2008;94:4277–81.

[41] Abramo M, Di Nola A, Amadei A. Kinetics of carbon monoxide migration and binding in solvated myoglobin as revealed by molecular dynamics simulations and quantum mechanical calculations. J Phys Chem B 2009;115:2436–46.

[42] Sabyashachi M, Meuwly M. Quantitative analysis of ligand migration from transition networks. Biophys J 2010;99:3969–78.

[43] Laio A, Parrinello M. Escaping free-energy minima. Proc Natl Acad Sci USA 2002;99:12562–66.

[44] Maragliano L, Vanden-Eijnden E. A temperature-accelerated method for sampling free energy and determining reaction pathways in rare events simulations. Chem Phys Lett 2006;426:168–75.

[45] Yu T, Lapelosa M, Vanden-Ejiden E, Abrams CF. Full kinetics of CO entry, internal diffusion, and exit in myoglobin from Transition-Path Theory simulations. J Am Chem Soc 2015;137:3041–50.

[46] Vanden-Eijnden E, Venturoli M. Markovian milestoning with Voronoi tessellation. J Chem Phys 2009;130:194101–113.

[47] Plattner N, Noe F. Protein conformational plasticity and complex ligand-binding kinetics explored by atomistic simulations and Markov models. Nat Commun 2015;6:7653.

3.2.2 **Artículo 6**: *Influence of Temperature on the Topological Features of Inner Cavities and Ligand Migration in Cytoglobin*

La citoglobina (Cygb) es el cuarto miembro de la familia de las globinas descubierto en humanos en diferentes tejidos. La unión de ligandos exógenos desencadena un cambio sustancial tanto en la dinámica de proteínas como en las cavidades internas, lo que concuerda con el patrón cinético complejo observado en los ensayos de recombinación de CO de Cygb bis-histidil hexacoordinado. En este trabajo, el interés se centra en la dependencia de la temperatura de las características topológicas de las cavidades internas de Cygb. Específicamente, nuestro objetivo es determinar el impacto de la temperatura en la dinámica de proteínas y el número y la naturaleza de las cavidades internas en Cygb tanto humano como psicrófilo, considerando la proteína en el pez antártico *Chaenocephalus aceratus*. Los resultados obtenidos a partir de simulaciones dinámicas moleculares se complementan con datos derivados de datos de rayos X y experimentos de “flash photolysis”. Se presenta una discusión detallada sobre la diferente plasticidad de las cavidades internas en C. aceratus y Cygb humano, que ilustra la ocurrencia de alteraciones estructurales drásticas inducidas por la temperatura en las características topológicas de las cavidades internas. Finalmente, también se examina el impacto de estos cambios en las vías de egresión del ligando.

Influence of Temperature on the Topological Features of Inner Cavities and Ligand Migration in Cytoglobin

Constantí Seira[a], Martino Bolognesi[a], Stefania Abbruzzetti, Cristiano Viappiani[b], F. Javier Luque[a], Axel Bidon-Chanal[b]

[a] *Department of Nutrition, Food Science and Gastronomy, Faculty of Pharmacy and Food Science, Institute of Biomedicine (IBUB), Universitat de Barcelona, Av. Prat de la Riba 171, Santa Coloma de Gramenet E-08921, Spain*

[b] *Departament of Biosciences, University of Milan,. Via Festa del Perdono, 7, 20122 Milano MI, Italy*

[c] *Dipartamento di Scienze Matematiche,Fisiche e Informatiche,University of Parma, Parco Area delle Scienze, 7/A - 43124 Parma, Italy*

Abstract:

Cytoglobin (Cygb) is the fourth member of the globin family discovered in humans in different tissues. Binding of exogenous ligands triggers a substantial change in both protein dynamics and inner cavities, which agrees with the complex kinetic pattern observed in CO rebinding assays of bis-histidyl hexacoordinated Cygb. In this work our interest is focused on the temperature dependence of the topological features of inner cavities of Cygb. Specifically, our aim is to ascertain the impact of temperature on the protein dynamics and the number and nature of inner cavities in both human and psycrophilic Cygb, considering the protein in the Antarctic fish *Chaenocephalus aceratus.* The results obtained from molecular dynamic simulations will be complemented with data derived from X-ray data and flash photolysis experiments. A detailed discussion is presented about the different plasticity of inner cavities in *C. aceratus* and human Cygb, which illustrates the occurrence of drastic temperature-induced structural alterations in the topological features of inner pockets. Also, the impact of these changes on the ligand egression pathways is also examined. Finally, the *Chaenocephalus aceratus* model is collated to another of *Dissostichus mawsoni* to study their similarity.

Keywords:

Cytoglobin, flash photolysis, CO binding kinetics, cavity, MDpocket, molecular dynamic simulations, tryptophan, mutation, temperature dependence, cavity, tunnel, icefish, model

Introduction

Cytoglobin (Cygb) is the fourth member of the globin family discovered in humans a few years ago located in different tissues[1]. It is made of 190 amino acids, showing extensions of about 20 amino acids at both C- and N-termini with respect to standard globins. The crystal structure suggests that Cygb has a typical globin-fold, generally similar to that of hemoglobin (Hgb) and myoglobin (Mgb). The amino acid sequence of Cygb is well conserved among other members of the globin family and is approximately 25% identical to that of neuroglobin (Ngb)[2]. A dimeric structure was reported for Cygb with intermolecular disulphide bonds[3] between two cysteine residues (Cys38 and Cys83) and previous studies have also suggested that Cygb could form an intramolecular disulphide bond that would permit different configurations and be critical for the physiological functions of Cygb.

The localization of Cygb might be indicative of a significant role in oxygen homeostasis and ischemia-induced cell signalling in human retinas and optic nerves. Its expression increases in response to different stress conditions, including hypoxia, oxidative stress and fibrotic stimulation, it is strongly up-regulated by hypoxia, which suggests that its expression is induced by hypoxia and that it promotes cell survival. Recent studies suggest that Cygb participate in scavenging of reactive oxygen species (ROS) in neurons[4,5] providing oxygen to enzymes in fibroblasts. The specific kinetics of this hexacoordinate globin is indicative of its role, aside from oxygen transporter and nitric oxide dioxygenase activities, as a temporary oxygen reservoir, which might provide a minimal, but continuous supply of intracellular oxygen during ischemic and anoxic conditions. Cygb might also participate in collagen synthesis and suppression of oncogenic transformation.

Cygb was the first example in humans and other vertebrates, together with Ngb, of hexacoordination with a histidine residue at the sixth coordination position of the heme iron as an endogenous ligand in both ferric and ferrous forms. For hexacoordinated globins there is a regulated equilibrium between hexacordinated (6c) and pentacoordinated states (5c)[6]. In the absence of exogenous ligands, the sixth heme iron coordination site is occupied by the distal HisE7 residue in both ferric and ferrous forms. Binding of exogenous ligands is possible only through the displacement of the distal HisE7, a regulatory mechanism that has been hypothesized demands a substantial conformational change. Thus, fine-tuning of the 6c ⇆ 5c equilibrium provides a mechanism to modulate ligand affinity, since the more displaced the equilibrium to the 5c state the higher the ligand affinity. However, the factors that modulate the 6c ⇆ 5c equilibrium are still unknown.[7]

The crystal structure of bis-histidyl hexacoordinated Cygb shows an extended apolar cavity, which appears to be dissimilar from the topology of inner cavities found in other haemoglobins. The internal volume and the topological nature of inner cavities are largely dependent on the coordination state of Cygb. In particular, a substantial change in both protein dynamics and inner cavities is observed upon transition from the CO liganded[8] to the pentacoordinated and bis-histidyl hexacoordinated species. This agrees with the complex kinetic pattern derived from carbon monoxide rebinding assays, which indicates the implication of distinct reaction intermediates, reflecting rebinding from temporary docking sites, second order recombination, and formation (and dissociation) of a bis-histidyl heme hexacoordinated reaction intermediate.[8]

The aim of this study is to understand the differences in the modulation of Cygb behaviour and ligand affinity in fish adapted to low temperatures and human. Specifically, our aim is to ascertain the impact of temperature on the protein dynamics and the number and nature of inner cavities. To this end, we want to characterize the structural, dynamical and topological properties of human Cygb with that of the Antarctic fish *Chaenocephalus aceratus* using both experimental and theoretical strategies[9,10]. Molecular dynamic simulations will be used, in conjunction with X-ray data and flash photolysis experiments to discuss the impact of temperature on the ligand migration properties of these two proteins. Besides, a mutated model of the human Cygb will be also examined to explore the effect of specific mutation on the topological properties of inner cavities. Finally, a *C. Aceratus* model is compared with another one of *D. mawsoni* proportioned by professor M. Bolognesi.

Materials and methods

Protein Expression and Purification. D. mawsonii and *C.aceratus* Cygb were cloned from retina and brain tissues, respectively, and the recombinant proteins expressed and purified as wild type (dmCygb-wt and caCygb-wt), in the presence of His-tag (dmCygb and caCygb) and as mutants in the presence of His-tag (dmCygb* and caCygb*), where Cys residues were replaced by Ser (C38S/C160S double mutants).

Oxygen affinity. Oxygen binding curves of caCygb were investigated at 20°C in 100 mM phosphate buffer, 1 mM EDTA, 5 mM DTT, at pH 7.0. Oxygen partial pressures in the range 0-7 Torr were generated with an Environics 4000 gas mixer using cylinders of pure helium, and 0.187% and 1.19% oxygen mixtures. The humidified gas was bubbled directly into the protein solution contained in cuvette (0.4-cm pathlength) endowed with a reservoir. A minimal amount of an antifoam agent was added to avoid denaturation. Cygb as purified is an oxy form, with a negligible amount of met form. Once deoxygenated, Cygb was equilibrated to oxygen partial pressures between 0 and 148 Torr and analyzed as a linear combination of the fully deoxy and fully oxy reference spectra.

CO-rebinding kinetics. For the study of CO-rebinding kinetics, flash photolysis experiments were performed using a laser photolysis system (Edinburg Instruments LP920) with a frequency-doubled Q-switched Nd:YAG laser (Spectra Physics Quanta-ray, 532 nm). Experiments were carried out at 20°C. CO-bounded samples were prepared in sealed 4x10 mm quartz cuvettes containing 1ml of 100mM potassium phosphate buffer/1 mM EDTA, at pH 7.0. The buffer was equilibrated with mixtures of CO and N_2 gas at different ratios to obtain different CO concentrations (200 µM CO, 400 µM CO, 600 µM CO, 800 µM CO). This was done with a High-Tech system (Bronkhorst). Saturated sodium dithionite solution (10 µl) was added to the buffer to scavenge residual oxygen. Protein was injected in a minimum amount to an end concentration of approximately 5 µM. The CO-ligated form was verified by using UV/Vis spectroscopy. CO was dissociated from the CO-ligated caCygb by a short laser pulse (5-8 ns). The recombination of the photo-dissociated CO-ligand was followed at different time scales, ranging from 2000 ns (geminate recombination) to 100 ms (bimolecular rebinding) at 436 nm. Exponential decays, from the different timescales, were joined together by using Matlab, to give the complete ligand-rebinding curve. Further analysis was performed by using Origin software. The rate of geminate rebinding K_{gem} was determined by fitting a single exponential curve through the data, obtained by the first 2000 ns measurements after photo dissociation.

Stopped flow. These measurements were performed to determine $k_{on,His}$ and $k_{off,His}$. Stopped flow measurements were performed at 20°C in 100 mM degassed potassium phosphate buffer and 1mM EDTA at pH 7.0, by using a thermostatted stopped flow apparatus (Applied Photophysics, Salisburry, UK). Sodium dithionite was added to both the protein solution and the CO solutions to a final concentration of 10mM. Measurements were carried out during 2 seconds at 430 nm. 20 mM protein solution was mixed with different CO concentrations (25 µM CO, 50 µM CO, 100 µM CO, 200 µM CO, 400 µM CO). Analysis was performed by using Origin software.

Molecular simulations. The model of caCygb was obtained from a homology model built with the program SWIS MODEL using the crystal structure of carbonmonoxy humnan cytoglobin with PDB ID 3AG0. This structure was used also as the model of human Cygb (hCygb_c1). The mutated variant of human Cygb was generated by rotating Trp151 (hCygb_c2), and introducing the mutation Met-Ser that differentiates hCygb_c2 from hCygb_S30M. For five- and six-coordinated states, protonation of distal HisE7 and proximal HisF8 was chosen to be in the Nδ position. Ligand bound Cygb structures were generated by introducing CO (caCygb) and O_2 (hCygb_c1, hCygb_c2 and hCygb_S30M) atoms to the five-coordinated state followed by several ns equilibration runns. For ligand-bound states, distal HisE7 was protonated in the Nε atom.

All molecular dynamics simulations were performed with the AMBER14 package. Simulations were performed at 283, 298 and 313 K and 1-bar pressure using Berendsen thermostat and barostat. The proteins were simulated in the ligand bound form for 1.5 μs at each temperature. The Amber99 force field (ff99SBildn[11,12]) was used for all residues, whereas previously developed and thoroughly tested parameters were used for the heme.

Every complex was immersed in an octahedral box of TIP3P water molecules and sodium ions were added to neutralize the system[13]. A minimum distance of 12 Å between any atom of the protein and the box limits was used to define the size of the simulated system. The system was energy minimized following a three-step protocol. First, the hydrogen atoms of the protein were minimized. Second, the orientation of water molecules was optimized. Finally, a global minimization was run in which all the atoms were let free to move. At this point, the system was thermalized to 283.15, 298.15 and 313.15 K in 4 steps of 50 ps each from an initial temperature of 100 K. The last snapshot from the thermalization procedure was used as starting point for MD simulations using the NPT ensemble, a 2 fs time- step, periodic boundary conditions and keeping frozen all the bonds implicating hydrogen atoms using SHAKE.[14]

Frames were collected at 1-ps intervals, taking the last 250 ns of every MD, which were subsequently used to analyze the trajectories with the MDPocket program representing inner tunnels found with a frequency level of at least the 50%.

Results

Oxygen affinity. The analysis of the equilibrium yielded a P_{50} of around 0.6 Torr (insert of Figure 1), indicating a very high oxygen affinity, much higher than that of mammalian Hb (26 Torr), and slightly higher than that of Mb (1 Torr).[15] Such high affinity indicates that oxygen transport is functionally unlikely, because the basic requirement of a respiratory protein employed in oxygen supply would not be fulfilled. For comparison, the oxygen binding curve of Cygb was measured under the same conditions (data not shown), yielding a P_{50} of 0.43 Torr, consistent with that reported in the literature.[16] Both the oxygen binding curve of Cygb and *ca*Cygb are sygmoidal, possibly indicating a degree of cooperativity. The fitting with the Hill equation yielded a Hill coefficient of 1.5. Oxygen affinity (measured as P_{50}) and cooperativity were calculated from the linearised Hill plot of log S/(1-S) against log pO_2 at half saturation, where S is the fractional oxygen saturation. Hill plots identify the transition between binding states in cooperativity, and the binding behaviour is different for cooperative and non-cooperative systems. Furthermore, the Hill plot gives a direct numerical measure of the degree of cooperativity from its maximum slope, which is called the Hill coefficient (nHill). Binding of oxygen to tetrameric Hb is an example of positive cooperativity and in this case the value of nHill is between 1 and 3.5. nHill value is usually 1 for monomeric proteins e.g. Mb, that does not show cooperativity.[16] A value above 1, as in the case of *ca*Cygb, could be due to an experimental variability or to the presence of the cooperative dimeric form. Further analyses are necessary to confirm these data.

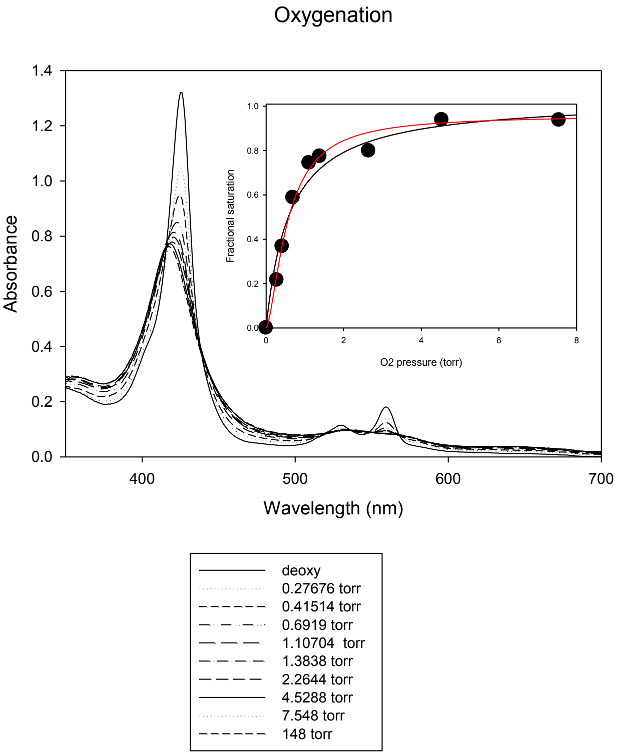

Figure 1. Oxygen binding to *ca*Cygb. Representative spectra collected at different oxygen partial pressures are reported. The inset shows the saturation fraction versus pO_2 (Torr): the fitting to a binding isotherm is in black. The fitting with a Hill equation with a Hill coefficient of 1.5 is in red.

CO-rebinding kinetics. The value of k_{obs} was determined according to:

$$k_{obs} = \frac{k_{off,H} k_{on,CO}[\mathrm{CO}]}{k_{off,H} + k_{on,H} + k_{on,CO}[\mathrm{CO}]}$$

assuming 1 mM CO.

The values reported in Table 1 show that for the cold adapted fish the k_{on} is much larger than human Cygb. This means that the protein binds CO much faster when starting from the fully bis-His hexacoordinated state, in the presence of a relatively high diatomic ligand concentration (comparable to the concentration of oxygen found at low temperatures).Antarctic fish Cygbs-1, with and without His-tag, do not show any differences between wt, ΔCys mutants and wt+DTT.

Table 1. Overview of the kinetic parameters on His-tagged proteins, except CYGBΔCys.[a]

His-tagged proteins	**$k_{on,\,CO}$ ($\mu M^{-1}s^{-1}$)**	**k_{gem} (10^{7} s^{-1})**	**F_{gem}(%)**	**$k_{on,His}$ (s^{-1})**	**$k_{off,His}$ (s^{-1})**	**K_{his}**	**k_{obs}(s^{-1})**
*dm*Cygb-1	3.52 ± 0.28	3.28 ± 1	27 ± 1	300 ± 133	30.5 ± 5	9.6 ± 2.8	27.9
*dm*Cygb-1*	3.14 ± 0.64	3.52 ± 1.06	29.0 ± 0.7	284 ± 65	40.5 ± 9	7.01 ± 0.02	36.7
*dm*Cygb-1 + 5mM DTT	4.42	2.55	23	ND		ND	--
*ca*Cygb-1	3.42 ± 0.26	5.2 ± 0.6	37 ± 3	436 ± 5	38.5 ± 2	11.34 ± 0.49	33.8
*ca*Cygb-1*	3.14 ± 0.20	5.49 ± 0.48	34 ± 3	334.5 ± 88	38.8 ± 5	8.56 ± 1.1	34.7
*ca*Cygb-1 + 1mM DTT	3.72	3.18	33	ND		ND	--
Cygb (without His-tag)	6.78 ± 0.13	2.75	20.0 ± 2.5	340.00 ± 9.94	0.40 ± 0.002	850	0.4
CygbΔCys (without His-tag)	4.91	3.9	22	319	0.66	483	0.6

[a] ND: Not determined

Molecular Simulation. Stable trajectories were obtained for caCygb, hCygb_c1, hCygb_c2 and hCygb_S30M structures at 283 K, 298 K and 313 K (Figure 2). The proteins were simulated in the oxygenated form for 1.5 μs at each temperature. Representation of the root mean square fluctuations of the backbone atoms highlights a distinct behaviour between the Cygb in the different models. CaCygb looks more rigid than the hCygb_c1 with an average r.m.s.d. of ~2.5Å for the highest simulated temperature, while it is significantly higher for the hCygb_c1 (> 3Å).

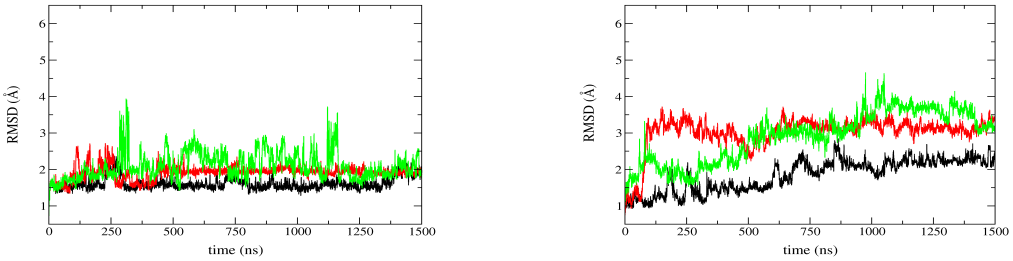

Figure 2. *RMSD representation of A) Chaenocephalus aceratus, B) Human. Black represents rmsd at 283. K, red represents rmsd at 298.95K and green represents rmsd at 313.15K.*

To get a more detailed view of the distinct flexibility of Cygb in both systems the performance of residue atomic fluctuations (RMSF) were computed along the trajectories (Figure 3). Clearly, caCygb shows lower fluctuations than hCygb_c1 and only increase with the temperature increment in the zone of residues 107 to 135.

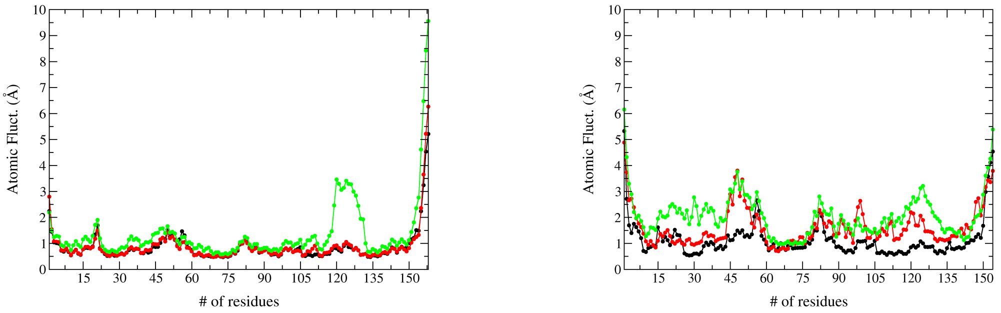

Figure 3*. Representation of the atomic fluctuations for 3 different temperatures 283.15 K, (black), 298.15 K (red) and 313.15 (green) of the hCygb_c1 ((right) and caCygb (left) proteins.*

Inner Cavities and Tunnels. Previous studies performed for hCygb_c1 at 298 K revealed that the oxygenated protein holds a big cavity. In the simulation started from the X-ray structure 4B3W there was no clear passage from the protein interior to the bulk solvent. However, the trajectory started from X-ray structure 3AG0 showed a well defined path that connects the primary docking site to the bulk solvent, passing through residues in loop AB and the final segment of helix G. The analysis also suggested the existence of a secondary path that involves the migration through distinct pocket sites and the exit via a passage between helix A and loop EF. Remarkably, the integrity of these paths is lost when simulations at 283 and 313 K are examined. In contrast to the preceding findings, simulations performed for caCygb reveal a well-shaped path through the protein matrix at 283 K, which is nevertheless disrupted when the temperature is raised to 298 (softly) and 313 K (sharply) as it is shown in Figure 4.

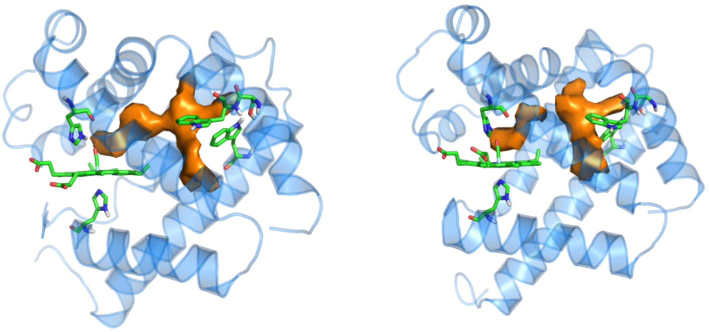

Figure 4. *Representation of the inner tunnel found in caCygb (corresponding to a frequency level of 50% as determined from MDpocket calculations; shown in orange) at 283 K (left) and 298 K (right). The protein backbone is shown in blue and the oxygenated haem is shown as green sticks together with the distal and proximal histidine residues.*

A comparison between the residues that shape the inner tunnel in caCygb and hCygb_c1/ hCygb_c2 suggests a seemingly key difference; the mutation of Met30 in hCygb_c1/ hCygb_c2 to Ser in caCygb. This change leads to the formation of a stable hydrogen-bond interaction between the Ser30 hydroxyl group and the indole NH unit of Trp151. This interaction fixes the orientation of Trp151, which in turn allows the formation of the tunnel in the interior of caCygb, especially at low temperatures. In contrast, the presence of Met instead of Ser in hCygb_c1 leads to an increased fluctuation of Trp151, thus contributing to blur the tunnel (Figure 5).

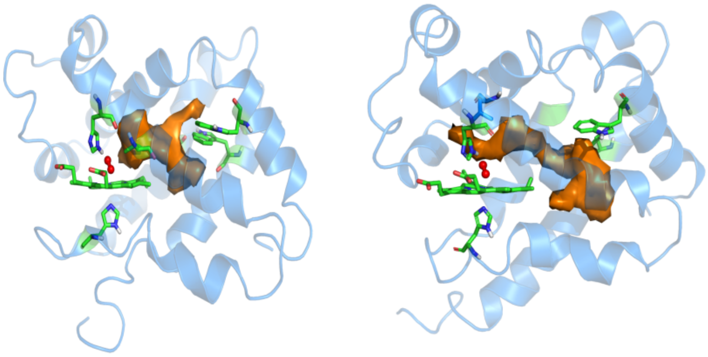

Figure 5. *Representation of the inner tunnel found in hCygb_c1 (corresponding to a frequency level of 50% as determined from MDpocket calculations; shown in orange). The image on the left shows the representation of the channel at 298 K, with the Trp151 in opposite orientation as CaCygb, while the image on the right respresents also the hCygb_c1, but at 283 K and the orientation of the Trp151 is "the same as caCygb. The protein backbone is shown in blue and the oxygenated heme is shown as green sticks, together with the distal and proximal histidine residues.*

To get a better understanding of the role of the two tryptophan residues in shaping the tunnel and modulating ligand migration through the inner cavities of the protein, a molecular dynamics simulation was carried out for the human protein but starting with the orientation of the tryptophan residues found in the *C. aceratus* structure (hCygb_c2). At low temperature (283.15 K), Trp151 is trapped in the initial conformation, thus the tunnel is kept during the simulation. However, the trajectories obtained for the other two temperatures show that increasing the temperature results in the rotation of this indole group to the same hCygb_c1 conformation fading away the tunnel and cutting it in two parts.

One of the reasonable motifs for this phenomenon might be that Trp151 is trapped in the starting orientation probably due to the lack of enough thermal energy to rotate and recover its usual conformation. At 298.15 K the original orientation of the human protein is very fast recovered at the beginning of the trajectory and does not go back to the caCygb conformation anymore (Figure 6).

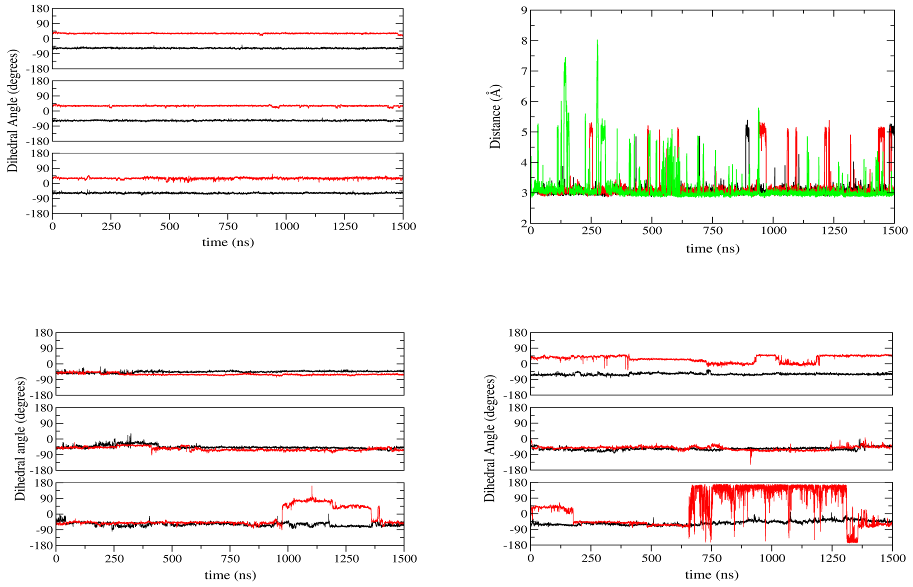

Figure 6 *Dihedral angles of Trp14 (black) and Trp134 (red). Top Left: caCygb Bottom Left: hCygb_c1. Top Right: Distance between Ser hydroxyl group and the indole NH unit of Trp151. Bottom Right: hCygb_c2 It can be clearly seen that the hydrogen bond is mantained during the whole trajectories at any of the three temperatures simulated for the Chaenocephalus aceratus: 283 (black), 298 (red) and 313 (green) and that this fact fixes the conformation of the Trp151.*

After our previous studies with *ca*Cygb, *h*Cygb_c1 and *h*Cygb_c2, we investigated the importance of the key mutation S30M in *h*Cygb. Simulations of the mutated human Cygb (*h*cygb_S30M) resulted in a notable increase of the size and the stability of the tunnels. Figure 7 shows a representation of the inner tunnels found for caCygb and hCygb_S30M at

283.15K. In both cases, the Ser30 is establishing a hydrogen bond interaction with the Trp151, allowing the formation of the tunnel.

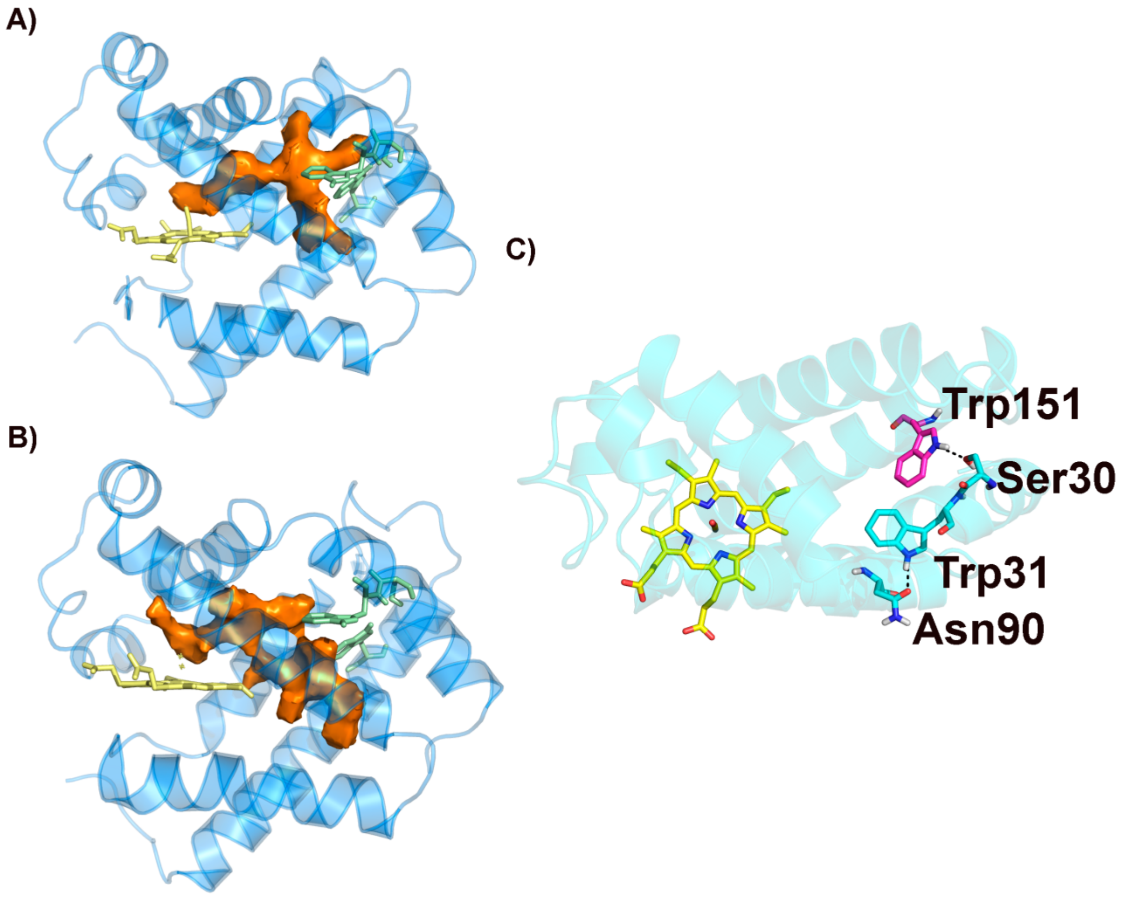

***Figure** 7. Representation of the inner tunnel found for A) caCygb and B) hCygb_S30M at 283.15 K (corresponding to a frequency level of 50% as determined from MDpocket calculations; shown in orange). C) In both systems the Trp151 shows the same orientation, allowing the hydrogen bond interaction with Ser30. The disposition of Trp151 in the hCygb_S30M is the opposite regarding to that expose in hCygb_c1.*

Representation of the root mean square fluctuations of the backbone atoms showed again a distinct behaviour between caCygb and hCygb_S30M. caCygb appeared more rigid than hCygb_S30M with an average RMSD at T283.15 K of ~1.62 Å for the while it is significantly higher at 313 K (~2.36 Å). Moreover the RMSF displayed a major fluctuation of residues in hCygb_S30M at both temperatures 283.15 and 298.15 K whilst in caCygb the fluctuations of residues is very low and remain more or less in the same values for both temperatures. Besides the stability provided by the hydrogen bond between Ser30 and Trp151 maintains the conformation of this latter residues almost unaltered in both models and in all the temperatures (Figure 8).

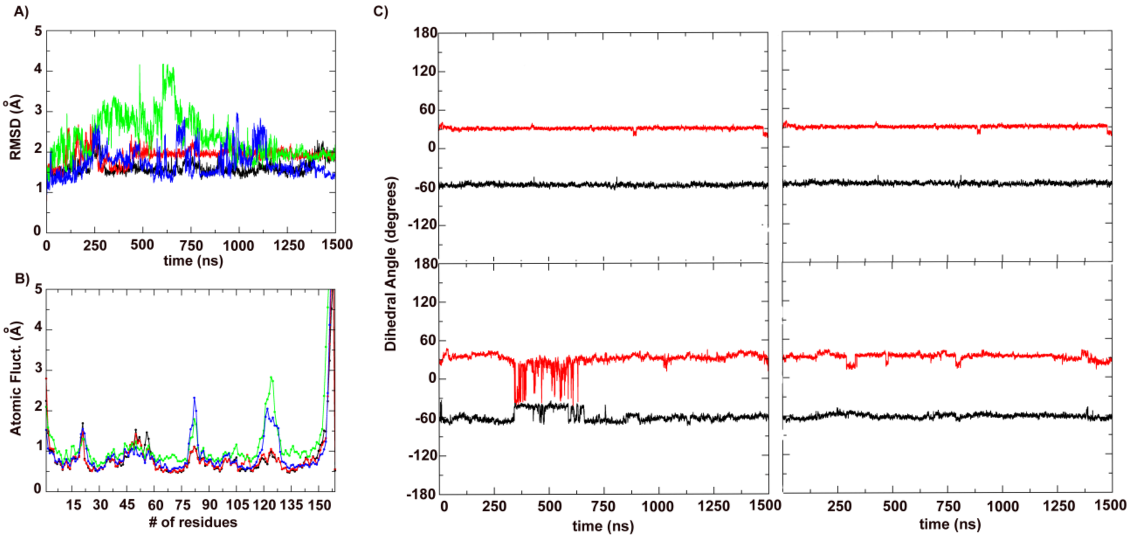

***Figure 8**. Representation of A) RMSD of caCygb at 283.15K (black) and 298.15K (red) and hCygb_S30M at 283.15K (green) and 298.15K (blue). B) RMSF of caCygb at 283.15K (black) and 298.15K (red) and hCygb_S30M at 283.15K (green) and 298.15K (blue). C) Dihedral angles of Trp31 (black) and Trp151 (red). Top Left: caCygb at 283.15 K. Top Right: hCygb_S30M at 283.15 K. Bottom Left: caCygb at 298.15 K. Bottom Right: hCygb_S30M at 298.15 K. The hydrogen bond is maintained during the whole trajectories for each temperature in both systems caCygb and hCygb_S30M.*

Ligand Migration in Cytoglobins. In order to get a deeper insight on the experimental results obtained by Prof. Viappiani about the photolysis of oxygen ligand in the heme group, we ran 20 short molecular dynamics simulations (of 50 ns) for each temperature (283.15K, 298.15K and 313.15K) and model, i.e., *ca*Cygb, *h*Cygb_c1, *h*Cygb_c2 and *h*Cygb_S30M. From these simulations we characterized the exit route followed by the ligand. Figure 9A displays the different exits paths obtained after the evaluation of all the simulations for each temperature and system. The percentage of exit followed by the ligand is indicated for each temperature at Figure 9B, considering all the model systems simulated. Additionally, we have considered the residence time of the ligand inside of each model system at 283.15K and 298.15K (Figure 9C). The results at 313.15K are not shown due to the lost of the tunnel in most of the model systems except *h*Cygb_S30M.

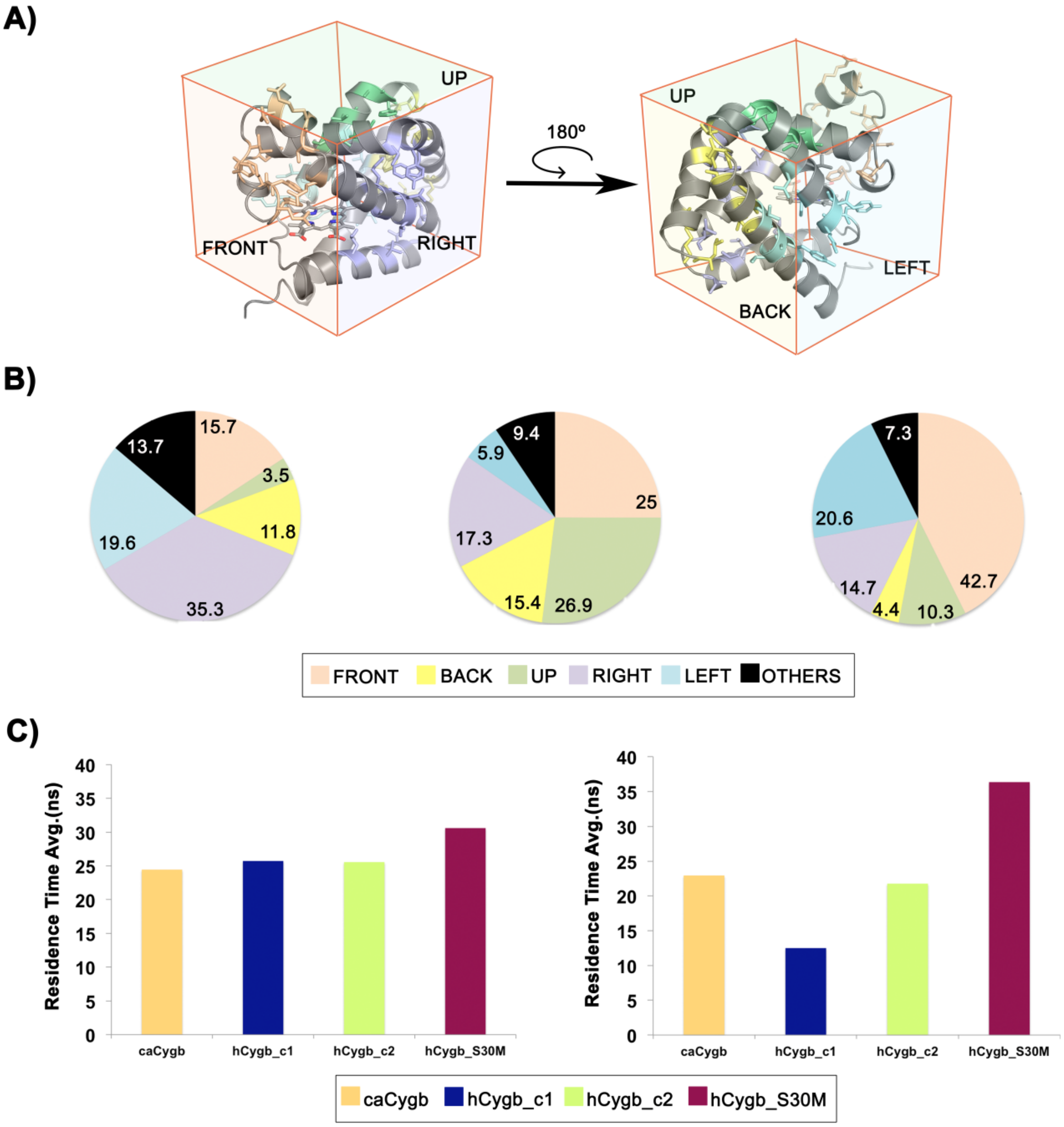

Figure 9. *Representation of A) exit sites of Cygb divided by zones as depicted by the cubic structure. B) Circular plots indicating the percentages of exit locations at the temperatures of 283.15 (left), 298.15 (middle) and 313.15K (right) for all the model systems simulated. C) Histogram of the residence time averages for caCygb, hCygb_1, hCygb_2 and hCygb_S30M at 283.15 (left) and 298.15K (right).*

The results support a different temperature sensitivity of caCygb and hCygb_c1/ hCygb_c2. In caCygb there seems to be an inner tunnel at 283 K, whereas in hCygb_c1 appears at 298 K, otherwise in hCygb_c2 the inner tunnel appears at 283 K losing its size and continuity because of the increase of the temperature and adopting a topology that resembles the distribution of cavities in hCygb_c1. In all the cases the tunnel is blurred upon increase of the temperature to 313 K with the exception of hCygb_S30M where it is kept also at 283 and 298 K. On the other hand, hCygb_S30M maintained the Ser-Trp hydrogen bond in all the temperatures as well as a stable tunnel. Finally, the short MD simulations performed in all the systems showed a substantially different behavior of the oxygen path and residence time after leaving its coordination with the heme group depending of the system and temperature.

*Comparison of ca*Gygb *and dm*Cygb. Comparison of the sequences of these two proteins reveal a limited number of changes, which correspond to the replacements shown in Table 2. All of these residues are located close to the surface, and hence one cannot expect a large influence on the topological features of the inner cavities. The only exception is the replacement of Met141 in caGygb by Ile142 in dmCygb, which locally contributes to define the shape of inner pockets (Figure 10).

Table 2. Residues that differ in the models of caGygb (blue) and dmGygb(green), with the convenient substitution of the CYS by SER in the latter protein (red).

Nº OF RESIDUE	C. ACERATUS	D. MAWSONI
7/8	**LYS**	**ARG**
21/22	**CYS**	**SER**
35/36	**LYS**	**ASN**
141/142	**MET**	**ILE**
143/144	**CYS**	**SER**
148/149	**ILE**	**VAL**

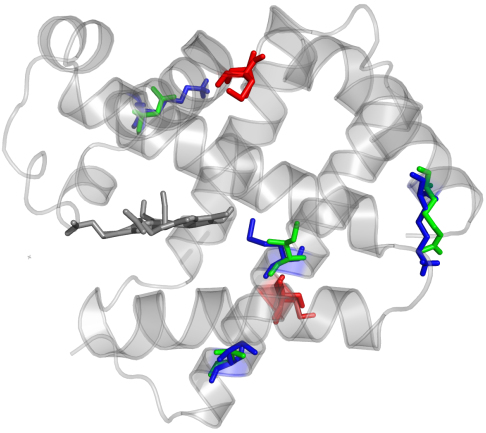

Figure 10 *Representation of the models of caGygb (blue) and dmGygb (green), with the change of the CYS by SER in the model of dmGygb in red.*

MD simulations were run at the 3 temperatures used previously for caGygb in order to explore the internal cavities with MDpocket and thus determine the influence of temperature on the topological changes in the channel(Figure 11). In contrast with caGygb, the results show the existence of well-defined tunnel, whose topological properties appear to be little affected by the changes in temperature. These results point out that the ligand can be trapped in multiple docking sites along the interior of the protein, which could contribute to retain the release to the bulk solvent. Future studies will be performed in order to evaluate the passage of the diatomic ligand along this tunnel and the potential release to the aqueous solution.

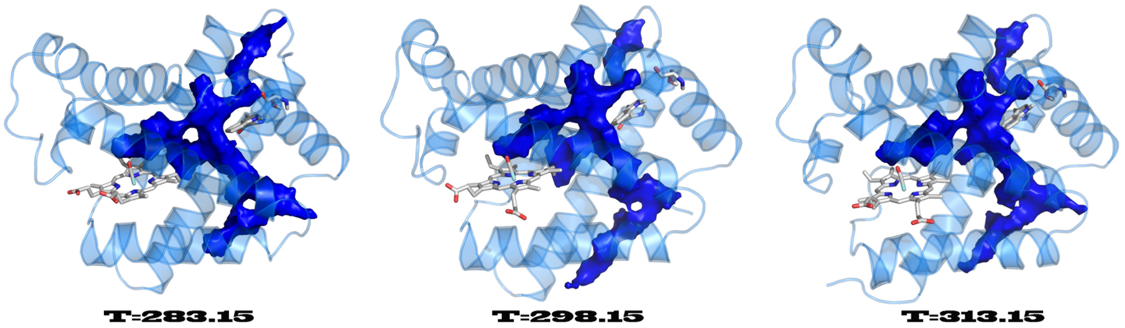

Figure 11 *Representation of the channel in the pentacoordinated form of D. Mawsoni with a 50% isosurface represented in blue in the final section between 1000 and 1250 ns at temperatures of 283, 298, 313 K.*

Conclusions

Comparison of caCygb and hCygb_c1/ hCygb_c2 points out that the Met30→Ser mutation might be a key factor in shaping the features of the tunnel in the interior of the proteins. Thus, the balance between the flexibility of residues in layers around the tunnel and the stability of specific interactions between residues seems to be critical for preserving the nature of the inner tunnel. Moreover the stability, length and size of the tunnels in hCygb_S30M at the three temperatures proposed, reinforce this hypothesis from S30M mutation is crucial for the stability of our models enhancing the size of the cavities and facilitating the connections between each other to form tunnels inside the protein structure.

With regard to the exit pathways followed by the diatomic ligand we could discern that the system *ca*Cygb exhibited the largest number of exits in comparison with the other models. In fact, only in *ca*Cygb and *h*Cygb_S30M is observed that the ligand pass through the exit site in the back of the protein due to superior length, size and stability of the channels in these models. On the other hand the increase of the temperature up to 298.15K promotes in many cases the diminution of the channel, making that the most frequent exit pathways neighboring the haemoglobin. This trend increase brusquely at 313.15 K, where most of the simulations display the majority of the exits close to the 2heme group, most probably because of the notable decrease of the channels in most of the systems.

It is also found that at 283.15 K the residence time was very similar for systems *ca*Cygb, *h*Cygb_c1 and *h*Cygb_2. However, for *h*Cygb_S30M system the residence time increment more than 10 ns, as a consequence of the increase of the size and length of the channels. Nevertheless at 298.15 K, the residence time for *ca*Cygb and *h*Cygb_c2 was similar to those observed at lower temperature, although the tunnels decreased for *h*Cyg_c2. In case of *h*Cygb_S30M, the residence time increases due to the augmentation of tunnels. Future studies will attempt to determine the kinetics migration of the small ligand through the Cytoglobin channels in order to calculate de diffusion rate of the ligands.

Finally, a channel was observed in D. Mawsoni that showed continuity and an increase in size and length in the three studied temperatures similar to that reported in hCygb_S30M. In contrast to caGygb, the topology of this channel is little affected by temperature, showing multiple docking sites that could trap the ligand in the interior of the protein.

References

[1] Schmidt, M., Gerlach, F., Avivi, A., Laufs, T., Wystub, S., Simpson, J. C., … Burmester, T. (2004). Cytoglobin is a Respiratory Protein in Connective Tissue and Neurons, Which Is Up-regulated by Hypoxia. *Journal of Biological Chemistry*, *279*(9), 8063–8069.

[2] Hankeln, T., Ebner, B., Fuchs, C., Gerlach, F., Haberkamp, M., Laufs, T. L., … Burmester, T. (2005). Neuroglobin and cytoglobin in search of their role in the vertebrate globin family. *Journal of Inorganic Biochemistry*. 2005, 99, 110-119.

[3] Tsujino, H., Yamashita, T., Nose, A., Kukino, K., Sawai, H., Shiro, Y., & Uno, T. (2014). Disulfide bondsregulate binding of exogenous ligand to human cytoglobin. *Journal of Inorganic Biochemistry*, *135*, 20–27. http://doi.org/10.1016/j.jinorgbio.2014.02.011

[4] Fordel, E., Thijs, L., Martinet, W., Lenjou, M., Laufs, T., Van Bockstaele, D., … Dewilde, S. (2006). Neuroglobin and cytoglobin overexpression protects human SH-SY5Y neuroblastoma cells against oxidative stress-induced cell death. *Neuroscience Letters*, *410*(2), 146–151.

[5] Yu, X., & Gao, D. (2013). Overexpression of cytoglobin gene inhibits hypoxic injury to SH-SY5Y neuroblastoma cells. *Neural Regeneration Research*, *8*(23), 2198–2203. http://doi.org/10.3969/j.issn.1673-5374.2013.23.010

[6] Pesce, A., De Sanctis, D., Nardini, M., Dewilde, S., Moens, L., Hankeln, T., … Bolognesi, M. (2004).
Reversible hexa- to penta-coordination of the heme Fe atom modulates ligand binding properties of neuroglobin and cytoglobin. *IUBMB Life*, *56*(11-12), 657–664.

[7] Bruno, S., Faggiano, S., Spyrakis, F., Mozzarelli, A., Abbruzzetti, S., Grandi, E., … Dominici, P. (2007). The

reactivity with CO of AHb1 and AHb2 from Arabidopsis thaliana is controlled by the distal HisE7 and internal hydrophobic cavities. *Journal of the American Chemical Society*, *129*(10), 2880–2889.

[8] Gabba, M., Abbruzzetti, S., Spyrakis, F., Forti, F., Bruno, S., Mozzarelli, A., … Dewilde, S. (2013). CO Rebinding Kinetics and Molecular Dynamics Simulations Highlight Dynamic Regulation of Internal Cavities in Human Cytoglobin. *PLoS ONE*, *8*(1).

[9] Boron, I., Capece, L., Pennacchietti, F., Wetzler, D. E., Bruno, S., Abbruzzetti, S., … Nadra, A. D. (2015). Engineered chimeras reveal the structural basis of hexacoordination in globins: A case study of neuroglobin and myoglobin. *Biochimica et Biophysica Acta - General Subjects*, *1850*(1), 169–177.

[10] Capece, L., Boechi, L., Perissinotti, L. L., Arroyo-Mañez, P., Bikiel, D. E., Smulevich, G., … Estrin, D. A. (2013). Small ligand-globin interactions: Reviewing lessons derived from computer simulation. *Biochimica et Biophysica Acta - Proteins and Proteomics*, *1834*(9), 1722–1738.

[11] K. Lindorff-Larsen, S. Piana, K. Palmo, P. Maragakis, J.L. Klepeis, R.O. Dror, D.E. Shaw, Improved side-chain torsion potentials for the Amber ff99SB force field, Proteins 78 (2010) 1950–1958.

[12] J.Wang, R.M. Wolf, J.W. Caldwell, P.A. Kollman, D.A. Case, Development and testing of a general force field, J. Comp. Chem. 25 (2004) 1157–1174.

[13] Jorgensen, W. L.; Chandrasekhar, J.; Madura, J. D.; Impey, R. W.; Klein, M. L. Comparison of simple potential functions for simulating liquid water. *J. Chem. Phys.* **1983**, *79* (2), 926–935.

[14] Ryckaert, J. P.; Ciccotti, G.; Berendsen, H. J. C. Numerical integration of the cartesian equations of motion of a system with constraints: molecular dynamics of n-alkanes. *J. Comput. Phys.* **1977**, *23* (3), 327–341.

[15] Burmester, T., B. Ebner, B. Weich & T. Hankeln, 2002. Cytoglobin:a novel globin type ubiquitously expressed invertebrate tissues. Molecular Biology and Evolution 19: 416–421.

[16] Fago, A.; Hundahl, C.; Dewilde, S.; Gilany, K.; Moens, L.; Weber, R. E. Allosteric regulation andtemperature dependence of oxygen binding in human neuroglobin and cytoglobin: Molecular mechanisms and physiological significance. *J. Biol. Chem.* **2004**, *279* (43), 44417–44426. Wittenberg, J.B.. *Physiol. Rev.* **1970** 50, 559

Discusión

4.1 Análisis de los inhibidores propuestos en la publicaciones de 11β-hidroxiesteroide deshidrogenasa tipo1

El acoplamiento de un ligando a su diana, descrito en adelante mediante el término *docking*, se ha convertido en una herramienta esencial en el diseño de fármacos para predecir el modo de unió del ligando teniendo en cuenta el ranking obtenido en base a las funciones de puntuación. La comprobación de dichas predicciones se lleva a cabo mediante el análisis de simulaciones de dinámica molecular (MD), que permiten distinguir entre diferentes modos de unión del ligando.[96]

En el caso de los compuestos analizados en esta tesis se realizaron 3 simulaciones independientes de MD para cada complejo ligando-receptor, de 50 ns cada una. La estabilidad del modo de unión del ligando, adoptando una determinada orientación en el centro de unión de la diana, viene determinada por el grado de preservación de las interacciones que dicho ligando efectúa, así como de su conformación inicial, asumiendo que la adopción de una orientación correcta debe preservar una integridad estructural superior a la de modos de unión incorrectos.

A lo largo de los diferentes estudios realizados en las publicaciones adjuntadas en esta tesis, se evaluaron diferentes aspectos del modo de unión de los compuestos propuestos como inhibidores de 11β-HSD1, así como las interacciones de enlace de hidrógeno con Ser 170 y Tyr183 (**Figura 14**). A este respecto, sin embargo, se observó una tendencia mayoritaria a perder la interacción del grupo hidroxilo de Tyr183 con el carbonilo común en todos los ligandos analizados en tanto que Tyr183 formaba un interacción con el cofactor, con la correspondiente modificación del sitio de unión hidrofóbico que este hecho conlleva. Estas interacciones fueron estudiadas para comprobar si se reproducía el mismo modo de unión observado en la estructura cristalográfica de PF-877443, que fue empleado como ligando de referencia en los primeros estudios, mediante análisis preliminares de docking con el programa Glide.

Cabe destacar que la elección de dicho programa de *docking* vino determinada por el hecho de proporcionar una mejor evaluación del sitio de unión, además de una clasificación de las conformaciones más razonables que las que se obtuvieron mediante un análisis comparativo con los programas rDock y Autodock. Por ello, en posteriores análisis únicamente se utilizó Glide en el proceso de *docking* para así homogeneizar el método empleado y evitar la posible disparidad de resultados motivada por el uso de diferentes programas.

Figura 14 *Representación del compuesto PF-877423 (izquierda) y EV22 (derecha). En la figura se resaltan las interacciones de los carbonilos con Ser171 y Tyr183, mostrando el cofactor NADPH al fondo de la cavidad.*

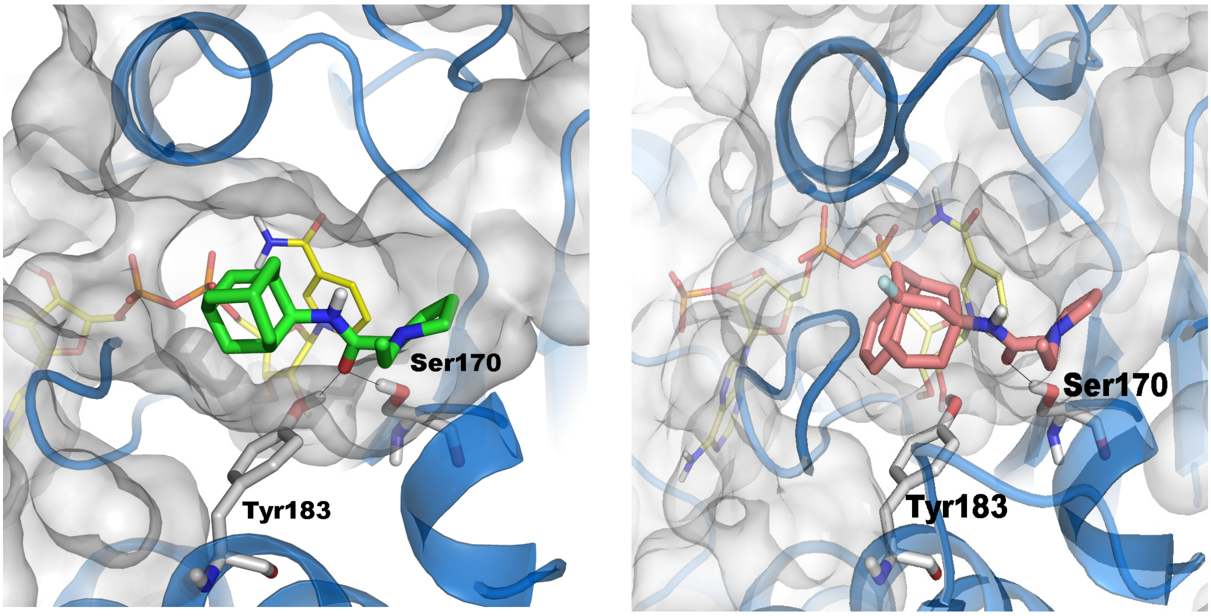

Como ejemplo de estos resultados, las puntuaciones de *docking* de los dos compuestos más potentes (EV15 y EV22) de nuestros primeros análisis mostraron resultados similares a los de PF-877423 **(Tabla 3)**. Sin embargo, el ensayo farmacológico de los compuestos EV15 y EV22 reveló que presentan una potencia entre 100 y 200 veces menor que PF877423 (IC_{50}= 4 nM). De este modo, la sustitución del grupo adamantano por el policiclo de mayor tamaño resultó perjudicial para la unión a la enzima. Ello puede reflejar en parte la limitada precisión de las funciones de puntuación, que podrían no permitir distinguir las diferencias de actividad entre estos compuestos, suponiendo que obedecen exclusivamente a diferencias en la interacción con el enzima.

***Tabla 3** Puntuaciones energéticas (en kcal/mol) de las mejores poses obtenidas para la unión de los ligandos PF877423, EV15 y EV22 al enzima 11β-HSD1.*

SOLUCIÓN/LIGANDO	**PF877423**	**EV15**	**EV22**
1	-7.75	-8.08	-8.21
2	-7.23	-7.82	-8.19
3	-7.23	-7.41	-7.83
4	-7.14	-7.33	-7.79
5	-7.13	-7.25	-7.38

Además los diferentes estudios y simulaciones de trayectorias mostraron que los ligando tienden a adoptar la misma conformación dentro de la cavidad, con el efecto beneficioso que implica la ocupación del adamantano (con los subtituyentes metilo y flúor en el caso de EV15 y EV22) en la zona hidrofóbica formada por las cadenas laterales de Leu126, Ala226, Val227 y el átomo de Cα de **Ser125 (**Figura 15**)**, permitiendo la formación de interacciones de Van der Waals.

Figura 15 *Representación de las interacciones entre el átomo de flúor (en EV22) en el bolsillo hidrofóbico formado por Ser125, Leu126, Ala226 y Val227(**A**, izquierda), y orientación espacial del anillo bencénico del compuesto EV15 y el grupo fosfato del cofactor NADP (**B**, derecha)*

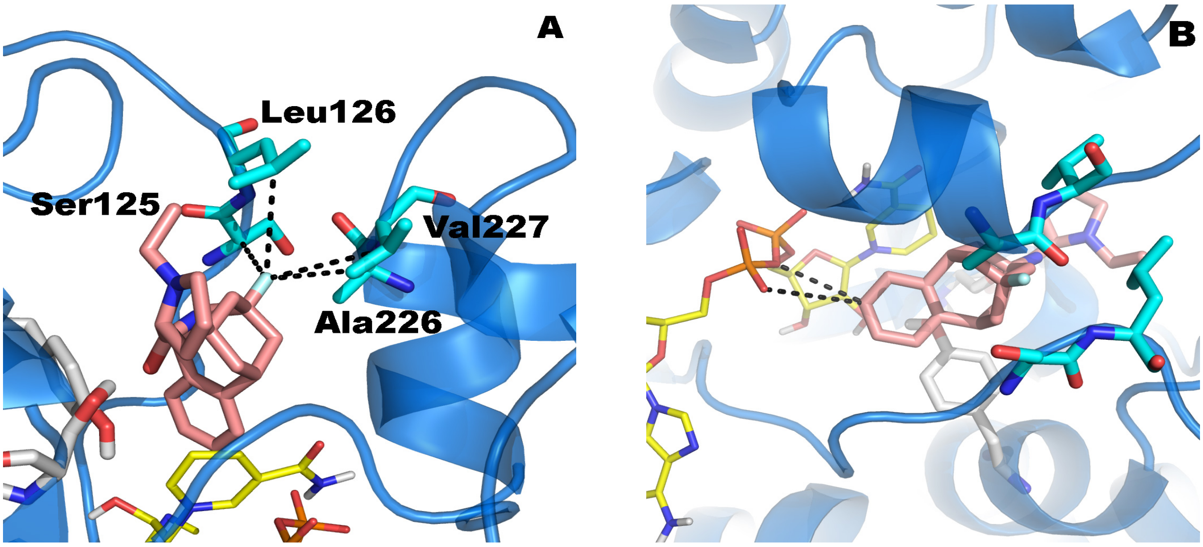

Aunque estos resultados apoyan la hipótesis de que la inserción del anillo bencénico pudiera ser beneficiosa para la unión, la disminución de la solubilidad en agua debido al aumento de la hidrofobicidad del policiclo también se sugirió como posible factor en la reducción de la potencia inhibitoria. En aras de discernir esta cuestión se determinó el coeficiente de reparto octanol/agua (log Po/w) a partir de cálculos QM-SCRF usando el modelo continuo de solvatación IEF/MST para PF-877423 y los compuestos más potentes. Tal y como se predijo, los resultados pusieron de manifiesto que la expansión del policiclo aumentaba el log Po/w en 1,5 y 0,9 unidades en relación con PF-877423. En consecuencia, es posible que la menor actividad refleje una disminución en la complementariedad hidrofóbica entre cofactor y ligando, dado que el coste debido a la expulsión de las moléculas de agua que hidratan los oxígenos del grupo fosfato del cofactor no se ven compensadas con interacciones favorables establecidas con el anillo de benceno del ligando.

4.1.1 Substitución en C1/C2

Los estudios realizados también persiguieron evaluar el efecto de la substitución del carbono C1/C2 en la disposición estérica del anillo de adamantano sobre las notables diferencias de actividad observadas en los compuestos RL103/RL106 **(Tabla 4)**.

Tabla 4 *Ligandos RL103 y RL106 con estructura C1/C2 respectivamente*

RL103 (C1)	RL106 (C2)
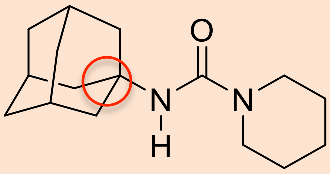	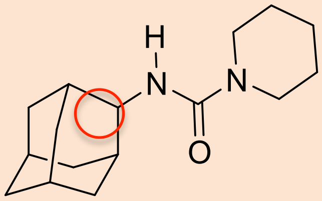

La actividad se incrementa en el caso de sustitución en C2 (RL106) debido a que ello condiciona tanto la movilidad del adamatano en el sitio de unión, como a su encaje en la cavidad, comparados con PF-877423 **(Figura 16)** .

Figura 16 *Representación de los complejos de 11β-HSD1 con PF-877423 (arriba a la izquierda), RL103 (arriba a la derecha), RL104 (abajo a la izquierda) y RL106 (abajo a la derecha), interaccionando con Ser170 y Tyr183*

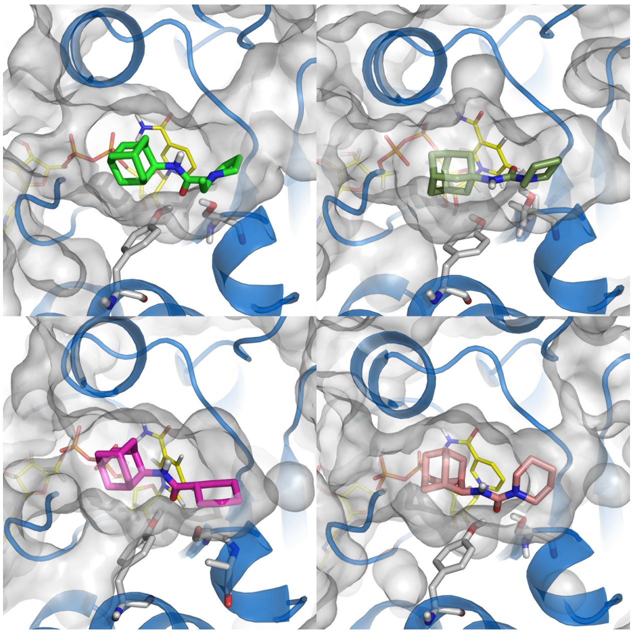

4.1.2 Inversión de N-pirrolidinas modificadas

Por otra parte, se ha examinado una serie de compuestos basados en la estructura de pirrolidina con una mayor potencia inhibidora en determinados compuestos por el anillo condensado, que debería reducir el coste conformacional aumentando la afinidad de unión de estos compuestos en comparación con otros más flexibles. Pese a que los resultados apoyaban el encaje en el bolsillo hidrofóbico, el hecho de mostrar una menor potencia inhibitoria podría sugerir que el tamaño del sustituyente policíclico permitido para la unión del ligando debería ser algo menor para no provocar distorsiones estructurales significativas en la cavidad.

Un ejemplo ilustrativo de ello serían los compuestos mostrados en la **Figura 17,** donde EV26 y EV28 que poseen una actividad mucho mejor (IC_{50} de 0,29 y 0,32 µM respectivamente) que RL116 (>100.000 µM) debido, en parte a su anillo fusionado de pirrolidina que facilita su acoplamiento en la cavidad hidrofóbica (pese a su mayor volumen). Por otra parte, el compuesto RL117, con un anillo policíclico de menor tamaño, exhibe una actividad 10 veces mayor (IC_{50} 0.029 µM) que EV26/EV28 con una diferente orientación de la amida respecto a RL116. También se detectó una escasa variación en las actividades de ligandos muy similares, tan sólo diferenciados por la presencia/ausencia de un doble enlace en su estructura (como muestra RL115 respecto a RL116 con una IC_{50} >100.000 μM, o RL117 respecto a RL118, con una IC_{50} de 0.019 μM)

Figura 17 *Representación del modo de unión de los compuestos EV28 (A), EV26 (B), RL116 (C) y RL118 (D) a la enzima 11β-HSD1 en las simulaciones MD.*

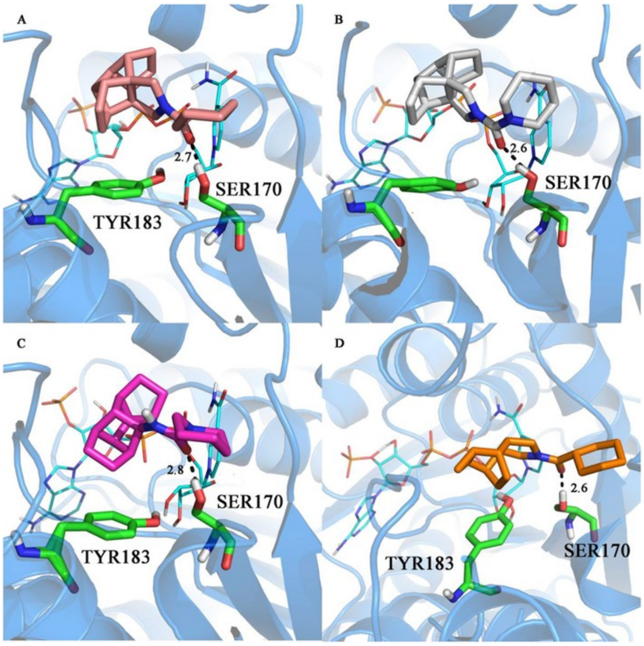
A
2.7
SER170
TYR183
B
2.6
SER170
C
2.8
SER170
TYR183
D
2.6
TYR183
SER170

Finalmente se evaluaron una serie de nuevos inhibidores de 11β-HSD1 que presentan una N-acilpirrolidina policíclica (**Tabla 5**).

***Tabla 5** Ligandos empleados en cada una de las estructuras cristal analizadas*

CRISTAL	3D5Q (RL144)	3CH6 (RL147)
COMPUESTO	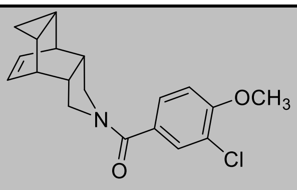	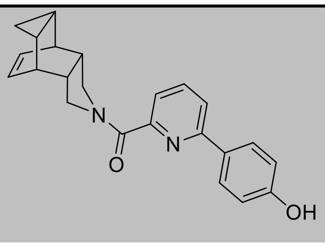
CRISTAL	4C7J (RL148)	4HFR (RL149)
COMPUESTO	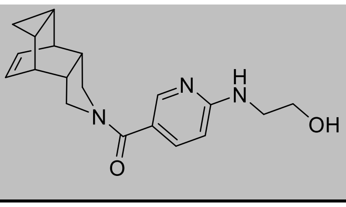	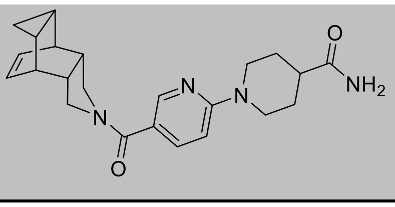

Los compuestos analizados, inspirados en los ligandos de la estructura cristalográfica de diferentes enzimas (al contrario que en estudios anteriores en los que sólo se partía de la estructura cristal 4BB6), proporcionaban potentes compuestos contra 11β-HSD1 humana.

De particular interés fueron los derivados de biarilo, de los cuales se desarrollaron varios compuestos, analizados previamente con un farmacóforo 3D-QSAR construido usando descriptores hidrofóbicos aprovechando la información disponible las estructuras de rayos X y la bibliografía que nos proporcionó ligandos derivados de las estructuras cristal hasta completar un “training set” de 41 ligandos **(Figura 18)**.[97,98,99,100]

***Figure 18**. Alineamiento del “training set” de ligandos .*

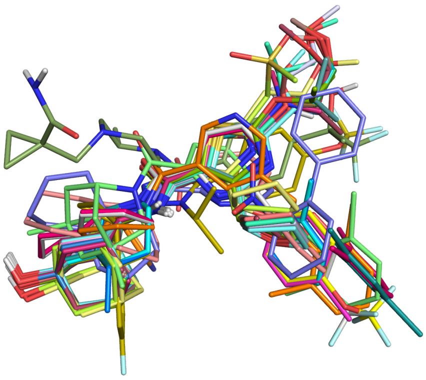

El análogo que contenía fenol (RL147), el compuesto más activo en la enzima humana con una IC_{50} nanomolar baja (14 nM en hHSD1), a pesar de no corresponderse con una potente actividad murina (77750 nM), debido al cambio conformacional del anillo de piridina-fenol, que tiene como consecuencia un tercer puente de hidrógeno con la Pro153. Ello puede relacionarse probablemente con la diferente orientación adoptada en el centro de unión. Se obtuvo un valor marcadamente inferior en el compuesto 3-cloro-4-metoxibenzoilo (RL144; $IC_{50} = 1003$ nM). Los compuestos RL148 y RL149 mostaron un 20 y 21 % de inhibición respectivamente a 10 µM, por lo que ya no se procedió a calcular sus valores de IC_{50}, pese a la interacción del alcohol de RL148 con el ASP234 **(Figura 19)**.

Figura 19 *Representación del modo de unión de los compuestos RL144 (A), RL147 (B), RL148 (C) y RL149 (D) a la enzima 11β-HSD1 en las simulaciones MD.*

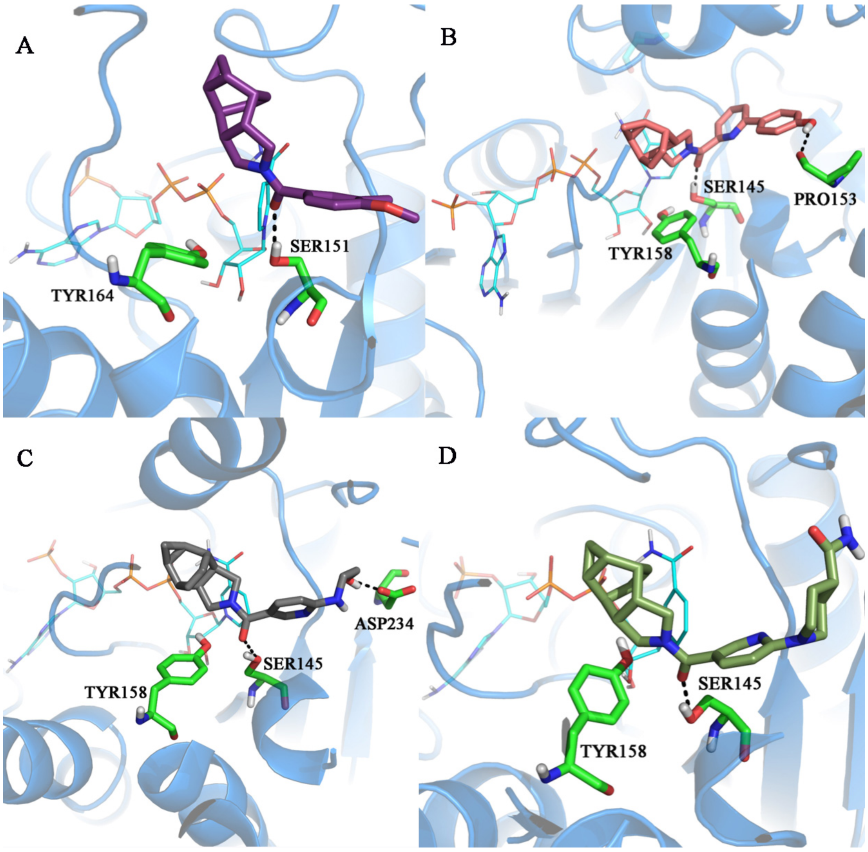

Los diferentes estudios llevados a cabo en la investigación de estos nuevos inhibidores han servido para analizarlos con más profundidad comprobando la afinidad y estabilidad de las diferentes conformaciones y su encaje en el sitio de unión, mostrando una manifiesta estabilidad del enlace de hidrógeno con la Ser170 en contrapunto con la pérdida, a lo largo del tiempo transcurrido en las simulaciones, del que se producía con la Tyr183, que generalmente se desplaza para interaccionar con el cofactor, dejando un espacio mayor que facilita el acople del ligando.

4.2 Estudio del proceso de migración de ligandos en globinas

4.2.1 Análisis de métodos para el estudio de la unión de ligandos con globinas en modelos de estado múltiple

Los progresos en técnicas experimentales, como la cristalografía de rayos X o ensayos cinéticos por flash-fotólisis, combinados con estudios estructurales basados en métodos computacionales, han permitido examinar las vías de migración a través del conjunto de cavidades internas en diferentes tipos de globinas. Su comprensión requiere una descripción muy precisa de todos los estados intermedios y el uso de modelos de estado múltiple. Se han desarrollado diferentes métodos de detección, aprovechando la mayor capacidad de procesamiento de los supercomputadores y GPU, facilitando la identificación y descripción energética de posibles vías de migración de ligandos (**Figura 20**).

Figura 20 *Factores que modulan la migración del ligando en diferentes hemoglobinas. (A) Superposición de las 350 estructuras de Mb encontradas en el PDB que muestran las diferentes disposiciones conformacionales adoptadas por HisE7. (B) Cavidades de unión con Xe encontradas en Mb a 7 bar de presión y 30 bar. (C) Representación superficial de trHbN de M. tuberculosis que muestra la ruta larga del túnel bloqueada por PheE15. (D) Representación superficial de mini-Hb de C. Lacteus que muestra el túnel continuo que conecta el sitio de unión al hemo con el disolvente.*

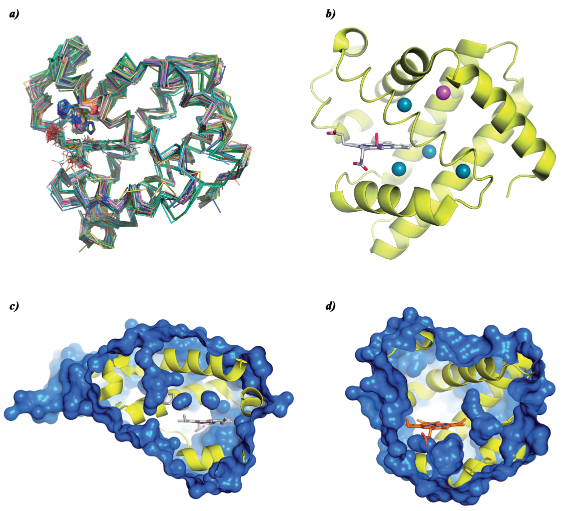

Esto resultados se muestran en concordancia con los hallazgos experimentales con respecto a la identificación de cavidades dentro de la matriz proteica y la identificación de residuos clave. Sin embargo, una de las principales dificultades de estos estudios ha sido la derivación de datos cinéticos, ya que requiere un estudio minucioso de todas las posibles transiciones de estado con una vía de migración de ligandos. Con los recientes avances en los métodos de muestreo MD mejorado acoplados a las técnicas de modelado del estado de Markov en diferentes formulaciones, se han obtenido constantes de tiempo así como constantes de velocidad cinética con un acuerdo cercano a valores medidos experimentalmente, demostrando la utilidad de descripciones markovianas para racionalizar eventos moleculares con transiciones aleatorias entre estados.

4.2.2 Influencia de la temperatura sobre las características topológicas del las cavidades internas en citoglobinas y estudio de la migración de ligandos diatómicos

Para determinar el impacto de la temperatura en las cavidades internas y migración de ligandos en citoglobinas se observó en los resultados un comportamiento diferente respecto a la temperatura de caCygb y hCygb_c1 / hCygb_c2. En caCygb existe un túnel interno a 283 K, mientras que en hCygb_c1 apareció a 298 K, de lo contrario en hCygb_c2 el túnel interno surgió a 283K perdiendo su tamaño y continuidad debido al aumento de la temperatura y adoptando una conformación hCygb_c1 debido a la rotación del Trp151 que, obviamente no interacciona con la Met30 **(Figura 21).**

Figura 21 *Representación del túnel interno que se encuentra en caCygb (con una frecuencia del 50%, en naranja determinado con MDPocket) a 283 K (A) y 298 K (B), hCygb_c1 a 298 K (C) con el Trp151 en orientación opuesta a CaCygb y hCygb_c2 a 283 K (D) donde la orientación del Trp151 es la misma que caCygb.*

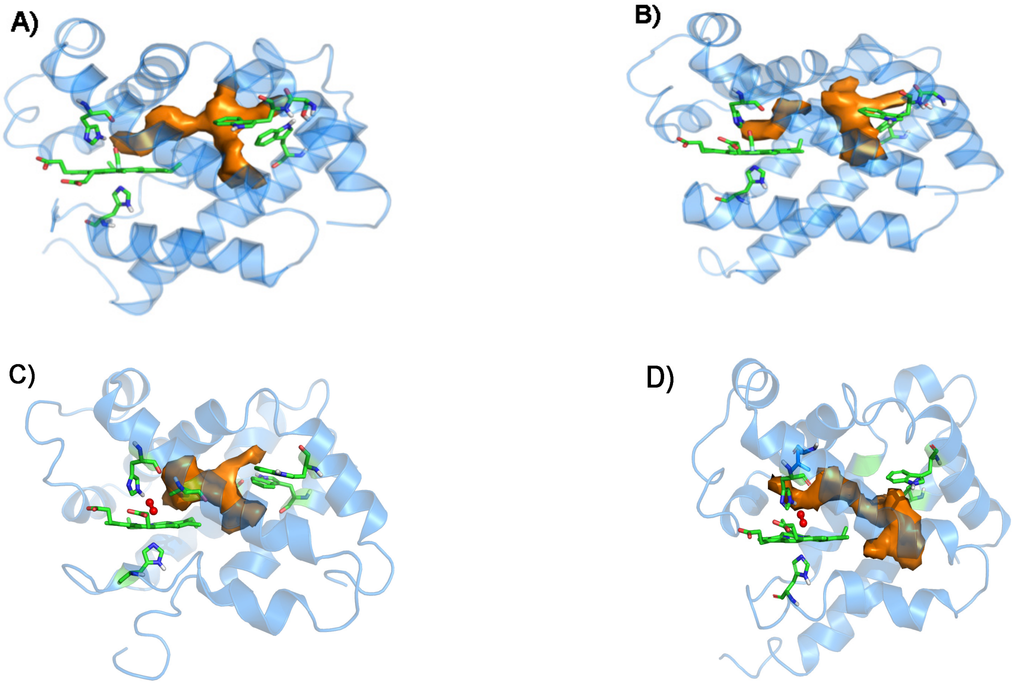

En todos los casos el túnel desapareció al aumentar la temperatura a 313 K excepto en hCygb_S30M donde se mantuvo, también en 283 y 298K. Mientras tanto, en hCygb_S30M se conservó el enlace de hidrógeno SER-TRP en todas las temperaturas, así como la estabilidad del túnel **(Figura 22).**

Figura 22 *Representación del túnel interno de A) caCygb y B) hCygb_S30M a 283.15 K (que corresponde a una frecuencia del 50%, en naranja, según lo determinado por los cálculos de MDPocket. C) En ambos sistemas, el Trp151 muestra la misma orientación, lo que permite la interacción del enlace de hidrógeno con Ser30. La disposición de Trp151 en hCygb_S30M es la opuesta respecto a la de hCygb_c1*

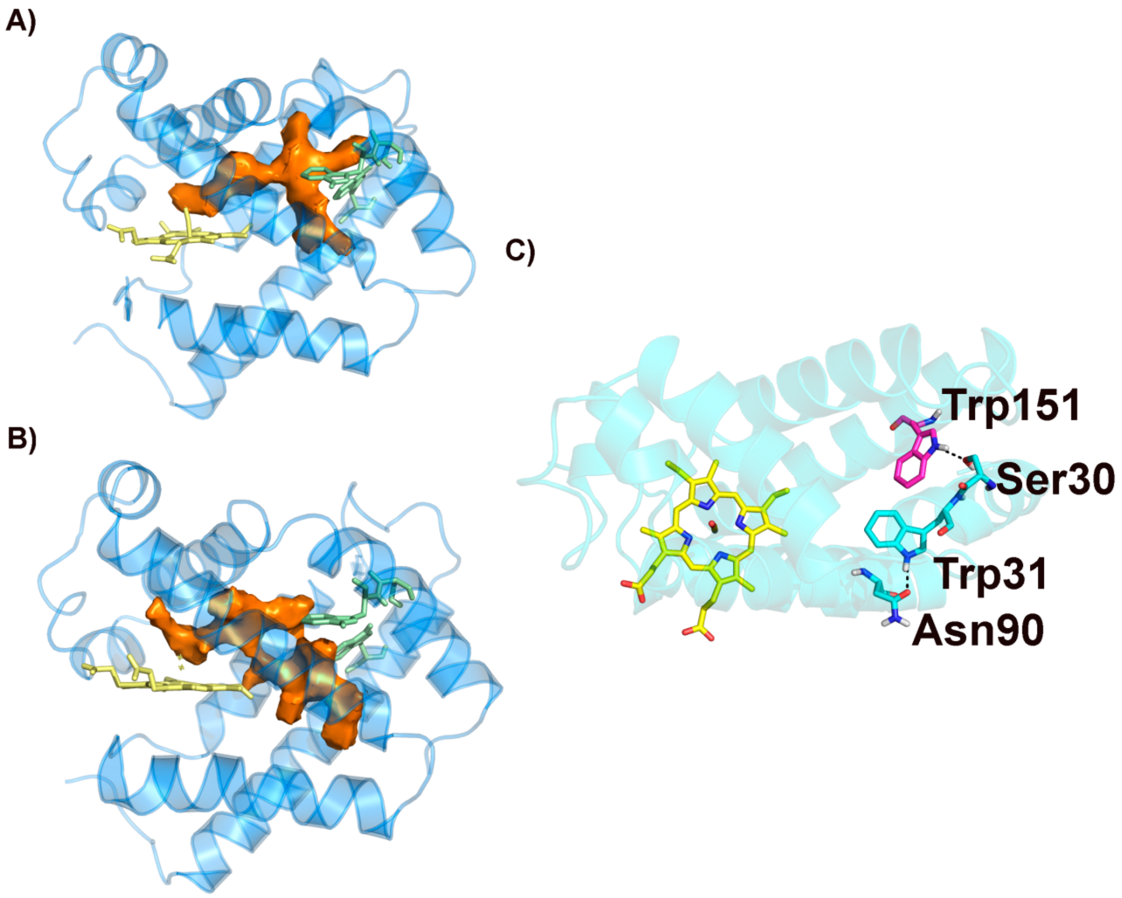

Por otro lado, las simulaciones de MD con ligando libre de ≤ 50 ns realizados en todos los sistemas mostraron un comportamiento sustancialmente diferente del oxígeno después de romper su coordinación con el grupo hemo dependiendo del sistema y de la temperatura, ya que esto implica una variación en la longitud, tamaño y continuidad de los canales haciendo más o menos accesible el paso de este ligando diatómico a través de la proteina**.**

La comparación de caCygb y hCygb_c1 / hCygb_c2 muestra que la mutación Met30 → Ser podría ser un factor clave en la configuración de las características del túnel en el interior de las citoglobinas. Por consiguiente, el equilibrio entre la flexibilidad de los residuos en capas alrededor del túnel y la estabilidad de las interacciones específicas entre los residuos parece ser crítico para preservar la naturaleza del túnel interior. Además, la estabilidad, longitud y tamaño de los túneles en hCygb_S30M a las tres temperaturas propuestas (único sistema que mantiene el túnel a 300 K), refuerzan esta hipótesis **(Figura 23)**.

Figura 23 *Representación de A) RMSD de caCygb a 283.15K (negro) y 298.15K (rojo) y hCygb_S30M a 283.15K (verde) y 298.15K (azul). B) RMSF de caCygb a 283,15 K (negro) y 298,15 K (rojo) y hCygb_S30M a 283,15 K (verde) y 298,15 K (azul). C) Diedros de Trp31 (negro) y Trp151 (rojo). Arriba a la izquierda: caCygb a 283,15 K. Arriba a la derecha: hCygb_S30M a 283,15 K. Abajo a la izquierda: caCygb a 298,15 K. Abajo a la derecha: hCygb_S30M a 298,15 K. El enlace de hidrógeno se mantiene durante todas las trayectorias para cada temperatura en ambos sistemas caCygb y hCygb_S30M .*

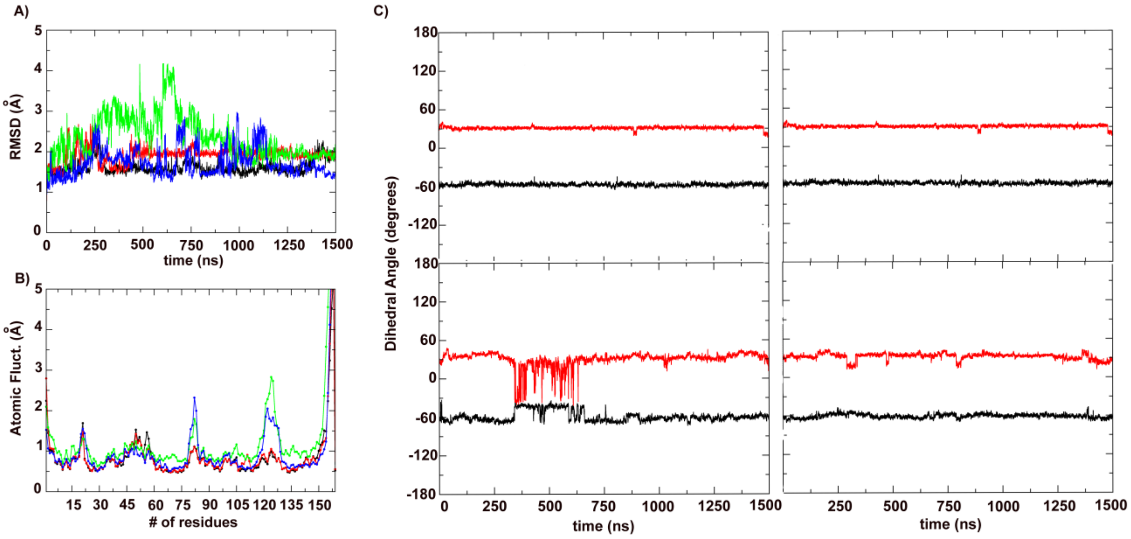

Con respecto a las vías de salida seguidas por el ligando diatómico, se pudo discernir que el sistema caCygb exhibió el mayor número de salidas en comparación con los otros modelos. De hecho, sólo en caCygb y hCygb_S30M se observa que el ligando pasa a través del sitio de salida en la parte posterior de la proteína debido a la longitud, el tamaño y la estabilidad superiores de los canales en estos modelos. Por otro lado, el aumento de la temperatura hasta 298.15K promueve en muchos casos (excepto hCygb_c1) la disminución del canal, haciendo que las vías de salida más frecuentes se sitúen próximos al grupo hemo. Esta tendencia aumenta bruscamente a 313.15 K, donde la mayoría de las simulaciones muestran vías de fuga cercanas al grupo hemo, muy probablemente debido a la notable disminución de los canales en la mayoría de los sistemas.

A propósito del tiempo de residencia del ligando dentro de la proteína, se dedujo que a 283,15 K el tiempo de residencia era muy similar para los sistemas caCygb, hCygb_c1 y hCygb_2. Sin embargo, para el sistema hCygb_S30M el incremento de tiempo de residencia es superior a 10 ns, como consecuencia del aumento del tamaño y longitud de los canales. Sin embargo, a 298,15 K, el tiempo de residencia para caCygb y hCygb_c2 fue similar a los observados a menor temperatura, aunque en el caso de hCyg_c2 los túneles disminuyeron (debido a la rotación de el TRP151 recuperando la conformación hCygb_c1).

En futuras investigaciones se tratará de determinar la constante cinética de la velocidad de migración del ligando diatómico a través de los canales de la citoglobina para calcular la velocidad de difusión de éstos **(Figura 24)**.

***Figura 24** Representación de A) zonas de salida de Cygb como se muestra en la estructura cúbica. B) Diagramas circulares que indican los porcentajes de los lugares por donde sale el oxígeno, temperaturas de 283,15 (izquierda), 298,15 (centro) y 313,15 K (derecha) para todos los sistemas modelo simulados. C) Histograma de promedios del tiempo de residencia para caCygb, hCygb_1, hCygb_2 y hCygb_S30M en 283.15 (izquierda) y 298.15K (derecha).*

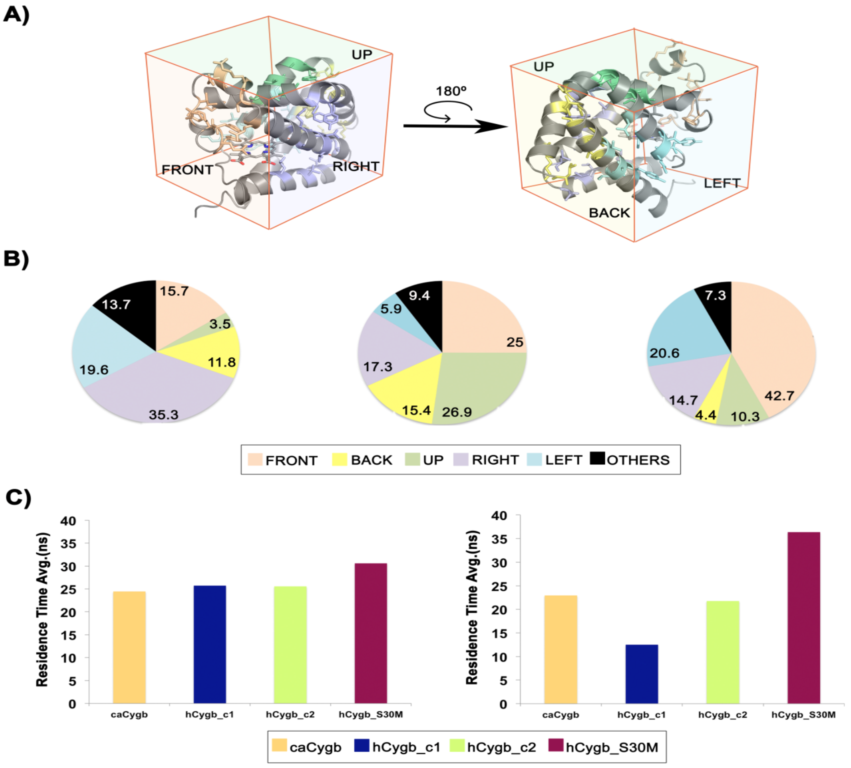

4.2.3 Estudio comparativo de los modelos de C. Aceratus y D. Mawsoni

Para ampliar los estudios anteriores se cotejó el anterior modelo de *C. Aceratus* con otro de *D. Mawsoni* proporcionado por el profesor Martino Bolognesi de la Universidad de Milano con el resultado mostrado en la **Tabla 4**, donde queda patente la similitud entre los 2 modelos, (puntualizar que las CYS se cambiaron por SER para evitar puentes disulfuro).

Tabla 4 *Residuos que difieren en los modelos de C. Aceratus (azul) y D. Mawson (verde), con la puntualización de la conveniente subtitución de las CYS por SER en el modelo de D. Mawsoni*

Nº DE RESIDUO	C. ACERATUS	D. MAWSONI
7/8	**LYS**	**ARG**
21/22	**CYS**	**SER**
35/36	**LYS**	**ASN**
141/142	**MET**	**ILE**
143/144	**CYS**	**SER**
148/149	**ILE**	**VAL**

Todos estos residuos se encuentran cerca de la superficie y, por lo tanto, no se espera una gran influencia en las características topológicas de las cavidades internas. La única excepción es la sustitución de Met141 en caGygb por Ile142 en dmCygb, que contribuye localmente a definir la forma de las cavidades interiores (**Figura 25**).

Figura 25 *Representación de los modelos de C. Aceratus (azul) y D. Mawson (verde), con el cambio de las CYS por SER en el modelo de D. Mawsoni en rojo ambas.*

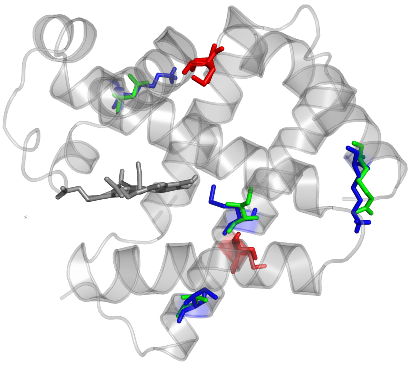

Para dejar patente esta similitud se procedió a realizar simulaciones de MD de la misma longitud y a las 3 temperaturas empleadas en *C. Aceratus* para posteriormente explorar también sus cavidades internas con MDpocket y así determinar una tendencia a la reducción del canal al aumentar la temperatura, tal y como se observó en *C. Aceratus*, aunque ahora, en *D. Mawsoni* se muestre un tamaño y continuidad similar en a las 3 temperaturas como se puede observar en la **Figura 26** donde se muestra la forma pentacoordinada. Así pues, para realizar un estudio estadístico en el canal interno se lanzaron dinámicas moleculares de ≤50 ns con un oxígeno en la cavidad interna en el último tramo entre 1250 y 1500 ns**,** para así poder comprobar que el ligando diatómico permanecía (o no) dentro de la cavidad y si se al desplazaba hacia otra parte de la proteína o al exterior.

Figura 26 *Representación del canal en la forma pentacoordinada de D. Mawsoni con una isosurface del 50% representada en azul en el tramo final entre 1000 y 1250 ns a las temperaturas de 283, 298, 313 K.*

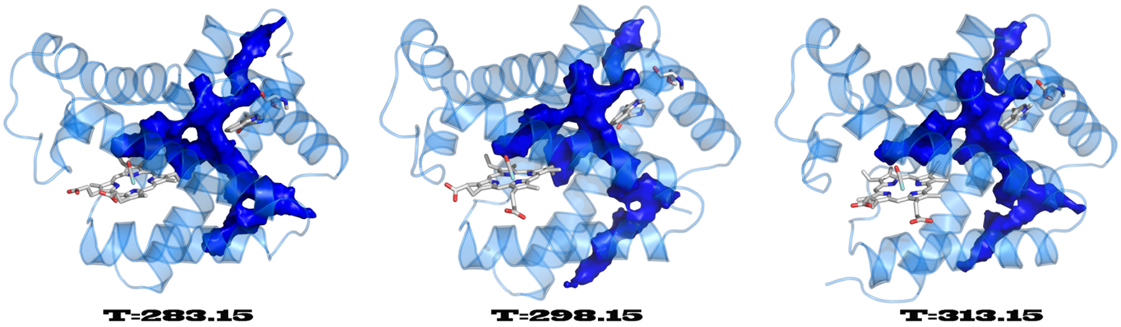

Conclusiones

5.1 Estudio computacional de la inhibición de 11β-HSD1

- Tomados en su conjunto, los resultados de los primeros estudios sugieren que el aumento de tamaño como estrategia pueden conducir a inhibidores efectivos de 11β-HSD1. Sin embargo, es necesario mantener un equilibrio adecuado para compensar la hidrofobicidad proporcionada por el policiclo de mayor tamaño y así optimizar su perfil farmacológico. Por tanto, la incorporación de un núcleo de una polaridad mayor podría considerarse como una estrategia adecuada para el desarrollo de nuevos inhibidores.

- Posteriormente, teniendo en cuenta los resultados farmacológicos, la actividad inhibidora de 11β-HSD1 en los adamantanos sustituidos en C2, debido a un menor impedimento estérico y una mayor libertad de rotación del anillo de adamtano, fue superior a la de sus equivalentes en C1. Además, n la introducción de un átomo de oxígeno en la estructura policíclica no conlleva una mejora en la actividad.

- La introducción de hidrocarburos policíclicos como por ejemplo, los basados en pirrolidina da lugar a potentes inhibidores de 11β-HSD1, y potencialmente estos sistemas con anillo/s alifático/s pueden ser considerados como alternativas al adamantilo.

- En la útlima serie de compuestos, se realizó un modelo de farmacóforo 3D-QSAR para predecir la actividad de la mayoría de ellos. Cabe destacar que, al ser estos de mayor tamaño que los anteriores, mostraron un mayor numero de interacciones, pese a que su encaje en la cavidad fue más dificultoso, principalmente debido a su mayor tamaño y a que las simulaciones de dinámica molecular fueron llevadas a cabo en diferentes sistemas con el fin de conseguir una mayor variedad de resultados debido a la mejor posibilidad de investigar diferentes conformaciones de los ligandos en diversos lugares de unión. Desafortunadamente no se consiguió (por el momento) obtener una selectividad de estos compuestos sobre 11β-HSD2 debido a la dificultad a la hora de contruir un modelo de homología con suficiente fiabilidad.

5.2.1 Análisis de métodos para el estudio de la unión de ligandos con globinas en modelos de estado múltiple

- La unión y migración de ligandos a globinas involucra la existencia de estados metaestables de larga duración, que deben ser considerados para describir la cinética del proceso global de unión.

5.2.2 Influencia de la temperatura sobre las características topológicas del las cavidades internas en citoglobinas y estudio de la migración de ligandos diatómicos

- La mutación S30M es crucial para la estabilidad de citoglobina, debido al enlace de hidrógeno establecido entre la Serina 30 y el Triptófano 134 incrementando el tamaño de las cavidades y facilitando las conexiones entre sí para formar túneles dentro de la estructura de la proteína.

- Respecto a la migración de oxígeno caCygb y hCygb_S30M se observa el paso del ligando a través de la Citoglobina con su salida por la parte posterior debido a la longitud, el tamaño y la estabilidad superiores de los canales en estos modelos.

- Se comprobó que en hCygb_S30M el tiempo de residencia aumenta de manera considerable debido al aumento de longitud y tamaño de los túneles en las 3 temperaturas propuestas motivado por la estabilidad proporcionada por el puente de hidrógeno SER-TRP.

5.2.3 Estudio comparativo de los modelos de C. Aceratus y D. Mawsoni

- No se encontraron diferencias remarcables entre los residuos de los 2 modelos.

- Se observo en D. Mawsoni un canal que mostró una continuidad y un aumento de tamaño y longitud en las 3 temperaturas estudiadas similar al que se reportó en hCygb_S30M.

Bibliografía

(1) Dallman, M. F.; Strack, A. M.; Akana, S. F.; Bradbury, M. J.; Hanson, E. S.; Scribner, K. A.; Smith,M.Feast_and_Famine:Critical_Role_of_Glucocorticodis_with_Insulin_in_Daily_Energy_Flow. pdf. *Front. Neuroendocrinol.* **1993**, *14* (No. 4), 303–347.

(2) Sapolsky, R. M.; Romero, L. M.; Munck, a. U. How Do Glucocorticoids Influence Stress Responses ? Preparative Actions *. *Endocr. Rev.* **2000**, *21* (April), 55–89.

(3) Rosen, E. D.; MacDougald, O. a. Adipocyte differentiation from the inside out. *Nat. Rev. Mol. Cell Biol.* **2006**, *7* (12), 885–896.

(4) Smoak, K. a.; Cidlowski, J. a. Mechanisms of glucocorticoid receptor signaling during inflammation. *Mech. Ageing Dev.* **2004**, *125* (10–11 SPEC. ISS.), 697–706.

(5) Arriza, J. L.; Weinberger, C.; Cerelli, G.; Glaser, T. M.; Handelin, B. L.; Housman, D. E.; Evans, R. M. Cloning of Human Mineralocorticoid Receptor Complementary DNA: Structural and Functional Kinship with the Glucocorticoid Receptor Cloning of Human Mineralocorticoid Receptor Complementary DNA: Structural and Functional IKinship with the Glucocorticoid Rec. *Source Sci. New Ser.* **1987**, *237222117* (17), 268–275.

(6) Dzyakanchuk, A. a.; Balázs, Z.; Nashev, L. G.; Amrein, K. E.; Odermatt, A. 11β-Hydroxysteroid dehydrogenase 1 reductase activity is dependent on a high ratio of NADPH/NADP+ and is stimulated by extracellular glucose. *Mol. Cell. Endocrinol.* **2009**, *301* (1–2), 137–141.

(7) Atanasov, A. G.; Nashev, L. G.; Gelman, L.; Legeza, B.; Sack, R.; Portmann, R.; Odermatt, A. Direct protein-protein interaction of 11β-hydroxysteroid dehydrogenase type 1 and hexose-6-phosphate dehydrogenase in the endoplasmic reticulum lumen. *Biochim. Biophys. Acta - Mol. Cell Res.* **2008**, *1783* (8), 1536–1543.

(8) Hardy, R. S.; Seibel, M. J.; Cooper, M. S. Targeting 11β-hydroxysteroid dehydrogenases: A novel approach to manipulating local glucocorticoid levels with implications for rheumatic disease. *Curr. Opin. Pharmacol.* **2013**, *13* (3), 440–444.

(9) Sandeep, T. C.; Walker, B. R. Pathophysiology of modulation of local glucocorticoid levels by 11beta-hydroxysteroid dehydrogenases. *Trends Endocrinol. Metab.* **2001**, *12* (10), 446–453.

(10) Zhang, J.; Osslund, T. D.; Plant, M. H.; Clogston, C. L.; Nybo, R. E.; Xiong, F.; Delaney, J. M.; Jordan, S. R. Crystal structure of murine 11 beta-hydroxysteroid dehydrogenase 1: an important therapeutic target for diabetes. *Biochemistry* **2005**, *44* (18), 6948–6957.

(11) Schuster, D.; Maurer, E. M.; Laggner, C.; Nashev, L. G.; Wilckens, T.; Langer, T.; Odermatt, A. The discovery of new 11??-hydroxysteroid dehydrogenase type 1 inhibitors by common feature pharmacophore modeling and virtual screening. *J. Med. Chem.* **2006**, *49* (12), 3454–3466.

(12) Odermatt, A.; Nashev, L. G. The glucocorticoid-activating enzyme 11β-hydroxysteroid dehydrogenase type 1 has broad substrate specificity: Physiological and toxicological considerations. *J. Steroid Biochem. Mol. Biol.* **2010**, *119* (1–2), 1–13.

(13) Mitić, T.; Andrew, R.; Walker, B. R.; Hadoke, P. W. F. 11β-Hydroxysteroid dehydrogenase type 1 contributes to the regulation of 7-oxysterol levels in the arterial wall through the inter-conversion of 7-ketocholesterol and 7β-hydroxycholesterol. *Biochimie* **2013**, *95* (3), 548–555.

(14) Odermatt, A.; Klusonova, P. 11β-Hydroxysteroid dehydrogenase 1: Regeneration of active glucocorticoids is only part of the story. *J. Steroid Biochem. Mol. Biol.* **2015**, *151*, 85–92.

(15) Kotelevtsev, Y.; Brown, R. W.; Fleming, S.; Kenyon, C.; Edwards, C. R.; Seckl, J. R.; Mullins, J. J. Hypertension in mice lacking 11beta-hydroxysteroid dehydrogenase type 2. *J. Clin. Invest.* **1999**, *103* (5), 683–689.

(16) Marchais-Oberwinkler, S.; Henn, C.; Möller, G.; Klein, T.; Negri, M.; Oster, A.; Spadaro, A.; Werth, R.; Wetzel, M.; Xu, K.; et al. 17??-Hydroxysteroid dehydrogenases (17??-HSDs) as therapeutic targets: Protein structures, functions, and recent progress in inhibitor development. *J. Steroid Biochem. Mol. Biol.* **2011**, *125* (1–2), 66–82.

(17) Bisschop, P. H.; Dekker, M. J. H. J.; Osterthun, W.; Kwakkel, J.; Anink, J. J.; Boelen, a.; Unmehopa, U. a.; Koper, J. W.; Lamberts, S. W. J.; Stewart, P. M.; et al. Expression of 11β-Hydroxysteroid Dehydrogenase Type 1 in the Human Hypothalamus. *J. Neuroendocrinol.* **2013**, *25* (5), 425–432.

(18) Kilgour, A. H. M.; Semple, S.; Marshall, I.; Andrews, P.; Andrew, R.; Walker, B. R. 11B-Hydroxysteroid Dehydrogenase Activity in the Brain Does Not Contribute To Systemic Interconversion of Cortisol and Cortisone in Healthy Men. *J. Clin. Endocrinol. Metab.* **2015**, *100* (2), 483–489.

(19) Robb, G. R.; Boyd, S.; Davies, C. D.; Dossetter, A. G.; Goldberg, F. W.; Kemmitt, P. D.; Scott, J. S.; Swales, J. G. Design of pyrazolo-pyrimidines as 11β-HSD1 inhibitors through optimisation of molecular electrostatic potential. *Med. Chem. Commun.* **2015**, *6*, 926–934.

(20) Masuzaki, H. A Transgenic Model of Visceral Obesity and the Metabolic Syndrome. *Science (80-.).* **2001**, *294* (5549), 2166–2170.

(21) Masuzaki, H.; Yamamoto, H.; Kenyon, C. J.; Elmquist, J. K.; Morton, N. M.; Paterson, J. M.; Shinyama, H.; Sharp, M. G. F.; Fleming, S.; Mullins, J. J.; et al. Transgenic amplification of glucocorticoid action in adipose tissue causes high blood pressure in mice. *J. Clin. Invest.* **2003**, *112* (1), 83–90.

(22) Kotelevtsev, Y.; Holmes, M. C.; Burchell, a.; Houston, P. M.; Schmoll, D.; Jamieson, P.; Best, R.; Brown, R.; Edwards, C. R. W.; Seckl, J. R.; et al. 11 -Hydroxysteroid dehydrogenase type 1 knockout mice show attenuated glucocorticoid-inducible responses and resist hyperglycemia on obesity or stress. *Proc. Natl. Acad. Sci.* **1997**, *94* (26), 14924–14929.

(23) Morton, N. M.; Paterson, J. M.; Masuzaki, H.; Holmes, M. C.; Staels, B.; Fievet, C.; Walker, B. R.; Flier, J. S.; Mullins, J. J.; Seckl, J. R. Novel Adipose Tissue – Mediated Resistance to Dehydrogenase Type 1 – Deficient Mice. *Mol. Med.* **2004**, *53*, 931–938.

(24) Morton, N. M.; Holmes, M. C.; Fiévet, C.; Staels, B.; Tailleux, A.; Mullins, J. J.; Seckl, J. R. Improved Lipid and Lipoprotein Profile, Hepatic Insulin Sensitivity, and Glucose Tolerance in 11β-Hydroxysteroid Dehydrogenase Type 1 Null Mice. *J. Biol. Chem.* **2001**, *276* (44), 41293–41300.

(25) Kershaw, E. E.; Morton, N. M.; Dhillon, H.; Ramage, L.; Seckl, J. R.; Flier, J. S. Adipocyte-Specific Glucocorticoid Inactivation Protects Against Diet-Induced Obesity. **2005**, *54* (Pt 24), 1023–1031.

(26) Morgan, S. a; Tomlinson, J. W. 11Beta-Hydroxysteroid Dehydrogenase Type 1 Inhibitors for the Treatment of Type 2 Diabetes. *Expert Opin Investig Drugs* **2010**, *19* (9), 1067–1076.

(27) Morton, N. M. Obesity and corticosteroids: 11??-Hydroxysteroid type 1 as a cause and therapeutic target in metabolic disease. *Mol. Cell. Endocrinol.* **2010**, *316* (2), 154–164.

(28) Joharapurkar, A.; Dhanesha, N.; Shah, G.; Kharul, R.; Jain, M. 11β-Hydroxysteroid dehydrogenase type 1: Potential therapeutic target for metabolic syndrome. *Pharmacol. Reports* **2012**, *64* (5), 1055–1065.

(29) Anderson, A.; Walker, B. R. 11??-HSD1 inhibitors for the treatment of type 2 diabetes and cardiovascular disease. *Drugs* **2013**, *73* (13), 1385–1393.

(30) McEwen B.S., Biron C.A., Brunson K.W., Bulloch K., Chambers W.H., Dhabhar F.S., GoldFarb R.H., Kitson R.P., Miller A.H., Spencer R.L., W. J. M. The role of adrenocorticoids as modulators of immune function. *Brain Res. Rev.* **1997**, *23*, 79–133.

(31) Yeager, M. P.; Guyre, P. M.; Munck, a. U. Glucocorticoid regulation of the inflammatory response to injury. *Acta Anaesthesiol. Scand.* **2004**, *48* (7), 799–813.

(32) Cooper, M. S.; Stewart, P. M. 11Beta-hydroxysteroid dehydrogenase type 1 and its role in the hypothalamus-pituitary-adrenal axis, metabolic syndrome, and inflammation. *J. Clin. Endocrinol. Metab.* **2009**, *94* (12), 4645–4654.

(33) Chapman, K. E.; Coutinho, A. E.; Gray, M.; Gilmour, J. S.; Savill, J. S.; Seckl, J. R. The role and regulation of 11β-hydroxysteroid dehydrogenase type 1 in the inflammatory response. *Mol. Cell. Endocrinol.* **2009**, *301* (1–2), 123–131.

(34) Hadoke, P. W. F.; Kipari, T.; Seckl, J. R.; Chapman, K. E. Modulation of 11β-hydroxysteroid dehydrogenase as a strategy to reduce vascular inflammation. *Curr. Atheroscler. Rep.* **2013**, *15* (5), 320.

(35) Jun, Y. J.; Park, S. J.; Hwang, J. W.; Kim, T. H.; Jung, K. J.; Jung, J. Y.; Hwang, G. H.; Lee, S. H.; Lee, S. H. Differential expression of 11??-hydroxysteroid dehydrogenase type 1 and 2 in mild and moderate/severe persistent allergic nasal mucosa and regulation of their expression by Th2 cytokines. *Clin. Exp. Allergy* **2014**, *44* (2), 197–211.

(36) Chapman, K. E.; Coutinho, A.; Gray, M.; Gilmour, J. S.; Savill, J. S.; Seckl, J. R. Local amplification of glucocorticoids by 11beta-hydroxysteroid dehydrogenase type 1 and its role in the inflammatory response. *Ann. N. Y. Acad. Sci.* **2006**, *1088*, 265–273.

(37) Chapman, K. E.; Seckl, J. R. 11??-HSD1, inflammation, metabolic disease and age-related cognitive (dys)function. *Neurochem. Res.* **2008**, *33* (4), 624–636.

(38) Hotamisligil, G. S. Inflammation and metabolic disorders. *Nature* **2006**, *444* (7121), 860–867.

(39) Sapolsky, R. M.; Pulsinelli, W. a. Glucocorticoids potentiate ischemic injury to neurons: therapeutic implications. *Science* **1985**, *229* (4720), 1397–1400.

(40) Beraki, S.; Litrus, L.; Soriano, L.; Monbureau, M.; To, L. K.; Braithwaite, S. P.; Nikolich, K.; Urfer, R.; Oksenberg, D.; Shamloo, M. A Pharmacological Screening Approach for Discovery of Neuroprotective Compounds in Ischemic Stroke. *PLoS One* **2013**, *8* (7), 1–13.

(41) Sandeep, T. C.; Yau, J. L. W.; MacLullich, A. M. J.; Noble, J.; Deary, I. J.; Walker, B. R.; Seckl, J. R. 11Beta-hydroxysteroid dehydrogenase inhibition improves cognitive function in healthy elderly men and type 2 diabetics. *Proc. Natl. Acad. Sci. U. S. A.* **2004**, *101* (17), 6734–6739.

(42) Meaney, M. J.; O'Donnell, D.; Rowe, W.; Tannenbaum, B.; Steverman, A.; Walker, M.; Nair, N. P. V.; Lupien, S. Individual differences in hypothalamic-pituitary-adrenal activity in later life and hippocampal aging. *Exp. Gerontol.* **1995**, *30* (3–4), 229–251.

(43) Yau, J. L. W.; Wheelan, N.; Noble, J.; Walker, B. R.; Webster, S. P.; Kenyon, C. J.; Ludwig, M.; Seckl, J. R. Intrahippocampal glucocorticoids generated by 11β-HSD1 affect memory in aged mice. *Neurobiol. Aging* **2015**, *36* (1), 334–343.

(44) de Quervain, D. J. F.; Poirier, R.; Wollmer, M. A.; Grimaldi, L. M. E.; Tsolaki, M.; Streffer, J. R.; Hock, C.; Nitsch, R. M.; Mohajeri, M. H.; Papassotiropoulos, A. Glucocorticoid-related genetic susceptibility for Alzheimer's disease. *Hum. Mol. Genet.* **2004**, *13* (1), 47–52.

(45) Martocchia, A.; Stefanelli, M.; Falaschi, G. M.; Toussan, L.; Ferri, C.; Falaschi, P. Recent advances in the role of cortisol and metabolic syndrome in age-related degenerative diseases. *Aging Clin. Exp. Res.* **2016**, *28* (1), 17–23.

(46) Katz, D. a; Liu, W.; Locke, C.; Jacobson, P.; Barnes, D. M.; Basu, R.; An, G.; Rieser, M. J.; Daszkowski, D.; Groves, F.; et al. Peripheral and central nervous system inhibition of 11β-hydroxysteroid dehydrogenase type 1 in man by the novel inhibitor ABT-384. *Transl. Psychiatry* **2013**, *3* (8), e295.

(47) Yau, J. L. W.; Noble, J.; Seckl, J. R. 11 -Hydroxysteroid Dehydrogenase Type 1 Deficiency Prevents Memory Deficits with Aging by Switching from Glucocorticoid Receptor to Mineralocorticoid Receptor-Mediated Cognitive Control. *J. Neurosci.* **2011**, *31* (11), 4188–4193.

(48) Green, K. N. Glucocorticoids Increase Amyloid-beta and Tau Pathology in a Mouse Model of Alzheimer's Disease. *J. Neurosci.* **2006**, *26* (35), 9047–9056.

(49) Sooy, K.; Noble, J.; McBride, A.; Binnie, M.; Yau, J. L. W.; Seckl, J. R.; Walker, B. R.; Webster, S. P. Cognitive and disease-modifying effects of 11β-hydroxysteroid

dehydrogenase type 1 inhibition in male Tg2576 mice, a model of Alzheimer's disease. *Endocrinology* **2015**, *156* (12), 4592–4603.

(50) Sun, W.; Chen, X.; Tong, Q.; Zhu, H.; He, Y.; Lei, L.; Xue, Y.; Yao, G.; Luo, Z.; Wang, J.; et al. Novel small molecule 11beta-HSD1 inhibitor from the endophytic fungus Penicillium commune. *Sci Rep* **2016**, *6* (April), 26418.

(51) Fotsch, C.; Askew, B. C.; Chen, J. J. 11beta-Hydroxysteroid dehydrogenase-1 as a therapeutic target for metabolic diseases. *Expert Opin. Ther. Pat.* **2005**, *15* (3), 289–303.

(52) Webster, S. P.; McBride, A.; Binnie, M.; Sooy, K.; Seckl, J. R.; Andrew, R.; Pallin, T. D.; Hunt, H. J.; Perrior, T. R.; Ruffles, V. S.; et al. Selection and early clinical evaluation of the brain-penetrant 11β-hydroxysteroid dehydrogenase type 1 (11β-HSD1) inhibitor UE2343 (Xanamem™). *Br. J. Pharmacol.* **2017**, *174* (5), 396–408.

(53) Webster, S. P.; Pallin, T. D. 11B-Hydroxysteroid Dehydrogenase Type 1 Inhibitors As Therapeutic Agents. *Expert Opin. Ther. Pat.* **2007**, *17* (12), 1407–1422.

(54) Hughes, K. a; Webster, S. P.; Walker, B. R. 11-Beta-hydroxysteroid dehydrogenase type 1 (11beta-HSD1) inhibitors in type 2 diabetes mellitus and obesity. *Expert Opin. Investig. Drugs* **2008**, *17* (4), 481–496.

(55) St. Jean Jr., D. J.; Wang, M.; Fotsch, C. Inhibitors of 11β -HSD1: A potential treatment for the metabolic syndrome. *Curr. Top. Med. Chem.* **2008**, *8* (17), 1508–1523.

(56) Boyle, C. D.; Kowalski, T. J. 11Beta-Hydroxysteroid Dehydrogenase Type 1 Inhibitors: a Review of Recent Patents. *Expert Opin. Ther. Pat.* **2009**, *19* (6), 801–825.

(57) Scott, J. S.; Goldberg, F. W.; Turnbull, A. V. Medicinal chemistry of inhibitors of 11??-hydroxysteroid dehydrogenase type 1 (11??-HSD1). *J. Med. Chem.* **2014**, *57* (11), 4466–4486.

(58) Stefan, N.; Ramsauer, M.; Jordan, P.; Nowotny, B.; Kantartzis, K.; Machann, J.; Hwang, J.-H.; Nowotny, P.; Kahl, S.; Harreiter, J.; et al. Inhibition of 11β-HSD1 with RO5093151 for non-alcoholic fatty liver disease: a multicentre, randomised, double-blind, placebo-controlled trial. *Lancet Diabetes Endocrinol.* **2014**, *2* (5), 406–416.

(59) Siu, M.; Johnson, T. O.; Wang, Y.; Nair, S. K.; Taylor, W. D.; Cripps, S. J.; Matthews, J. J.; Edwards, M. P.; Pauly, T. a.; Ermolieff, J.; et al. N-(Pyridin-2-yl) arylsulfonamide inhibitors of 11??-hydroxysteroid dehydrogenase type 1: Discovery of PF-915275. *Bioorganic Med. Chem. Lett.* **2009**, *19* (13), 3493–3497.

(60) Feig, P. U., S. Shah, A. Hermanowski-Vosatka , D. Plotkin, M. S. Springer, S. Donahue, C. Thach, E. J. Klein5, E. L. & K. D. K. Effects of an 11β -hydroxysteroid dehydrogenase type 1 inhibitor, MK-0916, in patients with type 2 diabetes mellitus and metabolic syndrome. *Int. J. Organ Transplant. Med.* **2011**, *13* (4), 498–504.

(61) Shah, S.; Hermanowski-Vosatka, A.; Gibson, K.; Ruck, R. A.; Jia, G.; Zhang, J.; Hwang, P. M. T.; Ryan, N. W.; Langdon, R. B.; Feig, P. U. Efficacy and safety of the selective 11??-HSD-1 inhibitors MK-0736 and MK-0916 in overweight and obese patients with hypertension.

J. Am. Soc. Hypertens. **2011**, *5* (3), 166–176.

(62) Waddell, S. T.; Balkovec, J. M.; Kevin, N. J.; Gu, X. Preparation of triazoles derivatives as inhibitors of 11β-hydroxysteroid dehydrogenase-1. WO 2007047625.

(63) Wang, H.; Robl, J. a.; Hamann, L. G.; Simpkins, L.; Golla, R.; Li, Y. X.; Seethala, R.; Zvyaga, T.; Gordon, D. a.; Li, J. J. Generation of 3,8-substituted 1,2,4-triazolopyridines as potent inhibitors of human 11??-hydroxysteroid dehydrogenase type 1 (11??-HSD-1). *Bioorganic Med. Chem. Lett.* **2011**, *21* (14), 4146–4149.

(64) Bauman, D. R.; Whitehead, A.; Contino, L. C.; Cui, J.; Garcia-Calvo, M.; Gu, X.; Kevin, N.; Ma, X.; Pai, L.; Shah, K.; et al. Evaluation of selective inhibitors of 11β-HSD1 for the treatment of hypertension. *Bioorg. Med. Chem. Lett.* **2013**, *23* (12), 3650–3653.

(65) Fordel, E.; Thijs, L.; Martinet, W.; Lenjou, M.; Laufs, T.; Van Bockstaele, D.; Moens, L.; Dewilde, S. Neuroglobin and cytoglobin overexpression protects human SH-SY5Y neuroblastoma cells against oxidative stress-induced cell death. *Neurosci. Lett.* **2006**, *410* (2), 146–151.

(66) Capece, L.; Boechi, L.; Perissinotti, L. L.; Arroyo-Mañez, P.; Bikiel, D. E.; Smulevich, G.; Marti, M. A.; Estrin, D. A. Small ligand-globin interactions: Reviewing lessons derived from computer simulation. *Biochim. Biophys. Acta - Proteins Proteomics* **2013**, *1834* (9), 1722–1738.

(67) Bruno, S.; Faggiano, S.; Spyrakis, F.; Mozzarelli, A.; Abbruzzetti, S.; Grandi, E.; Viappiani, C.; Feis, A.; Mackowiak, S.; Smulevich, G.; et al. The reactivity with CO of AHb1 and AHb2 from Arabidopsis thaliana is controlled by the distal HisE7 and internal hydrophobic cavities. *J. Am. Chem. Soc.* **2007**, *129* (10), 2880–2889.

(68) Uzan, J.; Dewilde, S.; Burmester, T.; Hankeln, T.; Moens, L.; Hamdane, D.; Marden, M. C.; Kiger, L. Neuroglobin and other hexacoordinated hemoglobins show a weak temperature dependence of oxygen binding. *Biophys. J.* **2004**, *87* (2), 1196–1204.

(69) Kawada, N.; Kristensen, D. B.; Asahina, K.; Nakatani, K.; Minamiyama, Y.; Seki, S.; Yoshizato, K. Characterization of a Stellate Cell Activation-associated Protein (STAP) with Peroxidase Activity Found in Rat Hepatic Stellate Cells. *J. Biol. Chem.* **2001**, *276* (27), 25318–25323.

(70) Hankeln, T.; Ebner, B.; Fuchs, C.; Gerlach, F.; Haberkamp, M.; Laufs, T. L.; Roesner, A.; Schmidt, M.; Weich, B.; Wystub, S.; et al. Neuroglobin and cytoglobin in search of their role in the vertebrate globin family. *Journal of Inorganic Biochemistry*. 2005, pp 110–119.

(71) Paramo, T.; East, A.; Garzón, D.; Ulmschneider, M. B.; Bond, P. J. Efficient characterization of protein cavities within molecular simulation trajectories: Trj-cavity. *J. Chem. Theory Comput.* **2014**, *10* (5), 2151–2164.

(72) Gabba, M.; Abbruzzetti, S.; Spyrakis, F.; Forti, F.; Bruno, S.; Mozzarelli, A.; Luque, F. J.; Viappiani, C.; Cozzini, P.; Nardini, M.; et al. CO Rebinding Kinetics and Molecular

Dynamics Simulations Highlight Dynamic Regulation of Internal Cavities in Human Cytoglobin. *PLoS One* **2013**, *8* (1).

(73) Giordano, D.; Boron, I.; Abbruzzetti, S.; van Leuven, W.; Nicoletti, F. P.; Forti, F.; Bruno, S.; Cheng, C. H. C.; Moens, L.; di Prisco, G.; et al. Biophysical Characterisation of Neuroglobin of the Icefish, a Natural Knockout for Hemoglobin and Myoglobin. Comparison with Human Neuroglobin. *PLoS One* **2012**, *7* (12).

(74) Boron, I.; Capece, L.; Pennacchietti, F.; Wetzler, D. E.; Bruno, S.; Abbruzzetti, S.; Chisari, L.; Luque, F. J.; Viappiani, C.; Marti, M. a.; et al. Engineered chimeras reveal the structural basis of hexacoordination in globins: A case study of neuroglobin and myoglobin. *Biochim. Biophys. Acta - Gen. Subj.* **2015**, *1850* (1), 169–177.

(75) Bisht, N. K.; Abbruzzetti, S.; Uppal, S.; Bruno, S.; Spyrakis, F.; Mozzarelli, A.; Viappiani, C.; Kundu, S. Ligand migration and hexacoordination in type 1 non-symbiotic rice hemoglobin. *Biochim. Biophys. Acta - Proteins Proteomics* **2011**, *1814* (8), 1042–1053.

(76) Pesce, A.; De Sanctis, D.; Nardini, M.; Dewilde, S.; Moens, L.; Hankeln, T.; Burmester, T.; Ascenzi, P.; Bolognesi, M. Reversible hexa- to penta-coordination of the heme Fe atom modulates ligand binding properties of neuroglobin and cytoglobin. *IUBMB Life* **2004**, *56* (11–12), 657–664.

(77) Pietra, F. On the pathways for CO egress from carboxy human cytoglobin. A molecular-dynamics investigation. *Chem. Biodivers.* **2013**, *10* (1), 86–95.

(78) Bustamante, J. P.; Radusky, L.; Boechi, L.; Estrin, D. a.; ten Have, A.; Martí, M. a. Evolutionary and Functional Relationships in the Truncated Hemoglobin Family. *PLoS Comput. Biol.* **2016**, *12* (1), 1–26.

(79) Abbruzzetti, S.; Spyrakis, F.; Bidon-Chanal, A.; Luque, F. J.; Viappiani, C. Ligand migration through hemeprotein cavities: insights from laser flash photolysis and molecular dynamics simulations. *Phys. Chem. Chem. Phys.* **2013**, *15* (26), 10686–10701.

(80) Yu, X.; Gao, D. Overexpression of cytoglobin gene inhibits hypoxic injury to SH-SY5Y neuroblastoma cells. *Neural Regen. Res.* **2013**, *8* (23), 2198–2203.

(81) Schmidt, M.; Gerlach, F.; Avivi, A.; Laufs, T.; Wystub, S.; Simpson, J. C.; Nevo, E.; Saaler-Reinhardt, S.; Reuss, S.; Hankeln, T.; et al. Cytoglobin Is a Respiratory Protein in Connective Tissue and Neurons, Which Is Up-regulated by Hypoxia. *J. Biol. Chem.* **2004**, *279* (9), 8063–8069.

(82) Bustamante, J. P.; Szretter, M. E.; Sued, M.; Martí, M. a.; Estrin, D. a.; Boechi, L. A quantitative model for oxygen uptake and release in a family of hemeproteins. *Bioinformatics* **2016**, *32* (12), 1805–1813.

(83) Acker, H. The oxygen sensing signal cascade under the influence of reactive oxygen species. *Philos. Trans. R. Soc. B Biol. Sci.* **2005**, *360* (1464), 2201–2210.

(84) Jackson, I. L.; Zhang, X.; Hadley, C.; Rabbani, Z. N.; Zhang, Y.; Marks, S.; Vujaskovic, Z.

Temporal expression of hypoxia-regulated genes is associated with early changes in redox status in irradiated lung. *Free Radic. Biol. Med.* **2012**, *53* (2), 337–346.

(85) Shivapurkar, N.; Stastny, V.; Okumura, N.; Girard, L.; Xie, Y.; Prinsen, C.; Thunnissen, F. B.; Wistuba, I. I.; Czerniak, B.; Frenkel, E.; et al. NIH Public Access. **2010**, *68* (18), 7448–7456.

(86) Tsujino, H.; Yamashita, T.; Nose, A.; Kukino, K.; Sawai, H.; Shiro, Y.; Uno, T. Disulfide bonds regulate binding of exogenous ligand to human cytoglobin. *J. Inorg. Biochem.* **2014**, *135*, 20–27.

(87) Beckerson, P.; Wilson, M. T.; Svistunenko, D. a; Reeder, B. J. Cytoglobin ligand binding regulated by changing haem-co-ordination in response to intramolecular disulfide bond formation and lipid interaction. *Biochem. J.* **2015**, *465* (1), 127–137.

(88) Isaksen, G. V.; Åqvist, J.; Brandsdal, B. O. Protein Surface Softness Is the Origin of Enzyme Cold-Adaptation of Trypsin. *PLoS Comput. Biol.* **2014**, *10* (8).

(89) Khan, S.; Farooq, U.; Kurnikova, M. Exploring protein stability by comparative molecular dynamics simulations of homologous hyperthermophilic, mesophilic, and psychrophilic proteins. *J. Chem. Inf. Model.* **2016**, *56* (11), 2129–2139.

(90) Siddiqui, K. S.; Cavicchioli, R. Cold-adapted enzymes. *Annu. Rev. Biochem.* **2006**, *75*, 403–433.

(91) Wells, S. a.; Crennell, S. J.; Danson, M. J. Structures of mesophilic and extremophilic citrate synthases reveal rigidity and flexibility for function. *Proteins: Structure, Function and Bioinformatics*. 2014.

(92) Wachtershauser, G. From volcanic origins of chemoautotrophic life to Bacteria, Archaea and Eukarya. *Philos. Trans. R. Soc. B Biol. Sci.* **2006**, *361* (1474), 1787–1808.

(93) Hamdane, D.; Kiger, L.; Dewilde, S.; Uzan, J.; Burmester, T.; Hankeln, T.; Moens, L.; Marden, M. C. Hyperthermal stability of neuroglobin and cytoglobin. *FEBS J.* **2005**, *272* (8), 2076–2084.

(94) Åqvist, J.; Kazemi, M.; Isaksen, G. V.; Brandsdal, B. O. Entropy and Enzyme Catalysis. *Acc. Chem. Res.* **2017**, acs.accounts.6b00321.

(95) Åqvist, J. Cold Adaptation of Triosephosphate Isomerase. *Biochemistry* **2017**, *56* (32), 4169–4176.

(96) Liu, K.; Kokubo, H. Exploring the Stability of Ligand Binding Modes to Proteins by Molecular Dynamics Simulations: A Cross-docking Study. *J. Chem. Inf. Model.* **2017**, acs.jcim.7b00412.

(97) Tu, H.; Powers, J. P.; Liu, J.; Ursu, S.; Sudom, A.; Yan, X.; Xu, H.; Meininger, D.; DeGraffenreid, M.; He, X.; Jaen, J. C.; Sun, D.; Labelle, M.; Yamamoto, H.; Shan, B.; Walker, N. P. C.; Wang, Z. *Bioorg. Med. Chem.* **2008**, *16*, 8922-8931

(98) Wang, H.; Ruan, Z.; Li, J. J.; Simpkins, L. M.; Smirk, R. A.; Wu, S. C.; Hutchins, R. D.; Nirschl, D. S.; Kirk, K. V.; Cooper, C. B.; Sutton, J. C.; Ma, Z.;Golla, R.; Seethala, R.; Salyan, M. E. K.; Nayeem, A.; Krystek Jr., S. R.; Sheriff, S.; Camc, D. M.; Morin, P. E.; Carpenter, B.; Robl, J. A.; Zahler, R.; Gordon, D. A.; Hamann, L. G. *Bioorg. Med. Chem. Lett.* **2008**, *18*, 3168-3172.

(99) Goldberg, F. W.; Dossetter, A. G.; Scott, J. S.; Robb, G. R.; Boyd, S.; Groombridge, S. D.; Kemmitt, P. D.; Sjögren, T.; Moretin Gutiérrez, P.; deSchoolmeester, J.; Swales, J. G.; Turnbull, A. V.; Wild, M. J. *J. Med. Chem.* **2014**, *57*, 970-986.

(100) Scott, J. S.; Bowker, S. S.; deSchoolmeester, J.; Gerhardt, S.; Hargreaves, D.; Kilgour, E.; Lloyd, A.; Mayers, R. M.; McCoull, W.; Newcombe, N. J.; Ogg, D.; Packer, M. J.; Rees, A.; Revill, J.; Schofield, P.; Selmi, N.; Swales, J. G.; Whittamore, P. R. O. *J. Med. Chem.* **2012**, 55, 5951-5964.